УНИВЕРЗИТЕТ У БЕОГРАДУ
МАШИНСКИ ФАКУЛТЕТ

Матија Н. Василев

Параметарско подешавање мреже у CFD прорачунима са применом у анализи енергетске ефикасности бродова

докторска дисертација

Београд, 2026

UNIVERSITY OF BELGRADE
FACULTY OF MECHANICAL
ENGINEERING

Matija N. Vasilev

Parametric Mesh Adjustment in CFD Calculations with Application to Ship Energy Efficiency Analysis

Doctoral Dissertation

Belgrade, 2026

Комисија за преглед, оцену и одбрану докторске дисертације

Ментор:	др Милан Калајџић, редовни професор, Универзитет у Београду, Машински факултет
Чланови комисије:	др Никола Момчиловић, ванредни професор Универзитет у Београду, Машински факултет
	др Дарко Раденковић, ванредни професор Универзитет у Београду, Машински факултет
	др Милан Калајџић, редовни професор Универзитет у Београду, Машински факултет
	др Стефан Рудаковић, доцент Универзитет у Београду, Машински факултет
	др Владислав Мараш, редовни професор Универзитет у Београду – Саобраћајни факултет

Датум одбране:

Изјаве захвалности

Као аутор, дугујем искрену захвалност коауторима свих радова на заједничком ангажовању у истраживању и писању, као и на драгоценим сугестијама које су пружили током израде ове докторске дисертације.

Посебну захвалност упућујем својој супрузи и деци, а потом и осталим члановима породице и пријатељима, на разумевању и подршци, као и инспирацији да уопште запловим у воде докторских студија бродоградње.

Резиме

Могло би се рећи да је трећа деценија 21. века која обухвата писање ове дисертације једна од веома значајних за савремену бродоградњу и то из више разлога. Са једне стране, постоји све већа потреба за све учесталијим транспортом добара између светске заједнице услед повећања броја људи на планети што резултира потребом изградње све већих бродова и чешћим пловидбама постојећих. Са друге стране, врши се велики притисак на бродовласнике како би се смањила емисија штетних гасова који доприносе ефектима стаклене баште тј. тражи се да бродови буду енергетски ефикаснији. Сам појам енергетске ефикасности је постао глобални тренд у свим економским секторима почетком 21. века. Иако бродови имају тек око 2,9%* удела у емисији угљен-диоксида (CO_2) на глобалном нивоу, регулативе које захтевају смањење испуштања овог гаса у атмосферу нису поштеделе ни овај вид транспорта што на први поглед делује веома апсурдно. Поготово што једна од регулатива има за циљ постизање нулте емисије до 2050. године. Стога је тема анализе енергетске ефикасности бродова веома популарна, нарочито правац који обухвата истраживања на пољу њеног побољшања. Пошто је временски рок веома кратак, траже се и многи помоћни (савремени софтверски) алати који би убрзали процес проналажења енергетски ефикасних решења. Зато је сада све актуелнија примена компјутерске динамике флуида (енг. Computational Fluid Dynamics - CFD), вештачке интелигенције (енг. Artificial Intelligence - AI), вештачких неуронских мрежа (енг. Artificial Neural Network - ANN) у циљу убрзања процеса пројектовања у савременој бродоградњи. Самим тим се отварају многе теме које до сада нису истраживане јер долази до повезивања мултидисциплинарних области са којима се класична бродоградња није сусретала. Зато је тему ове докторске дисертације било тешко дефинисати у једној реченици, а да покрије све области које су истражене, па се из тог разлога одлучило да ова дисертација има форму зборника више радова објављених у часописима различитих категорија као и радовима презентованим на међународним скуповима. У наслову је задржан кључан научни допринос који дисертација доноси, а односи се на параметарско подешавање мреже у CFD прорачунима. Појам енергетске ефикасности се прожима кроз скоро све радове, а обухваћена је кроз одређивање параметара енергетске ефикасности морских и речних бродова, примерима са применом емпиријских и нумеричких приступа са циљем побољшања енергетске ефикасности, развојем нових формула које убрзавају процесе поставки проблема у CFD софтверу, као и развој апликације за лакшу примену резултата добијених помоћу CFD софтвера и математичких модела добијених помоћу ANN. Кроз ову дисертацију, аутор описује опште појмове енергетске ефикасности бродова трудећи се да одговори на следећа питања: Како све бродови загађују околину? Када су бродови почели да загађују ваздух? Колико бродови заиста загађују ваздух? Како се одређује енергетска ефикасност бродова? Који је најбољи показатељ енергетске ефикасности бродова? Које су мере побољшања? Које су методе процене перформанси бродова? Која метода је најбоља и најпоузданија? Да ли су бродови током година заиста постали енергетски ефикаснији? Да ли су резултати истраживања спровођена на бродовима пре 70 година и данас актуелна? Како убрзати процесе пројектовања применом савремених софтверских алата и зашто је то важно? Зашто још увек не постоје јавно објављене смернице за поставку CFD симулација? Нека од ових питања су тривијална и одговори су веома јасни сваком читаоцу, док поједина питања захтевају веома дубоку анализу, како инжењерску, тако и економско-политичко-филозофску и због тога читалац можда неће наићи на конкретан одговор у овој дисертацији.

Кључне речи: енергетска ефикасност бродова, CFD, EEDI, EEXI, CII, ANN
Научна област: машинско инжењерство
Ужа научна област: бродоградња
УДК број:

* IMO, 2021. Fourth IMO Greenhouse Gas Study 2020. https://www.imo.org/.

Структура докторске дисертације

Концепт дисертације која се састоји из 13 радова је приказан на наредној слици:

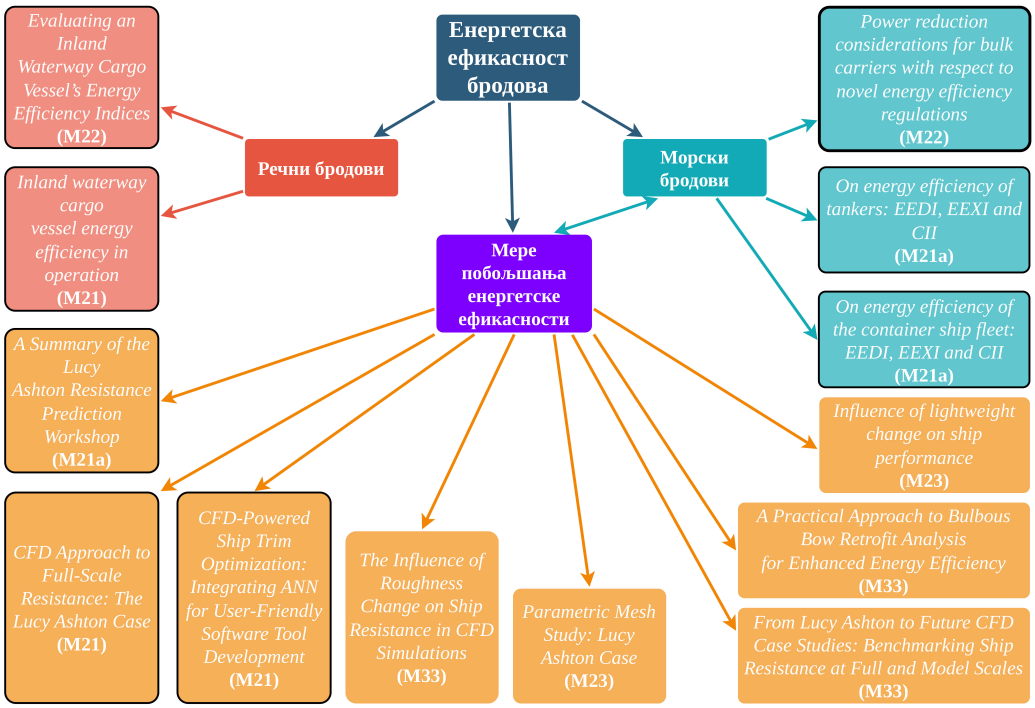

Слика 1: Структура докторске дисертације

Енергетска ефикасност бродова анализирана је код речних и морских бродова. У анализи речних бродова, објављена су два рада под називима: „*Evaluating an inland waterway cargo vessel's energy efficiency indices*“ [1] из категорије М22 и „*Inland waterway cargo vessel energy efficiency in operation*“ [2] из категорије М21. При анализи морских бродова, објављена су три рада који обухватају анализу енергетске ефикасности три типа брода: бродова за превоз расутог терета („*Power reduction considerations for bulk carriers with respect to novel energy efficiency regulations*“ [3] из категорије М22), танкера („*On energy efficiency of tankers: EEDI, EEXI and CII*“ [4] из категорије М21а) и контејнерских бродова („*On energy efficiency of the containership fleet: EEDI, EEXI and CII*“ [5] из категорије М21а). Када је реч о анализи мера за побољшање енергетске ефикасности, објављен је рад у часопису матичног факултета под називом „*Influence of lightweight change on ship performance*“ [6] из категорије М23. Главни фокус је заправо био на нумеричком приступу тј. употреби CFD софтвера у бродоградњи приликом чега су објављена четири рада у часописима и три рада саопштена на међународним скуповима. Носилац теме докторске дисертације је заправо рад под називом „*Parametric mesh study: Lucy Ashton case*“ [7] из категорије М23 објављен у часопису матичног факултета. Поред њега објављена су још три рада у часописима под називима „*CFD Approach to Full-Scale Resistance: The Lucy Ashton Case*“ [8] из категорије М21. као и „*A summary of the Lucy Ashton resistance prediction workshop*“ [9] из категорије М21а и „*CFD-powered ship trim optimization: integrating ANN for user-friendly software tool development*“ [10] из категорије М21. Из исте тематике, два рада саопштена на међународним скуповима носе називе „*A practical approach to bulbous bow retrofit analysis for enhanced energy efficiency*“ [11] и „*The influence of roughness change on ship resistance in CFD simulations*“ [12] из категорије М33. Рад на основу ког ће се темељити будућа CFD радионица је представљен кроз „*From Lucy Ashton to Future CFD Case Studies: Benchmarking Ship Resistance at Full and Model Scales*“ [13] из категорије М33. Поред наведених радова, написано је још пет радова из сличних области [14–18] који су саопштени

на међународним скуповима из категорије М33 и нису обједињени унутар резимеа дисертације. Наведени радови [1–13] се налазе у прилогу док су њихови најважнији доприноси приказани обједињено кроз наредна три главна поглавља.

Научни допринос ове дисертације огледа се у развоју методологије за параметарско дефинисање CFD мреже у симулацијама отпора депласманских бродова у мирној води. Предложени приступ заснива се на формулисању параметарских зависности које омогућавају систематско одређивање кључних параметара нумеричког модела, као што су величина прорачунског домена, величина основне ћелије, дебљина првог слоја ћелија у зони турбулентног граничног слоја и дистрибуција ћелија у критичним зонама око трупа брода. На тај начин унапређен је поступак постављања CFD симулација у бродоградњи, јер предложени параметарски приступ значајно смањује зависност од емпиријског подешавања параметара и метода „пробе и грешке“, који су често присутни у практичној примени CFD софтвера. У оквиру истраживања извршена је и детаљна нумеричка анализа утицаја скалирања, Фрудовог и Рејнолдсовог броја на процену отпора брода на основу експерименталних података за брод „Lucy Ashton“, чиме је омогућена нумеричка интерпретација експеримената који обухватају више различитих размера модела и мерења у стварној величини. Применљивост предложених параметарских формула потврђена је кроз валидацију CFD симулацијама на независном случају брода „Meteor“, што је показало да се предложена методологија може применити на бродове различитих геометријских размера и режима пловидбе. Поред тога, у дисертацији је приказана и практична примена CFD метода у анализи и унапређењу енергетске ефикасности бродова кроз разматрање конструктивних и оперативних мера, као што су оптимизација облика прамчаног дела, оптимизација трима и анализа утицаја обраштања трупа на отпор брода.

Summary

It could be said that the third decade of the 21st century, during which this dissertation was written, represents one of the most significant periods for modern shipbuilding, and this for several reasons. On the one hand, there is an ever-growing need for more frequent transportation of goods across the global community due to population growth, which results in the construction of larger ships and more frequent voyages of the existing ones. On the other hand, shipowners face increasing pressure to reduce the emission of harmful gases contributing to the greenhouse effect, i.e., to make ships more energy efficient. The very concept of energy efficiency became a global trend in all economic sectors at the beginning of the 21st century. Although ships contribute only about 2.9%* to global carbon dioxide (CO_2) emissions, regulations requiring a reduction of this gas's release into the atmosphere have not spared this mode of transport, which at first glance may seem paradoxical, especially considering that one of these regulations aims for zero emissions by 2050. Therefore, the topic of analyzing ship energy efficiency is highly relevant today, particularly in research focusing on its improvement.

Given the short timeframe for meeting these goals, there is an increasing demand for advanced (modern software) tools that accelerate the process of finding energy-efficient solutions. Hence, the application of Computational Fluid Dynamics (CFD), Artificial Intelligence (AI), and Artificial Neural Networks (ANN) has become increasingly prevalent to speed up the design process in modern shipbuilding. This has opened many new, previously unexplored research topics by linking multidisciplinary fields that classical shipbuilding had not previously encountered. For this reason, the topic of this doctoral dissertation could not easily be defined in a single sentence to encompass all investigated areas. Consequently, this dissertation has been structured as a collection of several published journal papers and conference contributions. The title retains the key scientific contribution of the dissertation – parametric mesh adjustment in CFD simulations. The concept of energy efficiency runs through almost all papers, covering: determination of energy efficiency parameters for both sea-going and inland vessels; examples combining analytical and numerical approaches aimed at improving energy efficiency; development of new formulas that accelerate the setup of CFD simulations; and the creation of an application that facilitates the use of CFD-based results and mathematical models obtained using ANN. Throughout this dissertation, the author discusses the general concepts of ship energy efficiency while attempting to answer the following questions: How do ships pollute the environment? When did they start polluting the air? How much do ships actually contribute to air pollution? How is ship energy efficiency determined? What is the best indicator of ship energy efficiency? What are the improvement measures? Which performance assessment methods exist? Which one is the most reliable? Have ships indeed become more energy-efficient over the years? Are research results from 70 years ago still relevant today? How can the design process be accelerated using modern software tools, and why is that important? Why are there still no publicly available guidelines for setting up CFD simulations? Some of these questions are rather straightforward, with obvious answers, while others require deep analysis, engineering, economic, political, and philosophical, and thus the reader may not find direct answers to all of them within this dissertation.

Keywords: Ship energy efficiency, CFD, EEDI, EEXI, CII, ANN
Scientific discipline: Mechanical Engineering
Scientific subdiscipline: Naval Architecture
UDC number:

* IMO, 2021. Fourth IMO Greenhouse Gas Study 2020. https://www.imo.org/.

Structure of the doctoral dissertation

The concept of the dissertation, which consists of 13 papers, is illustrated in the following figure:

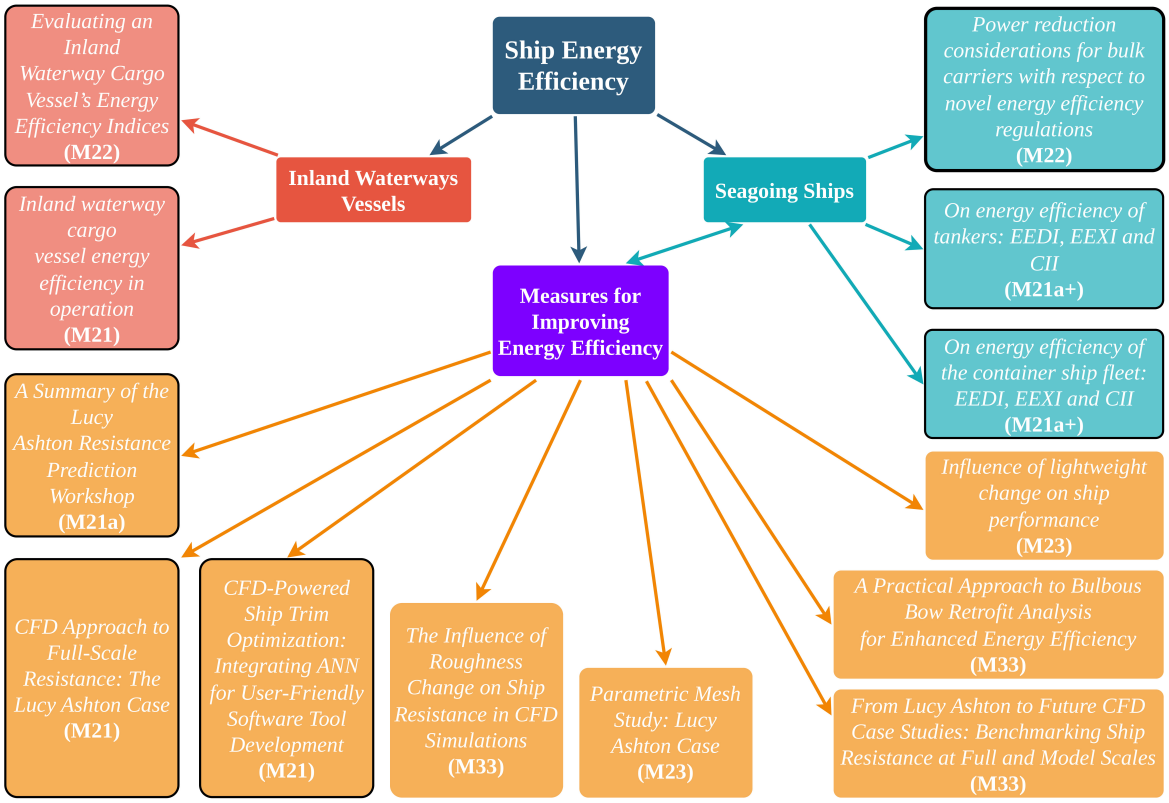

Figure 1: Structure of the Doctoral Dissertation

The energy efficiency of ships was analysed for both inland and seagoing vessels. In the analysis of inland vessels, two papers were published entitled: "*Evaluating an inland waterway cargo vessel's energy efficiency indices*" [1] (category M22) and "*Inland waterway cargo vessel energy efficiency in operation*" [2] (category M21). In the analysis of seagoing vessels, three papers have been published addressing the energy efficiency of two ship types: bulk carriers ("*Power reduction considerations for bulk carriers with respect to novel energy efficiency regulations*" [3], category M22), tankers ("*On energy efficiency of tankers: EEDI, EEXI and CII*" [4], category M21a) and containerships ("*On energy efficiency of the containership fleet: EEDI, EEXI and CII*" [5], category M21a). Regarding the analysis of measures for improving energy efficiency, the paper "*Influence of lightweight change on ship performance*" [6] (category M23) was published in the journal of the home faculty. The main focus, however, was on the numerical approach, i.e., the use of CFD software in shipbuilding, within which four journal papers and three conference papers were published. The main point of the doctoral dissertation is the paper entitled "*Parametric mesh study: Lucy Ashton case*" [7] (category M23), published in the journal of the home faculty. In addition, three more journal papers were published: "*CFD Approach to Full-Scale Resistance: The Lucy Ashton Case*" [8] (category M21), "*A summary of the Lucy Ashton resistance prediction workshop*" [9] (category M21a), and "*CFD-powered ship trim optimization: integrating ANN for user-friendly software tool development*" [10] (category M21). From the same research area, two papers presented at international conferences are titled "*A practical approach to bulbous bow retrofit analysis for enhanced energy efficiency*" [11] and "*The influence of roughness change on ship resistance in CFD simulations*" [12] (category M33). The paper forming the basis for the future CFD workshop was presented as "*From Lucy Ashton to Future CFD Case Studies: Benchmarking Ship Resistance at Full and Model Scales*" [13] (category M33).

In addition to the listed papers, five more papers [14–18] were written and presented at international conferences (category M33); these are not included within the dissertation. The aforementioned papers [1–13] are provided in the appendix, while their most important contributions are presented in an integrated manner through the following three main chapters.

The scientific contribution of this dissertation lies in the development of a methodology for the parametric definition of the CFD mesh in simulations of the calm-water resistance of displacement ships. The proposed approach is based on the formulation of parametric relationships that enable the systematic determination of key parameters of the numerical model, such as the size of the computational domain, the base cell size, the thickness of the first cell layer in the turbulent boundary layer region, and the distribution of cells in critical zones around the ship hull. In this way, the procedure for setting up CFD simulations in shipbuilding has been improved, as the proposed parametric approach significantly reduces the dependence on empirical parameter tuning and the "trial-and-error" methods that are often present in the practical application of CFD software. Within the scope of this research, a detailed numerical analysis of the influence of scaling, the Froude number, and the Reynolds number on the estimation of ship resistance was also carried out, based on experimental data for the ship *Lucy Ashton*, which enabled a numerical interpretation of experiments involving multiple model scales as well as full-scale measurements. The applicability of the proposed parametric formulas was confirmed through validation by CFD simulations on the independent case of the ship *Meteor*, demonstrating that the proposed methodology can be applied to ships of different geometric scales and operating conditions. In addition, the dissertation presents the practical application of CFD methods in the analysis and improvement of ship energy efficiency through the consideration of both design and operational measures, such as bow shape optimization, trim optimization, and the analysis of the influence of hull fouling on ship resistance.

Можда још увек ми (инжењери) не знамо како да направимо енергетски ефикасан брод, али је глобална агенда учинила нас саме ефикаснијима. Некада давно би за писање овакве дисертације био потребан и математичар и програмер и инжењер, али уз развој савремених софтверских алата и његово омогућено једноставно учење, дата нам је могућност бољег, лакшег и бржег усавршавања.

Садржај

Увод

Иако у свету влада глобални тренд повећања енергетске ефикасности са акцентом на смањењу емисије гасова који стварају ефекат стаклене баште, не могу се заобићи и остали типови загађења који потичу од бродова. Пре свега, бродови због кретања кроз два флуида (воду и ваздух), емитују штетну емисију и у воду и у ваздух. Поред CO_2 (одговоран за климатске промене) који има 96,4% удела у издувној емисији, ту су још и угљен-моноксид (CO) сумпорни (SO_x) и азотни оксиди (NO_x) (одговорни за смог и киселе кише), као и угљоводоници, честице чађи и тешки метали у малој количини. Наведени гасови настају као продукти потпуног и непотпуног сагоревања у главном погонском мотору, генераторима, инцинератору и осталим уређајима који као главни извор енергије користе угљоводонична горива. Такође, у атмосфери се може наћи и емисија од фреона или халогених гасова који потичу од расхладних система, а услед цурења на спојним местима, неправилним пуњењем или пражњењем система хлађења, оштећењем цевовода или размењивача топлоте или намерним испуштањем фреона (што је према тренутно важећим прописима забрањено). Током транспорта и претовара терета може долазити до испаравања нафтних деривата (бензин, дизел, керозин, деривати који садрже лако испарљиве супстанце), хемијских производа (метанол, етанол, стирен и др.) или течних гасова (течни природни гас (енг. Liquefied Natural Gas – LNG), течни нафтни гас (енг. Liqufied Petroleum Gas – LPG)). Испарљиве супстанце у атмосфери реагују са NO_x и стварају приземни озон и смог, неке испарљиве материје су канцерогене, а поједине паре могу бити запаљиве или чак и експлозивне. Вода се може загадити од стране бродова на много више начина. Бука и вибрације изазване мотором, а пренесене вратилом на пропелер, иако не испуштају директно супстанце у воду, утичу на морски екосистем. Отпадне воде садрже органске материје и патогене микроорганизме који смањују ниво кисеоника у води или доводе до еутрофикације. Чврсти отпад попут пластике, метала и папира је нажалост веома заступљен у води, а највећи проблем је микропластика која улази у ланац исхране. Услед неправилног одстрањивања зауљених вода може доћи до формирања уљаног филма на површини воде који спречава размену кисеоника. Код танкера или генерално приликом танковања брода може доћи до испуштања горива у воду. При судару, насукавању или оштећењу танкова, огромна количина терета или горива се могу наћи у води што доводи до дуготрајне еколошке катастрофе. Уколико се кањужна вода не пречисти добро, њеним испуштањем у воду долази до озбиљног загађења. Након транспорта нафте и хемикалија, резервоари се перу водом, а ако се заостала мешавина испусти у воду, уносе се велике количине угљоводоника и хемикалија. При узимању баласта, у танкове улазе микроорганизми и јединке из једног региона, а при испуштању у другом региону, они могу постати инвазивне врсте, угрозити екосистем и рибарство. Због тога данас постоје строга правила под окриљем Међународне поморске организације (енг. International Maritime Organization – IMO) која је основала 1973. године Интернационалну конвенцију о превенцији загађења са бродова (енг. International Convention for the Prevention of Pollution from Ships - MARPOL) и тиме покрила шест различитих аспекта загађења и то од уља (MARPOL Annex I – усвојен 1973. године, а ступио на снагу 1983.), штетних течних материја (MARPOL Annex II – усвојен 1973, године, а ступио на снагу 1983. године), штетних материја у пакованом облику (MARPOL Annex III – ступио на снагу 1978. године, а ступио на снагу 1992.), отпадних вода са бродова (MARPOL Annex IV – усвојен 1978, а ступио на снагу 2003.), смећа са бродова (MARPOL Annex V – усвојен 1978. године а ступио на снагу 1988.) и загађења ваздуха са бродова (MARPOL Annex VI – усвојен 1997. године, а ступио на снагу 2005.).

Више од 100 година је прошло од производње и поринућа првог брода са дизел мотором до усвајања анекса везаног за превенцију загађења ваздуха од стране бродова. Први практични комерцијални брод се звао Вулкан и изграђен је у Холандији 1910. године, а имао је два дизел мотора од 400 коњских снага. Према статистичким извештајима[1] 2005. године је светску флоту

[1] Equasis. *Equasis база података*. https://www.equasis.org/

чинило 61227 бродова (већих од 100 бруто тона), 2008. године 74814 бродова, а 2022. године тај број је порастао на 126947 бродова. Разлог зашто је настала оволика разлика у броју бродова у односу на 2005. и 2008. годину је у томе што тада рибарски бродови нису били урачунати. Чак 41% бродова светске флоте из 2022. је старије од 25 година што значи да бар 80-85% бродова који су постојали 2005. године су још увек пловили у то време. За наредне године, извештаји још увек нису објављени у време писања дисертације. Поред 2005. и 2022. године, наведен је податак и за 2008. годину која је веома значајна из разлога што се та година узима као референтна за ослобођену емисију гасова који стварају ефекат стаклене баште (енг. Greenhouse Gases – GHG) од стране бродова. IMO је кроз нове регулативе задао циљ да се 2050. године достигне нулта емисија GHG, а да се до 2030. године смањи емисија GHG у односу на 2008. годину најмање 20% (а тежећи 30%), а до 2040. године смањи емисија најмање 70% (а тежећи 80%).

2009. године први пут се уводи појам индекса енергетске ефикасности бродова и то кроз Оперативни индикатор енергетске ефикасности (енг. Energy Efficiency Operational Indicator – EEOI) изражен у количини емитованог CO_2 (у грамима) у атмосферу по једној превезеној тони терета и једној пређеној наутичкој миљи. Овај индикатор никада није постао обавезно применљив од стране регулаторног тела, већ је на добровољној бази могао показати колико је брод заправо користан. Овај показатељ се може применити на нивоу једне пловидбе, више пловидби, за један или више бродова. 2011. године се први пут уводи појам Пројектованог индекса енергетске ефикасности (енг. Energy Efficiency Design Index – EEDI), а односио се на све бродове веће од 400 бруто тона и изграђене након 1. јануара 2013. године или испоручене након 1. јануара 2015. Треба напоменути да готово половина светске флоте не подлеже IMO регулативи јер су испод 400 бруто тона или се ради о рибарским бродовима за које одређивање параметара енергетске ефикасности није применљиво. EEDI представља номиналну (теоријску) количину CO_2 (у грамима) емитовану у атмосферу по превезеној једној тони терета и пређеној једној наутичкој миљи. Сврха увођења овог индекса је да обавеже бродоградилишта и пројектанте да у нове бродове уграђују енергетски ефикасне технологије и моторе. Примењује се на тај начин што постигнути EEDI (енг. Attained EEDI) мора имати мању вредности од захтеване вредности (енг. Required EEDI). Захтевана вредност се одређује на основу референтне вредности, а референтна вредности је узета као просечна вредност EEDI-ја сличних бродова истог типа изграђених у периоду од 2000. до 2010. године. Пошто је број бродова изграђених пре 2013. године, а који се налазе у оперативи и даље веома велики поставило се питање како се они могу учинити ефикаснијима. Зато је 2019. године представљен Индекс енергетске ефикасности постојећих бродова (енг. Energy Efficiency for Existing Ship Index – EEXI), а који је ступио на снагу 2023. године. Он исто представља номиналну количину CO_2 (у грамима) емитовану у атмосферу по превезеној једној тони терета и пређеној једној наутичкој миљи, само важи за бродове изграђене пре 2013. године веће од 400 бруто тона. Примењује се на тај начин што постигнути EEXI (енг. Attained EEXI) мора имати мању вредност од захтеване вредности (енг. Required EEXI). Захтевана вредност EEXI-ја се рачуна исто на основу референтне вредности као код EEDI-ја. Суштинска разлика у захтеваним вредностима EEDI-ја и EEXI-ја је у другачијим факторима редукције. Наиме, код EEDI-ја, фактори редукције се разликују према типу брода и години производње брода и они су се мењали по фазама које су трајале од 2013. до 2025. године. Код EEXI-ја параметри редукције су од старта имали исту вредност у зависности од типа брода и они се у великој мери подударају са факторима редукције за EEDI из последње фазе. 2023. године ступа на снагу још један параметар енергетске ефикасности, а то је Индикатор заступљености угљеника (енг. Carbon Intensity Indicator – CII) који важи за бродове веће од 5000 бруто тона. Уведен је такође од стране IMO-а са циљем директног праћења емисије CO_2 и он представља стварну количину CO_2 (у грамима) емитовану у атмосферу по превезеној једној тони терета и пређеној једној наутичкој миљи. Од 2019. за сваки брод већи од 5000 бруто тона оператер брода (менаџмент) мора имати континуирано бележење количине потрошње горива, времена

проведеног у пловидби и пређеног пловног пута кроз тзв. Систем прикупљања података (енг. Data Collection System – DCS). Постигутни CII за текућу годину се рачуна на основу снимљених података за целу претходну годину. Постигнути CII (енг. Attained CII) се такође упоређује са захтеваном вредношћу CII-а (енг. Required CII) с тим што брод добија енергетски разред A, B, C, D или E у зависности од тога колико је далеко од захтеване вредности. Захтевана вредност CII-а се одређује према референтној вредности уз фактор редукције који се мења на сваке две године. Циљ је да брод има енергетски разред A, али је прихватљив и резултат који сврстава брод у разред C. Истовремено се поред постигнутог CII-а и одређеног разреда за текућу годину врши процена разреда и за наредне три године под претпоставком исте оперативности, те ако се деси да брод постиже три године заредом разред D или бар једну годину разред E, мора се направити детаљан план како оператер (менаџмент или сам бродовласник) планира да уз увођење одређених мера уштеде, достигне разред C.

Проблеми који се могу потенцијално јавити при одређивању номиналних параметара ефикасности (EEDI или EEXI) настају услед недостајања појединих, а кључних информација које директно утичу на њихову вредност. Првенствено се недостатак документације повезује са одређивањем EEXI-ја и то се односи на специфичну потрошњу горива и референтну брзину. Специфична потрошња горива изражена је у грамима по киловат-часу и најчешће је доступна у тзв. NO_x техничком документу који издаје произвођач мотора. Референтна брзина је брзина коју брод постиже при 75% максималне инсталисане снаге мотора или при 83% ограничене снаге мотора, ако брод има уграђен лимитатор као меру уштеде енергије, која год од те две вредности да је мања. Регулаторно тело је формирало два правца који се могу следити за одређивање недостајућих параметара, а то су статистички и директни приступ. Статистички приступ је заснован на препорученим формулама за одређивање података који недостају, а директни приступ се своди на директно, експериментално мерење тих параметара организацијом пробних вожњи бродова. Пробна вожња брода је заснована на директном мерењу брзине брода и обртног момента на вратилу, преко кога се уз измерену брзину обртања вратила добија ангажована снага мотора. Након обављене пробне вожње, уз кориговање измерених вредности за временске услове, стање мора и пливања брода, према стандардној процедури, добија се пропелерска крива на основу које се може одредити референтна брзина. Од 2022. године је званично прихваћен од стране регулаторног тела још један начин одређивања референтне брзине, а то је директна нумеричка симулација тј. CFD анализа. У дисертацији су одређени индекси енергетске ефикасности, помоћу статистички одређеним формулама (EEDI или EEXI), флоте коју чине 153 брода за превоз расутог терета [3], 426 танкера [4] и 162 контејнерска брода [5] изграђених у периоду од 2000. до 2020. године што је чинило укупно око 2,5% светске флоте ова три типа брода која подлежу IMO регулативи у том тренутку. Главни циљ код ових истраживања је био да се види да ли су нови бродови који су грађени током година заиста постајали енергетски ефикаснији. Додатна питања на која се могу наћи одговори у овој дисертацији су: Колики проценат бродова из разматране флоте (не) испуњава IMO регулативе? Који су економски најисплативији начини унапређења енергетске ефикасности? Колика је потребна редукција снаге главног мотора да би разматрани бродови испунили критеријуме номиналних параметара ефикасности (EEDI или EEXI)? Колике су просечне пројектоване брзине бродова за превоз расутог терета, танкера и контејнерских бродова а којом брзином они заправо плове? Колико је реално потребно смањити брзину пловидбе да би бродови испуњавали критеријуме CII-а?

Важно је напоменути да сви наведени показатељи енергетске ефикасности важе само за морске бродове, а када је реч о речним бродовима, до времена писања дисертације, не постоје обавезујуће међународне регулативе које налажу процену индекса енергетске ефикасности на унутрашњим пловним путевима. Централна комисија за пловидбу Рајном је 2018. године поставила сличне циљеве у погледу смањења емисије CO_2 до 2050. године, што је и у складу са Европском зеленом агендом из 2019. чији је циљ да Европа до 2050. године буде први

климатски неутралан континент. Постоје за сада два предлога за одређивање номиналних показатеља енергетске ефикасности и они су анализирани кроз дисертацију. Једна од метода је развијена управо на Машинском факултету Универзитета у Београду у оквиру докторске дисертације професора на Катедри за бродоградњу[2]. Метода је заснована на EEDI-ју морских бродова, дакле, исто се одређују постигнути и захтевани EEDI, при чему постигнути мора бити мањи од захтеваног. Разлика је у томе што се за речне бродове узима утицај дубине реке (ограничења пловног пута) и што се EEDI одређује за скуп брзина (код морских бродова се узима у обзир само референтна брзина). Друга метода је развијена у Развојном центру бродске технологије и транспортних система у Дуизбургу и она је такође заснована на принципима EEDI-ја морских бродова. И ова метода узима у обзир ограничења пловног пута с тим што у прорачун улази једна брзина која одговара прорачунској снази дефинисаној према методи. Међутим, ова метода узима у обзир и различите брзине реке. Када је реч о броју речних бродова, свака земља води сопствене регистре, а консолидоване међународне базе нису јавно доступне. Неким земљама (посебно у Азији, Африци или Латинској Америци) можда чак и недостају поуздани подаци. Према неким доступним извештајима за Европу, постоји податак да је регистровано око 15000 бродова унутрашњих пловних путева, а највећи број плови Рајном и Дунавом. Такође, скоро 40% бродова који плове Дунавом су стари преко 40 година, а само 1% регистрованих бродова је изграђено након 2010. године. Имајући у виду старост флоте, као и то да се многи велики градови налазе на рекама, несумњиво је да значајан утицај на загађење ваздуха имају и речни бродови, поготово што плове кроз насељена места. У раду [2] је анализирана количина CO_2 коју емитује један типичан самоходни речни брод на једној рути, за месец дана и за годину дана под одређеним претпоставкама и јавно доступним подацима. Према Европској зеленој агенди, циљ је да се 75% железничког и друмског транспорта преусмери на реке јер су бродови најефикаснији начин транспортовања по јединици пређеног пута и количини пренесеног терета.

Већ деценијама уназад долази до развоја разних метода и уређаја који имају за циљ побољшање енергетске ефикасности бродова. Начини на који се може доћи до уштеде енергије се могу поделити на четири групе: конструктивни, пропулзивни, технолошки и оперативни. Конструктивне мере се примењују најчешће на новим пловилима или при већим реконструкцијама. У те мере спадају оптимизација форме трупа, дизајн прамца, смањење отпора трења и оптимизација надградње и палубних уређаја. Оптимизацијом форме трупа смањује се отпор брода у води, а сама оптимизација се најчешће ради CFD анализом уз експерименталну валидацију. Дизајн или оптимизација прамца (постојање и облик булба, вертикалне статве) се такође врши CFD анализом и примењује се и у новоградњи, али и у реконструкцији брода јер може да се деси да се брод не експлоатише на онај начин на који је првобитно замишљено. То је веома чест случај када брод више пута мења власника или оперативни менаџмент. Смањење отпора трења се постиже премазима против обраштања (енг. anti-fouling coatings), самополирајућим премазима или премазима са ниским коефицијентом трења. Смањење тежине употребом лакших материјала, оптимизацијом простора и правилним конструктивним дизајном, може донети побољшања у уштеди енергије. Оптимизацијом надградних делова као што је нпр. конструктивни додак за заштиту од ветра код контејнерских бродова на прамцу може се смањити аеродинамички отпор, а самим тим и уштеди потребна енергија за кретање брода. Пропулзивне мере се фокусирају на побољшање рада пропелера и система за погон. Оптимизација пропелера подразумева прилагођавање његових геометријских карактеристика условима пловидбе брода са циљем постизања што већег степена корисности уз оптималну потрошњу горива погонског мотора. Додавање уређаја за уштеду енергије (енг. Energy Saving Device - ESD) најчешће је присутно код морских бродова, али се поједини користе и код речних бродова. Ти уређаји се постављају испред или иза пропелера (енд. pre-swirl/post-swirl). Уређаји који се постављају испред пропелера имају

[2] Симић, А. (2012). *Енергетска ефикасност речних самоходних теретних* (докторска дисертација, Универзитет у Београду, Машински факултет). http://doiserbia.nb.rs/phd/fulltext/BG20121101SIMIC.pdf

задатак да побољшају дострујавање воде пропелеру у заклоњеним зонама услед постојања трупа и то су нпр. Бекер Мевисова дострујна сапница (енг. Becker Mewis Duct), Шнеклутова дострујна сапница (енг. Schneekluth Wake Equalizing Duct), Мицубишијеве лопатице, (енг. Mitsubishi fins), дострујна крила, полу-сапнице и сл. Поред тога асиметрична крмена статва се понекад уграђује код једнопропелерних бродова иако је чест случај код двопропелерних бродова. Дострујни тунели и тзв. сукњице типични су за речне бродове. Уколико оперативне активности брода изискују уградњу пропелера већег пречника него што има места иза крмене статве, имајући у виду и ограничење газа, крма се укопава у форми тунела. Крмене сукњице се често уграђују да би се обезбедило боље дострујавање воде пропелеру и да би се спречило усисавање ваздуха са површине воде. Данас постоје и системи прекретних сапница које се отварају или затварају у зависности од газа брода. Пропелери у сапници су уобичајени код бродова код којих није могуће уградити пропелер довољно великог пречника, а постоји потреба за великом силом потиска као што је случај код реморкера и потискивача. Такође, сапница спречава преструјавање воде на врховима крила. Уређаји који се постављају иза пропелера имају задатак да искористе енергију вртлога који се формира ротацијом пропелера. Ту спадају контра кормила, узгонска крила на кормилу, булб на кормилу, крила на главчини пропелера (енг. Propeller Boss Cap Fin - PBCF). Гримово коло је уређај са сопственим лежајем који се монтира на главчину пропелера и обично је већег пречника од самог пропелера. Део крила који је у зони пропелера има улогу турбине чије лопатице покреће вода иза пропелера, а преостали део крила ствара додатни потисак. Тандем пропелери се користе уколико су пропелери веома оптерећени, па се оптерећење дели на више њих. Контра-ротирајући пропелери су пропелери који се обрћу у различитом смеру, а налазе се на истом вратилу. Главни недостатак свих статичних уређаја за уштеду енергије је што негативно утичу на отпор брода, а бенефити су свега пар процената, често и тешко мерљиви. Оперативне мере су најзаступљенији вид примене ради уштеде енергије на бродовима јер су економски најисплативије. Ту спадају смањење брзине (енг. slow steaming), отпимизација руте и брзине прилагођене временским приликама, редовно одржавање (чишћење) трупа и пропелера (чишћење), оптимизација логистике, оптимизација положаја пливања (енг. trim optimization). Смањење брзине је најчешћи вид унапређења енергетске ефикасности јер не захтева никаква улагања. Своди се на чињеницу да се за кретање мањом брзином савладава мањи отпор, при чему се троши мање горива, а тиме се смањује и издувна емисија. Главни проблем који се овде јавља јесте што овај вид уштеде има негативан ефекат на мотор јер ради на нижим температурама и тако долази до непотпуног сагоревања, кондензовања у издувном систему, појаве наслага чађи на лопатицама турбопуњача, појаве корозије и др. Оптимизација руте и брзине подразумева добру логистичку подршку са циљем избегавања подручја са лошим временским приликама. Редовно чишћење трупа и пропелера је веома значајно и ради се услед појаве обраштања. Обраштање је процес таложења и раста микроорганизама, алги, шкољки и других организама на подводном телу трупа брода. То је природна појава која настаје чим када је неко тело потопљено у воду. Постоји микрообраштање, када се на подводним деловима створи слој слузи и бактерија (тзв. биофилм), док макрообраштање је појава већих организама као што су шкољке, морске траве, алге и корали на подводним деловима брода. Било какве наслаге на трупу брода, повећавају храпавост површине, што доводи до повећања отпора брода који пропелер треба да савлада. Да би се одржала иста брзина пловидбе, брод мора да ангажује више снаге, а самим тим се повећава и потрошња горива, а потом и издувна емисија. Оптимизација логистике подразумева бољу испланираност времена проведеног на сидришту, у луци или количине транспортовања терета или подручја пловидбе. Под оптимизацијом положаја пливања се тражи положај при коме је отпор брода при одређеној брзини пловидбе минималан. Софтвери на бази CFD дају кључни допринос у примени ове оперативне мере у циљу побољшања енергетске ефикасности. Технолошке мере су економски најнеисплативији облик мера (уколико се ради о реконструкцији постојећег брода), али зато могу да допринесу највећом уштедом енергије. Ту спадају промена горива (LNG, метанол, амонијак, водоник), електрификација, рекуперација издувних гасова, испуштање мехурова ваздуха, уградња

соларних панела или ротора, постављањем једара. Предност промене горива се огледа у мањој количини штетних гасова који се добијају њиховим сагоревањем. Енергија добијена рекуперацијом издувних гасова се може користити за система грејања на броду. Смањење отпора брода се постиже и уградњом система за испуштање ваздуха испод трупа (енг. Air Lubrication System – ALS). Уређај ради на принципу испуштања мехурова ваздуха у зони равног дна и тиме се смањује трење. Парадоксално је што се испоставило да систем има бољи ефекат код контејнерских бродова који има мању површину равног дна и плове већим брзинама у односу на танкере и бродове за превоз расутог терета. Уградња ротора (високих ротирајућих цилиндара) на палуби омогућава стварање додатне силе потиска која се ствара Магнусовим ефектом. Једра користе енергију ветра, при чему се ствара додатна сила потиска. Међутим, ниједно од алтернативних горива нема толику количину енергије (калоричну моћ) по јединици масе као што има дизел гориво, зато се оно још увек налази на првом месту по употреби и зато се још увек праве бродови са погоном на ову врсту горива.

Кроз ову дисертацију анализиран је утицај конструктивних мера кроз оптимизацију облика прамчаног дела [11] и смањење тежине [6] и оперативних мера кроз смањење брзине [2, 3, 4, 5], редовно чишћење трупа [12] и оптимизацију положаја пливања тј. оптимизацију трима (енг. trim optimization) [10]. При анализирању наведених мера, смањење тежине и брзине је анализирано кроз статистичке формуле за одређивање параметара енергетске ефикасности као и праћењем смерница издатих од стране регулаторних тела. Оптимизација облика прамчаног дела, утицај редовног одржавања трупа и оптимизација трима су анализирани помоћу CFD софтвера, такође следећи смернице и препоруке за поставку симулација издатих од стране регулаторних тела.

Оптимизација облика прамчаног дела је подразумевала проверу различитих типова булбова и његовог постојања уопште код једног контејнерског брода [11] за који се анализом његових експлоатационих карактеристика испоставило да плови чак 40% нижом брзином него за коју је пројектован и да најчешће плови на знатно нижем газу, који одговара 60% уделу пројектованог депласмана.

Утицај обраштања на тотални отпор је знатан и та анализа је урађена кроз CFD симулације на примеру једног брода за превоз расутог терета [12] тј. колико се повећава отпор брода ако се он не би чистио пет година.

Трим оптимизација је обахватила анализу једног брода за превоз аутомобила [10] при чему су анализирана три газа, седам положаја пливања и три брзине, што је обухватило 63 симулације. Пошто брод у реалности може да плови и у стању које није анализирано нумеричким путем, изведен је математички модел процене брзине обртања вратила, ангажоване снаге мотора и дневне потрошње горива, помоћу вештачких неуронских мрежа. Помоћу математичког модела се тако може добити процена наведених параметара за било које међустање које је обухваћено дефинисаним границама применљивости тј. (урађеним симулацијама). Формуле добијене помоћу вештачких неуронских мрежа су веома комплексе, и за капетане и бродске официре нису погодне за дневну употребу. Стога је направљена посебна апликација у софтверском пакету „MATLAB“ која има једноставан графички интерфејс, а у позадини решаве комплексне математичке једначине.

Иако су тек 2022. године признате као званичан метод, нумеричке симулације (CFD) као начини решавања комплексних математичких једначина, користе се више деценија уназад за процене одређених параметара у бродоградњи. Најчешћа примена CFD-а у бродоградњи заснива се на процени пропелерске криве брода тј. процене отпора брода на мирној води, процена карактеристика пропелера, као и теста ауто-пропулзије брода у размери модела, али и у стварној величини. Поред тога, данас се CFD користи и за процену маневарских

способности, понашања брода на таласима, интеракције између флуида и конструкције, оптимизације трупа и пропелера ради побољшања енергетске ефикасности, кавитације пропелера, утицаја турбуленције и др. Примена CFD-а до 2022. године се заснивала искључиво у истраживачке сврхе ради развоја и оптимизације нумеричких алгоритама за решавање Навије-Стоксових једначина. До данас, не постоји јавно објављен документ који садржи процедуру за дефинисање поставки CFD симулација, а који гарантују поуздане резултате. Многи софтвери су непрактични за кориснике без претходног искуства јер имају сложен алгоритам и систем конфигурисања од минимум 50 параметара који директно утичу на резултате и зато су многа истраживања базирана на принципу пробе и грешке или само на утицају малог броја параметара.

Истраживања у овој дисертацији су усмерена на поједностављивање поставки CFD симулација увођењем параметарских формула. Параметарске формуле су добијене на основу анализе спроведених експеримената као и итеративним спровођењем CFD симулација све док није постигнута жељена тачност [7]. Фокус истраживања јесте дефинисање прорачунског домена, величине основне ћелије, дебљине првог слоја ћелија до трупа брода, дистрибуције ћелија у зони око трупа брода као и зона које треба представити финијом мрежом. Разлог зашто су ови параметри узети у разматрање јесте у томе што они највише утичу на резултате нумеричког прорачуна. У конкретном случају, под нумеричким прорачуном сматра се одређивање отпора брода у мирној води. Познато је да се у индустрији бродоградње процена отпора брода врши моделским испитивањима у базенима, а потом употребом екстраполатора издатог кроз Интернационалну конференцију базена за моделска испитивања (енг. International Towing Tank Conference – ITTC) 1978. године, врши прорачун отпора брода у стварној величини. У бродограђевној историји, позната су четири случаја експерименталног одређивања (мерења) отпора брода у стварној величини, а поред тога, за неке од њих постоје и подаци о моделским испитивањима у више различитих размера. Два од та четири случаја су анализирана кроз докторску дисертацију [7, 8, 9, 13]. Један случај представља пароброд „Lucy Ashton“ депласмана 390 тона који је био предмет истраживања још 1950. године од стране Истраживачке Асоцијације Британских Бродоградитеља (енг. British Ship Research Association – BSRA)[3] , а други случај је истраживачки брод „Meteor“ депласмана 2850 тона који је био предмет истраживања 1967. године[4]. Случај „Lucy Ashton“ садржи податке о измереном отпору брода у шест различитих размера модела, отпору брода у стварној величини, профилу брзина у граничном слоју за две брзине пловидбе на два места испод централне линије као и податке о храпавости површине трупа брода. Случај „Meteor“ садржи податке о измереном отпору брода у три различите размере модела, отпору брода у стварној величини, подацима о суструјном пољу у зони пропелера, као и пропелерску криву са пробне вожње. Важно је нагласати да уобичајена бродограђевна индустријска пракса обухвата извештај (у идеаланом случају) о подацима отпора брода у само једној размери модела, екстраполиране резултате отпора брода на стварну величину, процењене пропелерске криве за различите случајеве крцања терета, као и постигнуте пропелерске криве са пробне вожње приликом примопредаје брода бродовласнику. Најчешћи случај је да извештај који бродовласник добије садржи само

[3] Denny, M. E., 1951. B.S.R.A. Resistance Experiments on the Lucy Ashton, Part I – Full Scale Measurements, *International Conference of Naval Architects and Marine Engineers 1951*, Unwin Brothers, 40-57;
Conn, J. F. C., Lackenby, H., Walker, W. P., 1953. B.S.R.A. Resistance Experiments on the Lucy Ashton, Part II – The Ship-Model Correlation for the Naked Hull Conditions, *Spring Meeting of the Institution of Naval Architects*, March 25, 1953, 350-436;
Lackenby, H., 1955. Resistance Experiments on the Lucy Ashton, Part III – The Ship-Model Correlation for the Shaft-Appendage Conditions, *Quartetly Transactions of the Institution of Naval Architects*, 97(2), 109-166;
Smith, L., 1955. Resistance Experiments on the Lucy Ashton, Part IV – Miscellaneous Investigations and General Appraisal, *Quartetly Transactions of the Institution of Naval Architects*, 97(4), 525-561;

[4] Schuster, S., 1969. Schiffstechnische Meßfahrten mit dem Forschungsschiff "Meteor" 1967. Meteor Forschungsergebnisse: Reihe A, Allgemeines, *Physik und Chemie des Meeres*, 5, 72-84.

процењену и остварену пропелерску криву на пробној вожњи за пројектовани случај крцања терета и за брод у баласту. Извештаји о бродовима „Lucy Ashton“ и „Meteor“ су заправо веома сврсисходни за истраживање јер су веома обимни, а поготово занимљиви за истраживања на пољу CFD-а јер садрже релевантне податке о измереном отпору брода у више размера модела, па чак и у стварној величини.

Поузданост софтвера за добијање прихватљивих резултата се доказује упоређивањем резултата добијених нумеричким путем са подацима добијеним кроз моделска испитивања и/или са пробних вожњи. Према важећим регулативама, прихватљива су одступања података добијених нумеричким путем до 5% у односу на измерене вредности моделским испитивањима и/или са пробних вожњи. Ток развоја нумеричких алгоритама за решавање Навије-Стоксових једначина пратиле су тзв. CFD радионице. CFD радионице карактеришу се тиме што се експериментални подаци остају недоступни све док учесници не предају своје резултате нумеричких симулација организатору. Организатор радионице дужан је да свим учесницима достави основе податке о разматраном броду односно најмањи скуп података потребан за постављање симулације у неком CFD софтверу. Такође, организатор задржава право да анализира све пристигле податке и упореди их са експерименталним резултатима, а потом све резултате објави јавно. Овакав начин организовања радионица сматра се јединим исправним и валидним приступом. Током претходних деценија одржано је више оваквих радионица, почев од 1980. године а затим 1990, 1994, 2000, 2005, 2010, 2015, 2024, а две су организоване 2025. године. 2024. године је организована CFD радионица са бродом „Lucy Ashton“, а део тог истраживања је представљен кроз ову дисертацију [9].

Истраживање које обухвата дисертација, узимајући у обзир брод „Lucy Ashton“ је проширено у односу на CFD радионицу јер се бави нумеричком интерпретацијом експеримента који је спроведен у стварној величини [8]. Циљ истраживања био је да се испита утицај скалирања, Фрудовог и Рејнолдсовог броја на процену тоталног коефицијента отпора, као и да се упореде различити приступи нумеричком моделовању услова пловидбе у стварној величини. У посебној студији, анализиран је турбулентни гранични слој CFD симулацијама уз увођење додатних геометријских размера брода [7]. На тај начин се обухвата опсег режима рада савремених депласманских бродова дужине до 480 метара и Фрудових бројева од 0,1 до 0,3. Параметарске формуле добијене на основу експерименталних података за брод „Lucy Ashton“ и спроведених CFD симулација су подвргнуте валидацији спровођењем симулација процене отпора брода „Meteor“ [13].

Дискусија

Иако за бродове унутрашњих пловних путева (енг. Inland Waterways Vesells – IWV) још увек нису развијени званични прописи енергетске ефикасности, постоје општи показатељи ефикасности у незваничној форми. Они су углавном везани за хидродинамичке перформансе пловила и ефикасност транспорта, али не директно за енергетску ефикасност са аспекта заштите животне средине, као што је то случај са EEDI-јем или EEXI-јем. Предложени индекси енергетске ефикасности, посебно они разматрани за IWV, већ су систематски представљени у литератури, док су оригинална истраживања спроведена кроз неколико студија. Постоји веома мали број радова посвећених пловним путевима Европске Уније (ЕУ), док је број радова везаних за истраживања пловних путева Јужне Азије, далеко већи.

Предложене методе засноване су на EEDI концепту, према чему израчуната тј. процењена вредност EEDI-ја треба да буде нижа од захтеване вредности EEDI-ја. При оцени енергетске ефикасности у односу на приступ предложен од стране IMO-а, треба имати у виду да IWV обично имају веће моторе него што им је потребно за пројектовану брзину. Разлог томе лежи у додатним операцијама које речни бродови обављају у односу на морске – често се користе за гурање баржи или плове у комбинованим саставима. Због тога, једноставна примена IMO поступка за IWV није погодна, поготово што EEDI формула за поморске бродове разматра брзину при 75% инсталисане снаге мотора и то на мирној води. Осим тога, операције IWV веома зависе од услова пловидбе тј. плитке или дубоке воде. Такође, IWV ангажују мање снаге погонског мотора када плове низводно него узводно. Из тих разлога, индекси енергетске ефикасности IWV не могу се директно преузети из поморског сектора.

У раду [1] урађена је анализа енергетске ефикасности према две методе које се могу наћи у литератури за IWV, једна је названа модификовани EEDI (у раду приказана као Метода 1) развијена на Машинском факултету Универзитета у Београду[5], а друга DST EEDI (у раду приказана као Метода 2), развијена у Развојном центру бродске технологије и транспортних система у Дуизбургу[6].

Предложени индекси за IWV нису у формалном смислу индекси енергетске ефикасности за нова пловила, као што је то случај са IMO прописима за поморске бродове. Они су, заправо, више намењени постојећим бродовима, иако су означени као EEDI, и могу се користити на сличан начин. Као почетна база у истраживању, коришћена су 44 брода из базе података представљене у ранијим истраживањима. База садржи хидродинамичке карактеристике самоходних речних теретних бродова добијене током пловидбе и моделским испитивањима. Да би се израчунали индекси енергетске ефикасности према обема методама, било је потребно проценити криву зависности брзине и снаге за сваки од бродова. То је урађено помоћу сложеног математичког модела, развијеног и приказаног раније у литератури, а добијеног на основу ANN. Међутим, математички модел није могао да се примени у свим случајевима због ограничења саме методе. Метода 1 могла се применити код 32 брода из базе узимајући у обзир горњу границу корисне носивости (енг. deadweight – DWT) која износи 3000 тона. Са друге стране, иако ова граница код Методе 2 износи 6000 тона, ова метода се могла применити на само један брод. Разлог томе лежи у рестриктивној граници применљивости за газ брода која налаже да буде један и по пута већи од пречника пропелера. Међутим, имајући у виду да за примену Методе 2 није потребан пројектовани газ, узети су подаци који су доступни за газ

[5] Симић, А. (2012). *Енергетска ефикасност речних самоходних теретних* (докторска дисертација, Универзитет у Београду, Машински факултет). http://doiserbia.nb.rs/phd/fulltext/BG20121101SIMIC.pdf

[6] Development Centre for Ship Technology and Transport Systems (DST). (2020). *Evaluating the energy requirement of inland vessels using energy efficiency indices* (R&D project study, German Federal Ministry of Transport; CESNI). https://www.cesni.eu/wp-content/uploads/2021/03/cesnipt_energyindex_en.pdf

који одговара условима методе, па се из тих разлога, број анализираних бродова са једног, попео на четири.

Код Методе 1, за разлику од поморских бродова, где се EEDI рачуна при 75% снаге главног мотора, код IWV, модификовани EEDI није изражен једном вредношћу, већ се процењује за читав распон брзина кроз воду (10, 12, 14, 16, 18, 20 km/h). Сва четири брода испуњавају захтеве при нижим брзинама у условима дубоке воде. При вишим брзинама, постигнуте вредности модификованог EEDI-ја значајно премашују захтеване границе, што чини њихову пловидбу неефикасном. Занимљиво је да резултати сугеришу да су бродови у плиткој води ефикаснији него у дубокој, што је супротно очекиваним физичким понашањем бродова. За разлику од Методе 1, одређивање EEDI-ја према Методи 2 се врши за једну брзину брода, али при различитим брзинама тока воде. Према овој методи, за плитку воду постигнуте вредности EEDI-ја су у просеку око 40% ниже од захтеваних вредности, па метода делује неконзервативно у односу на Методу 1. За случај дубоке воде, захтеване вредности EEDI-ја су непроменљиве за три разматране брзине реке, јер зависе само од DWT, а не и од брзине воде. Дакле, Метода 1 даје распон постигнутих и захтеваних вредности за различите брзине брода кроз воду, док Метода 2 даје само једну специфичну вредност брзине брода која одговара предатој снази одређеној према формули методе. Зато су за потребе поређења метода, коришћене једне брзине брода (добијени према Методи 2), а при различитим брзинама река. Приликом поређења метода, испоставило се да само један брод испуњава све захтеве у свим размотреним случајевима. Метода 2 даје вредности EEDI-ја које су два до пет пута веће од оних које даје Метода 1 за исте услове. Иако је прорачунима коришћена различита специфична потрошња горива (200 g/kWh код Методе 1, 220 g/kWh код Методе 2), та разлика од 10% не може објаснити тако велики несклад резултата. Такође, обе методе немају исти критеријум дефинисања плитке воде – код Методе 1, граница је 5 метара, док Метода 2, узима да је плитка вода све испод 7,5 метара.

У раду [2] предложен је нови приступ дефинисању улазних података за постојеће две методе, при чему су коришћени оперативни подаци, а не пројектни. Дакле, рад пореди методе на основу оперативних улаза за конкретно путовање. Неки подаци су прибављени мерењем у реалном времену, а неки, за које аутори нису могли да прикупе мерења, процењени су за случај екстремних сценарија (услова пловидбе) тј. при најнижем и највишем очекиваном водостају (плитка вода и дубока вода). Студија случаја је представљена на примеру типичног самоходног теретног брода корисне носивости 1850 тона. Брод је пројектован за превоз расутог терета, а по потреби може да гура и друго пловило (баржу) или више њих. За период од једне године рада (15.01.2022-15.01.2023.) идентификоване су месечне пређене удаљености. За даљу анализу одабран је месец у којем је брод имао најинтензивнију употребу (највећа пређена дистанца). Прикупљени подаци укључују идентификацију стварних ограничења пловног пута на сваком сектору пловидбе и стварне брзине брода за одабрани месец, као и на годишњем нивоу. Енергетска ефикасност је процењена на основу Методе 1 и Методе 2, при чему је на тај начин процењена укупна емисија CO_2 за одабрани месец пловидбе и на годишњем нивоу. Путовања која нису задовољила захтеве енергетске ефикасности (према Методи 1 и према Методи 2), извршена је додатна анализа енергетске ефикасности у експлоатацији по секторима. За сваки од сектора је одређено потребно смањење брзине (а самим тим и потребно додатно време које брод проведе у пловидби) да би дошло до усклађивања са захтевима метода. Читава рута коју је брод прелазио током једне године се налази између луке Констанца (Румунија) и Аљмаша (Хрватска) и подељена је на 20 сектора услед различитих ограничења пловног пута, а током најфреквентнијег месеца, брод је пловио више пута на релацији Београд (Србија) – Свиштов (Бугарска). Та рута је подељена на девет сектора. Према резултатима, брод је током најфреквентнијег месеца испуњавао критеријуме Методе 2 за оба случаја водостаја (најнижег и највишег) током свих 11 путовања колико је забележено у том периоду, док према Методи 1, брод није испуњавао критеријуме енергетске ефикасности током три путовања и то

сва три у условима плитке воде и два од та три у условима дубоке воде. У условима плитке воде, да би брод задовољио критеријуме енергетске ефикасности, требало је смањити брзину пловидбе од 4,8% до 26% у зависности од сектора. Са друге стране, брзину брода, у условима дубоке воде, је требало смањити од 14,3% до 25,8%. Смањењем брзине, путовање би се продужило за додатних 10,7 сати у плиткој води, тј. 6,1 сат у дубокој води. Према грубој процени тј. екстраполацији на целу годину, брод би у служби провео 87 сати дуже у условима плитке воде тј. 49 сати дуже у дубокој води. Процењена емисија CO_2 за најфреквентнији месец (октобар) према Методи 1 је 24,6-24,9 тона у зависности од нивоа воде, док је према Методи 2 од 24,9 до 29,9 тона. Разлог зашто Метода 2 даје већи опсег процењене емисије лежи у начину прорачунавања (формулама) за случај плитке и дубоке воде. Према пређеној дистанци коју је брод остварио и количини терета коју је превозио током године, процењена емисија CO_2 за годину дана износи 197-199 тона према Методи 1 тј. 182-189 тора према Методи 2, у зависности од нивоа воде. Уколико би брод био експлоатисан током целе године као у најфреквентнијем месецу, емисија CO_2 би била 244-329 тона. Поређења ради, да би се иста количина терета превезла од Београда до Свиштова, потребно је чак 50 просечних шлепера (носивости 36 тона), при томе би шлепери превезли ту количину терета за 10 пута краће време од брода, али би при томе емитовали скоро дупло више CO_2, имајући у виду исту специфичну потрошњу горива. Метода 1 даје постигнуте и захтеване индексе енергетске ефикасности за читав распон брзина брода при мање рестриктивним условима него Метода 2. Највећи недостатак Методе 2 огледа се у услову да газ брода буде један и по пута већи од пречника пропелера, како би се метода могла применити. То би значило да за сваки брод мора да се спроведу нова испитивања сопствених перформанси тј. мерења брзине и снаге мотора на реци при том газу. С друге стране, иако Метода 1 није толико рестриктивна, она уопште не узима у обзир брзину реке. Такође постоји и разлика у специфичној потрошњи горива која директно улази у прорачун индекса енергетске ефикасности. Занимљиво је да према Методи 1, захтевани EEDI за плитку воду већи него за дубоку воду, што чини да су бродови енергетски ефикаснији у плиткој води него у дубокој, што у пракси делује невероватно. Ова ставка може бити и недостатак саме методе коју би требало додатно истражити. Један од највећих проблема обе методе јесте зависност од процене параметара брзине брода и ангажоване снаге мотора.

За разлику од речних бродова, за морске бродове су развијени многи показатељи енергетске ефикасности. Параметри који улазе у прорачун номиналних показатеља енергетске ефикасности се могу одредити на више начина, и то емпиријски, нумерички или експериментално. Регулативе дају могућност одабира сваком бродовласнику (менаџменту) који од ова три начина жели да примени. Може се десити да статистички начин да повољније вредности од експерименталног, што би дало погрешну слику о стварном стању. Са друге стране, манипулације током вршења експеримената неправилним баждарењем мерних уређаја, такође може да се добије нереална слика о издувној емисији. Нумерички приступ још увек није довољно савршен услед недовољно јасно дефинисаних правила и смерница, те даје простор за манипулацију уз већ присутну, нумеричку грешку. Имајући у виду све то, а поготово када је реч о номиналним параметрима ефикасности у којој заправо могу да фигуришу само теоријски параметри, реална слика може бити у потпуности другачија.

Кроз три независне студије [3, 4, 5], анализирани су индекси енергетске ефикасности и то оба типа, и номинални и експлоатациони. Све три студије се баве морским бродовима различитих категорија и то бродовима за превоз расутог терета [3], танкерима [4] и контејнерским бродовима [5]. Главни циљ ових радова се огледа у томе да се статистички одређеним параметрима енергетске ефикасности (кроз EEDI и EEXI) истражи да ли су бродови током година заиста постали ефикаснији, а да се кроз CII прикаже реалнија слика њихове оперативне учинковитости.

База бродова за превоз расутог терета [3] која је анализирана садржи 153 брода изграђених у периоду од 2000. до 2020. године који се и дан данас налазе у служби, дужина су од 107 до 362

метра, корисне носивости од 12588 до 400000 тона. Током година, установљено је да су се на бродове уграђивали све већи пропелери, док се брзина обртаја вратила смањивала, нарочито у другој деценији 21. века када су наступили нови прописи са циљем смањења издувне емисије. Зато је анализа раздвојена на бродове изграђене у периоду од 2000. до 2012. године и на млађе (изграђене током и након 2013. године). Пошто пре 2013. године није постојала ниједна регулатива, проверено је који проценат бродова би у том тренутку задовољио почетну фазу EEDI критеријума и добијено је да би свега 15% бродова из базе то остварило. За млађе бродове, чак 88% бродова би задовољило своју одговарајућу регулаторну фазу EEDI критеријума. Са друге стране, захтевани EEXI критеријум који је дефинисан регулативом са почетком применљивости у 2023. години, много је стриктнији и само један брод из базе га задовољава. Према томе, стандардни начин пројектовања бродова је добио значајан ударац. Истраживање је онда проширено како би се видело колико треба редуковати снагу мотора (уградњом лимитера снаге мотора – енг. Engine Power Limiter – EPL, или уградњом лимитера снаге вратила – енг. Shaft Power Limiter - ShaPoLi), а самим тим и смањити брзину, да би сви бродови из базе задовољили ригорозан EEXI критеријум. Анализа је спроведена помоћу статистичких формула и додатних формула за одређивање параметара који улазе у прорачун постигнутог EEXI-ја. Сам прорачун је додатно закомпликован увођењем многих коефицијената и додатних формула кроз неколико анекса издатих од стране регулаторног тела. Стога је у раду приказан поједностављен принцип одређивања усаглашености са EEXI критеријумом увођењем његове графичке верзије добијене решавањем свих формула и обједињавањем у зависност инсталисане снаге главног мотора (или референтне брзине), пет корекционих фактора и корисне носивости. На тај начин је критеријум знатно поједностављен за употребу јер је потребно одредити само пет корекционих фактора. Добијено је да снага главног мотора треба бити смањена у просеку чак 50% од инсталисане, при чему би бродови требало да смање референтну брзину око 15% (просечно). Додатно, бродови испод 200000 тона корисне носивости би требало да смање референтну брзину за око 18% у просеку, док би већи бродови требало да смање референтну брзину око 12%. Ако се узме у обзир да бродови већ плове при нижим брзинама тј. при 70-80% максималне снаге мотора где је и најнижа потрошња горива, реално смањење би било 10-14% и 3-7% за бродове испод и изнад 200000 тона носивости, респективно. Додатном анализом је утврђено да је просечна пројектована брзина бродова за превоз расутог терета из базе 14,5 чворова, просечна референтна брзина 13,8 чворова, а да је на основу анализе 25 бродова у својој оперативности постизало просечну брзину од 11,1 чвор. Реално смањење брзине да би CII критеријум био задовољен, тј. да брод има енергетски разред C у наредне три године је 8,8% што је значајно мање него што је добијено анализом статистичким путем EEXI критеријума (свих 25 бродова су мање носивости од 200000 тона). Када се узме у обзир колика је потребна бити нова (смањена) снага мотора у зависности од године изградње бродова, види се јасан тренд побољшања њихове ефикасности. За бродове из 2000. године, нова снага би била чак 58% мања од инсталисане, док је код бродова из 2020. године, та редукција сведена на 42%. Са тим трендом смањења, до 2050. године редукција би била око 17%, а тек 2071. године редукција снаге не би више морала бити увођена.

Када су у питању танкери [4], анализа енергетске ефикасности је урађена за њих 426 изграђених од 2000. до 2020. године. Сви разматрани танкери су подељени према типу и величини. За сваки од бродова су одређени постигнути и захтевани EEDI и EEXI, док су за 40 њих одређени и постигнути и захтевани CII. За све бродове који нису испунили EEXI критеријум, узето је обзир ограничавање снаге мотора као најзаступљенија и најекономичнија мера уштеде да би критеријум био задовољен. Сходно ограничењу снаге, одређено је и одговарајуће смањење брзине. Подела према типу је дефинисана према типу течног терета који танкер носи и то на: танкере за превоз хемијских/нафтних деривата (енг. chemical/oil tankers), танкере за превоз сирове нафте (енг. crude oil tankers), танкере за превоз течног природног гаса (енг. LNG tankers), танкере за превоз течног нафтног гаса (енг. LPG tankers) и танкере за друге врсте текућих терета (енг. product tankers). Када је у питању подела по

величини, танкери су подељени на: мале, средње, Панамакс, Афрамакс, Суецмакс, супертанкере и велике супертанкере (мамут-танкере). На основу двадесетогодишњег развоја танкера (од 2000. до 2020.) истиче се неколико трендова. Танкери су током времена постали дужи и шири, иако су LNG танкери постали краћи и ужи. Газ и корисна носивост су благо порасли код хемијских/нафтних танкера, LPG танкера и танкера за друге врсте текућих терета, док су танкери за сирову нафту и LNG показали минималне промене. Пројектоване брзине су значајно смањене код већине типова бродова, осим код LPG танкера који су постали бржи. Поред тога, Фрудов број је смањен током година, што одражава помак ка мањим брзинама (и/или дужим труповима) ради боље ефикасности и смањења емисије. Тренд у пројектовању бродова показује значајан пораст пречника пропелера код свих типова бродова осим код LNG танкера код којих је примећен пад, вероватно због специфичних оперативних захтева. Максимална инсталисана снага мотора показује различите трендове – повећање код LPG танкера и танкера за превоз других врста текућих терета, а смањење код танкера за превоз хемијских/нафтних деривата и танкера за сирову нафту, а нарочито код LNG танкера.

Удео бродова који испуњавају EEDI критеријуме наглашава утицај регулаторних мера на пројектовање бродова. На пример, 89,3% бродова изграђених 2013. и 2014. године испунило је критеријуме EEDI фазе 0, док је само 47,1% бродова изграђених 2020. испунило критеријуме фазе 2. Поређење бродова изграђених пре и после увођења EEDI стандарда показује пад неиспуњености критеријума са 39% на 27,2%. Овај пад наглашава ефикасност регулативе у подстицању енергетски ефикаснијег дизајна, али и указује на то да су даља побољшања неопходна. Посебно треба истаћи да само 14,8% бродова испуњава EEXI критеријуме, што показује да је придржавање овог строжег стандарда и даље велики изазов.

Анализа показује да су LNG танкери међу најефикаснијима по типу, док су мали бродови најефикснији по величини. Иако већи број мањих бродова испуњава EEXI критеријуме у поређењу са већима, мањи бродови (они који не испуњавају критеријум), су погођени драстичнијим редукцијама снаге. Супротно томе, танкери за превоз сирове нафте су најнеефикаснији по типу, а Панамакс бродови најмање ефикасни по величини.

Смањење снаге мотора, које директно доводи до смањења референтне брзине брода, јасно указује да су неопходне значајне промене како би се испунили EEXI критеријуми. Просечно потребно смањење снаге мотора за све размотрене танкере је 44%, уз просечно смањење брзине од 13,5%. Танкери за превоз других течних производа захтевају највеће смањење брзине (20,3%), док LNG танкери захтевају најмање (11,9%). Резултати показују да нема драстичних разлика у потребним редукцијама снаге и брзине по типу или величини танкера. тј. да су захтеви прилично уједначени. Варијације у потребним редукцијама ових параметара могу проистећи из различитих карактеристика уграђених мотора и пројектних брзина. Треба нагласити да номинални параметри ефикасности пре свега зависе од пројектних спецификација (намене за коју је брод изграђен), док оперативни параметри зависе од начина експлоатације самог брода.

Подаци указују да се у периоду од 2000. до 2020. године смањује број бродова код којих је потребно ограничење снаге мотора, док новији бродови захтевају и мање редукције снаге. Међутим, ако се 2013. година (када је EEDI критеријум ступио на снагу) узме као референтна, а анализира период до 2020. године, стопа раста редуковане снаге мотора је веома мала (испод 1%), што указује на незнатно побољшање ефикасности. Такође, у истом периоду, бележи се и пораст броја бродова којима су потребне корекције, али се оне незнатно мењају него у анализираном дужем периоду од 20 година.

Поређење између EEXI и CII критеријума открива значајну разлику од 8,1% у потребним редукцијама брзине да би дошло до испуњења критеријума. Ова разлика показује да бродови већ плове мањим брзинама него што је првобитно било претпостављено у оквиру EEDI и EEXI стандарда. Анализа CII-а показује да танкери користе само око 60% инсталисане снаге мотора

током путовања, што сугерише да се стварни оперативни услови разликују од референтних вредности коришћених у EEDI и EEXI проценама. Оптимизација бродова за њихове стварне брзине рада остаје важан аспект – посебно се поставља питање да ли су бродови оптимизовани за своје тренутне брзине, укључујући и ефикасност булба као и дизајн пропелера. Просечна пројектована брзина танкера из базе је 15,6 чворова, просечна референтна брзина 14,6 чворова, а просечна брзина коју бродови остварују је чак 25% мања од пројектоване.

Анализа базе података која се састоји од 162 контејнерска брода [5], а који су подељени према носивости (броју контејнера које могу да превезу) показује да само 12% целокупне флоте задовољава EEXI критеријум, иако је преко 83% њих задовољило EEDI критеријуме у времену у ком су настали. Потребна редукција снаге да би бродови задовољили EEXI критеријум значајно опада и то са 60% за бродове изграђене 2000. године до 5% за бродове из 2020. године. Узимајући у обзир и да се број бродова којима је потребна редукција снаге мотора смањио током година, несумњиво је да су контејнерски бродови постали доста ефикаснији што се и закључује на основу све мањих вредности постигнутих EEXI-ја. Потребно смањење снаге у просеку од 40% би се одразило кроз потребно смањење референтне брзине од 13% у односу на полазну, како би EEXI критеријум био задовољен.

Што се тиче начина пројектовања, не бележе се значајне промене у димензијама бродова током година, али се пројектована брзина свих типова контејнерских бродова временом смањивала што је праћено уградњом мотора мањих снага. Просечна пројектна брзина свих бродова из базе је 22 чвора, али анализом 21 брода за који су доступни подаци из оперативности, просечна остварена брзина је само 13,6 чворова. Као и код танкера и бродова за превоз расутог терета, остварена брзина од 13,6 чворова је мања од потребне референтне брзине која износи 18,9 чворова да би EEXI критеријум био задовољен. Додатно, и остварену брзину од 13,6 чворова је потребно још умањити за 7% да би бродови постизали одговарајуће енергетске разреде. Процене показују да би, под условом да сваки брод сваке године ради у истим оперативним условима, око 81% бродова испуњавало CII критеријум у референтној 2019. години. До 2030. године тај проценат би се смањио на мање од 10%, што указује да чак и благо пооштравање критеријума у складу са планираним факторима редукције (од 2% годишње), значајно утиче на ефикасност оперативности бродова. Просечна оперативна брзина је чак 30% мања од референтне пројектоване брзине, а када би се оперативна брзина усвојила као пројектована, само 5% бродова не би испунило најстрожи EEDI критеријум који је тренутно на снази (фаза 3).

Кроз једну од анализа енергетске ефикасности, проверен је утицај масе самог трупа код два брода за превоз расутог терета [6]. Из базе бродова за превоз расутог терета, издвојена су два брода која су слична по димензијама, али различита у облику трупа (један има булб, а други вертикалну статву). Један брод има скоро 20% већу корисну носивост, док је маса празног брода скоро идентична. Брод са вертикалном статвом има 19% мањи процењен отпор према емпиријској методи, иако је дужи и шири од брода са булбом. Размотрена су три различита случаја. Први случај узима у обзир смањење депласмана услед смањења масе уз исту корисну носивост и већу референтну брзину за исту ангажовану снагу мотора. Овим поступком би се умањио постигнути EEDI тј. EEXI за мање од 1% чак и са смањењем масе самог брода од 15%. Други случај је веома сличан првом, само што се узима у обзир иста референтна брзина, али мања потребна снага јер је мањи депласман. На овај начин постигнути EEDI тј. EEXI би се умањио и до 2,6%. Трећи случај узима у обзир повећање корисне носивости како се укупан депласман не би променио, и тиме се постиже побољшање енергетске ефикасности до 3,2%.

Да би се уопште могли проценити индекси енергетске ефикасности дефинисани од стране IMO-а, потребан је одређени број улазних параметара који се могу одредити експериментално или нумерички (CFD методом). Данас се све више користи нумерички приступ у ове сврхе јер је економски исплативије и ефикасније од традиционалног експерименталног приступа. Поред

одређивања улазних параметара за процену енергетске ефикасности бродова, нумерички приступ тј. CFD се све више користи и у фази пројектовања.

Пројектовање бродова представља мултидисциплинарни процес који обухвата хидростатичке, хидродинамичке (пропулзивне), конструктивне аспекте као и аспекте стабилитета, али и економске и експлоатационе параметре, безбедност пловидбе, утицај на животну средину, као и усклађеност са важећим међународним регулативама. Један од кључних изазова, са хидродинамичког аспекта, је предвиђање отпора трупа и обезбеђивање поузданих података за одређивање погонске снаге брода. Традиционално, овај проблем се решавао испитивањем модела брода у базенима, при чему се директно мерио отпор модела при истом Фрудовом броју као и на броду у стварној величини, а резултати се затим скалирају на реалне услове. Међутим, потпуно задовољавање динамичке сличности (Фрудовог и Рејнолдсовог броја) је практично немогуће, што доводи до потребе за корекцијама и додатним прорачунима чиме се уводи непоузданост у добијене резултате.

Са развојем рачунара, CFD је постао важан алат у бродоградњи јер омогућава детаљну анализу појава које је тешко или прескупо измерити експериментално. CFD се данас користи као допуна моделским испитивањима, а све чешће и као директан извор података из симулација у стварној величини. Ипак, ограничена количина доступних експерименталних података за реалне услове (у стварној величини) остаје препрека за потпуну валидацију и широку примену CFD-а у бродограђевној пракси.

Један од најефикаснијих начина за процену стања технике засноване на CFD-у су међунардоне радионице. На њима се учесницима дају једнаки почетни услови и геометрија, а добијени резултати се упоређују међусобно и са експерименталним подацима. На тај начин се могу идентификовати разлике између различитих софтвера и нумеричких приступа, као и утврдити ниво поузданости CFD метода. У поморској заједници, ова пракса постоји више деценија. Радионица заснована на случају брода „Lucy Ashton“ [9] представља важну прекретницу јер је први пут као тест случај коришћен брод за који постоје подаци о отпору трупа у стварној величини. Учесници нису знали о ком броду је реч, нити су имали приступ експерименталним резултатима пре предаје решења, што је омогућило објективну проверу предикцијских могућности различитих CFD софтвера.

У радионици је учествовало 40 самосталних истраживача, студената, представника институција или компанија чија је главна делатност употреба CFD софтвера у бродоградњи. Они су користили осам различитих софтвера (STAR-CCM+, OpenFOAM, FineMarine, ReFRESCO, HELYX-Marine, Ansys CFX/Fluent и др.). Радионица је обухватала три скупа случајева: студија непоузданости мреже за један Фрудов број у стварној величини (Сет 0), симулације процене отпора брода у стварној величини за више Фрудових бројева (Сет 1) и симулације процене отпора за један Фрудов број, а више размера модела (Сет 2). Анализа резултата показала је да су CFD прорачуни у просеку потцењивали отпор брода у свим условима, што је и очекивано јер нису моделовани утицаји храпавости трупа и динамичка померања (понирање и посртање). Упркос томе, распон резултата између различитих учесника био је релативно мали – медијанско апсолутно одступање за случај у стварној величини није прелазило 2,3%. Овај ниво слагања је упоредив са моделским испитивањима, што повећава поверење у примену CFD-а за случајеве у стварној величини. Учесници који су радили и додатне случајеве показали су мању дисперзију резултата, што указује да квалитетна припрема и више улагања времена воде поузданијим резултатима симулација. Такође, уочен је тренд да расипање резултата опада са порастом Фрудовог броја што указује да су нумерички модели стабилнији и поузданији за више брзине. Ово је значајан закључак за индустријску примену, јер управо у овим условима се доноси одлука о погонској снази брода и избору пропулзивног комплекса. Примећено је да је највеће одступање присутно код резултата добијених код учесника који су мање пажње посвећивали избору типа мреже и поставкама самих симулација. Квалитет генерисане мреже је један од најзначајнијих фактора који је утицао на дисперзију

добијених резултата. Учесници који су користили фино дискретизоване мреже постигли су боље слагање са медијаном и мању нумеричку непоузданост. Резултати добијени помоћу STAR-CCM+ софтвера, који је био најзаступљенији, показали су добру конзистентност, док су решења применом других CFD кодова, често била дисперзнија, али су ипак пала у оквире статистички прихватљивих вредности.

Додатна анализа [8], која се односи на предметни брод из претходно поменуте радионице, обухватила је све опционе случајеве (додатне брзине) који нису били обавезни за учеснике радионице. Симулације су спроведене уз омогућена динамичка померања, понирања (енг. sinkage) и трима (енг. trim), док су ефекти храпавости трупа и отпора ваздуха накадно укључени током постпроцесирања резултата (енг. post processing). Добијени резултати показују завидан ниво поузданости CFD симулација за предвиђање коефицијента тоталног отпора брода, како у размерама модела, тако и у стварној велични (видети Слику 2 и Слику 3). Упоређивањем CFD резултата са експерименталним подацима добијеним за брод „Lucy Ashton“ уочено је да одступања не прелазе 5% за процену коефицијента тоталног отпора брода. Наведена одступања су у складу са тренутно важећим смерницама ITTC-а што указује на погодну примену CFD-а у бродограђевној индустрији. Посебно је значајно што је CFD метода успешно репродуковала резултате у чак укупно шест различитих размера модела као и у стварној величини и то према два различита приступа (Приступ 1 и Приступ 2), чиме је показана универзалност методологије у погледу скалирања.

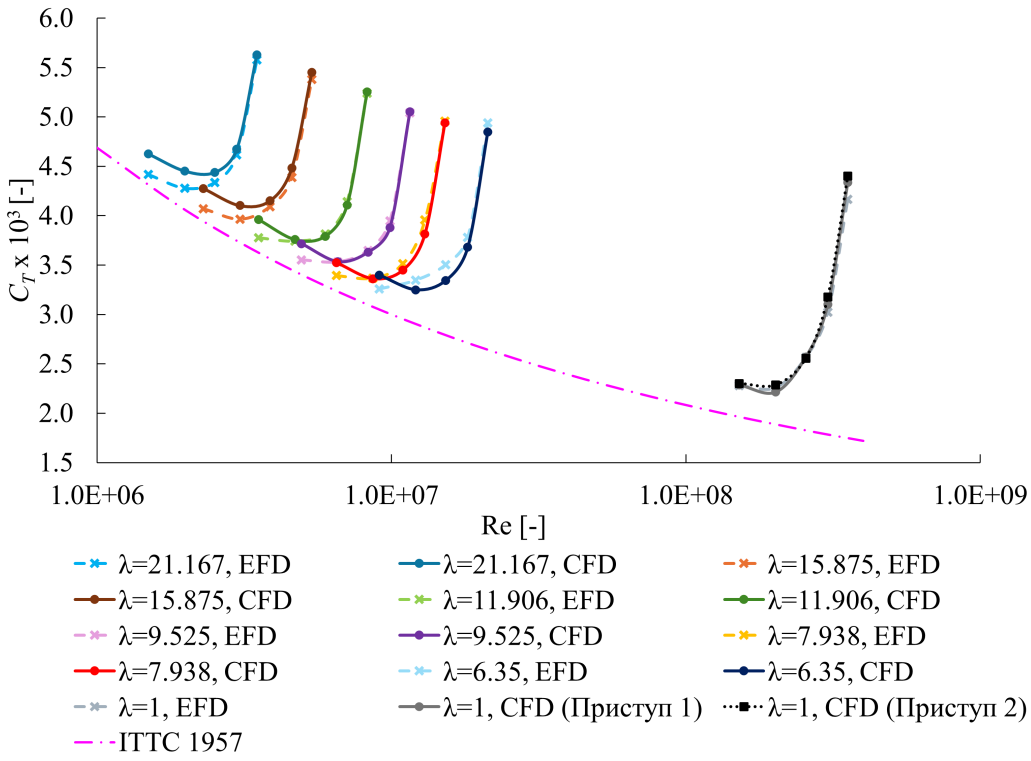

Слика 2: Коефицијент тоталног отпора одређени експериментално (EFD) и нумерички (CFD) у зависности од Рејнолдсовог броја за 6 размера модела и у стварној величини [8].

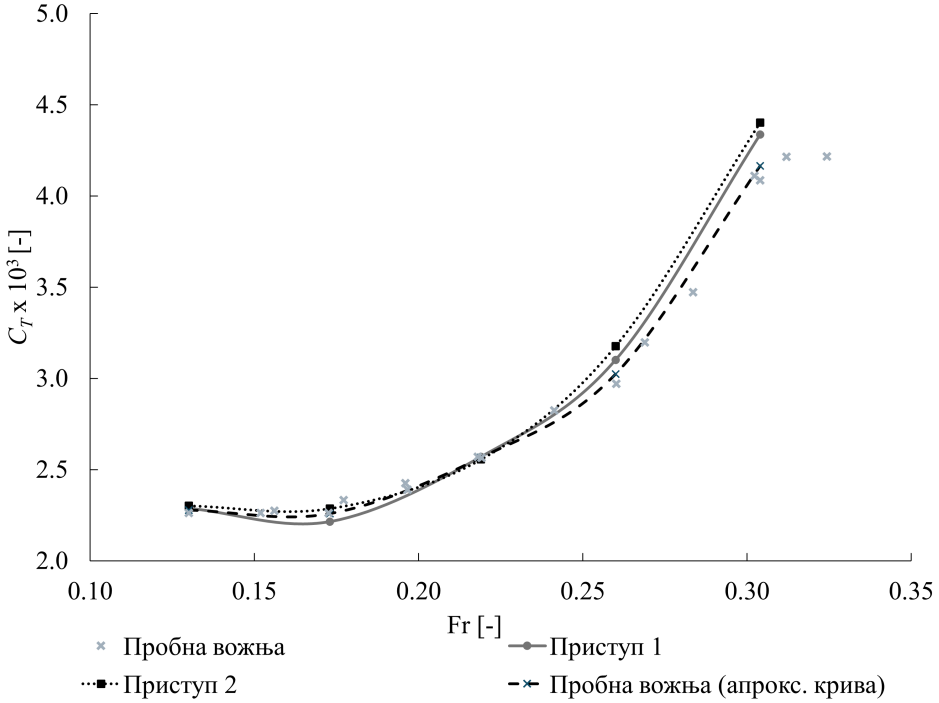

Слика 3: Коефицијент тоталног отпора одређен експериментално, током пробне вожње, и нумерички (Приступима 1 и 2) у зависности од Фрудовог броја у стварној величини [8].

У првом приступу (Приступ 1) брзина струјања је задавана као улазни услов, док је у другом приступу (Приступ 2) кретање брода одређено применом потисне силе која симулира рад млазних мотора коришћених током испитивања (у стварној величини). Боље слагање при већим брзинама у размерама модела и на нижим брзинама у стварној величини указује на одређена ограничења у моделовању одређених физичких појава, првенствено мислећи на турбуленцију. Укључивањем ефекта храпавости и отпора ваздуха у случајевима симулација у стварној величини постигнуто је боље слагање са експерименталним резултатима, што потврђује важност правилне корекције за добијање реалистичних предвиђања. Поређење два нумеричка приступа показало је да начин моделовања погона нема значајан утицај на процену тоталног отпора брода у стварној величини, док су разлике у динамичким померањима брода (понирање и трим) веома мале у апсолутном износу (Слика 4).

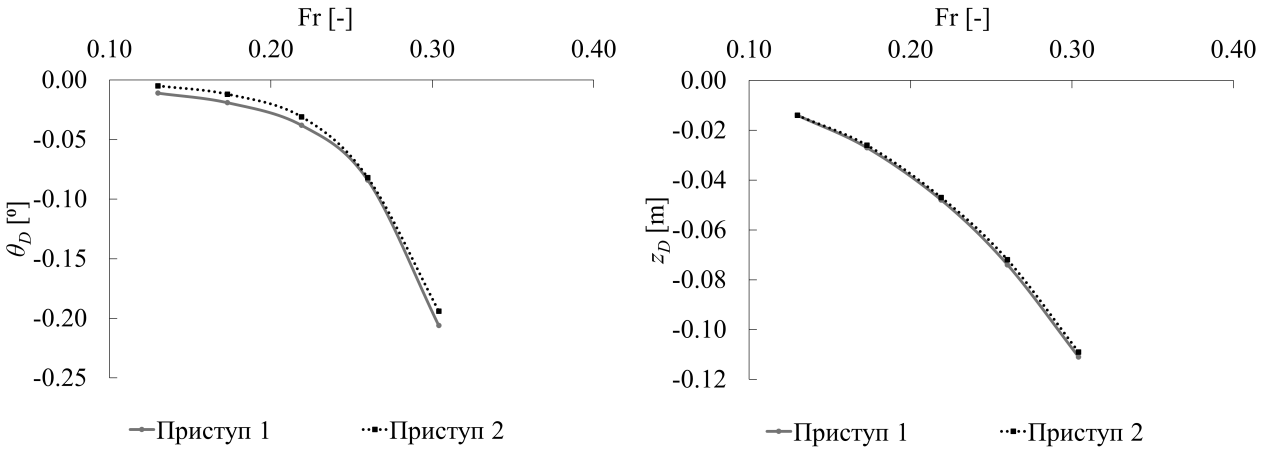

Слика 4: Разлике у динамичким померањима (трим – лево, понирање – десно) применом два различита приступа у нумеричким симулацијама [8].

Важан допринос дисертације заснива се на истраживању спроведеном на броду „Lucy Ashton“, које је усмерено на развој и верификацију предлога методологије за параметарско подешавање

мреже у CFD прорачунима, са посебним нагласком на зону у непосредној близини трупа у софтверу STAR-CCM+ [7]. Предложена методологија обухвата параметарски дефинисане зоне мреже (видети Табелу 1), величину основне ћелије, дебљину првог слоја ћелија уз труп брода и дистрибуцију ћелија у зони где су изражени велики градијенти брзине и притиска. Циљ је био да се ови параметри дефинишу у функцији познатих физичких карактеристика брода: дужине, ширине, газа, фактора форме, брзине за коју се процењује отпор или потисак, као и пречника и положаја пропелера. Све димензије дате у Табели 1 дефинисане су у односу на глобални координатни почетак који се налази у пресеку крменог перпендикулара, централне линије и кобилице брода (Слика 5) и односе се на дефинисање половине домена.

Брод „Lucy Ashton“ изабран је као референтни случај јер су експерименти спроведени на њему једни од најдетаљнијих од до сада јавно доступних у историји бродоградње. Његов недостатак је што потиче из 19. века и има форму која се знатно разликује од савремених бродова, јер је у питању пароброд. Због тога је предложена методологија додатно тестирана на другом историјски значајном броду – „Meteor“ [13], за који постоје подаци експерименталне процене отпора трупа у стварној величини. Добијени резултати се могу сматрати поузданим јер се забележена одступања, између CFD резултата и експерименталних резултата процене тоталног отпора, налазе у прописаним границама од 5%, што потврђује поузданост предложене методологије. Додатно, методологија се показала успешна и у CFD прорачунима ауто-пропулзије пошто су за брод „Meteor“ доступни подаци и са пробних вожњи. Што се тиче процене перформанси пропелера, одступања између CFD резултата и математичког модела (заснованог на експерименталним подацима) не прелазе 3% у зони оперативног рада пропелера. Важно је напоменути да резултати који су представљени у раду [13] нису приказани у потпуности (конкретне бројчане вредности).

Табела 1. Параметарски дефинисане димензије домена и запреминских зона финије мреже [7]. L_{pp} [m] – дужина између перпендикулара, λ [-] – размера брода (модела), B [m] – ширина брода, T [m] – газ брода.

	Крмена ивица	Прамчана ивица	Крмена страна	Прамчана страна	Доња екструзија	Горња екструзија
Домен	$-3.5 \cdot L_{pp} / \lambda$	$2 \cdot L_{pp} / \lambda$	$2 \cdot L_{pp} / \lambda$	$2 \cdot L_{pp} / \lambda$	$-2 \cdot L_{pp} / \lambda$	$0.5 \cdot L_{pp} / \lambda$
Зона слободне површине	$-3.5 \cdot L_{pp} / \lambda$	$2 \cdot L_{pp} / \lambda$	$2 \cdot L_{pp} / \lambda$	$2 \cdot L_{pp} / \lambda$	$0.9 \cdot T / \lambda$	$1.1 \cdot T / \lambda$
Крмена зона	$-0.15 \cdot L_{pp} / \lambda$	$0.2 \cdot L_{pp} / \lambda$	$0.6 \cdot B / \lambda$	$0.6 \cdot B / \lambda$	$-0.2 \cdot T / \lambda$	$1.3 \cdot T / \lambda$
Прамчана зона	$0.9 \cdot L_{pp} / \lambda$	$1.05 \cdot L_{pp} / \lambda$	$0.6 \cdot B / \lambda$	$0.6 \cdot B / \lambda - 0.15 \cdot L_{pp} / \lambda \cdot \mathrm{tg}(20^\circ)$	$-0.2 \cdot T / \lambda$	$1.3 \cdot T / \lambda$
Зона финије мреже Келвиновог клина	$-1.5 \cdot L_{pp} / \lambda$	$1.5 \cdot L_{pp} / \lambda$	$3 \cdot L_{pp} / \lambda \cdot \mathrm{tg}(20^\circ)$	$0.8 \cdot B / \lambda$	$0.7 \cdot T / \lambda$	$1.3 \cdot T / \lambda$
Зона грубље мреже Келвиновог клина	$-2.25 \cdot L_{pp} / \lambda$	$1.8 \cdot L_{pp} / \lambda$	$7.5 \cdot L_{pp} / \lambda \cdot \mathrm{tg}(20^\circ)$	$2 \cdot B / \lambda$	$0.5 \cdot T / \lambda$	$1.5 \cdot T / \lambda$

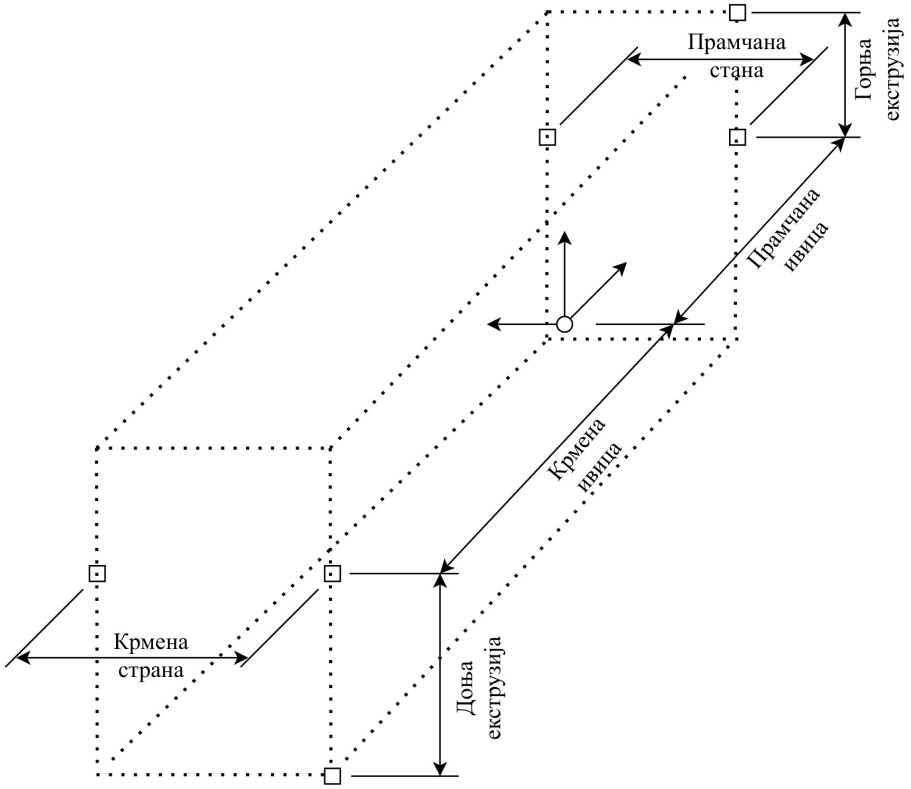

Слика 5: Дефинисање димензија домена и зона финије мреже у односу на глобални координатни систем према Табели 1.

Параметри као што су величина основне ћелије, димензија зоне са великим градијентима брзине и притиска и број слојева унутар те зоне представљају неопходне улазне податке за дефинисање мреже у софтверу STAR-CCM+ [7]. Процена дебљине првог слоја ћелија уз труп, броја слојева (ћелија) унутар зоне где се очекују велики градијенти брзине и притиска уз труп и фактора пропагације се врши нумерички уз додатне услове: 1) За групу симулација која може обухватити једну размеру, а више Фрудових бројева – дебљине последње ћелије у зони великих градијената брзине и притиска за све симулације су што приближније; 2) За групу симулација која обухвата више размера, а један Фрудов број – дебљине последње ћелије помножене фактором размере, у зони великих градијената брзине и притиска, за све симулације су што приближније. На овај начин се умањују разлике у мрежама између симулација, тј. постиже се да укупан број ћелија не варира пуно у симулацијама у случају једне размере, а више Фрудових бројева. Према класичној теорији турбулентног граничног слоја, са порастом Рејнолдсовог броја, однос дебљине граничног слоја и карактеристичне дужине опструјаваног тела, опада. Може се и рећи да за исту дужину карактеристичног опструјаваног тела, дебљина граничног слоја опада са порастом брзине. Пошто су највећи градијенти брзине и притиска присутни управо у граничном слоју, дебљина зоне у којој се они очекују узима се као претпостављена дебљина граничног слоја. Та зона се дефинише пре покретања симулације и не мора бити једнака стварној дебљини граничног слоја код конкретног брода. Симулације које су покривене студијом су рађене за димензије (дужине) бродова од 2 метра (што одговара размери модела приликом експерименталних испитивања у базенима), па све до 483 метара што је и дуже од највећег брода икада направљеног. До те димензије се дошло екстраполацијом геометријских параметара брода „Lucy Ashton“. Једна од предности избора овог брода је што су током експеримената мерене брзине струјања воде дуж централне линије трупа (на 49% и 62% дужине брода), што је омогућило процену дебљине граничног слоја у тим зонама. Коришћењем CFD метода добијене су додатне процене дебљине граничног слоја на 20%, 30%, 40% и 80% дужине брода. За референтну вредност узета је она код које брзина флуида достиже 99% брзине непоремећеног струјања. Пошто се дебљина граничног слоја

мења за неколико редова величина у зависности од дужине брода, било је неопходно прилагодити број ћелија (слојева) унутар граничног слоја тако да бездимензиона дистанца од зида (y^+) остане у прописаним границама (30–100). Код великих бродова то подразумева више од 20 ћелија у граничном слоју, док је код моделских размера довољно 5 или више. Ове границе су неопходне како би се осигурало да вискозни ефекти буду правилно третирани и код модела и код брода у стварној величини. Добијена формула за процену дебљине[7] зоне где се очекују високи градијенти брзине и притиска, уз сам труп, код опструјавања сложене бродске форме дата је у облику $\delta = 0.075L_{wl}/\mathrm{Re}^{0.15}$ што је сличан облик (зависност) као и код процене дебљине турбулентног граничног слоја при опструјавању равне плоче или струјања флуида кроз цеви, при чему су L_{wl} дужина на водној линији, а Re – Рејнолдсов број (Слика 6). Наведена формула јесте заснована на процени дебљине граничног слоја код брода „Lucy Ashton“ и она не мора да важи за остале сложене бродске форме, али се може користити као полазна процена улазних параметара које је неопходно дефинисати ради дефинисања мреже.

Величина основне ћелије мреже (*BS*) дата је формулом $BS=(L_{pp}\cdot r)/(30\cdot\lambda)$, где су L_{pp} – дужина између перпендикуалара, r – фактор резолуције мреже, а λ – размера брода у којој се поставља симулација. Приликом дефинисања мреже, посебну пажњу треба посветити броју слојева унутар граничног слоја и грубости мреже, јер претерано велика претпостављена дебљина граничног слоја може довести до непотребно великог броја ћелија и дужег времена трајања симулације. Практично је боље благо потценити дебљину граничног слоја него је преценити, јер се на тај начин постиже бољи однос између резултата, грубости мреже и рачунског времена. Дистрибуција дебљине граничног слоја у зони централне линије је јако добро апроксимирана полиномима четвртог степена, са максималном дебљином на 30%L_{pp}. Посматрањем утицаја размере показано је да ефекат размере има знатно већи утицај на дебљину граничног слоја него сама промена брзине.

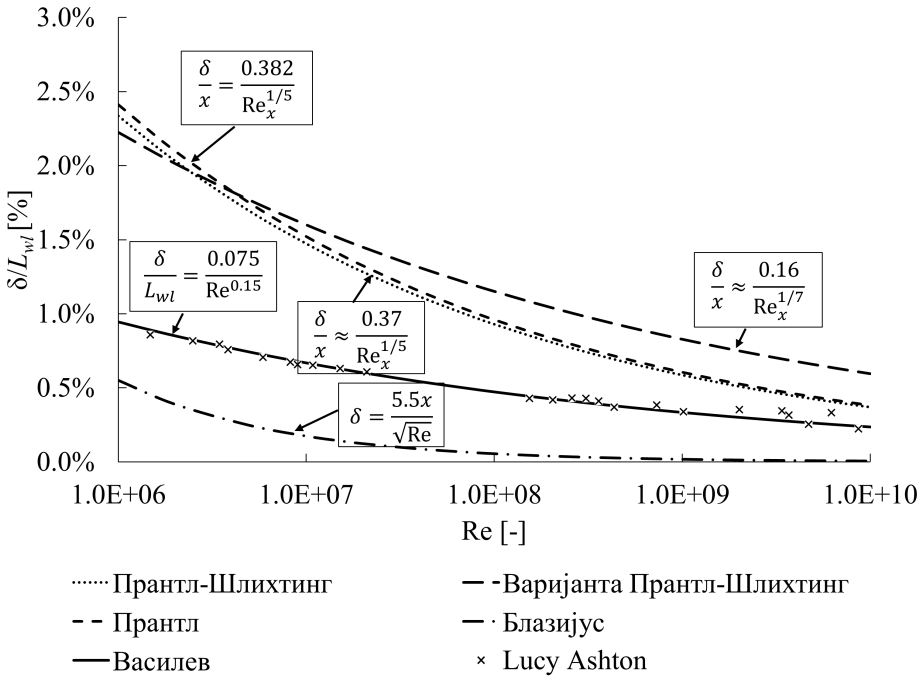

Слика 6: Поређење теоријских и емпиријских корелација за дебљину граничног слоја са нумерички добијеним подацима брода „Lucy Ashton“ [7].

Један од сегмената бродоградње у којој CFD алати још увек нису признати од стране регулаторних органа у смислу давања поузданих резултата јесте утицај храпавости на бродску

[7] Под дебљином сматра се димензија управна на површину трупа брода.

хидродинамику. Геометрија трупа која је предмет CFD анализе се у софтверу сматра идеално глатком површином, што је у стварности немогућ случај зато што постоје одређена одступања присуством заварених спојева и несавршено нанетом слоју фарбе, што уз девијацију лимова трупа доводи до повећања отпора трења, пре свега. Данас постоје уређаји који омогућавају мерење храпавости површине, али то у пракси, заправо, ником од бродовласника није потребно. Још један велики утицај на повећање отпора трења јесте појава обраштања што заправо представља насељавање површине трупа живим морским светом као што су микроорганизми, бактерије, алге, гљивице, шкољке и други организми. То је природна појава коју је немогуће избећи, али се њихова контаминација може успорити применом самополирајућих премаза, премазима који спречавају пријањење организама као и редовним чишћењем. У CFD прорачунима се не може директно имплементирати просечна вредност храпавости већ се утицај свих неправилности који утичу на отпор трења у граничном слоју узима преко тзв. еквивалентне храпавости. Суштински, она одређује законитост промене бездимензионе брзине у турбулентном граничном слоју. У литератури постоји математички описана зависност између средње висине храпавости и еквивалентне храпавости, међутим, она је заснована на мерењима која су спроведена на једном војном броду и то скоро пре две деценије. Додатно, постоје многа истраживања која се баве темом утицаја храпавости кроз CFD прорачуне, мада, валидна је само ITTC препорука која подразумева укључивање утицаја храпавости у пост-анализи резултата. У анализи која је спроведена кроз дисертацију [12] спрегнуте су препоруке ITTC-а са CFD-ом ради проналажења нове математичке везе (полиноми) између средње висине храпавости и еквивалентне храпавости. Разлог спровођења ове анализе лежи у скепси да садашњи полиноми дају изразито (чак и нереално) велике процене отпора са јако малим променама средње храпавости тј. порастом средње висине храпавости са идеално глатке површине на 600 микрометара, тотални отпор брода (у овом случају брода за превоз расутог терета корисне носивости око 50000 тона) порасте готово 50%. Још једна сумња у поузданост постојећег полинома лежи у томе што за вредности средње висине храпавости мање од 150 микрометара, тотални отпор брода такође расте. Резултати симулација са новодобијеним полиномом, показују мањи утицај храпавости на повећање отпора. Процењене вредности уштеде у снази мотора након петогодишњег чишћења трупа (од 6,6% до 15,7% у зависности од средње висине храпавости тј. нивоа обраслости трупа) добро корелирају са подацима из литературе новијих истраживања.

Други сегмент бродоградње у ком су CFD алати донели велики бенефит јесу истраживања која захтевају велики број провера варијацијом одређених параметара. Такав пример јесу трим оптимизација или оптимизација облика трупа. Експериментална провера ових параметара би била економски неисплатива, али је развој CFD-а неминовно омогућио унапређење енергетске ефикасности кроз примену ових мера.

Једна анализа утицаја облика трупа [11] на перформансе је урађена на контејнерском броду кроз оптимизацију облика прамчаног дела. Проблематика брода је заснована на лошој експлоатацији чијом анализом се испоставило да брод током свог трогодишњег путовања никада није пловио на пројектованом газу, нити је пловио пројектованом брзином. То се манифестовало постигнутим лошим енергетским разредом. Уз примену одређених ограничења, проверено је 10 различитих облика прамца и утврђено је да је за најучесталији положај пливања, оптимална вертикална статва (без постојања булба). Њоме би се могла постићи уштеда у дневној потрошњи горива и до 9% у односу на иницијални дизајн, а то аутоматски значи и бољи (виши) енергетски разред. Додатним симулацијама показало се да вертикална статва даје лошије резултате у односу на оригинални дизајн на пројектном газу. Овај резултат наглашава значај прилагођавања дизајна реалним оперативним условима.

Развојем рачунара високих перформанси и параметарског моделовања, могао би се проверити знатно већи број различитих варијација пројекта за релативно кратко време, квантитативно гледано, процена перформански око 150 различитих облика прамаца би се могла добити кроз свега неколико дана. Са друге стране, израда 150 физичких модела је економски неисплатива.

А развојем вештачке интелигенције и принципом адаптивног узорковања може се унапред предвидети да ли је уопште потребно спроводити CFD анализу за све случајеве или се и број случајева може редуковати, што би додатно уштедело и компјутерске ресурсе и време рада инжењера.

Једна од најефикаснијих оперативних мера за побољшање енергетске ефикасности јесте трим оптимизација јер она не изискује потребу за променом форме. Промена форме захтева додатна улагања у разраду потребне техничке документације као и проведено време у сувом доку, а тиме се спречава да брод зарађује.

Трим оптимизација је урађена на једном броду за превоз аутомобила (енг. RO-RO car carrier; RO-RO: roll on-roll off) [10]. Циљ трим оптимизације је био да се пронађе онај положај пливања за који брод остварује највећу уштеду у потребној снази мотора при кретању одређеном брзином на одређеном средњем газу. Поставка CFD симулација је обухватала процену предате снаге, њој одговарајући број обртаја пропелера и дневну потршњу горива за три брзине, три средња газа и седам тримова (положаја пливања). Због тога су урађене 63 CFD анализе. Изазов који се јавља при спровођењу великог броја симулација јесте и велики број података који се треба на неки начин анализирати и представити, а додатне потешкоће се огледају у томе како проценити резултате за случајеве за које нису рађене CFD симулације. Један од начина решавања овог проблема јесте линеарна интерполација међу-резултата, што се данас веома лако ради. Међутим, у зависности од нивоа дискретизације, број резултата се тако само повећава (у конкретном случаја на преко два милиона података) и на тај начин, табеларно приказивање резултата је бесмислено и практично неупотребљиво. Овако велики број података се онда може приказати графички, али је и то проблем јер су у конкретном случају варирана три параметра (брзина, трим и газ тј. депласман), па се ради о четвородимензионалном домену података. Зато се, у оваквим случајевима, од великог броја података који су међусобно зависни, може формирати математички модел помоћу вештачких неуронских мрежа (ANN). За тренирање ANN коришћени су депласман, брзина, трим и средњи газ као улазне величине, а резултати добијени CFD анализом – испоручена снага, број обртаја пропелера и дневна потрошња горива као излазне величине. Математичка интерпретација везе наведених параметара је тражена у облику сигмоидне функције зато што се њихова међусобна зависност (међусобна зависност параметара) добро подудара са обликом ове фунцкије.

Коначни математички модел за процену испоручене снаге, броја обртаја пропелера и дневне потрошње горива је веома комплексан и непогодан је за лаку примену јер се своди на серију матричних операција (множења и сабирања) и примену нелинеарних активационих функција. Међутим, овакви модели се могу лако испрограмирати и инкорпорирати у неку врсту апликације. Апликација која је развијена за специфичан случај разматраног брода захтева као улаз само један параметар, а то је депласман. Депласман је увек позната величина након утовара терета, а на основу четвородимензионалне матрице у којој сваком депласману одговара више вредности положаја пливања, брзине и средњег газа, може се брзо наћи оптималан сет ових параметара при којима се постиже најмања потребна предата снага. Ограничења примене апликације заснована су на границама у којима су рађени CFD прорачуни јер математички модели добијени на основу ANN су веома осетљиви на архитектуру мреже тј. како су распоређени параметри који су коришћени за њено тренирање.

У конкретном случају, након одрађене 63 симулације, процењено је да се највеће уштеде у потребној пренесеној снази постижу у положају пливања прамца на доле (претеге) 1,5 метар (негативни прамчани трим), с тим што се при газу од 7,5 метара добија оптимална брзина од 15,1 чвор, а при већим газовима – оптимална брзина од 12,5 чворова која је заправо и доња граница за коју је рађена оптимизација. Ред величине уштеде у потребној испорученој снази је до 10% што је веома оптимистичан резултат. Наравно, треба нагласити да су све CFD симулације рађене за случај мирне воде (без утицаја таласа, морских струја и ветра) и да се у реалности оволика уштеда не може остварити, али постоји могућност да уштеда свакако буде

значајна. Такође, велика промена трима може негативно утицати на маневарске способности брода, па и те случајеве треба додатно размотрити.

Закључак

Истраживања спроведа кроз радове обједињене кроз ову дисертацију показало је да постојеће методе за процену индекса енергетске ефикасности како речних [1, 2], тако и морских [3, 4, 5], су у значајној мери неусаглашене и недовољно прилагођене практичној примени. Методе за процену индекса енергетске ефикасности IWV би требало да буду усаглашеније и поједностављене, слично као што је случај код морских бродова, а у циљу ефикасне имплементације у пракси. Надлежни органи за пловидбу на унутрашњим пловним путевима требало би да у скоријем периоду понуде решења будући да је планирано да се значајан део транспорта добара пренесе на реке чиме би се значајно повећао удео емисије издувних гасова у градовима кроз које бродови плове. У протеклих десет година није ништа ново урађено поводом имплементације предложене две методе за процену индекса енергетске ефикасности IWV, чак није покушана ни њихова консолидација, а није предложена ниједна нова метода. Као једно од решења, могло би се увести континуирано мерење брзине и снаге мотора током сваке пловидбе, уз уградњу ограничивача снаге (као код поморских бродова). На тај начин би се могла управљати и оптимизовати снага мотора у реалном времену како би се постигла енергетска ефикасност под различитим условима пловидбе. Дакле, постигнута ефикасност би требало да се мери, а не само да се рачуна. На основу резултата анализе, предложене методе вероватно неће успети да подстакну развој нових технологија у области енергетске ефикасности IWV у скоријем периоду. Разлог је у томе што форме разматраних бродова практично нису мењане деценијама, а према тренутним критеријумима, бродови и као такви, већ задовољавају предложене захтеве.

Значај увођења оперативног индекса енергетске ефикасности код речних бродова, огледао би се у томе што би се имала јаснија представа о количини издувне емисије (првенствено CO_2). Према разматраним методама одређивања индекса енергетске ефикасности, а при модификованим улазним параметрима (користећи стварну пређену дистанцу и количину превезеног терета), један типичан IWV емитује 180-200 тона CO_2 годишње. Варијација количине издувне емисије зависи у великој мери од конфигурације реке, брзине реке, дубине воде, брзине брода и др. Смањењем брзине пловидбе, може се побољшати енергетска ефикасност до одређеног степена, а продужетак трајања пловидбе би на годишњем нивоу био занемарив. Такође, показано је да се испуњење критеријума може лако постићи применом контроле брзине пловидбе тј. ограничивачима снаге мотора уз континуирано праћење њиховог рада.

Код морских бродова заступљени су и номинални и оперативни критеријуми енергетске ефикасности кроз EEDI, EEXI (номинални) и CII (оперативни). Њиховом анализом у примени на флоти бродова за превоз расутог терета, танкера и контејнерских бродова, изграђених у двадесетогодишњем периоду, а који чине узорак од 2,5% од светске флоте који подлежу критеријумима енергетске ефикасности, уочавају се веома слични трендови. Чак ни начин пројектовања бродова са становишта промене главних параметара није значајно промењен током 20 година, осим што се уграђивао пропелер већег пречника, а да је његова брзина смањивана што доводи до закључка да је смањење брзине добила на значају као једна од мера за побољшање енергетске ефикасности. Иако је велики удео бродова из базе испуњавао пројектоване EEDI критеријуме у временима када су изграђени, велики број њих не испуњава EEXI критеријум. Потребно смањење брзине ради испуњења EEXI критеријума код сва три типа брода је веома слично (13-15%) и праћено је редукцијом снаге мотора за 40-50% што делује као огроман утицај. Међутим, анализом енергетске ефикасности бродова кроз оперативни индекс (CII), долази се до другачијих закључака. Просечне оперативне брзине су значајно мање од референтних брзина, такође и од пројектованих, што указује на неусаглашеност пројектованог и експлоатационог карактера бродова. Треба истаћи да, уколико се есплоатациони режим усвоји као пројектовани, тј. ако се брод заиста користи у

оперативном смислу на начин као што је пројектом и предвиђено, постоји могућност да велики број њих (бродова) испуњава чак и најстроже критеријуме процене номиналне енергетске ефикасности. Ово доводи до закључка да номинални и оперативни критеријуми енергетске ефикасности нису баш усаглашени јер у случају да сви бродови испуњавају EEXI критеријум, не значи да испуњавају и CII критеријум и обрнуто тј. иако је брод по једном критеријуму довољно ефикасан, по другом не мора бити.

Са становишта анализе поређења потребног процентуалног смањења снаге мотора, бележи се смањење броја бродова којима је редукција снаге мотора потребна уз квантитативно смањење удела у ограничавању снаге. Такође, бележе се и све ниже вредности номиналних параметара енергетске ефикасности у периоду од двадесет година што несумњиво указује да бродови заиста јесу постали ефикаснији.

Парадоксално је што је утврђено да се бродови крећу брзинама које одговарају снагама мотора које су већ испод граница на које треба ограничити инсталисане снаге мотора да би EEXI критеријуми били испуњени. Ово отвара питање колики ће бити стварни ефекат смањења емисије гасова у будућности. Суштински, ни танкери, ни бродови за превоз расутог терета, ни контејнерски бродови не плове брзинама за које су пројектовани. То оставља простор за унапређење постојећих бродова јер вероватно нису оптимизовани за рад под условима у којима се експлоатишу, а такође, указује и на потребну промену приступа у пројектовању. Нови бродови треба да се пројектују према стварним оперативним режимима. Кроз анализу мера побољшања енергетске ефикасности, утврђено је да почетни дизајн игра велику улогу у процени перформанси бродова и да у зависности од облика трупа [11], може се остварити значајна уштеда. Уштеде у енергетској ефикасности које су могу постићи у иницијалној фази пројектовања конструкције [6] су у рангу уштеда које остварује уградња појединих уређаја за уштеду енергије (ESD).

Веома велики допринос у развој енергетски ефикаснијих бродова је дао развој и имплементација CFD алата у бродоградњи. Његовом све већом применом, омогућено је брже и економски исплативије проналажење оптималног решења по питању иницијалног дизајна, али и оптимизације постојећег [10]. Питање валидности компјутерских симулација бродске хидродинамике је раније било веома упитно, али је све већи број јавно доступних експерименталних података указао да се уз пажљив одабир и методологију поставки симулација, могу добити поуздани резултати. Само у последње две године се бележи значајан пораст CFD радионица које управо омогућавају проверу и валидацију техника коришћења савремених алата. Један од најважнијих закључака које је донела CFD радионица, чији је предмет истраживања био брод „Lucy Ashton“, јесте тај да је CFD достигао ниво зрелости који омогућава његову примену (у бродоградњи) за случајеве процене отпора трупа у стварној величини уз услов да се поштују добри инжењерски сдандарди: адекватно генерисање мреже и правилан избор параметара приликом поставки симулација [9]. Осим тога, овакве радионице служе као платформа за размену искуства и едукацију, што доприноси целокупном напретку поморске индустрије. Посебно значајан резултат истраживања односи се на поређење два различита начина генерисања потиска [8]. Иако пропелер и млазни мотори представљају потпуно различите концепте погона и имају различит положај у односу на тежиште брода, показано је да ова разлика нема значајан утицај ни на процену укупног отпора брода нити на његова динамичка померања, као што су понирање и посртање. Добијени резултати указују да глобалне хидродинамичке карактеристике брода, у контексту процене отпора, остају практично непромењене без обзира на начин примене потиска.

Додатна истраживања која су спроведена на још једном броду („Meteor“), [13] за који су (аутору) доступни експериментални подаци процене отпора брода и теста ауто-пропулзије (теста мерења брзине и снаге мотора) у стварној величини, показала су да се у одређеном

опсегу Фрудових бројева могу добити поуздани резултати CFD симулација у стварној величини, уз одступања унутар граница прихватљивих за инжењерску праксу.

CFD има потенцијал да постане стандардни алат у раним фазама пројектовања, посебно у условима када су моделска испитивања прескупа или времески захтевна, а испитивања у стварној величини готово немогућа. Анализа брода „Meteor“ поставља основу за будућу CFD радионицу која ће први пут интегрисати све кључне области бродске хидродинамике – предвиђање отпора трупа у више размера, укључујући и стварну величину, тест испитивања карактеристика пропелера у слободној вожњи као и процену погонске снаге тј. пропелерске криве. Тиме ће се додатно допринети унапређењу поузданости CFD метода и њиховој све широј примени у поморској индустрији. У прилог доприносу ове радионице CFD заједници иде и то што се за њу пријавило више од 50 учесника, што ће саму радионицу чинити до сада најбројнијом икада.

Значај параметризације поставки проблема у било ком CFD софтверу је веома значајан јер се целокупан процес може убрзати са неколико сати на свега пар минута [7]. Методологија дефинисања прорачунске мреже у оквиру зоне великих градијената брзине и притиска уз сам труп даје добар иницијални оквир за добијање поузданих резултата при различитим размерама. Успостављање емпиријске функције и зависности физичких параметара омогућиле су доследно генерисање мреже и поузданост предвиђања хидродинамичких карактеристика. Спроведено истраживање доприноси унапређењу CFD метода у бродоградњи и представља корак ка ефикаснијим и стандардизованим поступцима у дефинисању прорачунске мреже бродских форми. Будућа истраживања би требало да се усмере на унапређење техника адаптивне мреже и проширење валидације на различитим типовима бродских форми.

Математичка интерпретација утицаја храпавости у CFD софтверима још увек представља велику енигму у процени вискозног отпора [12]. Недовољан број експерименталних испитивања доводи до немогућности верификације резултата добијених CFD анализом и зато данас постоје велике нелогичности у проценама тоталног отпора са укљученим ефектом храпавости јер се поставља логично питање да ли бродови са променом храпавости од само 0,5 милиметара имају и до 50% већи отпор?! Из праксе се може закључити да средња висина храпавости код обраслих бродова може бити и чак неколико центиметара и онда се поставља логично питање, ако би се таква проблематика уврстила у CFD софтвер, да ли би се такав брод уопште могао покренути?

Несумњиво је да је употреба CFD-а довела до пројектовања енергетски ефикаснијих бродова, али не само новоизграђених, већ је омогућила и унапређење постојећих. Бржим проналажењем ефикасних решења уз економску исплативност, развијена је потпуна нова област бродоградње која пре није постојала. Поред адекватног пројектовања, подједнако је битан и начин експлоатације брода тј. да ли брод плови предвиђеном брзином на газу и положају пливања (триму) као што је то пројектом и замишљено. Као резултат неусклађености пројектованог решења и експлоатације, бродови постају неефикаснији вид транспорта са становишта издувне емисије и пренешене количине терета.

Трим оптимизација [10] има значајан утицај на смањење потрошње горива, а самим тим и на емисију гасова, уз додатно смањење оперативних трошкова брода. Употребом вештачких неуронских мрежа добија се могућност да се за било који услов брзо одреди неки параметар без потреба за новим CFD симулацијама, што је посебно важно у оперативном планирању. У контексту трим оптимизације или било које хидродинамичке анализе, ANN „учи“ на основу скупа података добијених експерименталним путем или CFD симулацијама и формира функцију мапирања која за дати скуп улазних вредности предвиђа одговарајући излаз. Развијена додатна софтверска апликација је савремени корак напред ка дигитализацији

бродограђевне индустрије. Овакве апликације могу помоћи посади на броду да у реалном времену оптимизују брзину и уз оптимизацију руте остваре уштеде горива и побољшају енергетски разред брода. Међутим, највећи изазов није у самој примени математичких модела или софтверских алата, већ у почетном развоју и тренирању ANN, где је неопходно обезбедити квалитетне податке, правилно дизајнирати архитектуру мреже и извршити темељну валидацију.

Сумирајући спроведене анализе и резултате, закључује се да је енергетска ефикасност бродова једно мултидисциплинарно поље које захтева усклађен приступ регулатива, пројектовања и експлоатације. Систематична интеграција CFD метода, експерименталних испитивања и технолошки софистицираних алгоритама као што су вештачке неуронске мреже или вештачка интелигенција, може довести до отварања једног новог поглавља у начину пројектовања и експлоатације бродове. У будућности, напредак у области енергетске ефикасности зависиће од способности да се развију стандардизовани, флексибилни и транспарентни модели који могу лако да се провере, понове и користе у пракси. Под флексибилношћу се сматра да би методе требало да буду прилагодљиве различитим типовима бродова, режимима пловидбе и нивоима доступности података. Под транспарентношћу се сматра да резултати добијени савременим софтверским алатима треба да буду јасно документовани и проверљиви, тако да се могу користити и у инжењерске и у регулаторне сврхе. Само синергијом између регулаторних тела, истраживачке заједнице и индустрије могуће је обезбедити стварни напредак у правцу одрживе, технолошки, а потом и еколошки унапређене бродограђевне индустрије.

Завршна реч

Да ли ће и на који начин тренутна трећа деценија 21. века бити једна од историјских у бродограђевној индустрији остаје да се види. Несумњиво је да она више никада неће бити иста, традиционална. Данас, уз развој савремених софтверских алата, она постаје мултидисциплинарна област индустрије. Тежњом да се конвенционални начин пропулзије са дизел моторима у потпуности замени другим, алтернативним, након више од 100 година пловидбе, завршиће се једно велико поглавље овог вида транспорта.

Да ли ће вештачка интелигенција умањити значај рада инжењера бродоградње? Све док инжењер користи њу за развој личних вештина зарад разумевања физикалности појава и унапређења личне ефикасности, биће способан да буде испред ње.

Литература

[1] Kalajdžić M., Vasilev M., Momčilović, N.: Evaluating an Inland Waterway Cargo Vessel's Energy Efficiency Indices, - Polish Maritime Research, Sciendo, vol. 29 (Issue 2), pp. 27-34, 2022, ISSN 1233-2585, IF 2.0 DOI: https://doi.org/10.2478/pomr-2022-0014

[2] Kalajdžić M., Vasilev M., Momčilović N.: Inland waterway cargo vessel energy efficiency in operation, - Brodogradnja, vol.74, no. 3, pp. 71-89, 2023, ISSN 0007-215X, IF 3.9 DOI: https://doi.org/10.21278/brod74304 Д1.1.4

[3] Kalajdžić M., Vasilev M., Momčilović N.: Power reduction considerations for bulk carriers with respect to novel energy efficiency regulations, - Brodogradnja, vol.73, no. 2, pp. 79-92, 2022, ISSN 0007-215X, IF 1.8 DOI: https://doi.org/10.21278/brod74304

[4] Vasilev M., Kalajdžić M., Momčilović N.: On energy efficiency of tankers: EEDI, EEXI and CII, - Ocean Engineering, vol. 317, 120028, 2025, ISSN 0029-8018, IF 5.5 DOI: https://doi.org/10.1016/j.oceaneng.2024.120028.

[5] Vasilev M., Kalajdžić M., Momčilović N., Miltenović F.: On energy efficiency of containerships: EEDI, EEXI and CII, - Ocean Engineering, vol. 356, 125429, 2026, ISSN 0029-8018, IF 5.5 DOI: https://doi.org/10.1016/j.oceaneng.2026.125429.

[6] Vasilev M., Kalajdžić M.: Influence of lightweight change on ship performance. - FME Transactions, vol. 50, no. 4, pp. 615-622, 2022, ISSN 1451-2092, IF 1.6 DOI: https://doi.org/10.5937/fme2204615V.

[7] Vasilev M., Kalajdžić M.: Parametric mesh study: Lucy Ashton case. - FME Transactions, vol. 54, no. 2, pp. 45-61, 2026, ISSN 1451-2092, IF 1.2

[8] Vasilev M., Kalajdžić M., Ponkratov D.: CFD Approach to Full-Scale Resistance: The Lucy Ashton Case. Brodogradnja, vol.77, no. 3, 77307, 2026, ISSN 0007-215X, IF 4.2 DOI: https://doi.org/10.21278/brod77307

[9] Lopes R., Eslamdoost A., Bensow R., Ponkratov D., Kömpe A., Pekküçük Ç., Aydin C., Villa D., Ntouras D., Seo D. S., Rosano G., Vesting F., Bigini G., Chillcce G., Kaufmann J., Lin J., Muralha J., Kimmerl J., Ilter K., Lampropoulos D. S., Sagmo K., Lübke L., Kubota M., Vasilev M., Wheeler M., Sahid M., Grlj C. G., Kühl N., Crepier P., Joga R., Bilandi R. N., Boyd M., Toro A. del, Cunningham S., Bozzo S., Schumacher F., Melissaris T., Tissot V., Sorrentino V., Hoydonck W. V., Li Z. H.: A summary of the Lucy Ashton resistance prediction workshop, - Ocean Engineering, vol. 343, 122951, 2026, ISSN 0029-8018, IF 5.5 DOI: https://doi.org/10.1016/j.oceaneng.2025.122951

[10] Vasilev M., Kalajdžić M., Ivković I.: CFD-Powered Ship Trim Optimization: Integrating ANN for User-Friendly Software Tool Development. - Journal of Marine Science and Engineering, vol. 12, no. 8, 1265, 2024, ISSN 2077-1312, IF 2.8 DOI: https://doi.org/10.3390/jmse12081265

[11] Vasilev M., Kalajdžić M., Suvačarov A.: A Practical Approach to Bulbous Bow Retrofit Analysis for Enhanced Energy Efficiency, - Proceedings of 25th Numerical Towing Tank Symposium (NuTTS 2023), Ericeira, Portugal, October 2023

[12] Vasilev M., Kalajdžić M.: The Influence of Roughness Change on Ship Resistance in CFD Simulations, - Proceedings of 24th Numerical Towing Tank Symposium (NuTTS 2022), Zagreb, Croatia, October 2022

[13] Vasilev M., Kalajdžić M., Ponkratov D.: From Lucy Ashton to Future CFD Case Studies: Benchmarking Ship Resistance at Full and Model Scales, - Proceedings of 27th Numerical Towing Tank Symposium (NuTTS 2025), Zagreb, Croatia, September 2025

[14] Kalajdžić M., Vasilev M., Momčilović, N.: Energy Efficiency of Inland Vessels: Current Status, - Proceedings of 25th Symposium on the theory and practice of shipbuilding (SORTA 2022), Malinska, Croatia, September 2022

[15] Ivković I., Kalajdžić M., Vasilev M.: A CFD-Based Analysis of Bow Modification Influence on Ship Resistance and Energy Efficiency, - Proceedings of 26th Numerical Towing Tank Symposium (NuTTS 2024), Mulheim an der Ruhr, Germany, October 2024

[16] Kalajdžić M., Ivković I., Vasilev M.: Advancing CFD validation methods for self-propelled inland waterway vessels a workshop initiative, - The 26th Symposium on Theory and Practice of Shipbuilding (SORTA 2024), Zadar, Croatia, October 2024

[17] Kalajdžić M., Vasilev M.: CFD-Driven Ship Trim Optimization: Simplifying Complexity of ANN with User-Friendly Software, - 16th Symposium on High-Performance Marine Vehicles (HIPER 2024), Drübeck, Germany, June 2024

[18] Kalajdžić M., Vasilev M., Momčilović, N.: Exploring an Effect of Novel IMO Policies on Energy Efficiency of Existing Ships, - Book of Abstracts - 1st Kotor International Maritime Conference (KIMC 2021), Kotor, Montenegro, November 2021, ISBN 978-86-7664-205-2

ПРИЛОГ 1

sciendo

POLISH MARITIME RESEARCH 2 (114) 2022 Vol. 29; pp. 27-34
10.2478/pomr-2022-0014

EVALUATING AN INLAND WATERWAY CARGO VESSEL'S ENERGY EFFICIENCY INDICES

Milan Kalajdžić [1]
Matija Vasilev [2]
Nikola Momčilović *[1]

[1] University of Belgrade, Faculty of Mechanical Engineering, Department of Naval Architecture, Belgrade, Serbia
[2] Ocean Pro Marine Engineers LTD, Belgrade, Serbia

* Corresponding author: *nmomcilovic@mas.bg.ac.rs (N. Momčilović)*

ABSTRACT

Although the International Maritime Organization (IMO) introduced the energy efficiency requirements for ships more than a decade ago, to date, inland navigation has not been affected by corresponding regulations at all. Therefore, inland waterway vessels are left with no mandatory requirements that could push their technology into more energy efficient design. Fortunately, there are certain pioneering attempts to define energy efficiency criteria for inland vessels. This paper tries to gather and provide a review of such methods. Moreover, a typical Danube cargo inland vessel's data are used to evaluate their current energy efficiency levels with respect to provisional criteria. Consequently, two methods are found and used here. They are both based on IMO's energy efficiency concept but modified for the inland waterway vessels. The methods delivered a significant difference in applicability and were difficult to compare. Moreover, shallow and deep-water effects are explored in the same regard but provided unsound conclusions. The final results displayed discrepancies in energy efficiency levels for the same vessels and so the methodology should be improved and harmonised, if it is to be introduced as mandatory for inland waterway vessels. The analysis provided a glimpse into the current condition of the traditional design of the Danube inland fleet, with respect to the emerging energy efficiency policies.

Keywords: Inland vessels, Energy efficiency, Energy efficiency of inland vessels, EEXI, EEDI

INTRODUCTION

The reduction criteria for greenhouse gas emissions (GHG), issued by the International Maritime Organization (IMO), have been mandatory for newly built sea-going ships over 400 gross tonnage (GT) since 2013. In the case of existing ships, the corresponding requirements are set to start from 2023. These regulations, in the form of energy efficiency indices, are being implemented as a short-term measure and are intended to be strengthened over time to achieve the final long-term goal reductions. Therefore, the IMO introduced a set of energy efficiency indices through its Marine Environment Protection Committee (MEPC). The indices were intended to measure a ship's energy efficiency level. The first one, energy efficiency design index (*EEDI*), was first introduced in 2011 and applied two years later for new ships [1], while incrementally strengthening the criteria every five years. The *EEDI* value (attained *EEDI*) corresponds to the grams of carbon dioxide (CO_2) emissions per ship's capacity-mile and is to be calculated for each ship. Attained *EEDI* must be lower than the required *EEDI*, which is the criterion also imposed by IMO. Furthermore, following the Paris Agreement and the global need for GHG emission reduction, IMO presented a strategy for shipping. In general, it can be summarised as being: to strengthen requirements for *EEDI* over the years, to reduce the carbon intensity of ships (CO_2 per transport work

to at least 40% by 2030, reaching a 70% reduction by 2050) and to reduce GHG emissions to at least 50% by 2050, when compared to 2008 levels [2]. Moreover, IMO addressed the efficiency of existing ships in the same manner as in the case of EEDI, i.e., by introducing EEXI, which stands for 'energy efficiency of existing ships'. This requirement is set to start applying from 2023 [3].

In the meantime, ships are mostly fighting against the indices' criteria by slow steaming, while technological improvements like energy saving devices (ESD) and alternative fuels (and optimisation of the hull) still need some time to become fully applicable. Nevertheless, some authors have investigated the relation between fleets of existing ships and emerging indices: in cases of fleets of multi-purpose ships [4] and in cases of various ship classes [5]. Others have even recognised the 'energy efficiency gap' [6], labelling the industry's reluctance to address the use of novel technologies in order to reduce emissions.

Contrary to sea-going shipping, inland waterway vessel (IWV) regulations are much less unified. Depending on their navigation and cargo, IWV rely on various interconnected national, regional and international regulations. Unfortunately, these are not fully consolidated. However, the UN and EU are, indeed, trying to harmonise regulations on an international level [7, 8]. The EU inland fleet consists of 10,000 vessels registered in countries interfacing the Rhine, while an additional 3500 and 2300 vessels are registered along the Danube and in other EU countries, respectively, according to [9]. However, there are innovations that include energy efficient inland vessel designs. Reduced fuel consumption, air pollution and improved overall efficiency (considering specific waterway conditions) were investigated for merchant river vessels in [10]. Moreover, a high energy efficiency inland ferry concept was developed in [11], using hybrid propulsion. Similarly, the research in [12] explored hybrid propulsion as well, in addition to potential hull shape modification, to design a more energy efficient small inland passenger vessel.

Still, no mandatory requirements are available for the energy efficiency of IWV in any form. An explanation could be found in the much lower total GHG emissions of IWV transport when compared to road transport (in EU member states) and a conservative IWV industry. Yet industries that are not pursuing decarbonisation politics are risking exposure to social discontent.

Therefore, this paper aims to present a review of proposed and provisional methods for the calculation of energy efficiency indices for IWV. Furthermore, energy efficiency indices are calculated for typical Danube vessels. The results are expected to provide a perspective on current IWV designs regarding the initial energy efficiency criteria.

ENERGY EFFICIENCY INDICES FOR INLAND WATERWAY VESSELS

Although no energy efficiency regulations have been developed for IWV, overall efficiency indices are available in a non-regulatory form. They are mostly related to the hydrodynamic performance of the vessels and transport efficiency, but not directly to the energy efficiency from an environmental point of view, as in the case of *EEDI* or *EEXI*. Proposed energy efficiency indices, in particular, (explored for IWV and EU waterways) have already been systematically presented in [13], while the original research was delivered in [14, 15]. There are very few studies available regarding EU waterways but there is a study on this topic for waterways outside the EU, see [16, 17].

Proposed energy efficiency methods are based on the *EEDI* concept. Accordingly, the calculated or estimated so-called 'attained *EEDI*' should be lower than the required *EEDI* value. When evaluating energy efficiency performance with respect to the IMO's *EEDI* approach, it should be considered that IWV usually have larger engines than they need for the designed speed. This is because of the additional operations of IWV, compared to sea-going vessels. For instance, IWV are intended to push barges and to be coupled with other vessels. Therefore, using just the IMO procedure for IWV would not be suitable, since the *EEDI* formula for sea-going ships considers 75% of the engine power in still water. Moreover, inland vessel operations heavily depend on navigation conditions. This accounts for large variations of the draught between deep and shallow-draught vessels. The draught governs the propeller diameter and, thus, the installed power, which directly influences energy efficiency index. In addition, it should be noted that vessels use less power when operating downstream, compared to upstream. Consequently, IWV energy efficiency indices cannot just be transferred from the maritime sector.

MODIFIED EEDI

One of the first attempts to define the energy efficiency of IWV can be found in [13]. The method is based on IMO's *EEDI* approach and labeled as modified *EEDI* or *EEDI**. It was developed at the Department of Naval Architecture (University of Belgrade). The method presents a procedure for the calculation of attained *EEDI** and required *EEDI**. It can be used for existing vessels as well. The proposal presents the benchmark study, that can be comparable to phase 0 of the EEDI requirement, delivered for sea-going ships built after 2013, see [1]. The summary of the method, referred to here as Method 1, is presented in Table 1.

DST EEDI

DST (Development Centre for Ship Technology and Transport Systems), a Duisburg based institute, proposed equations for the assessment of energy efficiency of IWV, see [15]. The method classifies four vessel types: dry cargo/container self-propelled vessels, tankers, pushed convoys and passenger vessels. It also differentiates equations according to the navigation zones. Here, the procedure is given for cargo vessels carrying dry bulk or containers, considering the navigation in deep and shallow water. The method is presented in Table 2 and referred to as Method 2. Deep water corresponds to a water depth of 7.5 m

Tab. 1. Method 1

Indices	Attained *EEDI**	Required *EEDI**
Equation	$EEDI^* = P_{Bref} \cdot SFC \cdot CF / (m_{DWT} \cdot V)$	$EEDI^*_{Req} = a \cdot m_{DWT}{}^c$
Ranges	10 km/h ≤ V ≤ 22 km/h; 0.4 ≤ *Fnh* ≤ 0.65; 100 t ≤ m_{DWT} ≤ 3000 t	
Explanations and coefficients	*EEDI** – Modified energy efficiency design index [gCO_2/gFuel]; P_{Bref} – Reference engine power for achieving *V* [kW]; *SFC* – Specific fuel consumption, assumed 200 [g/kWh]; *CF* – carbon emission factor, 3.206 [gCO_2/gFuel]; m_{DWT} – mass of deadweight [t]; *V* – actual vessel speed through water [km/h].	Deep water: $a = 0.39554 \cdot V^2 - 11.27833 \cdot V + 111.69043$ Shallow water: $a = 93.712 \cdot F_{nh}{}^{-3} - 516.38 \cdot F_{nh}{}^{-2} + 886.54 \cdot F_{nh}{}^{-1} - 414.86$ Deep water: $c = -0.00114 \cdot V^2 - 0.05177 \cdot V + 0.70843$ Shallow water: $c = -0.4181 \cdot F_{nh}{}^{-3} + 2.5716 \cdot F_{nh}{}^{-2} - 5.2767 \cdot F_{nh}{}^{-1} + 3.3485$
Notes	- *V* is not governed on 75% of MCR like in IMO's *EEDI* approach, but poses an actual speed with reference to the water; - P_{Bref} is reference power, not based on MCR like in IMO's *EEDI* approach; - *EEDI** is to be assessed for all vessels in the same speed and river constraints (for instance: shallow water) to allow comparison.	- Benchmarking level formula is based on more than 10 year old vessels, but it is proposed that data should be collected from vessels built in the past 10 years; - *a, c* are functions of vessel type and *V* or Froude number F_{nh} in case of shallow water, *h* = 5 m; - The formula is proposed to be strengthened over the years for 10%, 20% and 30% like in the case of IMO's *EEDI*.

Tab. 2. Method 2

Indices	Attained EEDI ($EEDI_{IWV}$)					Required EEDI ($EEDI_{Req}$)			
Equation	Deep water: $P_D = \alpha_1 \cdot m_{DWT}$ P_D measure, V_s calculate $EEDI_{IWV}$ $EEDI_{IWV} = CF \cdot SFC \cdot P_D / (Vs \cdot m_{DWT})$					Deep water: $EEDI_{Req} = \alpha_4 + \beta_2 \cdot \exp(m_{DWT}/-\gamma_2) + \upsilon_1 \cdot \exp(m_{DWT}/-\delta_1)$			
	Shallow water: $P_D = (\alpha_6 + \beta_4 \cdot \exp(-\gamma_4 \cdot B) - \delta_2 \cdot \exp(h/-\varepsilon_1)) \cdot m_{DWT}$ P_D measure, V_s calculate $EEDI_{IWV}EEDI_{IWV} = CF \cdot SFC \cdot P_D / (Vs \cdot m_{DWT})$					Shallow water: $EEDI_{Req} = (\alpha_7 + \beta_5 \cdot V_c + \gamma_5 \cdot V_c{}^2) + (\delta_3 + \varepsilon_2 \cdot V_c - \zeta_1 \cdot V_c{}^2 + \eta_1 \cdot V_c{}^3) \cdot \exp(m_{DWT}/-\theta_1)$			
Ranges	Deep water: *T* = 1.5D; *T* = 2.0-3.2 m								
	Shallow water: *T* = 1.5D; *h* = 3.5-7.5 m; *T* = 2-2.8 m; *L* = 40-135 m; *B* = 5-17 m; m_{DWT} = 250-6000 t; V_c = 2-8 km/h; min(h/T) = 1.4								
Coefficients	Deep water:								
	α_1	α_3	α_4	β_1	β_2	γ_1	γ_2	δ_1	υ_1
	0.262	0.146	10	0.25	13	11	470	4500	8
	Shallow water:								
	α_6	α_7	α_8	α_9	β_4	β_5	β_7	β_8	
	0.375	21	18	0.375	0.0625	0.7	0.0625	2.5	
	γ_4	γ_5	γ_7	δ_2	δ_3	δ_5	δ_6	ε_1	
	0.13	0.28	8	0.5	11	0.5	0.75	2.8	
	ε_2	ε_4	ε_5	ζ_1	ζ_3	η_1	η_3	θ_3	
	0.78	2.8	0.25	0.46	0.375	0.154	3100	800	
Explanations	*D* – propeller diameter [m]; *B* – vessel breadth [m]; *h* – river depth [m]; *SFC* – specific fuel consumption, assumed to be 220 [g/kWh]; *CF* – carbon emission factor, 3.206 [gCO_2/gFuel]; *PD* – delivered power [kW]; $EEDI_{IWV}$ – attained (estimated energy efficiency design index [gCO_2/tkm]; $EEDI_{Req}$ – required energy efficiency designed index [gCO_2/tkm].								
Notes	For dry bulk and container vessels; For deep water (*h*>7.5m) and shallow water (zone 3) navigation; The method is proposed to be strengthened over the years for 15% and 25%.								

and above, while shallow water (which is defined as Zone 3 of the navigation conditions in EU inland waterways) accounts for the lower water depths.

ON MODELS AND THEIR APPLICABILITY

Proposed indices for inland vessels are not (formally speaking) energy efficiency indices for new vessels, as far as they correspond to those considered in IMO regulations for sea-going ships. They are, rather, indices for existing vessels, although they are labelled as *EEDI* here and could be used as such.

In this paper, a database consisting of 44 vessels was taken from the database in Method 1, published in [14] and used as a starting point for the analysis. The database contains hydrodynamic characteristics of self-propelled river cargo vessels obtained during the navigation and in model testing. Firstly, in order to evaluate energy efficiency indices for both methods, it was necessary to estimate the delivered power – speed curve for the vessels. Estimation of the delivered power – speed curve can be performed using the complex mathematical model developed in [14], via an artificial neural network approach. Respective input variables include: waterline length (L_{wl}), breadth (B_{wl}), draught (T), volumetric displacement (∇), ship speed through water (V), hydraulic radius (R_h), waterway breadth (b) and waterway depth (h). The output of the mathematical model is a coefficient of delivered power (CD) which is then used for the calculation of the delivered

power according to: $PD = CD \cdot (\rho \cdot g \cdot \nabla \cdot V)$. However, the mathematical model could not be applied for all cases because of the applicability limitations of the methods. Therefore, for the vessels that are 'out' of the limit and, moreover, their power – speed curve is not available as a part of the documentation, new river trials should be performed to obtain such dependency. Nonetheless, input variables for the required index are much less complex to acquire and include: Froude number based on water depth (*Fnh*) and deadweight (m_{DWT}) for Method 1; and speed of the river (*Vc*) and deadweight (m_{DWT}) for Method 2.

River speeds considered in the assessments were 2, 4 and 6 km/h, as this range corresponds to the applicability of the methods. The authors did not have all the parameters of the fleet that were required. Therefore, empirical equations given in [14] and recommendations from [18] were used to estimate missing data, which mostly concerned the deadweight values for some of the vessels.

Consequently, Method 1 can be applied to 32 vessels from the original database of 44, considering an upper boundary level of 3000 tons of DWT. In contrast, Method 2 only applicable for draught $T = 1.5 \cdot D$ (where D is the propeller diameter), which is very restrictive. Therefore, an original database consisting of 44 vessels was reduced to only one vessel, when Method 2 was considered. Hence, the vast difference between the methods' limitations was obvious from the start. Generally speaking, the draught required for Method 2 is not a design draught and, thus, a corresponding *DWT* will not be directly available for the analysis, in order to evaluate *EEDI* (attained and required). Therefore, this method commonly requires additional documentation, such as *Trim and Stability Booklet* for each specific vessel, where necessary input parameters for *EEDI* assessment can be found. Method 2 provides a limit of 6000 tons of *DWT* and covers all vessels in the database, when just a *DWT* is considered.

However, in order to achieve a comparison under an applicability limit for both methods, the assessment is performed for the vessels having an equal draught of 1.5*D*, taking into account the aforementioned, more restricted draught constraint of Method 2. This does not mean that the design draught of vessels is 1.5*D*, since it is quite the opposite for almost all the vessels except one, as previously mentioned. Despite the implication that the draught of all the vessels is, indeed, defined as 1.5*D*, for the purpose of the analysis and the corresponding volumetric displacement it is obtained according to the linear interpolation between parameters available for other draughts. Volumetric displacement is necessary for *DWT* evaluation and presents an input for *EEDI* calculations. Finally, after applied limitations and interpolation corrections, four cargo vessels remained for assessment, see Table 3.

Tab. 3. Vessels' main particulars

No.	L_{wl} [m]	B_{wl} [m]	T[m]	∇ [m³]	*DWT* [m]
1	109.3	14.00	2.78	3530.9	2771.8
2	110.0	11.40	2.40	2578.4	2024.0
3	82.9	9.50	2.32	1607.1	1261.6
4	93.3	11.5	2.40	2206.0	1607.0

The analysis of energy efficiency was performed according to the following constraints:

- Waterway depth - $h = 5$ m (for shallow water) and waterway breadth - $b = 400$ m;
- Waterway depth - $h = 8$ m (for deep water) and waterway breadth - $b = 400$ m.

RESULTS

In the following, the calculation of energy efficiency indices and the comparison of both methods are presented, based on the procedures described in previous sections.

METHOD 1

Attained energy efficiency index is dependent on brake power, not on delivered power. Hence, a shaft efficiency coefficient of 0.98 was applied to estimate the brake power of the vessels. Attained and required *EEDI** are not expressed as one value (as is the case for sea-going ships, where *EEDI* is calculated for 75% of main engine power). Here, both values of (attained and required) *EEDI** are estimated for a range of speeds. Therefore, various speeds (10, 12, 14, 16, 18 and 20 km/h) were applied, considering the method's limits of applicability. The comparison between attained and required energy efficiency index for shallow water was assessed according to Method 1, as shown in Table 4 and Fig. 1. Grey cells represent the cases in which the energy efficiency criteria are not satisfied – see 12 km/h and 14 km/h for vessels no. 1. At 18 and 20 km/h, corresponding Froude numbers exceed the applicability criteria, and so the consequent results are not shown. Moreover, results for the deep water condition are shown in Table 5 and Fig. 2, with grey cells representing the failed criteria.

The results show that all four vessels satisfy the requirements for a lower speed range when a deep water condition is considered. For higher speeds, attained *EEDI** values are significantly above the required limit, making their navigation less efficient. Therefore, it seems that, according to the results, vessels navigating deep-water conditions would be less effective than in shallow-water conditions, which is quite unsound.

Tab. 4. Energy efficiency for shallow water (Method 1)

No.	Attained *EEDI**				Required *EEDI**			
	10 km/h	12 km/h	14 km/h	16 km/h	10 km/h	12 km/h	14 km/h	16 km/h
1	3.74	4.98	7.39	11.45	3.80	4.65	7.14	11.93
2	3.27	4.50	6.39	9.58	4.14	5.05	7.74	12.78
3	3.66	4.88	7.41	11.76	4.71	5.72	8.73	14.16
4	3.93	5.25	7.84	12.18	4.41	5.37	8.21	13.43

Tab. 5. Energy efficiency for deep water (Method 1)

No.	Attained *EEDI**					
	10 km/h	12 km/h	14 km/h	16 km/h	18 km/h	20 km/h
1	3.74	4.98	6.63	8.88	11.98	16.35
2	3.27	4.50	6.06	8.06	10.69	14.30
3	3.66	4.88	6.53	8.75	11.78	16.02
4	3.93	5.25	7.02	9.41	12.67	17.24

No.	Required *EEDI**					
	10 km/h	12 km/h	14 km/h	16 km/h	18 km/h	20 km/h
1	3.80	4.65	7.74	7.05	8.67	11.31
2	4.14	5.05	6.24	7.64	9.36	12.13
3	4.71	5.72	7.06	8.62	10.51	13.47
4	4.41	5.37	6.63	8.10	9.91	12.77

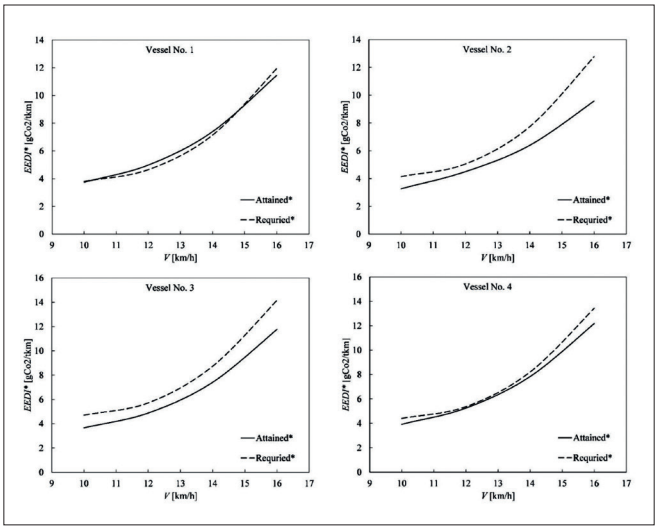

Fig. 1. Energy efficiency for shallow water (Method 1)

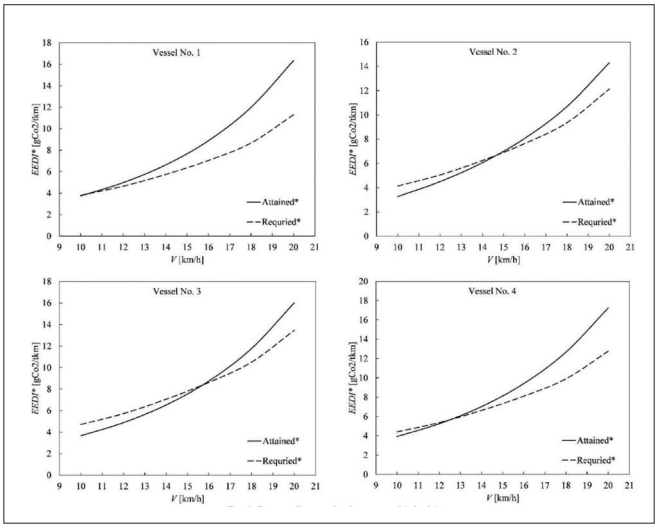

Fig. 2. Energy efficiency for deep water (Method 1)

METHOD 2

Energy efficiency indices assessed according to Method 2 are given in Table 6, for shallow and deep water, with grey cells representing the failed criteria. Note that river trial results (speed – power curves) have to be available prior to the *EEDI* estimation in order to evaluate the vessel's speed. Since the river trials results are not offered in the database, the delivered power was obtained using the mathematical model described and offered in [15]. Required EEDI is a function of the speed of the water, so the calculation was performed for 2, 4 and 6 km/h. However, the method is not able to consider the dependency between *EEDI* and the vessel speed, so the corresponding diagrams, as in the case of Method 1, could not be produced. Thus, this method allows calculation of energy indices for just one value of speed.

Method 2 appears to be less conservative than Method 1, when results for shallow water are considered, since attained *EEDI* values are approximately 40% less than required ones, on average. In the case of deep water, required *EEDI* values for all three water speeds are unchanged for each vessel, because they are only a function of *DWT* and not the speed of the river. Therefore, as the speed of the water is increased, an attained

Tab. 6. Energy efficiency for shallow and deep water (Method 2)

No.	Shallow water			Deep water		
	Speed of water – 2 km/h					
	V_s	Attained *EEDI*	Required *EEDI*	V_s	Attained *EEDI*	Required *EEDI*
1	14.23	14.93	23.89	14.97	12.34	14.36
2	14.79	14.56	24.47	15.50	11.92	15.28
3	14.21	15.35	25.99	15.11	12.23	16.93
4	14.08	15.35	25.12	14.73	12.55	16.02

No.	Shallow water			Deep water		
	Speed of water – 4 km/h					
	V_s	Attained *EEDI*	Required *EEDI*	V_s	Attained *EEDI*	Required *EEDI*
1	12.23	17.37	28.80	12.97	14.25	14.36
2	12.79	16.84	29.60	13.50	13.69	15.28
3	12.21	17.87	31.71	13.11	14.10	16.93
4	12.08	17.87	30.51	12.73	14.52	16.02

No.	Shallow water			Deep water		
	Speed of water – 6 km/h					
	V_s	Attained *EEDI*	Required *EEDI*	V_s	Attained *EEDI*	Required *EEDI*
1	10.23	20.77	36.29	10.97	16.85	14.36
2	10.79	19.96	37.86	11.50	16.07	15.28
3	10.21	21.37	41.97	11.11	16.63	16.93
4	10.08	21.41	39.63	10.73	17.22	16.02

EEDI is closer to the required limit. Hence, an attained *EEDI* is larger than that required for the 6 km/h speed of the river, for vessels no. 1, 2 and 4.

COMPARISON BETWEEN METHOD 1 AND METHOD 2

Method 1 gives a range of attained and required energy efficiency indices for various speeds of the vessel. However, Method 2 would provide the specific (one) attained and required energy efficiency value at delivered power for a specific speed. In order to compare the two methods, the specific attained and required *EEDI* values were obtained by applying the required speed (one value) derived from Method 2 into Method 1. This procedure was performed for three water speeds, while including shallow and deep-water conditions, see Table 7 (grey cells represent failed criteria). The difference between the two methods is illustrated in Fig. 3.

Since Method 1 is scaled to Method 2, both methods can be compared (Fig. 3): Method 1 (Table 7) vs. Method 2 (Table 6). Vessel No. 1 does not comply with the required *EEDI* in both shallow and deep-water conditions, in specific cases in Method 1. Despite this, the same vessel satisfies Method 2 in all cases, except deep water conditions where the water speed is 6 km/h. Furthermore, vessel No. 3 met the requirements in all cases and methods. Vessels No. 2 and No. 4 did not satisfy the Method 2 requirements for deep water conditions at a river speed of 6 km/h, but did comply with the requirements for the same river speed if Method 1 was considered. Nonetheless, for the same method, both vessels did not meet the required *EEDI* for 2 km/h of river speed, while vessel No. 4 did not even comply with the criterion when considering 4 km/h of river speed.

In general, as seen from the diagrams in Fig. 3, Method 2 provides two to five times larger values of energy efficiency indices (attained and required) than Method 1, for the river speeds of 2, 4 and 6 km/h and the same navigation conditions. Nonetheless, it should be noted that a different specific fuel consumption (SFC) was used in each method: 200 g/kWh for Method 1 and 220 g/kWh for Method 2. And yet, 10% of SFC difference could not lead to such a significant difference in energy efficiency indices.

Tab. 7. Energy efficiency for shallow and deep water (specific Method 1)

No.	Shallow water			Deep water		
	Speed of water – 2 km/h					
	V_s	Attained *EEDI**	Required *EEDI**	V_s	Attained *EEDI**	Required *EEDI**
1	14.23	7.73	7.53	14.97	7.64	6.35
2	14.79	7.28	9.30	15.50	7.51	7.27
3	14.21	7.70	9.15	15.11	7.68	7.91
4	14.08	7.96	8.36	14.73	7.81	7.14

No.	Shallow water			Deep water		
	Speed of water – 4 km/h					
	V_s	Attained *EEDI**	Required *EEDI**	V_s	Attained *EEDI**	Required *EEDI**
1	12.23	5.20	4.85	12.97	5.72	5.15
2	12.79	5.20	5.90	13.50	5.63	5.92
3	12.21	5.11	5.95	13.11	5.73	6.43
4	12.08	5.34	5.45	12.73	5.84	5.80

No.	Shallow water			Deep water		
	Speed of water – 6 km/h					
	V_s	Attained *EEDI**	Required *EEDI**	V_s	Attained *EEDI**	Required *EEDI**
1	10.23	3.82	3.81	10.97	4.30	4.18
2	10.79	3.64	4.28	11.50	4.16	4.79
3	10.21	3.69	4.71	11.11	4.30	5.22
4	10.08	3.95	4.41	10.73	4.37	4.72

CONCLUSION

Method 1 gives attained and required energy efficiency indices for a range of speeds and within less sensitive constraints than in Method 2. Therefore, such rigid limitations pose a great disadvantage in Method 2. This drawback is expressed through the draught requirement, which should be defined as 1.5*D* in order to use the method. Therefore, new

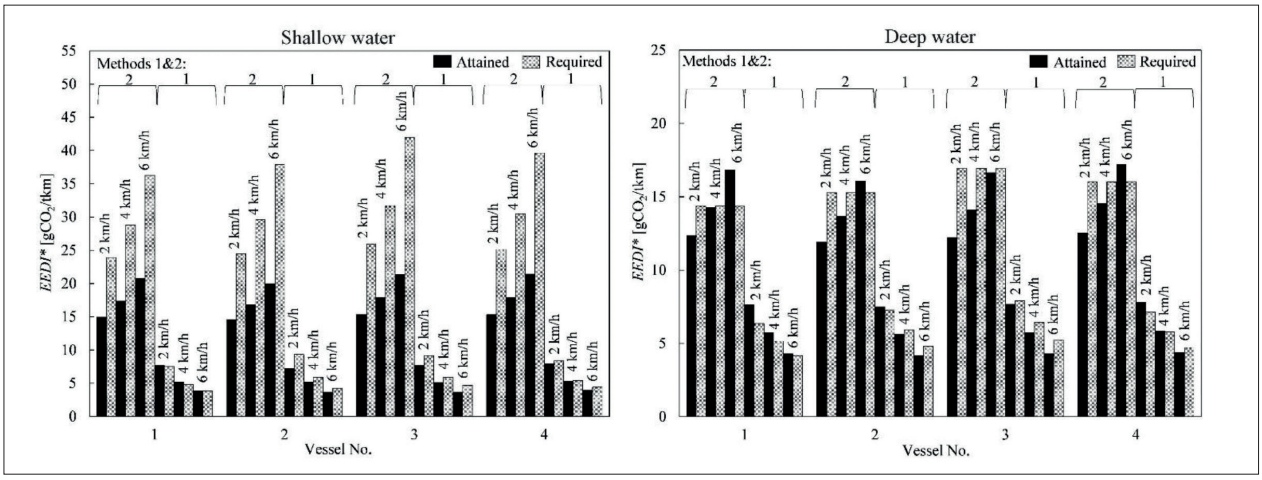

Fig. 3. Comparison between methods in shallow water conditions (left) and deep water conditions (right): 1 – specific Method 1 and 2 – Method 2

speed-power tests (river trials) should be conducted at this specific draught for the application of the method. Nonetheless, a potentially available speed-power curve would not be useful here. Although Method 1 is not so restrictive, it does not take into account the speed of the water. Moreover, there is a 10% difference in specific fuel consumption input between the methods, but this could not lead to a significant difference in the results. Furthermore, the results differ when both methods become comparable. It is interesting that, according to Method 2, shallow water required *EEDI* is quite large. In general, in a considerable number of cases, the vessels appear to be more energy efficient in shallow water than in deep water. This is quite improbable in practice, so the next step would be to address such a drawback within the methods.

Regarding the persistent issue arising from the power-speed curve estimation as an input, a real-time engine power measurement could be introduced during the navigation instead; followed by installation of an engine power limiter. Both could manage and optimise the real-time engine power to achieve energy efficiency under the limitations during the navigation. Therefore, in order to address the reliable navigation condition, attained energy efficiency should be measured rather than calculated.

It seems that the proposed regulations would not be able to induce the development of technology with respect to energy efficiency in years to come. The vessel designs considered here are the same as they were decades ago. This means that, according to the results, most of them do not need any improvements in terms of energy efficiency.

Nonetheless, the obvious conclusion is that inland waterway vessels' energy efficiency methods need to be harmonised when addressing the issues reported in this paper. Inland waterway authorities should provide more 'easy to use' solutions, such as in the maritime industry.

ACKNOWLEDGEMENTS

This work was partially supported by the Ministry of Education, Science and Technological Development (Project no. 451-03-68/2022-14/200105) of Serbia.

REFERENCES

1. IMO MEPC, "Resolution MEPC.203(62) – Amendments to the Annex of the Protocol of 1997 to amend the International Convention for the prevention of pollution from ships, 1973, as modified by the protocol of 1978 relating thereto.", International Maritime Organization (IMO), 2011/07/15. 2011. [Online]. Available: https://wwwcdn.imo.org/localresources/en/OurWork/Environment/Documents/Technical%20and%20Operational%20Measures/Resolution%20MEPC.203%2862%29.pdf. [Accessed: March 5, 2022].

2. IMO MEPC, "Resolution MEPC.304(72) – Initial IMO strategy on reduction of GHG emissions from ships", International Maritime Organization (IMO), 2018/04/13. 2018. [Online]. Available: https://wwwcdn.imo.org/localresources/en/KnowledgeCentre/IndexofIMOResolutions/MEPCDocuments/MEPC.304(72).pdf. [Accessed: March 5, 2022].

3. IMO ISWG-GHG, "Draft report of the eighth meeting of the Intersessional Working Group on Reduction of GHG Emissions from Ships (ISWG-GHG 8)", International Maritime Organization (IMO), Norway, 2021/05/28, 2021.

4. M. Kalajdžić and N. Momčilović, "A Step Toward the Preliminary Design of Seagoing Multi-Purpose Cargo Vessels", Brodogradnja/Shipbuilding, Vol. 71, No. 2, pp 75-89, 2020. doi: 10.21278/brod71205.

5. M. Kalajdžić, M. Vasilev and N. Momčilović, "Exploring an Effect of Novel IMO Policies on Energy Efficiency of Existing Ships", 1st Kotor International Maritime Conference (KIMC2021), Kotor, Montenegro, 27-28 November, 2021.

6. O. Konur, M. Bayraktar, M. Pamik, B. Kuleyin and M. Nuran, "The Energy Efficiency Gap in Turkish Maritime Transportation", Polish Maritime Research 3 (103), Vol. 26; pp. 98-106, 2019. doi:10.2478/pomr-2019-0050.

7. CESNI, "European Standard laying down Technical Requirements for Inland Navigation vessels (ES-TRIN)", European Committee for drawing up Standards in the field of Inland Navigation (CESNI), technical standard, 2021, [Online]. Available: https://www.cesni.eu/wp-content/uploads/2020/10/ES_TRIN_2021_en.pdf. [Accessed: March 6, 2022].

8. UNECE, "Recommendations on Harmonised Europe-wide Technical Requirements for Inland Navigation Vessels, Resolution No. 61, Revision 2", United Nations Economic Commission for Europe (UNECE), Geneva, 2020, [Online]. Available: https://unece.org/sites/default/files/2021-02/ECE-TRANS-SC3-172-r2e.pdf. [Accessed: March 6, 2022].

9. CCNR, "Annual Report 2021 – Inland avigation in Europe – Market Observation", Central Commission for The Navigation of the Rhine (CCNR), Report, 2021. [Online]. Available: https://www.ccr-zkr.org/files/documents/om/om21_II_en.pdf. [Accessed: March 6, 2022].

10. T. Abramowicz-Gerigk and Z. Burciu," Design and Operational Innovations in Adapting the Existing Merchant River Fleet to Cost-Effective Shipping", Polish Maritime Research 4 (104), Vol. 26; pp. 157-164, 2019. doi: 10.2478/pomr-2019-0078.

11. M. Kunicka and Wojciech Litwin, "Energy Efficient Small Inland Passenger Shuttle Ferry with Hybrid Propulsion – Concept Design, Calculations and Model tests", Polish Maritime Research 2 (102), Vol. 26; pp. 85-92, 2019. doi:10.2478/pomr-2019-0028.

12. A. Karczewski and M. Kunicka, "Influence of the Hull Shape on the Energy Demand of a Small Inland Vessel with Hybrid Propulsion", Polish Maritime Research 3 (111), Vol. 28; pp. 35-43, 2021. doi:10.2478/pomr-2021-0032.

13. D. Radojčić, A. Simić, N. Momčilović, M. Motok and B. Friedhoff, Design of Contemporary Inland Waterway Vessels – The Case of the Danube River. Springer, 2021. ISBN: 978-3-030-77324-3, doi: 10.1007/978-3-030-77325-0.

14. A. Simić, "Energy Efficiency of Inland Self-Propelled Cargo Vessels". Doctoral dissertation, University of Belgrade, Faculty of Mechanical Engineering, Belgrade, 2012. [Online]. Available: http://doiserbia.nb.rs/phd/fulltext/BG20121101SIMIC.pdf. [Accessed: March 7, 2022].

15. DST, "Evaluating the Energy Requirement of Inland Vessels using Energy Efficiency Indices", DST, German Federal Ministry of Transport, CESNI, R&D project study, 2020. [Online]. Available: https://www.cesni.eu/wp-content/uploads/2021/03/cesnipt_energyindex_en.pdf. [Accessed: March 6, 2022].

16. M. M. Karim and S. M. R. Hasan, "Establishment of EEDI Baseline for Inland Ship of Bangladesh", Procedia Engineering, Vol. 194, pp. 370-377, 2017. doi: 10.1016/j.proeng.2017.08.159.

17. N. M. G. Zakaria and S. Rahman, "Energy Efficiency Design Index (EEDI) for Inland Vessels in Bangladesh", Procedia Engineering, Vol. 194, pp. 362-369, 2017. doi: 10.1016/j.proeng.2017.08.158.

18. A. Papanikolaou, "Ship Design – Methodologies of Preliminary Design". Springer, 2014. ISBN: 978-94-017-8750-5, doi: 10.1007/978-94-017-8751-2, 2014.

CONTACT WITH THE AUTHORS

Milan Kalajdžić
e-mail: mdkalajdzic@mas.bg.ac.rs

University of Belgrade
Faculty of Mechanical Engineering
Department of Naval Architecture, Belgrade
Serbia

Matija Vasilev
e-mail: matija@oceanpro.eu

Ocean Pro Marine Engineers LTD
Belgrade
Serbia

Nikola Momčilović
e-mail: nmomcilovic@mas.bg.ac.rs

University of Belgrade
Faculty of Mechanical Engineering
Department of Naval Architecture, Belgrade
Serbia

ПРИЛОГ 2

Brodogradnja/Shipbuilding/Open access Volume 74 Number 3, 2023

Milan Kalajdžić
Matija Vasilev
Nikola Momčilović

http://dx.doi.org/10.21278/brod74304

ISSN 0007-215X
eISSN 1845-5859

Inland waterway cargo vessel energy efficiency in operation

UDC 629.55:621.182.3:629.542
Original scientific paper

Summary

Inland waterways vessels (IWV) have no mandatory regulations regarding their energy efficiency, as sea-going ships have. So far, there are just two proposed design energy efficiency evaluation methods, both based on IMO EEDI approach and data on EU inland navigation. Operational indicators and real-time navigation measurements from available literature do not exist. Therefore, this paper aims to introduce the energy efficiency in operation (EEO), assessed for the typical Danube cargo vessel. Firstly, an operational profile is acquired by tracking the vessel's voyages, and by identifying actual constraints of each sector the vessel has sailed during the designated time. Secondly, EEO is incorporated within two available methods and calculated based on acquired operational data considering different navigational conditions. The paper shows how the energy efficiency vastly depends on variables such as water depth, current speed, draught, deadweight, river constraints. Analysis is performed for the most employed month of the vessel navigation, and annually. Depending on water level scenarios and during the selected month of sailing, the total amount of CO_2 emitted is estimated to be between 22.7 t and 29.9 t, while the necessary average speed reduction (i.e., slow steaming) per sectoral voyage for the requirement compliance is calculated to be in between 4.8%-26%. Slow steaming is assessed to extend the time of voyage for 6.1-10.7 hours on monthly basis and 49-87 hours annually.

Key words: *energy efficiency design index; energy efficiency in operation; inland vessel efficiency, inland waterway vessels; operational profile, slow steaming.*

1. Introduction

Energy efficiency indicators for sea-going ships intended for international voyages are used for a decade and are provided by the International Maritime Organization (IMO). They can be divided into design and operational ones. Firstly, a design indicator labelled as energy efficiency design index (EEDI) became mandatory for new ships over 400 GT built between 2013 and 2015 [1], under the MARPOL Annex VI. EEDI criterion has been strengthened over the years, namely in 2015, 2020, and expected to be strengthened in 2025. In 2023, existing ships faced the IMO's regulatory examination through the compulsory requirements of the energy efficiency existing ship index (EEXI), see calculation guidelines in [2]. The main disadvantage of the design-based indicators is that they do not represent an actual

navigational nature of shipping. They use design or nominal inputs, acquired as a single value from the calculation procedures defined in [1, 2]. Therefore, energy efficiency is evaluated using single value for deadweight (DWT), speed, engine power, etc. In order to represent the real sailing conditions during the voyages over a period of time, a carbon intensity indicator (CII) has been set as mandatory measure starting from 2023 [3]. CII is an operational indicator applied for ships over 5000 GT and is projected to provide an actual operational emission estimation. Based on CII results obtained for the whole year, ships will be rated by grades: A, B, C, D, E (A – the highest grade, E – the lowest grade). Ship with lower annual rating (for instance, D or E) must provide a plan to improve rating and its energy efficiency. Fortunately, fuel consumption recording during the navigation has become mandatory from 2019, for ships over 5000 GT, as set by IMO. It is achieved by implementing the data collection system (DCS) [4]. Moreover, IMO has already provided an operational tool (although not an actual criterion and not mandatory) called energy efficiency operational indicator (EEOI) [5]. EEOI is planned to help ship operators to supervise the energy efficiency performance of their fleets over time and thus, to identify increased emission sequences and to quantify the effect of modifications on their voyage efficiency. All these indicators' aims were to provide short-term measures in order to achieve mid- and long-term greenhouse gas (GHG) reduction goals, which IMO presented in its studies. Most recent study from 2020 [6] targeted the following: to reduce CO_2 emissions per transport work (carbon intensity) in shipping, on average, to 40% until 2030 (compared to 2008), to reduce emissions per transport work (carbon intensity) in shipping, on average, to 70% until 2050 (compared to 2008), to achieve peak emissions from shipping as soon as possible, and to reduce annual GHG emissions from shipping to at least 50% until 2050, (compared to 2008). Literature data on energy efficiency of ships followed the regulation adoption and have been increasing over the years. Energy efficiency level for most prominent multipurpose ships and bulk carriers built from 2000 until 2020 is evaluated in [7, 8], respectively. As slow steaming has become the most used operational measure to improve EEDI and EEXI levels, paper [9] additionally gave an estimation for the ships' power reduction needs to comply with novel requirements. Slow steaming benefits for various navigation conditions are investigated in [10]. The paper emphasized the importance of considering actual sailing routes for a specific container ship in energy efficiency evaluations. In [11], the real voyage data for general cargo ship were used to estimate CII, based on different engine loads and slow steaming rate. Besides extensively researched slow steaming, some other measures for existing designs have been analysed, such as the influence of biofilm on energy savings [12].

In contrast, inland waterway vessels (IWV) are not regulated by IMO and thus, not falling under their mandatory requirements. Nevertheless, in Europe alone, more than 15000 IWV are in operation, while most of them are registered in Rhine and Danube countries, 63% and 22%, respectively, according to data from 2021 [13]. As of 2017, nearly 40% of the Danube vessels is more than 40 years old, while less than 1% of them are built after 2010 [14]. In Danube countries, the largest quantity of goods carried within national territories is achieved in Romania (37.5%) and Serbia (13.3%) [14]. From 2017 until 2020, the rate of change of goods in major Danube ports in these two countries increased by 10.5%, whereas in all other Danube ports decreased by 7.3%, on average [15]. Dry cargo IWV represent the major ship type, with a 73% share on Rhine, and 76% share on Danube. They compete in freight transport over land with road and rail modes, while sea-going ships have no competition in that sense. Moreover, IWV pass through the large cities and urban areas and are emitting harmful pollutants. Nonetheless, they are considered as a cleaner mode of transport, expressed in ton per km of freight transport, as shown in [16]. Therefore, 2019 EU Green Deal [17] addressed IWV, by implying that around 75% of the road and rail transport should be moved to IWV. Moreover, European Commission's Naiades III action plan from

2020 [18], being in line with EU Green Deal, set a goal to increase inland and short-sea shipping by 25% and 50% until 2030 and 2050, respectively. In order to counter GHG emissions from IWV, Central Commission for the Navigation of the Rhine (CCNR) published a roadmap in 2022, similar to IMO goals [19], in which it was aimed to reduce GHG emissions from IWV by at least 35% until 2035, compared to 2015 level, and to almost eliminate GHG and other pollutant emissions until mid of the century.

Although IWV policies exists from recently, IWV have no mandatory regulations regarding the energy efficiency, except evaluations proposals given in two methods from [20] and [21]. These methods used data on European inland navigation. They are based on IMO EEDI approach; however, they are different in their nature, see detailed their comparison in [22]. Other methods that targeted European waterways are also available, but they are more developed to evaluate transport rather than energy efficiency. Their systematic description and comparison are given in [16].

On the other hand, there were some rare attempts to establish "similar to IMO EEDI" assessments outside European waterways. Energy efficiency attained values and requirement line have been evaluated for rivers in Bangladesh, as they represent important transport path in the region. Study in [23] applied IMO EEDI procedure to general cargo, oil tanker and passenger IWV. It was concluded that EEDI assessments should be region based rather than generalized for the world's inland fleets, due to the diversity of inland navigation. Furthermore, paper [24] investigated an influence of design features on energy efficiency of IWV. The study concluded that the service speed decrease and draught increase lowered EEDI values, which is in compliance to the European IWV performances, see [16]. These attempts have been revised in [25] to account for the field study performed by measuring actual MCR for 15 IWV. The research stated that the effect of shallow water on energy efficiency of studied IWV is significant, and varied between 19.30% and 21.10%, on average. Other efforts to include energy efficiency in inland navigation has been more directed towards the hydrodynamically optimised design for the particular river with respect to the high flow and low depth constraints, as presented in [26] for Magdalena river in Colombia. To conclude, an average age of IWV on Danube is much larger than in case of sea-going ships. Moreover, IWV are left behind with no compulsory design-based energy efficiency regulations or requirements, while operational ones are also neglected. This can be alarming since IWV include highly diversified operations and large fleets. In addition, literature dealing with energy efficiency of IWV is very rare. There are no available energy efficiency assessments of IWV using instantaneous and actual fairway constraint change, as well as operational data of any kind (real-time, averaged or estimated), as delivered in this paper. Therefore, the objective of this paper is to perform energy efficiency assessments for a typical self-propelled IWV taking into account:

- energy efficiency design indices delivered by two methods proposed so far and given in [20, 21], and
- energy efficiency in operation using operational data for the selected vessel.

2. Assessment methodology

The following methodology for assessments is used for the case study vessel:

- for a year of service, identified are monthly travelled distances,
- a month in which the vessel had the most frequent usage (distance covered) is selected for further analysis,

- input data gathered for evaluation include identification of actual constraints of the fairway on each sector of the navigation and actual speed of the vessel for a selected month of sailing and annually, as elaborated in sect. 2.1.
- energy efficiencies are evaluated based on two methods from [20, 21], and only ones proposed so far for IWV, as given in sect 2.2,
- the total CO_2 emitted by the vessel is evaluated for the selected month of sailing and annually, based on two available methods.
- voyages that did not satisfy energy efficiency requirements has been selected and their energy efficiency in operation is evaluated by the sector,
- the necessary reduction of speed is calculated for the critical voyages (and their corresponding sectoral sailings) to comply with the requirements,
- the additional time for navigation is calculated for the vessel to comply with regulations by means of slow steaming.

Note that the paper is not providing a new method. It is delivering the new approach for inputs for existing methods. It uses operational and not the design data as inputs. Moreover, the paper compares methods based on operational input data for the particular voyage. This is not performed so far in the literature related to IWV. Some of the operational data are obtained in real-time and some, for which authors could not acquire data, are estimated using extreme scenarios, which is thoroughly described in sect. 2.1.

2.1 Operational profile

Compared to sea-going voyages, in general, IWV operational profile is more complex as its navigation additionally considers shallow water effects, current speed, bank effects, the presence of the bridges, etc. The vessel considered in this paper operated on Danube between port of Constanta (Romania) and Aljmas (Croatia), during the period starting from 15 January 2022 until 15 January 2023. The voyage data are extracted from Marine Traffic website [27]. Nonetheless, the data from the website were not sufficient for precise representation of the navigation conditions. Thus, more accurate and detailed pilot charts of Danube are employed. They are published by the Danube Commission in [28] and are included within six documents: Pilot Charts of the Danube I, II, III(1), III(2), IV and V. Pilot charts cover the Danube from its confluence into the Black Sea (0 km) to the Hungarian-Serbian border (1433 km from the confluence). The raw data from the charts are divided into 171 sectors ranging from 2 to 12 km in length, with average sector having 5 km in length. This division was too large to analyse, so simplified river model is created meaning that 171 sectors are regrouped into 20 sectors, separated by major Danube ports. Going upstream, these ports are: Constanta (Romania), Agigea (Romania), Murfatlar (Romania), Medgidia (Romania), Cernavoda (Romania), Silistra (Bulgaria), Ruse/Giurgiu (Bulgaria/Romania), Svishtov (Bulgaria), Vidin/Calafat (Bulgaria/Romania), Prahovo (Serbia), Drobeta Turnu Severin (Romania), Orsova (Romania), Moldova Veche (Romania), Veliko Gradište (Serbia), Smederevo (Serbia), Pancevo (Serbia), Belgrade (Serbia), Sremski Karlovci (Serbia), Novi Sad (Serbia), Vukovar (Croatia), Aljmas (Croatia).

The exact water levels and current speeds during navigation of the vessel could not be obtained from the available data, since there is no available historical data on real-time tracking of such parameters, according to the best of authors knowledge. Hence, navigation is modelled according to the two extreme scenarios in which the vessel could potentially sail:

- during the lowest navigable water levels (LNWL) for the sector and
- during the highest navigable water levels (HNWL) for the sector.

This means that actual vessel water level could have been only evaluated in between these two extreme values of LNWL and HNWL. Both, LNWL and HNWL change as the vessel is passing through the each of the sector. LNWL and HNWL also produce two extreme current speeds. Therefore, by analysing the vessel navigation at LNWL and HNWL (and corresponding current speeds), we assumed that its consequent and actual energy efficiency could have been only evaluated in between two energy efficiencies: one calculated for LNWL and one calculated for HNWL condition. LNWL and HNWL data and their corresponding current speeds are obtained statistically. Namely, data from [28] includes LNWL and HNWL values for every 3 km of the Danube sector. These data were averaged by the sector to obtain each of the sector's average LNWL and HNWL, which is used for further analyses. Correspondingly, the current speeds for both scenarios were determined following the same procedure and sector division. In such way, the energy efficiency of the vessel can be considered to be within the bandwidth given by two extremes. Therefore, the following parameters for the Danube sectors are extracted from [28, 29]: river kilometre, LNWL, HNWL, current speed at LNWL and HNWL. During the period of one year (Fig. 1), the vessel had 106 voyages and covered the distance of 21531 km. Vessel spent 138 days in navigation, 210 days in ports, while during 17 days the vessel was idle. In August 2022, there was no navigation. However, in October 2022, the vessel was most frequently employed and thus, travelled the largest distance compared to other months. Therefore, October 2022 was chosen for detailed assessment. The reason that the whole year is not assessed by real-time operation data, as the case was for October 2022, is because some of the data were unavailable and unreliable for certain months. Therefore, annual estimation of energy efficiency and CO_2 emissions are performed using extrapolation of the October 2022 sailings.

During October 2022, the total of 11 voyages were recorded along with the distances travelled, transit and port calls periods, and respective draughts. In that month, the vessel sailed to 10 ports on a Danube between Belgrade (Serbia) and Svishtov (Bulgaria). October 2022 sailings are divided into 9 sectors, as in Fig. 2. Sectors' average water depths and current speeds are given in Fig. 3.

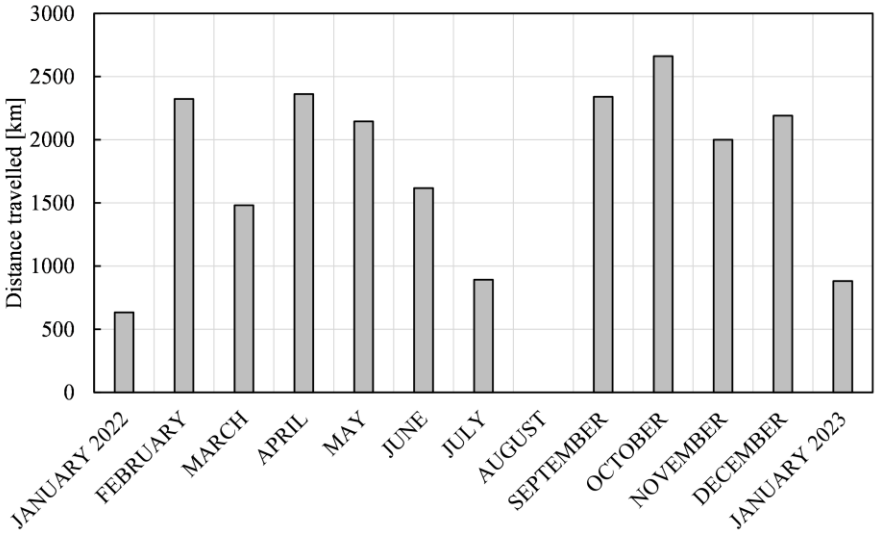

Fig. 1 Distance covered by the vessel navigation for each month during the year

Fig. 2 October 2022 route: map

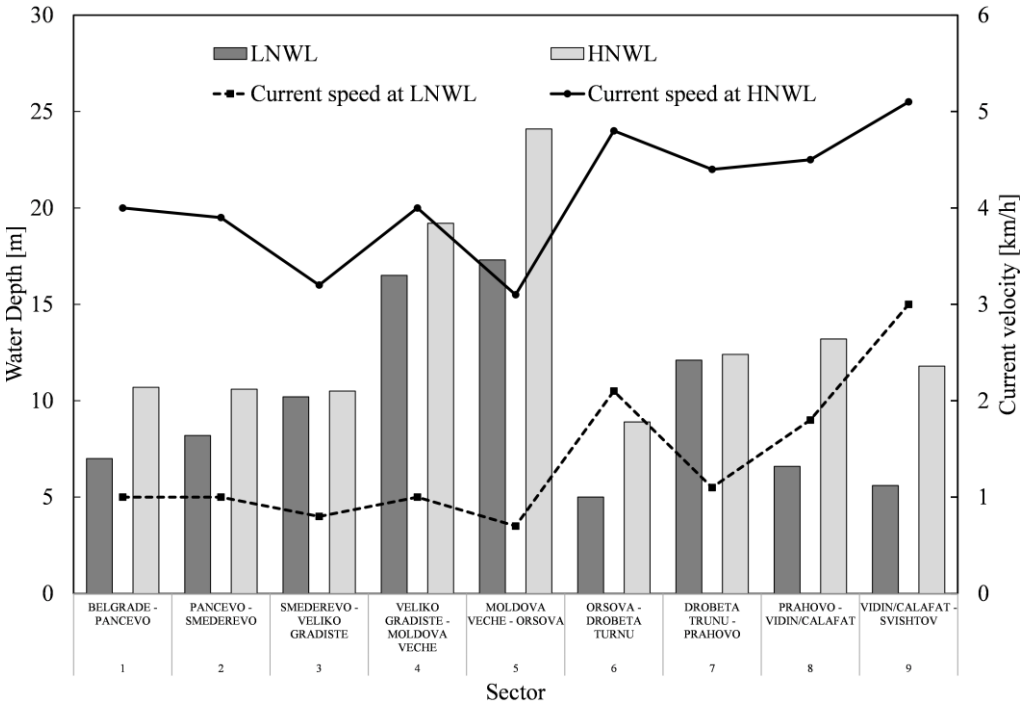

Fig. 3 October 2022 route: water depths and current speeds

Additionally, width of the river for each location is extracted from the documents in [29], which provides a maximum fairway width that is guaranteed by the Danube Commission, throughout the entire year. Based on service draught and available vessel documentation, specifically Trim and Stability Booklet, the displacement and the deadweight are determined. The average sailing speed (speed over ground - SOG) for each voyage was calculated by dividing the distance travelled between the starting and ending destination by the time obtained from subtracting the duration spent in port from the total duration of a certain route. Finally, voyage data for October 2022 navigation are presented in Table 1.

Table 1 Voyages data for October 2022

Voyage no. and port calls	Distance [km]	Draught [m]	DWT [t]	Duration [h]	Speed over ground (SOG) [km/h]
1. Veliko Gradište - Belgrade	108	2.4	1548.5	57.81	1.87
2. Belgrade - Pančevo	15	2.4	1548.5	0.80	18.75
3. Pančevo - Drobeta Turnu Severin	223	2.4	1548.5	10.98	20.30
4. Drobeta Turnu Severin - Svishtov	372	1.7	851.0	29.68	12.53
5. Svishtov – Veliko Gradište	502	2.5	1650.1	88.28	5.69
6. Veliko Gradište - Belgrade	108	2.5	1650.1	11.03	9.79
7. Belgrade	105	2.5	1650.1	92.70	1.13
8. Belgrade - Svishtov	610	1.7	851.0	36.28	16.81
9. Svishtov	9	1.7	851.0	9.33	0.96
10. Svishtov – Veliko Gradište	502	2.2	1346.9	87.03	5.77
11. Veliko Gradište - Belgrade	108	2.2	1346.9	7.33	14.73

Furthermore, the following matrix is created to represent the operation of the vessel during the October 2022, see Fig. 4. During voyages 7 and 9 (crossed cells), the vessel sailed within the area of the port or city. The vessel deadweight varied between 851 t and 1650.1 t.

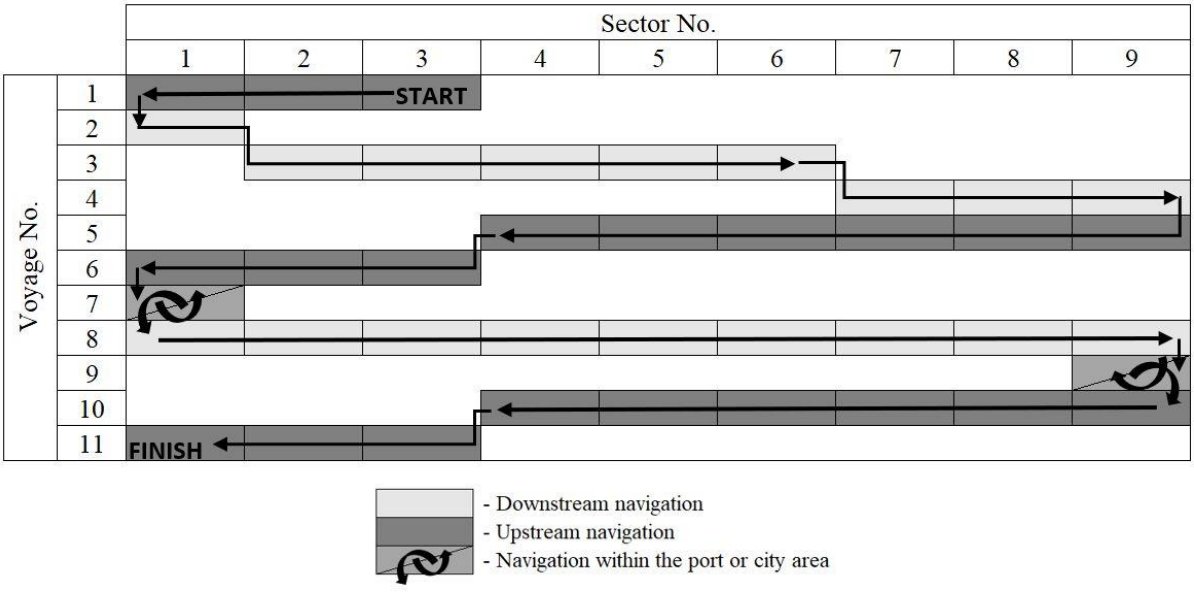

Fig. 4 October 2022 navigation matrix

2.2 Energy efficiency design indices

Energy efficiency design indices are evaluated using two methods proposed so far delivered for European IWV. The first one is called modified energy efficiency design index (EEDI*) [20, 30], and the second one is delivered by DST ($EEDI_{IWV}$) [21]. Both are similar to IMO's EEDI method, so that an attained level of energy efficiency has to be lower than required level of energy efficiency, in order for the vessel to satisfy criteria. The summary of calculation procedures for both methods is shown in Table 2. Their detailed comparison, advantages and disadvantages are comprehensively assessed in [22].

Table 2 Energy efficiency design index proposals for IWV

Index	EEDI*	$EEDI_{IWV}$
Equations	Attained EEDI: $EEDI^* = P_{Bref} \cdot SFC \cdot CF / (m_{DWT} \cdot V)$ Required EEDI: $EEDI^*_{Req} = a \cdot m_{DWT}{}^{c}$ For deep water: $a = 0.39554 \cdot V^2 - 1.27833 \cdot V + 111.69043$ $c = -0.00114 \cdot V^2 - 0.05177 \cdot V + 0.70843$ For Shallow water (h < 5 m): $a = 93.712 \cdot F_{nh}^{-3} - 516.38 \cdot F_{nh}^{-2} + 886.54 \cdot F_{nh}^{-1} - 414.86$ $c = -0.4181 \cdot F_{nh}^{-3} + 2.5716 \cdot F_{nh}^{-2} - 5.2767 \cdot F_{nh}^{-1} + 3.3485$	Attained EEDI: For deep water: $P_D = \alpha_1 \cdot m_{DWT}$ P_D to be measured, V_s to calculate $EEDI_{IWV}$ $EEDI_{IWV} = CF \cdot SFC \cdot P_D / (V_s \cdot m_{DWT})$ For shallow water (h < 7.5 m): $P_D = (\alpha_6 + \beta_4 \cdot exp(-\gamma_4 \cdot B) - \delta_2 \cdot exp(h/-_1)) \cdot m_{DWT}$ P_D to be measured, Vs to calculate $EEDI_{IWV} = CF \cdot SFC \cdot PD / (Vs \cdot m_{DWT})$ Required EEDI: For deep water: $EEDI_{Req} = \alpha_4 + \beta_2 \cdot \exp(m_{DWT}/-\gamma_2) + \upsilon_1 \cdot \exp(m_{DWT}/-\delta_1)$ For shallow water (h < 7.5 m):: $EEDI_{Req} = (\alpha_7 + \beta_5 \cdot V_c + \gamma_5 \cdot V_c^2) + (\delta_3 + \varepsilon_2 \cdot V_c - \zeta_1 \cdot V_c^2 + \eta_1 \cdot V_c^3) \cdot \exp(m_{DWT}/-\theta_1)$ Coefficients are given in [22].
Constraints	10 km/h ≤ V ≤ 22 km/h 0.4 ≤ F_{nh} ≤ 0.65 100 t ≤ m_{DWT} ≤ 3000 t	For deep water: T = 1.5D; T =2.0-3.2 m. For shallow water (h < 7.5 m): T = 1.5D; h = 3.5-7.5 m; T = 2-2.8 m; L = 40-135 m; B = 5-17 m; m_{DWT} = 250-6000 t; Vc = 2-8 km/h; min(h/T) = 1.4.
Notes	$EEDI^*$ – modified energy efficiency design index [gCO_2/gFuel]; P_{Bref} – Reference engine power for V [kW]; SFC – Specific fuel consumption [g/kWh]; CF – carbon emission factor, 3.206 [gCO_2/gFuel]; m_{DWT} – mass of deadweight [t]; V – actual vessel speed through water (not on 75% of MCR like in IMO's EEDI) [km/h].	$EEDI_{IWV}$ – energy efficiency design index [gCO_2/tkm]; D – propeller diameter [m]; B – vessel breadth [m]; h – river depth [m]; SFC – specific fuel consumption [g/kWh]; CF – carbon emission factor, 3.206 [gCO_2/gFuel]; m_{DWT} – mass of deadweight [t]; P_D – delivered power [kW].

2.3 Energy efficiency in operation

In order to evaluate energy efficiency of the vessel in operation, an energy efficiency in operation (EEO) index is introduced and calculated. EEO differs from EEOI, since the latter one is delivered by IMO as voluntary tool for sea-going ships and considers already established procedures for sea-going ships, see [5]. On the other hand, EEO takes into account diversified operation of the IWV with respect to shallow water and current speed, which is not considered within IMO's energy efficiency indices. Therefore, EEO is calculated using operational profile inputs (from sect. 2.1), for the specified vessel, into two proposed methods elaborated in sect. 2.2: EEDI* and $EEDI_{IWV}$, see equation (1).

$$EEO_1 = EEDI^* \qquad EEO_2 = EEDI_{IWV}. \tag{1}$$

For the purpose of the analysis, the following assumptions are made:

- required engine power is calculated as ratio of the delivered power and shaft efficiency and taken to be 0.98,
- delivered power is available based on real time measurements during sailings at different draughts,
- the specific fuel oil consumption used in this study is assumed to be 210 g/kWh, and it was obtained as an average value from both methods (the method [20] proposes 200 g/kWh and the method from [21] proposes 220 g/kWh),
- carbon emission factor for diesel fuel is 3.206 g CO_2/g fuel,
- calculation is carried out for both cases of river depth (the lowest and the highest level) in order to obtain the range of CO_2 emissions since there were no available data on water depth during voyages.

3. Case study

The case study is represented by the typical self-propelled cargo vessel with general arrangement and particulars as shown in Fig. 5 and Table 3, respectively. The vessel is designed to carry bulk cargo and additionally, if necessary, push other vessels (barges).

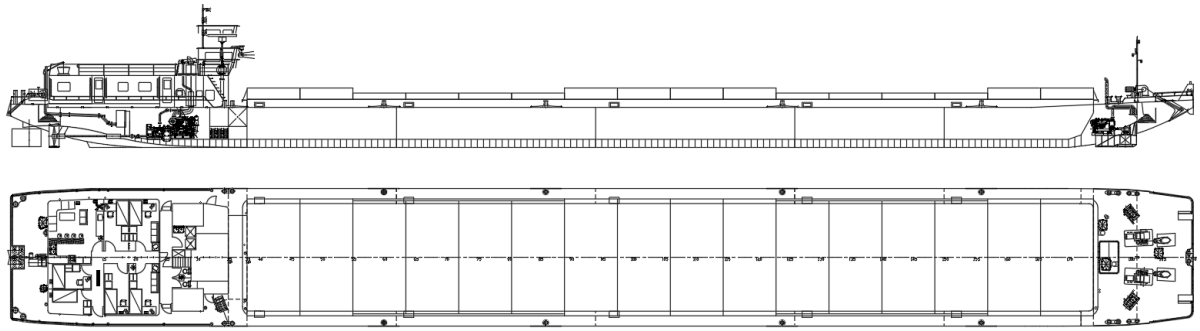

Fig. 5 General arrangement of the vessel

Table 3 Vessel particulars

Length	95 m
Width	11 m
Height	3.2 m
Draught	2.7 m
Deadweight mass	1850 t
Lightweight mass	637 t
Engine power	2 x 638 kW
Propeller diameter	2 x 1.6 m

4. Results and discussion

Results are evaluated for October 2022 navigation for the lowest (LNWL) and the highest (HNWL) water depths, as a function of speed through water (STW). Each of the 11 voyages are divided into the nine sectoral voyages (9 in total, see Fig. 4.) for which an energy efficiency is assessed. During each of the sector passings, the vessel had the corresponding: draught (ranging between 1.7 m and 2.4 m), deadweight, STW, distance covered. EEO is calculated according to equation (1). In addition, EEO results are compared to the requirements of the energy efficiency design indices, given by two methods (EEDI* and $EEDI_{IWV}$). EEDI* requirement is labelled here as $EEOI_{1,\ req}$. On the following diagrams, this requirement is represented by the curve separating the right area (coloured in grey, on the right side of diagrams), meaning that the vessel has unsatisfactory energy efficiency; and the left side, in which the vessel has met the requirement. Furthermore, $EEDI_{IWV}$ method can have multiple requirements: $EEOI_{2,\ req\ i}$ - requirement for the sector i; and (or) $EEOI_{2,\ req\ j,\ k,\ l}$ – requirement for the sectors j, k, l. The area above these lines represents the energy efficiency not satisfied by the vessel. $EEDI_{IWV}$ can have multiple criteria, compared to EEDI* single curve requirement. This is due to fact that $EEDI_{IWV}$ has different definition of the shallow water. Water is considered to be shallow if the depth is less than 5 m according to EEDI* method; and less than 7.5 m, according to the $EEDI_{IWV}$ method. In all sectors considered (see Fig. 3), the actual water depth was recorded to be above 5 m, meaning that it was defined as deep water by EEDI*, and single corresponding calculation procedure is used (see Table 2). Instead, although being above 5 m in depth, in some sectors, the water depth was recorded to be lower or higher than 7.5 m, so that the different requirement formula is used when $EEDI_{IWV}$ method was applied. Thus, energy efficiency requirements are different by sector because they depend on navigation conditions, as shown in formulas given in Table 2. Therefore, EEO are given as averaged values per voyage. Diagrams of energy efficiency for each of 11 voyages, for LNWL and HNWL are presented in Fig. 6 and Fig. 7, respectively.

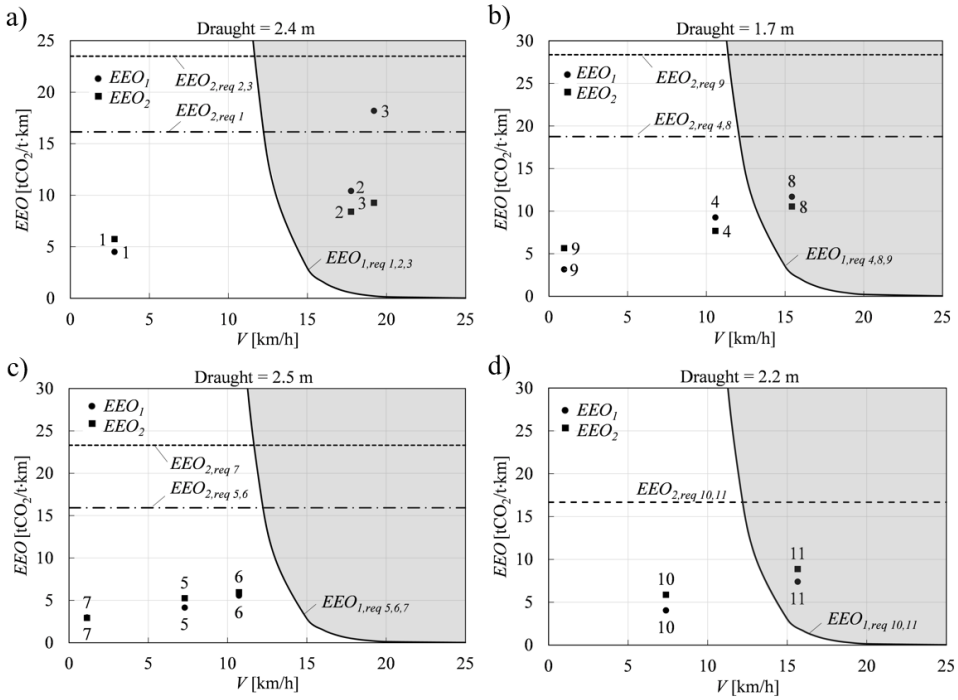

Fig. 6 Energy efficiency for October 2022 navigation for LNWL, for voyages no.: a) 1,2,3, b) 4,8,9, c) 5,6,7, d) 10, 11

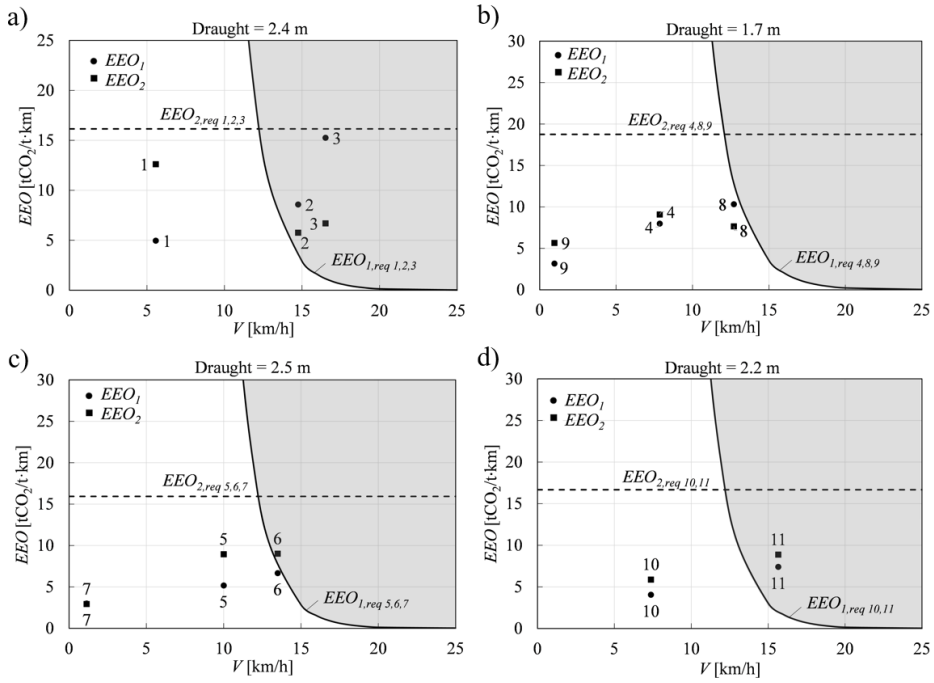

Fig. 7 Energy efficiency for October 2022 navigation for HNWL, for voyages no.: a) 1,2,3, b) 4,8,9, c) 5,6,7, d) 10, 11

When sailing at LNWL, the vessel meets $EEDI_{IWV}$ requirements, while EEDI* is not satisfied for voyages 2, 3, 8 and 11. Based on the EEDI* requirement curve, the vessel sailing above 13-15 km/h (almost for all deadweights) will always be in prohibited zone, independent of the draught, meaning that the vessel will not be an energy efficient for those speeds. Therefore, decreasing the speed (and engine power) can result in a more energy efficient performance, as such is the case for sea-going ship as well, see also [8]. In contrast, there is

no speed limit for the $EEDI_{IWV}$ approach, with respect to deadweight. Note that typical speed of IWV on Danube River is between 12 and 20 km/h, depending on various factors such as water levels, current speeds, vessel type and traffic density. In case of the scenario in which the vessel is sailing at HNWL, EEDI* criterion is not satisfied for voyages no. 2, 3 and 11 (voyage 6 is at the limit). Voyage no. 8, which did not meet the requirement at LNWL, is now energy efficient. This is due to fact that, according to this method, the definition of the shallow water is different, and hence, the requirement criterion, implying that the vessel is now sailing in deep water and therefore, more efficient. Unlike to results from Fig. 6, $EEDI_{IWV}$ method has only one requirement at HNWL, as vessel operates in high water conditions. Methods are insensitive to the deadweight change, which is a disadvantage and not representing the realistic navigation conditions. Also, the definition of the shallow water plays a significant role in final results, as the different calculation procedures for requirement curves are included.

Furthermore, based on previous results, the total amount of CO_2 emissions released in October 2022 is calculated by multiplying the EEO with the distance travelled and DWT, see Table 4.

Table 4 Total amount of CO_2 emissions for October 2022

	At LNWL		At HNWL	
	Based on EEO_1	Based on EEO_2	Based on EEO_1	Based on EEO_2
Total amount of CO_2 emitted [t]	24.6	22.7	24.9	29.9

According to EEO_1, the total emitted CO_2 in October 2022 is between 24.6 t and 24.9 t, while considering EEO_2, the range is wider: 22.7 t – 29.9 t. The result of the EEO_2 at HNWL is a bit larger than other three, as $EEDI_{IWV}$ method has different calculation procedure and requirement for the deep-water case. Authors could not perform the same analysis for the whole year as for October 2022, due to the time-consuming acquirement of the unsystematically available data for remaining months. In addition, there were periods in which the vessel was completely unemployed, as in August. Thus, the October 2022 emissions were scaled up to the whole year: the annual CO_2 emissions are calculated according to the deadweight and distance travelled for other months during sailing, as shown in Table 5.

For the whole year of sailing (extrapolated from October 2022 results and including distance travelled and deadweight for remaining months), the total released CO_2 is 197-199 t according to EEO_1 and 182-189 t according to EEO_2. Here, the assumption is made that the vessel performed through the whole year as in its most employed month. Moreover, assuming that the vessel had sailed during all months of the year like in October 2022 (now, not taking into account actual deadweight and distance travelled of remaining months), the amount of CO_2 emissions is calculated to be in between 244-329 t (excluding August, in which the vessel was idle). Note that IWV compete with rail and road cargo for freight transport over land. For the sake of comparison, a single heavy-duty truck (which carries 30 t) emits around 36 tons of CO_2 annually, when data from [31] are used. This means that, annually, 5-6 of them would emit the same amount of CO_2 as the selected vessel.

Table 5 Total CO_2 emissions for the whole year

Month	Distance travelled [km]	DWT [t]	Total amount of CO_2 emitted [t]			
			At LNWL		At HNWL	
			Based on EEO_1	Based on EEO_2	Based on EEO_1	Based on EEO_2
January 2022	633	1003.6	4.3	4.0	4.4	4.0
February	2323	1571.8	25.0	23.0	25.3	23.0
March	1482	1462.3	14.8	13.7	15.0	13.7
April	2362	1198.8	19.4	17.9	19.6	17.9
May	2145	1334.1	19.6	18.0	19.9	18.0
June	1618	1605.3	17.8	16.4	18.0	16.4
July	892	1130.7	6.9	6.4	7.0	6.4
August	0	0	0	0	0	0
September	2341	1127.9	18.0	16.7	18.3	16.7
October	2662	1349.3	24.6	22.7	24.9	29.9
November	2000	1185.9	16.2	15.0	16.2	15.0
December	2191	1387.3	20.8	19.2	20.8	19.2
January 2023	882	1650.1	9.9	9.2	9.9	9.2
Total	**21531**	**/**	**197**	**182**	**199**	**189**

Moreover, additional analyses are performed to identify sectoral EEO. Thus, critical voyages from Fig. 6 and Fig. 7 are extracted, in which energy efficiency requirement was not satisfied. EEDI* requirement was chosen for further analysis as this is more restrictive method. $EEDI_{IWV}$ criteria was passed in previous analyses. In the next step, voyages are separated into the sectoral voyages. They include four voyages performed during the LNWL and three voyages during the HNWL conditions. During the LNWL, voyages included are: no. 2 (sector: 1), no. 3 (sectors: 2-6), no. 8 (sectors: 1-9) and no. 11 (sector: 1-3). During the HNWL conditions identified are critical voyages: no 2 (sector: 1), 3 (sector: 2-6) and no. 11 (sector: 1-3). Their EEO results are presented in Fig 8. Label "i/j" corresponds to the voyage no. i, on a sector no. j. In all voyages with criterion unsatisfied, their corresponding energy efficiency by each of the sector also proved to be unsatisfactory by the requirement. Results shows that energy efficiency of the vessel depends whether the navigation is performed during upstream or downstream navigation. Voyage no. 2 and 3 was carried out while downstream and was more efficient in deep water. In contrast, voyage no. 11 was performed upstream and thus, is less efficient. It is due to fact that diagrams are given as a function of STW, not SOG speeds. For the same SOG, the vessel had to use more power upstream because of the increased current speed. Therefore, energy efficiency of the vessel depends on the downstream or upstream sailings. Note that $EEDI_{IWV}$ method does not consider the direction of the river flow.

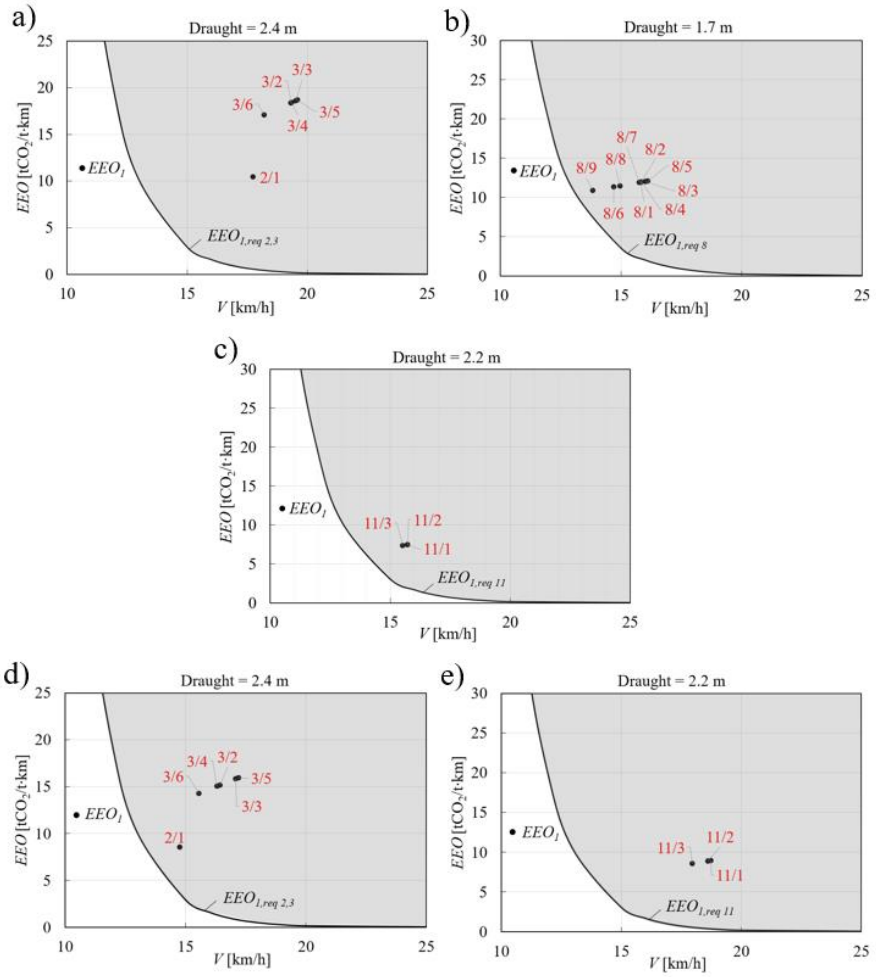

Fig. 8 Energy efficiency for October 2022 navigation at LNWL (a, b, c) and at HNWL (d, e), for voyages with respect to sector

In all sectors, speed had to be decreased (i.e., perform slow steaming) for the vessel to meet the energy efficiency criterion. Therefore, calculated are necessary sectoral speed over ground reductions by voyage. They are given in the following Table 6. At LNWL, the average speed reduction by sectors is in between 4.8% and 26%. In case of HNWL sailing, the speed reduction varies between 14.3% and 25.8%.

If the speed was reduced, the sailing time would be extended, so the additional time that the vessel spent in navigation has also been calculated on a monthly basis, and then the estimated extension of time has been evaluated on an annual basis. Results are shown in the Table 7.

Table 6 Reduction of the speed over ground in km/h and percentages

		Sectors								
		1	2	3	4	5	6	7	8	9
Voyage no. at LNWL	2	4.25 (22.6%)								
	3		6.6 (32.5%)	6.8 (33.5%)	6.7 (33.0%)	6.9 (34.0%)	5.5 (27.1%)			
	8	2.71 (16.1%)	2.71 (16.1%)	2.91 (17.3%)	2.81 (16.7%)	3.01 (17.9%)	1.61 (9.6%)	2.71 (16.1%)	1.91 (11.4%)	0.81 (4.8%)
	11	1.93 (13.1%)	1.93 (13.1%)	1.73 (11.8%)						
Average by sector at LNWL		17.3%	20.6%	20.9%	24.9%	26%	18.4%	16.1%	11.4%	4.8%
Voyage no. at HNWL	2	1.25 (6.6%)								
	3		3.8 (18.7%)	4.4 (21.7%)	3.6 (17.8%)	4.5 (22.2%)	2.9 (14.3%)			
	11	4.83 (32.8%)	4.83 (32.8%)	4.13 (28.1%)						
Average by sector at HNWL		19.7%	25.8%	24.9%	17.8%	22.2%	14.3%			

Table 7 Additional time needed for the compliance with the EEDI* requirements by means of slow steaming

Additional time for navigation [h]		
Month	At LNWL	At HNWL
January 2022	2.6	1.5
February	9.4	5.3
March	6.0	3.4
April	9.5	5.4
May	8.7	4.9
June	6.5	3.7
July	3.6	2.0
August	0.0	0.0
September	9.4	5.4
October	10.7	6.1
November	8.1	4.6
December	8.8	5.0
January 2023	3.6	2.0
Total	**87**	**49**

If the vessel had slowed down at certain sectors in order to meet the criterion, it would have sailed an additional 10.7 h or 6.1 h depending on the water depth, during October 2022. On an annual basis, the estimated extension of travel time would be 87 h and 49 h at LNWL

and HNWL, respectively. This appears as negligible additional sailing when considering the total number of days vessel spent in transit. However, one should note that this is also governed by the fact that the vessel was already slow and did not navigate extensively, which is not accounted within the available method and therefore, can be improved.

This study represents an initial step towards the development of energy efficiency assessments that take into account the operational data and actual fairway constraint changes for IWV. By considering operational data, this research provides a more explicit evaluation of the energy performance for typical IWV, which is still unaddressed in the literature. Hence, these findings could set a benchmark for the actual vessel energy efficiency and could pave the way for the development of future mandatory regulations for improving the energy efficiency of IWV and reducing their environmental impact.

5. Conclusions

Energy efficiency regulations, corresponding mandatory indicators and requirements do not exist in inland navigation. Moreover, literature data is almost negligible compared to the sea-going ships. This is disturbing considering that IWV represents the large sector responsible for harmful emissions released while navigating through the urban areas. Compared to the sea-going ships which have no competition in international deep-sea freight transport, IWV transport cargo “over land”, while competing directly with rail and road modes. IWV navigation is diverse, and their energy efficiency, unlike for sea-going ships, depends on additional parameters, such as water depth, current speeds, fairway constraints, etc. Therefore, this paper aims to fill the gap and deliver one of the first attempts to quantify the energy efficiency of the vessel in actual navigation using real-time data. Moreover, it aims to provide an analysis of energy efficiency in operation (EEO) of the typical cargo vessel navigating on Danube. EEO is evaluated based on operational data for a most employed month of navigation during the year, between January 2022 and January 2023. Only two proposed methods are used to calculate and assess EEO for different voyages during the designated period of one month, and annually. These methods are only available for EU waterways, they are published, but still did not achieve mandatory status.

Results showed that for the same voyage, EEO and CO_2 emitted significantly differs with respect to sector of navigation. That is because each of the sector has different fairway constraints, largely depending on the level of water depth. In general, low water depth generally decreases the energy efficiency of the vessel. The total CO_2 emitted is delivered and is in between 22.7 and 29.9 tons for the most employed month of sailing and between 182 and 199 tons, annually, if the vessel has sailed according to the designated distance travelled and deadweights for remaining months. The actual speed reduction by sectors, necessary for the requirement compliance, is estimated to be 4.8%-26% for sailing at LNWL and 14.3%-26% when sailing at HNWL.

By introducing regulations aimed at limiting CO_2 emissions from vessels and reducing the speed of navigation, energy efficiency could be improved to certain extent, and the extension of the duration of a voyage would be only slightly longer, as assessed in the paper. This can easily be achieved by implementing cruise control on vessels, which can also be equipped with diagrams like those presented in this study, in which it is possible to oversee in real-time whether the vessel satisfied the requirements. Further research should conduct a more detailed investigation for other months, as well as research for other vessels and zone of navigations. Parallel efforts should be made to harmonize the methods for determining the energy efficiency of IWV, as they have not yet officially entered into force. Furthermore, due to diverse operation of the IWV, only real-time measurement during the navigation thought the different conditions would represent the actual energy efficiency of the vessel, as the

energy efficiency of the IWV vastly depends on the river configuration, water depths, precipitation, locks dimensions, river curvature, the existence of the hydropower plants, speed of the vessel, fuel oil consumption, etc.

ACKNOWLEDGEMENTS

This work was supported by Ministry of Education, Science and Technological Development of Serbia (Project no. 451-03-47/2023-01/ 200105 from 3 February 2023). Authors want to express special thanks to company "Ocean Pro Marine Engineers" for the technical support given during this study.

ABBREVIATIONS

CCNR	Central Commission for the Navigation of the Rhine
CII	Carbon Intensity Indicator
DCS	Data Collection System
DST	Duisburg's Development Centre for Ship Technology and Transport Systems (*DST Entwicklungszentrum für Schiffstechnik und Transportsysteme*)
DWT	Deadweight
EEDI	Energy Efficiency Design Index
EEDI*	Modified Energy Efficiency Design Index (for IWV)
$EEDI_{IWV}$	Energy Efficiency Design Index (for IWV)
EEO	Energy Efficiency in Operation
EEOI	Energy Efficiency Operational Indicator
EEXI	Energy Efficiency Existing Ship Index
EU	European Union
GHG	Greenhouse Gas
GT	Gross Tonnage
HNWL	Highest Navigable Water Level
IMO	International Maritime Organization
IWV	Inland waterway Vessel
LNWL	Lowest Navigable Water Level
SOG	Speed over ground
STW	Speed through water

REFERENCES

[1] IMO MEPC, 2011. Resolution MEPC.203(62). *International Maritime Organization (IMO)*, 2011/07/15, London, UK.

[2] IMO MEPC, 2021. Resolution MEPC.333(76) – 2021 Guidelines on the Method of Calculation of the Attained Energy Efficiency Existing Ship Index (EEXI) - Annex 7. *International Maritime Organization (IMO)*, London, UK.

[3] IMO MEPC, 2022. Resolution MEPC.352(78) – 2022 Guidelines on Operational Carbon Intensity Indicators and the Calculations Methods (CII Guidelines, G1) - Annex 14. *International Maritime Organization (IMO)*, London, UK.

[4] IMO MEPC, 2016. Resolution MEPC.278(70). *International Maritime Organization (IMO)*, London, UK.

[5] IMO, 2009. Guidelines for voluntary use of the ship energy efficiency operational indicator (EEOI). *International Maritime Organization (IMO)*, London, UK.

[6] IMO, 2020. Forth IMO Greenhouse Gas Study. *International Maritime Organization (IMO)*, London, UK.

[7] Kalajdžić, M., Momčilović, N., 2020. A step toward the preliminary design of seagoing multi-purpose cargo vessels. *Brodogradnja*, 71(2), 75-89. https://doi.org/10.21278/brod71205

[8] Kalajdžić, M., Vasilev, M., Momčilović, N., 2022. Power reduction considerations for bulk carriers with respect to novel energy efficiency regulations. *Brodogradnja*, 73(2), 79-92. https://doi.org/10.21278/brod73205

[9] Farkas, A., Degiuli, N., Martić, I., Grlj, C.G., 2022. Is slow steaming a viable option to meet the novel energy efficiency requirements for containerships? *Journal of Cleaner Production*, 374, 133915. https://doi.org/10.1016/j.jclepro.2022.133915

[10] Farkas, A., Degiuli, N., Martić, I., Mikulić, A., 2023. Benefits of slow steaming in realistic sailing conditions along different sailing routes. *Ocean Engineering*, 275, 114143. https://doi.org/10.1016/j.oceaneng.2023.114143

[11] Zincir, B., 2023. Slow steaming application for short-sea shipping to comply with the CII regulation. *Brodogradnja*, 74(2), 21-38. https://doi.org/10.21278/brod74202

[12] Farkas, A., Degiuli, N., Martić, I. and Ančić, I., 2022. Energy savings potential of hull cleaning in a shipping industry. *Journal of Cleaner Production*, 374, 134000. https://doi.org/10.1016/j.jclepro.2022.134000

[13] CCNR, 2022. Annual Report 2022 – Inland Navigation in Europe Market Observation. *Central Commission for the Navigation of the Rhine*.

[14] Danube Commission, 2017. Danube Navigation Statistics in 2015-2016. *Danube Commission*, Report.

[15] CCNR, 2021. Annual Report 2021 - Inland navigation in Europe - Market Observation. *Central Commission for The Navigation of the Rhine (CCNR)*, Report.

[16] Radojčić, D., Simić, A., Momčilović, N., Motok, M., Friedhoff, B., 2021. Design of Contemporary Inland Waterway Vessels - The Case of the Danube River. *Springer*. https://doi.org/10.1007/978-3-030-77325-0

[17] EC, 2019. Communication from the Commission to the European Parliament, the European Council, the Council, the European Economic and Social Committee and the Committee of the Regions - The European Green Deal. *European Commission*, Brussels.

[18] EC, 2021. NAIADES III: Boosting future-proof European inland waterway transport. *European Commission*, Brussels.

[19] CCNR, 2022. CCNR Roadmap for reducing inland navigation emissions. *Central Commission for the Navigation of the Rhine*.

[20] Simić, A., 2014. Energy efficiency of inland waterway self-propelled cargo ships. *Conference on Influence of EEDI on Ship Design*, London, UK. https://doi.org/10.3940/rina.eedi.2014.04

[21] DST, 2020. Evaluating the Energy Requirement of Inland Vessels using Energy Efficiency Indices. *DST, German Federal Ministry of Transport, CESNI, R&D project study*.

[22] Kalajdžić, M., Vasilev, M., Momčilović, N., 2022. Evaluating an Inland Waterway Cargo Vessel's Energy Efficiency Indices. *Polish Maritime Research*, 29(2), 27-34. https://doi.org/10.2478/pomr-2022-0014

[23] Karim, M.M., Hasan, S.M.R., 2017. Establishment of EEDI Baseline for Inland Ship of Bangladesh. *Procedia Engineering*, 194, 370-377. https://doi.org/10.1016/j.proeng.2017.08.159

[24] Zakaria, N.M.G., Rahman, S., 2017. Energy Efficiency Design Index (EEDI) for Inland Vessels in Bangladesh. *Procedia Engineering*, 194, 362-369. https://doi.org/10.1016/j.proeng.2017.08.158

[25] Hasan, S.M.R., Karim, M., 2022. Reanalysis of the revised EEDI parameters for inland ships of Bangladesh. *Proceedings of the Institution of Mechanical Engineers Part M Journal of Engineering for the Maritime Environment*, 14750902221131418. https://doi.org/10.21203/rs.3.rs-1362921/v1

[26] Alvarado, D.R., Paternina, L.A., Paipa, E.G., 2022. Synthesis model for the conceptual design of inland cargo vessels to operate on the Magdalena river. *Brodogradnja*, 73(4), 13-37. https://doi.org/10.21278/brod73402

[27] Marine Traffic website. https://www.marinetraffic.com. accessed 18st January 2023.

[28] Danube Commission, Pilot Charts of the Danube, I-V, 1987-1997.

[29] Interreg, 2018. Common Danube report 2018. *Danube Transnational Programme*, Report.

[30] Simić, A., 2012. Energy efficiency of inland waterway self-propelled cargo vessels. *University of Belgrade, Faculty of Mechanical Engineering*, Doctoral dissertation, Belgrade, Serbia.

[31] EEA, 2020. Monitoring CO2 emissions from Heavy Duty Vehicles in 2018. *European Environment Agency*.

Submitted: 07.04.2023.
Accepted: 15.05.2023.

Milan Kalajdžić
University of Belgrade, Faculty of Mechanical Engineering, Department of Naval Architecture, Kraljice Marije 16, 11120 Belgrade 35, Serbia, mdkalajdzic@mas.bg.ac.rs
Matija Vasilev
Ocean Pro Marine Engineers LTD, 8 Stasnoja Glavaša, 11000 Belgrade, Serbia
Nikola Momčilović
University of Belgrade, Faculty of Mechanical Engineering, Department of Naval Architecture, Kraljice Marije 16, 11120 Belgrade 35, Serbia

ПРИЛОГ 3

Milan Kalajdžić
Matija Vasilev
Nikola Momčilović

http://dx.doi.org/10.21278/brod73205

ISSN 0007-215X
eISSN 1845-5859

POWER REDUCTION CONSIDERATIONS FOR BULK CARRIERS WITH RESPECT TO NOVEL ENERGY EFFICIENCY REGULATIONS

UDC 629.546.2:629.5.01
Original scientific paper

Summary

After introducing an energy efficiency design index (*EEDI*) in 2011, International Maritime Organization (IMO) pursued their short- and long-term goals to reduce greenhouse gas (GHG) emissions from ships by presenting, among others, an energy efficiency existing ship index (*EEXI*). Contrary to *EEDI* which is used for new ships solely, *EEXI* is addressing an energy efficiency of already built ships and is set to become formally applicable starting from 2023. Existing designs cannot be essentially and rapidly changed to comply the criterion. The only main particular from the preliminary design phase that can be meaningly optimized "post festum" is a required engine power, and thus, the speed. Therefore, the paper explores the effect of *EEXI* policy on a fleet of 153 bulk carriers built between 2000 and 2020 in order to address their near future and prompt design changes, specifically considering the power reduction. For that purpose, an attained and a required *EEXI* are calculated for each ship. The results showed that only 15% of the ships built in 2000-2012 satisfied 2013-2014 IMO criterion. This impacted the design of ships built in 2013-2022, as they complied the same criterion by 88% of share. However, no ship from the whole database satisfied the present day *EEDI* requirement and only one ship fulfilled the contemporary *EEXI* requirement meaning that the current designs are not able to match the emerging criteria to a large extent. In order to meet an energy efficiency criterion, a main engine power reduction and speed are predicted assuming that the engine power and shaft limiter are installed. The investigation showed that *MCR* reduction of the total fleet taken into account had to be reduced by 50% and speed by 15% on average in order for ships to meet current requirements. Moreover, a graphic method is developed for the estimation of *EEXI* by using only deadweight (*DWT*) and maximum continuous rating (*MCR*). The proposed simplified method based on average values could be used on existing bulk carriers with an aim to satisfy novel regulation with application of "easy to use" approach. Additionally, authors discussed other options to reliably evaluate an energy efficiency of existing ships.

Key words: *energy efficiency; EEXI; EEDI; ship design; bulk carriers*

1. Introduction

Following the Paris Agreement on climate change and global emission reduction goals, IMO presented an initial strategy for the decarbonization of ships in 2018, see [1]. It included three levels of ambitions, considering both short- and long-term predictions. In the first one, IMO detailed and reviewed already implemented *EEDI* requirements for ships, which were introduced in 2011 and set in use starting from 2013 [2]. Since 2015, *EEDI* requirements are planned to be strengthened every five years. Before 2015 (i.e., phase 0), a required *EEDI* reference line was the criterion, so that ships built in the period 2013-2014 had to achieve their own attained *EEDI* lower than required *EEDI* reference line. In the phase 1, ships built in 2015-2019 had to satisfy the same *EEDI* reference line, but reduced by 10%. In the phase 2, for the ships which are being built in 2020-2024, the reduction of the *EEDI* reference line criterion is obliged to be 20%; whereas for the ship built after the 2025, the reduction is set to be 30% of the reference line. In the second level of ambition, IMO aim was to reduce CO_2 emissions per transport work, on average for shipping, to 40% until 2030 while trying to reach even 70% until 2050, when compared to the 2008 values. The third level included a desire to achieve peak of GHG emissions more rapidly and to reduce total annual GHG emissions until 2050 by at least 50%, comparing to the 2008. In the meantime, *EEDI* criteria, and consequently the slow steaming approach, already reduced an installed power, lowered shaft speed and increased propeller diameter of new ships, see [3].

Furthermore, in order to address emissions from existing ships, IMO [4] introduced *EEXI* requirements for ships falling under the MARPOL Annex VI, and over 400 GT, such was in case of *EEDI*. Likewise, a calculated (attained) *EEXI* of the ship has to be lower than required *EEXI* reference. *EEXI* requirement will be used from 2023 for existing ships such as bulk carriers, tankers, container ships, etc. Final *EEXI* calculation procedure is adopted at MEPC meeting in 2021 [5], while next IMO review of the criteria is expected to be in 2026. *EEXI* very much corresponds to *EEDI* second and third phase criteria. Although these recent short-term measures with respect to *EEDI* and *EEXI* governed the power reduction of the main engine, the long-term IMO ambitions are expected to potentially propel the use of alternative solutions (alternative fuels, optimization solutions, use of wind, etc.). Furthermore, this could also drive to lower speeds, but not so necessarily or directly, because certain ship types are already navigating at reduced speed and engine power. Therefore, the main challenge currently appears to be the estimation of power and speed to comply to *EEXI* requirements.

A review of the IMO energy efficiency policy from the beginning can be found in [6]. Study [7] presented a comprehensive review of technical changes and fuel consumption trends for bulk carriers built from 1970 until 2006. Particularly, an effect of slow steaming on a bulk carrier fleet is examined in [8]. Paper [9] concluded that bulk carriers built between 2005 and 2014 showed no significant performance improvement. Somewhat the same was noted in [10**,** 11] implying that the implementation of efficiency measures for bulk carriers were almost negligible. Paper [12] identified 2014-2016 as years from which the bulk carriers delivered lower *EEDI* since they were impacted by the IMO policy. Furthermore, energy efficiency improvements for bulk carriers are examined in [13]. More on ship optimization with respect to EEDI, potential emission reduction measures and energy saving device analysis can be found in [14], [15], [16], respectively.

Authors of this paper have been exploring energy efficiency measures effect on ship design in the case of multi-purpose cargo vessels, see [17]. Results showed that most of the present fleet designs could not meet even the first phase of *EEDI* criterion let alone the second and the third phase requirements, except for the ships with lower speeds. Furthermore, the

analogous was shown in [18], where *EEXI* calculation is performed on four existing ships type representatives (container ship, bulk carrier and oil tanker).

This paper presents the investigation on how the bulk carrier fleet of 153 ships built in the past 20 years (2000-2020) are relating to the novel energy efficiency policies. Furthermore, while examining the share of ships that could not comply to current *EEXI* criterion, authors studied the effect of meeting such requirements on ship's installed power and speed. Therefore, assuming that the engine power limiter is installed, a reduction of power and speed is predicted for each ship. Also, a graphic method is proposed to estimate *EEXI* of bulk carriers by using just two parameters: *DWT* and *MCR*. Besides, authors discussed a possibility for more reliable evaluation of energy efficiency of existing ships.

2. Database

Most ships are conducted from the RINA's Significant Ships [19] journal and moreover, updated with additional bulk carriers for which the authors had obtained reliable data from the shipyards. Ships having lesser deadweight than 12000 t were eliminated from the database since they have been mostly related to the sea-river navigation. Furthermore, certain ships had additional "booster" engines installed (shaft generators), but those were excluded from analysis in order to achieve more uniform database with respect to power source. Finally, the gathered database used for the analysis consists of 153 bulk carriers built from 2000 until 2020. Particulars have the following ranges, in terms of L_{OA}, *DWT*, *GT*, respectively: 107 m - 362 m, 12588 t - 400000 t and 5686 – 203403. More detailed particulars are presented in Figures 1-5. Authors did not have all the data needed for each ship. Therefore, for instance (and for some ships), a block coefficient is estimated according to displacement and *L*, *B*, *T*.

Figures 1-4 are showing the ships' particulars as a function of deadweight. In Figure 5, as similarly observed in [3], one can note the tendency of increasing the propeller diameter and reducing the shaft speed of ships in years (2010-2012) in which the energy efficiency regulations started to emerge. Shaded areas present the 95% and 94% of the ships from the database in terms of *D* an *n*, respectively.

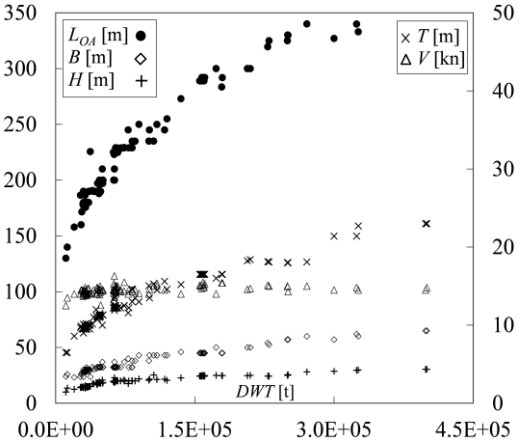

Fig. 1 L_{OA}, *B, H, T, V vs. DWT*

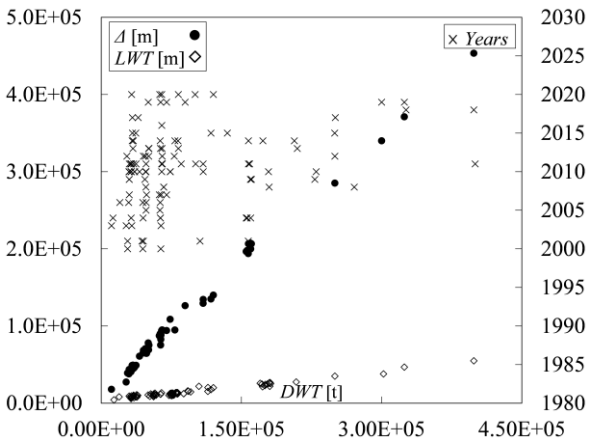

Fig. 2 *Δ, LWT, Years* vs. *DWT*

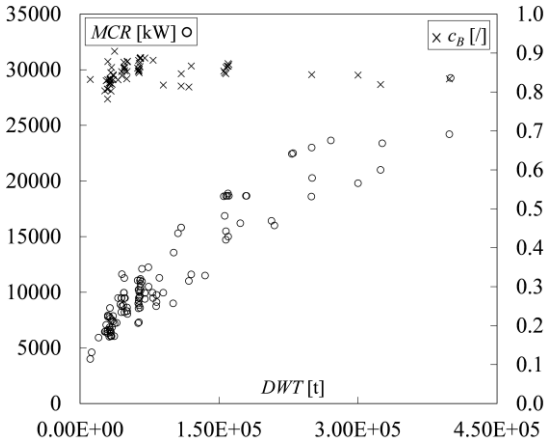

Fig. 3 *MCR*, c_B vs. *DWT*

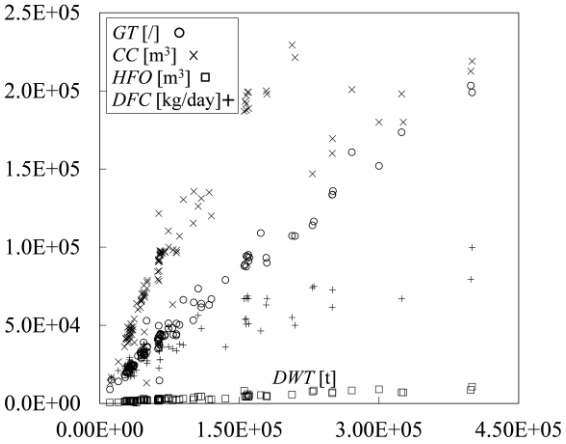

Fig. 4 *GT*, *CC*, *HFO*, *DFC* vs. *DWT*

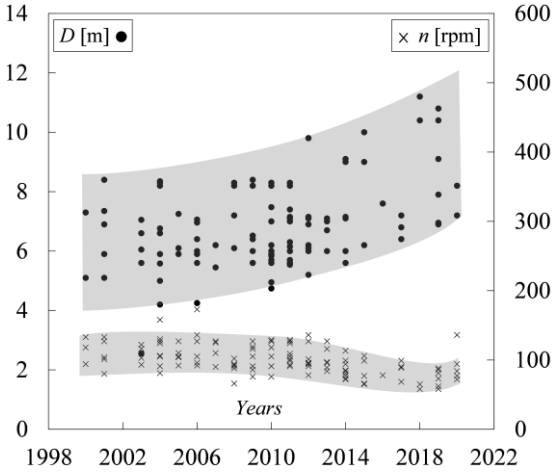

Fig. 5 *D*, *n* vs. *DWT*

3. Methodology

For each ship, an attained *EEXI* and a required *EEXI* are calculated, according to [20] and [21], respectively. This means that an attained *EEXI* should be lower than a required *EEXI*, see equation (1), in order that the ship could be considered as energy efficient. In the following sections, a full procedure for the calculation of EEXI is described.

$$\text{Attained } EEXI \leq \text{Required } EEXI \tag{1}$$

3.1 Attained *EEXI*

General method to calculate an attained *EEXI* is given in equation (2) and taken from [20].

$$\text{Attained } EEXI = \frac{\left[\begin{array}{l}\left(\prod_{j=1}^{n} f_j\right)\left(\sum_{i=1}^{n_{ME}} P_{ME(i)} \cdot C_{FME(i)} \cdot SFC_{ME(i)}\right) + \left(P_{AE} \cdot C_{FAE} \cdot SFC_{AE*}\right) + \\ \left(\left(\prod_{j=1}^{n} f_j \cdot \sum_{i=1}^{n_{PTI}} P_{PTI(i)} - \sum_{i=1}^{n_{eff}} f_{eff(i)} \cdot P_{AEeff(i)}\right) \cdot C_{FAE} \cdot SFC_{AE}\right) - \\ \left(\sum_{i=1}^{n_{eff}} f_{eff(i)} \cdot P_{eff(i)} \cdot C_{FME} \cdot SFC_{ME**}\right)\end{array}\right]}{f_i \cdot f_c \cdot f_l \cdot Capacity \cdot f_w \cdot V_{ref} \cdot f_m} \tag{2}$$

A report from [20] provides detailed explanations for equation (2). Namely, a subscript "*" means that, if part of the normal maximum sea load is provided by shaft generators, SFC_{ME} and C_{FME} may, for that share of the power, be used instead of SFC_{AE} and C_{FAE}. Additionally, subscript "**" requires that, in case of $P_{PTI(i)} > 0$, an average weighted value of ($SFC_{ME} \cdot C_{FME}$) and ($SFC_{AE} \cdot C_{FAE}$) should be used for the calculation of P_{eff}. Note that all 153 ships have one main engine and no shaft generators. Moreover, they have no innovative mechanical energy efficient technologies applied on main nor auxiliary engines. Hence, Table 1 summarizes the assumptions made corresponding to equation (2).

Table 1 Assumptions used for equation (2)

One engine (main)	$\sum_{i=1}^{n_{ME}} P_{ME(i)} = P_{ME(1)}$
No shaft generator	$\sum_{i=1}^{n_{PTI}} P_{PTI(i)} = 0$
No innovative energy efficient technologies on main engine	$\sum_{i=1}^{n_{eff}} f_{eff(i)} \cdot P_{eff(i)} = 0$
No innovative energy efficient technologies on auxiliary engine	$\sum_{i=1}^{n_{eff}} f_{eff(i)} \cdot P_{AEeff(i)} = 0$

Consequently, an equation (2) is being transformed to equation (3).

$$\text{Attained } EEXI = \frac{P_{ME} \cdot C_{FME} \cdot SFC_{ME} + P_{AE} \cdot C_{FAE} \cdot SFC_{AE}}{f_i \cdot f_c \cdot f_l \cdot Capacity \cdot f_W \cdot V_{ref} \cdot f_m} \tag{3}$$

Engine power (P_{ME}) is defined as 75% of the maximum continuous rating (MCR). Auxiliary engine power (P_{AE}) is calculated according to [22] recommendation, see equation (4), and taking into account that there is no shaft generator.

$$\begin{aligned} P_{AE} &= 0.5 \cdot MCR \ (MCR < 10000\,\text{kW}) \\ P_{AE} &= 0.025 \cdot MCR + 250 \ (MCR \geq 10000\,\text{kW}) \end{aligned} \tag{4}$$

Since there is no full list of available data for each ship from the database, authors used a detailed estimation procedure published in [20] to estimate the particulars presented as follows. Accordingly, the following is approximated: $SFC_{ME,app}$ = 190 g/kWh, $SFC_{AE,app}$ = 215 g/kWh, $C_{F,app}$ = 3.114 t CO_2/t·fuel. The subscripts "$_{ME}$" and "$_{AE}$" refer to the main and auxiliary engine, respectively. For the purpose of calculation, it is more reliable to obtain a reference speed (V_{ref}) from speed-power curve, but such is not disclosed to the authors. Nevertheless, V_{ref} is determined from equation (5) from [20]. Furthermore, authors also used the same report for the estimation of $V_{ref,,avg}$ and MCR_{avg}, which is based on ship type and DWT. The same recommendations define a performance margin (m_v) as minimum among 5% of $V_{ref,avg}$ and 1 kn. Additionally, $Capacity$ is defined as DWT for scantling draught, while the correction factors (f_i, f_c, f_l, f_w, f_m) are calculated from the procedure presented in [22].

$$V_{ref,app} = V_{ref,avg} - m_v \left[\frac{P_{ME}}{0.75 MCR_{avg}} \right]^{1/3} \tag{5}$$

Apart from speed-power data, the database does not include sea trial report with *EEDI* calculation, nor draft at design load condition. Both could be useful since they already include parameters needed for the calculation of *EEXI*. Moreover, reference [18] states that ships, if applicable, can use their previously calculated attained *EEDI* instead of attained *EEXI*, if attained *EEDI* is equal or less than attained *EEXI*.

3.2 Required *EEXI*

The required *EEXI* is calculated considering the procedure given in [21] for bulk carriers, see equation (6), with corresponding parameters shown in Table 2.

$$\text{Required } EEXI = \left(1 - \frac{Y}{100}\right) \cdot \text{Reference line}$$
$$\text{Reference line} = a \cdot b^{-c} \tag{6}$$

Table 2 Parameters for the calculation of required *EEXI*

Y (reduction factor)	*a*	*c*	*b*
15 ($DWT \geq 200000$) 20 ($20000 \leq DWT < 200000$) 0-20[1] ($10000 \leq DWT < 20000$)	961.79	0.477	*DWT* ($DWT \leq 279000$) 279000 ($DWT > 279000$)

[1]Regarding the bulk carriers with DWT between 10000-20000 t, the reduction factor *Y* should be linearly interpolated between two values.

4. Results

The ships from the database are assessed with respect to the energy efficiency criteria developed since 2011. The aim was to investigate their energy efficiency level and its influence on power and speed from the start of energy efficiency indices application. Firstly, the database is divided into two categories; the ships built in 2000-2012 and 2013-2020. The first category of ship designs (built in 2000-2012) could be only applied to the IMO resolution [2] issued in 2011 for new ships (became mandatory for the years 2013-2014), since there were no energy efficiency requirements for existing ships at the time. Therefore, an attained *EEXI* calculated from sect. 3.1 is assessed to the phase 0 required *EEDI* [2]. Such required *EEDI* used the same reference line and reduction factors as in the case of required *EEXI*, defined as in equation (6) and Table 2. This comparison could be performed since attained *EEXI* (sect. 3.1) and attained *EEDI* from [2] are supposed as equal and defined according to equation (3), if an equivalent assumption were adopted (see Table 1), as stated by [21]. Such assessment provides a view on how 2000-2012 period designs would relate to the firstly introduced energy efficiency criterion.

The results are plotted in Figure 6 showing that only 15% of ships built in the period 2000-2012 would satisfy phase 0 *EEDI* criterion that were used for 2013-2014. Since there was no need, no energy efficiency measures were considered before the regulations were introduced. However, a share of 88% of the ships built in 2013-2020 satisfied the same criteria. The design change followed the introduction of IMO mandatory requirement and almost exclusively included slow steaming, i.e., power and speed reduction during the navigation. Slow steaming appeared to be only solution that could be promptly applied. Furthermore, *EEDI* requirements tightened over the years following the reduction of the criterion from phase 0 (applied in 2013-2014), to phase 1 (applied in 2015-2019) and phase 2

(started in 2020 until 2024). Phase 2 required *EEDI* is defined by the same reference line criterion from equation (6), as in the case of phase 0 required *EEXI* criterion. However, instead of *Y* from Table 2 used in the phase 0, a new reduction factors are introduced: *Y* = 20 (for ships with DWT equal or above the 20000 t) and *Y* = 0 - 20 (for ships with DWT of 10000 t and above but less than 20000 t). Therefore, the criterion remains the same for lighter ships, but strengthened for ones having DWT over the 200 000 t, see Figure 6. Contrary to the ships built in 2012-2020 that could mostly satisfy the *EEDI* 2013-2014 requirement, no ship is complying with the current *EEDI* reference line. Moreover, only one ship satisfied *EEXI* requirement and is represented by one of largest, an ultra large crude carrier with 398595 t of *DWT*. Thus, in a 7-year period, the standard designs became unacceptable from the energy efficiency point of view. This has been expected to make a huge impact on ship design.

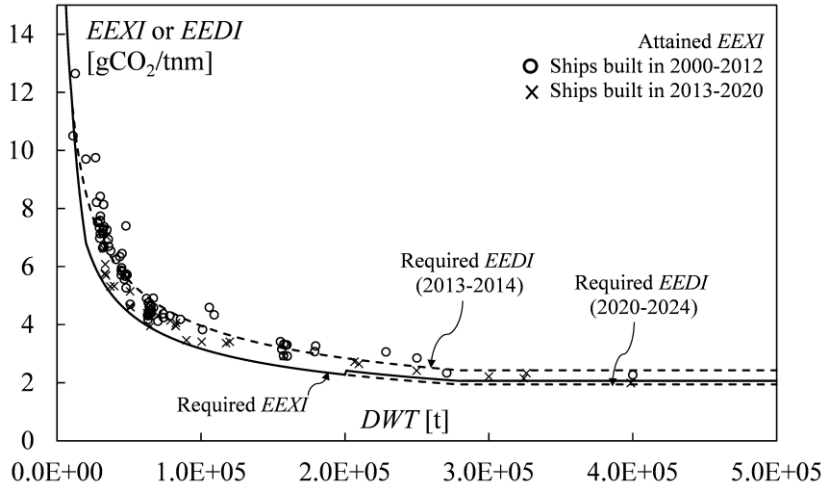

Fig. 6 Energy efficiency indices

Therefore, authors investigated the extent of possible solution in reduction of power/speed of the ships. This could be performed, as per IMO suggestion, by an installation of engine/shaft power limiter (EPL/ShaPoLi) system as most easy to install solution to reduce attained *EEXI*, see more on their application and types in [23]. EPL limits maximum engine power, both mechanically and electronically, while SHaPoLi limits the shaft power.

4.1 Power reduction

According to [23], the installation of EPL/SHaPoLi system requires the power of the main engine (P_{ME}) to be calculated as in equation (7), and limited installed power (MCR_{lim}) as in equation (8).

$$P_{ME} = \min(0.83 \cdot MCR_{\text{lim}}; 0.75 \cdot MCR) \tag{7}$$

$$MCR_{\text{lim}} = EPL_x \cdot MCR \tag{8}$$

MCR_{lim} cannot be calculated analytically, so the iterative approach has been used by varying EPL_x for each ship between 0 and 1, where EPL_x = 1 means that an attained *EEXI* is already equal or less than the required *EEXI* and that there is no need for power limitation. The Figure 7 shows the required percentage of EPL for each ship in order to reach *EEXI* requirement, where EPL_x =1 stands for EPL_x = 100%. It seems that new policies have larger impact on lighter ships since they require larger power reduction. *MCR* should be decreased for nearly 50% on average to comply with *EEXI* requirement, indicating that many of the

ships should navigate significantly slower from 2023. Larger ships with *DWT* above 200000 t are in a more favourable position in that regard. RMS lines are showing the corresponding tendency in which the newer ships (built in 2013-2020) would need less power reduction than in case of older ones (built in 2000-2012), with a difference in EPL_x change varying from around 10% for lighter to 15% for larger ships. When evaluating the results, it should be considered that the database is uneven with respect to *DWT*, with much larger number of ships with DWT below the 150000 t.

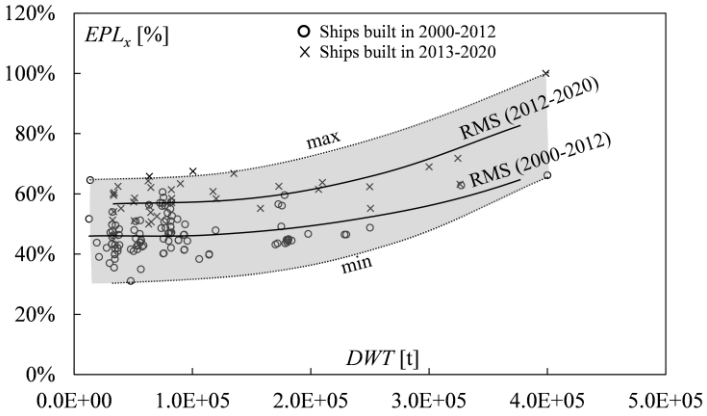

Fig. 7 EPL value for existing ships in database

4.2 Simplification of EEXI evaluation

Evaluation of *EEXI* requires a lot of inputs. Most of them cannot be obtained directly from ship navigation conditions and need to be estimated, which is indeed allowed by IMO resolutions, see sect. 3.1. Although estimations simplify the procedure, they also reduce the calculation time. Thus, in order to allow easy to use energy efficiency check authors proposed simplification of calculation for attained *EEXI* by using only *MCR* and reference speed ($V_{ref,\ app}$) proposed in [20]. The method is based on the general procedure, assumptions and the equations explained in sect. 3.1 and 3.2. Nonetheless, equation (3) presents the starting point. Following the aforesaid, an assumption is made here regarding the correction factors. Specifically, product of correction factors, which was performed for all 153 ships, is approximated as: $f = f_i \cdot f_c \cdot f_l \cdot f_W \cdot f_m$.

Furthermore, for *MCR* that equals to 10000 kW or above, using equations (3) to (6) and assumptions from Table 1, a new nonlinear equation is derived. Such equation is nonlinear and cannot be solved analytically. However, the solution is obtained in Matlab software by using Newton-Raphson method for finding the roots of the equation. It was based on solving 481 equations for DWT = 1000 – 500 000 t with step of 1000 t. Consequently, $MCR/f^{1.5}$ as a function of *DWT* is calculated for each ship from the database, with ship specific *f* value, and the results are shown in Figure 8 for entire fleet of 153 ships. The boundary line is the required *EEXI* limit from sect. 3.2, which is here recalculated to $MCR/f^{1.5}$ – *DWT* trend, where f =1 is assumed. Stepped line segments correspond to the change in reduction factor explained previously. This dependency can be used to predict the attained *EEXI* based on ship's *MCR* and *DWT*. As shown, ships below the boundary line satisfy the *EEXI* requirement and the ones over - do not. It can be observed that only one ship from the entire fleet can comply with the requirement. Figure 8 corresponds to Figure 6 (see attained and required *EEXI*) and therefore it is validated accordingly. In both figures, ships are correspondingly distanced from the required reference line. The only ship that was able to comply with the requirement in Figure 6 is the same one to do so in Figure 8.

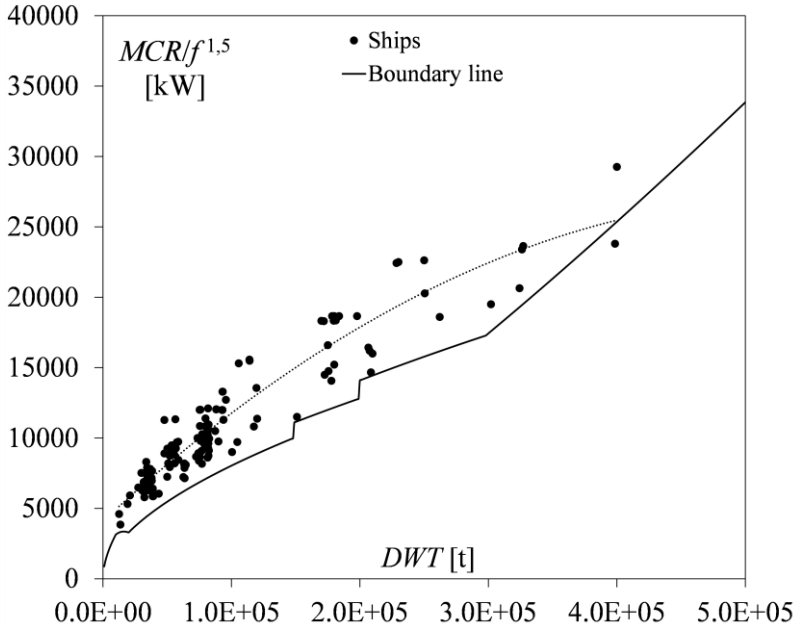

Fig. 8 Simplification of EEXI evaluation

4.3 Simplification of EEXI evaluation with EPL/SHaPoli effect

As in sect. 4.2, authors introduced $V_{ref,app}/f^{0.5}$ as a function of *DWT*. The dependency covers the range of *DWT* = 1000 – 400000 t. Contrary to *MCR* and *DWT* inputs form Figure 8, one could estimate ship's *EEXI* performance using $V_{ref,app}$ and MCR. The derivation is performed in the same manner as in sect. 4.2: by using equations and assumptions from sect. 3.1 to produce single nonlinear equation that is solved numerically. The only difference is that $V_{ref,app}$ is used instead of *MCR*. Therefore, Figure 8 is transferred to Figure 9. The derivation of attained *EEXI* data here is performed for each ship without (current status) and with EPL/SHaPoLi, taking into account equations (5) and (7). Similarly, if the speed and *DWT* positions the ship above the reference line, the ship is not energy efficient with respect to *EEXI* criterion. In terms of *EEXI* performance for the fleet, the diagram corresponds to the Figure 8 and 6. Parameter $V_{ref,app,\mathrm{lim}}/f^{0.5}$ is also shown in Figure 9 and it presents approximated reference speed after EPL/SHaPoLi installation in order to see the speed reduction. Additionally, EPL/SHaPoLi analysis show that ships would need to reduce their speed according to data below (approximately between 12-18%) to comply with EEXI reference line. Approximated speed reduction is obtained from (RMS/trendlines) prior and after EPL/SHaPoLi installation for a range of *DWT* = 1000 – 400000 t; 18% reduction corresponds for ships less than 200000 *DWT* and 12% speed reduction corresponds for ships larger than 200000 *DWT*.

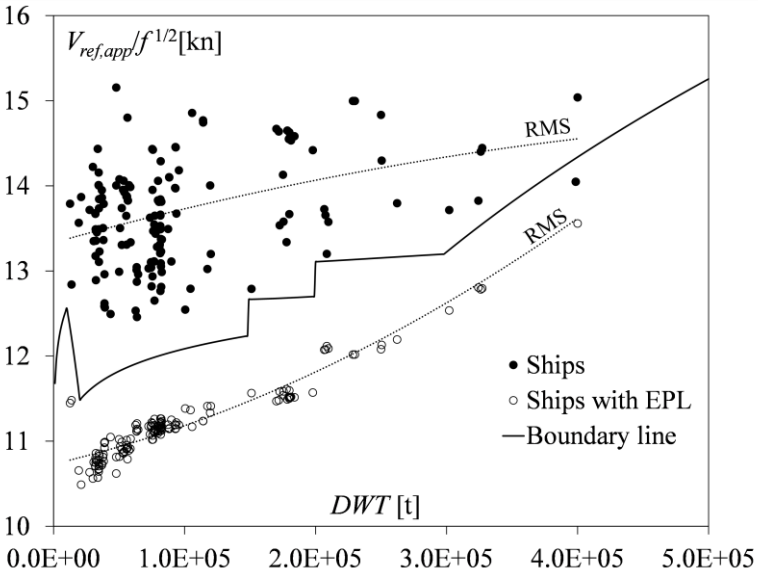

Fig. 9 Simplified EEXI evaluation: before and after the EPL/SHaPoLi

Both reference lines $MCR/f^{1.5}$ and $V_{ref,app}/f^{0.5}$ can be used only for checking the *EEXI* requirements prior the installation of EPL/SHaPoLi. Boundary lines in Figures 8 and 9 are not generic and these lines become ship specific after limiter system integration according to equations (7) and (8) and that is why lower points ($V_{ref,app,\mathrm{lim}}/f^{0.5}$) are not on the boundary line in Figure 9.

4.4 Discussion notes

According to [24], the lowest fuel consumption rate for three engine manufacturers (Wärtsilä, Caterpillar and MAN) is between 70-80% of the engine load. Considering that many ships intended to comply with EEXI requirements have been already sailing in such regime, the actual speed reduction after EPL/SHaPoLi installation should be less than previously mentioned by 12-18%, when ships sail under fully loaded main engine. Regarding the aforementioned sailing regime, the paper shows that the actual speed reduction could be 10-14% for small and 3-7% for large ships according to Figure 9, depending on whether 70% or 80% of engine load is used. Therefore, the speed obtained by sea trials instead of IMO approximated reference speed could be more suitable for *EEXI* calculation because real reference speed can be larger than suggested approximated speed in [20]. In most cases, the existing sea margin could be lost after EPL/SHaPoLi installation, but this wouldn't affect the operation of the ship. Nevertheless, both methods presented here (sect. 4.2 and 4.3), based on *MCR* or $V_{ref,app}$, provide direct solution on the amount on power and speed reduction needed for the *EEXI* compliance. Such could not be obtained in original *EEXI* procedure, see sect. 3.1 and 3.2.

5. Conclusion

Energy efficiency policies that have been developing over the years appeared to had impact on bulk carriers built in the past 20 years, according to the database of 153 ships presented here. The study here showed that:

- 15% of the bulk carriers built in 2000-2012 complied the 2013-2014 *EEDI* IMO criterion, and 88% of the bulk carriers built in 2013-2020 complied the 2013-2014 *EEDI* IMO criterion,

- no bulk carrier complied the present day *EEDI* criterion and only one bulk carrier complied the present day *EEXI* criterion (largest by DWT).

Therefore, current designs cannot satisfy the contemporary energy efficiency requirements. In the interregnum in which the industry was waiting for the alternative fuel solutions, power (speed) reduction has been governing *EEXI* compliance for most of the ships. For presented fleet, roughly, *MCR* reduction is estimated to be 50%, followed by the 15% of speed reduction. *EEXI* analysis is performed using statistical estimations, especially regarding speed, which is allowed and proposed by respective IMO resolutions. Nonetheless, *EEXI* prediction should not deviate significantly. However, in order to address energy efficiency evaluation in more reliable manner, an actual speed-power curve should be obtained, not by estimations, but by sea trials as most accurate method. Furthermore, a graphical method is derived to evaluate *EEXI* performance of bulk carriers. Contrary to the original procedure with numerous particulars needed for the assessment, the method is based solely on *MCR* and *DWT* or $V_{ref,app}$ and *DWT* for easy check. The method instantly provides an amount of power or speed reduction for the criterion fulfilment. Therefore, due "user-friendly" approach, this method can be used onboard to allow energy efficient navigation during each loading condition change, so EPL/ShaPoLi would not be needed.

Nomenclature

B – breadth [m];

Capacity – equal to deadweight [t];

c_B – block coefficient [/];

CC – cargo capacity [m^3];

$C_{F,app}$ – approximated conversion factor between fuel consumption and CO_2 emission for main engine and auxiliary engine [tCO_2 / t·Fuel];

C_{FAE} – conversion factor between fuel consumption and CO_2 emission for auxiliary engine [tCO_2 / t·Fuel];

C_{FME} – conversion factor between fuel consumption and CO_2 emission for main engine [tCO_2/ t·Fuel];

D – propeller diameter [m];

DFC – daily fuel consumption [kg/day];

DO – diesel oil capacity [m^3];

DWT – deadweight mass [t];

$EEDI$ – energy efficiency design index [gCO_2/tnm];

$EEXI$ – energy efficiency existing ship index [gCO_2/tnm];

EPL_x – reduction coefficient for *MCR* [/].

f – total correction factor [/];

fc – cubic capacity correction factor [/];

f_{eff} – innovative mechanical energy efficient technology factor [/];

f_i – capacity correction factor [/];

f_l – factor for general cargo ships equipped with cranes and other cargo-related gear [/];

f_m – factor for ice-classed ships having IA Super and IA [/];

f_w – factor for speed reduction at sea [/];

GT – gross tonnage [/];
H – height [m];
HFO – heavy fuel oil capacity [m^3];
L – length between perpendiculars [m];
L_{OA} – length over all [m];
LWT – lightweight mass [t];
MCR – maximum continuous rating [kW];
MCR_{avg} – average maximum continuous rating [kW];
MCR_{lim} – maximum continuous rating after installing EPL [kW];
m_v – performance margin [kn];
n – shaft speed [rpm];
n_{ME} – number of main engines [/];
n_{PTI} – number of shaft engines [/];
P_{AE} – power of auxiliary engine [kW];
$P_{AE,eff}$ – innovative mechanical energy efficient technology for auxiliary engine [kW];
P_{eff} – innovative mechanical energy efficient technology for main engine [kW];
P_{ME} – power of main engine [kW];
P_{PTI} – power of shaft engine [kW];
SFC_{AE} – specific fuel oil consumption for auxiliary engine [g/kWh];
$SFC_{AE,app}$ – approximated specific fuel oil consumption for auxiliary engine [g/kWh];
SFC_{ME} – specific fuel oil consumption for main engine [g/kWh];
$SFC_{ME,app}$ – approximated specific fuel oil consumption for main engine [g/kWh];
T – draught [m];
V – design speed [kn];
V_{ref} – reference speed [kn];
$V_{ref,app}$ – approximated reference speed [kn];
$V_{ref,app,lim}$ – approximated limited reference speed [kn];
$V_{ref,avg}$ – average reference speed [kn];
Y – reduction factor [/];
Δ – displacement [t];
η_{DWT} - deadweight ratio [/].

Acknowledgements

This work was partially supported by Ministry of Education, Science and Technological Development (Project no. 451-03-68/2022-14/200105) of Serbia.

REFERENCES

[1] IMO, 2018. Resolution MEPC.304(72). Initial IMO Strategy on Reduction of GHG Emissions from Ships.

[2] IMO, 2011. Resolution MEPC.203(62). Inclusion of regulations on energy efficiency for ships in MARPOL Annex VI.

[3] Pang, E., Barber, D., 2021. Ship's Power Limitation in the context of the IMO Short Term GHG Measures. Lecture/Webinar, RINA IMO Committee, The Royal Institution of Naval Architects, 11 March 2021. https://www.youtube.com/watch?v=XFsyi4IdSOk. accessed 10th of February 2021.

[4] IMO, 2020. IMO MEPC 75, Amendments to MARPOL Annex VI. Virtual Session, 16-20 November 2020. Meeting summary: https://www.imo.org/en/MediaCentre/MeetingSummaries/Pages/MEPC-75th-session.aspx. accessed 10th of February 2021.

[5] IMO, 2021. IMO MEPC 76, remote session, 10-17 June 2021. Meeting summary: https://www.imo.org/en/MediaCentre/MeetingSummaries/Pages/MEPC76meetingsummary.aspx. accessed 10th of February 2021.

[6] Liu, S., Papanikolaou, A., Shang, B., 2022. Regulating the safe navigation of energy-efficient ships: A critical review of the finalized IMO guidelines for assessing the minimum propulsion power of ships in adverse conditions. *Ocean Engineering*, 249, 111011. https://doi.org/10.1016/j.oceaneng.2022.111011

[7] Chen, S., Frouws, K., van de Voorde, E., 2010. Technical changes and impacts on economic performance of dry bulk vessels. *Maritime Policy & Management*, 37, 305-327. https://doi.org/10.1080/03088831003700710

[8] Cepeda, M.A.F., Assis, L.F., Marujo, L.G., Caprace, J.D., 2017. Effects of slow steaming strategies on a ship fleet. *Marine Systems & Ocean Technology*, 12, 178-186. https://doi.org/10.1007/s40868-017-0033-3

[9] Pruyn, J., 2017. Are the new fuel-efficient bulkers a threat to the old fleet?. *Maritime Business Review*, 2(3), 224-246. https://doi.org/10.1108/MABR-01-2017-0002

[10] Rehmatulla, N., 2015. Assessing the implementation of technical energy efficiency measures in shipping. Survey Report, UCL Energy Institute.

[11] Rehmatulla, N., Calleya, J., Smith, T., 2017. The implementation of technical energy efficiency and CO_2 emission reduction measures in shipping. *Ocean Engineering*, 139, 184-197. https://doi.org/10.1016/j.oceaneng.2017.04.029

[12] Pruyn, J.F.J, 2020. Benchmarking bulkers delivered between 2010 and 2016, identifying the effect of the EEDI introduction. *Journal of Shipping and Trade*, 5. https://doi.org/10.1186/s41072-020-00063-1

[13] Ancic, I., Theotokatos, G, Vladimir, N., 2018. Towards improving energy efficiency regulations of bulk carriers. *Ocean Engineering*, 148, 193-201. https://doi.org/10.1016/j.oceaneng.2017.11.014

[14] Hang, H.Y., Xiao, L., Yang, M.X., 2018. Hull Lines Reliability-Based Optimization Design for Minimum EEDI. *Brodogradnja*, 69(2), 17-33. https://doi.org/10.21278/brod69202

[15] Ammar, N.R., 2019. Environmental and Cost-Effectiveness Comparison of Dual Fuel Propulsion Options for Emissions Reduction Onboard LNG Carriers. *Brodogradnja*, 70(3), 61-77. https://doi.org/10.21278/brod70304

[16] Kang, J.G., Kim M.C., Shin, R.I., Jin W.S., 2021. Feasibility Study on Effect of Structural Flexibility of Asymmetric Pre-Swirl Stator on Propulsion Performance for Kriso Container Ship (KCS). *Brodogradnja*, 72(4), 103-119. https://doi.org/10.21278/brod72406

[17] Kalajdžić, M., Momčilović, N., 2020. A Step Toward the Preliminary Design of Seagoing Multi-Purpose Cargo Vessels, *Brodogradnja*, 71(2), 75-89. https://doi.org/10.21278/brod71205

[18] Kalajdžić, M., Vasilev, M., Momčilović, N., 2021. Exploring an Effect of Novel IMO Policies on Energy Efficiency of Existing Ships. KIMC conference, Kotor, Montenegro, 28-29th November 2021.

[19] RINA, 2000-2020. Significant Ships. Journal of the Royal Institution of Naval Architects (RINA), issues from 2000 to 2020, London.

[20] IMO, 2021. Consideration of the Report to MEPC 76. Draft Report of the Eighth Meeting of the Intersessional Working Group on Reduction of GHG Emissions from Ships (ISWG-GHG 8), 28th May 2021.

[21] IMO, 2021. Resolution MEPC. 328(76). Annex 1, Amendments to the Annex, 2021 Revised MARPOL Annex VI, 2021.

[22] IMO, 2018. Resolution MEPC. 308(73). 2018 Guidelines on the Method of Calculation of the Attained Energy Efficiency Design Index (EEDI) for new ships.

[23] IMO, 2021. Resolution MEPC. 335(76). Annex 9, 2021 Guidelines on the Shaft/Engine Power Limitation.

[24] Jalkanen, J.P., Johansson, L., Kukkonen, J., Brink, A., Kalli, J., Stipa, T., 2012. Extension of an assessment model of ship traffic exhaust emissions for particulate matter and carbon monoxide. *Atmospheric Chemistry and Physics*, 12, 2641–2659. https://doi.org/10.5194/acp-12-2641-2012

Submitted: 18.03.2022.
Accepted: 11.05.2022.

Milan Kalajdžić, University of Belgrade, Faculty of Mechanical Engineering, Department of Naval Architecture, Associate Professor,
mdkalajdzic@mas.bg.ac.rs
Matija Vasilev, Ocean Pro Marine Engineers LTD, MSc Naval Architect
Nikola Momčilović, University of Belgrade, Faculty of Mechanical Engineering, Department of Naval Architecture, Associate Professor

ПРИЛОГ 4

Ocean Engineering 317 (2025) 120028

Contents lists available at ScienceDirect

Ocean Engineering

journal homepage: www.elsevier.com/locate/oceaneng

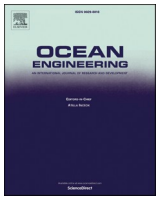

Research paper

On energy efficiency of tankers: EEDI, EEXI and CII

Matija Vasilev *, Milan Kalajdžić, Nikola Momčilović

Department of Naval Architecture, Faculty of Mechanical Engineering, University of Belgrade, 11120 Belgrade, Serbia

ARTICLE INFO

Keywords:
Energy efficiency design index (EEDI)
Energy efficiency existing ship index (EEXI)
Carbon intensity indicator (CII)
Tankers
Slow steaming

ABSTRACT

This paper aims to extensively analyze the energy efficiency of large tanker fleets, focusing on their compliance with the International Maritime Organization (IMO) requirements through the evaluation of design and operational indices. Despite an increase in energy efficiency studies, few have assessed large tanker fleets and their subgroups systematically, leaving a significant gap regarding the impact of regulations on different tanker sizes. The paper evaluates the energy efficiencies of tankers concerning Energy Efficiency Existing Ship Index (EEXI), Energy Efficiency Design Index (EEDI), and Carbon Intensity Indicator (CII), differentiating ships by size and type. It further explores and provides the potential reductions in speed and power for each subgroup of tankers, required to meet current and future energy efficiency requirements. The outcome shows that regulatory measures like EEDI, EEXI, and CII have significantly improved energy efficiency, but compliance remains challenging, with only 14.8% of ships meeting the EEXI criteria, especially for smaller ships, which face greater power reductions than larger ones. The results also indicate that the considered fleet of tankers does not operate at more than 60% of the available engine power and that the ships are already sailing at 8% lower speed than for which they were designed.

1. Introduction

More than ten years have passed after the International Maritime Organization (IMO) set as compulsory the first globally applicable energy efficiency requirement for new built ships intended for international voyages, labelled as energy efficiency design index (EEDI) (IMO, 2011). In reality, shipping decarbonization process was started by enforcing the EEDI phase 0 regulation for new ships built in between 2013 and 2015 and having 400 GT or above. Afterwards, the EEDI requirement curve has been strengthened every several years. The EEDI phase 1 of the regulation was prescribed for new ships built between 2015 and 2019, where the corresponding EEDI requirement curve was reduced by 10% for tankers, compared to the original criterion from EEDI phase 0. Furthermore, tankers built from 2020 have been falling under the EEDI phase 2 criterion, which was reduced by 20% compared to the EEDI phase 0 requirement curve. EEDI phase 2 is expected to last until 2025 and its requirement for tankers is strengthened by 30% compared to the original criterion from 2013. All mentioned reductions are related to the tankers having 20000 *DWT* and above. However, for the lesser ones, reductions vary according to factors defined in (IMO, 2011). Guidelines for the calculation of EEDI were updated over the years, see (IMO, 2018). On the other hand, ships already navigating the seas have been addressed recently, through the enforcement of the energy efficiency existing ship index (EEXI), starting from 2023 (IMO, 2022b, 2022c).

Both EEDI and EEXI are design indices, meaning that they are based on the designated or single value of the deadweight, speed, power, etc. However, during navigation, these parameters change so the designated values are not representing the actual physicality of the sailing conditions nor delivering actual emissions during the timeframe. IMO tried to counter such shortcoming by setting the CII in 2023, for ships with 5000 GT or above (IMO, 2022d, 2022e). CII is intended to quantify annual ship emissions (IMO, 2022f). Starting from 2024, ships will be graded based on their CII results for the previous year. Ships can obtain the following grades: A, B, C, D and E (A is the highest, E is the lowest grade). For instance, ships having grade D for three consecutive years or E at least one year will have to present a plan for improving their energy efficiency in order to achieve higher grade (IMO, 2022g). As agreed on MEPC 76, an annual reduction of CII compared to 2019 was proposed to be 5%, 7%, 9% and 11% for 2023 until 2026, respectively, with a revision expected in 2026 (IMO, 2021a; Psaraftis, 2021).

In order to help reach a proper level of energy efficiency, IMO presented several tools. Along with EEDI phase 0 in 2013, the Ship Energy Efficiency Management Plan (SEEMP) was enforced to help operators

* Corresponding author.
E-mail address: matija@oceanpro.eu (M. Vasilev).

https://doi.org/10.1016/j.oceaneng.2024.120028
Received 29 August 2024; Received in revised form 13 November 2024; Accepted 3 December 2024
Available online 9 December 2024

manage energy efficiency of fleets in a real-time manner (IMO, 2011). SEEMP updated guidelines are given in (IMO, 2022g). Recordings on fuel oil consumption, along with traveled distance became mandatory from 2019 by means of using Data Collection System (DCS), for ships having 5000 GT or above (IMO, 2016). When it comes to non-mandatory tools that are applied in the past ten years, an energy efficiency operational indicator (EEOI), presented back in 2009 (IMO, 2009), is introduced to help operators manage ship in-situ energy efficiency level when modifications were performed, such as slow steaming, weather routing, hull cleaning, etc.

All abovementioned measures and tools are provided by IMO and defined under MARPOL Annex VI (IMO, 2022h). Employing SEEMP, DCS and EEOI can help improve EEDI, EEXI and CII, especially on operational level. The last three are used to evaluate a ship's level of energy efficiency with respect to the designated criterion. The IMO set an ambitious approach to reach net-zero emissions by around 2050 with indicative checkpoints around 2030 and 2040 (IMO, 2023): to reduce the total annual GHG emissions from international shipping by at least 20%, striving for 30%, by 2030 and by at least 70%, striving for 80%, by 2040 compared to 2008. Moreover, peak emissions should be reached as soon as possible, and the reduction of annual GHG emissions has to reach net-zero by 2050, compared to 2008.

However, the maritime community has no definite perception of the level of energy efficiency progress that particular fleets have achieved with respect to their main particulars change or slow steaming practice. In addition, the impact of EEDI, EEXI and CII regulations on ships' levels of energy efficiency in the future is still uncertain. While EEDI or EEXI might present better energy efficiency level for the particular ship, CII could deliver a different outcome. Compared to other large cargo ship types, various tankers fleets still remain poorly investigated in energy efficiency related literature. This concerns considering that tankers represent 14.9% and 31.9% of the world merchant fleet by a number of ships and gross tonnage (GT), respectively, according to data from 2021 (Equasis, 2021). Moreover, from 2020 to 2021, the size of tankers increased by 2.05% in numbers of ships and by 1% in GT (Equasis, 2020, 2021), and by 2.4% in GT in between 2022 and 2023 (UNCAD, 2023). After decades of growth, in the past several years carbon intensity of tankers is almost constant, whilst their total emission of CO_2 is on persistent rise (UNCAD, 2022; UNCAD, 2023).

The majority of the cargo ship energy efficiency studies dealing with major ship types investigate containerships rather than bulk carrier and tankers. It is driven by the fact that average design speed of containerships is larger than for other two types, so the potential for the most used approach, i.e., slow steaming, appears to be the most promising for containerships. A study of a general cargo ship with its real voyage data shows that the total voyage expenses may be decreased by up to 23.3% with applied slow steaming (Zincir, 2023). However, slow steaming may not be always an effective measure to improve energy efficiency (Rehmatulla et al., 2015; Nian and Yuan, 2017). This might not be the case for gas tankers which have the largest design speeds within all tanker fleets. Nonetheless, study on 88 tankers and their noon reports state that speed reduction has its limits and is often overestimated (Berthelsen and Nielsen, 2021), suggesting that it is better to optimize speed rather than reduce it. Energy efficiency of tankers was assessed taking into account sailing on various sea states and realistic sailing conditions, see (Lu et al., 2015; Lindstad and Bo, 2018). Fuel consumption reduction due to speed optimization is performed on a complete voyage (Berthelsen and Nielsen, 2021). Study on a 48000 dwt oil tanker navigating on irregular winds and waves on the particular route stated that speed optimization during the navigation can produce fuel savings of 32.63% leading to the improvement of energy efficiency (Li et al., 2018). However, it was noted that besides an environmental concern, the extent of slow steaming is also influenced on the price of the fuel and market. A study conducted on an example of chemical tankers showed that 10% of the speed reduction leads towards the 19.6% of the fuel consumption reduction (Yuan et al., 2019). Nonetheless, an investigation performed in (Taskar and Andersen, 2020) showed that speed reduction potential with respect to emissions highly depends on weather conditions. While analyzing the chemical tanker (Sui et al., 2019), acknowledged that speed reduction is a pathway to improve energy efficiency, noting that it would lead to the selection of smaller size main engines in the preliminary design phase. Despite, adverse sailing conditions are the ones leading the selection of larger engines. To conclude, speed reduction remains the largely applied measure due to its simplicity.

Study from (Lindstad and Bo, 2018) showed that the most energy and cost competitive solutions to meet EEDI phase 2 requirements for Aframax tanker are found to be ones having a conventional engine and more slender hulls. Adding hybrid propulsion instead of diesel engine to the previous design can produce meeting even the future EEDI phase 3 requirement. It is concluded that these solutions produced larger GHG than EEDI reductions, making the latter a more conservative approach. The similar discrepancy is also noted in (Trivyza et al., 2020), where Aframax tanker attained EEDI was decreased by employing various main engine modifications, which decreased attained EEDI by 9–30% and led to 32%–54% of the lifetime CO_2 emission reductions. Optimization of existing engine was also found to be sufficient to meet EEDI requirements for the 30000 dwt oil tanker, along with improvement of the engine-propeller system, according to (Amoraritei, 2019). An emerging type of ship, labelled as liquified hydrogen tanker, was analyzed employing various propulsion systems to comply with EEDI requirements (Ahn et al., 2017). Namely, it was found that a solution steam turbine having hydrogen boil-off gas boiler can even meet EEDI phase 3 criteria. On the other hand, the study on dual-fuel diesel electric propulsion for LNG tankers stated that such solution provided better EEOI level compared to steam turbine propulsion (Boumediene et al., 2024).

An approach using the effect of periodic hull cleaning on oil tankers energy efficiency changes is examined in (Adland et al., 2018). By tracking the data from 2012 to 2016, it was concluded that periodic hull cleaning significantly lowers fuel consumption and improves energy efficiency especially for ship sailing in laden conditions. More innovative solution was proposed by (Stec et al., 2021), in which the findings showed that the post-combustion carbon capture for the 47000 dwt tanker lowers the attained EEDI so that even the strictest EEDI phase 3 requirement are expected to be satisfied with a sufficient margin. Another innovative approach to improve energy efficiency included the application of molten carbonate fuel cell system on a chemical tanker (Inal and Deniz, 2021). Based on 27 voyages data recorded in 2018, such solution is estimated to reduce onboard CO_2 emissions by 33% compared to conventional propulsion leading also to the significant EEDI drop. In the study provided by (Prados et al., 2024), hydrogen is introduced as an energy carrier capable of meeting decarbonization goals by 2050, however significant challenges remain, including storage issues, insufficient supply infrastructure and the need for advancements in technology and regulations.

When it comes to more systematic studies, and besides the slow steaming approach (Jia et al., 2017), assessed the potential of other operational measures to save fuel and improve energy efficiency. Authors of this research tracked VLCC tankers through the AIS data in between 2013 and 2015 and concluded that just by reducing the excess port time and use it for sailing could deliver fuel savings in between 7% and 19% on average across the examined ships. IMO (IMO, 2021b) estimated the archived power reductions in fleets for the period in between 2012 and 2018, which is the period that covers EEDI phase 0 and EEDI phase 1. Average main engine loads reduction has been recorded for oil tankers with up to 4999 dwt, followed by 20000–59999 dwt and larger than 200000 dwt sizes. Reductions were 16.4%, 12.1% and 11.1%, respectively. However, an average design speed reduction trend across the whole tanker fleet in the recorded period is noted to be approximately up to 5%. In addition to the IMO study, the European Commission (EC) performed a comprehensive investigation on energy

efficiency of fleets considering IMO database (EC, 2021) and delivered predictions for the future of shipping. EC stated that introduction of EEDI improved overall energy efficiency level, whilst the plateau has been reached in 2015. Similarly to (IMO, 2021b), EC stated that the reference speed changes were not particularly perceptible for tanker fleet indicating that better EEDI score was a result of a design improvements. Oil tankers had worse EEDI score than their gas tanker counterparts, indicating that EEDI phase 3 criteria could be unreachable for those designs. For instance, Aframax oil tankers EEDI levels were better before 2015 than after 2015, when the score is evaluated by the corresponding criterion at the time. The explanations lay in stricter regulations, verification and trail correction procedures for those sizes. In contrast to the rest of the fleet, tankers having less than 50000 dwt are expected to meet EEDI phase 3 criteria. Although gas tankers had a better EEDI score than oil tankers, such was not the case with smaller LPG tankers (ethylene carriers), who appeared unable to meet EEDI requirements. The study argued that even with LNG as a power source, small LPG tankers would not comply with a future EEDI phase 3 requirement. Larger gas tankers are expected to meet EEDI phase 3, due to their larger speed and thus, slow steaming potential. In general, according to (EC, 2021), tanker EEDI improvements are so far achieved by increasing the propeller diameter, reducing the engine rpm, use of energy saving devices (ESD), improved engine specific fuel oil consumption (SFOC), while the reference speeds remained almost constant. Conclusions obtained from (EC, 2021) for gas tankers were similar to the finding obtained from the study on 212 LNG tankers performed by (Ekanem Attah and Bucknall, 2015). This study showed that newly built gas tankers came with larger design improvements, and along with their slow steaming potential, they are expected to comply with energy efficiency regulations, even with EEDI phase 3. However, their actual energy efficiency is significantly affected by the methane slip phenomenon and its methods of incorporation into the evaluations. More specifically, (Ekanem Attah and Bucknall, 2015) stated that methane slip can increase EEDI level by up to 115%. Nonetheless, the high demand growth of the gas tanker fleet leads to the growth of their CO_2 emissions, as recorded in China-oriented maritime transport form 2000 until 2017 (Yang and Ma, 2019). In a review of ship energy efficiency (Barreiro et al., 2022) stated that EEDI phase 3 will be satisfied by 26% of oil tankers and only 13% of gas tankers built in between 2013 and 2017. Oil tankers improved their energy efficiency by 35%, whilst gas tankers by 42%, compared to the original EEDI requirement curve from 2013. Furthermore, the study acknowledged the improvement in optimization of main design parameters as a consequence of EEDI introduction, as most of the studies did (EC, 2021). The study (Barreiro et al., 2022) noted the block coefficient increase and length to displacement ratio decrease over the past decades. It was concluded that EEDI has led to minimizing the EEDI score rather than minimizing the fuel and energy consumption. When ships are built, they should already comply with EEDI, and therefore, with corresponding EEXI targets (Rutherford et al., 2020). EEXI regulations emerged recently for ships already at sea, so their main design particulars could not be changed at the site. Study (Bortuzzo et al., 2022) assessed EEXI for 5 tanker ships (109143–163591 dwt) and found that the requirement was exceeded by 17.5–23.6%. In order to meet EEXI, ships had to reduce *MCR* in between 23 and 30%. The paper proposed that tankers with smaller EEXI requirement exceedance, might use engine modifications, hull modifications, engine recovery and deadweight increase; while for ones with exceedance of 15% or more, an installation of Engine Power Limiter (EPL) and Shaft Power Limiter (ShaPoLi) can be employed. Their aim is to limit engine or shaft power, respectively, and finally to slow steam, as this is the simplest measure for ships already operating. Investigations from (Bayraktar and Yuksel, 2023; Chuah et al., 2023) also concluded that tankers EEXI is satisfied with a use of EPL. Nevertheless, IMO presented guidelines for EPL use to meet EEXI (IMO, 2021d) to help the designers. Existing technology resources are not sufficient to allow full adjustment in meeting future EEXI requirements for cargo ships, including tankers, although the designs are improving. Current regulations discriminate smaller ships, as partially loaded larger ships will comply, according to (Czermanski et al., 2022). EEDI and EEXI measures, contrary to the effect of the fleet growth, influenced the carbon intensity levels of tankers. Energy intensities of product tankers, in China-oriented maritime transport increased in between 1999 and 2017 (Yang and Ma, 2019), as the fleet experienced growth and demand in past two decades in Asia. Study in (Sou et al., 2022) concluded that, due to effect of energy efficiency design indices, the carbon intensity of ship fleets decreased, with reduction being higher in 2012–2015 than in 2015–2018. EEXI and CII for older tankers found to have more challenges in compliance considering their cost during the lifetime (Chuah et al., 2023). Oil and gas tankers are assessed using scenario-based assessment of EEXI and CII. Compliance with those regulations is found to be hard with conventional fuels (MDO and HFO) and without EPL, although ships are close to requirement limits. Alternative fuels surely will solve the issue. Still, EPL can be a solution to comply with CII (Bayraktar and Yuksel, 2023).

Alternative evaluation procedure for energy efficiency is proposed by semi-empirical assessment, called Energy Performance indicator (EEPI), introduced for oil tanker case study, but stated that can be applicable for liquid chemical tankers as well. In short, EEPI is defined as ratio of CO_2 emissions per specific period/voyage transport work (Zhang et al., 2019). Somewhat the similar is proposed in (Lu et al., 2015) by proposing energy efficiency in operation indicator defined as main engine fuel consumption to unit of transport work ratio. Tanker ships designs were also used to assess the IMO guidelines for assessing the minimum propulsion power of ships in adverse conditions, and would meet energy efficiency regulations IMO, by criticizing simplistic procedures for tankers and bulk carriers (Liu et al., 2022).

1.1. Research gap

Since EEDI has a longer history, most of the research is directed towards EEDI than toward novel regulations with respect to EEXI or CII. Although under investigated compared to other major fleets, there are studies that evaluate tankers' energy efficiency levels. However, these are dispersed and in the most cases, not systematically given with respect to the particular phase of the EEDI introduction or compared with the EEXI or CII levels. They investigated their EEDI levels in the majority of studies. However, studies that compare energy efficiency level of the same tankers with respect to EEDI, EEXI and CII thorough the history of the introduction of these measures are missing, according to the best of authors knowledge. They explored the effects of the particular technology solution in some cases (hull cleaning, engine modifications), or the reduction of speed (i.e., slow steaming). However, consequent results are related to single tanker or fleet of similar tankers, and hardly can be attributed to larger tanker fleets.

Although the number of studies related to energy efficiency of ships have been increased over the recent years, rare have been assessing large fleets of tankers and their subgroups. The extensive comparison of design- and operational-based energy efficiencies, as well as the actual slow steaming to meet IMO requirements, is not found in literature for those fleets in a manner analyzed here, according to the best of author knowledge. This leaves a gap in identification of the actual effect regulations have on particular tanker ships deadweights, their environmental impact, when it comes to operational and design modifications.

1.2. Key contributions

Therefore, the goal of the paper is to deliver an extensive study regarding energy efficiencies of tankers with respect to EEDI, EEXI and CII, in order to identify the level of progress according to each of the measure and sizes. Energy efficiencies are separated by the size and type of the tankers. In addition, the necessary reduction of the tankers' speed and power (i.e., slow steaming) potentials are evaluated to satisfy current and future energy efficiency criteria.

2. Database

A database consists of 426 sea-going tankers built between 2000 and 2020, designed to carry liquified cargo such as: oil, chemicals, LNG, LPG, methanol, palm oil, bitumen, fruit juice, sulphur, ethylene, and similar. Thus, ships are grouped into categories according to their class: chemical/oil products tankers, crude oil tankers, LNG tankers, LPG tankers and products tankers. Furthermore, they are also divided in terms of their deadweight size into the most common categories used in practice: Small, Medium, Panamax, Aframax, Suezmax, Very Large Crude Carriers (VLCC) and Ultra Large Crude Carriers (ULCC), see Table 1. The majority of the data for ships are obtained from Significant Ships journal published by The Royal Institution of Naval Architects (RINA) from 2000 to 2020 (RINA, 2000), in which the most significant ships (by their design) built in those years are selected by industry peers. In this study, ships built after 2020 were not considered due to the outbreak of the COVID-19 pandemic, which significantly impacted the entire maritime industry. Furthermore, the source for the database were acquired by shipyard data disclosed to the authors, and other sources such as: official websites of ship operators or owners, AIS tracking websites, etc. (see Fig. 1a and b). Some of the ships have more than one classification notation. Note that sampling was performed by random nature according to the availability of substantial number of data needed for such analyses. Indeed, the database does not reflect the nature of the overall tanker fleets population. Consequently, conclusions are only related to the tanker fleets provided in this paper.

Ships are categorized here according to their primary type of liquified cargo and *DWT*. Note that with varying degrees of accuracy for each source of data, any errors within the data input source will extend to the results, resulting in decreasing overall reliability of the results. Ships' main specifics are provided in Fig. 2 depending on their respective *DWT*. In Fig. 2a-h, characteristic trends in parameter changes as a function of *DWT* can be observed. The relationship between the overall length, breadth, height, draft, speed, propeller diameter and *DWT* is practically logarithmic, while the relationship between displacement and *DWT* is linear. For *MCR* and *DWT*, a clear dependency trend cannot be observed for all types of ships (especially not for LNG tankers); the best fit is power fit. Additionally, each of the aforementioned figures includes a mathematical interpretation of the trendline for each type of ship individually. The dependency that gives a coefficient of determination as close to 1 as possible is adopted for the mathematical formulas. These mathematical interpretations can be used in the initial phase of ship design when selecting the main dimensions of tankers, but for *MCR*, regression equations should be taken with caution because the coefficient of determination is about 0.5. Similar equations exist in (Papanikolau, 2014), but only with considered tankers built in the period from 2000 to 2005.

The following analysis examines the development of ships over the years, specifically how key parameters such as length, width, draft, *DWT*, designed speed, and engine power have changed from 2000 to 2020. In Fig. 3, data for different ship types are represented with markers of various shapes and colors. Dashed lines show the linear trends for each of the eight parameters, separately for each ship type. The trends are not results of this study but given just in order to provide insight into the nature of database we gathered, which are inputs we used for analyses of EEDI, EEXI and CII. Fig. 3a and b shows the overall length and width of ships, respectively, indicating that ships have generally become longer and wider over the years. However, LNG carriers have become shorter and narrower. Fig. 3c and d displays the draft and *DWT*. For chemical/oil products, LPG, and products tankers, both draft and *DWT* have slightly increased, while for crude oil tankers and LNG carriers, these parameters have changed only slightly. Fig. 3e shows the designed speed, which has significantly decreased for all ship types over the years, except for LPG tankers, which have become faster. Fig. 3f presents the *MCR*, which has slightly increased over the years for LPG and products tankers. For chemical/oil products tankers, it has slightly decreased, while for crude oil and LNG tankers, it has decreased more noticeably, particularly for LNG tankers. The propeller diameter (Fig. 3g) has significantly increased over time for all types of ships except for LNG tankers, where it has decreased, while the Froude number has decreased for all types of ships (Fig. 3h).

3. Methodology

3.1. Research approach

The introduction provides a detailed analysis of the current IMO regulations regarding ship energy efficiency, with an emphasis on EEDI, EEXI, and CII as the three most important indices. A review of extensive literature revealed that there are currently no research results on large fleets of the same type of ships (tankers) built in the first and second decades of the 21st century. In the following chapters, the calculation methodology for each of the three energy efficiency indices is presented and applied to a database of 426 sea-going tankers. All considered ships are classified by type and size based on *DWT* and all obtained results were analyzed according to this classificaiton. For each ship, the attained and required EEDI and EEXI were determined, while for 40 ships from the database, the attained and required CII were also calculated, as the authors had sufficient data to determine CII for only these 40. For all ships from the database that do not meet the EEDI/EEXI criteria, EPL was determined as one of the simplest methods to meet EEDI/EEXI requirements. In accordance with engine power limitations, the corresponding speed reduction was calculated, both individually and for tankers divided by type and size. Through comprehensive analysis, the rate of energy efficiency improvement for the entire fleet during the period from 2000 to 2020 was also determined. Summarizing, this section presents the streamlined guidance depicted in Fig. 4 as a flowchart.

3.2. EEXI

For a ship to pass the IMO criterion, attained EEXI has to be lower than required EEXI, see Eq. (1). Both attained and required EEXI score is assessed using IMO procedures for tankers described in (IMO, 2018,

Table 1
Number of ships according to the type and size.

Size	*DWT* range	Type of tankers					Total
		Chemical/Oil	Crude	LNG	LPG	Products	
Small	−25000	66	1	12	15	4	**98**
Medium	25000–50000	73	2	3	8	11	**97**
Panamax	50000–75000	28	12	6	13	3	**62**
Aframax	75000–120000	6	31	52	0	1	**90**
Suezmax	120000–200000	2	39	4	0	0	**45**
VLCC	200000–320000	0	28	0	0	0	**28**
ULCC	320000 -	0	6	0	0	0	**6**
Total		**175**	**119**	**77**	**36**	**19**	**426**

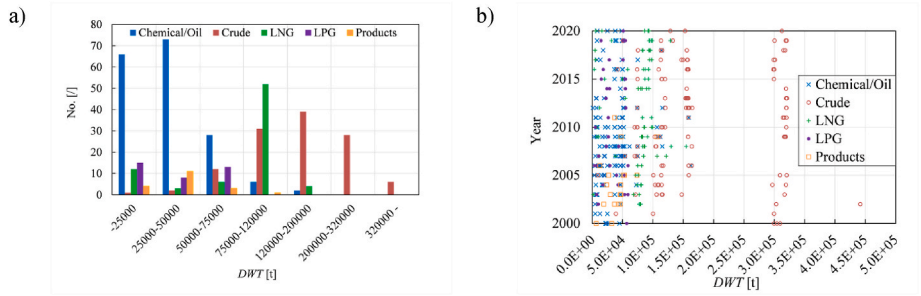

Fig. 1. Database ships specific parameters depending on a deadweight: a) number of ships, b) year of built.

2021c, 2022i), and given in Eqs. (2) and (3), and Tables 1 and 2, respectively. In Eq. (2), subscript "*" points that SFC_{ME} and C_{FME} can replace SFC_{AE} and C_{FAE}, respectively. This can be performed if part of the normal maximum load is delivered by shaft generators. Subscript "**" means that an average weighted value of (SFC_{ME}•C_{FME}) and (SFC_{AE}•C_{FAE}) is to be applied of the calculation of P_{eff}. The subscripts "$_{ME}$" and "$_{AE}$" relate to the main and auxiliary engine, respectively. Since the power-speed curve from the trails was not available, we calculated the reference speed using a proposed equation given in Table 2. According to this, V_{ref}, along with MCR_{avg} depends on ship type and deadweight. Capacity values are taken as respective deadweights for scantling drafts. All inputs explanations and respective sources for the calculation of attained EEXI are given in Table 2. Required EEXI is calculated using (IMO,2021c) Table 3 and Table 4.

$$\text{Attained EEXI} = \frac{\left[\left(\prod_{j=1}^{n} f_j\right)\left(\sum_{i=1}^{n_{ME}} P_{ME(i)} \cdot C_{FME(i)} \cdot SCF_{ME(i)}\right) + (P_{AE} \cdot C_{FAE} \cdot SCF_{AE^*}) + \left(\left(\prod_{j=1}^{n} f_j \cdot \sum_{i=1}^{n_{PTI}} P_{PTI(i)} - \sum_{i=1}^{n_{eff}} f_{eff(i)} \cdot P_{AEeff(i)}\right) \cdot C_{FAE} \cdot SCF_{AE} - \left(\sum_{i=1}^{n_{eff}} f_{eff(i)} \cdot P_{eff(i)} \cdot C_{FME} \cdot SCF_{ME^{**}}\right)\right]}{f_i \cdot f_c \cdot f_l \cdot Capacity \cdot f_W \cdot V_{ref} \cdot f_m} \quad (1)$$

$$\text{Attained EEXI} \leq \text{Required EEXI} \quad (2)$$

$$\text{Required EEXI} = \left(1 - \frac{Y}{100}\right) \cdot \text{Reference line} \quad (3)$$

$$\text{Reference line} = a \cdot b^{-c} \quad (4)$$

According to the methodology described in (Kalajdzic et al., 2022), the required EPL and consequently the new reference speed ($V_{ref,app,lim}$) is determined to ensure that each ship in the database meets the EEXI criterion. Moreover, the relative difference between the approximated speeds ($V_{ref,app}$ and $V_{ref,app,lim}$) before and after the installation of the EPL is also provided to see how much ships need to slow down in order to meet the EEXI criteria.

3.3. EEDI

Assessment of EEDI is analogous to assessment of EEXI: the lower attained EEDI score means that the ship is considered as more energy efficient, attained value has to be lower than required value of EEDI. The calculation is performed using (IMO, 2018) and amended with (IMO, 2019) indicating that a similar formula is used as for EEXI, see Eqs. (5)–(7). The required EEDI criterion is strengthened over the years and as such is incorporated in calculation using reduction factors, as given in (IMO, 2021c). All inputs explanations and respective sources for the calculation of attained EEDI are given in Table 2. Required EEDI is calculated using (IMO,2021c), Tables 3 and 5.

$$\text{Attained EEDI} \leq \text{Required EEDI} \quad (5)$$

$$\text{Required EEDI} = \left(1 - \frac{X}{100}\right) \cdot \text{Reference line} \quad (6)$$

While Reference line is depicted as Eq. (4).

3.4. CII

In addition to EEDI and EEXI, a group of ships are extracted from the database and chosen for the calculation of their CII rating, see Eqs. (7)–(11). It is performed for the total of 40 ships for which the authors had reliable data for the evaluation: IMO DCS data on annual fuel consumption for 2022 per fuel type, number of hours spent under way and distance traveled. Note that starting from the January 1, 2023 all ships have to have a three-year plan in which the explanation of proper CII achievement will be given (IMO, 2022g). Consequently, attained CII is calculated according to (IMO, 2022d), reference CII (CII_{ref}) is evaluated as per (IMO, 2022e) for 2019 and reduction factor Z is extracted from (IMO, 2021a). All input explanations and respective sources for the calculation of attained CII are given in Table 6. Parameters for determining the specific reference line and reduction factors are given in Table 7 and Table 8.

$$\text{Required CII} = M/W \quad (7)$$

$$M = FC_j \cdot C_{F_j} \quad (8)$$

$$W = C \cdot D_t \quad (9)$$

$$\text{Attained CII} \leq \left(1 - \frac{Z}{100}\right) \cdot \text{CII}_{\text{ref}} \quad (10)$$

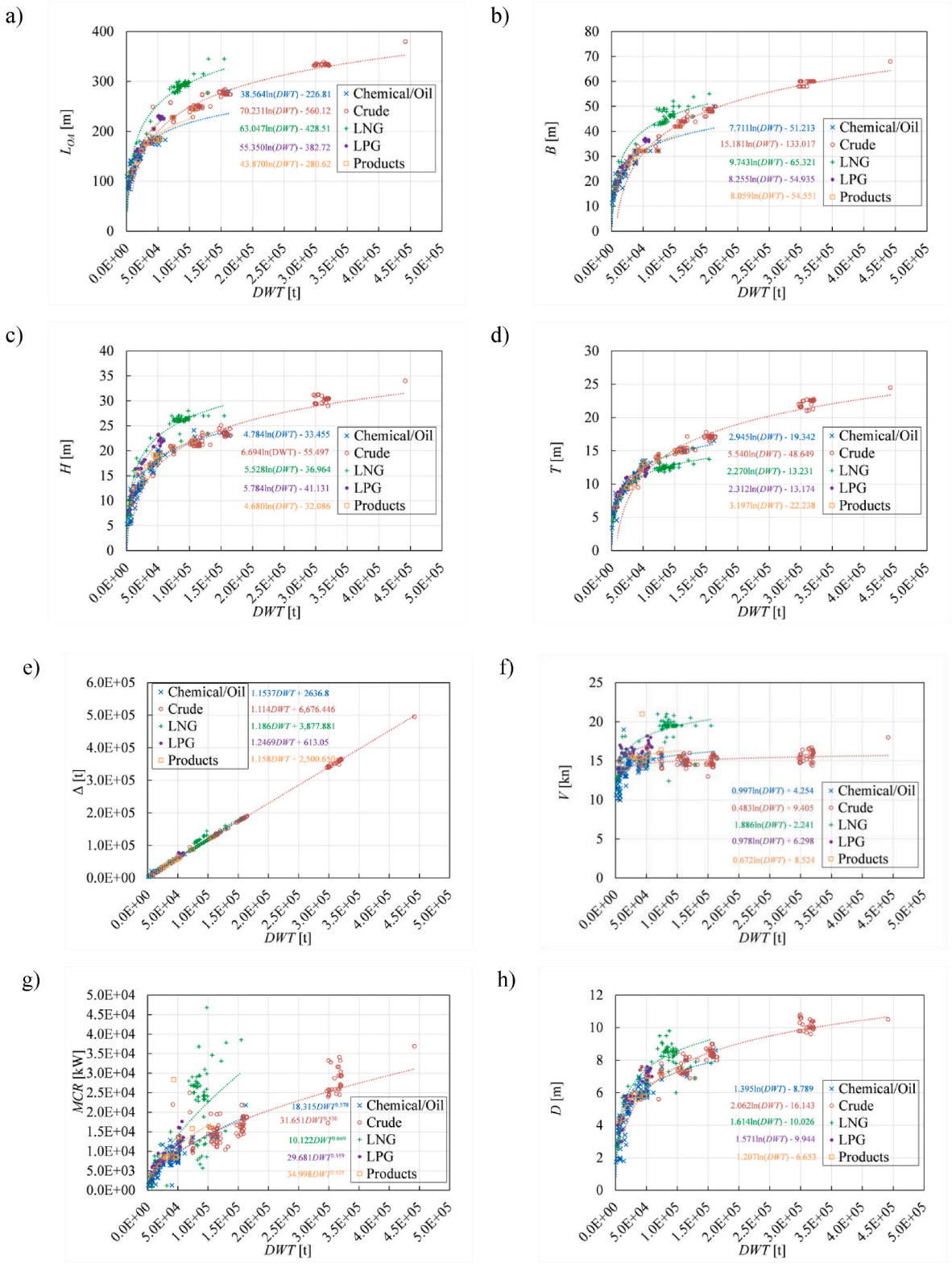

Fig. 2. Database ships specific parameters depending on a deadweight: a) length overall, b) breadth, c) height, d) scantling draft, e) displacement (fully loaded), f) design speed, g) *MCR* power, h) propeller diameter.

$$CII_{ref} = a \cdot Capacity^{-c} \tag{11}$$

The idea of developed rules and guidelines is to determine the rank for each ship. The operational carbon intensity rating classifies ships into five grades (A, B, C, D, and E) based on their annual operational carbon intensity indicator. This ranking system indicates the vessel's performance level, ranging from major superior to minor superior, moderate, minor inferior, or inferior (IMO, 2022f). To facilitate the evaluation process, annual rating assignments from 2023 to 2030 involve the definition of four distinct boundaries within the five-grade rating framework: superior, lower, upper, and inferior boundary. This

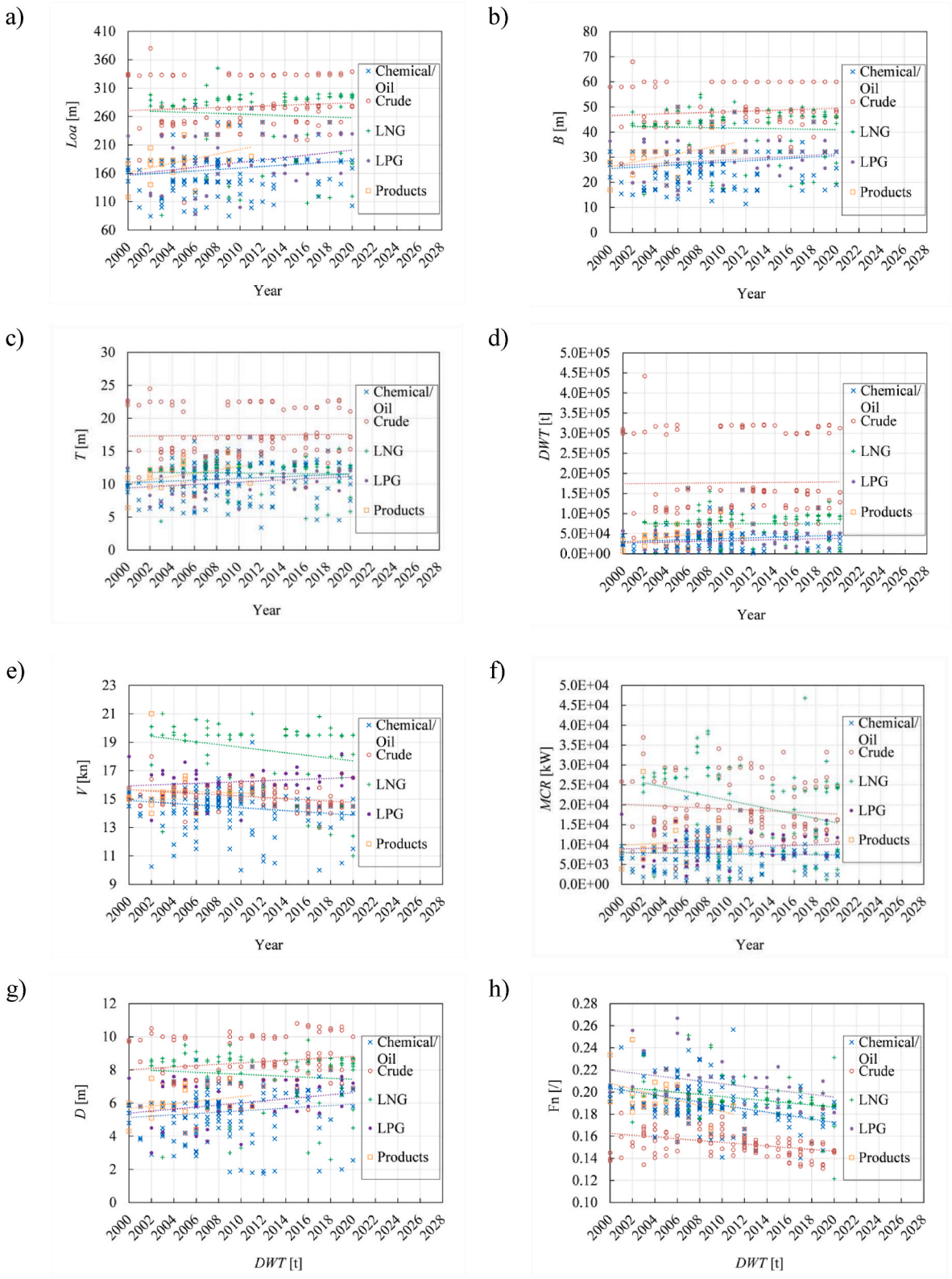

Fig. 3. Development of ships parameters over the years: a) Length overall - *Loa*, b) Breadth - *B*, c) Scantling draft - *T*, d) Deadweight - *DWT*, e) Design speed - *V*, f) Maximum engine power - *MCR*, g) Propeller diameter - *D*, h) Froude number based on length - Fn.3.

allows for the assessment of a ship's annual operational CII by comparing it to these specified boundary values. The determination of these boundaries is rooted in the distribution of individual ships' CIIs in the year 2019. The boundaries for performance ratings over time are synchronized while maintaining the consistent relative distance between them. Notably, a ship's rating is determined by its achieved CII concerning predetermined boundaries, independent of the CII levels of other ships. The establishment of these boundaries involves considering the required annual operational CII in conjunction with vectors denoted as dd vectors, signifying both the direction and magnitude of deviation

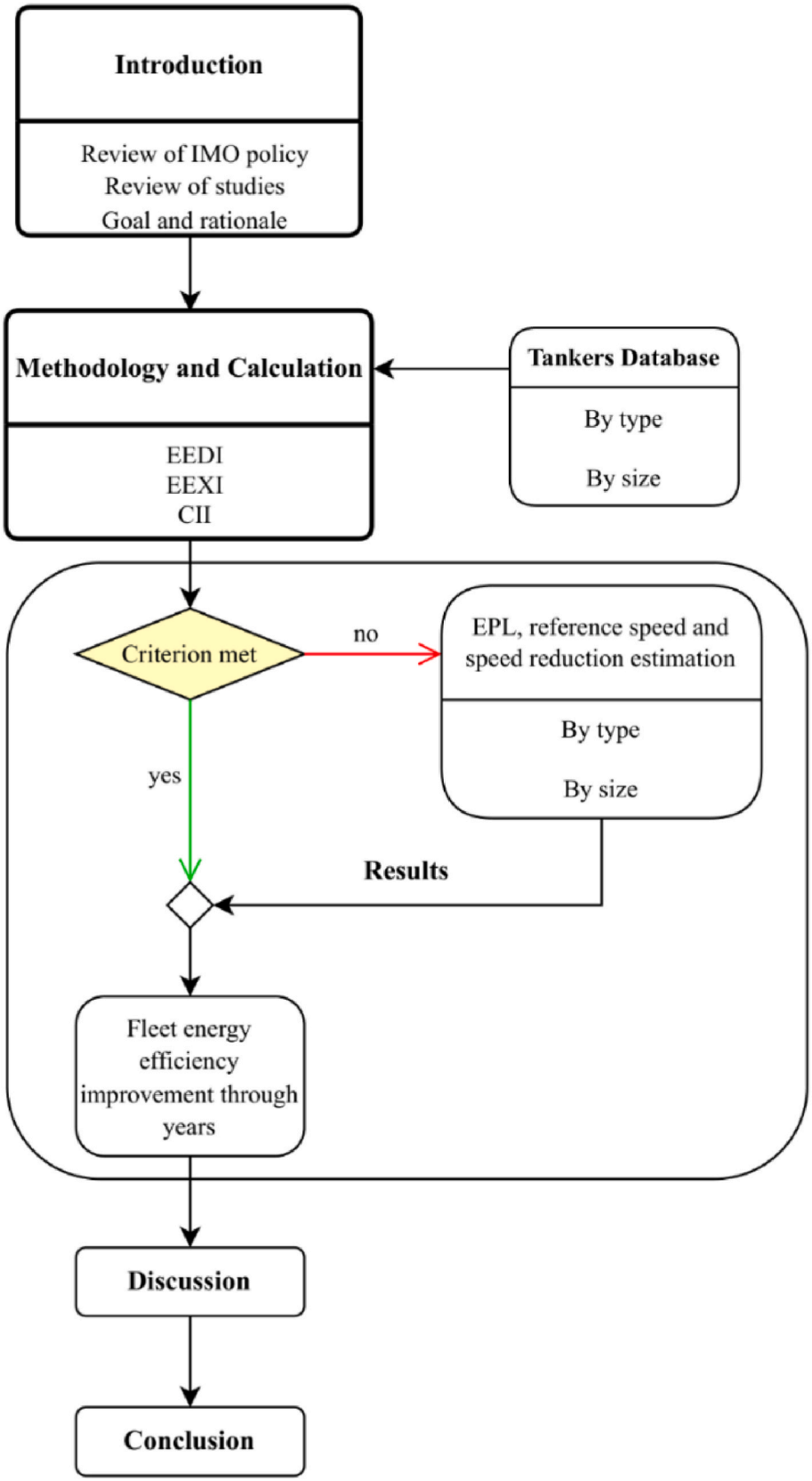

Fig. 4. Research approach.

Table 2
Inputs for the calculation of attained EEXI.

Input	Methodology	Comments (explanations/sources)
Main engines	$\sum_{i=1}^{n_{ME}} P_{ME(i)}$	75% of the maximum continuous rating (*MCR*). This is to be taken as 83% of limited installed power (MCR_{lim}) or 75% of *MCR*, whichever is lower (IMO, 2022i).
Shaft generators	$\sum_{i=1}^{n_{PTI}} P_{PTI(i)} = 0$	No shaft generators
Innovative energy efficient devices on main engine	$\sum_{i=1}^{n_{eff}} f_{eff(i)} \cdot P_{eff(i)} = 0$	No innovative energy efficient devices on main engine
No innovative energy efficient devices on auxiliary engine	$\sum_{i=1}^{n_{eff}} f_{eff(i)} \cdot P_{AEeff(i)} = 0$	No innovative energy efficient devices on auxiliary engine
P_{AE}	$P_{AE} = 0.5 \cdot MCR$ ($MCR < 10000$ kW) $P_{AE} = 0.025 \cdot MCR + 250$ ($MCR \geq 10000$ kW)	For *MCR* >10 000 kW MCR (IMO, 2018)
SCF_{FME}	190 g/kWh	This is assumed for engines that have no NOx Technical File and verified manufacturer's data (IMO, 2022i),
SFC_{AE}	215 g/kWh	
C_{FME}	3.114 t CO_2/t•fuel - for HFO	
C_{FAE}	3.206 t CO_2/t•fuel - for diesel	
$V_{ref,app}$, $V_{ref,app,lim}$	$V_{ref,avg} - m_v \left[\frac{P_{ME}}{0.75 MCR_{avg}}\right]^{1/3}$	Where there is no power speed curve available or there are no EEDI from sea trials, the formula represents the statistical mean of distribution of ship speed and engine power (IMO, 2022i)
MCR_{avg}	$D \cdot E^F$ $D = 22.8415$ – tankers $D = 21.4704$ – gas carriers $D = 20.7096$ – LNG $E = DWT$ $F = 0.55826$ – tankers $F = 0.59522$ – gas carriers $F = 0.63477$ – LNG	Depends on ship type (IMO, 2022i)
mv	min ($V_{ref,avg}$, 1 kn)	IMO (2022i)
$V_{ref,avg}$	$V_{ref,avg} = A \cdot B^C$	Parameters A, B, C are given in (IMO, 2022i)
Capacity	*DWT*	IMO (2018)
f_j	Ship specific design elements – the power correction factor for ice-classed ships: the greater value of f_{j0} and $f_{j,min}$ but not greater than $f_{j,max} = 1$	IMO (2018)
f_i	Capacity correction factor	IMO (2018)
f_c	Cubic capacity correction factor	IMO (2018)
f_l	Factor for general cargo ships equipped with cranes. $f_l = 1$	IMO (2018)
f_w	Factor for speed reduction at sea. $f_w = 1$	IMO (2018)
f_m	Factor for ice-classed ships	IMO (2019)

Table 3
Inputs for the calculation of EEDI Reference line (IMO, 2021c).

Ship type	*a*	*b*	*c*
Gas carrier	1120	*DWT*	0.456
Tanker	1218.8	*DWT*	0.488
LNG carrier	2253.7	*DWT*	0.474

from the required value. dd vectors for determining the rating boundaries are shown in Table 9.

One of the most popular and easiest methods for meeting the CII criteria is reducing speed. Therefore, in this case, the relative difference between the average sailing speed of each ship over one year and the speed at which the ship should sail to meet the CII criteria for the same period and distance traveled has also been determined.

In Table 10 are outlined the main differences and similarities between EEDI, EEXI and CII:

This multi-dimensional evaluation perspective based on calculating EEDI, EEXI and CII helps to more comprehensively judge the energy efficiency level of tankers, identify shortcomings in design and operation, and provide more details about energy saving and emission reduction from a large tanker fleet.

Table 4
Reduction factor *Y* for the required EEXI compared to the EEDI reference line (IMO, 2021c).

Ship type	Size	Reduction factor
Gas carrier	$DWT \geq 15000$	30
	$10000 \leq DWT < 15000$	20
	$2000 \leq DWT < 10000$	0–20[a]
Tanker	$DWT \geq 200000$	15
	$20000 \leq DWT < 200000$	20
	$4000 \leq DWT < 20000$	0–20[a]
LNG carrier	$DWT \geq 10000$	30

[a] The reduction factor *Y* should be linearly interpolated between two values dependent upon ship size.

4. Results

Firstly, for each basic type of ship (Gas Carrier, Tanker, LNG Carrier – according to IMO classification), reference values for the required EEDI have been determined according to phases, with criteria becoming stricter over the years. Therefore, in Fig. 5, the EEDI reference line (green - phase 0, blue - phase 1, purple - phase 2, orange - phase 3) shifts downward. The EEXI reference line is shown in Fig. 5 with a black line, and it largely coincides with the orange EEDI reference line (whose reduction coefficient corresponds to phase 3). Each point (square, circle, rhomb, triangle) represents one of the ships from the database with its attained EEDI/EEXI. The color of the point is defined according to the colors of the reference lines. 89.3% of ships built during the period 2013–2014 meet the EEDI criteria corresponding to Phase 0, 72.5% of those built during 2015–2019 meet the criteria corresponding to Phase 1, while 47.1% of ships built in 2020 meet the criteria for Phase 2. In Fig. 4, the attained EEXI for ships older than 2013 is shown by triangles. For newer ships, the attained EEDI and attained EEXI are equal. Since the EEXI regulations came into force in 2023, all ships were considered for compliance with the regulation. Only 14.8% of ships meet the EEXI criteria, which corresponds to 63 out of 426 ships from the database. It can be seen that the EEXI and EEDI (Phase 3) criteria are practically the same for Gas Carriers and LNG Carriers, while the EEXI criterion for

Table 5
Reduction factor *X* for required the EEDI relative to the EEDI reference line (IMO, 2021c).

Ship type	Size	Phase 0	Phase 1	Phase 2	Phase 2	Phase 3	Phase 3
		1 Jan 2013–31 Dec 2014	1 Jan 2015–31 Dec 2019	1 Jan 2020–31 Mar 2022	1 Jan 2020–31 Dec 2022	1 Apr 2022 and onwards	1 Jan 2025 and onwards
Gas carrier	$DWT \geq 15000$	0	10	20		30	
	$10000 \leq DWT < 15000$	0	10		20		30
	$2000 \leq DWT < 10000$	Not applicable	0–10[a]		0–20[a]		0–30[a]
Tanker	$DWT \geq 20000$	0	10		20		30
	$4000 \leq DWT < 20000$	Not applicable	0–10[a]		0–20[a]		0–30[a]
LNG carrier[b]	$DWT \geq 10000$	Not applicable	10[c]	20		30	

[a] Regarding the tankers with *DWT* between 4000 and 20000 t, the reduction factor *Y* should be linearly interpolated between two values.
[b] Reduction factor applies to those ships delivered on or after 1 Sep 2019.
[c] Phase 1 commences for those ships on 1 Sep 2015.

Table 6
Inputs for the calculation of attained CII.

Note	Symbol	Comments (explanations/sources)
Mass of CO_2 emissions	M	Total mass of CO_2 in grams from all the fuel oil consumed on board a ship in a given calendar year
Mass of consumed fuel oil	FC	Total mass in grams of consumed fuel oil type *j* in the calendar year, as reported in IMO DCS Annual emissions report
Fuel oil type	j	HFO, LFO, MDO/MGO, LPG, LNG
Conversion factor	C_{Fj}	Fuel oil mass to CO_2 mass conversion factor for fuel oil type: 3.114, 3.151, 3.206. 3.030, 2.750 for each fuel oil type above respectively. (IMO, 2022i; ISO, 2024)
Transport work	W	The supply-based transport work (IMO, 2022d)
Ship's capacity	C	Deadweight
Traveled distance	D_t	Total distance traveled in nautical miles as reported in IMO DCS Annual emissions report

tankers largely overlaps with the EEDI (Phase 2) reference line.

In 2013, the EEDI came into force according to the IMO. Ships built before that time were not subject to this criterion, but if the rules had applied to them, 39% of ships would not have met the criteria. Since the EEDI came into effect, the proportion of ships not meeting the EEDI criterion has decreased to 27.2%. This means that the introduced regulations have influenced the design of more energy-efficient ships in the initial phase, but the percentage has not yet reached zero.

Table 7
Inputs for determining the specific 2019 CII reference lines (IMO, 2022e).

Ship type		*Capacity*	*a*	*c*
Gas carrier	$DWT \geq 65000$	*DWT*	$14405 \cdot 10^7$	2.071
	$DWT < 65000$	*DWT*	8104	0.639
Tanker		*DWT*	5247	0.610
LNG carrier	$DWT \geq 100000$	*DWT*	9.827	0.000
	$100000 > DWT \geq 65000$	*DWT*	$14479 \cdot 10^{10}$	2.673
	$DWT < 65000$	65000	$14779 \cdot 10^{10}$	2.673

Table 8
Reduction factor Z for the CII relative to the 2019 CII reference line (IMO, 2021a).

Year	Reduction factor relative to 2019
2023	5%
2024	7%
2025	9%
2026	11%
2027 and onwards	a

[a] *Z* factors for the years 2027 and onwards will be introduced after review of the current measure.

Table 9
dd vectors for determining the rating boundaries of ship types (IMO, 2022f).

Ship type		*Capacity*	*dd* vectors			
			Exp (d_1)	Exp (d_2)	Exp (d_3)	Exp (d_4)
Gas carrier	$DWT \geq 65000$	*DWT*	0.81	0.91	1.12	1.44
	$DWT < 65000$	*DWT*	0.85	0.95	1.06	1.25
Tanker		*DWT*	0.82	0.93	1.08	1.28
LNG carrier	$DWT \geq 100000$	*DWT*	0.89	0.98	1.06	1.13
	$DWT < 100000$	*DWT*	0.78	0.92	1.10	1.37

It can be observed from Fig. 5c that there is only 3 LNG tankers classified according to the IMO in this category. This classification includes LNG tankers with unconventional propulsion in this group, while LNG tankers with conventional propulsion are classified as Gas Carriers.

Table 10
EEDI, EEXI, CII – main differences and similarities.

Feature	EEDI	EEXI	CII
Purpose	Measures energy efficiency of new ships	Measures energy efficiency of existing ships	Evaluates operational carbon intensity of all ships
Implementation Date	Introduced in 2013	Applicable since 2023	Effective from January 2023
Calculation Basis	Based on design specifications	Based on design specifications	Based on actual fuel consumption and distance traveled
Assessment Criteria	Attained EEDI must be less than required EEDI	Attained EEXI must be less than required EEXI	Attained CII rating is compared to reference CII
Ship Type Consideration	Different for ship types (tankers, gas carriers, LNG)	Different for ship types (similar to EEDI)	Different for ship types (varies with capacity)
Reduction Factors	Reduction factors applied over time	Reduction factors based on ship type	Reduction factors based on annual goals
Rating System	Not a rating system, just a score	Not a rating system, just a score	Five-grade rating system (A to E)
Compliance Monitoring	Monitored at the time of delivery	Monitored periodically for existing ships	Annual monitoring based on fuel reports
Focus	Design phase energy efficiency	Existing design energy efficiency	Operational carbon intensity and emissions

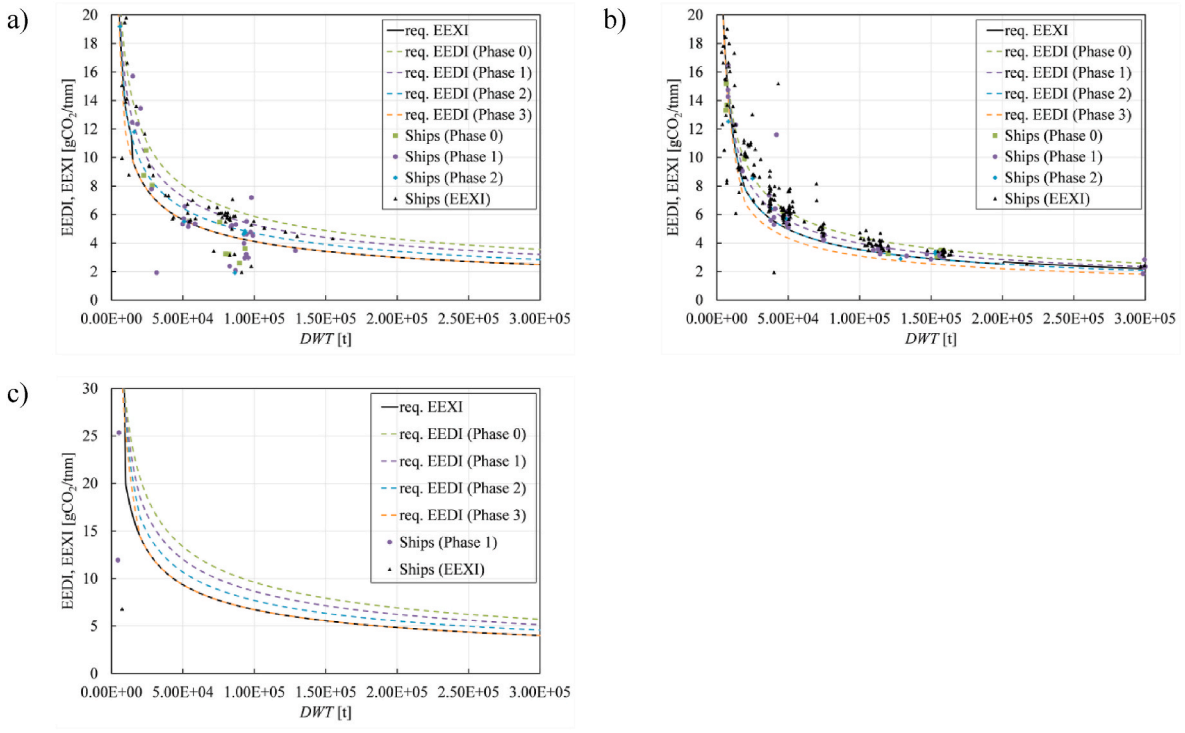

Fig. 5. Attained and required EEDI/EEXI: a) Gas carriers, b) Tankers, c) LNG carriers.

Table 11
Number of ships that meet EEXI criteria based on size and type.

	Chemical/Oil	Crude	LNG	LPG	Products	Total
Small	22	0	7	2	1	32
Medium	3	0	2	2	0	7
Panamax	0	0	1	2	0	3
Aframax	0	1	15	0	0	16
Suezmax	0	2	1	0	0	3
VLCC	0	2	0	0	0	2
ULCC	0	0	0	0	0	0
Total	25	5	26	6	1	63

Therefore, further analysis of tanker energy efficiency was conducted based on the EEXI and CII criteria, with ships classified by type as chemical/oil products, crude, LNG, LPG and products tankers and by size as Small, Medium, Panamax, Aframax, Suezmax, VLCC and ULCC. In Table 11 are shown numbers of ships that meet EEXI criteria. In Table 11, the numbers of ships that meet the EEXI criterion are provided according to size and type, as well as the total number of ships in these categories.

According to the results, LNG tankers stand out as the most efficient by type, while small ships are the most efficient by size. On the other hand, crude tankers are the least efficient by type, and Panamax ships are the least efficient by size.

The estimated EPL is expressed as a percentage and represents the ratio between the new limited power (MCRlim) and the designed MCR. The results are shown in Fig. 6a, which displays the EPL by ship type, and in Fig. 6b, which shows the EPL by ship size. According to type, the EPL for product tankers deviates more than the others by almost 10%. In terms of size, the largest ships require the smallest percentage of power reduction to meet the EEXI criteria, while the power reduction on the smallest ships will account for a significantly larger proportion.

The relationship between speed reduction and power reduction to meet the specified criteria is interconnected. Given that engine power is proportional to the cube of speed, a slight decrease in speed leads to a substantial reduction in the power needed to maintain that speed, which in turn lowers the EEDI/EEXI. In Fig. 7a and b, the average designed speeds, approximated reference speeds, and approximated limited reference speeds based on ship type and size are shown, respectively. The average designed speed of the entire tanker fleet is 15.6 knots, while the average approximated reference speed is 14.6 knots and average approximated limited reference speed is 12.6 knots.

Fig. 8a and b shows the required percentage reduction in reference speed to meet the EEXI criterion, categorized by ship type and ship size, respectively. The biggest speed reduction of 20.3% is needed for

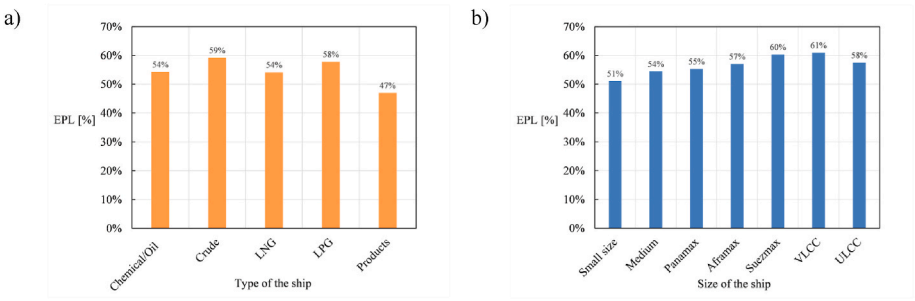

Fig. 6. EPL estimation: a) per ship type, b) per ship size.

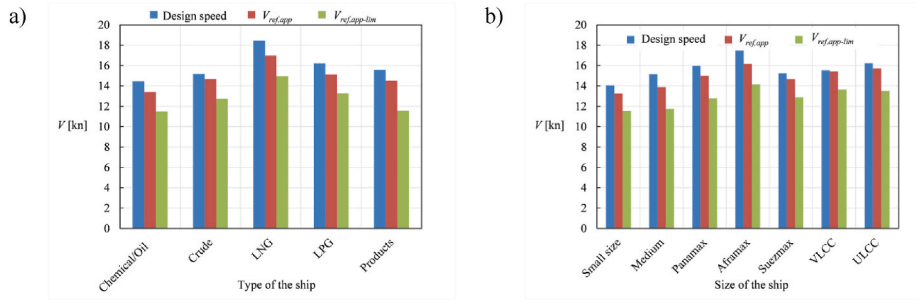

Fig. 7. Speed estimation: a) per ship type, b) per ship size.

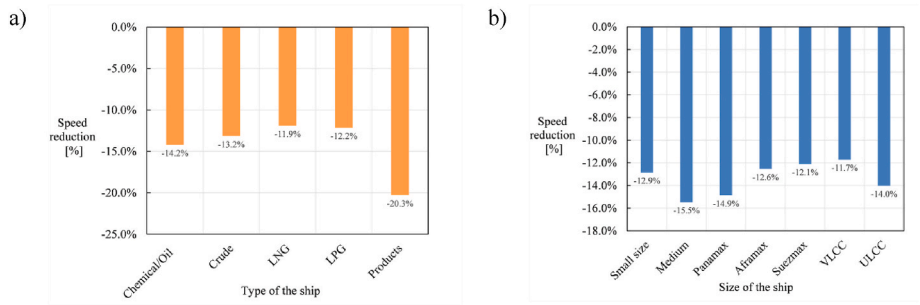

Fig. 8. Speed reduction estimation: a) per ship type, b) per ship size.

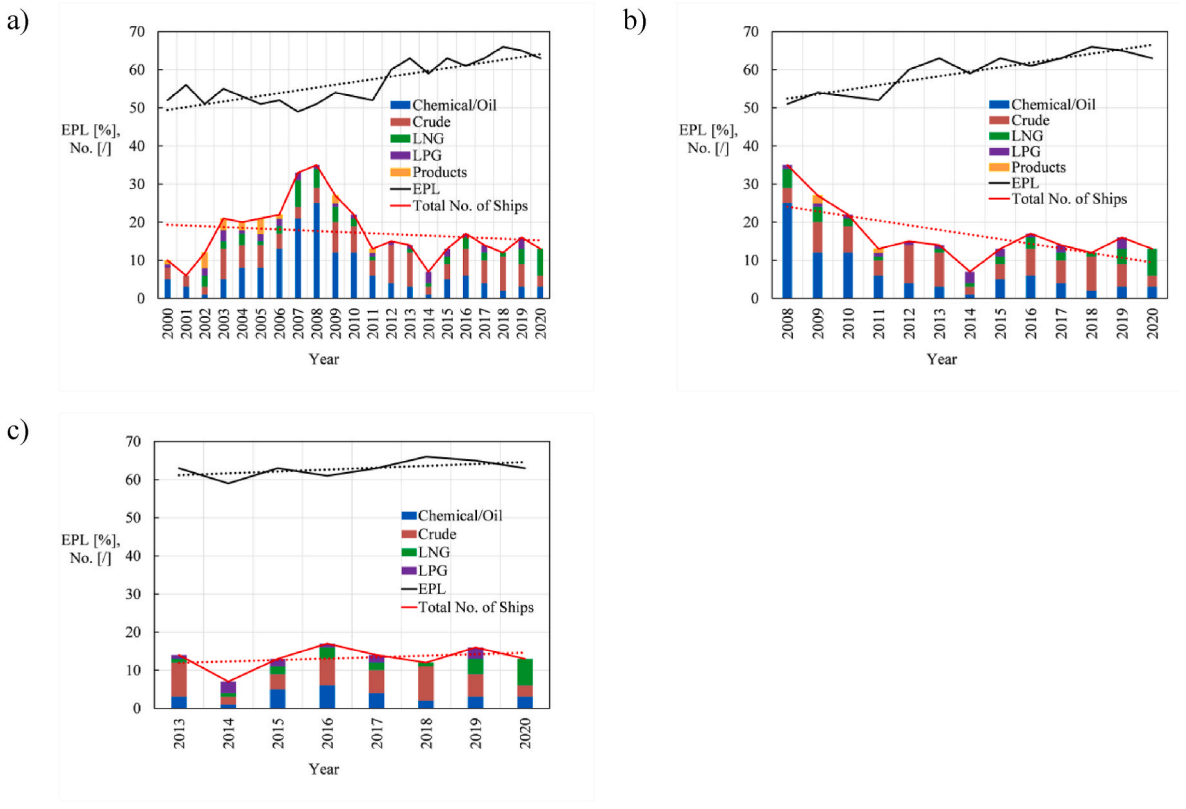

Fig. 9. Fleet energy efficiency improvement through the years: a) from 2000 to 2020, b) from 2008 to 2020, c) from 2013 to 2020.

products tankers, while the least reduction is required for LNG tankers (11.9%), based on ship type. Regarding ship size, the speed needs to be reduced by 11.7% for VLCCs and down to 15.5% for medium size tankers.

The average EPL for all tankers in the database is 56% i.e., the new maximum power is even 44% lower than the original, and the average speed reduction required to meet the EEXI criterion is 13.5%.

The ships have also been sorted by year of construction to gain a clearer view of the trend in fleet improvement over a 20-year period. Fig. 9a shows the number of ships requiring a reduction in engine power

by type for each year of construction. The black solid line represents the average EPL in % for all ship types by year of construction. The dashed lines illustrate the linear trend of the decreasing number of ships needing EPL over the years (red colored), as well as the trend of increasing EPL itself (black colored). Fig. 8a shows that the highest number of ships in the database requiring EPL was built in 2008. This year is used as the reference point for aiming to reduce emissions of exhaust gases. The same year also saw a major economic crisis, which significantly impacted all sectors of industry. Consequently, the decline in the number of ships requiring EPL was accompanied by a reduction in the number of ships built in the subsequent three years (especially chemical/oil products tankers). Generally, since 2008, there has been a decreasing number of ships needing EPL, with a reduction rate of 7.5%, while the EPL has increased at a rate of 2% over the 12-year period (Fig. 9b). However, if 2013 was considered as the reference year, since the EEDI officially came into force then, the rate of EPL increase would be less than 1% (Fig. 9c). In fact, there has been a recorded increase in the number of ships requiring EPL since that year (Fig. 9c).

EEDI and EEXI are nominal energy efficiency parameters and cannot accurately reflect the actual GHG caused by ships, as they are determined using a single speed (reference speed) and engine power based on scantling *DWT*. A more realistic efficiency parameter is CII, which considers the distance traveled, time spent underway, and the actual fuel consumed over a year. By accounting for the distance traveled and the total time spent underway, the average speed of the ship over a year is determined. In this case, the average speed of the tanker fleet is 11.2 knots, meaning the actual speed of the tankers is nearly 30% lower than the designed speed. It should be noted that the entire fleet of 426 ships was reduced to 40, specifically chemical/oil products tankers, as data for determining CII is only available for these ships. With this in mind, the CII analysis was conducted based solely on ship size. As much as 83.3% of ships meet the CII 2023 criteria, having a C rating, while 52.8% are expected to maintain a C rating over the next three years. For the remaining ships to also achieve at least a C rating during the next three years, the average speed needs to be reduced by 5.4%. The average speed reduction needed to meet the same requirement, divided by ship size, is shown in Fig. 10.

When comparing the necessary speed reductions to meet EEXI and CII criteria, an average difference of 8.1% is found. This indicates that ships are already operating at lower speeds (slow steaming) than originally assumed when EEDI and EEXI were introduced as energy efficiency indicators. According to IMO guidelines, the reference speed is achieved at 75% of the engine's MCR. However, the CII analysis shows that tankers are using only about 60% of the maximum available engine power during their voyages.

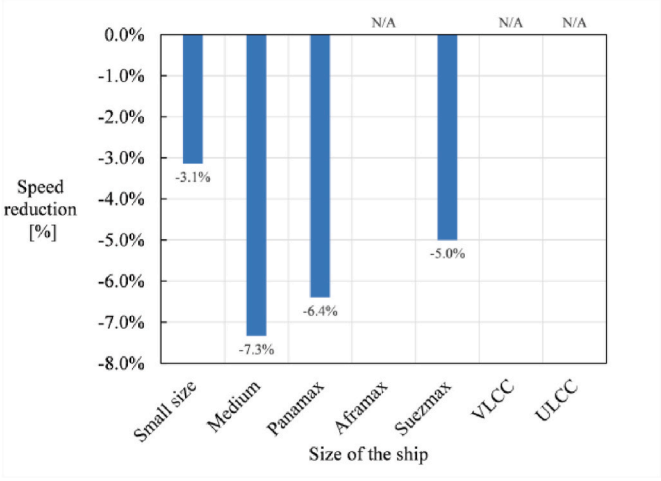

Fig. 10. Necessary speed reduction to reach C grade for the next three years by size of the ship.

5. Discussion

The examination of ship development from 2000 to 2020 highlights several trends. Ships have become longer and wider, though LNG carriers have become shorter and narrower. The draft and *DWT* have increased slightly for chemical/oil products, LPG, and products tankers, while crude oil and LNG carriers have seen minimal changes. Designed speeds have decreased significantly across most ship types, except for LPG tankers, which have become faster. The *MCR* has shown varying trends, with increases for LPG and products tankers and decreases for chemical/oil products and crude oil tankers, particularly for LNG tankers. The trend in ship design shows a significant increase in propeller diameter for all ship types except LNG tankers, which have seen a decrease, possibly due to specific operational requirements. Additionally, the Froude number has decreased across all ship types, reflecting a shift towards lower speeds (and/or longer length) for greater fuel efficiency and reduced emissions.

The analysis of ship energy efficiency through the EEDI and EEXI criteria reveals significant trends in maritime industry practices over the past decades. The data demonstrates that the reference (required) values for EEDI have become increasingly stringent over time. The EEDI reference lines show a downward shift, indicating more rigorous standards with each phase. The EEXI reference line aligns closely with the Phase 3 EEDI reference line for Gas and LNG carriers and Phase 2 EEDI reference line for Tankers, suggesting a convergence towards stricter efficiency requirements.

The proportion of ships meeting these criteria highlights the impact of regulatory measures on ship design. For example, 89.3% of ships built between 2013 and 2014 met the EEDI Phase 0 criteria, while only 47.1% of ships built in 2020 met the Phase 2 criteria. The comparison of ships built before and after the EEDI's introduction shows a decrease in non-compliance from 39% to 27.2%. This decrease underscores the effectiveness of the regulations in promoting more energy-efficient designs, though it also highlights that further improvements are necessary. The significant drop-in compliance rates for more recent ships suggest that while regulations have improved ship design efficiency, they have also become more challenging to meet.

Notably, only 14.8% of ships meet the EEXI criteria, demonstrating that adherence to this more stringent standard remains a significant challenge.

The conducted analysis of EEDI and EEXI calculations are based on statistical models and IMO-proposed formulas rather than actual sea trial data. This methodological approach may affect the accuracy of efficiency assessments, suggesting that real-world measurements could provide a more precise evaluation of ship efficiency.

The analysis shows that LNG tankers are among the most efficient by type, while small ships are the most efficient by size. Although a greater number of smaller ships meet the EEXI criteria compared to larger ships, the smaller ships (those that do not meet the criteria) are affected by more drastic power reductions than the larger ones. Conversely, crude oil tankers are the least efficient by type, and panamax ships are the least efficient by size.

The required EPL and associated reference speeds reveal the need for significant speed reductions to meet EEXI criteria. The average EPL for all tankers is 56%, with a required average speed reduction of 13.5% to comply with EEXI standards. Products tankers require the highest speed reduction (20.3%), while LNG tankers require the least (11.9%). The results indicate that there are no drastic differences in the required reductions in power and speed based on the type or size of the tanker i.e., the required reductions are of the same order of magnitude. Variations in the necessary reductions of these parameters may arise from the variability of the installed engines and the speeds for which they were designed. It should be noted that the nominal efficiency parameters primarily depend on the design specifications, meaning the intended

purpose for which each ship was designed, while the operational efficiency parameters depend on how the ship is operated.

Trends in EPL and the number of ships requiring it over time are shown through the data analysis. The data shows a decline in the number of ships needing EPL since 2008, reflecting improvements in ship efficiency over the years. However, if 2013, when the EEDI officially came into effect, were used as a reference, the rate of EPL increase would have been lower (less than 1%), indicating ongoing improvements in efficiency but also a rising number of ships requiring adjustments. Dynamic research over time provides important highlights into trends and changes within the maritime sector, revealing how factors like economic events and regulatory changes affect the fleet improvements.

The comparison between EEXI and CII criteria reveals a notable difference of 8.1% in the required speed reductions. This discrepancy indicates that ships are already operating with slow steaming than initially anticipated under EEDI and EEXI standards. The CII analysis shows that tankers use only about 60% of their maximum engine power during voyages, suggesting that actual operational conditions differ from the reference values used in EEDI and EEXI assessments. The optimization of ships for their actual operating speeds remains an important consideration. Specifically, questions arise regarding whether ships are optimized for their current speeds, including factors like the efficiency of the bulbous bow and propeller design.

While EEDI and EEXI are nominal efficiency parameters, they are limited in their ability to reflect real-world performance as they rely on theoretical calculations. In contrast, the CII provides a more accurate measure of a ship's efficiency by accounting for actual fuel consumption, time spent underway, and distance traveled. This makes CII a more reliable indicator of true operational efficiency and environmental impact.

6. Conclusion

The analysis of EEDI and EEXI criteria over time underscores the evolving nature of maritime efficiency standards and their impact on ship design. The stricter reference values introduced over the years have led to improved energy efficiency in ship design, although achieving full compliance remains challenging.

The proportion of ships meeting EEDI criteria has improved since its introduction, reflecting the effectiveness of regulatory measures. However, compliance with EEXI remains limited, indicating that further advancements are needed.

LNG tankers are the most efficient by type, while small ships are the most efficient by size. However, the smaller ships that do not meet the criteria are affected by more drastic power reductions than the larger ones. Conversely, crude oil tankers and Panamax ships are among the least efficient. This variability highlights the need for targeted approaches to improve efficiency across different ship types and sizes in general.

The reliance on statistical models and IMO-proposed formulas for EEDI and EEXI calculations may not fully capture real-world efficiency. Incorporating data from sea trials could enhance the accuracy of efficiency assessments.

Significant speed reductions are required to meet EEXI criteria, with the largest reductions needed for products tankers. The CII analysis indicates that ships operate at lower speeds and use less engine power than assumed, suggesting that operational conditions and efficiency assessments need to be aligned more closely. Considering that ships operate using no more than 60% of the engine's power and that the average EPL is 56%, it is concluded that ships do not actually need to sail significantly slower than they currently do. This raises the question of how much the actual reduction in GHG emissions will be in the future. This essentially means that ships are not actually sailing at the speeds for which they were designed. This leaves room for improvement of existing ships, as they are likely not optimized to operate under these conditions.

The analysis from 2000 to 2020 reveals trends towards larger and wider ships, with notable exceptions such as LNG carriers. Designed speeds have decreased, while MCR trends vary by ship type. These changes reflect ongoing efforts to improve ship efficiency and adapt to regulatory requirements. The peak of vessels needing EPL occurred in 2008. Since then, EPL demand has decreased by 7.5%, while average EPL rose by 2%. However, from 2013, when the EEDI took effect, EPL increases have slowed to under 1%, with a resurgence in the number of ships requiring EPL.

For the first time, this study provided a concrete insight into the impact of global mandatory IMO measures (EEDI, EEXI, CII) on the energy efficiency performance across various tanker types and sizes.

While there have been significant improvements in ship efficiency and design, ongoing efforts are needed to address challenges in achieving regulatory compliance and optimizing ship performance. Future research and regulatory updates should focus on integrating real-world data, addressing variability across ship types, and continuing to advance efficiency standards. It is crucial to expand the database with more ships for deeper CII analysis which will provide a better view of fleet performance. To obtain a clearer understanding of overall energy efficiency in the maritime sector, it is important to broaden the research to cover additional types of ships within the commercial fleet.

CRediT authorship contribution statement

Matija Vasilev: Writing – review & editing, Visualization, Validation, Software, Investigation, Formal analysis, Data curation. **Milan Kalajdžić:** Writing – review & editing, Supervision, Resources, Project administration, Funding acquisition, Data curation, Conceptualization. **Nikola Momčilović:** Writing – review & editing, Writing – original draft, Supervision, Project administration, Methodology, Conceptualization.

Declaration of competing interest

The authors declare that they have no known competing financial interests or personal relationships that could have appeared to influence the work reported in this paper.

Acknowledgements

This work was supported by Ministry of Education, Science and Technological Development of Serbia (Project no. 451-03-65/2024-03/200105 from February 5, 2024). Authors would like to acknowledge Ocean Pro for its help in collecting data for the ship database.

Data availability

Data will be made available on request.

References

Adland, R., Cariou, P., Jia, H., Wolff, F.-C., 2018. The energy efficiency effects of periodic ship hull cleaning. J. Clean. Prod. 178, 1–13. https://doi.org/10.1016/j.jclepro.2017.12.247.

Ahn, J., You, H., Ryu, J., Chang, D., 2017. Strategy for selecting an optimal propulsion system of a liquefied hydrogen tanker. Int. J. Hydrogen Energy 42 (8), 5366–5388. https://doi.org/10.1016/j.ijhydene.2017.01.037.

Amoraritei, M., 2019. A preliminary propulsive performance evaluation for an oil tanker to meet EEDI challenge. The Annals of "Dunarea de Jos" University of Galati - Fascicle Xi - Shipbuilding 42, 103–108.

Barreiro, J., Zaragoza, S., Dias-Casas, V., 2022. Review of ship energy efficiency. Ocean Eng. 257. https://doi.org/10.1016/j.oceaneng.2022.111594.

Bayraktar, M., Yuksel, O., 2023. A scenario-based assessment of the energy efficiency existing ship index (EEXI) and carbon intensity indicator (CII) regulations. Ocean Eng. 278. https://doi.org/10.1016/j.oceaneng.2023.114295.

Berthelsen, F.H., Nielsen, U.D., 2021. Prediction of ships' speed-power relationship at speed intervals below the design speed. Transport. Res. Transport Environ. 99. https://doi.org/10.1016/j.trd.2021.102996.

Bortuzzo, V., De Domenico, M., Bucci, V., 2022. Strategies for ship decarbonisation: technical measure for reducing energy efficiency existing ship index. In: Rizzuto, E., Ruggiero, V. (Eds.), Technology and Science for the Ships of the Future, vol. 6, pp. 632–640.
Boumediene, K., Belhenniche, S.E., Beladjine, B.M., 2024. DFDE and steam turbine propulsion system, energy efficiency operational index comparison on board LNG carrier. J. Marit. Res. 21 (2), 373–380.
Czermanski, E., Oniszczuk-Jastrząbek, A., Spangenberg, E.F., Kozłowski, L., Adamowicz, M., Jankiewicz, J., Cirella, G.T., 2022. Implementation of the energy efficiency existing ship index: an important but costly step towards ocean protection. Mar. Pol. 145. https://doi.org/10.1016/j.marpol.2022.105259.
Chuah, L.F., Mokhtar, K., Ruslan, S.M.M., Bakar, A.A., Abdullah, M.A., Osman, N.H., Bokhari, A., Mubashir, M., Show, P.L., 2023. Implementation of the energy efficiency existing ship index and carbon intensity indicator on domestic ship for marine environmental protection. Environ. Res. 222. https://doi.org/10.1016/j.envres.2023.115348.
EC, 2021. Decarbonisation of Shipping, Technical Study on the Future of the Ship Energy Efficiency Design Index. Publications Office of the European Union. Report.
Equasis, 2020. The 2020 World Merchant Fleet - Statistics from Equasis. Report.
Equasis, 2021. The 2021 World Merchant Fleet - Statistics from Equasis. Report.
Ekanem Attah, E., Bucknall, R., 2015. An analysis of the energy efficiency of LNG ships powering options using the EEDI. Ocean Eng. 110 (Part B), 62–74. https://doi.org/10.1016/j.oceaneng.2015.09.040.
IMO, 2009. MEPC.1/Circ.684, Guidelines for Voluntary Use of the Ship Energy Efficiency Operational Indicator (EEOI). IMO, London, England.
IMO, 2011. Resolution MEPC.203(62. Amendments to the Annex of Protocol of 1997 to Amend the International Convention for the Prevention of Pollution from Ships, 1973, as Modified by the Protocol of 1978 Relating Thereto (Inclusion of Regulations on Energy Efficiency for Ships in MARPOL Annex VI). IMO, London, England. Available online. https://docs.imo.org/. (Accessed 9 April 2023).
IMO, 2016. Resolution MEPC.278(70. Amendments to the Annex of Protocol of 1997 to Amend the International Convention for the Prevention of Pollution from Ships, 1973, as Modified by the Protocol of 1978 Relating Thereto (Data Collection System for Fuel Oil Consumption of Ships). IMO, London, England. Available online. https://docs.imo.org/. (Accessed 9 April 2023).
IMO, 2018. Resolution MEPC.308(73). 2018 Guidelines on the Method of Calculation of the Attained Energy Efficiency Design Index (EEDI) for New Ships. IMO, London, England. Available online. https://docs.imo.org/. (Accessed 9 April 2024).
IMO, 2019. Resolution MEPC. 322(74. Amendments to the 2018 Guidelines on the Method of Calculation of the Attained Energy Efficiency Design Index (EEDI) for New Ships. IMO, London, England. Available online. https://docs.imo.org/. (Accessed 9 April 2024).
IMO, 2021a. Resolution MEPC.338(76). 2021 Guidelines on the Operational Carbon Intensity Reduction Factors Relative to Reference Lines (CII Reduction Factors Guidelines, G3). IMO, London, England. Available online. https://docs.imo.org/. (Accessed 9 April 2024).
IMO, 2021b. Fourth IMO greenhouse gas study 2020. Available online. https://www.imo.org/. (Accessed 9 April 2024).
IMO, 2021c. Resolution MEPC. 328(76. Amendments to the Annex of Protocol of 1997 to Amend the International Convention for the Prevention of Pollution from Ships, 1973, as Modified by the Protocol of 1978 Relating Thereto (2021 Revised MARPOL Annex VI). IMO, London, England. Available online. https://docs.imo.org/. (Accessed 9 April 2024).
IMO, 2021d. Resolution MEPC 335(76). 2021 Guidelines on the Shaft/Engine Power Limitation System to Comply with the EEXI Requirements and Use of a Power Reserve. IMO, London, England. Available online. https://docs.imo.org/. (Accessed 9 April 2024).
IMO, 2022a. Resolution MEPC.364(79). 2022 Guidelines on the Method of Calculation Od the Attained Energy Efficiency Design Index (EEDI) for New Ships. IMO, London, England. Available online. https://docs.imo.org/. (Accessed 9 April 2024).
IMO, 2022b. Resolution MEPC.350(78). 2022 Guidelines on the Method of Calculation of the Attained Energy Efficiency Existing Ship Index (EEXI). IMO, London, England. Available online. https://docs.imo.org/. (Accessed 9 April 2024).
IMO, 2022c. Resolution MEPC.351(78). 2022 Guidelines on Survey and Certification of the Attained Energy Efficiency Existing Ship Index (EEXI). IMO, London, England. Available online. https://docs.imo.org/. (Accessed 9 April 2024).
IMO, 2022d. Resolution MEPC.352(78). 2022 Guidelines on Operation Carbon Intensisty Indicators and the Calculation Methods (CII Guidelines, G1). IMO, London, England. Available online. https://docs.imo.org/. (Accessed 9 April 2024).
IMO, 2022e. Resolution MEPC.353(78). 2022 Guidelines on the Reference Lines for Use with the Operational Carbon Intensity Indicators (CII Reference Lines Guidelines, G2). IMO, London, England. Available online. https://docs.imo.org/. (Accessed 9 April 2024).
IMO, 2022f. Resolution MEPC.354(78). In: 2022 Guidelines on the Operational Carbon Intensisty Rating of Ships (CII Rating Guidelines, G4). IMO, London, England. Available online. https://docs.imo.org/. (Accessed 9 April 2024).
IMO, 2022g. Resolution MEPC.346(78). 2022 Guidelines for the Development of a Ship Energy Efficiency Management Plan (SEEMP). IMO, London, England. Available online. https://docs.imo.org/. (Accessed 9 April 2024).
IMO, 2022h. MARPOL Annex VI. Regulations for the Prevention of Air Pollution from Ships. Available online. https://www.imo.org/. (Accessed 5 March 2024).
IMO, 2022i. Consideration of the Report to MEPC 78, Report of the Twelfth Meeting of the Intersessional Working Group on Reduction of GHG Emissions from Ships (ISWG-GHG 12), 24th May 2022. https://www.imo.org/. (Accessed 1 October 2023).
ISO, 2024, seventh ed.. Products from Petroleum, Synthetic and Renewable Sources – Fuels (Class D) – Specifications of Marine Fuels. International Standard Organization, Geneva, Switzerland. ISO 8217:2024-05.
Inal, O.B., Deniz, C., 2021. Emission analysis of LNG fuelled molten carbonate fuel cell system for a chemical tanker ship: a case study. Marine Science and Technology Bulletin 10 (2), 118–133. https://doi.org/10.33714/masteb.827195.
Jia, H., Adland, R., Prakash, V., Smith, T., 2017. Energy efficiency with the application of Virtual Arrival policy. Transport. Res. Transport Environ. 54, 50–60. https://doi.org/10.1016/j.trd.2017.04.037.
Kalajdžić, M., Vasilev, M., Momčilović, N., 2022. Power reduction consideration for bulk carriers with respect to novel energy efficiency regulations. Brodogradnja 73 (2), 79–92. https://doi.org/10.21278/brod72205.
Li, X., Sun, B., Zhao, Q., Li, Y., Shen, Z., Du, W., Xu, N., 2018. Model of speed optimization of oil tanker with irregular winds and waves for given route. Ocean Eng. 164, 628–639. https://doi.org/10.1016/j.oceaneng.2018.07.009.
Lindstad, E., Bo, T.I., 2018. Potential power setups, fuels and hull designs capable of satisfying future EEDI requirements. Transport. Res. Transport Environ. 63, 276–290. https://doi.org/10.1016/j.trd.2018.06.001.
Liu, S., Papanikolau, A., Shang, B., 2022. Regulating the safe navigation of energy-efficient ships: a critical review of the finalized IMO guidelines for assessing the minimum propulsion power of ships in adverse conditions. Ocean Eng. 249. https://doi.org/10.1016/j.oceaneng.2022.111011.
Lu, R., Turan, O., Boulougouris, E., Banks, C., Incecik, A., 2015. A semi-empirical ship operational performance prediction model for voyage optimization towards energy efficient shipping. Ocean Eng. 110 (Part B), 18–28. https://doi.org/10.1016/j.oceaneng.2015.07.042.
Nian, V., Yuan, J., 2017. A method for analysis of maritime transportation systems in the life cycle approach – the oil tanker example. Appl. Energy 206, 1579–1589. https://doi.org/10.1016/j.apenergy.2017.09.105.
Papanikolaou, A., 2014. Ship Design – Methodologies of Preliminary Design, first ed. Springer, Dordrecht. https://doi.org/10.1007/978-94-017-8751-2.
Prados, J.M.M., Fernandez, I.A., Gomez, M.R., Parga, M.N., 2024. The decarbonisation of the maritime sector: horizon 2050, 75 (2), 1–26.
Psaraftis, H.N., 2021. Shipping decarbonization in the aftermath of MEPC 76. Cleaner Logistics and Supply Chain 1. https://doi.org/10.1016/j.clscn.2021.100008.
Rehmatulla, N., Smith, T., 2015. Barriers to energy efficiency in shipping: a triangulated approach to investigate the principal agent problem. Energy Pol. 1 (84), 44–57. https://doi.org/10.1016/j.enpol.2015.04.019.
RINA, 2000. Significant Ships. Publications of the Royal Institution of Naval Architects (RINA), London, 2023.
Rutherford, D., Mao, X., Comer, B., 2020. Potential CO2 reductions under the energy efficiency existing ship index. International Council on Clean Transportation 1–18. Working Paper 2020-27 1020.
Sou, W.S., Goh, T., Lee, X.N., Ng, S.H., Chai, K.-H., 2022. Reducing the carbon intensity of international shipping – the impact of energy efficiency measures. Energy Pol. 170. https://doi.org/10.1016/j.enpol.2022.113239.
Stec, M., Tatarczuk, A., Iluk, T., Szul, M., 2021. Reducing the energy efficiency design index for ships through a post-combustion carbon capture process. Int. J. Greenh. Gas Control 108. https://doi.org/10.1016/j.ijggc.2021.103333.
Sui, C., Stapersma, D., Visser, K., de Vos, P., Ding, Y., 2019. Energy effectiveness of ocean-going cargo ship under various operating conditions. Ocean Eng. 190. https://doi.org/10.1016/j.oceaneng.2019.106473.
Taskar, B., Andersen, P., 2020. Benefit of speed reduction for ships in different weather conditions. Transport. Res. Transport Environ. 85. https://doi.org/10.1016/j.trd.2020.102337.
Trivyza, N.L., Rentizelas, A., Theotokatos, G., 2020. A comparative analysis of EEDI versus lifetime CO2 emissions. J. Mar. Sci. Eng. 8 (61). https://doi.org/10.3390/jmse8010061.
UNCAD, 2022. Review of Maritime Transport 2022 – Navigating Stormy Water. UN. https://doi.org/10.18356/9789210021470.
UNCAD, 2023. Review of Maritime Transport 2023 – towards a Green and Just Transition. UN. https://unctad.org/system/files/official-document/rmt2023_en.pdf. (Accessed 24 September 2023).
Yang, H., Ma, X., 2019. Uncovering CO2 emissions patterns from China-oriented international maritime transport: decomposition and decoupling analysis. Sustainability 11 (10). https://doi.org/10.3390/su11102826.
Yuan, J., Nian, V., He, J., Yan, W., 2019. Cost-effectiveness analysis of energy efficiency measures for maritime shipping using a metamodel based approach with different data sources. Energy 189. https://doi.org/10.1016/j.energy.2019.116205.
Zhang, S., Li, Y., Yuan, H., Sun, D., 2019. An alternative benchmarking tool for operational energy efficiency of ships and its policy implications. J. Clean. Prod. 240. https://doi.org/10.1016/j.jclepro.2019.118223.
Zincir, B., 2023. Slow steaming application for short-sea shipping to comply with the CII regulation. Brodogradnja 74 (2), 21–38. https://doi.org/10.21278/brod74202.

ПРИЛОГ 5

Ocean Engineering 356 (2026) 125429

Contents lists available at ScienceDirect

Ocean Engineering

journal homepage: www.elsevier.com/locate/oceaneng

Research paper

On energy efficiency of the container ship fleet: EEDI, EEXI and CII

Matija Vasilev *, Milan Kalajdžić, Nikola Momčilović, Filip Miltenović

Department of Naval Architecture, Faculty of Mechanical Engineering, University of Belgrade, 11120, Belgrade, Serbia

ARTICLE INFO

Keywords:
Shipping decarbonization
Energy efficiency
EEDI
EEXI
CII
Container ships

ABSTRACT

The maritime sector has gained significant experience in complying with regulations supporting global decarbonization and reducing greenhouse gas emissions from shipping. Key instruments driving this transition are the International Maritime Organization's (IMO) Energy Efficiency Design Index (EEDI), Energy Efficiency Existing Ship Index (EEXI), and Carbon Intensity Indicator (CII). While many studies address individual vessels or small fleets, large-scale analyses combining all three indices remain scarce, especially for container ships, which play a major role in global trade. This study reviews existing literature on compliance and the effectiveness of technical and operational measures for container ships, then evaluates 162 vessels built between 2000 and 2020, from small feeders to ultra-large container ships (ULCS). The analysis includes EEDI and EEXI for all vessels and CII for 21, examining trends in key design parameters. Results show that most ships initially met EEDI limits, but compliance has declined, while EEXI and CII performance remain considerably lower. The main adaptation strategy is slow steaming, with an average speed reduction of 33%. Overall, findings suggest that future compliance with IMO decarbonization goals will require major design changes and the adoption of alternative fuels, as existing operational measures are nearing their limits.

1. Introduction

To pursue the decarbonization of shipping, international regulations have increasingly mandated compliance with progressively stricter criteria, fundamentally influencing ship design, operational practices, and fleet management strategies. A systematic evaluation of how energy efficiency measures have shaped compliance, ship design, and performance across different fleet size categories is of growing importance for both industry and policy makers (DNV, 2025). This is particularly relevant for container ships, as they represent one of the most significant fleet segments driving the maritime sector, emissions from shipping, and global trade. In fact, the container ship fleet increased by 9.7% in deadweight between 2024 and 2025, representing by far the largest growth among all ship types, and accounting for the largest share of newbuilds in 2024 (41.3%), (UNCAD, 2024; UNCAD, 2025).

Accordingly, this section examines prior work and is organized into three main parts. The first part presents a focused review of the IMO regulatory framework on energy efficiency, with a special focus on three mandatory instruments that directly shape the energy efficient-based design of ships: EEDI, EEXI and CII. The second part reviews literature addressing the progress of energy efficiency and compliance with these regulations, while the third identifies existing research gaps and outlines the key contributions of this study.

1.1. Review of IMO's energy efficiency regulatory framework

The concept of ship energy efficiency indices was first introduced in 2009 with the Energy Efficiency Operational Indicator (EEOI), expressed as the amount of CO_2 emitted (in grams) per ton of cargo transported per nautical mile (IMO, 2009). Although never made mandatory, the EEOI was promoted as a voluntary tool for assessing a ship's actual operational efficiency and served as a precursor to forthcoming mandatory measures. It could be applied to a single voyage, multiple voyages, or to one or more ships, and it represented the first step toward quantifying operational efficiency.

In 2011, the International Maritime Organization (IMO) adopted the EEDI which became mandatory for all ships above 400 gross tons built after January 1, 2013, or delivered after January 1, 2015 (IMO, 2011). The EEDI measures the nominal (theoretical) amount of CO_2 emitted per ton of cargo per nautical mile (IMO, 2018; IMO, 2019; IMO2022a). Compliance requires that the attained EEDI of a ship be lower than the required value, which is calculated from a reference line based on the average efficiency of similar ships built between 2000 and 2010. Despite its wide application, almost half of the world fleet remains outside the

* Corresponding author.
E-mail addresses: matija.vasilev@gmail.com, matija@oceanpro.eu (M. Vasilev).

https://doi.org/10.1016/j.oceaneng.2026.125429
Received 3 November 2025; Received in revised form 31 March 2026; Accepted 1 April 2026
Available online 4 April 2026

scope of EEDI, as ships below 400 gross tons and fishing vessels are exempt (Equasis, 2020).

As the number of pre-2013 ships in operation had remained high and unaddressed in terms of energy efficiency, the IMO introduced the EEXI in 2019, which entered into force in 2023 (IMO, 2022b). Similar in concept to the EEDI, the EEXI represents the nominal CO_2 emitted per ton of cargo per nautical mile but applies to ships above 400 gross tons built before 2013. As with EEDI, compliance requires that the attained value does not exceed the required value, which is determined relative to reference lines for each ship type. The key difference between the two indices lies in the reduction factors (IMO, 2021a). For EEDI, reduction factors vary by ship type and year of construction, and have been phased in gradually since 2013, tightening progressively until 2025. In contrast, EEXI reduction factors were fixed from the outset, depending on ship type, and largely aligned with the final-phase EEDI values.

However, because EEDI and EEXI are based on nominal design values, they do not reflect the operational realities of navigation. To address this limitation, the IMO introduced the CII in 2023, applying to ships above 5000 gross tons (IMO, 2022c; IMO, IMO, 2022d; IMO, 2022e). This measure represents the actual amount of CO_2 (in grams) emitted per ton of cargo transported per nautical mile and has been designed to encourage the monitoring of emissions during operation. Note that, prior to the introduction of CII, the IMO established the Data Collection System (DCS) in 2019, under which operators of ships above 5000 gross tons were required to record fuel consumption, sailing time, and distance traveled (IMO, 2016).

The attained CII for a given year is calculated from the operational data recorded in the previous year and is compared with the required CII, which is derived from a reference value adjusted by a reduction factor that changes every two years. Consequently, each ship is assigned with an energy rating of A, B, C, D, or E based on its deviation from the required value. While an A rating is desirable, ratings of B or C are also considered acceptable. At the same time, the rating for the next three years is also projected in addition to that of the current year. If a ship is rated D for three consecutive years, or E in any single year, the operator must prepare a corrective plan outlining measure to achieve at least a C rating.

EEDI, EEXI and CII measures are presented in MARPOL Annex VI (IMO, 2022f). Utilizing DCS and EEOI can enhance the operational dimension of improving EEDI, EEXI, and CII. Specifically, the targets aim to reduce total annual GHG emissions from international shipping by at least 20% (working towards 30%) by 2030, and by at least 70% (working towards 80%) by 2040, relative to 2008 levels, according to (IMO, 2023). Furthermore, global emissions are expected to peak as soon as possible, with the ultimate goal of achieving net-zero emissions by 2050.

To conclude, the main difference between EEDI, EEXI, and CII lies in their underlying approach. The first two indices are based on nominal input parameters and therefore do not fully reflect the operational nature of ship navigation. However, their calculation procedures and required inputs are simpler, making them suitable for estimating energy efficiency levels, particularly in qualitative analyses. In contrast, although CII requires more extensive operational data, which are often not readily available, it has the potential to provide a more accurate assessment of the actual energy efficiency of container ships.

1.2. Literature review

A substantial body of research has emerged over the past decade addressing ship energy efficiency measures from multiple perspectives, ranging from operational and design measures to digital optimization tools. Collectively, these studies demonstrate the breadth of strategies available for compliance with IMO regulations. Accordingly, this subsection begins with a general overview of the current position of container ship fleets in the context of decarbonization. It then examines two of the most widely adopted operational strategies for improving energy efficiency, slow steaming and voyage optimization, which are primarily applied to existing ships. The following part discusses ship design considerations, emphasizing hull form and propulsion system optimization, as well as the use of energy-saving technologies (ESTs). While hull form and propulsion optimization are generally associated with newbuilds, ESTs are applicable to both new and existing ships due to their ease of retrofit. Furthermore, the ship design approach with the highest potential for achieving full decarbonization lies in the adoption of alternative fuels. Finally, two measures relevant to maintenance and operational phases, hull cleaning and the application of deep learning techniques, are examined.

The scope of this review excludes less established technologies, such as wind-assisted or nuclear propulsion, due to insufficient data and limited available evidence regarding their energy efficiency performance. It should be noted that numerous other studies have been conducted on this topic, many of which report similar or overlapping findings. However, we believe that the literature reviewed here is sufficient to support the conclusions presented, as the inclusion of additional works would not materially alter the findings of this study.

1.2.1. Overview

Analysis of the modern merchant fleet by (Lysyy et al., 2018) revealed a substantial increase in both the number and size of container ships, with the average carrying capacity of vessels built between 2015 and 2018 growing by nearly 2.8 times compared with those built 15-19 years earlier. This expansion, combined with the tendency of container ships to operate at maximum speeds regardless of weather conditions, has resulted in higher propulsion power demands, greater fuel consumption, and increased emissions. According to (Olmer et al., 2017), CO_2 emissions from container ships amount to approximately 205 million tons, representing about 23% of total shipping emissions. Study by (Tran and Tran, 2023) examined the emissions of a global container ship fleet and their environmental impacts on regional ports. Using a bottom-up modeling approach based on voyage data, the study analyzed Maersk Line's fleet of 653 ships (3.52 million TEU capacity) operating over 1,043,845 nautical miles per week. The fleet was estimated to generate 683,428 tonnes of CO_2 and other pollutants weekly, corresponding to an external cost of approximately €202.3 million. Emissions were concentrated along major East–West shipping routes linking East Asia, Europe, and North America, with the highest in-port emissions observed in East Asia, Europe, and the Mediterranean due to the concentration of operations at key strategic ports. Assessment of a Turkish container ship by (Tokuşlu, 2020) confirmed compliance with IMO EEDI regulation. However, this is a single case study made for the IMO requirements at the time. In contrast (Serra and Fancello, 2020), stated that while no single measure can achieve full decarbonization, combinations of current technologies, supported by policies, financial incentives, and research, can make significant progress.

1.2.2. Slow steaming

Since the introduction of energy efficiency regulations, slow steaming has been the predominant fleet-wide response, particularly among container ships, which typically operate at higher speeds than other major ship types and therefore offer greater potential for speed reduction. Modeling by (Sames and Köpke, 2012) confirmed that slow steaming is the most effective short-term measure for reducing fuel consumption and emissions without technological modification. The analysis further confirmed that larger container ships achieve lower CO_2 emissions per transported TEU and increase their energy efficiency, reflecting the benefits of economies of scale. In addition (Meyer et al., 2012), demonstrated that reducing speed substantially lowers fuel costs and allows determination of an optimal operating speed that maximizes both economic and environmental efficiency. Although the optimal speed varies with route, ship type, and operating conditions, the overall trend confirms that slower, strategically planned sailing maximizes energy efficiency while supporting IMO emission reduction targets,

according to (Woo and Moon, 2014). The same study also showed that by optimizing speed relative to fuel prices, ship design, and carbon costs, shipping companies can achieve both economic and environmental benefits. Similar conclusions were reached by (Kontovas and Psaraftis, 2011; Elkafas et al., 2023) who likewise highlighted the dual advantages of speed optimization for emissions reduction, energy efficiency compliance and profitability. In addition (Kontovas and Psaraftis, 2011), emphasized that minimizing port time is critical for improving overall energy efficiency of container ships. They examined the relationship between engine load, fuel consumption, and ship speed using regression analysis to model emission reductions along the maritime intermodal container chain at the time.

More focused case studies have quantified the actual benefits of slow steaming. For example (Elkafas and Shouman, 2021), assessed the environmental and energy efficiency benefits of speed reduction using a medium-sized container ship as a case study. A 12.6% decrease in ship speed resulted in a 36% reduction in CO_2 emissions, a 31.7% improvement in EEDI, and a 26.5% reduction in EEOI, satisfying both current and future IMO energy efficiency requirements. Moreover (Elkafas et al., 2023), evaluated the technical, environmental, and economic impacts of service speed reduction for container ships ranging from 2500 to 15,000 TEU. The study found that smaller vessels can meet EEXI requirements at approximately 19 knots, while larger ships require speeds of 21.5 knots or lower. Maintaining speeds at or below 19.5 knots keeps CII ratings within the A–C range, and the accompanying operational and economic analyses demonstrated how speed reduction affects annual profit margins depending on ship size and carbon taxation. Further evidence is provided by (Woo and Moon, 2014), who analyzed the effects of slow steaming on environmental performance in liner shipping, showing that reducing voyage speeds to 15–18 knots on major routes can significantly lower fuel consumption and CO_2 emissions. Beyond low or moderate speed reductions (Woo and Moon, 2014), examined more substantial cases of speed reduction. On the Asia–North Europe route, they reported that by 2011 approximately 93% of liner services had adopted slow steaming, reducing average voyage speeds from 23 to 25 knots in 2008 to 15–18 knots, a practice often referred to as ultra-slow steaming (Kalajdžić et al., 2022a). assessed the energy efficiency of existing cargo ships, including three container vessels, and determined the exact Maximum Continuous Rating (*MCR*) reduction required for each ship to comply with EEXI regulations. More importantly, the authors demonstrated that different methods for determining input parameters can affect the results. For example, statistically derived inputs and sea-trial data can lead to significantly different energy efficiency scores. Slow steaming is primarily achieved through the implementation of Engine Power Limitation (EPL) (Kalajdžić et al., 2022a; Bayraktar and Yüksel, 2023a).

In summary, slow steaming has proven to be the most effective short-term measure for reducing fuel consumption and therefore complies with IMO's energy efficiency regulations in container shipping, largely due to the higher operating speeds of these vessels compared with other ship types and the absence of design modifications. In that context, EPL is the most widely used approach. However, as decarbonization efforts progress and regulatory requirements tighten, slow steaming has reached its practical limits, as the margin for further speed reduction without compromising transport efficiency is nearly exhausted. Moreover, many ships are now operating at speeds for which they were not originally designed, resulting in a loss of optimal performance.

1.2.3. Voyage optimization

Improving optimization techniques for voyage planning has been shown to enhance CII ratings (Gałecka, 2024; Rauca and Batrinca, 2023) indicated that applying current CII methods may not always reduce overall emissions, suggesting a potential need for revised metrics, such as calculating an average CII at the company level rather than per ship. Case studies on container ships, bulk carriers, and tankers show that CII is highly influenced by idle and laden voyages (Vasilev et al., 2025). Effective cooperation between shipowners and charterers, reduction of port and anchoring times, and just-in-time scheduling can be critical for optimizing CII performance, highlighting the importance of detailed voyage planning and operational adjustments. The research by (Kim and Eom, 2023) has proposed operational strategies, such as a just-in-time arrival policy, to reduce emissions by converting waiting time at ports into voyage time. Case studies at the Pusan International Container Terminal demonstrated reductions in carbon emissions by an average of 45.8% and up to 91%, with 87% of ships improving their CII rank. The approach also extended compliance with carbon regulations by an average of eleven years, emphasizing the potential of operational measures to decarbonize shipping without modifying propulsion systems. Another investigation by (Sevgili et al., 2025) evaluated the effect of cold ironing (CI) on container ships' CII performance using projected data from 183 voyages between 2023 and 2030. Results show that CII compliance declines sharply over time, with only 19.7% of voyages meeting the reference value by 2030 without additional measures. CI eliminates over 12,500 tons of fuel consumption during port stays, significantly lowering emissions. In addition, optimizing a ship's trim during navigation has been found to have a notable effect on overall energy efficiency (Vasilev et al., 2024; Gatin et al., 2024).

Optimized voyage planning influences operational efficiency and thus has a direct impact on CII. Improved routing and port scheduling may yield modest reductions in fuel consumption and emissions, supporting, though not ensuring, regulatory compliance.

1.2.4. Ship design considerations: hull form, propulsion systems and energy saving technologies (ESTs)

Ship design plays a central role in achieving energy efficiency and meeting environmental requirements, particularly in the case of newbuild vessels. Thus (Garbatov and Georgiev, 2021), emphasized the need for a paradigm shift in conceptual design to balance regulatory compliance with end-of-life costs, identifying EEDI requirements as key drivers of optimization, as studies on tankers (Vasilev et al., 2024) and bulk carriers (Kalajdžić et al., 2022b) further demonstrate that main dimensions, propulsion design, seakeeping, and maneuverability must be balanced with energy efficiency and freight rates to achieve optimal designs.

Apart from the operational measures adopted through the slow steaming approach, efforts to enhance energy efficiency were also supported by a hull form design optimization for the resistance reductions, engine and propeller modifications, and incorporation of energy-saving devices.

(Kim and Park, 2015) demonstrated that hull form optimization for ultra-large container ships (ULCS) can reduce resistance and enhance propulsion efficiency, as verified through CFD simulations and model testing. The study employed a four-step approach: reviewing design procedures with environmental and economic considerations, analyzing single and twin-skeg hulls, optimizing hull forms through CFD and experimental validation, and refining them for operational draught and speed. The results confirmed measurable gains in energy efficiency.

(Constantin and Amoraritei, 2018) showed that achieving EEDI compliance requires a careful balance of propulsive performance parameters. Analyses of two container ships (800 and 1805 TEU) highlighted the need to optimize main engine selection and redesign propellers to meet power requirements. The results further emphasized that compliance with IMO energy efficiency standards depends on balancing ship capacity, engine power, speed, and fuel consumption. In line with previous findings for EEDI (Wiliyan et al., 2023), indicated that nearly 80% of ClassNK container ships will require technical adjustments, primarily to the propulsion system, to achieve EEXI compliance, with EPL highlighted as a principal solution. Engine sizing, together with speed reduction, has also been identified as a major factor in achieving IMO compliance (Bayraktar and Yüksel, 2023a). Moreover, the use of larger slow-speed two-stroke diesel engines, propeller redesign, and waste heat recovery systems such as the Organic Rankine Cycle

(ORC) can improve propulsion performance and reduce energy losses. Implementing ORC systems has been shown to enhance overall efficiency and lower fuel consumption (Elkafas, 2024), with demonstrated installations recovering heat from engine exhaust or jacket water even at relatively low temperatures (Sellers, 2017).

Quantified gains in energy efficiency have been achieved through the application of energy-saving technologies (ESTs) in propeller design (Jin et al., 2023). investigated the optimization of blade position on an asymmetric pre-swirl stator (PSS) applied to a 2500 TEU LNG-fueled feeder container ship. Using a potential-based program, the study optimized blade position, pitch angle, and spacing, achieving a 0.59% efficiency gain compared with the initial design and an additional 0.13% through tip rounding. When combined with a rudder bulb, the total efficiency improvement reached 3.56%. Moreover (Nadery and Ghassemi, 2020), numerically investigated the hydrodynamic performance of a propeller with and without a wake equalizing duct (WED) installed ahead of the propeller to improve wake flow and efficiency on a KCS model with a KP505 propeller. The results showed that a well-designed WED can increase efficiency by up to 1.67%, whereas a poorly designed duct may decrease it by 3.25%. More than 1800 ships are currently equipped with Propeller Boss Cap Fins (PBCF) (Nojiri et al., 2011), which reduce hub vortex energy loss and can lower fuel consumption by approximately 5% at constant speed or increase vessel speed by about 2% for the same fuel use (Lim et al., 2014). investigated Propeller Boss Cap Fin (PBCF) and hub cap designs for a 6000 TEU container ship to improve propulsion efficiency. The results showed that a divergent hub cap increased open-water efficiency by approximately 2% compared with a conventional cap, confirming the CFD predictions. However, attaching PBCF models to the divergent hub cap reduced efficiency due to a higher torque coefficient. Retrofitting older ships (Katelieva, 2023) through modifications to propeller (Cicek and Yilmaz, 2023) and bow design (Vasilev et al., 2023), can enhance energy efficiency and provide additional benefits, such as reduced underwater noise (ZoBell et al., 2023). Ships are increasingly equipped with ESTs to meet environmental regulations and enhance energy efficiency by recovering rotational energy from the propeller.

Hull form optimization and modifications to propulsion systems can yield measurable improvements in energy efficiency scores; however, the gains are relatively small for ships that are already well optimized. ESTs have proven suitable as retrofits for existing ships seeking compliance with EEXI and CII requirements at the moment. Nevertheless, their combined benefits, together with those of hull form optimization and propulsion system modifications, are insufficient on their own to meet future IMO energy efficiency targets.

1.2.5. Fuels

More radical efforts to improve energy efficiency have been focused on investigating the potential of alternative fuels (Bayraktar and Yüksel, 2023a). assessed the impact of EEXI and CII regulations on five ship types, including bulk carriers, gas carriers, tankers, general cargo, and container ships, across seven operational scenarios. The results showed that compliance is highly challenging for ships operating on conventional fuels (MDO, HFO) without EPL, which provides a significant compliance advantage, as previously discussed in relation to slow steaming. Switching to alternative fuels such as LNG or methanol is effective in meeting regulatory thresholds. Dual-fuel engines, particularly those using LNG, were found to be sensitive to primary fuel specifications and mixing ratios, whereas converting conventional engines to methanol substantially reduces EEXI values and improves CII ratings. Similarly (He et al., 2024), assessed four marine fuels (VLSFO, MGO, LNG, and Methanol) with respect to EEXI and CII requirements for a container ship. Results indicate that Shipboard Carbon Capture and Storage (SCCS) can substantially reduce operational emissions, with VLSFO ships achieving a 61% reduction. While fossil methanol lowers combustion emissions, its life-cycle emissions are 17.5–19.6% higher than conventional fuels. Overall, SCCS improves EEXI and CII ratings, enabling VLSFO- and MGO-fueled ships to comply with IMO greenhouse gas targets until 2030 (IMO, 2020) and LNG- and Methanol-fueled ships beyond 2030.

Transitioning from conventional heavy fuel oil to LNG or dual-fuel engines can lead to significant reductions in CO_2, SO_x, and NO_x emissions (Elkafas et al., 2021; Park et al., 2023) examined technical measures to improve the EEDI for a 50K DWT container ship in line with IMO CO_2 reduction regulations. The results showed that switching from diesel oil to LNG reduced EEDI by approximately 27%, while speed reduction provided an additional 22% improvement. The study concluded that a combination of LNG fuel conversion, speed reduction, energy-saving devices, and CO_2 capture is required to achieve full compliance with future IMO regulations. Different alternative fuels were investigated in relation to achieving compliance with CII requirements by (Zhang et al., 2024) who found that larger ships using LNG or methanol, as well as zero-carbon fuels such as hydrogen and ammonia, are consistent with IMO CII targets. Similar conclusions were reached by (Bayramoglu, 2024), who showed that methanol significantly improves EEXI performance, while hydrogen and ammonia can fully satisfy IMO energy efficiency targets (Elmallah et al., 2025). through a case study on the container ship, demonstrated that dual-fuel engines operating on 89% natural gas and 11% methanol, or 91% methanol and 9% MDO, can meet EEDI requirements (Ahn et al., 2023). evaluated EPL, energy-saving devices, and alternative fuels based on marginal abatement cost. Among the five case studies, LNG fuel retrofit emerged as the most effective solution for meeting EEXI and CII requirements for the Korean container fleet. This is particularly important given South Korea's "2030 Green Ship-K Initiative," which aims to introduce 140 environmentally friendly merchant ships and promote sustainable shipping. In another paper (Lehmann et al., 2025) analyzed operational data from 16 container ships monitored between 2018 and 2021 and found that more than half of the fleet will need to transition to alternative fuels to achieve CII compliance.

(Ammar and Seddiek, 2020) examines the impact of emission reduction strategies on container ships, focusing on the improved EEDI from both environmental and economic perspectives. Using A19 and A7 class container ships as case studies, three combined strategies were evaluated: natural gas use, exhaust treatment equipment, and speed reduction. The A19 achieved the lowest annual emissions per transported cargo, with 18.9 kg/TEU NO_x, 0.93 kg/TEU SO_x, and 1.8 kg/TEU CO_2. For the A7, reducing ship speed by 22.5% enables compliance with all three IMO EEDI phases, achieving CO_2 reduction at a cost-effectiveness of 52.54 $/ton CO_2. Additionally, utilizing the A19's dual-fuel engine improves energy efficiency by 10.13% and yields annual fuel savings of 23.73 million USD.

In addition, hybrid systems incorporating batteries or photovoltaic (PV) solar panels can enhance energy savings and reduce emissions, particularly in supplying auxiliary power (Piazza et al., 2024).

A recent study by (Uygur et al., 2026) employed a system dynamics model to evaluate different decarbonization pathways in container shipping, showing that operational measures such as speed reduction can provide short-term emission reductions, while significant long-term decarbonization requires large-scale adoption of alternative fuels such as LNG, methanol, and hydrogen. Traditional fuels have reached their limits within the slow steaming approach. To meet IMO energy efficiency requirements under EEDI, EEXI, and CII, a substantial portion of the container ship fleet will need to transition to at least dual-fuel engines operating on LNG or methanol, with zero-carbon fuels representing the ultimate pathway toward full decarbonization.

1.2.6. Hull cleaning

Timely hull cleaning has also been shown to optimize fuel consumption, according to (Vasilev and Kalajdžić, 2022). Ship resistance, particularly the frictional component, increases over time due to biofouling, leading to higher fuel consumption and power demand. This deterioration directly impacts compliance with mandatory EEXI and CII

requirements (Bayraktar and Yüksel, 2023b). examined the impact of anti-fouling systems on EEXI and CII ratings using a container ship case study. Scenarios representing high, medium, and low anti-fouling effectiveness showed that while high-performance coatings can maintain compliance with reference values in the short term, biofouling significantly challenges energy efficiency over time. The results indicated that without effective anti-fouling measures, a ship may sustain a CII rating of C only until 2026, after which performance declines to D–E levels. The study underscores the importance of robust anti-fouling strategies for maintaining energy efficiency and long-term regulatory compliance. AIS data indicate that idling among container ships has increased sharply in recent years, with many vessels remaining idle for more than 30 days (Hoffmann, 2022), particularly in biofouling-prone regions. In such conditions, effective antifouling coatings are essential for maintaining hull performance during extended idle periods. Proper biofouling management enables operators to reduce fuel consumption, enhance energy efficiency, and maintain compliance with evolving environmental regulations. Moreover, containerships were shown to be particularly affected by biofouling during long idle periods in warm waters, which increases hydrodynamic drag, fuel consumption, thereby degrading CII ratings (Bayraktar and Yüksel, 2023a).

Hull cleaning can serve as an effective maintenance strategy to improve energy efficiency ratings; however, it should be considered only as a complementary measure to more substantial interventions.

1.2.7. Deep learning

Wang et al., (2024) proposed a Long Short-Term Memory model with a self-attention mechanism (SA-LSTM) to forecast hourly fuel consumption and CII, as well as annual CII ratings for a 2400 TEU container ship. Compared with ten alternative models, the SA-LSTM achieved the highest prediction accuracy, reducing fuel consumption errors by up to 20% and providing the most reliable estimates of annual CII performance. Furthermore (Alshareef and Alghanmi, 2024), explored the application of deep reinforcement learning (DRL) to optimize maritime energy efficiency across various ship types and operational scenarios. By dynamically adjusting engine parameters and integrating alternative fuels such as bio-LNG and hydrogen, DRL-based approaches achieved notable improvements in fuel efficiency, EEXI, and CII performance compared with conventional optimization methods. Reported benefits include fuel efficiency gains of up to 10%, reductions in EEXI values by 8–15%, and CII improvements of 10–30%, demonstrating the potential of DRL to reduce emissions and enhance operational performance under diverse cargo loads and operating conditions. Data collection, AI-based predictive models, and artificial neural networks (ANNs) have been shown to enhance energy management and emission forecasting by utilizing real-time operational data, including weather, load conditions, and main engine parameters (Ozsari, 2023; Wang et al., 2021) shows that simply requiring a ship's annual CII to remain below a reference value could paradoxically increase emissions. This highlights the need for more sophisticated models, informed by real operational data to assess CII effectiveness.

Overall, the integration of deep learning techniques has so far provided a framework for enhancing ship energy efficiency, improving prediction accuracy, and supporting compliance with IMO energy efficiency regulations, although still on a limited scale.

1.2.8. General conclusions

The reviewed literature demonstrates that achieving compliance with IMO's EEDI, EEXI, and CII regulations requires an integrated approach that combines operational, technical, and design measures. For existing container ships, slow steaming, voyage optimization, trim control, and hull maintenance have proven to be the most practical short-term strategies for improving energy efficiency. However, these measures alone are insufficient to meet forthcoming regulatory targets. For newbuilds, hull form and propulsion optimization, along with the integration of ESTs, provide incremental efficiency gains but remain limited in scale. Emerging deep learning methods are expected to play an increasingly important role in operational planning and performance forecasting. In contrast, transitioning to alternative fuels, and ultimately, zero-carbon fuels like hydrogen and ammonia offers the most substantial long-term potential for compliance.

1.3. Key contribution and research gap

While several studies and regulatory reports have analyzed EEDI, EEXI and CII individually or in the context of specific fleets, most existing analyses rely on heterogeneous datasets, often including vessels of widely varying design quality, or focus on limited case studies and operator-specific fleets. In contrast, the present study evaluates a carefully selected dataset of 162 modern container ships built between 2000 and 2020, primarily representing well-designed and technologically advanced vessels. This enables a more realistic assessment of the actual limits for further improvements in energy efficiency in already optimized ships. The analysis is performed within a consistent methodological framework and structured across multiple vessel size categories, allowing a more practical interpretation of compliance trends as a function of ship capacity. In addition, both historical and current regulatory requirements are considered, providing points into the evolution of energy efficiency standards over time. Finally, the study offers a combined and consistent evaluation of design-based indices (EEDI and EEXI) and operational performance (CII), while also quantifying the engine power limitation required for regulatory compliance, based on a dataset of this size and quality, which is currently lacking in the available literature. By analyzing ships built over a 20-year period, the study seeks to determine whether container ships have become more energy-efficient and operationally effective over time. The analysis examines changes in key design parameters, such as principal dimensions, engine power, speed, and cargo capacity, to understand how design standards and priorities have evolved. Furthermore, it investigates the actual operational performance of these vessels to assess whether they are used in accordance with their original design intent. The outcomes of this research are expected to provide insights into the relationship between design evolution and real-world performance, identify trends in operational speed, and highlight where design assumptions align or diverge from practical operation. These findings can inform future ship design, energy efficiency strategies, operational planning, and policy development. Moreover, the review of regulations and accompanying literature synthesis presented in this section provide a valuable contribution to this research, as they directly interpret and consolidate the key insights reported to date on this topic. Similar comprehensive analyses have been conducted for tankers (Vasilev et al., 2025) and bulk carriers (Kalajdžić et al., 2022b).

The main limitation of this study lies in the nature of the fleet sample. Ships built after 2020 were excluded from the analysis due to the distorting effects of the COVID-19 pandemic on global shipbuilding trends. Although sampling was influenced by data availability and therefore does not represent the entire population of container ships, the conclusions drawn apply reliably to the sample analyzed. It is also important to note that the selected fleet was not entirely random. The vessels were deliberately chosen from a reliable source and were built in some of the most advanced shipyards at the time of construction. The sample excludes ships equipped with alternative fuels or significant energy-saving technologies (ESTs), allowing the assessment to focus on conventional, baseline designs. Consequently, the selected vessels represent some of the most proven and efficient designs in the industry from a traditional naval architecture perspective. This approach provides a clearer understanding of how well proven conventional ship designs comply with energy-efficiency regulations, ensuring that the influence of novel technologies does not obscure the broader assessment of baseline design performance.

2. Database

The database used in this study comprises 162 seagoing container ships built between 2000 and 2020, all designed for the carriage of standard TEU containers. Ships were classified by TEU capacity into Small Feeder, Feeder, Feedermax, Panamax, Post-Panamax, Neo-panamax, and ULCS categories (Table 1). The primary data source for this study was *Significant Ships* (RINA, 2000-2020), an annual publication of the Royal Institution of Naval Architects (RINA) that features the most notable ships delivered each year. Supplementary data was obtained from shipyard records, operator and owner websites, AIS tracking information, and other publicly available sources (see Figs. 1 and 2).

The Significant Ships database primarily includes vessels representing notable technological developments or important deliveries in a given year. As a result, the dataset may contain a slight bias toward technologically advanced designs compared with the global fleet average. Nevertheless, because these ships originate from a wide range of shipyards and operators worldwide, they still provide a meaningful representation of mainstream container ship design trends.

The relationships between deadweight (*DWT*) and key design parameters of the analyzed fleet, including length overall (L_{OA}) – Fig. 3, breadth (*B*) – Fig. 4, height (*H*) – Fig. 5, scantling draft (*T*) – Fig. 6, propeller diameter (*D*) – Fig. 7, displacement (Δ) – Fig. 8, design speed (*V*) – Fig. 9 and main engine power (*MCR*) in Fig. 10 are shown. The relationships for L_{OA}, *B*, *H*, *T*, and *D* exhibit a near-logarithmic increase with *DWT*, reflecting the natural scaling of ship geometry as carrying capacity grows. Displacement shows a linear correlation with *DWT*, consistent with expectations since *DWT* and displacement are related through constant lightweight and reserve buoyancy assumptions.

More variability is observed in the correlations for design speed and *MCR*. The *DWT*–*MCR* relationship shows a moderate correlation ($R^2 \approx 0.84$), capturing the general trend of increasing installed power with higher carrying capacity but also revealing significant scatter that reflects variations in engine selection, hull form and design philosophy among shipbuilders. The *DWT*–*V* relationship is even less pronounced ($R^2 \approx 0.58$), indicating that speed is a function not only of size but also of evolving operational profiles, with many ships designed for lower service speeds in the later years of the sample. These findings suggest that while principal dimensions scale predictably with *DWT*, propulsion power and speed are subject to greater variability driven by market conditions and regulatory influences.

Temporal evolution of principal containership parameters over the 2000–2020 period is presented in Fig. 11 – L_{OA}, Fig. 12 – B, Fig. 13 – H, Fig. 14 – T, Fig. 15 – D, Fig. 16 – V, Fig. 17 – MCR, Fig. 18 – DWT, and in Fig. 19 Froude number – Fr. Each figure provides insight into how ship designs evolved over two decades. Length overall has remained nearly constant across all ship sizes. Variations are within ±3 % for most of the database, showing that designers maintained optimal hull length-to-beam ratios while respecting port and canal constraints and longitudinal strength by the early 2000s. The absence of a significant upward trend indicates that capacity growth during this period was not achieved by simply lengthening hulls. Breadth also shows high stability, with a slight widening observed after 2016 for Panamax ships, corresponding to the Panama Canal expansion. Height and draft remain relatively stable throughout the time series. This reflects port access and dredging limitations as the main governing factor. The stability of draft also implies that additional capacity was accommodated by improved internal arrangement and depth increases rather than deeper loading. A clear downward trend is observed, with design speeds declining by several knots over the two decades. This reflects the widespread industry shift toward slow steaming, initially adopted in response to rising fuel costs after 2008 and later reinforced by EEDI/EEXI/CII regulatory

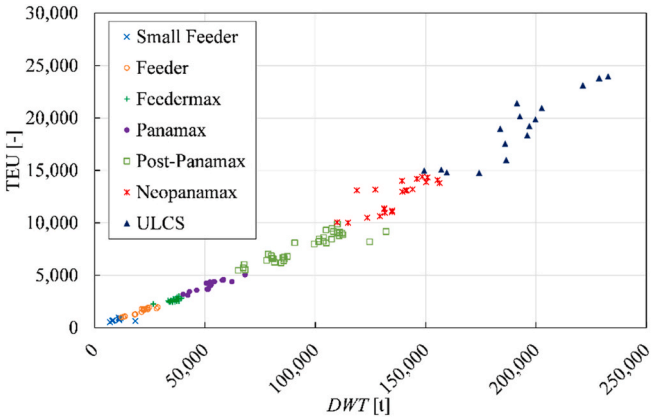

Fig. 1. Database ships capacity in TEU per size depending on a *DWT*.

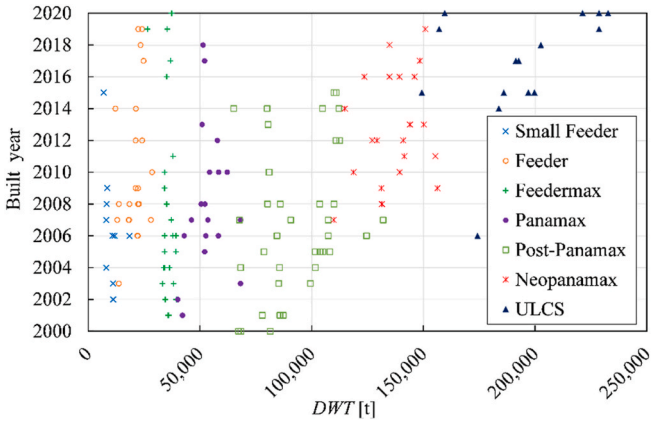

Fig. 2. Database ships built year per size depending on a *DWT*.

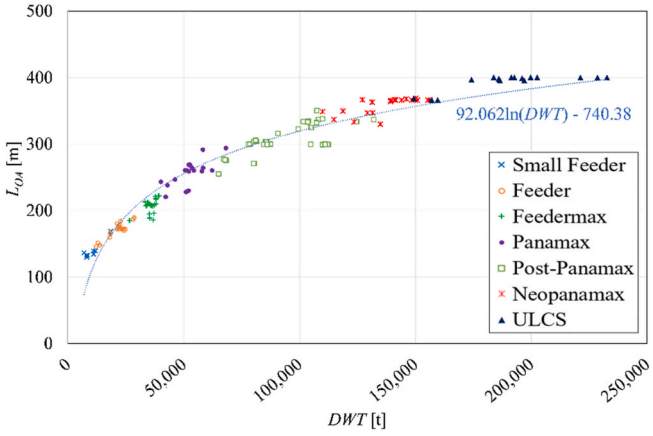

Fig. 3. Database ships L_{OA} per size depending on a *DWT*.

Table 1
Number of ships in database according to the size.

Size	TEU range	Total
Small Feeder	Up to 1000	11
Feeder	1001-2000	25
Feedermax	2001-3000	30
Panamax	3001-5100	19
Post-Panamax	5101-10000	38
Neopanamax	10001-14500	22
ULCS	14501 and higher	17
Total		**162**

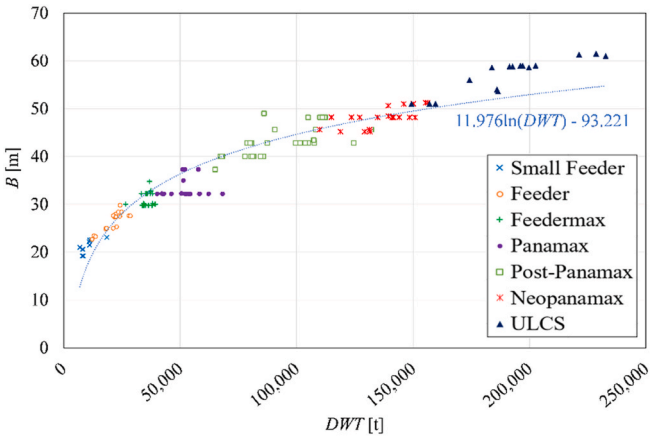

Fig. 4. Database ships *B* per size depending on a *DWT*.

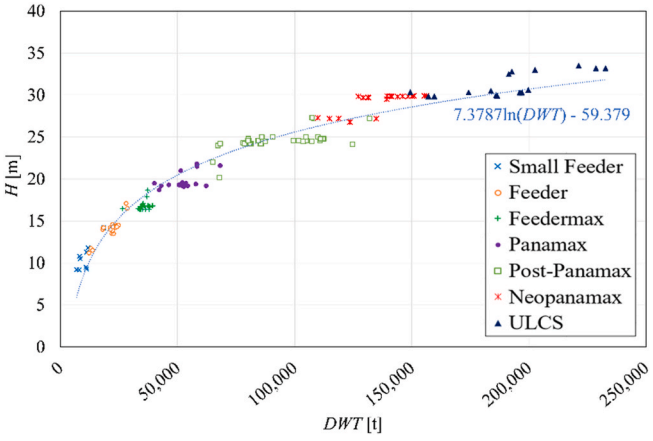

Fig. 5. Database ships *H* per size depending on a *DWT*.

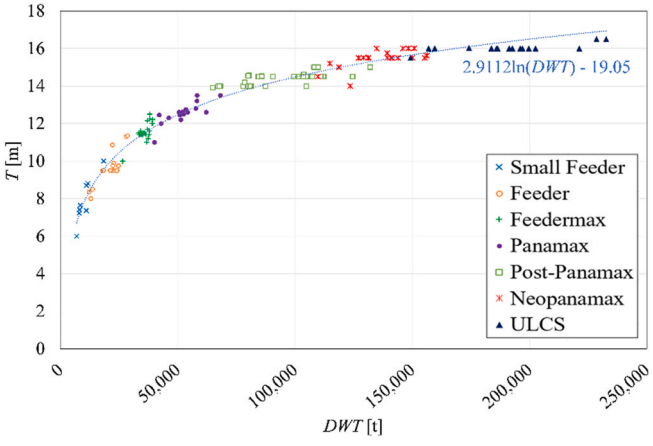

Fig. 6. Database ships *T* per size depending on a *DWT*.

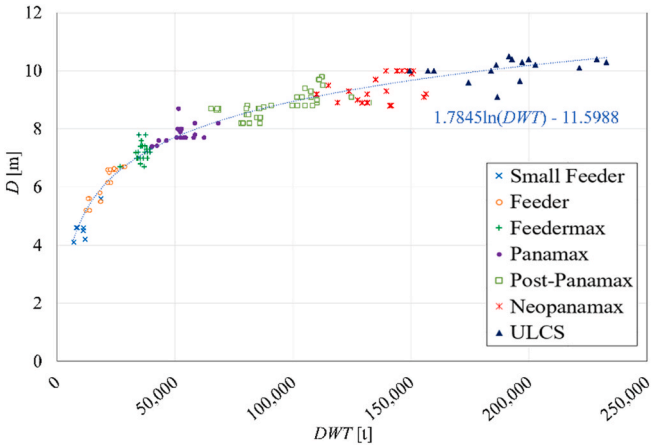

Fig. 7. Database ships *D* per size depending on a *DWT*.

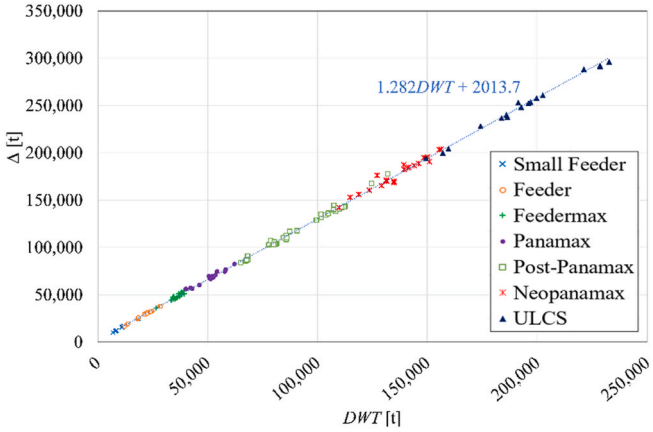

Fig. 8. Database ships Δ (fully loaded) per size depending on a *DWT*.

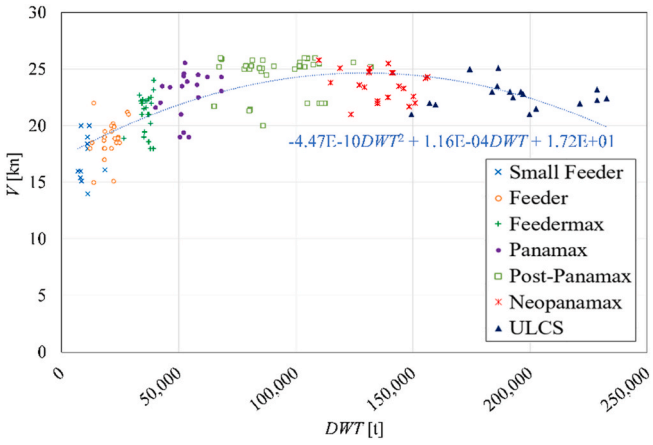

Fig. 9. Database ships *V* per size depending on a *DWT*.

requirements. *MCR* shows a marked decline over time, closely following the reduction in design speed. Since required propulsive power scales approximately with the cube of speed, even moderate speed reductions allowed substantial engine downsizing. This trend shows a conscious effort by designers to optimize installed power for lower operational profiles, reducing capital cost, fuel consumption and emissions. The simultaneous increase in propeller diameter for lower-speed ships suggests a design shift toward larger, slower-turning propellers to maintain propulsive efficiency with derated engines. The observed decline in Froude number confirms that ships transitioned to lower speed regimes, reducing wave-making resistance and improving hydrodynamic efficiency.

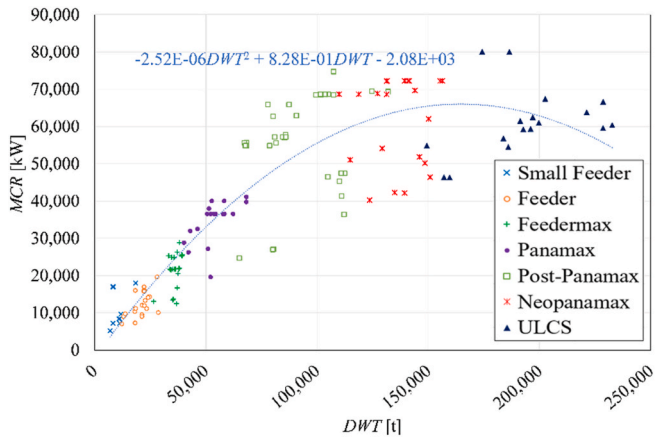

Fig. 10. Database ships *MCR* per size depending on a *DWT*.

3. Methodology

3.1. Research approach

The introduction provides a detailed review of current IMO regulations on ship energy efficiency, with particular emphasis on the three key indices: EEDI, EEXI, and CII. A comprehensive literature review revealed a lack of studies analyzing large fleets of container ships built during the first two decades of the 21st century.

The subsequent sections present the calculation methodology for each of the three indices and apply it to a database of 162 seagoing container ships. All ships were classified by TEU capacity, and results were analyzed according to this classification. For each ship, the attained and required EEDI and EEXI values were determined. For 21 ships, sufficient operational data was available to calculate the attained and required CII. For ships that did not comply with EEDI/EEXI criteria, the required EPL was determined as a practical compliance measure, and the associated speed reduction was calculated individually for each ship. This approach enabled an assessment of energy efficiency improvements across the entire fleet over the 2000–2020 period.

Fig. 20 presents the methodological framework of the study. It begins with the introduction, which includes a review of IMO policies, relevant literature, and the research objectives. This is followed by the creation of a container ship database, which serves as the basis for the analysis. In the methodology, the ships are evaluated using two regulatory approaches: EEDI/EEXI and CII. For each ship, it is checked whether the required efficiency criteria are met. If the EEDI/EEXI criterion is not satisfied, the required EPL and corresponding reference speed reduction is estimated. If the CII criterion is not met, the required operational speed reduction is calculated. The results from both pathways are then combined to assess the improvement of fleet energy efficiency over the years, followed by the discussion and conclusion of the study.

3.2. EEXI

For a ship to comply with IMO requirements, its attained EEXI must be lower than the required EEXI (Eq. (1)). The attained and required EEXI values were calculated following the IMO standard procedures for containerships (IMO, 2018; IMO, 2021a; IMO, 2022g), as defined by Eqs. (2) and (3) and summarized in Tables 2 and 3. In Eq. (2), the subscript "*" indicates that SFC_{ME} and C_{FME} may replace SFC_{AE} and C_{FAE}, but only if part of the normal maximum load is supplied by shaft generators. The subscript "**" specifies that a weighted average of $(\cdot C_{FME})$ and $(\cdot C_{FAE})$ should be used when calculating P_{eff}. The subscripts "ME" and "AE" denote main and auxiliary engines, respectively. Because power–speed curves from sea trials were unavailable for the ships in the database, the reference speed V_{ref} was estimated using the empirical formula provided in Table 2. This formula expresses V_{ref} and MCR_{avg} as functions of ship type and deadweight, with capacities derived from the corresponding deadweight at scantling draft. Explanations of all inputs and their respective data sources for the attained EEXI calculation are provided in Table 2. The required EEXI values were calculated according to the IMO procedures summarized in Tables 3 and 4 (IMO, 2021a).

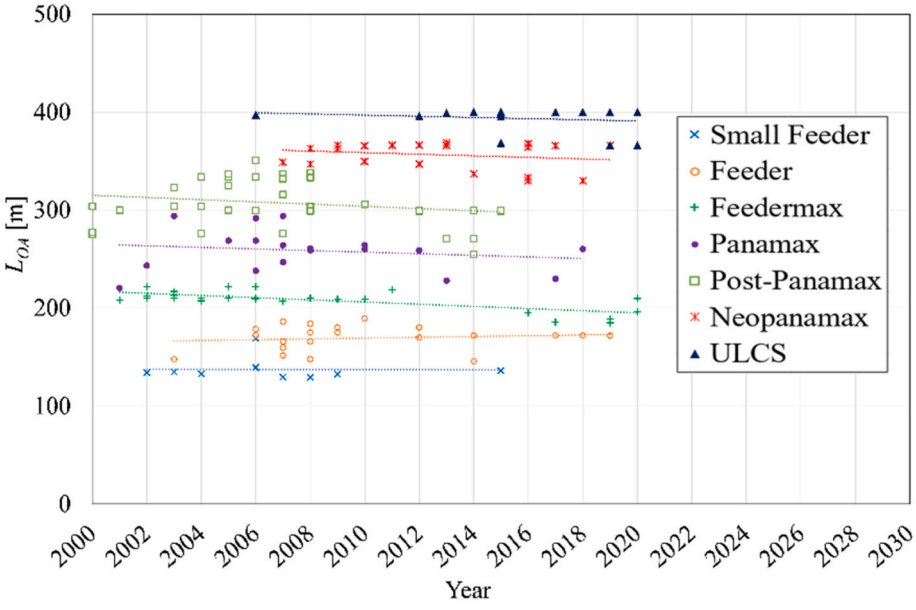

Fig. 11. Development of ships L_{OA} over the years.

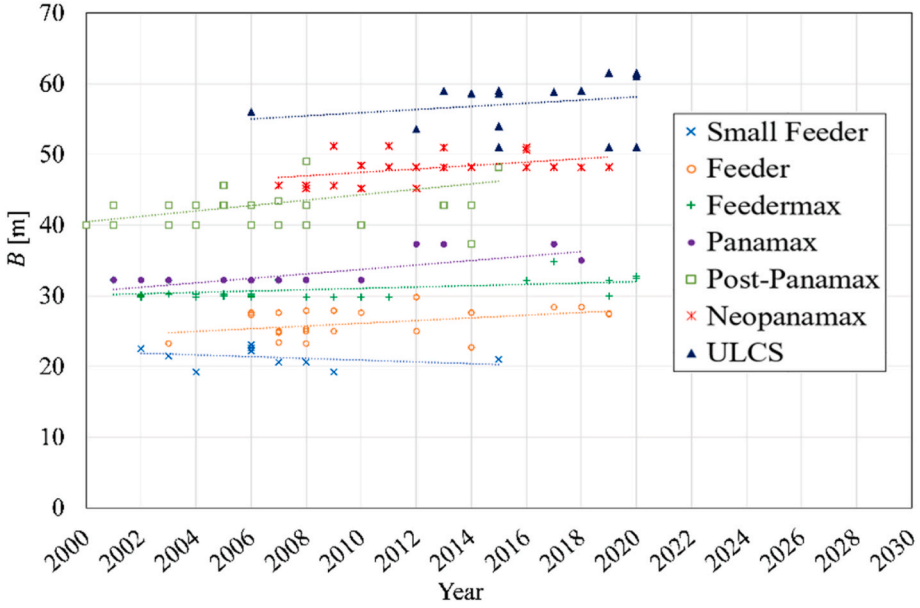

Fig. 12. Development of ships *B* over the years.

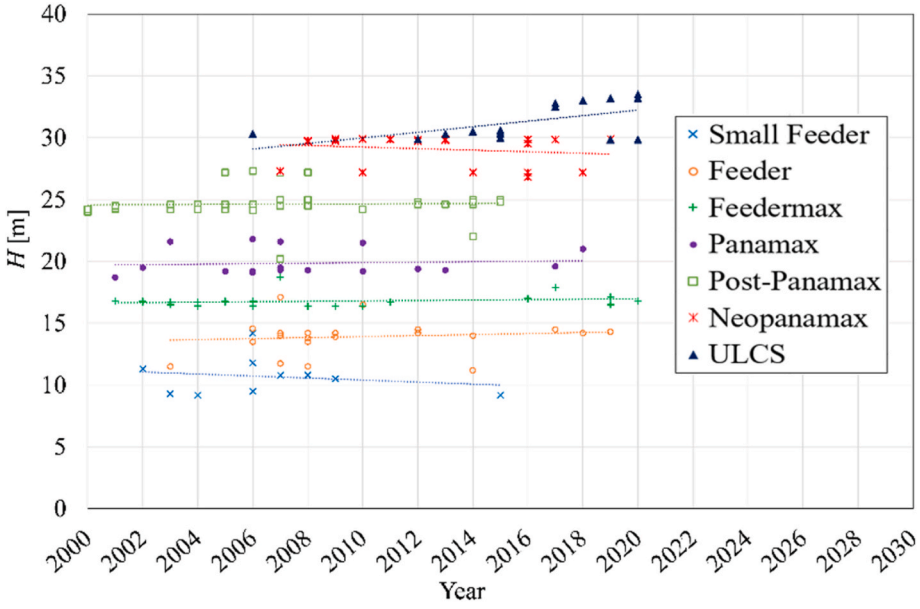

Fig. 13. Development of ships *H* over the years.

$$Attained\ EEXI = \frac{\left[\begin{array}{c}\left(\prod_{j=1}^{n} f_j\right)\left(\sum_{i=1}^{n_{ME}} P_{ME(i)} \cdot C_{FME(i)} \cdot SCF_{ME(i)}\right) + (P_{AE} \cdot C_{FAE} \cdot SFC_{AE^*}) + \\ \left(\left(\prod_{j=1}^{n} f_j \cdot \sum_{i=1}^{n_{PTI}} P_{PTI(i)} - \sum_{i=1}^{n_{eff}} f_{eff(i)} \cdot P_{AEeff(i)}\right) \cdot C_{FAE} \cdot SCF_{AE} - \\ \left(\sum_{i=1}^{n_{eff}} f_{eff(i)} \cdot P_{eff(i)} \cdot C_{FME} \cdot SCF_{ME^{**}}\right)\end{array}\right]}{f_i \cdot f_c \cdot f_l \cdot f_w \cdot f_m \cdot Capacity \cdot V_{ref}} \quad (1)$$

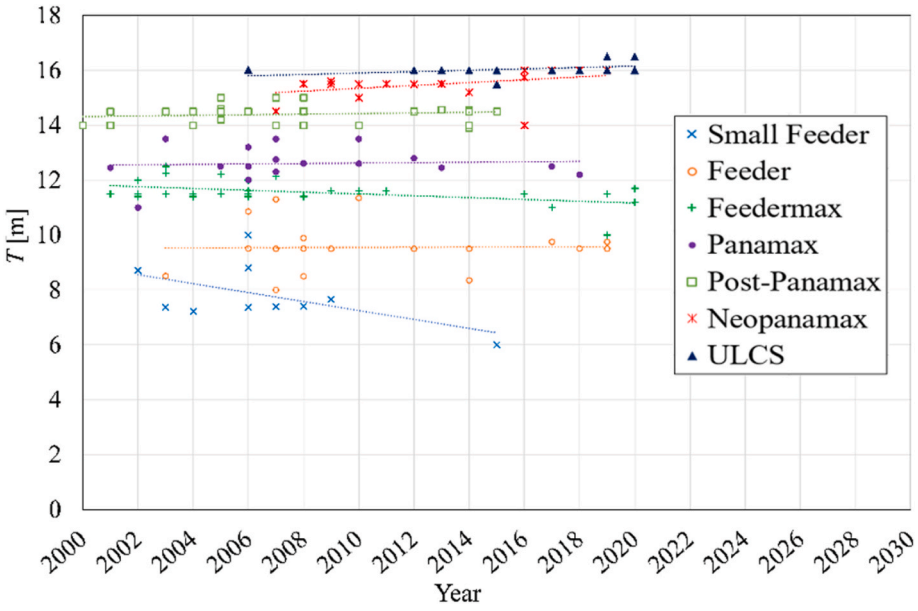

Fig. 14. Development of ships T over the years.

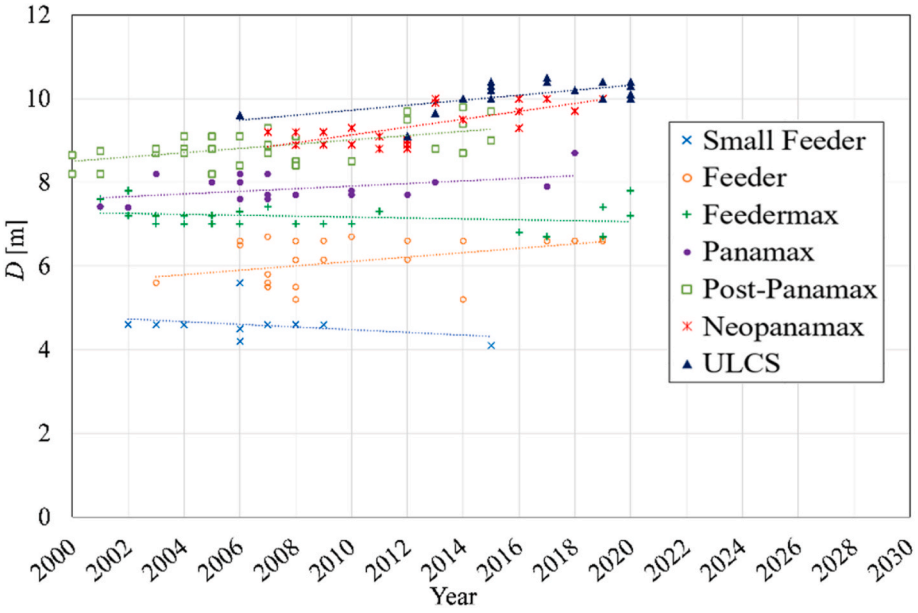

Fig. 15. Development of ships D over the years.

$$Attained\ EEXI \leq Required\ EEXI \tag{2}$$

$$Required\ EEXI = \left(1 - \frac{Y}{100}\right) \cdot Reference\ line \tag{3}$$

$$Reference\ line = a \cdot b^{-c} \tag{4}$$

Following the methodology described by (Kalajdžić et al., 2022b), the required EPL and the corresponding new reference speed ($V_{ref,app,lim}$) were calculated to ensure that every ship in the database complies with the EEXI criterion. For ships that did not satisfy the required EEXI criterion, the required EPL was determined iteratively by progressively reducing the available main engine power until the recalculated attained EEXI value satisfied the regulatory requirement. The corresponding limited reference speed was then estimated using the Admiralty relationship between ship speed and propulsion power. The relative speed reduction was calculated as the percentage difference between the original reference speed and the limited reference speed.

3.3. EEDI

The assessment of EEDI closely parallels that of EEXI. A lower attained EEDI indicates higher energy efficiency under this regulation, just as for EEXI, where the attained value must not exceed the required threshold. The calculations follow the methodology outlined in (IMO, 2018) and are updated according to (IMO, 2019), which provides a similar formula for EEXI (see Eqs. (5) and (6)). Over the years, the required EEDI criteria have been progressively tightened, and this is accounted for in the calculations through reduction factors, as specified in (IMO, 2021a). All necessary input data, explanations, and sources for calculating the attained EEDI are provided in Table 2, while the required

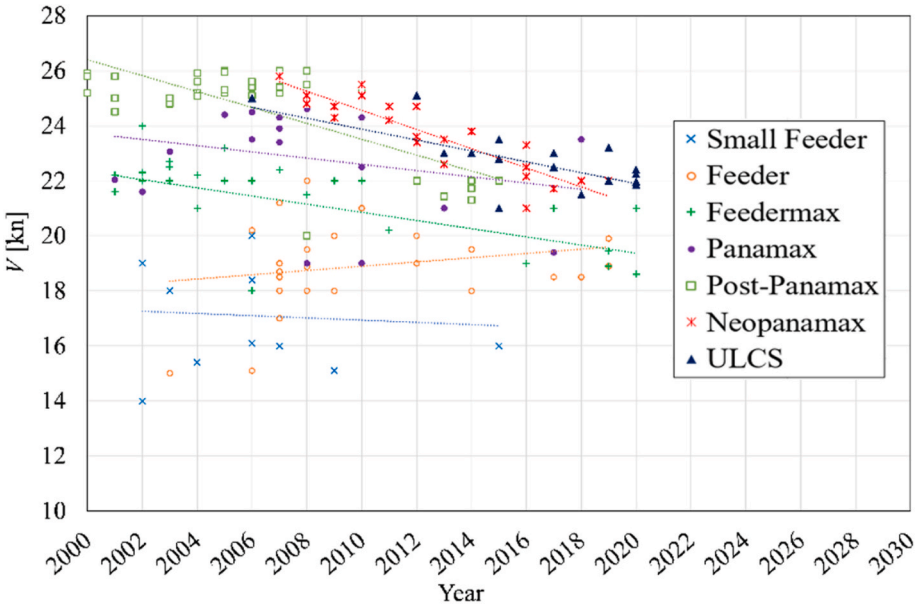

Fig. 16. Development of ships *V* over the years.

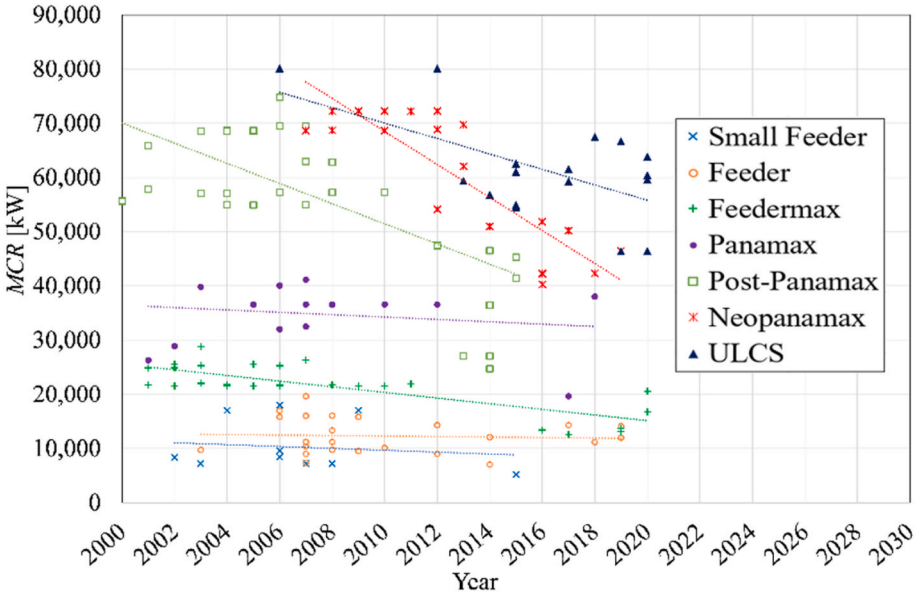

Fig. 17. Development of ships *MCR* over the years.

EEDI is determined according to (IMO, 2021a) and presented in Tables 3 and 5.

$$Attained\ EEDI \leq Required\ EEDI \tag{5}$$

$$Required\ EEDI = \left(1 - \frac{X}{100}\right) \cdot Reference\ line \tag{6}$$

The Reference line is given in Eq. (4).

3.4. CII

In addition to calculating EEDI and EEXI for all ships in the database, a subset of 21 ships was selected for the calculation of their CII rating (see Eqs. (7)–(11)). These ships were chosen due to the availability of reliable data, including IMO DCS records of annual fuel consumption by fuel type for 2022, hours spent underway, and distance traveled. Although this subset does not fully represent the global container ship fleet, it provides useful insights into operational efficiency trends among ships with verified data availability. Consequently, the results of the CII analysis should be interpreted as indicative rather than statistically representative of the entire fleet. It is important to note that, starting from 1 January 2023, all ships are required to have a three-year plan outlining how they will achieve the CII targets (IMO, 2022h). The attained CII is calculated according to the methodology in (IMO, 2022c) while the reference CII (CII_{ref}) is determined as per (IMO, 2022d) for 2019, with the reduction factor *Z* taken from (IMO, 2021b; IMO, 2022a). Explanations and sources for all inputs required in the CII calculation are provided in Table 6, and all parameters for determining the specific reference line along with their reduction factors are presented in Tables 7 and 8.

$$Attained\ CII = \frac{M}{W} \tag{7}$$

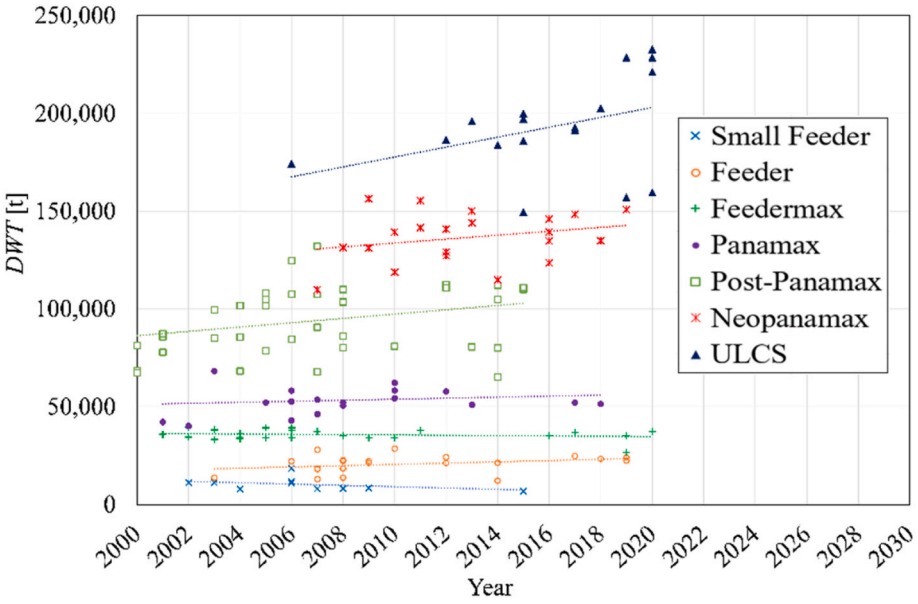

Fig. 18. Development of ships *DWT* over the years.

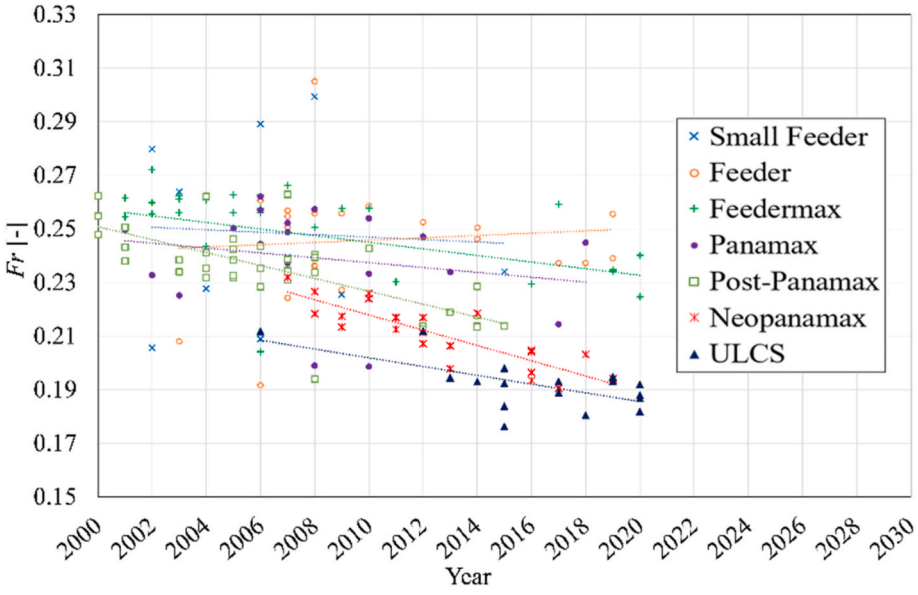

Fig. 19. Development of ships Fr over the years.

$$M = FC_j \cdot C_{F_j} \tag{8}$$

$$W = C \cdot D_t \tag{9}$$

$$Required\ CII \leq \left(1 - \frac{Z}{100}\right) \cdot CII_{ref} \tag{10}$$

$$CII_{ref} = a \cdot Capacity^{-c} \tag{11}$$

The primary purpose of these developed rules and guidelines is to determine the rating for each ship. The CII rating classifies ships into five grades – A, B, C, D, and E – based on their annual operational CII, with performance levels ranging from major superior to inferior (IMO, 2022e). To streamline the evaluation process, annual ratings from 2023 to 2030 define four boundaries within the five-grade framework: superior, upper, lower, and inferior. This system allows a ship's annual operational CII to be assessed by comparison with these boundaries. These limits are derived from the distribution of individual ships' CIIs in 2019, ensuring that performance ratings over time remain synchronized while maintaining consistent relative distances. A ship's rating is determined solely by its achieved CII relative to the predetermined boundaries, independent of other ships' CII values. The establishment of these boundaries considers the required annual operational CII in relation to vectors denoted as dd vectors, which indicate both the direction and magnitude of deviation from the required value, as shown in Table 9.

The most widely used method for meeting the CII criteria is to reduce the speed. Therefore, in this case, the relative difference between the average sailing speed of each ship over one year and real speed at which the ship should sail to meet the CII criteria for the same period and distance traveled has also been determined.

In addition to the EEXI-based assessment, the operational speed reductions required to satisfy the CII criterion were also estimated. For each vessel with available operational data, the average operational

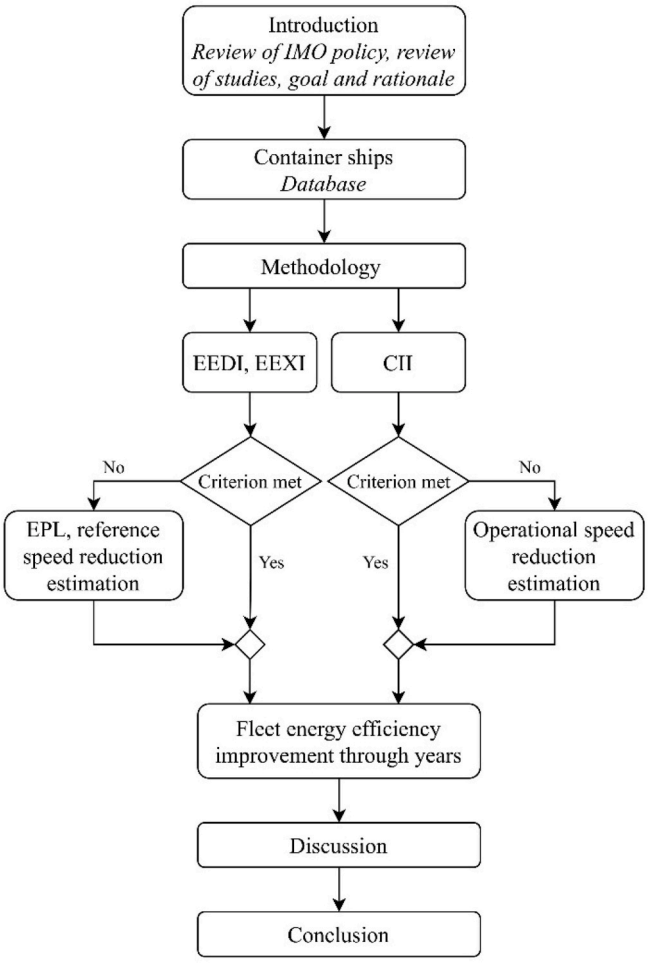

Fig. 20. Research approach.

speed was determined from AIS-derived voyage information and reported annual operational data. The required speed necessary to achieve at least a C rating was then estimated under the assumption that the vessel performs the same annual transport work, meaning that the same total distance is traveled and the same cargo capacity is maintained. Under this assumption, a reduction in sailing speed implies a longer voyage duration while covering the same distance. The corresponding decrease in propulsion power was estimated using the classical propulsive relationship between ship speed and required propulsion power, while the associated fuel consumption was assumed to vary proportionally with engine power through the specific fuel consumption of the main engine. The required speed reduction was then expressed as the relative difference between the current operational speed and the recalculated speed that satisfies the required CII value.

4. Results

First, reference values for the required EEDI were determined for each ship in the database according to IMO phase criteria, which have become progressively more stringent over time. As illustrated in Fig. 21, the EEDI reference line shifts downward from Phase 0 (dashed green) to Phase 1 (dashed purple), Phase 2 (dashed blue) to Phase 3 (dashed orange), reflecting these tightening requirements. The EEXI reference line is shown in black solid line. Each point in Fig. 21 (square, circle, rhomb, triangle) represents one ship from the database with its attained EEDI and EEXI value, color-coded according to the phase to which it corresponds.

Overall, all ships built in 2013 and 2014 from database meet the Phase 0 EEDI criterion, 90% of ships built between 2015 and 2019 meet Phase 1 and 83 % of ships built in 2020 meet Phase 2. For consistency, ships built before 2013 (before EEDI became mandatory) were assessed against the EEXI criterion and only 4.4% meet it. For recently built ships, the attained EEDI and EEXI are identical, but all ships from the database

Table 2
Inputs for the calculation of attained EEXI.

Input	Methodology	Explanation/sources
Main engines	$\sum_{i=1}^{n_{ME}} P_{ME(i)}$	75% of the maximum continuous rating (*MCR*). This is to be taken as 83% of limited installed power (MCR_{lim}) or 75% of *MCR*, which ever is lower (IMO, 2022g)
Shaft generators	$\sum_{i=1}^{n_{PTI}} P_{PTI(i)} = 0$	No shaft generators
Innovative energy efficient devices on main engines	$\sum_{i=1}^{n_{eff}} f_{eff(i)} \cdot P_{eff(i)} = 0$	No innovative energy efficient devices on main engine
No innovative energy efficient devices on auxiliary engine	$\sum_{i=1}^{n_{eff}} f_{eff(i)} \cdot P_{AEeff(i)} = 0$	No innovative energy efficient devices on auxiliary engine
P_{AE}	$P_{AE} = 0.5 \cdot MCR\ (MCR < 10000kW)$ $P_{AE} = 0.025 \cdot MCR + 250\ (MCR \geq 10000kW)$	Power of auxiliary engines (IMO, 2018)
SCF_{ME}	190 g/kWh	This is assumed for engines that have no NOx Technical File and verified manufacturer's data (IMO, 2022g)
SCF_{AE}	215 g/kWh	
C_{FME}	3.114 t CO_2/t•fuel – for HFO	
C_{FAE}	3.206 t CO_2/t•fuel – for diesel	
$V_{ref.app}, V_{ref.app.lim}$	$V_{ref.avg} - m_v \left[\frac{P_{ME}}{0.75 MCR_{avg}}\right]^{1/3}$	Where there is no power speed curve available or there are no EEDI from sea trials, the formula represents the statistical mean of distribution of ship speed and engine power (IMO, 2022g)
MCR_{avg}	$D \cdot E^F$ $D = 0.5042$ $E = DWT$ $F = 1.03046$	IMO (2022g)
m_v	$\min(0.05 \cdot V_{ref.app}, 1\ kn)$	IMO (2022g)
$V_{ref.avg}$	$V_{ref.avg} = A \cdot B^C$	Parameters A,B, C are given in (IMO, 2022g)
Capacity	0.7•*DWT*	IMO (2018)
f_j	Ship specific design elements – the power correction factor for ice – classed ships: the greater value of f_{j0} and $f_{j,min}$ but not greater than $f_{j,max} = 1$	IMO (2018)
f_i	Capacity correction factor	IMO (2018)
f_c	Cubic capacity correction factor	IMO (2018)
f_l	Factor for general cargo ships equipped with cranes. $f_l = 1$	IMO (2018)
f_w	Factor for speed reduction at sea. $f_w = 1$	IMO (2018)
f_m	Factor for ice – classed ships	IMO (2018)

Table 3
Inputs for calculation of EEDI Reference line (IMO, 2021a).

a	b	c
174.22	DWT	0.201

Table 4
Reduction factor Y for required EEXI compared to the EEDI reference line (IMO, 2021a).

Ship size	Reduction factor Y
200,000 DWT and above	50
120,000 and above but less than 200,000 DWT	45
80,000 and above but less than 120,000 DWT	35
40,000 and above but less than 80,000 DWT	30
15,000 and above but less than 40,000 DWT	20
10,000 and above but less than 15,000 DWT	0-20[a]

[a] The reduction factor Y should be linearly interpolated between two values dependent upon ship size.

Table 5
Reduction factor X for required EEDI (IMO, 2021a).

Size	Phase 0	Phase 1	Phase 2	Phase 2	Phase 3	Phase 3
200,000 DWT and above	1 Jan 2013 – 31 Dec 2014	1 Jan 2015 – 31 Dec 2019	1 Jan 2020 – 31 Mar 2022	1 Apr 2022 and onwards	1 Apr 2022 and onwards	1 Jan 2025 and onwards
200,000 DWT and above	0	10	20		50	
120,000 and above but less than 200,000 DWT	0	10	20		45	
80,000 and above but less than 120,000 DWT	0	10	20		40	
40,000 and above but less than 80,000 DWT	0	10	20		35	
15,000 and above but less than 40,000 DWT	0	10	20		30	

*Regarding the containerships between 10000 and 15000 t, the reduction factor X should be linearly interpolated between two values.

were checked against EEXI requirements as this became mandatory in 2023. Only 12% of the database - 20 out of 162 ships - meet the EEXI criterion without modifications (see Fig. 22). Ships were further classified into seven TEU-based size categories and Fig. 22 presents the ships per size that meet EEXI requirements. The most efficient categories are Feeders and ULCS, with one quarter of ships in compliance, followed by the Feedermax, Post-Panamax and Panamax. The least efficient categories are Small Feeders and Neopanamax, with no ships in these groups meeting the EEXI threshold.

For noncompliant ships, the required EPL was calculated. EPL is expressed as a percentage ratio between the new limited power MCR_{lim} and the original MCR. Fig. 23 presents the EPL distribution by ship size.

Fig. 24 compares the designed speed, approximated reference speed

Table 6
Inputs for the calculation of attained CII.

Symbol	Note	Explanation/source
M	Mass of CO_2 emissions	Total mass of CO_2 in grams from all the fuel oil consumed on board a ship in a given calendar year.
FC	Mass of consumed fuel oil	Total mass in grams of consumed fuel oil type j in the calendar year, as reported in IMO DCS Annual emissions report.
j	Fuel oil type	HFO, LFO, MDO/MGO, LPG, LNG
C_{F_j}	Conversion factor	Fuel oil mass to CO_2 mass conversion factor for fuel oil type: 3.114, 3.151, 3.206, 3.030, 2.750 for each fuel oil type above respectively
W	Transport work	The supply-based transport work (IMO, 2022c)
C	Ship's capacity	Deadweight
D_t	Traveled distance	Total distance traveled in nautical miles as reported in IMO DCS Annual emissions report

Table 7
Inputs for calculating the specific 2019 CII reference lines (IMO, 2022d).

Capacity	*a*	*c*
DWT	1984	0.489

Table 8
Reduction factor Z for the CII relative to the 2019 CII reference line (IMO, 2021b; IMO, 2022a).

Year	Reduction factor relative to 2019
2020	1%
2021	2%
2022	3%
2023	5%
2024	7%
2025	9%
2026	11%
2027	13.625%
2028	16.250%
2029	18.875%
2030	21.500%

Table 9
dd vectors for determining the rating extremities of containerships (IMO, 2022e).

Capacity in CII calculation	*dd* vectors (after exponential transformation)			
	$\exp(d_1)$	$\exp(d_2)$	$\exp(d_3)$	$\exp(d_4)$
DWT	0.83	0.94	1.07	1.19

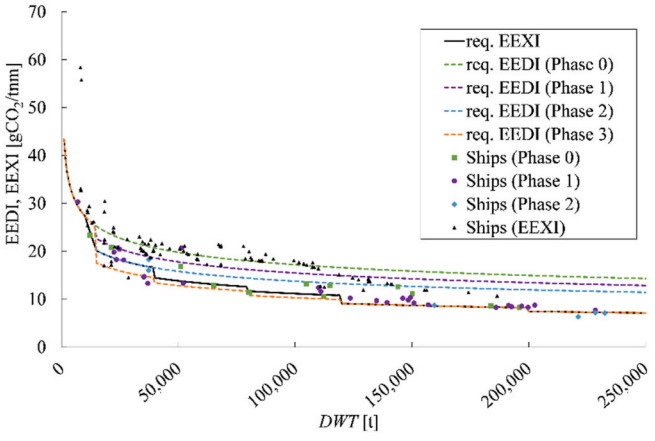

Fig. 21. Attained and required EEDI and EEXI according to phases.

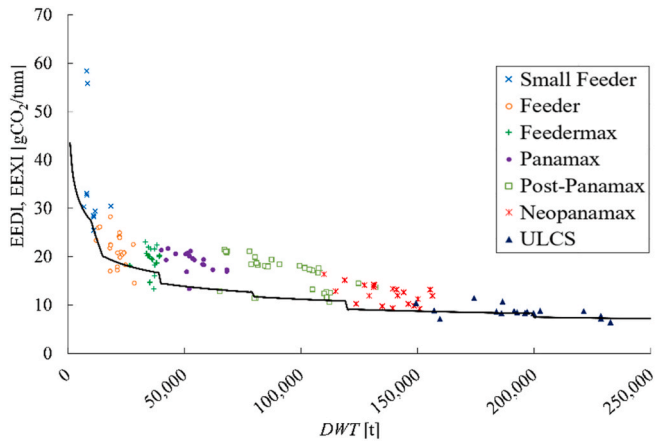

Fig. 22. Attained EEDI and EEXI according to ships' size against required EEXI.

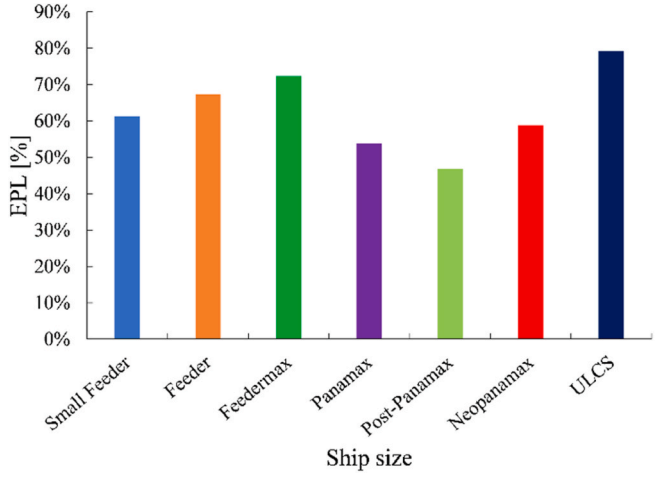

Fig. 23. EPL estimation by ship size.

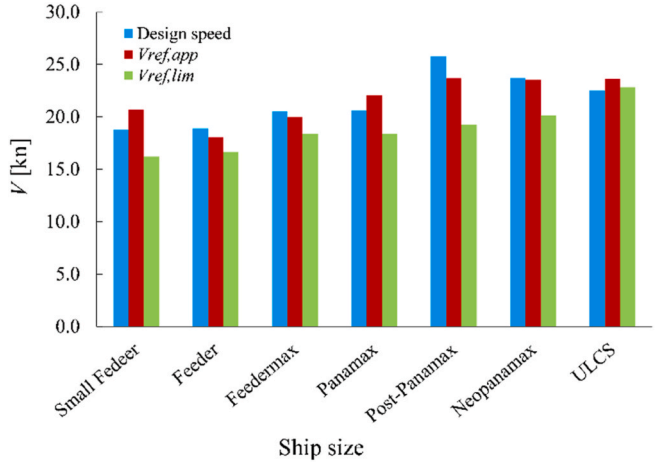

Fig. 24. Design speed, approximated reference speed and limited reference speed by ship size.

and limited reference speed by ship size. The fleet-wide average designed speed is 22 kn, while the average reference speed is slightly lower at 21.6 kn. After applying EPL, the average limited reference speed decreases to 18.9 kn.

Fig. 25 illustrates the percentage speed reduction required to meet EEXI by ship size. Small Feeders require the highest reductions (22%), while ULCS require the least (4%). Across the entire database, the

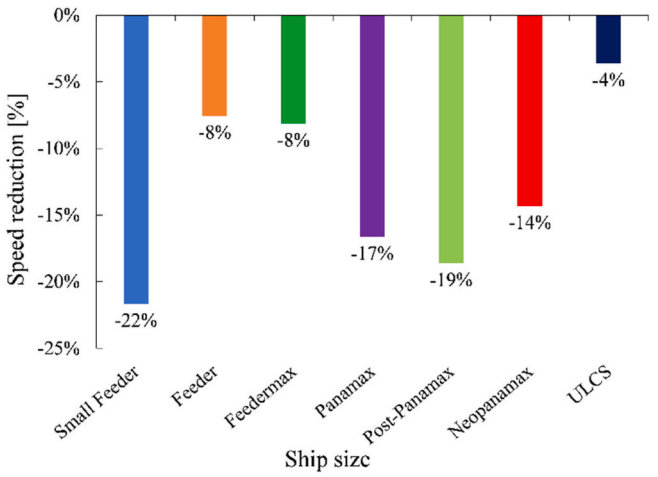

Fig. 25. Speed reduction by ship size to meet EEXI criteria.

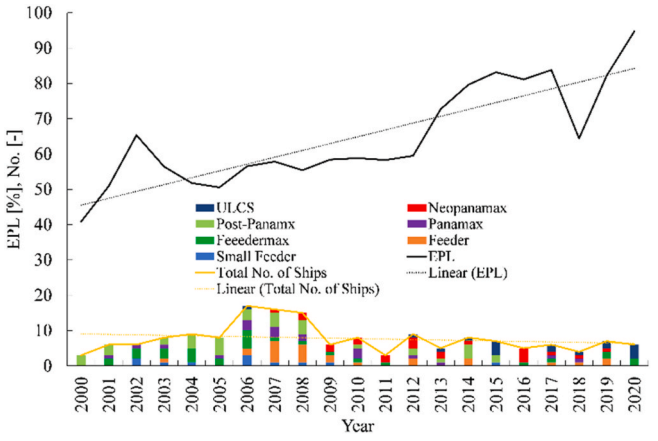

Fig. 26. Fleet energy efficiency improvement through from 2000 to 2020.

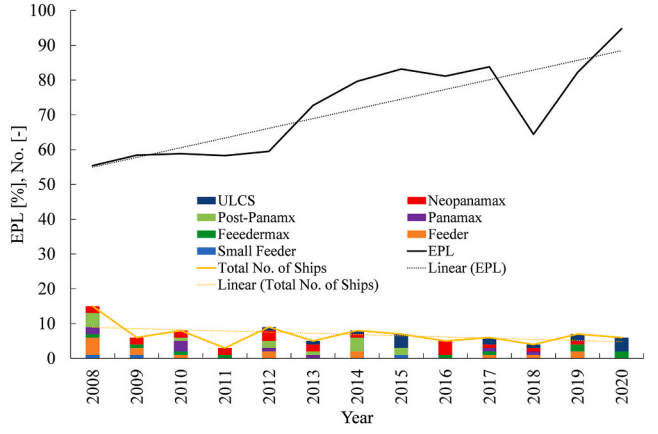

Fig. 27. Fleet energy efficiency improvement through from 2008 to 2020.

average EPL is 60%, corresponding to a 40% reduction in maximum engine power and an average speed reduction of 13%.

To assess temporal trends, ships were also sorted by year of construction. Fig. 26 shows the number of ships requiring EPL by year with a solid yellow line, while black solid line represents the average EPL across all sizes per year. A peak in the number of ships requiring EPL is observed in 2006, followed by a marked decline after the 2008 economic crisis, which also saw a drop in newbuild deliveries. While the number of ships requiring EPL has decreased slightly since 2000, the average EPL

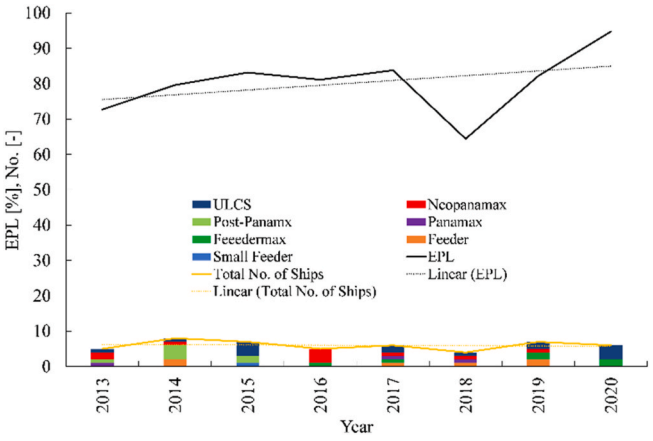

Fig. 28. Fleet energy efficiency improvement through from 2013 to 2020.

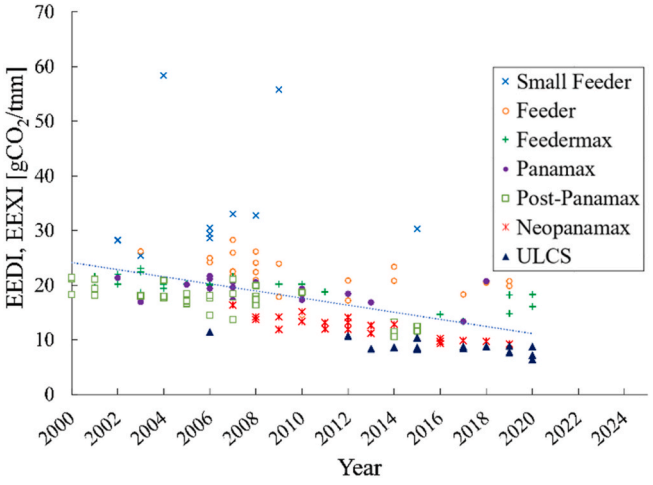

Fig. 29. Energy efficiency evolution.

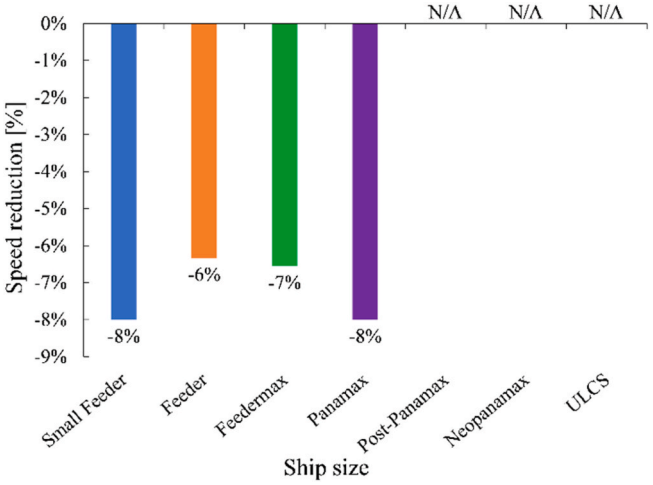

Fig. 30. Necessary speed reduction to reach C grade for the next three years by size of the ship.

itself has risen by approximately 37% between 2000 and 2020. If 2008 is taken as a reference year, since then, EPL has risen for 33% (Fig. 27) and if 2013 (the year EEDI entered into force) is taken as the baseline, the EPL increase is less than 10% (Fig. 28).

Fig. 29 shows the achieved EEDI and EEXI values for all ship types by size, arranged according to their year of construction. Over the course of

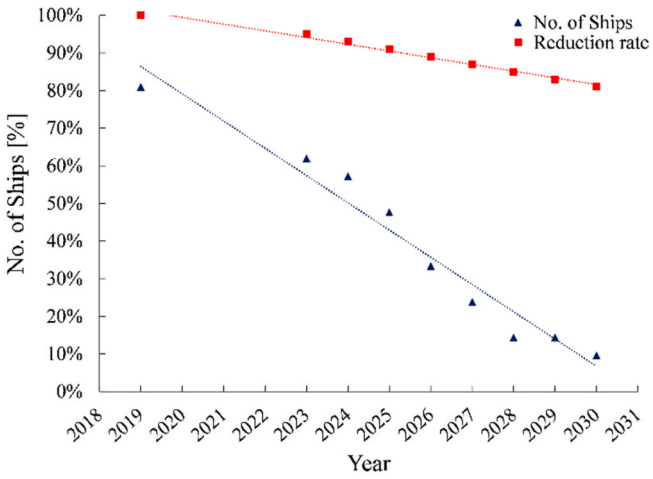

Fig. 31. CII ratings compliance.

20 years, a decreasing trend in energy efficiency indices can be observed, indicating that ships have indeed become more efficient over time.

Because both EEDI and EEXI are nominal indices based on a single reference speed and engine power at scantling draft, they do not reflect actual GHG emissions. To address this limitation, CII was introduced as a more realistic operational indicator, as it accounts for distance traveled, time underway and annual fuel consumption. For the 21 ships in the database with sufficient operational data, the average annual operating speed is 13.6 kn, approximately 33% lower than the designed speed, confirming widespread slow steaming. Of these 21 ships, 48% already meet the 2025 CII requirement, but only 14% are projected to maintain a positive CII rating over the next three years without operational changes. The remaining ships would need to reduce their average speed by 7% to achieve at least a C rating. Fig. 30 shows the required speed reductions by ship size where Small Feeder and Panamax ships have to decrease the speed for about 8% while Feeders and Feedermax ships have to reduce the speed for approximately 6% and 7%, respectively. For the other ship sizes, data for CII evaluation were not available.

Comparing EEXI- and CII-based speed reductions reveals an average difference of 6%, demonstrating that ships are already operating below their EEXI reference speeds.

Fig. 31 shows the percentage of ships (relative to the total number in the database) that would meet the CII criterion over the years, assuming that each ship operates under the same conditions every year (blue triangles). Thus, in 2019, which is taken as the reference year, 81% of the

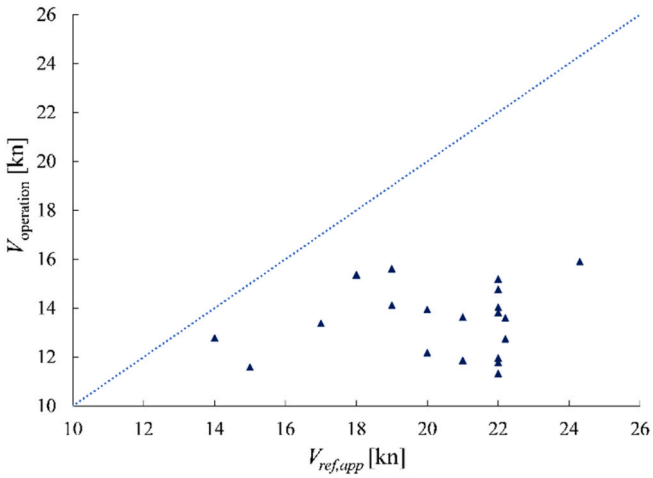

Fig. 32. Difference between operational speed and reference speed.

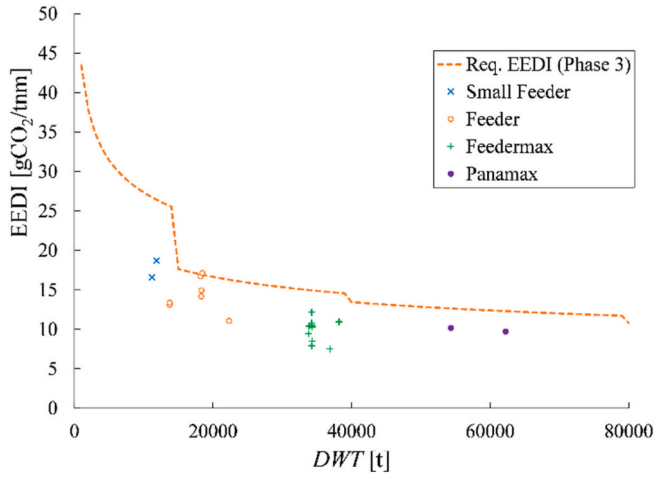

Fig. 33. EEDI values when operational speeds are considered as reference speeds.

ships in the database would have met the then-current CII criterion, while by 2030 this percentage would drop to below 10%. The same figure also shows, with red squares, the rate of tightening of the criterion compared to the reference year 2019, which actually corresponds to the reduction factors presented in Table 8.

By comparing the reference speeds ($V_{ref,app}$) with the average operational speeds ($V_{operation}$), it can be seen that none of the ships in the database actually operate at their design speeds (see Fig. 32); instead, their operating speeds are on average 30% lower.

For this reason, an additional analysis was carried out to answer the following question: would the ships in the database meet the current EEDI criterion (Phase 3) if the reference speed used in the attained EEDI evaluation were taken as the actual operational speed ($V_{ref,app} = V_{operation}$)? The main engine power (P_{ME}) and the corresponding installed power (*MCR*) were estimated based on the equality of the Admiralty constants. In this way, it was concluded that container ships typically use only about 37% of their available engine power in service. The attained EEDI values in this case, along with the corresponding reference EEDI values, are shown in Fig. 33.

Only 5% of the ships (1 out of 21) did not meet the EEDI Phase 3 criterion, while according to Fig. 21, less than 5% of the ships would have satisfied the same criterion if they had been built after 2022.

5. Discussion

The analysis of 162 seagoing container ships built between 2000 and 2020 highlights both design evolution and operational efficiency trends in the global container fleet. Although the database does not represent the entire global container fleet, it includes vessels recognized as technologically notable designs delivered by leading shipyards. As such, the dataset reflects prevailing design practices and efficiency strategies among modern container ships rather than the statistical average of the global fleet. Consequently, the results should be interpreted as indicative of design and regulatory trends within the most representative conventional designs, rather than as a direct description of the entire fleet population. The database reveals that principal dimensions: length overall, breadth, height and draft – scale predictably with *DWT*, following near-logarithmic or linear trends. This indicates that shipbuilders have adhered to well-established hull scaling rules over the two decades. Displacement correlates linearly with *DWT*, consistent with expectations, while variation in propeller diameter, design speed, and installed main engine power (*MCR*) reflects diverse operational profiles and evolving market and regulatory pressures.

Temporal analysis shows that length overall, breadth and draft remained largely stable over the 2000–2020 period, suggesting that increases in capacity were primarily achieved via internal volume optimization rather than enlarging hull dimensions. Notably, a slight widening of Panamax ships post-2016 aligns with the Panama Canal expansion, while height and draft stability point to persistent port and dredging constraints. Conversely, the marked reduction in design speeds over time illustrates the widespread adoption of slow steaming, initially in response to rising fuel costs post-2008 and subsequently reinforced by IMO regulations, including EEDI, EEXI and CII requirements. Engine downsizing and larger, slower-turning propellers complement this operational trend, enabling improved hydrodynamic efficiency and reduced fuel consumption, consistent with the observed decline in Froude numbers.

EEDI compliance reveals a strong trend of improvement in ship energy efficiency over time. All ships built in 2013–2014 meet the Phase 0 EEDI criterion, 90% of 2015–2019 ships meet Phase 1 and 83% of 2020 ships meet Phase 2, demonstrating that the gradual tightening of EEDI requirements has driven tangible design improvements. However, ships built prior to the EEDI mandate largely fail to meet the required energy efficiency thresholds, confirming that policy-driven regulation has been the main catalyst of innovation, rather than spontaneous market evolution. EEXI compliance, however, paints a more restrictive picture: only 12% of the fleet meets current thresholds without modification. Small Feeders and Neopanamax ships show the lowest compliance, while Feeders and ULCS are comparatively more efficient. EPL calculations indicate an average required reduction of 40% in *MCR*, translating into a 13% decrease in maximum speed. These adjustments underscore the growing tension between legacy design intent and modern operational reality. Smaller ships require the largest relative reductions, up to 22%, reflecting the greater mismatch between older design speeds and current energy efficiency targets.

The analysis of linear trends describing the limitation of installed engine power across different timeframes provides data into the evolution of energy efficiency in container ships. The regression model for the period 2000–2020 shows a moderate improvement trend, indicating that, on average, ships had to restrict their installed power by approximately 1.9% annually. This baseline period captures the long-term trajectory of technological and regulatory developments. In contrast, the model for 2008–2020 exhibits a significantly steeper slope, meaning that from 2008 onward, ships increasingly adopted design and operational improvements, requiring more stringent EPL values. The year 2008 is particularly relevant since the IMO established it as the reference year against which reductions in emissions and energy efficiency improvements are measured. Therefore, trends from this year onward reflect both regulatory expectations and industry responses to rising environmental concerns. The 2013–2020 trend suggests that the most substantial progress had already occurred in the preceding years, after which improvements plateaued – a signal that conventional optimization approaches are reaching saturation. The shift from design-oriented to operation-oriented compliance also becomes evident: ships today no longer operate at their design speed but at an “operational compliance speed,” dictated by regulatory and fuel efficiency constraints. This represents a structural change in how ships are conceived, operated, and evaluated. By 2013, many container ships already complied with higher EPL thresholds, with average restrictions starting at approximately 74%. The lower slope compared to the 2008–2020 regression indicates that much of the rapid progress had already occurred in the preceding years. This choice of 2013 as a reference is not coincidental: it marks the entry into force of the EEDI, which imposed mandatory efficiency standards for new ships. Thus, the flatter trend after 2013 suggests a stabilization effect, as ships were increasingly designed from the outset to meet these regulatory benchmarks. Overall, the comparison across the three time periods highlights two critical aspects: the acceleration of efficiency improvements after 2008, driven by regulatory and environmental pressures and the consolidation of these improvements after 2013, when EEDI standards became mandatory for new designs. These results confirm that regulatory frameworks have directly shaped the trajectory

of EPL restrictions and consequently, the operational and design practices of container ships.

CII-based assessments, which account for actual operational data including fuel consumption, distance traveled and time underway, confirm that ships are already operating below their EEXI reference speeds. The average operating speed of 13.6 kn is roughly 33% lower than design speed, demonstrating widespread slow steaming. While 48% of the 21 ships with sufficient operational data meet the 2025 CII requirements, only 14% are projected to maintain a positive CII rating over the next three years without further speed reductions. The required adjustments to achieve at least a C rating are modest (7%), indicating that operational measures rather than extensive retrofitting are generally sufficient for compliance. However, most vessels already operate significantly below their design speeds, leaving limited room for further reductions through speed optimization alone. As the CII requirements become progressively stricter in the coming years, speed reduction is therefore likely to become insufficient as a standalone compliance measure. Thus, the potential for further emission reduction through speed reduction alone is becoming increasingly limited. Consequently, additional improvements will likely require more substantial technological changes such as alternative fuels, hybrid propulsion systems or advanced energy-saving technologies. It should be noted that the CII analysis is based on a subset of 21 ships for which sufficiently detailed operational data were available. Because such data are rarely publicly accessible, the operational dataset remains relatively limited compared with the design dataset used for EEDI and EEXI analyses. Consequently, the CII results should be interpreted primarily as indicative of operational trends rather than as statistically representative of the entire container fleet.

Similarly, Feeder and Feedermax ships require remarkably similar speed reductions when assessed according to both the EEXI and CII criteria. This suggests that these ships typically operate at speeds close to those for which they were originally designed, reflecting a good alignment between design intent and operational profile. In contrast, Small Feeder and Panamax ships exhibit much larger discrepancies between the speed reductions required by the two criteria, indicating that their actual operational speeds often deviate significantly from their design speeds, possibly due to varying operational patterns or trading routes.

According to the conducted analysis, it can be observed that even a slight tightening of the CII criterion, by only 2% per year starting from 2022, has a significant impact on the CII performance of ships. This essentially means that ships will need to change their operational patterns in order to continue meeting the CII requirements. On the other hand, if the ships had been designed according to the way they are actually operated, a large number of them would have satisfied even the strictest criteria currently in force.

Overall, the combined EEDI/EEXI and CII analyses illustrate the dual importance of design optimization and operational management in achieving energy efficiency. While EEDI and EEXI capture potential efficiency at design stage, CII provides a more accurate reflection of real-world performance. The observed discrepancy between design and operational speeds emphasizes the effectiveness of slow steaming and other operational measures in reducing emissions, suggesting that regulatory strategies combining both design and operational targets are essential for sustainable fleet management. Further improvements in energy efficiency will likely depend increasingly on technological innovation. In addition to propulsion optimization and energy-saving devices, this includes the gradual adoption of alternative fuels such as LNG, methanol, ammonia or hydrogen, as well as hybrid propulsion concepts and partial electrification of auxiliary power systems. Such solutions are increasingly being considered as part of broader strategies to achieve the long-term IMO greenhouse gas reduction targets.

The results also have broader implications for key actors in the maritime supply chain. Since operational measures such as speed reduction directly influence voyage duration and schedule reliability, regulatory requirements such as CII increasingly affect not only shipowners but also charterers, cargo owners and logistics operators. In liner shipping in particular, slower operating speeds may influence service frequency, fleet deployment strategies and overall supply-chain planning. Consequently, compliance with energy efficiency regulations is gradually becoming a shared responsibility across the entire maritime transport chain rather than solely a technical issue for ship designers and operators.

6. Conclusion

The analysis of 162 seagoing container ships built between 2000 and 2020 provides a detailed picture of design evolution, energy efficiency trends, and regulatory compliance in the global container fleet.

The study demonstrates that container ships have achieved progressive improvements in energy efficiency, as reflected in the increasing EPL values across successive periods. Between 2000 and 2020, efficiency improvements were steady, but after 2008, the rate of EPL increase almost doubled, reflecting intensified global regulatory and environmental focus. The year 2008, serving as the IMO reference year for emission reductions, represents a turning point where stronger improvements were observed. By 2013, when EEDI regulations entered into force, the baseline EPL values were significantly higher and subsequent improvements occurred at a slower rate, signaling regulatory-driven stabilization.

This analysis confirms that EPL trends not only reflect technological advancement but also the strong influence of regulatory frameworks such as the IMO's efficiency measures. The results provide evidence that container ship design and operation have become progressively more energy efficient, with the steepest gains occurring in periods aligned with major regulatory milestones. In general, ships have achieved progressively lower EEDI and EEXI values over the years, which clearly indicates that they have become more energy efficient.

Furthermore, the analysis of ship operational profiles revealed that the actual sailing speeds of the analyzed vessels are already below the levels required to satisfy the EEXI criterion, which raises questions about the overall relevance and practical effectiveness of this regulatory measure. This also indicates that the potential for further emission reductions through speed reduction alone is limited, since most vessels already operate well below their design speeds. On the other hand, if ships had been designed more closely in accordance with their actual operational profiles, a significant number of them would have satisfied even the most stringent regulations currently in force. However, as the CII requirements are expected to become progressively stricter in the coming years, speed reduction may eventually become insufficient as a standalone compliance measure. Future studies should expand the operational dataset by incorporating a larger number of ships and longer time series of operational data in order to improve the statistical robustness of fleet-level assessments of operational carbon intensity. This research therefore highlights the need for a fundamental shift in ship design philosophy – from compliance-driven optimization toward a holistic decarbonization strategy that aligns design, operation and energy systems. The concept of design speed is progressively being replaced by an operational compliance speed, defining the actual regime at which ships are designed to function efficiently within environmental and regulatory boundaries. Such a transformation requires integration of alternative fuels, hybrid propulsion systems, energy-saving devices and data-driven optimization tools that collectively enable genuine emission reduction rather than temporary compliance.

In conclusion, while existing measures such as EEDI, EEXI, and CII have played a pivotal role in steering the industry toward higher efficiency, they represent only transitional instruments on the path to zero-carbon shipping. The broader implication of this study lies in demonstrating that future progress depends on a systemic reconfiguration of design and operational paradigms, positioning the maritime sector not merely to comply with regulations but to actively lead the global decarbonization transition. In this context, the findings of the present

study suggest that regulatory mechanisms such as EEDI, EEXI and CII have already significantly influenced ship design and operational practices. However, achieving deeper emission reductions in the coming decades will likely require a combination of regulatory pressure, technological innovation and operational optimization across the entire maritime transport system.

CRediT authorship contribution statement

Matija Vasilev: Writing – original draft, Visualization, Validation, Software, Investigation, Formal analysis, Data curation. **Milan Kalajdžić:** Writing – review & editing, Supervision, Resources, Project administration, Funding acquisition, Data curation, Conceptualization. **Nikola Momčilović:** Writing – review & editing, Writing – original draft, Supervision, Project administration, Methodology, Conceptualization. **Filip Miltenović:** Writing – original draft, Methodology, Investigation, Formal analysis.

Funding sources

This research did not receive any specific grant from funding agencies in the public, commercial, or not-for-profit sectors.

Declaration of competing interest

The authors declare the following financial interests/personal relationships which may be considered as potential competing interests: Matija Vasilev reports administrative support was provided by Ocean Pro Marine Engineers LTD. If there are other authors, they declare that they have no known competing financial interests or personal relationships that could have appeared to influence the work reported in this paper.

Acknowledgements

The research is supported by Ministry of Science, Technology Development and Innovation of Republic of Serbia, Contract No. 451-03-34/2026-03/200105. Authors would like to acknowledge Ocean Pro Marine Engineers LTD for its help in collecting data for the ship database.

References

Ahn, J., Seong, S., Lee, J., Yun, Y., 2023. Energy efficiency and decarbonization for container fleet in international shipping based on IMO regulatory frameworks: a case study for South Korea. J. Int. Maritime Safety Environ. Affairs Shipping 7, 2–3. https://doi.org/10.1080/25725084.2023.2247832.

Alshareef, M.H., Alghanmi, A.F., 2024. Optimizing maritime energy efficiency: a machine learning approach using deep reinforcement learning for EEXI and CII compliance. Sustainability 16, e10534. https://doi.org/10.3390/su162310534.

Ammar, N.R., Seddiek, I.S., 2020. An environmental and economic analysis of emission reduction strategies for container ships with emphasis on the improved energy efficiency indexes. Environ. Sci. Pollut. Res. 27, 23342–23355. https://doi.org/10.1007/s11356-020-08861-7.

Bayraktar, M., Yüksel, O., 2023a. A scenario-based assessment of the energy efficiency existing ship index (EEXI) and carbon intensity indicator (CII) regulations. Ocean Eng. 278, e114295. https://doi.org/10.1016/j.oceaneng.2023.114295.

Bayraktar, M., Yüksel, O., 2023b. Investigation of the effect of anti-fouling systems on meeting energy efficiency regulations. Marine Sci. Technol. Bull. 12 (2), 172–181. https://doi.org/10.33714/masteb.1276367.

Bayramoglu, K., 2024. The effects of alternative fuels, cruising duration and variable generators combination on exhaust emissions, energy efficiency existing ship index (EEXI) and carbon intensity rating (CII). Ocean Eng. 302, e117723. https://doi.org/10.1016/j.oceaneng.2024.117723.

Cicek, I., Yilmaz, N., 2023. Modeling and analysis of container-type ships marine propeller for engine load conditions. J. ETA Maritime Sci. 11 (1), 14–27. https://doi.org/10.4274/jems.2023.81568.

Constantin, G., Amoraritei, M., 2018. Analysis of the energy efficiency design index for two container ships and EEDI influence on propulsion performances. Ann. "Dunarea de Jos" Univ. Galati. Fascicle XI Shipbuilding. https://doi.org/10.35219/ANNUGALSHIPBUILDING.2018.41.19.

DNV, 2025. Maritime forecast to 2025. https://www.dnv.com/maritime/maritime-forecast/. (Accessed 20 September 2025).

Elkafas, A., 2024. Thermodynamic analysis and economic assessment of organic rankine cycle integrated with thermoelectric generator onboard container ship. Processes 12 (2), e355. https://doi.org/10.3390/pr12020355.

Elkafas, A.G., Shouman, M.R., 2021. Assessment of energy efficiency and ship emissions from speed reduction measures on a medium sized container ship. Trans. R Inst. Nav. Archit. A: Int. J. Marit. Eng. 163, 121–132. https://doi.org/10.5750/ijme.v163iA3.805.

Elkafas, A., Khalil, M.I., Shouman, M., ElGohary, M.M., 2021. Environmental protection and energy efficiency improvement by using natural gas fuel in maritime transportation. Environ. Sci. Pollut. Res. Int. 28, 60585–60596. https://doi.org/10.1007/s11356-021-14859-6.

Elkafas, A.G., Rivarolo, M., Massardo, A.F., 2023. Environmental economic analysis of speed reduction measure onboard container ships. Environ. Sci. Pollut. Control Ser. 30 (21), 59645–59659. https://doi.org/10.1007/s11356-023-26745-4.

Elmallah, M., Madariaga, E., Almeida, J.A.G., Alghaffari, S., Saadeldin, M.A., Ghoneim, N.I., Shouman, M., 2025. Decarbonization potential of alternative fuels in container shipping: a case study of the EVER ALOTVessel. Environments 12 (9), 306. https://doi.org/10.3390/environments12090306.

Equasis, 2020. The 2020 World Merchant Fleet - Statistics from Equasis. https://www.equasis.org/EquasisWeb/restricted/Stat?fs=HomePage. (Accessed 22 September 2025).

Gałecka, O., 2024. Case studies examining the impact of employing robust voyage optimization techniques on enhancing a vessel's CII rating. In: Proceedings of 16th Symposium on High Performance Marine Vehicles (HIPER'24). Drubeck, Germany, pp. 29–35. June 2024.

Garbatov, Y., Georgiev, P., 2021. Advances in conceptual ship design accounting for the risk of environmental pollution. Ann. J. Techn. Univ. Varna 5 (1), 25–41. https://doi.org/10.29114/ajtuv.vol5.iss1.227. Bulgaria.

Gatin, I., Keser, R., Vukčević, V., 2024. Deep dive into trim optimisation: physical phenomena behind the fuel savings. In: Proceedings of 9th Hull Performance & Insight Conference (HullPIC'24), Tullamore. Ireland, pp. 18–24. March 2024.

He, Z., Tanhaei, M., Huang, K.W., Ibrahim, I., Liu, M., Yin, X., 2024. Evaluating environmental impact and the significance of shipboard carbon capture and storage for emission reduction in maritime sector. J. Phys. Conf. 2867 (1), e012004. https://doi.org/10.1088/1742-6596/2867/1/012004.

Hoffmann, M., 2022. The impact of 'fouling idling'on ship performance and Carbon Intensity Indicator (CII). In: Proceedings of 7th Hull Performance & Insight Conference (HullPIC'22), pp. 161–168. Tullamore, Ireland, May 2022.

IMO, 2009. MEPC.1/Circ.684, Guidelines for Voluntary Use of the Ship Energy Efficiency Operational Indicator (EEOI). https://docs.imo.org/. (Accessed 22 September 2025).

IMO, 2011. Resolution MEPC.203(62). Amendments to the Annex of Protocol of 1997 to Amend the International Convention for the Prevention of Pollution from Ships, 1973, as Modified by the Protocol of 1978 Relating Thereto (Inclusion of Regulations on Energy Efficiency for Ships in MARPOL Annex VI). https://docs.imo.org/. (Accessed 22 September 2025).

IMO, 2016. Resolution MEPC.278(70). Amendments to the Annex of Protocol of 1997 to Amend the International Convention for the Prevention of Pollution from Ships, 1973, as Modified by the Protocol of 1978 Relating Thereto (Data collection system for fuel oil consumption of ships. https://docs.imo.org/. (Accessed 22 September 2025).

IMO, 2018. Resolution MEPC.308(73). 2018 guidelines on the method of calculation of the attained Energy Efficiency Design Index (EEDI) for new ships. https://docs.imo.org/. (Accessed 22 September 2025).

IMO, 2019. Resolution MEPC. 322(74). Amendments to the 2018 guidelines on the method of calculation of the attained Energy Efficiency Design Index (EEDI) for new ships. https://docs.imo.org/. (Accessed 22 September 2025).

IMO, 2020. Fourth IMO Greenhouse Gas Study. International Maritime Organization.

IMO, 2021a. Resolution MEPC. 328(76. Amendments to the Annex of Protocol of 1997 to Amend the International Convention for the Prevention of Pollution from Ships, 1973, as Modified by the Protocol of 1978 Relating Thereto (2021 Revised MARPOL Annex VI). https://docs.imo.org/. (Accessed 22 September 2025).

IMO, 2021b. Resolution MEPC.338(76). 2021 guidelines on the operational carbon intensity reduction factors relative to reference lines. CII Reduction Factors Guidelines, G3). https://docs.imo.org/. (Accessed 22 September 2025).

IMO, 2022a. Resolution MEPC.364(79). 2022 Guidelines on the method of calculation od the attained Energy Efficiency Design Index (EEDI) for new ships. https://docs.imo.org/. (Accessed 22 September 2025).

IMO, 2022b. Resolution MEPC.350(78). 2022 guidelines on the method of calculation of the attained energy Efficiency Existing Ship Index (EEXI). https://docs.imo.org/. (Accessed 22 September 2025).

IMO, 2022c. Resolution MEPC.352(78. 2022 Guidelines on Operation Carbon Intensity Indicators and the Calculation Methods (CII Guidelines, G1). IMO, London, England. https://docs.imo.org/. (Accessed 22 September 2025).

IMO, 2022d. Resolution MEPC.353(78). 2022 guidelines on the reference lines for use with the operational carbon intensity indicators. CII Reference Lines Guidelines, G2). https://docs.imo.org/. (Accessed 22 September 2025).

IMO, 2022e. Resolution MEPC.354(78). 2022 guidelines on the operational carbon intensity rating of ships (CII rating guidelines, G4). https://docs.imo.org/. (Accessed 22 September 2025).

IMO, 2022f. MARPOL annex VI. Regulations for the prevention of air pollution from ships. https://www.imo.org/. (Accessed 25 September 2025).

IMO, 2022g. Consideration of the report to MEPC 78, report of the twelfth meeting of the intersessional working group on reduction of GHG emissions from ships (ISWG-GHG 12). https://www.imo.org/. (Accessed 24 September 2025).

IMO, 2022h. Resolution MEPC.346(78). 2022 guidelines for the development of a Ship Energy Efficiency Management Plan (SEEMP). https://docs.imo.org/. (Accessed 24 September 2025).
IMO, 2023. Resolution MEPC.377(80). 2023 IMO Strategy on Reduction of GHG Emissions from Ships. https://docs.imo.org/. (Accessed 12 March 2026).
Jin, W.S., Kim, M.C., Kang, J.G., Shin, Y.J., Lee, K.W., 2023. Optimization of blade position on an asymmetric pre-swirl stator used in container ships. J. Mar. Sci. Eng. 11 (1), e50. https://doi.org/10.3390/jmse11010050.
Kalajdžić, M., M, 2022. The influence of roughness change on ship resistance in CFD simulations. In: Proceedings of 24th Numerical Towing Tank Symposium (NuTTS 2022). Zagreb, Croatia, October 2022.
Kalajdžić, M., Vasilev, M., Momčilović, N., 2022a. Assessment of energy efficiency for the existing cargo ships. J. Maritime Sci. (JMS) 23 (1). https://doi.org/10.56080/jms220502.
Kalajdžić, M., Vasilev, M., Momčilović, N., 2022b. Power reduction considerations for bulk carriers with respect to novel energy efficiency regulations. Brodogradnja 73 (2), 79–92. https://doi.org/10.21278/brod72205.
Katelieva, E., 2023. Technical retrofits for energy efficiency improvement of ships. In: Proceedings of 15th Electrical Engineering Faculty Conference (BulEF), 2023. https://doi.org/10.1109/BulEF59783.2023.10406254. Varna, Bulgaria, September 2023.
Kim, S.W., Eom, J.O., 2023. Ship carbon intensity indicator assessment via just-in-time arrival algorithm based on real-time data: case study of pusan new international port. Sustainability 15, e13875. https://doi.org/10.3390/su151813875.
Kim, M., Park, D., 2015. A study on the green ship design for ultra large container ship. J. Korean Soc. Marine Environ. Safety 21 (5), 558–570. https://doi.org/10.7837/kosomes.2015.21.5.558.
Kontovas, C., Psaraftis, H.N., 2011. Reduction of emissions along the maritime intermodal container chain: operational models and policies. Marit. Pol. Manag. 38 (4), 451–469. https://doi.org/10.1080/03088839.2011.588262.
Lehmann, N., Panagakos, G., Barfod, M.B., 2025. Impact assessment of regulations on container shipping decarbonization: an evidence-based case study. Transp. Res. Part D 146, e104902. https://doi.org/10.1016/j.trd.2025.104902.
Lim, S.S., Kim, T.W., Lee, D.M., Kang, C.G., Kim, S.Y., 2014. Parametric study of propeller boss cap fins for container ships. Int. J. Nav. Archit. Ocean Eng. 6 (2), 187–205. https://doi.org/10.2478/IJNAOE-2013-0172.
Lysyy, A., Kotenko, V., Yakovtsev, S., 2018. Conceptual scheme for ensuring the energy efficiency principle in modern container. EUREKA: Phys. Eng. 6, 41–47. https://doi.org/10.21303/2461-4262.2018.00749.
Meyer, J., Stahlbock, R., Voß, S., 2012. Slow steaming in container shipping. In: Proceedings of the 45th Hawaii International Conference on System Sciences, Maui, HI, USA, 4–7 January, pp. 1306–1314.
Nadery, A., Ghassemi, H., 2020. Numerical investigation of the hydrodynamic performance of the propeller behind the ship with and without wed. Pol. Marit. Res. 27 (4), 50–59. https://doi.org/10.2478/pomr-2020-0065.
Nojiri, T., Ishii, N., Kai, H., 2011. Energy saving technology of PBCF (propeller boss cap fins) and its evolution. Mar. Eng. 46 (3), 350–358. https://doi.org/10.5988/jime.46.350.
Olmer, N., Comer, B., Roy, B., Mao, X., Rutherford, D., 2017. Greenhouse gas emissions from global shipping. Int. Council Clean Transport. https://theicct.org. (Accessed 23 September 2025).
Ozsari, I., 2023. Predicting main engine power and emissions for container, cargo, and tanker ships with artificial neural network analysis. Brodogradnja 74 (2), 77–94. https://doi.org/10.21278/brod74204.
Park, J., Jung, J., Seo, Y., 2023. Investigation of applying technical measures for improving Energy Efficiency Design Index (EEDI) for KCS and KVLCC2. J. Ocean Eng. Technol. 37 (2), 58–67. https://doi.org/10.26748/KSOE.2023.001.
Piazza, M.C.D., Pucci, M., Iafrati, A., 2024. Status and future trends of electrification-based solutions for efficiency-oriented ship retrofitting. IEEE International Conference on Electrical Systems for Aircraft, Railway, Ship Propulsion and Road Vehicles & International Transportation Electrification Conference (ESARS-ITEC), pp. 1–6. https://doi.org/10.1109/ESARS-ITEC60450.2024.10819870. Naples, Italy, November 2024.
Rauca, L., Batrinca, G., 2023. Impact of carbon intensity indicator on the vessels' operation and analysis of onboard operational measures. Sustainability 15, e11387. https://doi.org/10.3390/su151411387.
RINA, 2000. Significant Ships. Publications of the Royal Institution of Naval Architects (RINA), London.
Sames, P.C., Köpke, M., 2012. CO_2 emissions of the container world fleet. Proced. Soc. Behav. Sci. 48, 1–11. https://doi.org/10.1016/j.sbspro.2012.06.982.
Sellers, C., 2017. Field operation of a 125kW ORC with ship engine jacket water. Energy Proc. 129, 495–502. https://doi.org/10.1016/j.egypro.2017.09.168.
Serra, P., Fancello, G., 2020. Towards the IMO's GHG goals: a critical overview of the perspectives and challenges of the main options for decarbonizing international shipping. Sustainability 12 (8), e3220. https://doi.org/10.3390/su12083220.
Sevgili, C., Bayraktar, M., Seyhan, A., Yüksel, O., 2025. Cold ironing impact on voyage carbon intensity in container shipping: economic and regulatory insights. Sustainability 17 (12), e5556. https://doi.org/10.3390/su17125556.
Tokuşlu, A., 2020. Analyzing the Energy Efficiency Design Index (EEDI) performance of a container ship. Int. J. Electron. Govern. 7 (2), 114–119. https://doi.org/10.30897/ijegeo.703255.
Tran, N.K., Tran, T.A.T., 2023. Environmental effects of Maersk Line's global container shipping operation. Supply Chain Forum Int. J. 24 (2), 170–181. https://doi.org/10.1080/16258312.2022.2159277.
UNCTAD, 2024. Review of Maritime Transport. United Nations Conference on Trade and Development. https://www.iims.org.uk/unctad-review-of-maritime-transport-2024-navigating-maritime-chokepoints/. (Accessed 20 September 2025).
UNCTAD, 2025. Review of Maritime Transport. United Nations Conference on Trade and Development. https://unctad.org/publication/review-maritime-transport-2025. (Accessed 20 September 2025).
Uygur, S., Bolat, P., Kayışoğlu, G., Düzenli, E., Bolat, F., Arslan, O., Wei, R., Zhou, F., Wang, Y.W., 2026. Modelling maritime GHG emission measures impact assessment: a case study for container shipping by system dynamics. Brodogradnja 77 (2), 77207. https://doi.org/10.21278/brod77207Vasilev.
Vasilev, M., Kalajdžić, M., Suvačarov, A., 2023. A practical approach to bulbous bow retrofit analysis for enhanced energy efficiency. In: Proceedings of 25th Numerical Towing Tank Symposium (NuTTS 2023). Ericeira, Portugal, October 2023.
Vasilev, M., Kalajdžić, M., Ivković, I., 2024. CFD-Powered ship trim optimization: integrating ANN for user-friendly software tool development. J. Mar. Sci. Eng. 12 (8), e1265. https://doi.org/10.3390/jmse12081265.
Vasilev, M., Kalajdžić, M., Momčilović, N., 2025. On energy efficiency of tankers: EEDI, EEXI and CII. Ocean Eng. 317, e120028. https://doi.org/10.1016/j.oceaneng.2024.120028.
Wang, S., Psaraftis, H.N., Qi, J., 2021. Paradox of international maritime organization's carbon intensity indicator. Commun. Transport. Res. 1, e100005. https://doi.org/10.1016/j.commtr.2021.100005.
Wang, Z., Lu, T., Han, Y., Zhang, C., Zeng, X., Li, W., 2024. Improving ship fuel consumption and carbon intensity prediction accuracy based on a long short-term memory model with self-attention mechanism. Appl. Sci. 14 (18), e8526. https://doi.org/10.3390/app14188526.
Wiliyan, R., Ariana, I.M., Widhi, D., 2023. Evaluation of energy Efficiency Existing Ship Index (EEXI) on container ship in Indonesian shipping. IOP Conf. Ser.: Earth Environ. Sci. Surabaya. https://doi.org/10.1088/1755-1315/1198/1/012025. Indonesia, November 2023.
Woo, J.K., Moon, D.S.H., 2014. The effects of slow steaming on the environmental performance in liner shipping. Marit. Pol. Manag. 41, 176–191. https://doi.org/10.1080/03088839.2013.819131.
Zhang, J., Zhang, Z., Liu, D., 2024. Comparative Study of different alternative fuel options for shipowners based on carbon intensity index model under the background of green shipping development. J. Mar. Sci. Eng. 12 (11), e2044 doi.org/10.3390jmse12112044.
ZoBell, V.M., Gassmann, M., Kindberg, L.B., Wiggins, S.M., Hildebrand, J.A., Frasier, K. E., 2023. Retrofit-induced changes in the radiated noise and monopole source levels of container ships. PLoS One 18 (3), e0282677. https://doi.org/10.1371/journal.pone.0282677.

ПРИЛОГ 6

Influence of Lightweight Change on Ship Performance

Matija Vasilev
University of Belgrade
Faculty of Mechanical Engineering
Ocean Pro Marine Engineers LTD

Milan Kalajdžić
University of Belgrade
Faculty of Mechanical Engineering
Associate professor

An influence assessment of lightweight change on Energy Efficiency Existing Ship Index/Energy Efficiency Design Index performance for two supramax bulk carriers is presented in this paper. The study covers a variation of lightweight from 100% to 85% with the step of 5% reduction. The influence on ship performance is determined through deadweight, reference speed, and engine load. In one part of the work, deadweight is considered to be constant, so the study covers the impact of displacement change on ship speed and power, while in the other one, displacement was kept the same so that the direct influence of deadweight on performance indices was considered. Due to displacement change, a new power curve should be derived, and for this purpose, the Holtrop-Mennen method has been used to predict total resistance. Estimated results show that an increase in speed can be up to 0,7% for the same power and a reduction in power up to 2,6% for the same speed. An increase of a deadweight affects the performance indices up to 3,2%.

Keywords: *energy efficiency, EEDI, EEXI, lightweight*

1. INTRODUCTION

Displacement of the ship consists of lightweight (*LWT)* and deadweight (*DWT)*. Lightweight is a term that represents the total weight of an empty ship (mass without cargo, fuel, lubricating oil, water (ballast, fresh, potable, stores, people (passengers and crew)). Deadweight is defined as a variable load that a ship can carry. One of the most important things in the initial design stages is to estimate the LWT as precisely as possible. Lightweight can be roughly separated into the weight of the hull (steel weight), the weight of the machinery (equipment weight), and the weight margin. There are a lot of approximate formulas for determining the weight of the hull and machinery. Some of the empirical formulas for direct calculation of previously mentioned groups of weight have been in use for decades and can be found in [1-3]. Weight margin or tolerance of uncertainty in the initial design stage is 3% of the deadweight according to [2], 1-2% for simple structures (tankers and bulk carriers), and 2-3% for more complex ships [3]. Nevertheless, the initial *LWT* assessment can be based on a non-dimensional coefficient [3], such as ratios between certain weight groups, including *the DWT- Δ* ratio for a particular type of ship. As the most common and precise procedure nowadays, it can be considered as the conversion of weights from the parent ship to the designed ship [4]. It is interesting that in the last 50 years, the *LWT* has had a decreasing trend of roughly 20% for some ship types [5], and according to [6], the average efficiency has improved by 22-28% within a decade. Also, according to [7], the *LWT-LBD* ratio (where *L* – length, *B* – breadth, *H* – depth) is decreasing for larger *DWT*, which means that smaller ships are usually heavier, which is one of the reasons why larger ships are being built.

On the other hand, over the decades, supply and demand have increased globally due to society's deve–lopment and civilization's progress. Consequently, there was a need for a greater and more frequent exchange of goods between more distant countries. This led to the design and construction of larger ships [7,8]. Larger ships also required the installation of larger engines, while larger engines required a larger amount of fuel, and combustion of a larger amount of fuel leads to greater pollution from greenhouse gases. Even though in 2011 Marine Environment Protection Committee rele–ased a resolution [9] in order to prevent pollution from newbuilt ships falling under the MARPOL Annex VI and over 400 GT through *EEDI* that set-in use from 2013, the global trend of CO_2 is still rising [10]. Also, International Maritime Organization (IMO) has introduced an energy efficiency parameter [11] for existing ships through *EEXI* that will enter into force in 2023. and it is based on *EEDI*. This regulation covers only seagoing ships, while some of the first evaluations of inland waterways cargo ships' efficiency indices are described in [12].

The overtaken work has to give an answer how extensive can be the benefit in energy efficiency if the *LWT* is reduced and whether it could be compared with other energy-saving measures such as the installation of Energy Saving Devices (ESD), optimized operational strategies, fuel changes, hull cleaning, and anti-fouling paint application, propeller polishing, etc. The ESD can improve the overall efficiency by 6-14% with pre-swirl ducts [13] or 2-5% with post-swirl devices [14]. Opti–mized operational strategies such as optimum trim, speed, and routing can save up to 5% in power [14]. The effect of different fuel types on the environment can be found in [15,16], while the anti-fouling application and polishing could have a significant influence [17, 18].

Received: June 2022, Accepted: September 2022
Correspondence to: Matija Vasilev
Ocean Pro Marine Engineers LTD,
Takovska 45, 11000 Belgrade, Serbia
E-mail: matija@oceanpro.eu
doi: 10.5937/fme2204615V

2. METHODOLOGY

Two ships are considered in this paper: bulk carrier 1 and bulk carrier 2. The main particulars are shown in Table 1:

Table 1. Main particulars

	Bulk Carrier 1		Bulk Carrier 2	
	Scantling	Design	Scantling	Design
year	2011		2010	
Loa [m]	197		189.9	
Lpp [m]	194		182.7	
B [m]	32.26		30.5	
H [m]	18		17.5	
T [m]	12.65	11.3	12.8	11
WS [m^2]	10084	9508	9054	8305
AT [m^2]	25.6	5.2	6.05	0
LCB [%]	1.14	1.54	1.93	2.38
KB [m]	6.571	5.861	6.637	5.686
Cb [-]	0.853	0.844	0.831	0.819
Cp [-]	0.855	0.847	0.835	0.823
Cw [-]	0.929	0.925	0.915	0.891
Δ [t]	69179	61150	60796	51498
DWT [t]	58675	50646	50136	40838
LWT [t]	10504		10660	
MCR [kW]	8630		9480	
V_{des} [kn]	14.5		14.5	

They have different bow types: bulk carrier 1 has an unusual bow with a vertical stem, while bulk carrier 2 has a bulbous bow. Their non-dimensional resistance $Rt/(\Delta \cdot g)$ in the function of Froude number (based on length) is shown in the following figure:

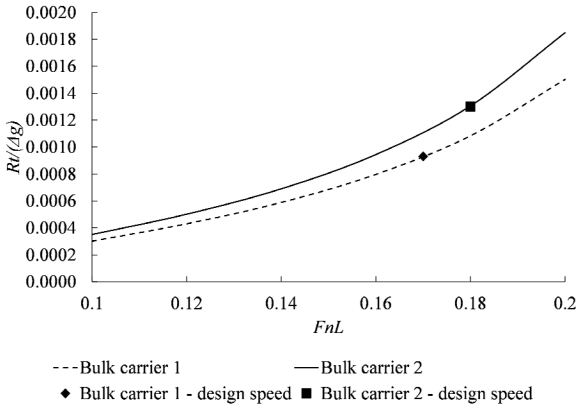

Figure 1. Non-dimensional total resistance vs. speed comparison

Bulk carrier 1 has approximately 19% (average) better performance for the same speed (Figure 1). Also, bulk carrier 1 has approximately 10% larger wetted surface, which is a dominant part of viscous resistance at low speeds. This means that pressure resistance is significantly less because the total resistance of this ship is less. Both ships were completed (built) within a year, but the keel of bulk carrier 2 was laid in 2004. while the keel of bulk carrier 1 was laid in 2010. It seems that in a period of 6 years, design in the shipping industry has significantly progressed. Ships have become lighter, could carry more cargo, and go faster even with a less powerful engine.

Both ships are made from the same steel grade (mild steel); although bulk carrier 1 is longer and wider, she is also lighter. The capacity of bulk carrier 1 is greater by approximately 10000t at the design draft. So, it was interesting to find out, could bulk carrier 2 be faster if she had been made lighter.

Figure 2 are shown 3D models of both considered bulk carriers, while characteristic sections are shown at the end of this topic.

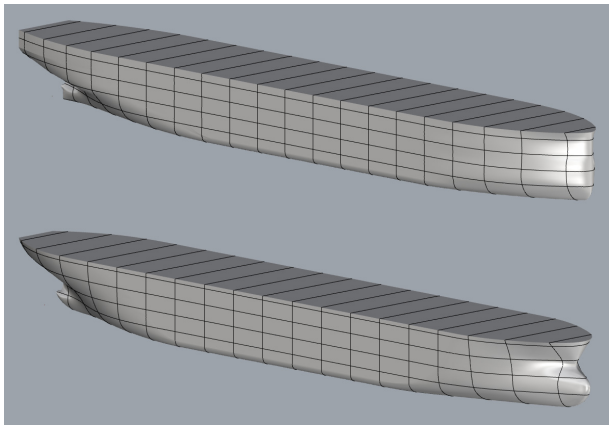

Figure 2. Hull shape - bulk carrier 1 (up), bulk carrier 2 (down)

The reduction of *LWT* in this paper refers to the reduction of steel weight, but this information is not given in the ship's documentation. So, the steel weight and machinery weight for both ships are approximated as an average value derived from the following formulas also given in [3]:

$$m_1 = 0,1 \cdot X \cdot e^{-5,7310^{-7} \cdot X}, X = \frac{1}{12} \cdot L^2 \cdot B \cdot \sqrt[3]{C_B} \quad (1)$$

$$m_2 = \frac{1}{6} \cdot C_B^{2/3} \cdot L \cdot B \cdot H^{0,72} \cdot \left[0,002 \cdot \left(\frac{L}{H} \right)^2 + 1 \right] \quad (2)$$

$$m_3 = 0,03325 \cdot L^{1,65} \cdot \left(B + H + 0,5 \cdot T \right) \cdot (0,5 \cdot C_B + 0,4) \quad (3)$$

$$m_4 = 0,032 \cdot E^{1,36}, E = L \cdot \left(B + T \right) + 0,85 \cdot L \cdot \left(H - T \right) \quad (4)$$

$$m_5 = \left[0,07 + 0,064 \cdot e^{-\left(0,5 \cdot u + 0,1 \cdot u^{2,45} \right)} \right] \cdot L \cdot B \cdot H,$$

$$u = \log \left(\frac{\Delta}{100} \right) \quad (5)$$

$$m_6 = 0,78 \cdot LWT. \quad (6)$$

Average approximated data are given in Table 2:

Table 2. Estimation of group weights

	Bulk carrier 1	Bulk carrier 2
W_{steel} [t]	9130	8251
$W_{\text{machinery}}$ [t]	1292	1305
LWT_{app} [t]	10422	9555
LWT [t]	10504	10660
ΔLWT	-1%	-10%

Approximated LWT_{app} of bulk carrier 1 is within the proposed margin, while *the* LWT_{app} of bulk carrier 2 is underestimated by 10%. The proposed reduction rate for

steel weight is 5, 10, and 15% in accordance with previous observations and achieved possible reductions described in [19]. After applying reduction rates, total *LWT* is decreased for 4, 9, and 13% (bulk carrier 1) and 4, 8, and 12% (bulk carrier 2). In order to simplify the procedure and further calculation, the estimated new *LWT* equals to original reduced by 5, 10, and 15%. This means that reduction is not directed to steel weight only but to total *LWT*.

The influence of *LWT* reduction was determined through three parameters, and the estimation procedure is summarized in Table 3:

Table 3. Overall calculation procedure

	LWT	*DWT*	*Δ*	V_{ref}	*Engine Load*
Case 1	100%	original	original	original	original
	95%	const.	reduced	to estimate	const.
	90%				
	85%				
Case 2	100%	original	original	original	original
	95%	const.	reduced	const.	to estimate
	90%				
	85%				
Case 3	100%	original	original	original	original
	95%	increased	const.	/	/
	90%				
	85%				

The term 'original' in the previous table means that *DWT* and *Δ* are taken from the ship's Stability Booklet.[1] For scantling and design draughts, while original speed represents reference speed, and the original engine load is engine power load which corresponds to reference speed. Reference speed is needed for attained *EEXI* and attained *EEDI* calculation. Full form of attained *EEXI* and attained *EEDI* formulas are given in [19] and [20], respectively, but here, these parameters are evaluated according to simplified form:

$$att.EEXI = \frac{P_{ME} \cdot C_{FME} \cdot SFC_{ME,app} + P_{AE} \cdot C_{FAE} \cdot SFC_{AE,app}}{f \cdot Capacity \cdot V_{ref,EEXI}} \quad (7)$$

$$att.EEDI = \frac{P_{ME} \cdot C_{FME} \cdot SFC_{ME,app} + P_{AE} \cdot C_{FAE} \cdot SFC_{AE,app}}{f \cdot Capacity \cdot V_{ref,EEDI}} \quad (8)$$

All parameters from (10) and (11) are described in [11,18,19]. The required *EEXI* and *EEDI* are calculated in accordance with [11]:

$$req.EEXI = req.EEDI = a \cdot DWT^{-c} \cdot \left(1 - \frac{Y}{100}\right) \quad (9)$$

where for bulk carriers a = 961,79; c = -0,477 and Y = 20 [11]. Attained *EEXI* and *EEDI* have to be below their required *EEXI* and *EEDI*. $V_{ref,EEDI}$ is defined as the speed at 75% of Maximum Continuous Rating (*MCR*), while $V_{ref,EEXI}$ is calculated in accordance with the following equation given in [19]:

$$V_{ref,EEXI} = k^{\frac{1}{3}} \cdot \left(\frac{DWT_{S,service}}{Capacity}\right)^{\frac{2}{9}} \cdot V_{S,service} \cdot \left(\frac{P_{ME}}{P_{S,service}}\right)^{\frac{1}{3}} \quad (10)$$

Service power ($P_{S,service}$) is equal to 85% of *MCR* and with no sea margin included. $DWT_{S,service}$ corresponds to design deadweight, while $V_{S,service}$ is the sea-trial service speed under the design draught corresponds to $P_{S,service}$. k is scale coefficient and equals 0,97 [20]. Reference speed for *EEDI* is evaluated in accordance with the [21] and it is a speed that corresponds to 75% of maximum installed power (*MCR*).

In cases 1 and 2, *DWT* was kept constant, so the *Δ* is reduced because of a reduced *LWT*. The effect of the lighter ship is determined via the expected speed increase for the same power for case 1 and vice versa for case 2. In case 3, *DWT* is increased to compensate for the *LWT* reduction in order to keep the *Δ* constant. The power curve stayed the same in this case, so the effect of this change on *EEXI*/*EEDI* can be directly estimated.

A change in *Δ* is manifested by a change in a draught, so the ship has different *LCB*, *Cb*, *Cp*, *Cw*, *WS*, etc. Previously mentioned parameters are given in Stability Booklets for different draughts. For each new *Δ*, these parameters have been linearly interpolated. Due to variations in main particulars, the total resistance is different and, therefore, power curves. To estimate new total resistance, Holtrop-Mennen (HM) method has been used where resistance due to bulb presence is separated from total resistance. In order to verify results, they are compared with available data from Model Test[2] Reports for considered ships. If there is an average deviation greater than 5% in total resistance between calculated and Model Test data, a residual resistance coefficient in the HM method is calibrated until average differences become less than 5% in the area where the model test had been performed. The residual resistance coefficient is derived as the difference between the total resistance coefficient and the frictional resistance coefficient (with roughness allowance included). All formulas for HM method can be found in [22], [23], [24], [25] and [26]. The calibration coefficient is evaluated for scantling and design draughts. For other draughts, calibration coefficients are linearly interpolated for draughts between design and scantling and linearly extrapolated for less-than-design draughts. After total resistance assessment, the engine load is evaluated in accordance with the following equation:

$$P_b = \frac{V \cdot 0,5144 \cdot R_T}{\eta_D \cdot \eta_S} \quad (11)$$

where η_D is the quasi-propulsive coefficient and η_s is shaft efficiency. These coefficients are usually given in Model Test reports, but for bulk carrier 1 are not available and therefore they are assumed to be 0,7 as per [27] for each speed. For shaft efficiency, 0,985 is applied for both ships.

After evaluation of power curves, speeds at 75% (usual reference speed) and 85% (the usual speed at Nominal Continuous Rating (*NCR*)) of *MCR* can be

[1] Each ship should be provided with a stability booklet, approved by the Administration, which contains sufficient information to enable the master to operate the ship in compliance with the applicable requirements.

[2] Ship model testing can protect shipowners and shipbuilders from costly and preventable mistakes. It's used to check systems and specs on a new design, assess midlife upgrades or renovations, determine the outside limits of a vessel's capabilities, or troubleshoot problems.

determined, and thereafter reference speed. As the attained *EEDI* and attained *EEXI* formulas are prac–tically the same (7) and (8) where reference speed is stated in denominators like *DWT* (i.e., *Capacity*); direct influence on these energy efficiency parameters can be assessed in cases 1 and 3. In case 2, an engine power load reduction for initial reference speed is evaluated.

3. RESULTS

Compared obtained and calibrated results (total resistance) from the HM method for scantling and design draught (100% *LWT*) together with model test data, are shown in the following figures (bulk carrier 1 – Figure 3, bulk carrier 2 – Figure 4):

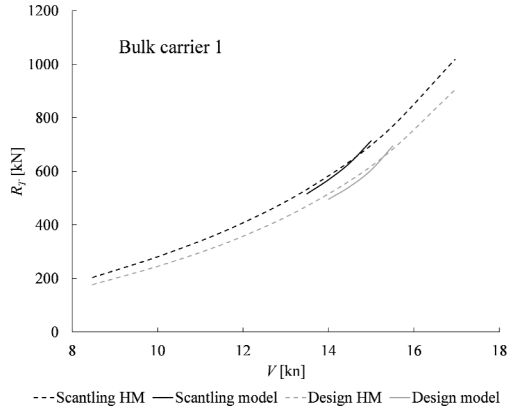

Figure 3. Estimated total resistance and model test results for scantling and design draught (bulk carrier 1)

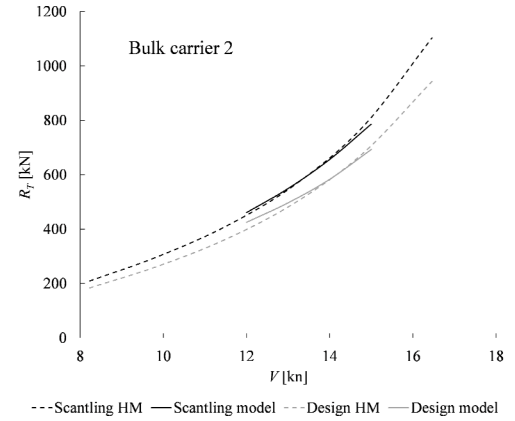

Figure 4. Estimated total resistance and model test results for scantling and design draught (bulk carrier 2)

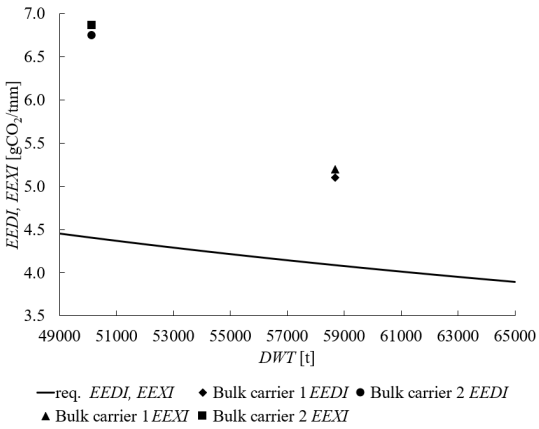

Figure 5. Attained and required *EEDI*/*EEXI*

Input parameters for the HM method, together with estimated total resistance and engine load for all cases, are summarized in tables at the end of the paper. Table 4 are presented input data for attained and required *EEDI* and *EEXI* with calculated relative differences between them for scantling and design draught with 100% of *LWT*.

Table 4. Initial energy efficiency parameters

Parameter	Bulk carrier 1	Bulk carrier 2
P_{ME} [kW]	6472,5	7110
P_{AE} [kW]	431,5	474
C_{FME} [tCO_2/tFuel]	3.206	3,206
C_{FAE} [tCO_2/tFuel]	3.206	3,206
SFC_{ME} [g/kWh]	190	190
SFC_{AE} [g/kWh]	215	215
f [-]	1	1
Capacity [t]	58675	50136
$V_{ref\ EEDI}$ [kn]	14,16	13,77
$V_{ref\ EEXI}$ [kn]	13,90	13,53
(Attained) *EEDI* [gCO_2/tnm]	5,105	6,746
(Attained) *EEXI* [gCO_2/tnm]	5,200	6,864
req. *EEDI* [gCO_2/tnm]	4,089	4,408
req. *EEXI* [gCO_2/tnm]	4,089	4,408
Δ*EEDI* [%]	24,8%	53,1%
Δ*EEXI* [%]	27,2%	55,7%

Attained *EEDI* and *EEXI* are also presented graphically in the following figure:
From the standpoint of energy efficiency, bulk carrier 1 is approximately 25% better than bulk carrier 2, but both are very far from the required indices. The influence of *LWT* change is checked for both energy efficiency parameters for the following reasons:

- *LWT* can only be changed in the initial design phase; therefore *EEDI* has been calculated;
- To assess how far these ships would be today from required (*EEXI*) values if they had been built lighter.

Case 1: $DWT = const.$, Δ is reduced due to a reduction in *LWT*; hence new reference speeds (V_{ref_EEDI} and V_{ref_EEXI}) are evaluated. Results are shown in Table 5.

If the *LWT* is reduced by 5-15%, a possible speed increase of 0,2-0,5% for scantling draught and 0,2-0,6% for design draught could be expected. In the following table, direct influence on *EEXI* and *EEDI* is calculated, where in the *EEXI* improvement column, V_{ref} for different percentages of *LWT* is compared against V_{ref} for full *LWT*. In *EEDI* improvement column, *V* at 75% MCR (Table 6) for scantling (95%, 90%, 85% *LWT*) draught are compared against original *LWT* (100% *LWT*).

Table 5. Speed assessment at 75% and 85% of *MCR*

		Bulk carrier 1		Bulk carrier 2	
	% *LWT*	*V* @75% *MCR*	*V* @85% *MCR*	*V* @75% *MCR*	*V* @85% *MCR*
Design	100%	14,63	15,12	14,44	14,92
	95%	14,64	15,14	14,47	14,96
	90%	14,67	15,16	14,50	14,98
	85%	14,68	15,18	14,53	15,02
Scant.	100%	14,16	14,64	13,77	14,21
	95%	14,20	14,69	13,80	14,24
	90%	14,22	14,71	13,83	14,28
	85%	14,26	14,74	13,84	14,29

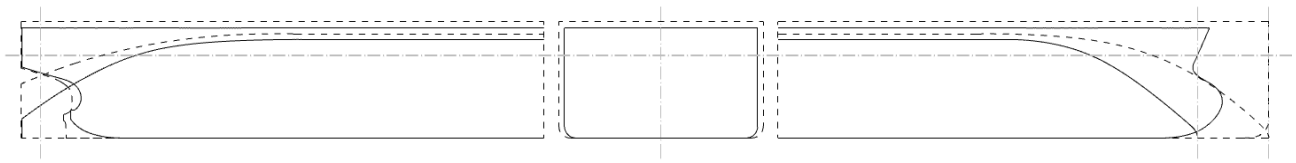

Figure 6. characteristic sections at midship, center line, and water line (dashed line – bulk carrier 1, solid line – bulk carrier 2)

Table 6. *EEXI*/*EEDI* improvement assessment

	Bulk carrier 1			Bulk carrier 2		
% *LWT*	V_{ref}	*EEXI* improve.	*EEDI* improve.	V_{ref}	*EEXI* improve.	*EEDI* improve.
100%	13,90	-	-	13,53	-	-
95%	13,91	0,1%	0,3%	13,57	0,2%	0,2%
90%	13,93	0,3%	0,5%	13,59	0,4%	0,4%
85%	13,95	0,4%	0,7%	13,62	0,6%	0,5%

Case 2: $DWT = const.$, Δ is reduced due to a reduction in *LWT*; hence new power for the same reference and design speed is evaluated for design and scantling draught when 5, 10, and 15% of *LWT* decrease is applied. Results for bulk carrier 1 are shown in Table 7, and for bulk carrier 2 in Table 8.

Table 7. Brake power reduction – bulk carrier 1

	V_{ref} = 13,9 kn		V_{des} = 14,5 kn	
% *LWT*	ΔPb [%] Scantling	ΔPb [%] Design	ΔPb [%] Scantling	ΔPb [%] Design
95%	-1,0%	-0,4%	-1,1%	-0,4%
90%	-1,8%	-1,0%	-1,8%	-1,0%
85%	-2,6%	-1,4%	-2,6%	-1,4%

Table 8. Brake power reduction – bulk carrier 2

	V_{ref} = 13,53 kn		V_{des} = 14,5 kn	
% *LWT*	ΔPb [%] Scantling	ΔPb [%] Design	ΔPb [%] Scantling	ΔPb [%] Design
95%	-0,9%	-0,8%	-0,9%	-0,9%
90%	-1,7%	-1,4%	-1,8%	-1,5%
85%	-2,1%	-2,2%	-2,1%	-2,4%

Case 3: In the previous two cases, Δ was reduced due to the reduction of *LWT*, while *DWT* was kept the same. In this case, when the *LWT* is being decreased, *DWT* is increased to keep the Δ constant (original). Consequently, the original power curves are the same because the draught has not been changed. However, the effect on *EEDI*/*EEXI* is present. As it is stated earlier that *DWT* (*Capacity=DWT*) is in the denominator in *EEDI*/*EEXI* formula (7), (8) direct influence of *DWT* change can be obtained just by comparing new *DWT* with the original. Results are shown in Table 9:

Table 9. Influence of *DWT* change on *EEDI*/*EEXI*

	Bulk carrier 1		Bulk carrier 2	
% *LWT*	New *DWT* [t]	ΔDWT [%]	New *DWT* [t]	ΔDWT [%]
95%	59085	0,9%	50669	1,1%
90%	59610	1,8%	51202	2,1%
85%	60135	2,7%	51735	3,2%

Table 10. Input parameters for HM method (bulk carrier 1)

	Bulk carrier 1							
	100% *LWT*		95% *LWT*		90% *LWT*		85% *LWT*	
	Design	Scantling	Design	Scantling	Design	Scantling	Design	Scantling
DWT [t]	50550	58560	50550	58560	50550	58560	50550	58560
LWT [t]	10504	10504	9979	9979	9454	9454	8928	8928
Δ [t]	61054	69064	60529	68539	60003	68013	59478	67488
T [m]	11.30	12.65	11.21	12.59	11.12	12.48	11.03	12.37
LCB [%]	1.57%	1.16%	1.60%	1.18%	1.63%	1.18%	1.65%	1.24%
WS [m^2]	9495	10084	9457	10047	9418	10000	9380	9952
Cb [-]	0.842	0.851	0.842	0.849	0.841	0.850	0.840	0.851
Cp [-]	0.845	0.854	0.845	0.852	0.844	0.853	0.844	0.853
Cw [-]	0.922	0.927	0.922	0.927	0.922	0.926	0.921	0.926
AT [m^2]	5.2	25.7	4.1	24.7	3.0	22.8	2.0	21.0

Table 11. Input parameters for HM method (bulk carrier 2)

	Bulk carrier 2							
	100% *LWT*		95% *LWT*		90% *LWT*		85% *LWT*	
	Design	Scantling	Design	Scantling	Design	Scantling	Design	Scantling
DWT [t]	40838	50136	40838	50136	40838	50136	40838	50136
LWT [t]	10660	10660	10127	10127	9594	9594	9061	9061
Δ [t]	51498	60796	50965	60263	50432	59730	49899	59197
T [m]	11.00	12.80	10.90	12.70	10.79	12.60	10.69	12.46
LCB [%]	2.38%	1.93%	2.41%	1.95%	2.44%	1.98%	2.46%	2.01%
WS [m^2]	8305	9054	8263	9012	8216	8971	8173	8913
Cb [-]	0.820	0.832	0.819	0.831	0.818	0.831	0.818	0.832
Cp [-]	0.823	0.835	0.822	0.834	0.822	0.833	0.821	0.835
Cw [-]	0.892	0.916	0.890	0.915	0.889	0.913	0.887	0.912
AT [m^2]	0.0	6.1	0.0	5.5	0.0	4.9	0.0	4.2

Table 12. Total resistance and brake power – design and scantling draught – bulk carrier 1

Design	100% *LWT*	95% *LWT*	90% *LWT*	85% *LWT*	100% *LWT*	95% *LWT*	90% *LWT*	85% *LWT*
V [kn]	*Rt* [kN]	*Rt* [kN]	*Rt* [kN]	*Rt* [kN]	*Pb* [kW]	*Pb* [kW]	*Pb* [kW]	*Pb* [kW]
14.00	526	523	520	518	5489	5468	5436	5414
14.50	579	577	573	571	6259	6237	6199	6174
15.00	635	633	629	627	7111	7087	7043	7015
15.50	696	694	689	687	8049	8023	7972	7939
16.00	760	758	753	750	9076	9048	8989	8952
16.50	828	826	820	817	10196	10167	10099	10057
Scantling	100% *LWT*	95% *LWT*	90% *LWT*	85% *LWT*	100% *LWT*	95% *LWT*	90% *LWT*	85% *LWT*
V [kn]	*Rt* [kN]	*Rt* [kN]	*Rt* [kN]	*Rt* [kN]	*Pb* [kW]	*Pb* [kW]	*Pb* [kW]	*Pb* [kW]
13.50	539	534	530	525	5432	5378	5337	5288
14.00	594	588	584	579	6209	6145	6100	6047
14.50	654	647	642	637	7072	6995	6948	6890
15.00	717	709	705	699	8025	7934	7885	7822

Table 13. Total resistance and brake power – design and scantling draught – bulk carrier 2

Design	100% *LWT*	95% *LWT*	90% *LWT*	85% *LWT*	100% *LWT*	95% *LWT*	90% *LWT*	85% *LWT*
V [kn]	*Rt* [kN]	*Rt* [kN]	*Rt* [kN]	*Rt* [kN]	*Pb* [kW]	*Pb* [kW]	*Pb* [kW]	*Pb* [kW]
12.00	393	391	388	385	3552	3527	3505	3480
13.00	486	482	479	475	4738	4702	4673	4636
14.00	595	590	586	581	6255	6203	6164	6112
15.00	720	713	709	702	8161	8087	8037	7963
16.00	862	853	848	840	10650	10547	10481	10379
Scantling	100% *LWT*	95% *LWT*	90% *LWT*	85% *LWT*	100% *LWT*	95% *LWT*	90% *LWT*	85% *LWT*
V [kn]	*Rt* [kN]	*Rt* [kN]	*Rt* [kN]	*Rt* [kN]	*Pb* [kW]	*Pb* [kW]	*Pb* [kW]	*Pb* [kW]
12.00	443	439	436	433	4150	4114	4084	4059
13.00	551	547	542	540	5638	5588	5543	5518
14.00	681	674	669	667	7517	7448	7384	7362
15.00	831	823	815	814	9921	9826	9736	9718
16.00	1002	992	982	981	13058	12930	12804	12794

Compared to case 1, the effect of *DWT* change (Case 3) has a greater influence on *EEDI*/*EEXI* than speed increase due to Δ reduction. That was to be expected due to the higher order of magnitude of *DWT* than V_{ref}.

4. CONCLUSIONS

The influence of possible *LWT* reduction on ship performance has been carried out in this paper. Reduction rates were assessed to be 5, 10, and 15% based on *LWT* (original and approximated) comparison of two bulk carriers. If one ship is larger than the other in terms of *L*, *B*, *T*, or Δ it doesn't necessarily mean that she is heavier. The structural design dates from different, but again, very close periods and the improvement is significant – 19% better performance in terms of total resistance. It turned out that an unusual bow with a vertical stem is more efficient for current Froude numbers. In addition, *the LWT* of compared ships are similar, so it was interesting to point out whether the bulk carrier 2 had had better performance, in case less steel was used.

Results are based on *EEDI*/*EEXI* (case 1 and case 3) performance check and possible reduction in brake power for design and reference speed (case 2). Study shows that *DWT* change has a greater influence (depending on *LWT* reduction rate) on *EEDI*/*EEXI* performance (up to 3,2%) than a change in reference speed (up to 0,7%), while brake power reduction can be 0,4-2,6% for the same speed. This reduction is equivalent to the pollution of 1000 cars per year. The reduction is negligible in terms of *EEDI*/*EEXI* because there are 1.4 billion motor vehicles worldwide. However, from the ship owner's point of view, every percentage of reduction that will imply money-saving is significant. Nevertheless, *LWT* change is only one step in the initial design phase of how we can improve ship performance, and some of the additional ways are described in [28].

The benefit of lighter ships could be achieved by paying attention in the design construction stage. Savings that can be accomplished during the initial design process are equal to the savings that are very difficult to achieve by installing some of the ESD. However, there is still space for possible further improvement with ESDs.

ACKNOWLEDGMENT

This work was partially supported by the Ministry of Education, Science and Technological Development (Project no. 451-03-68/2022-14/200105) of Serbia.

REFERENCES

[1] Watson, D.: Practical Ship Design, Elsevier Ocean Engineering Book Series, Vol. 1, 2002.

[2] Schneekluth, H., Bertram, V.: Ship Design for Efficiency and Economy, Butterworth Heinemann, Second edition, 1998.

[3] Papanikolaou, A.: Ship Design – Methodologies of Preliminary Design, Springer, 2014.

[4] Roh, M. I., Lee, K. Y.: Computational Ship Design, Springer, 2018.

[5] Chen, S., Frouws, K., Van de Voorde, E.: Technical changes and impacts on economic performance of dry bulk vessels, Maritime Policy & Management: The flagship journal of international shipping and port research, 2010.

[6] Faber, J., Hoen, M.: Historical trends in ship design efficiency, CE Delft, Delft, 2015.

[7] Kristensen, H., Lutzen, M.: Existing Design Trends for Tankers and Bulk Carriers – *Design changes for Improvement of the EEDI in the Future*, Technical Information Center of Denmark, IMDC2012, Glasgow, 2012.

[8] Kalajdžić, M., Vasilev, M., Momčilović, N.: Power reduction consideration for bulk carriers with respect to novel energy efficiency regulations, Brodogradnja, Vol. 73 No. 2, 2022.

[9] IMO MEPC, Resolution MEPC.203(62): Amendments to the Annex of the Protocol of 1997 to amend the International Convention for the prevention of pollution from ships, 1973, as modified by the protocol of 1978 relating thereto.: IMO, 2011/07/15, 2011.

[10] IMO, Fourth IMO Greenhouse gas study, International Maritime Organization, 2021.

[11] IMO MEPC, Resolution MEPC.328(76): Amendments to the Annex of the Protocol of 1997 to amend the International Convention for the prevention of pollution from ships, 1973, as modified by the protocol of 1978 relating thereto.: IMO, 2021.

[12] Simić, A., Radojčić, D.: On Energy Efficiency of Inland Waterway Self-Propelled Cargo Vessels, FME Transactions, Vol. 41 No. 2, 2013.

[13] Mancini, S., Vitiello, L., Bilandi, R. N., De Carlini, M.: Shipping Decarbonization: An Overview of the Different Stern Hydrodynamic Energy Saving Devices, Journal of Marine Science and Engineering, 2022.

[14] Molland, A.F., Turnock, S. R., Hudson, D. A., Utama, I. K. A. A.: Reducing Ship Emissions: A Review of Potential Practical Improvements in the Propulsive Efficiency of Future Ships, Transition of the Royal Institution of Naval Architects Part A: International Journal of Marine Engineering, 2014.

[15] Brynolf, S., Baldi, F., Johnson, H.: Energy Efficiency and Fuel Changes to Reduce Environmental Impacts, Shipping and the Environment, Springer, 2016.

[16] Jafarzadeh, S., Schjolberg, I.: Emission Reduction in Shipping Using Hydrogen and Fuel Cells, *Proceedings of the ASME 2017 36th International Conference on Ocean*, Offshore and Arctic Engineering, OMAE2017, 25-30.06.2017, Trondheim, 2017.

[17] Townsin, R. L.: The Ship Hull Fouling Penalty, Biofouling: The Journal of Bioadhesion and Biofilm Research, Taylor & Francis, 2003.

[18] Khor, Y. S., Xiao, Q.: CFD simulations of the effects of fouling and antifouling, Ocean Engineering, Vol. 38, Issue 10, 2011.

[19] Momčilović, N., Motok, M.: Estimation of Ship Lightweight Reduction by Means of Application of Sandwich Plate System, FME Transactions, Vol. 37 No. 3, 2009.

[20] Intersessional Working Group. Draft report of the eight meeting of he Intersessional Working Group on Reduction of GHG Emissions from Ships (ISWG-GHG 8). Norway: IMO, 2021/05/28

[21] IMO MEPC, Resolution MEPC.308(73): Guidelines on the Method of Calculation of the attained Energy Efficiency Design Index (EEDI) for new ships: IMO, 2018/10/26, 2018.

[22] Holtrop, J.: A statistical analysis of performance test results, International Shipbuilding Progress, Vol. 24, No. 270, 1977.

[23] Holtrop, J. Mennen, G.G.J.: A statistical power prediction method, International Shipbuilding Progress, Vol. 25, No. 290, 1978.

[24] Holtrop, J. Mennen, G.G.J.: An approximate power prediction method, International Shipbuilding Progress, Vol. 29, No. 335, 1982.

[25] Holtrop, J.: A statistical re-analysis of resistance and propulsion data, International Shipbuilding Progress, Vol. 31, 1984.

[26] Molland A. F., Turnock S. R., Hudosn D. A.: Ship resistance and propulsion: Practical Estimation of Ship Propulsive Power, Cambridge University Press, 2011.

[27] International Standard, ISO 15016-2015: Ships and marine technology – Guidelines for the assessment of speed and power performance by analysis of speed trial data, ISO 2015, 2015.

[28] Kalajdžić, M., Vasilev, M., Momčilović, N.: Assessment of Energy Efficiency for the Existing Cargo Ships, Journal of Maritime Sciences, Vol. 1 No. 1, 2022.

NOMENCLATURE

AT [m^2]	wetted transom area
B [m]	breadth
Capacity [t]	*DWT* at scantling draught
Cb [-]	block coefficient
C_{FAE} [tCO_2/tFuel]	Conversion factor between fuel consumption and CO_2 emission for auxiliary engine
C_{FME} [tCO_2/tFuel]	Conversion factor between fuel consumption and CO_2 emission for main engine
Cp [-]	prismatic coefficient
Cw [-]	water plane coefficient
DWT [t]	deadweight
$DWT_{S,service}$ [t]	design deadweight
EEDI [gCO2/tnm]	Energy Efficiency Design Index
EEXI [gCO2/tnm]	Energy Efficiency of Existing Ship Index
f [-]	correction factor
g [m/s^2]	gravitational constant, g=9.81
H [m]	depth
k [-]	scale coefficient
KB [m]	vertical center of buoyancy
LCB [%]	longitudinal center of buoyancy
Loa [m]	length overall
Lpp [m]	length between perpendiculars

LWT [t]	lightweight
LWT_{app} [t]	approximated lightweight
MCR [kW]	maximum continuos rating
NCR [kW]	nominal continuos rating
P_{AE} [kW]	Power of auxiliary engine
Pb [kW]	Brake power
P_{ME} [kW]	Main engine power (75% of MCR)
$P_{S,service}$ [t]	power of main engine corresponds to $V_{S,service}$
Rt [kN]	Total resistance
SFC_{AE} [g/kWh]	Specific fuel oil consumption for auxiliary engine
SFC_{ME} [g/kWh]	Specific fuel oil consumption for main engine
T [m]	draught
V [kn]	speed
V_{des} [kn]	design speed
V_{ref} [kn]	reference speed
V_{ref_EEDI} [kn]	Reference speed for $EEDI$ calculation (speed at 75% of MCR)
$V_{ref\ EEXI}$ [kn]	Reference speed for $EEXI$ calculation
$V_{S,service}$ [kn]	service speed under design draught
$W_{machinery}$ [t]	machinery weight
WS [m^2]	wetted surface
W_{steel} [t]	steel weight
Δ [t]	Displacement
ΔDWT [%]	relative deadweight difference
$\Delta EEDI$ [%]	Relative $EEDI$ difference
$\Delta EEXI$ [%]	Relative EEXI difference
ΔLWT [%]	relative lightweight difference
ΔPb [%]	relative brake power difference
η_D [-]	quasi-propulsive coefficient
η_S [-]	shaft efficiency

УТИЦАЈ ПРОМЕНЕ МАСЕ ПРАЗНОГ БРОДА НА СОПСТВЕНЕ ПЕРФОРМАНСЕ

М. Василев, М. Калајџић

Утицај промене масе празног брода на Индекс енертетске ефикасности постојећих и нових бродова за два „supramax“ брода за превоз расутог терета је приказан у овом раду. Рад обухвата редукцију масе празног брода од 100% до 85%, са кораком од 5%. Утицај на перформансе брода је одређен кроз преосталу масу, референтну брзину и оптерећење мотора. У једном делу рада, преостала маса је сматрана константном, те је разматран утицај промене депласмана на брзину брода и потребну ангажовану снагу, док је у другом делу, депласман сматран константним, па је размотрен директан утицај преостале масе на индексе енергетске ефикасности. Услед промене депласмана, било је потребно одредити нову криву снаге, па је за потребе процене тоталног отпора коришћена метода Холтроп-Менен. Добијени резултати показују да је могуће остварити повећање брзине до 0,7% за исту снагу, док редукција снаге за исту брзину може достићи до 2,6%. Повећање преостале масе побољ–шава индексе енергетске ефикасности до 3,2%.

ПРИЛОГ 7**

**У тренутку писања резимеа докторске дисертације, DOI још није додељен овом раду, па је из тих разлога у прилог додат Сертификат о публикацији.

FME TRANSACTIONS

Journal of
Faculty of Mechanical Engineering
University of Belgrade

Kraljice Marije 16, 11120 Belgrade 35

5 March, 2026
Belgrade

Paper No: **FME-026-2212**

http://www.mas.bg.ac.rs/transactions/index.html

CERTIFICATE OF PUBLICATION

I confirm, that the paper by Matija Vasilev and Milan Kalajdžić, entitled:

PARAMETRIC MESH STUDY: LUCY ASHTON CASE

is accepted for publication in the scientific journal FME Transactions, and will be printed in Vol. 54 No 2, pp. 45-61 in June 2026. The electronic version of paper is available online from 15 of May 2026 on the link: https://www.mas.bg.ac.rs/istrazivanje/fme/start

Editor in chief of the journal

Prof. Dr Boško Rašuo

Parametric mesh study: Lucy Ashton case

Matija Vasilev
Research Assistant
University of Belgrade
Faculty of Mechanical Engineering

Milan Kalajdžić
Full Professor
University of Belgrade
Faculty of Mechanical Engineering

This study considers the ship Lucy Ashton, a benchmark case providing full-scale measurements of total ship resistance and boundary layer thickness. A series of CFD simulations was carried out for several different scales and Froude numbers, with the aim of reproducing experimental data on ship resistance and the boundary layer. The results showed agreement with the measurements, with ship resistance predictions within ±5% and realistic boundary layer profiles along the hull. Based on these findings, practical formulas for boundary layer thickness and base mesh cell size were derived. Although these formulas were developed considering only the Lucy Ashton case, they represent a promising basis for application to other ships, particularly at model scale. Further studies are recommended to confirm their reliability for different full scale hull forms.

Keywords: *mesh, boundary layer, full-scale, model scale, resistance prediction.*

1. INTRODUCTION

1.1 CFD mesh

Computational Fluid Dynamics (CFD) has become very useful tool in the last decade for improving ship hydrodynamics and reducing operational costs in the shipping industry. CFD enables detailed analysis of ship hull and propeller performance, directly addressing economic and regulatory pressures to minimize fuel consumption and therefore, improve energy efficiency. In addition to the CFD (numerical) approach commonly used for the analysis of ship energy efficiency, analytical methods are also available [1], [2].

Parametric mesh studies in ship CFD are essential for ensuring accuracy while optimizing computational efficiency. Research shows that mesh generation and resolution directly impact simulation results. When studying ship resistance, researchers have successfully used multiple mesh configurations ranging from coarse to fine grids, comparing results to validate the computational approach [3]. Similarly, analysis of mesh resolution effects demonstrates that mesh configuration directly impacts numerical results in velocity fields, with finer meshes showing convergence improvements of up to 6.4% [4]. One comprehensive study conducted over 50 iterations of heaving sphere simulations by varying mesh configurations and simulation parameters, achieving good agreement with experimental data while maintaining computational efficiency through axisymmetric exploitation [5]. In resistance prediction studies, parametric analysis has revealed that wavelength ratio significantly influences the pattern of resistance in waves, with added resistance behaviour varying non-linearly with wave height [6]. Grid-independence studies are essential to establish which mesh configurations provide adequate accuracy, and modern approaches increasingly employ machine learning to guide parametric optimization searches efficiently [7]. Grid sensitivity (or grid convergence) studies evaluate how variations in mesh resolution affect simulation results. The standard approach uses Richardson extrapolation methods to assess mesh convergence. In ship hydrodynamics, researchers typically conduct systematic grid convergence studies based on multiple grid resolutions to predict uncertainties in numerical solutions [8]. A key protocol involves performing sensitivity analyses on each operating condition, with particular attention paid to critical flow regions like the free-surface and wake fields in the propeller plane. When conducting grid refinement studies, researchers evaluate sensitivity for each operating condition separately. For example, in full-scale ship trials, grid refinement sensitivity is systematically assessed for each power setting, and time-step effects are also evaluated for the selected grids. The simulated results showed good agreement with test data, illustrating the capability of numerical methods to determine ship performance at full scale [9]. Studies investigating ship resistance and self-propulsion often verify grid convergence through comparison with experimental data, examining the influence of factors like mesh density, time steps, and turbulence models [10]. The free-surface region and wake flow require particular mesh refinement. Grid independence studies should assess both overall domain resolution and local refinement at critical areas [11]. Additionally, research on ship design operations in confined waters has utilized detailed grid independence checks at different design stages to optimize both accuracy and computational efficiency [12].

A comprehensive study by [13]. developed best practices for self-propulsion simulation of ship models in calm water. Extensive convergence studies were carried out to examine effects of various propeller modelling

Received: February 2026, Accepted: March 2026
Correspondence to: Matija Vasilev
Faculty of Mechanical Engineering,
Kraljice Marije 16, 11120 Belgrade, Serbia
E-mail: mnvasilev@mas.bg.ac.rs

methods and parameters, including non-dimensional wall distance, grid resolution/distribution, and turbulence model selection. The study examined both bare-hull resistance and propeller open-water performance initially, then applied two different propeller modelling methods: a simplified body-force method and a detailed propeller modelling approach to predict wake fraction and propeller performance behind the hull. The difference in accuracy between these methods was quantified through convergence studies, allowing researchers to establish best modelling practices. Validation was performed on the KRISO Container Ship (KCS) model, where the effective wake fraction determined from CFD was compared with experimental effective wake fraction data. A detailed numerical study on full-scale ship self-propulsion performance demonstrates how grid convergence is incorporated into validation procedures [14]. The research included simulations using RANS method with both double-model and Volume-of-Fluid (VOF) models for scale effect analysis. Verification of grid convergence was performed through global mesh refinements, and a series of sea trials were conducted to collect reliable data for validating predictions. The study demonstrated that grid convergence studies are critical for understanding hull-propeller interaction, where boundary layer separation is the main source of wake variation. Notably, the research found that simplification of free surface treatment does not only affect wave-making resistance of the bare hull but also induced drag, which can produce up to 5% uncertainty in power prediction. A numerical study of two-propeller hydrodynamic performance demonstrates systematic grid convergence methodology [15]. The research conducted standardized mesh and time-step convergence studies following ITTC recommendations. The hydrodynamic results for the KP505 propeller were compared with experimental data to validate the reliability of the method. Over 40 propeller arrangements with varying transverse and longitudinal spacing were then simulated. The study revealed that the high-speed wake generated by the upstream propeller significantly affects the downstream propeller's hydrodynamic performance, with this interaction diminishing as transverse spacing increases. An uncertainty quantification study of self-propulsion analyses with RANS-CFD examined a small-size product/oil tanker at model scale [16]. The methodology involved open water propeller predictions and model scale computations for minimum two different loadings to determine the self-propulsion point and respective parameters. To expedite computations, cases were solved using a single-phase approach. Resistance predictions were compared with experimental findings, and uncertainty associated with thrust prediction was quantified. The comparison between CFD predictions and full-scale sea trials conducted on the subject ship indicated that CFD computation could predict performance with sufficient accuracy at acceptable computational cost. A study on Flettner rotors as wind-assisted propulsion demonstrated grid convergence methodology for preliminary design assessment [17]. RANS-based CFD evaluated aerodynamic performance of various rotor configurations. A grid convergence study was conducted as part of the CFD results verification process. Initially, isolated 2D and 3D rotors at model scale were simulated for various operating conditions. A cargo ship fitted with Flettner rotors was then simulated to compute resistance and evaluate rotor-to-rotor interaction, demonstrating how grid convergence studies enable confidence in subsequent design evaluations.

These examples demonstrate that grid sensitivity studies are essential at every stage of ship CFD analysis, from preliminary design through validation against sea trials. The studies consistently show that proper mesh convergence procedures establish confidence in propulsion performance predictions, enable accurate scale effects analysis, and support design optimization with quantified uncertainty bounds.

1.2 Boundary layer

The boundary layer forms on the ship's hull surface because of the fluid's viscous effects, causing the fluid velocity to change from zero at the solid surface to the value of the undisturbed flow velocity. The exact characteristics of the boundary layer depend on factors such as the Reynolds number, ship geometry, speed and fluid properties. Its study is crucial for determining the frictional resistance coefficient, which represents a significant component of the ship's total resistance. It is known that when the hull is subjected to water flow, turbulent flow occurs and consequently, the boundary layer that forms is called the turbulent boundary layer. The boundary layer thickness is defined as the position where the flow velocity reaches 99% of the undisturbed flow velocity, measured from the wall where the flow velocity is zero [18].

Research in the field of boundary layer velocities dates back more than 120 years [19], [20], [21] and initially focused on pipe flow. It was concluded that the velocity near the wall during turbulent flow varies with 1/7 power of the distance from the wall. It should be noted that this exponent holds only for smooth pipes (up to $\mathrm{Re} = 10^5$), but for larger Reynolds numbers, it decreases to 1/10. However, in the case of rough pipes, the exponent for increasing relative roughness rises from 1/7 to 1/4 [22]. As early as 1927, Prandtl proposed an expression for the thickness of the turbulent boundary layer in pipes [20]:

$$\frac{\delta}{x} \approx \frac{0.37}{\mathrm{Re}_x^{1/5}}. \tag{1}$$

For flow over a flat plate, the following expressions were obtained [23]:

$$\frac{\delta}{x} \approx \frac{0.16}{\mathrm{Re}_x^{1/7}}, \tag{2}$$

or [24]:

$$\frac{\delta}{x} = \frac{0.382}{\mathrm{Re}_x^{1/5}}. \tag{3}$$

Since a ship has an extraordinarily complex geometric structure, the turbulent boundary layer that forms is highly irregular in shape [25]. In 1948, one of the first formulations for the boundary layer thickness on ships appeared [26], [27]:

$$\delta = \frac{5.5x}{\sqrt{\mathrm{Re}}}. \tag{4}$$

By the 1970s, research emerged focusing on methods for solving three-dimensional turbulent

boundary layer flow on ships [28] which later led to the organization of the first workshop in 1980 [29]. The greatest challenge when solving flow around a ship's hull arises in the stern region where flow separation occurs [30]. In [31] authors conducted experiments in a wind tunnel on a 10ft long Wigley hull to study the flow in the boundary layer and a wake over the stern. Study by [32] presents experimental results from towing-tank tests examining propeller-hull interaction using the Series 60 C_b = 0.6 hull form. Measurements included mean-velocity and pressure fields for conditions both with and without a propeller. Data were collected upstream, downstream and in the near-wake region, alongside surface-pressure distributions, wave profiles, resistance and self-propulsion tests. Results highlight key differences in flow behaviour when a propeller is present. The interaction between the propeller and the hull's boundary layer and wake is analysed using a propeller-performance program, revealing that most interaction effects stem from the propeller's response to the three-dimensional non-uniform inflow.

Boundary layer phenomena are critical in maritime applications as they affect resistance, propulsion set and manoeuvrability. Accurate simulation of these phenomena requires sufficiently refined and well-structured meshes that capture the near-wall effects effectively. The advances in mesh generation techniques have notable implications for maritime CFD analyses. In [33] authors discussed how the future landscape of CFD will rely on high-performance computing and improved mesh adaptability, proposing that real-time simulations will depend on the efficiency and quality of generated meshes. This interdependence inherently calls for innovative solutions to align meshing techniques with complex geometries and fluid interactions in maritime settings.

One critical challenge in ship hydrodynamics is managing the significant difference in boundary layer thickness between model-scale and full-scale ships. A novel approach to address this is the Boundary Layer Similarity (BLS) model, where only the stern part of the hull is extracted and lengthened to make its boundary layer thickness equivalent to that of a full-scale ship [34]. CFD simulations of energy-saving fin performance demonstrated that the BLS model is capable of predicting full-scale performance through model-scale simulations, with flow fields affected by fins showing similar characteristics to those of full-scale ships

Different turbulence models have varying capabilities for capturing boundary layer characteristics. Research comparing eight turbulent viscous models revealed that model selection significantly affects the prediction of pressure distribution, velocity distribution, and boundary layer characteristics around ship hulls [35].

The boundary layer separation around the hull is a primary source of wake variation and affects propeller performance. Research on full-scale ship self-propulsion demonstrated that the difference in hull boundary layer separation is the main source of wake characteristics [14]. This finding links boundary layer behaviour directly to propulsive efficiency. In shallow water operations, the boundary layer interactions become even more complex; studies found that the ship's manoeuvring characteristics in shallow water are linked to complex interactions between the hull wake, boundary layer, propeller, vortices, and the seabed [36].

Currently, the literature does not provide specific guidance on the mesh resolution of the near-wall region for ship applications. The need for such guidance arises from the fact that CFD software often requires this value as an input when generating the mesh. Three key parameters are commonly used as inputs when defining the mesh in the near-wall region: the prism layer total thickness, the number of layers and either the aspect ratio or the thickness of the first layer. The number of layers determines how many individual mesh layers are included within near-wall region. A higher number of layers can improve the resolution of the velocity profile but may increase computational costs. Conversely, too few layers may result in insufficient resolution, compromising simulation accuracy.

Some studies provide guidance on the appropriate size of the base cell. The base cell size plays a significant role in defining the overall mesh structure and balancing computational efficiency with solution accuracy. In the study that involves estimating the resistance of a catamaran using CFD software [37] it is suggested that a grid size of about 6.0‰ of the waterline length can be used as the mesh size for the catamaran surface. The study [38] identifies that a grid size of 0.34% of the waterline length optimizes resistance prediction accuracy without increasing computational cost and resistance results remain stable with y^+ values between 11.5 and 200. Additionally, while the grid distribution ratio has minimal impact under these conditions, a smaller ratio is recommended for improved accuracy.

This study focuses on the Lucy Ashton benchmark, selected due to the availability of extensive experimental data, including resistance measurements at multiple model scales, full-scale resistance data, and boundary layer thickness measurements. Results from the Workshop are summarized in [39], while other research based on this ship are presented in [40], [41]. Lucy Ashton, a former paddle steamer built in 1888, was extensively modified after 1949 for full-scale resistance experiments, including hull fairing and the installation of four jet engines to provide steady, well-controlled thrust. The experimental database originates from 1950s sea trials conducted at multiple speeds and under different surface conditions; for the workshop, the smoothest configuration (faired seams with aluminium paint) was adopted as the reference case, without roughness modelling in CFD. Ship speed and boundary-layer characteristics were measured using pitot logs mounted at two longitudinal positions along the hull. The measured velocity profiles confirmed the expected growth of the boundary layer downstream and yielded frictional resistance estimates consistent with direct resistance measurements.

Based on the results of conducted Lucy Ashton case, the objectives of this study are defined as follows:

- To analyze the boundary layer thickness of the Lucy Ashton case through CFD results and compare its variation with Reynolds number against classical theoretical formulations (1-4);

- To determine an appropriate distribution of layers in the near-wall region for accurate CFD resolution of flow close to the surface;
- Formulation of an expression for the base cell size in the mesh;
- Validation of the developed methods using experimental data from the Lucy Ashton ship in various model scales and full scale.

2. METHODOLOGY

2.1 Case description

The Lucy Ashton case is particularly well suited for addressing the points outlined above due to the availability of experimental data. This includes total resistance measurements from model tests at six different scales and across multiple speeds λ = [21.167, 15.875, 11.906, 9.525, 7.938, 6.35], total resistance data for several speeds in full scale (λ = 1), and boundary layer thickness measurements at a speed of 10.18 knots, taken at 49% of the ship length from the stern along the centerline. The basic data and dimensions of the Lucy Ashton ship are provided in the following Table 1.

Table 1. Ship particulars

L_{pp} [m]	58.1
L_{wl} [m]	59.49
B [m]	6.4
T [m]	1.584
H [m]	2.1844
WS_{total} [m^2]	417
Δ [t] (sw)	390
C_b [-]	0.685
C_p [-]	0.705
C_m [-]	0.972

2.2 CFD setup and simulation conditions

The initial speeds considered for the CFD analysis in this study are the same as those used in the workshop, with Fr = [0.130, 0.173, 0.219, 0.260, 0.304] for the full-scale ship and Fr = 0.219 for the model scale. For the CFD calculations, the software STAR-CCM+ developed by Siemens was used. In wall-resolved mesh generation, three key parameters are commonly defined to control the near-wall discretization: the number of prism (inflation) layers, the near-wall (first-layer) thickness and the total prism layer thickness. There is a mathematical relationship between these three parameters, which is based on geometric progression:

$$\delta_{\text{pltt}} = \frac{Y_1\left(1-SF^{n_{\text{lay}}}\right)}{1-SF}, \tag{5}$$

where δ_{pltt} is the prism layer total thickness, Y_1 is the thickness of the first cell layer, SF is the stretch factor and n_{lay} is the number of layers, representing four unknown quantities. Since there are no recommendations for the prism layer total thickness of complex geometric shapes, recommendations for boundary layer thickness in pipes or flat plates (1-4) are usually used, where x is the length of the ship at the waterline (L_{wl}) and Re is the Reynolds number based on the length at the waterline. This region is defined prior to running the simulation and does not need to match the actual boundary layer thickness for a specific ship. This is the reason why the same symbol is used for the total prism layer thickness (δ_{pltt}) and boundary layer thickness (δ). There are no direct recommendations for determining the thickness of the first cell layer, but there is a relationship between this parameter and the dimensionless thickness of the first cell layer, y^+.

$$y^+ = \frac{Y_1 u^*}{\nu}, \tag{6}$$

where u^* is the friction velocity and ν is the kinematic viscosity of water. The kinematic viscosity can be determined based on the temperature of the water at which the experiments were conducted. In this case, it was determined based on known values for density and dynamic viscosity (given in Table 2).

Table 2. Water and air properties

	Full scale	Model scale
ρ_w [kg/m^3]	1026.02	998.8
ρ_a [kg/m^3]	1.225	1.242
η_w [Pas]	1.22E-03	1.27E-03
η_a [Pas]	1.79E-05	1.77E-05

The friction velocity can be determined using the following expression:

$$u^* = \sqrt{\frac{\tau_w}{\rho_w}}, \tag{7}$$

where τ_w is the wall shear stress (viscous force stress on the wall or ship hull), which can be determined using the following expression:

$$\tau_w = \frac{1}{2} C_V \rho_w u^2, \tag{8}$$

where C_V is the coefficient of viscous resistance and u is the free-stream velocity of water (i.e., the speed of the ship). The coefficient of viscous resistance, according to the ITTC 1978, is determined by the following formula [42]:

$$C_V = (1+k)C_F, \tag{9}$$

where k is the form factor and C_F is the friction coefficient for an equivalent flat plate, which can be determined using the ITTC formula [42]:

$$C_F = \frac{0.075}{(\log Re - 2)^2}, \tag{10}$$

Form factor is extracted with Prohaska's method as indicated in the [43]. If data for the form factor is not available, empirical formulas given in [44] can be used, or recommendations provided in [45]. Also, CFD double body simulations can be used to determine the form factor [46].

2.3 Mesh parameterization

Based on the current guidelines and recommendations [47], which emphasize that y^+ should remain within the range of 30 to 100 for CFD simulations in ship hydrodynamics if wall functions are used, the

question arises of how to determine the parameters used as input for setting up such simulations. This study demonstrates one possible approach to defining these parameters. In addition to y^+, there is a specified *SF* in [47] to be 1.2 and number of layers (n_{lay}) to be 15, but in this research, an investigation is extended to cover a range of *SF* from 1.2 to 1.4 and the range for n_{lay} from 7 to 25. An additional reason for extending the ranges lies in the author's experience: simulations aimed at predicting the resistance of complex ship forms for certain ship types either failed or required excessive computational time due to poor mesh quality, which resulted directly from using a fixed number of layers in the near-wall region. Removing prism layers near the hull, according to the author's observations, led to unreliable results that did not match experimental measurements. Moreover, key parameters, such as y^+, would fall outside the limits defined by official ITTC and IACS guidelines.

By extending (6) and multiplying by L_{wl}/Fr:

$$\frac{y^+ L_{wl}}{Y_1 \text{Fr}} = \frac{u^* L_{wl}}{\upsilon \text{Fr}} = f(\lambda)\,, \tag{11}$$

A graphical representation of the dependency $\frac{y^+ L_{wl}}{Y_1 Fr}(\lambda)$ for ships of different scales can be obtained. Similarly, the dependence $\frac{y^+ L_{wl}}{Y_1 \lambda}(Fr)$ for ships of the same scale but at different speeds can also be plotted:

$$\frac{y^+ L_{wl}}{Y_1 \lambda} = \frac{u^* L_{wl}}{\upsilon \lambda} = g(Fr), \tag{12}$$

The functions $f(\lambda)$ and $g(Fr)$ can be represented in the form $a\cdot\lambda^b$ and $c\cdot Fr^d$, respectively, where the coefficients *a*, *b*, *c* and *d* are determined by using logarithmic transformation and linear regression with the least squares method:

$$a = \exp\left(\frac{\sum_j\left(\ln\frac{y^+ L_{wl}}{Y_1}(j)\right) - b\cdot\sum_j(\ln\lambda(j))}{l}\right), \tag{13}$$

$$b = \frac{l\sum_j\left(ln\,\lambda(j)\cdot ln\frac{y^+ L_{wl}}{Y_1}(j)\right) - \sum_j(\ln\lambda(j))\cdot\sum_j\left(\ln\frac{y^+ L_{wl}}{Y_1}(j)\right)}{l\sum_j(\ln\lambda(j))^2 - \left(\sum_j\ln(\lambda(j))\right)^2}, \tag{14}$$

$$c = \exp\left(\frac{\sum_j\left(\ln\frac{y^+ L_{wl}}{Y_1}(j)\right) - d\cdot\sum_j(\ln Fr(j))}{l}\right), \tag{15}$$

$$d = \frac{l\sum_j\left(\ln Fr(j)\cdot\ln\frac{y^+ L_{wl}}{Y_1}(j)\right) - \sum_j(\ln Fr(j))\cdot\sum_j\left(\ln\frac{y^+ L_{wl}}{Y_1}(j)\right)}{l\sum_j(\ln Fr(j))^2 - \left(\sum_j\ln(Fr(j))\right)^2}, \tag{16}$$

where *l* is the number of speeds (*Fr*) i.e., number of scale factors in specific case. For Lucy Ashton case, *l*=7 for *Fr*=idem=0.219 and *l*=5 for λ=idem=1. Counter *j* goes from 1 to *l*.

Based on the prism layer total thickness, stretch factor, the number of layers and using the geometric sum formula for finite number of array elements, the first layer thickness can be evaluated.

$$Y_1 = \frac{\delta_{\text{pltt}}(1-SF)}{1-SF^{n_{\text{lay}}}}, \tag{17}$$

From (11) and (12), y^+ can be expressed as:

$$y^+ = \frac{Y_1\cdot Fr}{L_{wl}} f(\lambda) = \frac{Y_1\cdot Fr}{L_{wl}}\cdot a\cdot\lambda^b, \tag{18}$$

$$y^+ = \frac{Y_1\cdot\lambda}{L_{wl}} g(Fr) = \frac{Y_1\cdot\lambda}{L_{wl}}\cdot c\cdot Fr^d. \tag{19}$$

The thickness of the last layer (Y_{last}) can be expressed as:

$$Y_{\text{last}} = Y_1\cdot SF^{n_{\text{lay}}-1}\,. \tag{20}$$

When the size of the base cell (*BS*) is taken to be equal to the size of the last cell in the prism layer divided by zone refinement factor (*ZR*), the following relationship applies:

$$BS = Y_{\text{last}}/ZR. \tag{21}$$

Zone refinement is a factor that depends on the degree of fineness of the local mesh. Zonal refinement is essential for achieving accurate predictions of hydrodynamic forces by concentrating mesh resolution in regions near the hull and in wave-making zones, where flow gradients are highest. This approach optimizes computational efficiency, enabling detailed analysis of complex geometries and advanced turbulence models without prohibitive resource costs.

Figure 1 illustrates the refinement zones, parametrically defined as functions of the principal dimensions (L_{pp}, *B*, *T*). The volumetric dimensions of these refinement zones are provided in Table 3 together with domain size (refer to the end of the paper). All dimensions in Table 3 are specified with respect to the global coordinate system, located at the aft perpendicular and the keel centerline. Positive values are oriented in the positive *x*-axis direction, i.e., toward the bow. In this manner (Table 3), the zones are defined for half of the ship, which can be applied in cases where the ship is symmetric, as in the present case. Table 4 presents the relative percentages of the base cell size along the *x*, *y*, and *z* directions, respectively.

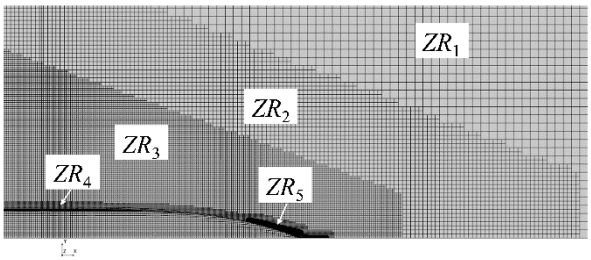

Figure 1. Zone refinements

Table 4. Zone refinements – Relative from base cell size

	ZR [% *BS*]		
	x	*y*	*z*
Domain	600	600	600
Free Surface	50	50	12.5
Stern refinement	12.5	12.5	12.5
Fore refinement	3.125	3.125	3.125
Fine cone refinement	12.5	12.5	6.25
Coarse cone refinement	25	25	12.5

In this specific case, it is applied that the degree of fineness of the last cell in the near-wall region is four, which means that the dimension of the last cell in the near-wall region is 6.25% of the base cell dimensions, i.e., it is $1/2^4$ times smaller.

The baseline equation for estimating the prism layer total thickness is given as (1), while assuming that the near-wall region thickness (i.e. prism layer total thickness) is equal to the boundary layer thickness and it was applied in first iteration. Alongside it, there are three other (17), (18) or (19) and (20) and five unknown

variables (y^+, Y_1, SF, n_{lay}, Y_{last}), the system is not closed and cannot be solved analytically. However, since the ranges for y^+, SF and n_{lay} are defined, the system of equations can be solved by adding one additional condition. For a constant Fr and different scales, the one condition is that the product $Y_{last} \cdot \lambda$ should remain approximately constant across scales. This condition ensures that the physical size of the last layer in the near-wall region remains consistent in real dimensions across different scales, thereby maintaining similar wall resolution. In contrast, for constant scale and varying Fr, the last cells' sizes in the near-wall region i.e., the base cell size should remain approximately constant ($BS \approx const.$). In this way, one solution is selected for each scale or for each Fr. The resulting solution defines mesh parameters BS, y^+, Y_1 and n_{lay}, i.e., the full prism layer setup needed to generate an appropriate mesh.

The cell size in each case will be different (for different speeds or scales), so an additional analysis was performed to potentially develop a simple formula for determining its dimensions. The idea is to come up with a formula in the form $BS = f(L_{pp}, r, \lambda, m)$ where r is refinement level which according to [48] equals $\sqrt{2}$ (or 2, $2\sqrt{2}$,…) and m is the scaling parameter, which is sought such that it provides the largest cell dimension without significantly affecting the results. Specifically, m will be determined as a local minimum or maximum of the $h(\lambda)$ where h is approximated function for specific Fr:

$$h(\lambda) = BS \cdot \lambda / (L_{pp} \cdot r). \tag{22}$$

Thus, the suggested simple expression for the size of the base cell dimension will be in the form:

$$BS = (L_{pp} \cdot r / \lambda) \cdot m^s, \tag{23}$$

where:

$$s = \begin{cases} 1, & \text{if } h'(\lambda) = 0 \text{ and } h''(\lambda) < 0 \text{ (local maximum)} \\ -1, & \text{if } h'(\lambda) = 0 \text{ and } h''(\lambda) > 0 \text{ (local minimum)} \\ 0, & \text{otherwise} \end{cases}$$

and m is the local minimum or maximum of the function h.

2.4 Validation and boundary layer evaluation

As an output from the CFD analysis, two parameters are selected: the total resistance of the ship ($R_{T,CFD}$) and the dimensionless boundary layer thickness $\delta_{CFD}/L_{wl}(Re)$. An acceptable solution is considered to be the total resistance value that lies within ±5% (or less if possible) of the measured value during experimental testing.

In CFD simulations, for all cases, velocity profiles were determined at 20%, 30%, 40%, 49%, 62% and 80% of L_{pp} along the centre line. At 100%L_{pp}, the boundary layer thickness is considered to be zero. The boundary layer thickness at each defined longitudinal position (%L_{pp}) was taken as the vertical distance from the ship's hull where the velocity reaches 99% of u_∞ with u_∞ being the free-stream velocity. An illustrative representation of the determined velocity profiles is shown in Figure 2. The dots in Figure 2 denote the calculated boundary layer thickness at each cross-section. The resulting set of points can be approximated using a n^{th} degree polynomial via least squares regression, where the residual sum of squares (RSS) is minimized. Subsequently, the maximum value of the polynomial within the ship's length boundaries is identified and adopted as the boundary layer thickness for the entire ship.

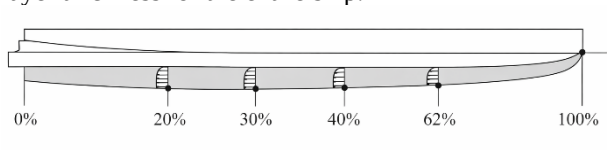

Figure 2. Boundary layer thickness evaluation

The boundary layer thickness determined by the CFD analysis is considered good if it is within the range of values obtained during the experiment or as close as possible. According to the notes from [49] it was often difficult to obtain satisfactory readings in the boundary layer and many of them are discounted, so this was the reason why only for one speed, the data about velocity profile is available. If the two conditions mentioned above (for total resistance and boundary layer thickness) are not met, the simulation setup parameters are adjusted until the results are considered valid, i.e., until both conditions are satisfied for all considered speeds and all scales (11 cases in total). The entire process is iterative and based on the principle of trial and error, adjusting the boundary layer thickness formula according to the results of the CFD analysis. Since the Lucy Ashton ship is relatively small by today's standards (58.1m), additional simulations were conducted with extrapolated ship dimensions using factors of 0.5, 0.18 and 0.12, for several speeds according to the matrix shown in the following table (Table 5). The "o" symbols indicate the originally conducted simulations corresponding to the cases defined through the workshop, while the "x" symbols indicate the additional simulations to extend the boundary layer formula to cover the range of the largest ship ever built (The Seawise Giant).

The ratio $\delta_{CFD}/L_{wl}(Re)$ was found in the form of $e \cdot Re^h$, where e and h were determined in the same way as coefficients a, b, c and d (see (13-16)).

Table 5. Conducted simulation cases

λ	Fr=0.13	Fr=0.173	Fr=0.219	Fr=0.26	Fr=0.304
21.167	x		o		x
15.875			o		
11.906			o		
9.525			o		
7.938			o		
6.35	x		o		x
1	o	o	o	o	o
0.5	x		x		x
0.18	x		x		x
0.12	x		x		x

After conducting new simulations, the boundary layer thickness formula was further calibrated until the conditions for completing the calibration were met. The algorithm for determining the boundary layer thickness formula based on data for the Lucy Ashton ship is given in the Figure 3 (refer to end of paper). The dashed arrow in the same figure shows the possible calibration of other

parameters during a single CFD calculation. Other parameters include domain size, turbulence model and its parameters, boundary conditions, solver, time step and others, which may affect the results. It is important to note that in the calculations for this study, these parameters were not changed compared to how they were defined for the Lucy Ashton workshop case and in previously published paper by authors [41].

Based on algorithm in Figure 3 (refer to the end of paper), a short code is developed in MATLAB software for evaluation of y^+, SF, n_{lay} and BS. As noted in Figure 3, range for y^+ is defined to be from 60 to 200. This is because, in a computational mesh, y^+ is evaluated at the centre of the first cell – corresponding to half of its thickness – rather than at the cell boundaries, which represent the full cell thickness.

The numerical models, boundary conditions, grid uncertainty analysis, and post-processing procedures were performed in accordance with the methodology described in the paper [41].

3. RESULTS

The results obtained according to the methodology defined in the previous chapter are presented below.

For all tables mentioned below, please refer to the end of paper.

In Table 6 are shown values obtained with (7-10). In Table 7, initial values for defining near-wall region parameters are provided for $Fr = 0.219$ at different scales. Table 8 and Table 9 (corresponding to Tables 6 and 7) also provide initial values for defining near-wall region parameters but for the full-scale ship at different Fr.

In Figure 4 the graphical representation of evaluated function $f(\lambda) = a \cdot \lambda^{b}$ is shown in accordance with data from Table 7.

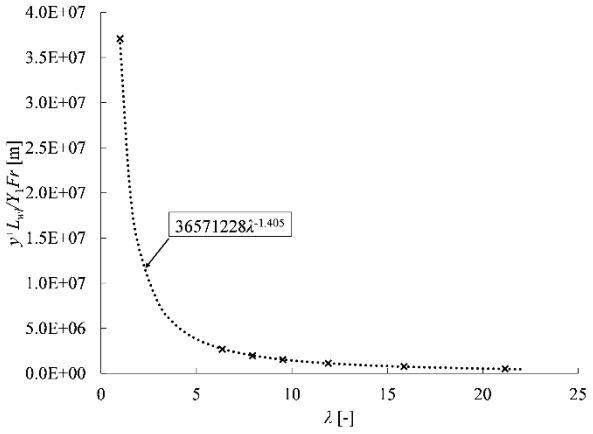

Figure 4. Graphical representation of evaluated (11) – (Lucy Ashton case Fr=0.219)

In Figure 5 graphical representation of evaluated function $g(Fr) = c \cdot Fr^{d}$ is shown in accordance with data from Table 7.

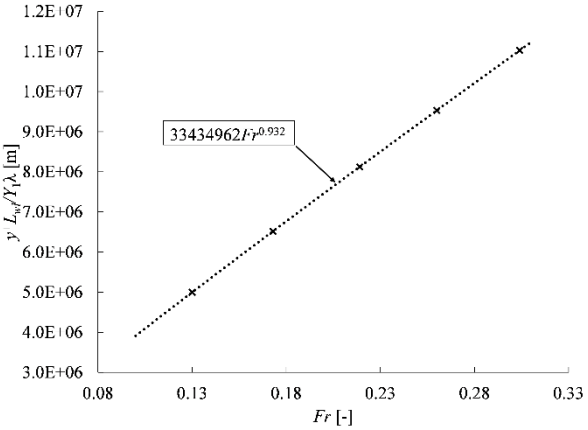

Figure 5. Graphical representation of evaluated (12) – (Lucy Ashton case $\lambda = 1$)

Based on (22), the h function could be evaluated for a range of Fr. The form of the function h is presented in Figure 6. The dots in Figure 6 present values of function h for a $Fr = 0.219$. The bars indicate the ranges within which the function h varies depending on another Fr. The approximated curve passes through the lowest sides of bars and is exponential in nature:

$$h(\lambda) \approx 43.79\exp(-0.2794 \cdot \lambda) + 29.85\exp(0.002018 \cdot \lambda) \quad (24)$$

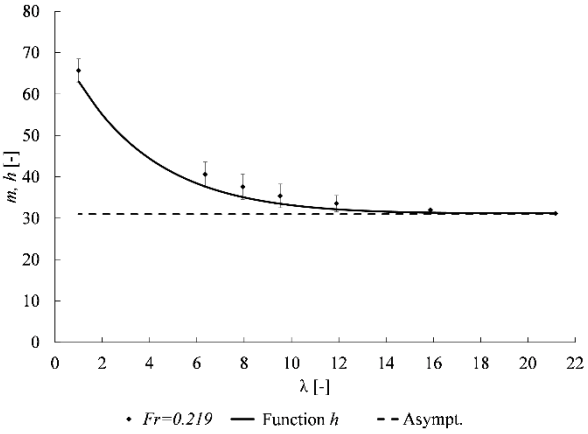

Figure 6. Evaluation of parameter function h and parameter m

The function h has a global minimum and it occurred at approximately $\lambda \approx 18.88$ with a minimum value of about 31.23. For the sake of simplicity in notation, the parameter value $m = 30$ was adopted. Consequently, (23) takes its final form:

$$BS=(L_{pp} \cdot r)/(30 \cdot \lambda). \quad (25)$$

The velocity profile obtained from CFD analysis can only be compared with one set of experimental measurement data, specifically at a speed of 10.18 kn ($Fr \approx 0.219$) at 49% of the ship's length along the centre line. A comparative velocity profile, expressed in terms of boundary layer thickness (δ) and the ratio of disturbed to undisturbed flow velocity (u/u_∞), is shown in Figure 7. In the figure, experimental data [49] are represented by "o" symbols, while a dashed line represents the approximated velocity profile based on experimental data analysis. The gray shaded area denotes the zone encompassing the velocity profile when accounting for all measured values.

Data obtained from the CFD analysis are marked with "x" and the velocity profile is approximated with a solid line. A vertical dotted line indicates the 99%u_∞ level, which is defined as the boundary layer thickness at 49%L_{pp}.

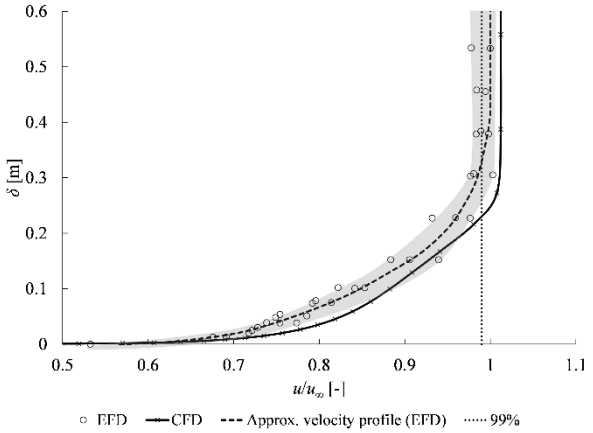

Figure 7. Velocity profile at CL at 49%L_{pp}, $Fr \approx 0.219$

According to the methodology described, the boundary layer thickness determination procedure was applied to all transverse cross-sections at selected distances from the aft perpendicular (AP). These values were then approximated using an *n*-th degree polynomial along the ship's length. The process was repeated for each analyzed speed. By evaluating second-, third- and fourth-degree approximation polynomials, it was found that fourth-degree polynomials yield the smallest RSS. Results from the initial 11 CFD simulations related to boundary layer thickness are presented in Figure 8 and Figure 9.

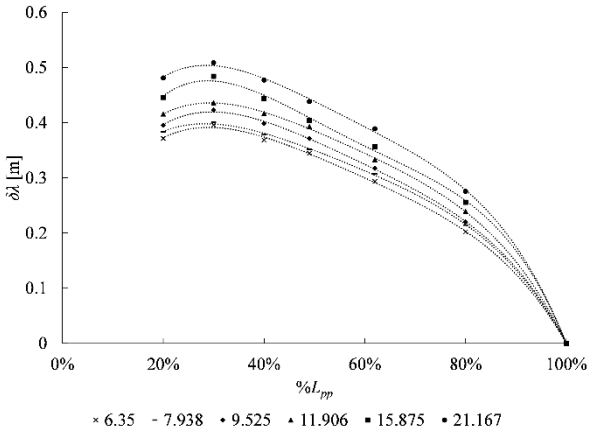

Figure 8. Boundary layer thicknesses for different λ (Fr = 0.219)

Figure 8 illustrates the boundary layer thickness distribution from 20% L_{pp} to 100% L_{pp} for different ship scales at Fr = 0.219. Here, the boundary layer thickness was multiplied by corresponding scaling factors to clearly display all six cases (scales) on a single diagram. Figure 9 shows the boundary layer thickness distribution along the ship's length for the full-scale ship at various Fr. Dashed lines in Figure 8 and Figure 9 represent the fourth-degree approximation polynomials.

By solving the first derivative equation of the fourth-degree polynomial, it was determined that the maximum boundary layer thickness occurs at approximately 30%L_{pp} from the AP. The analysis further revealed that the effect of scale variation has a greater influence on boundary layer thickness than changes in speed.

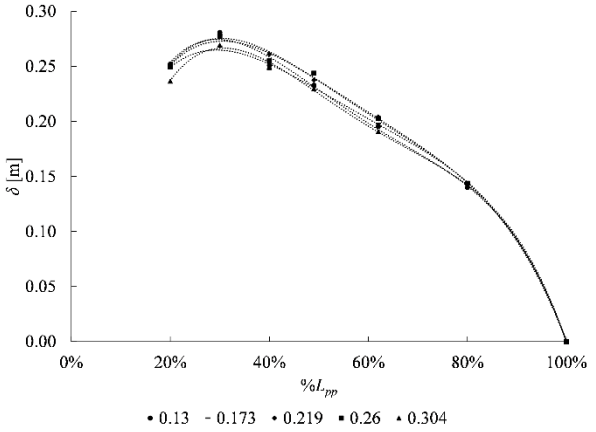

Figure 9. Boundary layer thicknesses for different Fr (λ=1)

The maximum of the fourth-degree polynomial, i.e., the maximum boundary layer thicknesses expressed in the dimensionless ratio (δ/L_{wl}) plotted as a function of Re, are shown in Figure 10 for all cases examined in Table 5 (denoted with "x" for entire conducted simulations for Lucy Ashton case).

The final formula for boundary layer thickness evaluation is given below:

$$\frac{\delta}{L_{wl}} = \frac{0.075}{Re^{0.15}}. \tag{26}$$

In Figure 10 are also given $\delta/L_{wl}(Re)$ lines obtained with (1-4) and (26).

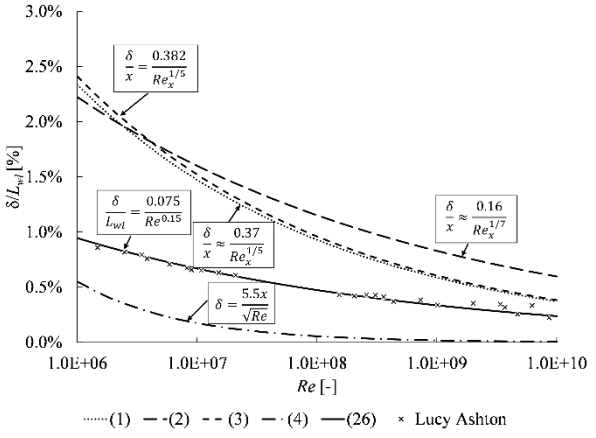

Figure 10. Non-dimensional boundary layer thickness change for different Re (1-4, 26)

The estimated total resistance coefficients obtained from CFD simulations using coarse, medium, and fine meshes are summarized in Table 10 and Table 12, together with the corresponding EFD data and relative errors. The associated grid, data, and validation uncertainties for the Lucy Ashton case are reported in Table 11 and Table 13, covering various scales at a single speed and multiple speeds at full scale, respectively.

Table 11. Validation for Lucy Ashton case (various scales, one speed (same Fr))

U_G %S_1	U_D %D	U_V %

7.04	1	7.1

Table 13. Validation for Lucy Ashton case (various speeds, full scale)

U_G %S_1	U_D %D	U_V %
6.4	1	6.5

In Table 14 and Table 15, the predicted y^+ values and the y^+ values obtained from CFD analysis are listed for cases of different scales at a constant *Fr*, as well as for the full-scale ship at varying *Fr*.

Table 14. y^+ values Lucy Ashton case (various scales, one speed)

λ [-]	target y^+ [-]	obtained y^+ [-]
21.167	35	38
15.875	44	43
11.906	37	36
9.525	38	37
7.938	48	47
6.35	48	47

Table 15. y^+ values Lucy Ashton case (various speeds, full scale)

Fr [-]	target y^+ [-]	obtained y^+ [-]
0.13	43	43
0.173	41	41
0.219	39	42
0.26	44	44
0.304	39	39

4. DISCUSSION

Although the parameter *m* for the full-scale case (λ=1) deviates by up to 100% from the adopted value (*m*=30) in (25), the obtained results are sufficiently reliable, as seen in Table 12 for the Lucy Ashton case. This also needs to be further tested with other types of full-scale ships because it has been observed that extrapolated ships (λ = 0.12 and λ = 0.18) exhibit oscillations in the residuals, as the cell aspect ratio is considerably large. This could be indicated in Figure 5, where the parameter for $\lambda < 1$ would be significantly greater than 30, while already at model scales the parameter *m* does not deviate substantially from 30. The next immediate step would be to verify the entire procedure and the derived formulas for other benchmark cases, including the Meteor case, for which full-scale measurements of total resistance exist and others benchmark cases such as JBC, KCS, DTC and others.

For cases where $\lambda > 10$, the parameter *m* is shown not to change drastically. The development of the formula (26) is also heavily influenced by the parameter *ZR*, i.e., the definition of refinement zones around the ship.

The observed deviation of the parameter *m* for the full-scale case indicates that the parameter may depend not only on the *Re* but also on hull geometry and mesh refinement strategy. This suggests that the adopted value *m* = 30 should be interpreted as a practical engineering approximation rather than a universal constant. Nevertheless, the results demonstrate that the proposed mesh parameterization remains sufficiently robust even when deviations in *m* occur.

According to Figure 7, the velocity profile obtained from CFD analysis partially lies outside the gray zone bounded by EFD data and exhibits an irregular shape. Additionally, the ratio of the water velocity in the disturbed flow zone to the constant velocity used as input in the simulation is greater than one, meaning the uniform flow velocity outside the boundary layer is higher than the undisturbed flow velocity and remains constant far from the ship's hull. The discrepancy in the velocity profile may stem from the neglect of hull roughness in the CFD simulations. While neglecting hull roughness is a plausible explanation, other factors such as turbulence modeling limitations (e.g., reliance on RANS vs. LES) may amplify discrepancies.

The number of cells in near-wall region is more influenced by scale than by changes in the *Fr*, as evidenced by the parameter n_{lay} in Table 7 and Table 9. This behavior is expected because the *Re* changes significantly with scale, directly affecting viscous effects and boundary layer development. In contrast, variations in the *Fr* primarily influence the wave system rather than the viscous flow close to the hull. Based on Figure 8, there is no geometric similarity in boundary layer thickness across different scales, even though dynamic similarity (*Fr* = *idem*) is satisfied. However, the trend in boundary layer thickness distribution remains similar. The non-dimensional boundary layer thickness decreases with increasing *Re* as a classical theory based on earlier experiments with pipes and flat plates. For all cases, a 4th-degree polynomial (Figure 8 and Figure 9) provides a good approximation of the boundary layer thickness distribution along the centerline. The position of maximum boundary layer thickness depends on the geometry of the flat bottom and the location of the stern shoulders and in this case is about 30% of L_{pp} towards the bow. Notably, the boundary layer does not exhibit a uniformly increasing trend along the centerline. Below 20% of L_{pp}, a sharp increase in boundary layer thickness occurs. The non-uniform growth of the boundary layer along the hull can be explained by the pressure gradients generated by the hull geometry. In the forward part of the hull, the flow is subjected to favorable pressure gradients which delay boundary layer thickening, while the stern region is characterized by adverse pressure gradients and wake formation that accelerate boundary layer growth.

The estimation of form factors is well executed, resulting in accurate predictions of y^+ values, as seen in Table 14 and Table 15.

Regarding the total resistance coefficient obtained from CFD analysis, deviations for individual cases (speeds) are below 4%, (Table 10 and Table 12). Grid uncertainty analysis, involving three different grids, validated CFD results, as $E\%D < U_V$. The grid uncertainty analysis was performed for only one speed (see Table 10, Table 11, Table 12, Table 13).

The choice of formula for estimating prism layer total thickness does not play a critical role in obtaining valid

results. Equation (1) was employed in the first iteration as an initial approximation for the estimation of characteristic parameters, providing a necessary starting point for the iterative procedure. In subsequent iterations, alternative formulations were applied; however, only the results corresponding to the initial and final iterations are presented herein, as inclusion of intermediate steps would unnecessarily extend the discussion without providing additional insight. Following the methodology described, a number of layers within the estimated prism layer total thickness (near-wall region) are shown in Table 16 and Table 17.

Table 16. Number of layers (Lucy Ashton - various scales, *Fr* = 0.219)

	Eq. (26)	Eq. (1)
λ [-]	n_{lay} [-]	n_{lay} [-]
21.167	7	8
15.875	7	9
11.906	8	11
9.525	9	12
7.938	9	12
6.35	10	13

Table 17. Number of layers (Lucy Ashton – full scale, various *Fr*)

	Eq. (26)	Eq. (1)
Fr [-]	n_{lay} [-]	n_{lay} [-]
0.130	17	20
0.173	18	20
0.219	19	20
0.260	19	21
0.304	20	21

The number of layers defined according to (1) results up to 30% more layers, thereby increasing the total cell count in the mesh and directly extending the simulation runtime. What gives (26) an advantage is that the total thickness is almost twice as small compared to (1), which allows for a bigger number of layers in the region with a high velocity gradient.

In Figure 11, the cell distribution and velocity profile in the near-wall region are shown, with the boundary layer thickness estimated using (1) (top) and (26) (bottom) at 49% of L_{pp} of the Lucy Ashton in full scale for Fr = 0.219.

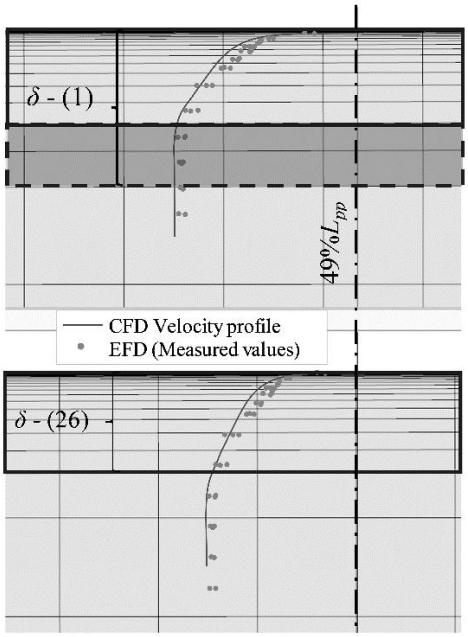

Figure 11. Comparison of cell distribution and velocity profiles (evaluated through CFD and EFD) in the near-wall region obtained with (1) and (26) at 49%L_{pp} of Lucy Ashton in full scale for *Fr* = 0.219.

The velocity profiles obtained from CFD analysis are shown with a solid line, while the measured velocities from EFD are indicated with dots. The estimated boundary layer thickness based on CFD results is marked with a solid line rectangle, while the absolute difference between the prism layer total thickness estimated by (1) and boundary layer thickness determined through CFD is marked with a grey zone in dashed rectangle (in the upper part of the figure). In the lower there is no dashed rectangle because prism layer total thickness and boundary layer are the same.

According to Table 17, the estimated number of layers in the near-wall region based on (1), n_{lay}, is 20. However, based on CFD results, 18 layers are sufficient to cover the entire boundary layer. According to (26), the number of layers in the near-wall region is n_{lay} = 19, and there are no additional layers that would increase the total number of cells and thus prolong the simulation time.

In any case, this difference in the number of cells is negligible and has practically no effect on the resistance prediction in CFD simulations in full scale.

In Figure 12, the cell distribution and velocity profile in the near-wall region are shown, with the prism layer total thickness estimated using (1) (top) and (26) (bottom) at 49% of L_{pp} of the Lucy Ashton in model scale (λ = 21.167) for Fr = 0.219.

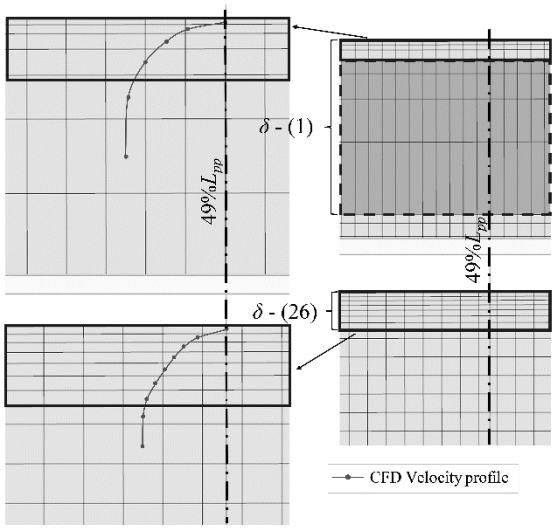

Figure 12. Comparison of cell distribution and velocity profiles (evaluated through CFD and EFD) in the near-wall region obtained with (1) and (26) at 49%L_{pp} of Lucy Ashton in model scale (λ=21.167) for Fr=0.219

The velocity profiles obtained from the CFD analysis are shown with a solid line. The estimated boundary layer thickness based on CFD results is marked with a solid line rectangle, while the absolute difference between the prism layer total thickness estimated by (1) and that determined through CFD is marked with a grey zone in dashed rectangle (Figure 12, top right).

According to Table 16, the estimated number of layers in the near-wall region based on (1), n_{lay}, is 8. However, according to the CFD results, 4 to 5 layers are sufficient to cover the entire boundary layer. In the additional three layers, one cell dimension compared to the other is large (grey zone in dashed rectangle in Figure 12, top right), i.e., the height of the last cell (Y_{last}) is exceptionally large (the aspect ratio is large), which can lead to numerical instability.

To avoid numerical instability, the cell size in the other dimension (lengthwise) should match the height of the last cell. However, this would mean that the ship hull would be represented with a very coarse mesh in model scale, leading to larger deviations in resistance prediction from CFD compared to EFD.

On the other hand, to maintain the same cell dimension along the length, it is possible to increase the number of layers n_{lay} in the near-wall region, but this would significantly prolong the simulation time due to the unnecessary increase in the total number of cells.

According to (26), the number of layers in the near-wall region is n_{lay} = 7, which represents the balance between result reliability, boundary layer thickness estimation, and simulation runtime.

Table 18 provides the standard deviation of the differences between CFD and EFD results for Lucy Ashton using two distinct formulas ((26) and (1)). In both examined cases, the use of (26) yielded results with slightly smaller standard deviations and shorter simulation times.

Table 18. Standard deviation between CFD and EFD with implementation of (26) and (1).

	Lucy Ashton	
	Various λ	Various Fr
Eq. (26)	2.2	2.1
Eq. (1)	2.6	2.3

From a practical perspective, the advantage of (26) lies in the more balanced distribution of cells within the near-wall region. By reducing unnecessary prism layer thickness, the method allows a greater portion of the mesh resolution to be concentrated in regions with strong velocity gradients. This leads to improved numerical stability while maintaining comparable accuracy in resistance prediction.

The additional analysis includes verification of the use of (4); however, according to the described methodology and the defined limits for *SF*, n_{lay} and y^+, it was not possible to determine these three parameters. For this reason, the CFD analysis was not conducted for this case.

The main contribution of the present study lies in the systematic parameterization of CFD mesh parameters based on boundary layer characteristics. Unlike previous investigations of the Lucy Ashton case [39, 40, 41], this work focuses on establishing relationships between the *Re*, boundary layer thickness and key mesh parameters used in CFD simulations.

5. CONCLUSION

This study investigated the relationship between boundary layer characteristics and mesh parameterization in CFD simulations of ship resistance using the Lucy Ashton benchmark case. The analysis included six model scales and full-scale conditions for which experimental resistance data and boundary layer measurements are available. The objective was to examine the influence of scaling, *Fr* and *Re* on boundary layer development and to evaluate their implications for mesh definition in the near-wall region.

A methodology was proposed for estimating key mesh parameters in the near-wall region, including the prism layer total thickness, number of layers and first cell height. Initial mesh parameters were defined for different scales and *Fr*, allowing a systematic setup of CFD simulations. The comparison of velocity profiles demonstrated a reasonable agreement between CFD and experimental data, with the predicted boundary layer thickness falling within the expected experimental range.

The results showed that scale effects have a stronger influence on boundary layer development than variations in *Fr*, while the nondimensional boundary layer thickness decreases with increasing *Re*, consistent with classical theoretical expectations. CFD predictions of the total resistance coefficient showed deviations below 3.8% compared with experimental data, confirming the reliability of the numerical setup.

The comparison of different formulations for estimating prism layer total thickness indicated that (26) provides a more balanced compromise between numerical accuracy and computational efficiency for the investigated case. The proposed procedure therefore

provides practical guidance for defining near-wall mesh parameters in CFD simulations of ship flows.

It should be noted that the methodology was developed based on a single hull form and simulations performed using STAR-CCM+. Although the results demonstrate promising agreement with experimental data, further validation on additional benchmark hull forms is required in order to confirm the broader applicability of the proposed approach.

Future work should focus on extending the validation to other benchmark cases, including ships with different geometrical characteristics, as well as exploring advanced mesh adaptation strategies and optimization techniques to further improve computational efficiency.

ACKNOWLEDGMENT

The research is supported by Ministry of Science, Technology Development and Innovation of Republic of Serbia, Contract No. 451-03-34/2026-03/200105. Authors would like to acknowledge Ocean Pro Marine Engineers LTD for its help in guidance and support for CFD assessment.

REFERENCES

[1] Simić, A. and Radojčić, D.: On energy efficiency of inland waterway self-propelled cargo vessels, FME Transactions, Vol. 41, No. 2, 2013.

[2] Vasilev, M. and Kalajdžić, M.: Influence of lightweight change on ship performance, FME Transactions, Vol. 50, No. 4, 2022. doi:10.5937/fme2204615V

[3] Elhadad, A.M., El-Ela, A.M.A. and Hussien, M.M.: MATLAB implementation using Holtrop and Mennen method of bare hull resistance prediction for a surface combatant ship coupled with CFD, CFD Letters, Vol. 15, No. 10, pp. 1–11, 2023. doi:10.37934/cfdl.15.10.111

[4] Widiawaty, C.D., Siswantara, A.I., Budiyanto, M.A., Andira, M.A., Adanta, D., Hilman, M., Syafei, G., Farhan, T.A. and Rizianiza, I.: Analysis of mesh resolution effect on numerical results of CFD-ROM turbulent flow in stationary parallel plates, CFD Letters, Vol. 16, No. 8, pp. 1–17, 2024. doi:10.37934/cfdl.16.8.117

[5] Davidson, J., Nava, V., Andersen, J. and Kramer, M.: Exploiting axisymmetry to optimize CFD simulations—heave motion and wave radiation of a spherical buoy, Symmetry, Vol. 16, No. 9, 1252, 2024. doi:10.3390/sym16091252

[6] Zeraatgar, H., Ghaemi, M. and Sadeghi, M.: Analysis of instantaneous ship resistance increase in waves using CFD-URANS, Polish Maritime Research, Vol. 32, No. 1, 2025. doi:10.2478/pomr-2025-0001

[7] Liu, J., Hu, L., Zhang, B., Zhang, K., Bi, J. and Zheng, Q.: Enhancing ship hydrodynamic performance via machine-learning-driven CFD parametric optimization, Engineering Applications of Computational Fluid Mechanics, Vol. 19, No. 1, 2025. doi:10.1080/19942060.2025.2565801

[8] Mandru, A., Rusu, L., Bekhit, A. and Pacuraru, F.: Numerical study of a model- and full-scale container ship sailing in regular head waves, Inventions, Vol. 9, No. 1, 22, 2024. doi:10.3390/inventions9010022

[9] Mikulec, M. and Piehl, H.: Verification and validation of CFD simulations with full-scale ship speed/power trial data, Brodogradnja, Vol. 74, No. 1, 2022. doi:10.21278/brod74103

[10] Yang, C., Zeng, K., Chu, J., Han, Y. and Gu, M.: Study of influencing factors on CFD methods and separated flow by the virtual static captive test, *IOP Conference Series: Materials Science and Engineering*, Vol. 1288, 012049, 2023. doi:10.1088/1757-899X/1288/1/012049

[11] Espaa, R.E., Alvarez, L.V. and Samarasinghe, J.T.: Grid-independence studies applied to a field-scale CFD model using the DES technique along the Colorado River, Earth Surface Processes and Landforms, 2025. doi:10.1002/esp.70030

[12] Wu, P.-C.: A CFD-based correction for ship mass and longitudinal center of gravity to improve resistance simulation, Mathematics, Vol. 13, No. 11, 1788, 2025. doi:10.3390/math13111788

[13] Jin, S., Peng, H., Qiu, W., Oldfield, C. and Stockdill, B.: Best modeling practice for self-propulsion simulation of a ship model in calm water, Physics of Fluids, Vol. 35, 2023. doi:10.1063/5.0167387

[14] Sun, W., Hu, Q., Hu, S., Su, J., Xu, J., Wei, J. and Huang, G.: Numerical analysis of full-scale ship self-propulsion performance with direct comparison to sea trial results, Journal of Marine Science and Engineering, Vol. 8, No. 1, 24, 2020. doi:10.3390/jmse8010024

[15] Wang, X., Ma, Y., Feng, D., Yao, C. and Cai, Z.: Numerical study of the hydrodynamic performance of a two-propeller configuration, Journal of Marine Science and Engineering, Vol. 13, No. 5, 992, 2025. doi:10.3390/jmse13050992

[16] Saydam, A.Z., Koksu, G.N., Insel, M. and Gokay, S.: Uncertainty quantification of self-propulsion analyses with RANS-CFD and comparison with full-scale ship trials, Brodogradnja, Vol. 73, No. 4, 2022. doi:10.21278/brod73406

[17] Moon, M.H., Zaman, S.A., Hussain, M.D. and Uddin, M.M.: Preliminary assessment of power savings by Flettner rotors installed on a cargo ship, MIST International Journal of Science and Technology, Vol. 13, No. 1, pp. 73–82, 2025. doi: 10.47981/j.mijst.13(01)2025.508

[18] Schlichting, H. and Gersten, K.: *Boundary-Layer Theory*, 9th ed., Springer, Berlin, 2017.

[19] Prandtl, L.: On fluid motion with very small friction, *Proc. 3rd Int. Math. Congress*, Heidelberg, 1904 (English translation).

[20] Prandtl, L.: Ergebnisse der Aerodynamischen Versuchsanstalt Göttingen, Vol. 3, 1927.

[21] Nikuradse, J.: Investigations on velocity distribution in turbulent flows, Forschungsheft, No. 281, 1926.

[22] Nikuradse, J.: Laws of flow in rough pipes, *VDI-Forschungsheft*, No. 361, 1933.

[23] White, F.M. and Majdalani, J.: *Viscous Fluid Flow*, 4th ed., McGraw-Hill, New York, 2021.

[24] Kothandaraman, C.P. and Rudramoorthy, R.: *Fluid Mechanics and Machinery*, 2nd ed., New Age International, New Delhi, 2007.

[25] Pena, B., Muk-Pavic, E. and Fitzsimons, P.: Detailed analysis of the flow within the boundary layer and wake of a full-scale ship, Ocean Engineering, Vol. 218, 108022, 2020. doi:

10.1016/j.oceaneng.2020.108022

[26] Garthune, R.S., Rosenberg, B., Cafiero, D. and Olson, C.R.: The performance of model ships in restricted channels in relation to ship canal design, Defense Documentation Center for Scientific and Technical Information, Alexandria, VA, 1948.

[27] Klemm, V.P. and Buckingham, W.L.: *Investigation of the scale effect of appendage resistance of DD-710 class ship models*, M.Sc. Thesis, Webb Institute of Naval Architecture, Glen Cove, NY, 1954.

[28] Larsson, L.: Calculation method for three-dimensional turbulent boundary layers on ship-like bodies, *Proc. 1st Int. Conf. on Numerical Ship Hydrodynamics*, Washington, D.C., 1975.

[29] Larsson, L.: *SSPA-ITTC Workshop on Ship Boundary Layers—Proceedings*, Liber Distribution, Vällingby, Sweden, 1980.

[30] Cebeci, T., Chang, K.C. and Kaups, K.: General method for calculating three-dimensional laminar and turbulent boundary layers on ship hulls, Ocean Engineering, Vol. 7, No. 2, pp. 229–280, 1980. doi:10.1016/0029-8018(80)90058-X

[31] Patel, V.C. and Sarda, O.P.: Mean-flow and turbulence measurements in the boundary layer and wake of a ship double model, Experiments in Fluids, Vol. 8, No. 6, pp. 319–335, 1990. doi:10.1007/BF00217197

[32] Toda, Y., Stern, F., Tanaka, I. and Patel, V.C.: Mean-flow measurements in the boundary layer and wake of a Series-60 (C_B=0.6) model ship with and without propeller, Journal of Ship Research, Vol. 34, No. 4, pp. 225–252, 1990.

doi:10.5957/jsr.1990.34.4.225

[33] Chawner, J.R., Dannenhoffer, J. and Taylor, N.J.: Geometry, mesh generation and the CFD-2030 vision, *Proc. 46th AIAA Fluid Dynamics Conference*, Washington, D.C., 2016. doi:10.2514/6.2016-3485

[34] Sadakata, K., Hino, T. and Takagi, Y.: Estimation of full-scale performance of energy-saving devices using a boundary-layer similarity model, Journal of Marine Science and Technology, Vol. 29, 2024. doi:10.1007/s00773-023-00981-2

[35] Nguyen, H.V. and Nguyen, V.H.: Viscous resistance acting on a symmetrical hull with different turbulent models, *Proc. NICS*, 2022. doi:10.1109/NICS56915.2022.10013465

[36] Tezdogan, T., Kim, D. and Incecik, A.: Hydrodynamic analysis of ship manoeuvrability at ports using CFD, International Maritime Transport and Logistics Journal, Vol. 12, No. 1, pp. 213–225, 2023. doi:10.21622/marlog.2023.12.1.213

[37] Deng, R., Huang, D., Li, J., Cheng, X. and Lei, Y.: Discussion of grid generation for catamaran resistance calculation, Journal of Marine Science and Application, Vol. 9, No. 2, pp. 187–191, 2010. doi:10.1007/s11804-010-9080-2

[38] Deng, R., Huang, D., Zhou, G.L., Sun, H., Chang, L. and Ma, C.: Research on mesh generation affecting resistance calculation, Applied Mechanics and Materials, Vols. 138–139, pp. 886–893, 2011. doi:10.4028/www.scientific.net/AMM.138-139.886

[39] Lopes, R., Eslamdoost, A., Bensow, R.E., Ponkratov, D. *et al.*: Summary of the Lucy Ashton resistance prediction workshop, Ocean Engineering, Vol. 343, 122951, 2026.

doi: 10.1016/j.oceaneng.2025.122951

[40] Lopes, R., Eslamdoost, A., Johansson, R., RoyChoudhury, S., Bensow, R.E., Hogstrom, P. and Ponkratov, D.: Resistance prediction using CFD at model and full scale and comparison with measurements, Ocean Engineering, Vol. 321, 120367, 2025.

doi: 10.1016/j.oceaneng.2025.120367

[41] Vasilev, M., Kalajdžić, M. and Ponkratov, D.: CFD approach to full-scale resistance – The Lucy Ashton case, Brodogradnja, Vol. 77, No. 3, 77307, 2025. doi:10.21278/brod77307

[42] ITTC: 1978 ITTC performance prediction method, *ITTC Quality System Manual*, Recommended Procedures and Guidelines, 2021.

[43] ITTC: Final report of the specialist committee on powering performance prediction, *Proc. 25th ITTC*, Fukuoka, Japan, 2008.

[44] Molland, A.F., Turnock, S.R. and Hudson, D.A.: *Ship Resistance and Propulsion*, Cambridge University Press, Cambridge, 2011.

[45] Vasilev, M., Kalajdžić, M. and Ivković, I.: CFD-powered ship trim optimization integrating ANN for user-friendly software development, Journal of Marine Science and Engineering, Vol. 12, 1265, 2024. doi:10.3390/jmse12081265

[46] Korkmaz, K.B., Werner, S., Sakamoto, N. *et al.*: CFD-based form factor determination method, Ocean Engineering, Vol. 220, 108451, 2021. doi: 10.1016/j.oceaneng.2020.108451

[47] ITTC: Practical guidelines for ship CFD applications, *ITTC Quality System Manual*, 2024.

[48] ITTC: Uncertainty analysis in CFD verification and validation, *ITTC Quality System Manual*, 2024.

[49] Smith, L.: Resistance experiments on the Lucy Ashton—Part IV, Quarterly Transactions of the Institution of Naval Architects, Vol. 97, No. 4, pp. 525–561, 1955.

NOMENCLATURE

Sym.	Unit	Name
∇	m^3	Displacement volume
a	-	Coefficient of function $f(\lambda)$
B	m	Breadth
b	-	Exponent of function $f(\lambda)$
BS	m	Cell base size
c	-	Coefficient of function $g(Fr)$
C_b	-	Block coefficient
C_F	-	Friction resistance coefficient
$C_{F,\mathrm{ITTC}}$	-	Friction resistance coefficient based on ITTC guidelines
C_m	-	Midship coefficient
C_p	-	Prismatic coefficient
C_T	-	Total resistance coefficient
C_V	-	Viscous resistance coefficient
D	-	EFD data
d	-	Exponent of function $g(Fr)$
e	-	Coefficient
E	-	Comparison error
f	-	Wall-resolution control function based on λ
Fr	-	Froude number
g	-	Wall-resolution control function based on Fr
H	m	Depth
h	-	Mesh scaling function
i	-	Exponent
j	-	Counter
k	-	Form factor
l	-	Number of cases
L_{pp}	m	Length between perpendiculars
L_{wl}	m	Waterline length
n_{lay}	-	Number of layers in boundary layer
r	-	Refinement factor
Re	-	Reynolds number
$R_{T,\mathrm{CFD}}$	N	Total resistance based on CFD analysis
$R_{T,\mathrm{EFD}}$	N	Total resistance based on EFD analysis
S	-	CFD solution
s	-	Exponent of parameter m
SF	-	Stretch factor
T	m	Draft
u	m/s	Fluid speed
u^*	m/s	Friction velocity
u_∞	m/s	Undisturbed stream velocity
U_D	-	Data uncertainty
U_G	-	Grid uncertainty
U_V	-	Validation uncertainty
WS	m^2	Wetted surface without rudder
WS_{total}	m^2	Wetted surface with rudder
x	m	Length / Cell length in x direction
y	-	Cell length in y direction
y^+	-	Non-dimensional wall distance
Y_1	m	First cell thickness in the boundary layer
Y_{last}	m	Last cell thickness in the boundary layer
z	-	Cell length in z direction
ZR	-	Zone refinement factor
δ	m	Boundary layer thickness
δ_{CFD}	m	Boundary layer thickness based on CFD analysis
δ_{pltt}	m	Prism layer total thickness, near-wall region thickness
$\Delta_{(\mathrm{sw})}$	t	Displacement in sea water
ΔC_F	-	Roughness allowance
η_a	kg/ms	Dynamic viscosity of air
η_w	kg/ms	Dynamic viscosity of water
λ	-	Scale
ρ_a	kg/m^3	Air density
ρ_w	kg/m^3	Water density
τ_w	N/m^2	Shear stress
υ	m^2/s	Kinematic viscosity of water

Table 3. Domain and zone refinements dimensions

	Aft edge	Fore edge	Aft Side	Fore Side	Bottom extrusion	Top extrusion
Domain	$-3.5 \cdot L_{pp} / \lambda$	$2 \cdot L_{pp} / \lambda$	$2 \cdot L_{pp} / \lambda$	$2 \cdot L_{pp} / \lambda$	$-2 \cdot L_{pp} / \lambda$	$0.5 \cdot L_{pp} / \lambda$
Free surface refinement	$-3.5 \cdot L_{pp} / \lambda$	$2 \cdot L_{pp} / \lambda$	$2 \cdot L_{pp} / \lambda$	$2 \cdot L_{pp} / \lambda$	$0.9 \cdot T / \lambda$	$1.1 \cdot T / \lambda$
Stern refinement	$-0.15 \cdot L_{pp} / \lambda$	$0.2 \cdot L_{pp} / \lambda$	$0.6 \cdot B / \lambda$	$0.6 \cdot B / \lambda$	$-0.2 \cdot T / \lambda$	$1.3 \cdot T / \lambda$
Fore refinement	$0.9 \cdot L_{pp} / \lambda$	$1.05 \cdot L_{pp} / \lambda$	$0.6 \cdot B / \lambda$	$0.6 \cdot B / \lambda - 0.15 \cdot L_{pp} / \lambda \cdot \tan(20)$	$-0.2 \cdot T / \lambda$	$1.3 \cdot T / \lambda$
Fine cone refinement	$-1.5 \cdot L_{pp} / \lambda$	$1.5 \cdot L_{pp} / \lambda$	$3 \cdot L_{pp} / \lambda \cdot \tan(20)$	$0.8 \cdot B / \lambda$	$0.7 \cdot T / \lambda$	$1.3 \cdot T / \lambda$

Coarse cone refinement	$-2.25 \cdot L_{pp} / \lambda$	$1.8 \cdot L_{pp} / \lambda$	$7.5 \cdot L_{pp} / \lambda \cdot \tan(20)$	$2 \cdot B / \lambda$	$0.5 \cdot T / \lambda$	$1.5 \cdot T / \lambda$

Table 6. Initial values for near-wall region setup obtained with (7-10): (Lucy Ashton case, *Fr* = 0.219)

λ [-]	k [-]	V [m/s]	Re [-]	$C_{F,\mathrm{ITTC}}$x10^3 [-]	C_vx10^3 [-]	τ_w [Pa]	u^* [m/s]
21.167	0.029	1.136	2511991	3.8739	3.9863	2.571	0.05073
15.875	0.035	1.312	3867554	3.5639	3.6886	3.172	0.05635
11.906	0.034	1.515	5954677	3.2896	3.4014	3.9	0.06249
9.525	0.042	1.694	8321652	3.0981	3.2282	4.627	0.06806
7.938	0.046	1.856	10938061	2.9538	3.0897	5.314	0.07294
6.35	0.051	2.075	15287850	2.7904	2.9328	6.305	0.07945
1	0.058	5.228	261594245	1.821	1.9266	27.018	0.16227

Table 7. Initial values for near-wall region setup obtained with MATLAB code: (Lucy Ashton case, *Fr* = 0.219)

λ [-]	δ [m]	y^+L_{wl}/Y_1Fr [-]	SF [-]	n_{lay} [-]	y^+ [-]	Y_1 [m]	Y_{last} [m]
21.167	0.02311	512086	1.20	7	35	0.00179	0.00534
15.875	0.02889	758417	1.24	7	44	0.00198	0.00718
11.906	0.03610	1121320	1.30	8	37	0.00151	0.00950
9.525	0.04292	1526621	1.29	9	38	0.0014	0.01073
7.938	0.04943	1963082	1.28	9	48	0.00168	0.01213
6.35	0.05876	2673162	1.28	10	48	0.00152	0.01404
1	0.24372	37073875	1.29	19	36	0.00056	0.05523

Table 8. Initial values for near-wall region setup obtained with (7-10): (Lucy Ashton case, λ =1)

Fr [-]	V [m/s]	Re [-]	$C_{F,\mathrm{ITTC}}$x10^3 [-]	C_vx10^3 [-]	τ_w [Pa]	u^* [m/s]
0.130	3.104	155284255	1.9567	2.0702	10.23	0.09985
0.173	4.130	206647508	1.8805	1.9896	17.411	0.13027
0.219	5.228	261594245	1.8210	1.9266	27.018	0.16227
0.260	6.207	310568510	1.7794	1.8826	37.212	0.19044
0.304	7.258	363126257	1.7428	1.8439	49.825	0.22037

Table 9. Initial values for near-wall region setup obtained with MATLAB code: (Lucy Ashton case, λ =1)

Fr [-]	δ [m]	$y^+L_{wl}/Y_1\lambda$ [-]	SF [-]	n_{lay} [-]	y^+ [-]	Y_1 [m]	Y_{last} [m]
0.130	0.26355	4995928	1.29	17	43	0.00102	0.06004
0.173	0.25249	6517776	1.29	18	41	0.00076	0.05735
0.219	0.24372	8119179	1.29	19	39	0.00056	0.05523
0.260	0.23752	9528551	1.29	19	44	0.00055	0.05382
0.304	0.23202	11025758	1.29	20	39	0.00042	0.05248

Table 10. Results of Lucy Ashton case (various scales, one speed (same *Fr*))

			CFD			
	λ [-]	EFD	Coarse (S_3)	Medium (S_2)	Fine (S_1)	E %D
C_T x 10^3 [-]	21.167	4.3	4.495	4.444	4.404	-2.4
	15.875	4.038	-	-	4.125	-2.2
	11.906	3.838	-	-	3.808	0.8
	9.525	3.643	-	-	3.634	0.3
	7.938	3.621	-	-	3.482	3.8
	6.35	3.467	-	-	3.351	3.3

No. of cells x 10^6	-	-	0.63	1.311	2.637	-

Table 12. Results for Lucy Ashton case (various speeds, full scale)

			CFD			
	Fr [-]	EFD	Coarse (S_3)	Medium (S_2)	Fine (S_1)	*E* %*D*
C_T x 10^3 [-]	0.13	2.278	-	-	2.287	-2.4
	0.173	2.259	-	-	2.214	-2.2
	0.219	2.566	-	-	2.57	0.8
	0.26	3.024	-	-	3.101	0.3
	0.304	4.165	4.425	4.385	4.353	3.8
No. of cells x 10^6	-	-	0.846	1.633	3.481	-

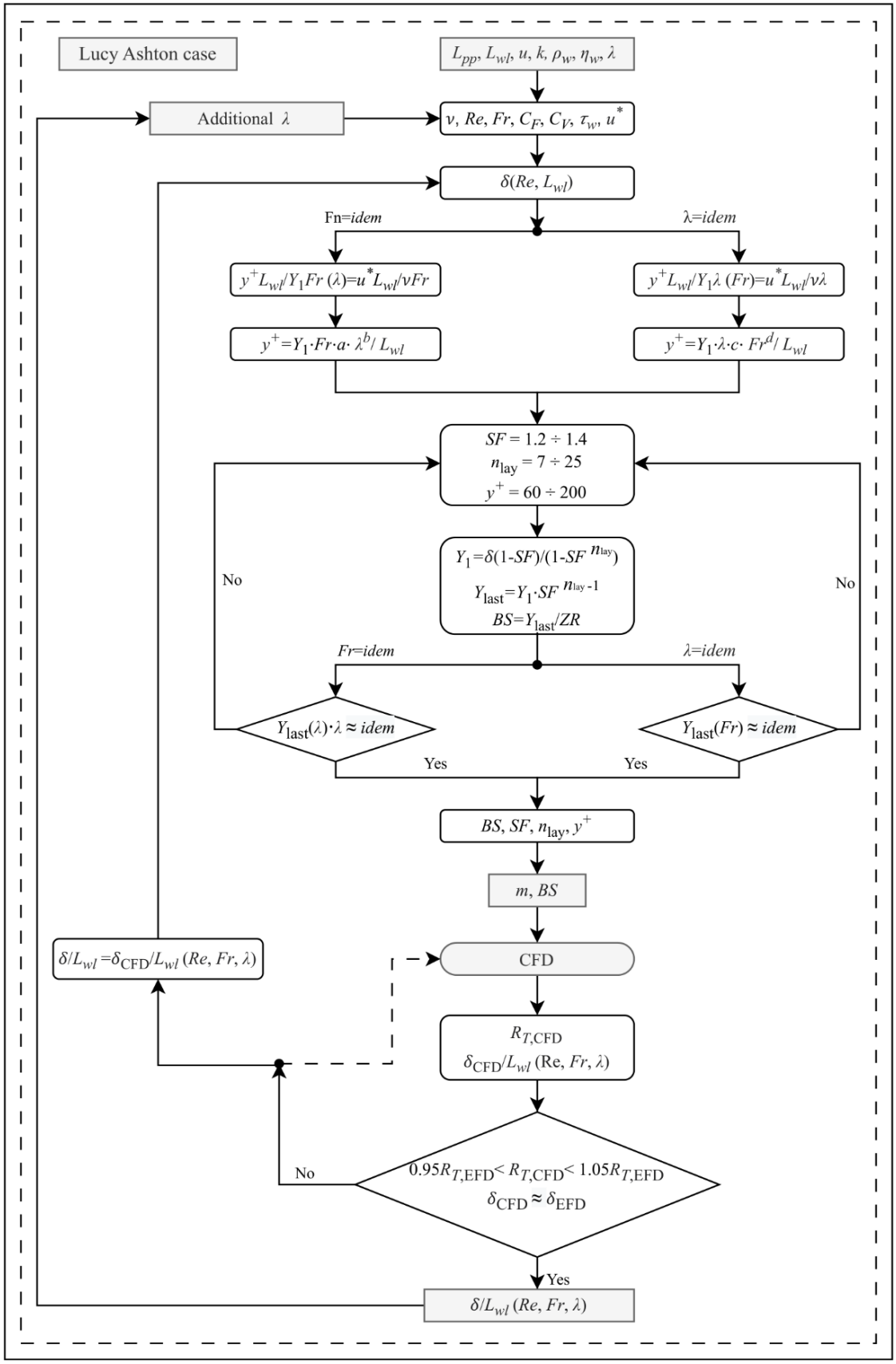

Figure 3. Methodology algorithm

ПАРАМЕТАРСКО ДЕФИНИСАЊЕ МРЕЖЕ: СТУДИЈА СЛУЧАЈА – ЛУСИ ЕШТОН

Ова студија обухвата брод Луси Ештон (енг. *Lucy Ashton*), јединствен референтни случај који пружа податке о мереном тоталном отпору брода у стварној величини и мерења дебљине граничног слоја. Спроведена је серија CFD симулација за више различитих размера и Фрудових бројева, са циљем репродукције експерименталних података о отпору брода и граничном слоју. Резултати су показали одлично слагање са мерењима, при чему су прогнозе отпора брода биле у оквиру ±5%, а профили граничног слоја дуж трупа реалистични. На основу ових налаза изведене су практичне формуле за дебљину граничног слоја и величину основне ћелије мреже. Иако су ове формуле изведене узимајући у обзир само брод Луси Ештон, они представљају обећавајућу основу за примену и на другим бродовима, поготов у раземри модела. Препоручују се даља истраживања ради потврде њихове поузданости за различите форме трупа у стварној величини.

ПРИЛОГ 8

University of Zagreb
Faculty of Mechanical
Engineering and Naval
Architecture

journal homepage: www.brodogradnja.fsb.hr

Brodogradnja

An International Journal of Naval Architecture and
Ocean Engineering for Research and Development

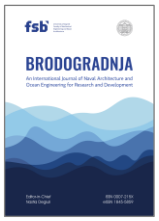

CFD approach to full-scale resistance: The Lucy Ashton case

Matija Vasilev[1,2*], *Milan Kalajdžić*[1,2], *Dmitriy Ponkratov*[3]

[1]*Department of Naval Architecture, Faculty of Mechanical Engineering, University of Belgrade, 11120 Belgrade, Serbia*
[2]*Ocean Pro Marine Engineers LTD, Belgrade, 11120 Belgrade, Serbia*
[3]*Siemens Digital Industries Software, London, UK*

ARTICLE INFO

Keywords:
Full-scale
Model scale
Resistance prediction

ABSTRACT

Accurate prediction of ship resistance remains a major challenge in Computational Fluid Dynamics (CFD), particularly when translating results from model to full scale. This study investigates the prediction of total resistance for the historic vessel Lucy Ashton using CFD across six model scales and full scale. Experimental resistance data were harmonized using third-order polynomial fits, enabling consistent comparison with CFD results. Two full-scale approaches were evaluated: Setup 1 with prescribed inflow and Setup 2 incorporating surge motion with applied thrust to emulate deck-mounted jets used during sea trials. Across all scales, CFD predictions showed strong agreement with experiments, with deviations typically within ±5%, consistent with accepted validation standards. Dynamic motions (heave and pitch) were also examined, and both setups produced nearly identical trends, with absolute differences negligible for resistance assessment. The results demonstrate that both CFD methodologies provide reliable full-scale resistance estimates.

1. Introduction

The improvement of ship performance (energy efficiency) as a global agenda goal was first presented in 2018 through [1]. The adoption of [2] finally defined the goal set by the International Maritime Organization (IMO), which is to reduce global greenhouse gas (GHG) emissions to net-zero by 2050. Checkpoints have also been introduced for 2030 and 2040, by which time total annual GHG emissions from international shipping should be reduced by at least 20%, striving for 30%, by 2030 and by at least 70%, striving for 80%, by 2040 compared to 2008 levels. Moreover, peak emissions should be reached as soon as possible and the reduction of annual GHG emissions must achieve net-zero by 2050, compared to 2008. According to available data from [3] and [4], the reduction rate of CO_2 emissions from ships in global emissions for the period from 2008 to 2018 was 0.3%. The current phase involves the analysis of the post-2018 period, with the latest CO_2 emission data expected to be published in the Fifth IMO Greenhouse Gas Study 2025. Using another available source for now [5], the share of international shipping in global emissions was 7.5% in 2023, which is significantly higher than in 2018 when it was 2.89%.

* Corresponding author.
E-mail address: matija@oceanpro.eu

https://doi.org/10.21278/brod77307
Received 23 September 2025; Received in revised form 15 December 2025; Accepted 21 December 2025
Available online 28 December 2025
ISSN 0007-215X; eISSN 1845-5859

Due to the rapid increase in the share of global emissions, modern software tools are increasingly used in the shipbuilding industry, such as CFD [6], Artificial Neural Network (ANN) [7, 8] and since 2018, Artificial Intelligence (AI) [9] to accelerate ship optimization solutions. In addition to these approaches, various optimization algorithms have also been developed and successfully applied to ship design problems in order to further improve hydrodynamic performance and energy efficiency [10]. One of the biggest challenges in using CFD software is the reliability of the results, i.e., how trustworthy the computer-generated solutions are. In shipbuilding practice, model tests have been conducted for decades and their results have never been questioned. The results obtained from model tests are then extrapolated to full-scale dimensions following the guidelines provided in [11]. CFD software have been under development for over five decades and supporting guidelines are issued by the International Towing Tank Conference (ITTC) under reference document number 7.5-03, which covers resistance, propulsion and maneuverability. It was only in 2022 that the IMO included numerical calculations as an acceptable method for determining the reference speed for the Energy Efficiency for Existing Ship Index (EEXI) regulation framework [12, 13] with direct guidelines published in [14].

Of the 14 papers considered as benchmarks for CFD validation [15], only one vessel has full-scale data available - the general cargo ship Regal. This vessel was also the subject of the first CFD workshop related to a full-scale ship, organized by Lloyd's Register in 2016 [16]. The same author previously worked on a similar topic, validating CFD results against full-scale sea trial measurements [17, 18]. CFD workshops are characterized by the fact that measurement data (whether from model tests or full-scale) are not shared publicly until participants submit their results to the organizer. The workshop organizer holds the right to analyze all submitted data and compare it with experimental results. This method of organizing workshops is considered the only valid and correct approach. Over the past decades, several such workshops have been held, starting in 1980, followed by events in 1990, 1994, 2000, 2005, 2010, 2015, 2024 and another is known to be planned for 2025. The analysis of published results from the Lloyd's Register workshop showed that the mean comparison error of the predicted power was 13% for all submitted results, with only three out of 27 participants achieving errors below 3% for all considered speeds [16]. A deviation of up to 16% in total resistance between participants was also reported in another results analysis of the Lloyd's Register workshop [19].

Among the guidelines issued by the ITTC, one document specifically addresses uncertainty analysis in CFD verification and validation [20] in this document, numerical error is divided into four components: (iteration number, grid size, time step and other parameters). Among these, the grid size error is identified as the most significant contributor. Grid uncertainty stems from multiple factors related to grid generation, such as cell type and refinement strategy. These factors significantly influence the accuracy of flow field representation in maritime environments, making proper grid resolution a critical aspect in CFD analysis for ship hydrodynamics.

In the paper [21], the authors investigated the influence of grid size (ranging from 5 to 11 million cells) on the predicted self-propulsion propeller revolutions rate for two ships. The study resulted in a 0.15% uncertainty for the general cargo ship Regal and 4.02% uncertainty for the car carrier. However, the authors did not follow the guidelines for uncertainty analysis as specified by ITTC in [20] where it is recommended that the grid refinement ratio should be uniform and equal to $\sqrt{2}$. In the study by [22] the grid refinement ratio value of $\sqrt{2}$ was used for grid sensitivity analysis, covering four grids (12.3, 25.4, 41.1 and 62.5 million cells). This study again examined the Regal ship, but it remains unclear why the authors conducted analyses of the grid size effect on the total resistance coefficient, as the total resistance for this ship was not directly measured but was an average value from workshop participants. The authors reported deviations of the total resistance coefficient from the average value ranging from -6.27% to +0.44% between the coarsest and finest grids. The group of authors [23] in their study also performed a grid uncertainty analysis for the KVLCC2 ship using three grids (0.897, 1.69 and 3.077 million cells). They obtained an uncertainty of 2.49%, with results varying between -1% and +2% compared to experimental data. An extensive verification and validation study of ship scale CFD self-propulsion simulations is presented in [24]. As a part of the study, a speed and power test were conducted with a research vessel for three different power settings. Numerical uncertainties

due to the finite number of cells were assessed according to the grid convergence index (GCI) method. The observed uncertainty values were low, ranging from 0.54% to 4.52% (for grid ranges from 1.75 to 11.52 million of cells). The propeller revolution results aligned well with the trial data, with relative errors between -2.46% and -4.40% when compared to the corrected trial values. However, significantly larger errors were noted in the delivered power comparison, varying from -30.15% to -41.93%. In [25] RANS-CFD analyses employed to predict resistance, open water propeller performance and self-propulsion for a tanker ship, with results compared to experimental data and sea-trial measurements of three sister ships. The proposed methodology showed good agreement with full-scale power predictions, achieving a maximum error of 4.13%. Numerical uncertainty on resistance and thrust was approximately 0.5% for a grid of 9.9, 15.5 and 22.6 million cells, while the propeller torque uncertainty, identified as the major contributor, was calculated at 5%.

In the article written by [17] an optimized setup was determined based on Regal test case, balancing computational cost and accuracy, with an optimal mesh density of around 11 million cells. The findings emphasize the need for a separate full-scale ship CFD guideline, as using model scale parameters can lead to unnecessary computational resource waste. The study [26] combines numerical simulations and experimental tests to predict self-propulsion points and required brake power for a bulk carrier at full scale under different load conditions. The numerical results using the RKE turbulence model and a coarse mesh (4.1 million cells) showed good agreement with extrapolated towing tank data.

In [27] CFD simulations of delivered power are validated for a full-scale ship and verifies the numerical method through systematic grid refinement for both model and full-scale cases. With a validation uncertainty of 7% and an average comparison error of 1% in the speed range of 12.5 to 14.5 knots, the results highlight the accuracy of the simulations, particularly considering surface roughness effects on the hull and propeller.

In [28] the feasibility of full-scale CFD predictions for self-propulsion characteristics is demonstrated, applying a methodology to the KRISO container ship (KCS) that includes three full-scale simulations: open water, towed and self-propelled cases. It highlights key differences between model and full-scale simulations, particularly due to Reynolds number effects, with a thinner boundary layer in full scale leading to improved propeller performance and higher efficiency.

In [29] the nominal wake at full scale for a Handymax bulk carrier using CFD simulations with and without wall functions is assessed. A verification study showed small numerical uncertainties for frictional resistance and three turbulence models (RKE, SSTKO and RSM) were tested, with RSM providing the best agreement with experimental wake data. Significant scale effects were observed, with numerically obtained effects exceeding extrapolated ones, particularly when using wall functions at model scale.

The literature review highlights several studies that compare the performance of different types of ships, using both CFD analysis and experimental methods. These studies often involve model testing, as well as full-scale measurements of ship speed and power. Additionally, many of these works consider the influence of various factors, such as the number of cells and cell size in CFD simulations, on the accuracy of the results. The problem in estimating resistance in full scale lies in the method used to extrapolate results from model tests to real-world conditions. Today, two well-established methods known as ITTC 57 and ITTC 78, dating back over 50 years, are still commonly used for this purpose [11]). These methods, although originating in the past, continue to be relevant and widely applied in current practice. So, CFD results are not directly compared with measured data but rather with extrapolated values. It is true that these methods have been used in shipbuilding practice for decades and that designed ships have shown that extrapolators can be trusted. However, whether a specific numerical value, such as the engine power required at a given sailing speed, can be trusted is quite difficult to determine due to numerous parameters (such as the effect of the propeller's operation behind the ship and weather conditions) that can influence the ship's performance. Therefore, the best method of comparison is to conduct direct resistance measurements of the full-scale ship alongside CFD results.

One of the main challenges in full-scale resistance measurement is the difficulty in directly measuring resistance on a full-size ship. To address this, one common approach involves towing the ship (without a propeller) with one or two tugboats and measuring the force exerted on the towline. However, a major

limitation of this method is that the tugboats pulling the ship affect the resistance measurement. Their wake and wave patterns, generated as they move ahead of the towed ship, influence the resistance of the ship being towed. This interaction introduces a level of complexity that must be accounted for when interpreting the results, but it is not clear how.

An alternative method to measure ship resistance involves the installation of jet engines on the ship's deck. This approach creates thrust, simulating propulsion, while eliminating the influence of the tugboats' waves. Two historical cases of such experiments, which were conducted several decades ago, are documented in the literature and published in two separate papers [30, 31].

The primary goal of the measurements of the hull resistance of the Lucy Ashton [30] was to gather data for comparing ship resistance with the resistance predicted from model tests across a wide range of speeds. By obtaining accurate resistance values, the comparisons could be made between these values and the corresponding model test resistance, which would help clarify the effectiveness of various methods used for skin friction correction between the model and ship. Additionally, the tests aimed to explore how factors like fairing seams, different ship surfaces, paint deterioration and appendages such as twin-screw bossings or "A" brackets with shafts affect resistance. The research program was developed with these objectives in mind, with some adjustments based on experience gained during testing. The analysis and testing have been further expanded and published in three additional parts. The paper [32] focuses on correlating the measured full-scale resistance of the Lucy Ashton with the results from tests on six geometrically similar models, ranging from 9 to 30 feet in length. The translation of model test results to full scale was done using Froude's skin-friction coefficients and skin-friction formulations. The study specifically correlates resistance for four naked hull conditions, including tests with two different paint surfaces and the effect of fairing the seams of the shell plating. The paper also describes the various corrections applied to the ship results and provides an analysis of the hull surface roughness measurements. Next part [33] examines the resistance increments caused by twin-screw shaft appendages (bossings and shaft brackets) on the Lucy Ashton, correlating full-scale ship results with those from six geometrically similar models. The study focuses on measuring additional resistance due to these appendages, marking the first time this has been done on a full-size ship. The findings are analyzed in the context of scale effects on appendage resistance. This final part [34] presents additional investigations on the Lucy Ashton, covering the effects of fouling on resistance, acceleration and retardation trials to determine the ship's virtual mass and Pitot traverses in the frictional belt to study velocity distributions under various hull-surface conditions.

The Lucy Ashton case is investigated through the paper published by [35]. In this study numerical simulations were performed across various Froude numbers and scaling ratios, primarily assuming a smooth hull and fixed position. A major challenge identified was the smearing of the free surface near the hull, which led to underpredicted resistance values-especially at full scale-due to artificially low viscosity. Including effects like surface roughness and freedom in heave and pitch improved agreement with experimental data. The study also highlighted limitations of the double-body approach at higher Froude numbers and found inconsistencies in form factor estimation using Prohaska's method. The ITTC 78 scaling procedure matched full-scale results well when roughness and air resistance were excluded. The study [36] found that CFD generally predicted lower resistance than 1950s experimental data due to assumptions of a smooth hull and no heave or pitch. Scatter in full-scale resistance decreased with increasing Froude number, with a median absolute deviation up to 2.3%, and the variability was similar to that observed at model scale, supporting confidence in full-scale CFD predictions.

In 1967, the R.V. Meteor [31] conducted full-scale tests in the Baltic Sea to validate the extrapolation of model test results to full-scale conditions for large, fast vessels. The tests included a model family of the ship at scales of 1:25, 1:19 and 1:13.75, with the aim of completing the series with full-scale data. Key measurements focused on resistance, propeller thrust, propeller power demand and the wake both in the absence and presence of the propeller. Boundary layer velocity distribution and ship behavior during maneuvering were also studied. After completing the measurement of speed and power trials, the propeller was removed to measure the total resistance. The Meteor was equipped with three jets (inspired by Lucy Ashton case) with a total power of 12000 HP. Jet thrust was measured by a strain gauges installed in the

supporting frame of each jet. Other measurements included wake using pitot tubes, boundary layer data with Prandtl tubes, rudder forces with a balance on the rudder shaft and ship speed through calibrated current meters. The results indicated that the ITTC 1957 line, commonly used for frictional resistance extrapolation, had too small a slope. The total efficiency of the model and prototype were identical and the thrust deduction fraction showed no dependence on scale. The study confirmed laboratory values for the boundary layer law, with $K = 0.41$ and $C = 5.0$.

The subject of this study is the Lucy Ashton case because it was used for the blind CFD workshop organized in 2024 by Chalmers University of Technology, in which the authors participated. The Lucy Ashton, originally a Clyde paddle steamer built in 1888, was modified for ship resistance experiments after its retirement in 1949. The vessel underwent significant alterations, including the removal of paddle wheels, machinery and deckhouses, followed by the addition of sand ballast and structural reinforcements. The hull was cleaned, smoothed with fairing material and sharpened at the plate edges to improve hydrodynamic performance. To achieve the required thrust for resistance tests, four Rolls Royce Derwent V jet engines were installed on a specially constructed gantry. These engines provided a combined thrust exceeding six tons, enabling the ship to reach speeds of about 15 knots. Since the jet engines could not reverse thrust, large steel flaps were added beneath the gantry to act as emergency water brakes, effectively slowing the vessel. A soundproof cabin was constructed to protect the crew from the intense noise. Accurate thrust measurement systems were installed using strain gauges on the engine mounts to ensure precise resistance readings. The choice of jet engines provided a steady and controllable thrust, overcoming issues like wake interference and unstable towing forces seen in alternative methods. Additional fuel tanks were fitted to extend operational range and ensure uninterrupted test runs on the measured mile.

The workshop cases were chosen based on data from 1950s sea trials, which included tests at various speeds and with four different surface conditions. These conditions involved two types of coatings: aluminum paint and red oxide paint, along with sharp and faired seams. For the workshop, participants were instructed not to include roughness modeling in their CFD simulations. Consequently, the smoothest experimental condition - faired seams with aluminum paint - was used as the reference for comparison. This condition was also used to determine the specific speeds selected for the simulations.

Two pitot logs were installed on the hull: one 72 ft 6 in. and the other 97 ft 4 in. aft of the forward perpendicular. These logs measured both static and dynamic pressure heads, connected to a mercury manometer to determine water speed. The logs could extend up to 3 ft from the hull's surface for boundary layer velocity measurements. Although their primary purpose was boundary layer investigation, these logs were also used to measure speed during acceleration and retardation trials. The calibration process involved taking readings during double runs on the measured mile, adjusting the log's position along the way. While fully extended readings were stable, issues arose with unstable data during traversing. Results were only considered reliable if the data scatter was within ±3% and enough readings were available for a mean curve. The data showed a thicker boundary layer (18 in.) at the No. 2 log's position compared to the No. 1 log's position (12 in.), reflecting the expected increase in boundary layer thickness along the hull at a speed of 10.18kn (unfortunately, data are available only for this speed) at the center line. Frictional-resistance coefficient derived from this velocity profile aligned well with direct resistance measurements.

Based on the results of conducted Lucy Ashton case, the objectives of this study are defined as follows:

- To compare CFD predictions with full-scale experimental measurements and scale-model tests performed with two degrees of freedom (heave and pitch) using the classical simulation approach in which the inflow passes around a fixed-speed ship.
- To compare CFD predictions with full-scale experimental measurements conducted with three degrees of freedom (surge, heave, and pitch) while explicitly accounting for the thrust generated by the jet engines.

2. Methodology

2.1 Case description

The Lucy Ashton case is highly suitable for developing the points mentioned earlier for several reasons:

- Data on total resistance from model tests is available for six different scales and multiple speeds: λ = [21.167, 15.875, 11.906, 9.525, 7.938 and 6.35];
- Data on total resistance for multiple speeds in full scale (λ = 1);

The basic data and dimensions of the Lucy Ashton ship are provided in the following Table 1, while the lines plan is provided in Fig. 1:

Table 1 Ship particulars

L_{pp} [m]	58.1
L_{wl} [m]	59.49
B [m]	6.4
T [m]	1.584
H [m]	2.1844
WS_{total} [m^2]	417
Δ [t] (sw)	390
C_b [-]	0.685
C_p [-]	0.705
C_m [-]	0.972

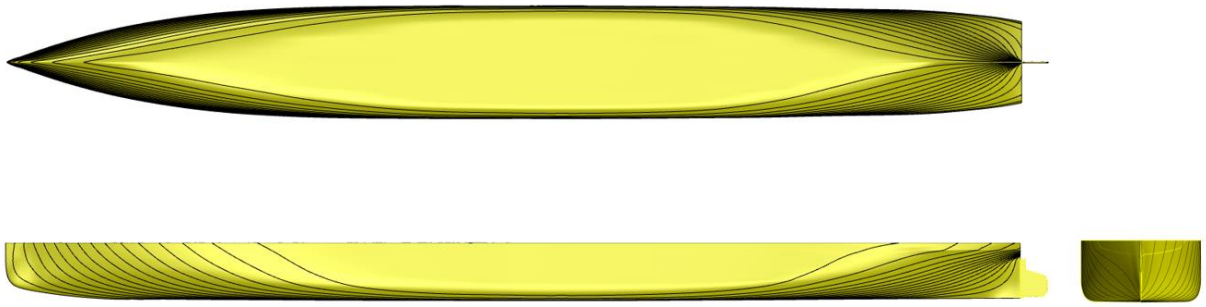

Fig. 1 Lines plan (Lucy Ashton)

2.2 CFD setup and simulation conditions

Setup 1: In the first (classical) CFD configuration, the ship has two degrees of freedom (heave and pitch), while the inflow velocity is imposed and water flows around the hull. The simulation is terminated when the total resistance, heave and pitch exhibit convergence. This setup is applied to all model scales and full-scale ship.

Setup 2: In the second CFD configuration, the ship has three degrees of freedom (surge, heave and pitch).The water domain is static, and a prescribed force, corresponding to the total thrust produced by the jet engines is applied at the location where the jets were mounted during the experiments. The entire computational domain translates with the vessel. The simulation stops once the ship speed, total resistance, heave and pitch converge. This setup is applied only for full-scale ship.

The cases considered in the workshop for the full-scale ship resistance prediction included following Fr = [0.130, 0.173, 0.219, 0.260, 0.304] and Fr = 0.219 for the model scales resistance prediction. In this

study, the number of conducted simulations were increased to contain all cases. Another distinction between this study and the simulations performed during the workshop is the inclusion of dynamic motions, specifically heave and pitch, which are now fully accounted for. For the CFD calculations, the software STAR-CCM+ developed by Siemens was used. In Table 2, "o" marked cells contain simulations conducted during the workshop, while with "x" are denoted additional simulations carried out in this study. Forces that are applied in Setup 2 are F=[2.25 kN, 4 kN, 7.5 kN, 12.5 kN, 23.5 kN] and it is important to note that values correspond to half-body. The location point where each force is applied is 19m from the aft perpendicular, in centerline and 3.216m above keel. The force location point moves together with a ship.

Table 2 Conducted simulations

λ	Fr=0.130	Fr=0.173	Fr=0.219	Fr=0.26	Fr=0.304
21.167	x	x	o, x	x	x
15.875	x	x	o, x	x	x
11.906	x	x	o, x	x	x
9.525	x	x	o, x	x	x
7.938	x	x	o, x	x	x
6.35	x	x	o, x	x	x
1	o, x	o, x	o, x	o, x	o, x

The kinematic viscosity can be determined based on the temperature of the water in which the experiments were conducted. In this case, it was determined based on known values for density and dynamic viscosity (given in Table 3).

Table 3 Water and air properties

	Full scale	Model scale
ρ_w [kg/m^3]	1026.02	998.8
ρ_a [kg/m^3]	1.225	1.242
η_w [Pas]	1.22E-03	1.27E-03
η_a [Pas]	1.79E-05	1.77E-05

2.3 Numerical models

The governing equations are discretized using the collocated Volume of Fluid (VOF) multiphase method integrated within the software. This method is designed for large-scale two-phase flows, specifically involving water and air, commonly encountered in naval hydrodynamics. The model describes a two-phase, incompressible, turbulent and viscous flow.

The VOF multiphase Eulerian model in STAR-CCM+ belongs to the interface-capturing methods category, which predicts the distribution and movement of the interface between immiscible phases. This approach assumes that the mesh resolution is adequate to capture the position and shape of the phase interface accurately. For more detailed insights into the VOF method, refer to [37]. A key characteristic of immiscible phase systems, such as air and water, is that the fluids remain separated by a distinct interface. To replicate the convective transport of immiscible fluid components, the High-Resolution Interface Capturing (HRIC) scheme is employed, ensuring precise tracking of sharp interfaces.

Fluid domain dimensions are defined as follows (from Aft Perpendicular):

- Inlet: 2.5 L_{pp} - defined as velocity inlet;
- Outlet: 3 L_{pp} - defined as pressure outlet with wave damping boundary option included;
- Bottom: 1.5 L_{pp} - defined as velocity inlet;
- Top: 1 L_{pp} - defined as velocity inlet;
- Port Side: 2 L_{pp} - defined as velocity inlet with wave damping boundary option included;

• Starboard Side: at centerline of the ship defined as symmetrical plane.

The wave damping length (*WDL*) is defined as two wave lengths (*WL*), where the wave length is calculated as per:

$$WL = 2\pi \cdot Fr^2 \cdot L_{pp} \tag{1}$$

The hull is considered as a no-slip wall as per [14] and a blended wall function is set as a default physics setting in the used software when *all y+ wall treatment* model is activated. In the user manual of used software is noted that *all y+ wall treatment* approach should be chosen whenever is available when complex geometries are being considered.

Principally, the flow is calculated only around the Port side of the ship to reduce computational resource consumption due to the large number of simulations and this condition was also defined through the workshop. The difference compared to the workshop guidelines is that dynamic pitch and heave are enabled, so the results obtained in this study are more reliable and differ from those sent by the authors to the organizers for participation in the workshop.

The turbulence model that is applied in this study is *k-ω* SST [38].

2.4 Grid uncertainty and post-processing

A grid convergence study is performed to assess the convergence of the results by systematically refining the base cell size by multiplying with $1/\sqrt{2}$ and 1/2. The convergence ratio is defined as:

$$R = \frac{\varepsilon_{21}}{\varepsilon_{32}} \tag{2}$$

where ε_{21} is the difference between the solution obtained using medium and fine mesh and ε_{32} is the difference between the solution obtained using coarse and medium mesh. *R* is used for the estimation of the convergence conditions: monotonic convergence is achieved when $0 < R < 1$, oscillatory convergence is achieved when $-1 < R < 0$ and divergence is achieved when $|R|>1$. The numerical uncertainty (U_G) and error (E) for monotonic convergence conditions is estimated as per ITTC [20]. The estimated order of accuracy (p_{RE}) and error (δ_{RE}) is calculated as per:

$$p_{RE} = \frac{\ln\left(\varepsilon_{32}/\varepsilon_{21}\right)}{\ln\sqrt{2}} \tag{3}$$

$$\delta_{RE} = \frac{\varepsilon_{21}}{\left(\sqrt{2}\right)^{p_{RE}} - 1} \tag{4}$$

To estimate the grid uncertainty U_G, a safety factor approach is employed [39], defining U_G as:

$$U_G = FS \cdot \left|\delta_{RE}\right| \tag{5}$$

where *FS* is a safety factor estimated as per [40]:

$$FS = 2.45 - 0.85P \text{ for } 0 < P \leq 1 \tag{6}$$

$$FS = 16.4P - 14.8 \text{ for } P > 1 \tag{7}$$

where *P* is the ratio of the estimated order of accuracy to the theoretical order of accuracy (p_{th}) which is two:

$$P = p_{RE}/p_{th} \tag{8}$$

Numerical uncertainty (U_{SN}) in this case is adopted to be equivalent to grid uncertainty:

$$U_{SN} = U_G \tag{9}$$

To determine if validation has been achieved, comparison error E is compared to validation uncertainty U_V given by:

$$U_V^2 = U_D^2 + U_{SN}^2 \tag{10}$$

where U_D is data uncertainty, but in Lucy Ashton case U_D is not available, therefore in this case validation uncertainty is equal to grid uncertainty. The comparison error is given by difference in the data D and simulation S values:

$$E = D - S \tag{11}$$

If $|E| < U_V$, the validation is achieved at the U_V level.

In the Lucy Ashton case grid uncertainty analysis had been done for two different scales in Lucy Ashton case (λ=21.167 and λ=1) and one speed.

In the numerical simulations conducted for Lucy Ashton full scale study, the direct consideration of the roughness effects is not included. However, this effect is accounted for in the post-processing stage by following the recommended procedures and guidelines outlined in [41]. The ITTC guidelines provide specific methodologies for incorporating the effects of the roughness and air resistance into the analysis, allowing for an assessment of the overall performance and characteristics of the ship. The roughness allowance (ΔC_F) is calculated as per [42]:

$$\Delta C_F = 0.044\left[\left(\frac{k_s}{L_{wl}}\right)^{\frac{1}{3}} - 10\mathrm{Re}^{-\frac{1}{3}}\right] + 0.000125 \tag{12}$$

where k_s is the surface roughness and it is known for Lucy Ashton (5.842×10^{-5}m) [34]. However, this value gives negative ΔC_F calculated as per Eq. 12, so the other approach is set because there is available the allowance on C_F, i.e., ΔC_F necessary to complete the full-scale ship-model balance, in the same document. Roughness allowances are given in Table 4 for each considered speed:

Table 4 Roughness allowances

Fr [-]	$\Delta C_F \times 10^3$ [-]
0.130	0.0181
0.173	0.0169
0.219	0.1303
0.260	0.2421
0.304	0.2979

The air resistance was neglected, as the superstructure had been removed prior to the sea trials. The additional structure installed to support the jet engines was lattice steel construction, resulting in minimal aerodynamic influence.

3. Results

The experimental datasets were fitted using third-order polynomial curves, achieving an R^2 value greater than 0.999 for each scale. This fitting procedure was necessary to enable a direct and consistent comparison between the CFD-based results and the experimental measurements. All experimental measurements of total resistance, both for the model and the full-scale ship, were converted into the non-dimensional total resistance coefficient using the available density values for fresh and seawater. The wetted surface area was estimated from the 3D hull model and consistently applied in the evaluation of the total resistance coefficient for both the experimental data and the CFD results. Furthermore, the standard deviation of the discrepancy between the polynomial-based values and the corresponding experimental measurements was determined for each scale, providing a quantitative measure of the fitting accuracy. The calculated standard deviations for all scales are presented in Table 5.

Table 5 Standard deviation of residuals between polynomial-fitted and experimental total resistance coefficients for each scale

λ [-]	σ [%]
21.167	2.20
15.875	2.30
11.906	2.90
9.525	2.30
7.938	1.20
6.350	2.00
1	3.10

3.1 Model scales

This section presents the CFD results obtained using Setup 1. In this context, the CFD results correspond to the total resistance coefficient evaluated for the half-hull at five Froude numbers. These coefficients are directly compared (relative error is given) with the experimental total resistance coefficients, which were obtained by applying the fitted polynomial to the measured total resistance data in each model scale.

In Tables 6-11 are given total resistance coefficients (C_T x 10^3) evaluated through Experimental Fluid Dynamics (EFD) and CFD for each *Fr* and relative error for model scales of 21.167, 15.875, 11.906, 9.525, 7.938 and 6.35, respectively.

Table 6 Results of Lucy Ashton case (model scale – λ=21.167)

Fr [-]	$C_{T,\mathrm{EFD}}\cdot 10^3$ [-]	$C_{T,\mathrm{CFD}}\cdot 10^3$ [-]	*E* %*D*
0.130	4.417	4.625	−4.7
0.173	4.278	4.451	−4.0
0.219	4.337	4.439	−2.3
0.260	4.615	4.675	−1.3
0.304	5.578	5.628	−0.9

Table 7 Results of Lucy Ashton case (model scale – λ=15.875)

Fr [-]	$C_{T,\mathrm{EFD}}\cdot 10^3$ [-]	$C_{T,\mathrm{CFD}}\cdot 10^3$ [-]	*E* %*D*
0.130	4.070	4.276	−5.1
0.173	3.963	4.102	−3.5
0.219	4.091	4.150	−1.4
0.260	4.388	4.484	−2.2
0.304	5.379	5.451	−1.3

Table 8 Results of Lucy Ashton case (model scale – λ=11.906)

Fr [-]	$C_{T,\mathrm{EFD}}\cdot 10^3$ [-]	$C_{T,\mathrm{CFD}}\cdot 10^3$ [-]	*E* %*D*
0.130	3.775	3.969	−4.6
0.173	3.741	3.758	−0.4
0.219	3.813	3.791	0.6
0.260	4.140	4.107	0.8
0.304	5.240	5.252	−0.2

Table 9 Results of Lucy Ashton case (model scale – λ=9.525)

Fr [-]	$C_{T,EFD}\cdot10^3$ [-]	$C_{T,CFD}\cdot10^3$ [-]	E %D
0.130	3.552	3.717	−4.6
0.173	3.533	3.534	0.0
0.219	3.648	3.629	0.5
0.260	3.947	3.878	1.7
0.304	5.041	5.051	−0.2

Table 10 Results of Lucy Ashton case (model scale – λ=7.938)

Fr [-]	$C_{T,EFD}\cdot10^3$ [-]	$C_{T,CFD}\cdot10^3$ [-]	E %D
0.130	3.393	3.524	−3.9
0.173	3.468	3.362	3.1
0.219	3.515	3.449	1.9
0.260	3.956	3.815	3.6
0.304	4.958	4.940	0.4

Table 11 Results of Lucy Ashton case (model scale – λ=6.350)

Fr [-]	$C_{T,EFD}\cdot10^3$ [-]	$C_{T,CFD}\cdot10^3$ [-]	E %D
0.130	3.257	3.399	−4.4
0.173	3.346	3.250	2.9
0.219	3.505	3.344	4.6
0.260	3.781	3.680	2.7
0.304	4.938	4.848	1.8

The grid uncertainty analysis was performed for the smallest model (λ=21.167) and the lowest speed (Fr=0.130), using three different cell sizes to generate the coarse, medium and fine meshes. The resulting total resistance coefficients obtained from these three mesh densities, along with the corresponding number of cells in the computational domain covering the half-hull, are presented in Table 12.

Table 12 Grid uncertainty analysis (λ=21.167, Fr=0.130)

	Coarse (S_3)	Medium (S_2)	Fine (S_1)
$C_{T,CFD}$ x 10^3 [-]	4.625	4.498	4.412
No. of cells x 10^6	0.63	1.311	2.637

Grid uncertainty in this case is 7.7% and since it is bigger than comparison error (4.7%), the validation is achieved.

3.2 Full-scale

Two different simulation setups were carried out to compare the CFD-based predictions of ship resistance, expressed through the total resistance coefficient. In both cases (Setup 1 and Setup 2), the computed total resistance coefficients were compared with the corresponding values obtained from the fitted polynomial representation of the experimental data (see Table 13 and Table 14). In addition to the resistance results, the dynamic motions (heave and pitch) were also evaluated, and the differences between the two setups are presented as well in Table 15. Index 1 in $z_{D,1}$ and $\theta_{D,1}$ refers to Setup 1, while index 2 in $z_{D,2}$ and $\theta_{D,2}$ refers to Setup 2. A negative sign in the heave motion indicates downward movement of the ship, while a negative sign in the pitch motion indicates trim by the stern.

Table 13 Results of Lucy Ashton case (full-scale – λ=1, Setup 1)

Fr [-]	$C_{T,EFD}\cdot10^3$ [-]	$C_{T,CFD}\cdot10^3$ [-]	E %D
0.130	2.278	2.287	−0.4
0.173	2.259	2.214	2.0
0.219	2.566	2.570	−0.2
0.260	3.024	3.101	−2.6
0.304	4.165	4.336	−4.1

Table 14 Results of Lucy Ashton case (full-scale – λ=1, Setup 2)

Fr [-]	$C_{T,EFD}\cdot10^3$ [-]	$C_{T,CFD}\cdot10^3$ [-]	E %D
0.130	2.278	2.302	−1.0
0.173	2.259	2.287	−1.2
0.219	2.566	2.556	0.4
0.260	3.024	3.177	−5.1
0.304	4.165	4.402	−5.7

Table 15 Dynamic motions and relative comparison of them between Setup 1 and Setup 2

Fr [-]	$z_{D,1}$ [m]	$\theta_{D,1}$ [deg]	$z_{D,2}$ [m]	$\theta_{D,2}$ [deg]	δz_D [%]	$\delta\theta_D$ [%]
0.130	−0.014	−0.011	−0.014	−0.005	0.0	54.5
0.173	−0.027	−0.019	−0.026	−0.012	3.7	36.8
0.219	−0.048	−0.038	−0.047	−0.031	2.1	18.4
0.260	−0.074	−0.084	−0.072	−0.082	2.7	2.4
0.304	−0.111	−0.206	−0.109	−0.194	1.8	5.8

The grid uncertainty analysis was performed for Setup 1 and the maximum considered speed (Fr=0.304), using three different cell sizes to generate the coarse, medium and fine meshes. The resulting total resistance coefficients obtained from these three mesh densities, along with the corresponding number of cells in the computational domain covering the half-hull, are presented in Table 16.

Table 16 Grid uncertainty analysis (λ=1, Fr=0.304)

	Coarse (S_3)	Medium (S_2)	Fine (S_1)
$C_{T,CFD}$ x 10^3 [-]	4.336	4.207	4.128
No. of cells x 10^6	0.846	1.633	3.481

Grid uncertainty in this case is 5.3% and since it is bigger than comparison error (4.1%), the validation is achieved.

4. Discussion

All EFD and CFD results listed in Tables 6–11 and Tables 13–14 are presented graphically in Fig. 2 as functions of the Reynolds number, plotted on a logarithmic scale. The solid lines represent the CFD-predicted total resistance coefficients obtained with Setup 1, the dashed lines correspond to the experimental data, and the dotted line denotes the full-scale CFD results obtained with Setup 2. The long dash dotted line represents ITTC 1957 friction line. This graphical comparison provides a clear assessment of the consistency between CFD and EFD results across all geometric scales, particularly at higher speeds.

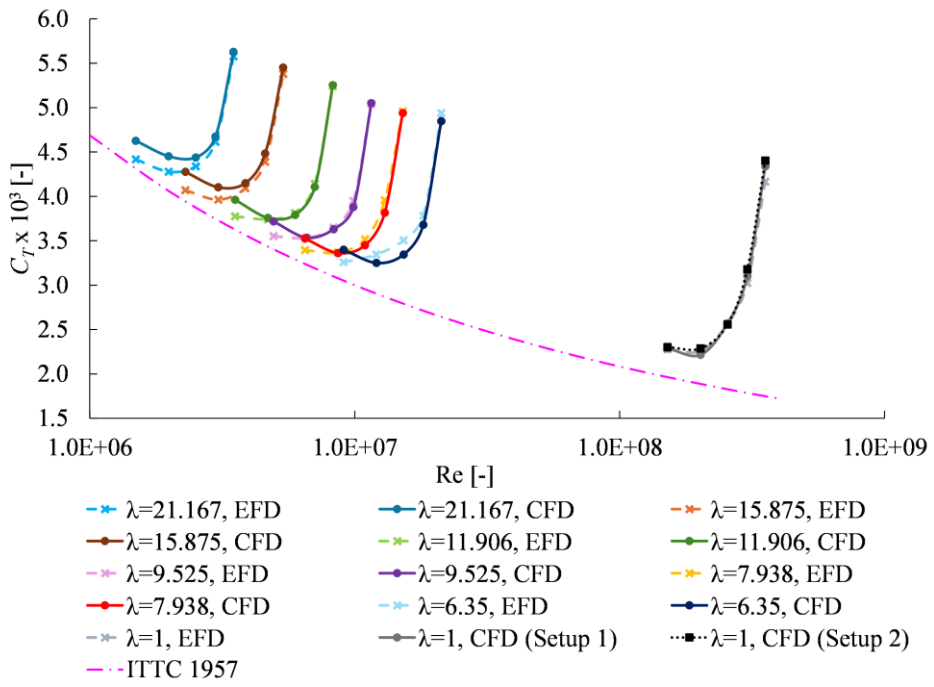

Fig. 2 Total resistance coefficients for all geometric scales

The largest discrepancies between CFD predictions and experiments occur at the lowest speed (*Fr*=0.130) for all model scales. This systematic behaviour suggests that the turbulence-modelling strategy may require adjustment for low-speed conditions. It should be noted that the same simulation configuration, Setup 1, was used for all scales and all Froude numbers.

The main distinction between Setup 1 and Setup 2 is the inclusion of the surge degree of freedom in Setup 2. Instead of prescribing a uniform inflow velocity, a reference point was attached to the hull and allowed to move relative to the vessel while being subjected to a thrust force. This formulation was used to emulate the effect of the jet engines installed on the deck during the full-scale tests.

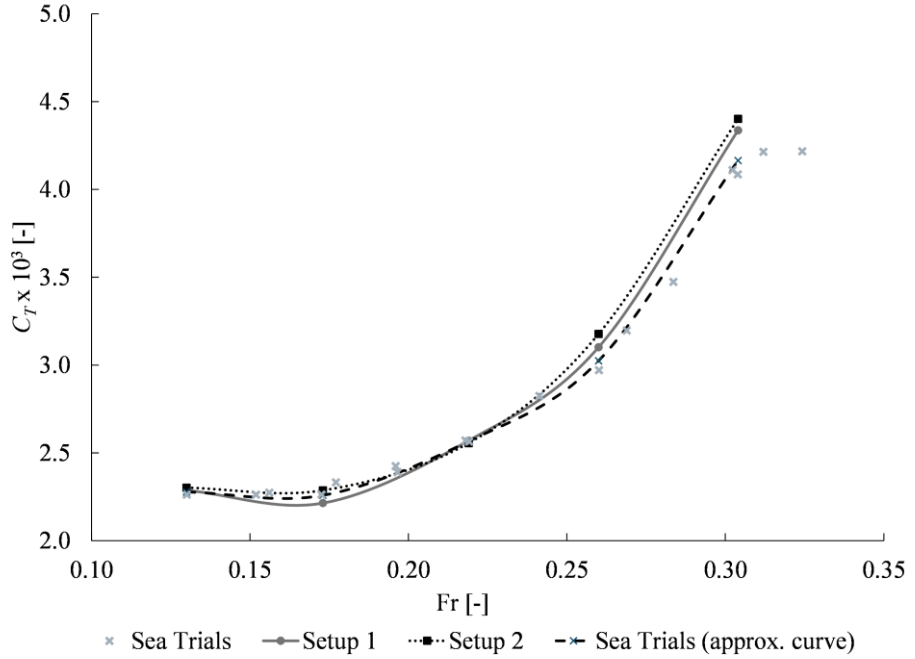

Fig. 3 Total resistance coefficients for full-scale. Sea Trials (EFD) data and CFD data based on Setup 1 and Setup 2 approaches

Fig. 3 presents the full-scale total resistance coefficients only as a function of *Fr*: the experimental measurements (tabulated values, marked with ‘x’), the fitted polynomial (dashed line), and the CFD results

obtained using Setup 1 (solid line) and Setup 2 (dotted line). A closer agreement between CFD and EFD results is observed at lower speeds, while the differences increase at higher speeds. Despite employing two fundamentally different modelling approaches, both setups produce comparable predictions of the total resistance.

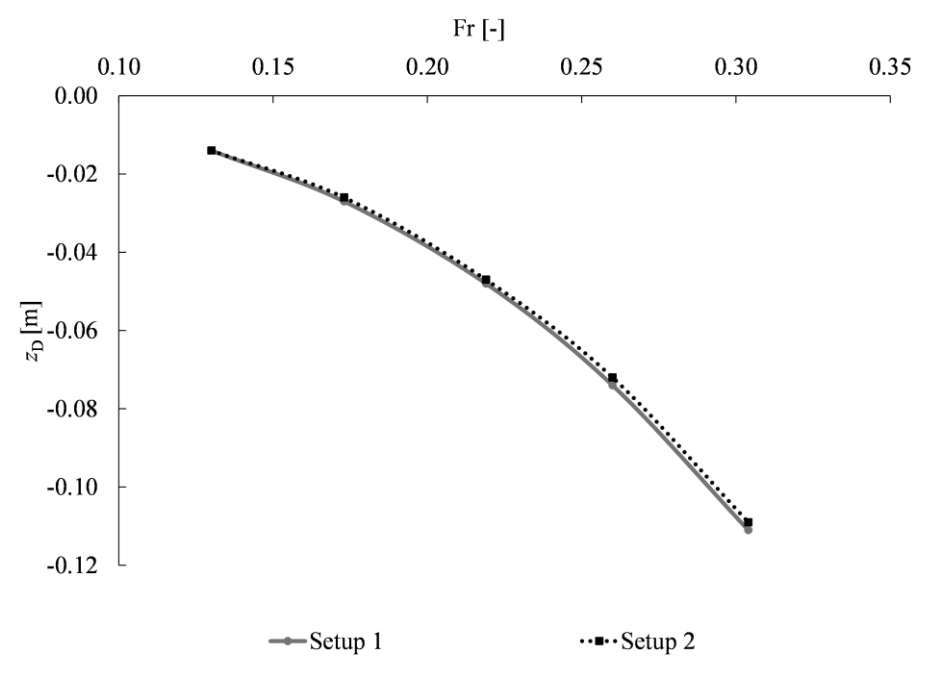

Fig. 4 Dynamic heave. Comparison between Setup 1 and Setup 2

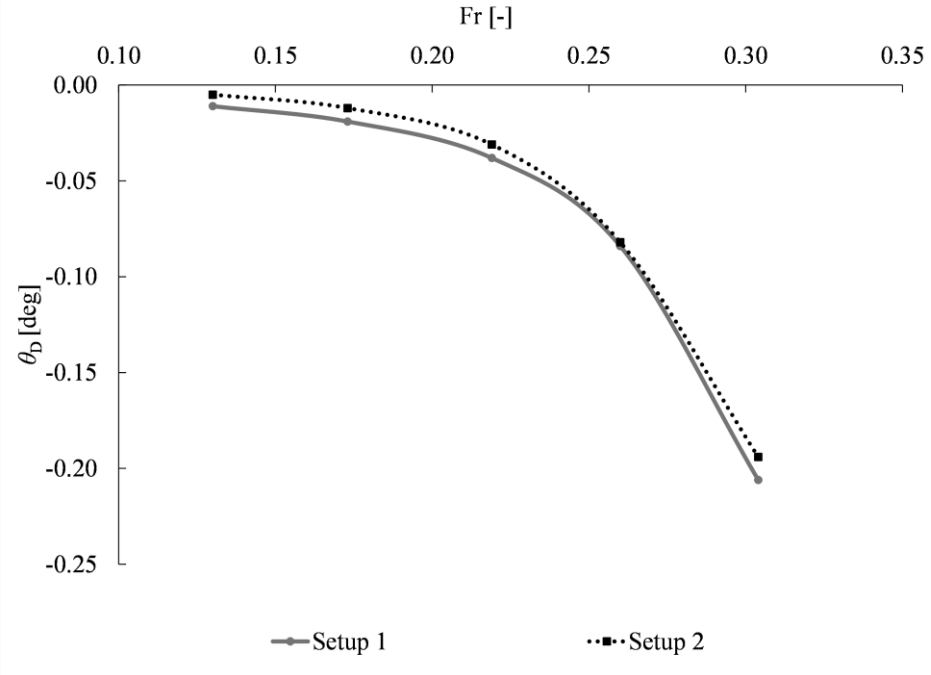

Fig. 5. Dynamic pitch. Comparison between Setup 1 and Setup 2

Because Lucy Ashton was originally propelled by large paddle wheels mounted on the sides, it is reasonable to examine whether the shift in the location and type of thrust affects the dynamic motions (heave and pitch). Mechanically, the moment generated by the deck-mounted jet thrust differs from that produced by the paddle-wheel blades, which could influence the vessel's response. However, the CFD results show that both modelling approaches (Setup 1 and Setup 2) produce similar trends in heave and pitch, as shown in Fig. 4 and Fig. 5. Moreover, the configuration with deck-mounted jets results in slightly smaller dynamic motions.

The magnitude of these differences is negligible in practice. Although the relative difference in heave reaches up to 4%, the physical displacement is only about 2 mm. For pitch, the relative deviation at the lowest speed is around 55%, yet the absolute value remains extremely small, on the order of 10^{-3} degrees, indicating that the effect is practically insignificant for resistance evaluation.

Both setups show a standard deviation of approximately 2% when compared with the experimental data. Considering that the standard deviation introduced by recalculating the full-scale resistance into the non-dimensional total resistance coefficient at a given Froude number is 3.1%, the results strongly suggest that both CFD approaches are robust. The difference in how thrust is applied (paddle-wheel mechanism versus jet-thrust representation) does not meaningfully affect the predicted total resistance, and both setups can be considered reliable for assessing full-scale hydrodynamic performance.

5. Conclusion

This study aimed to evaluate total resistance coefficient estimation for unique ship hull using CFD simulations. The research encompassed Lucy Ashton, for which the resistance measurements in six different model scales and in full scale are available. A focus on investigating is how scaling, *Fr* number and *Re* number affect total resistance predictions.

The resistance coefficient validation demonstrated that CFD simulations yielded results with an error margin within about 5% when compared to experimental data. The total resistance coefficient deviations fall within accepted industry tolerances for CFD validation (typically ±5%).

The comparison of two simulation strategies for the full scale (Setup 1 and Setup 2) showed that the difference in thrust modeling, uniform inflow versus thrust-driven surge, does not significantly influence the predicted total resistance. Although noticeable relative deviations appear in small dynamic motions such as heave and pitch, their absolute magnitudes remain extremely small (on the order of millimeters or 10^{-3} degrees). Both setups achieve a standard deviation of approximately 2% when compared with the fitted experimental values, confirming the robustness of the CFD methodology.

Despite the encouraging results, several limitations should be acknowledged. The standard deviation of the fitted polynomial is approximately 3%, which is more than twice the 1.3% deviation observed between the two estimation methods. This indicates that the methods are mutually consistent with relatively small and stable differences, whereas the larger scatter relative to the polynomial suggests that the approximation model is not optimal or that the data exhibit nonlinear behavior that the chosen polynomial cannot adequately capture. The largest discrepancies occur at the lowest speeds (Fr = 0.130), suggesting that the turbulence model or near-wall treatment may require refinement for these flow regimes for each scale. There is also concern about possible turbulence triggering in the model scale experiments at lower speeds, since this aspect is not described in the reports and CFD well predict total resistance in a full-scale condition at lower speeds. Only one CFD code (STAR-CCM+) and one general meshing approach were used; cross-validation using alternative solvers or mesh-generation technologies was not performed.

Future work should focus on improving turbulence-modeling strategies for low-speed regimes. Extending the grid-convergence analysis to a broader range of *Fr* numbers would further strengthen the numerical validation. Finally, incorporating scale effects through advanced wall-modeling or hybrid RANS–LES approaches could provide additional view into the sources of discrepancy between model- and full-scale predictions.

Overall, the results confirm that both CFD approaches used in this study are reliable for estimating the total resistance of the Lucy Ashton hull across all scales, supporting the broader applicability of CFD as a predictive tool in ship hydrodynamics, especially in full-scale.

NOMENCLATURE

∇	m^3	Displacement volume
B	m	Breadth
C	-	Additive constant
C_b	-	Block coefficient
C_m	-	Midship coefficient
C_p	-	Prismatic coefficient
C_T	-	Total resistance coefficient
$C_{T,\mathrm{CFD}}$	-	Total resistance coefficient based on CFD analysis
$C_{T,\mathrm{EFD}}$	-	Total resistance coefficient based on EFD analysis
D	-	EFD data
E	-	Comparison error
Fr	-	Froude number
FS	-	Factor of safety
H	m	Depth
K	-	Von Karman constant
k_s	m	Surface roughness
L_{pp}	m	Length between perpendiculars
L_{wl}	m	Waterline length
P	-	Distance metric to the asymptotic range
p_{RE}	-	Order of accuracy
p_{th}	-	theoretical order of accuracy
R	-	Convergence ratio
Re	-	Reynolds number
S	-	CFD solution
T	m	Draft
U_D	-	Data uncertainty
U_G	-	Grid uncertainty
U_{SN}	-	Numerical uncertainty
U_V	-	Validation uncertainty
WDL	m	Wave damping length
WS	m^2	Wetted surface without rudder
WS_{total}	m^2	Wetted surface with rudder
z_{D}	m	Dynamic heave
$\Delta_{(\mathrm{sw})}$	t	Displacement in sea water
ΔC_F	-	Roughness allowance
δ_{RE}	-	Error estimate
δz_{D}	%	Relative change in dynamic heave
$\delta\theta_{\mathrm{D}}$	%	Relative change in dynamic pitch
ε_{21}	-	Difference between solutions obtained using medium and fine mesh
ε_{32}		Difference between solutions obtained suing coarse and medium mesh
η_a	kg/ms	Dynamic viscosity of air
η_w	kg/ms	Dynamic viscosity of water

θ_D	deg	Dynamic pitch
λ	-	Scale
π	-	Pie
ρ_a	kg/m^3	Air density
ρ_w	kg/m^3	Water density
υ	m^2/s	Kinematic viscosity of water

ABBREVIATIONS

AI	Artificial Intelligence
ANN	Artificical Neural Network
CFD	Computational Fluid Dynamics
EEXI	Energy Efficiency for Existing Ship Index
EFD	Experimental Fluid Dynamics
GCI	Grid Convergence Index
GHG	Greenhouse Gas
HRIC	High-Resolution Interface Capturing
IMO	International Maritime Organization
ITTC	International Towing Tank Conference
KCS	KRISO Container Ship
KVLCC2	KRISO Very Large Crude Carrier 2
RKE	Realizable k-ε (turbulence model variant)
RSM	Reynolds Stress Model
SST	Shear Stress Transport (turbulence model)
SSTKO	Shear Stress Transport (variant of SST model)
VOF	Volume of Fluid

ACKNOWLEDGMENTS

The research is supported by Ministry of Science, Technology Development and Innovation of Republic of Serbia, Contract No. 451-03-137/2025-03/200105. Authors would like to acknowledge Ocean Pro Marine Engineers LTD for its help in guidance and support for CFD assessment.

REFERENCES

[1] IMO, 2018. Resolution MEPC.304(72). Initial IMO Strategy on Reduction of GHG Emissions from Ships. IMO, London, England. URL https://docs.imo.org/. (accessed 5th March 2025)

[2] IMO, 2023. Resolution MEPC.377(80). 2023 IMO Strategy on Reduction of GHG Emissions from Ships. IMO, London, England. Available online. https://docs.imo.org/. (Accessed 5th March 2025)

[3] IMO, 2014. Third IMO Greenhouse Gas Study 2014. https://www.imo.org/. (accessed 5th March 2025)

[4] IMO, 2021. Fourth IMO Greenhouse Gas Study 2020. https://www.imo.org/. (accessed 5th March 2025)

[5] Statista, 2025. https://www.statista.com/statistics/1185535/transport-carbon-dioxide-emissions-breakdown/, (accessed 5th March 2025)

[6] Zhi-Rong, Z., Hui, L., Song-Ping, Z., Feng, Z., 2006. Application of CFD in ship engineering design practice and ship hydrodynamics. *Journal of Hydrodynamics*, 18(3), 315-322. https://doi.org/10.1016/S1001-6058(06)60072-3

[7] Tang, H., Zhu, R., Wan, Q., Ren, D., 2025. Short-term prediction of trimaran load based on data driven technology. *Brodogradnja*, 76 (1), 76101. https://doi.org/10.21278/brod76101

[8] Meng, L., Gan, H., Liu, H., Lu, D., 2025. Deep learning-based research on fault warning for marine dual fuel engines. *Brodogradnja*, 76 (3), 76303. https://doi.org/10.21278/brod76303

[9] Xiao, G., Yang, D., Xu, L., Li, J., Jiang, Z., 2024. The Application of Artificial Intelligence Technology in Shipping: A Bibliometric Review. *Journal of Marine Science and Engineering*, 12, 624. https://doi.org/10.3390/jmse12040624

[10] Guo, S., Zhang, B., Tian, Z., Liu, J., Tang, H., 2024. Automatic Optimal Design Method for Minimum Total Resistance Hull Based on Enhanced FFD Method. *Brodogradnja*, 74 (4), 75407. https://doi.org/10.21278/brod75407

[11] ITTC, 2021. 7.5-02-03-01.4. 1978 ITTC Performance Prediction Method, ITTC Quality System Manual, Recommended Procedures and Guidelines; International Towing Tank Conference, *Propulsion Committee of the 29th ITTC*. https://www.ittc.info/media/8017/75-02-03-014.pdf (accessed 6th March 2025)

[12] IMO, 2022. Resolution MEPC.350(78). 2022 Guidelines on the Method of Calculation of the Attained Energy Efficiency Existing Ship Index (EEXI). IMO, London, England. https://docs.imo.org/ (accessed 6th March 2025)

[13] IMO, 2022. Resolution MEPC.351(78). 2022 Guidelines on Survey and Certification of the Attained Energy Efficiency Existing Ship Index (EEXI). IMO, London, England. https://docs.imo.org/ (accessed 6th March 2025)

[14] IACS, 2024. EEXI Implementation Guidelines, Recommendation No. 172. London, England. https://iacs.org.uk (6th March 2025)

[15] ITTC, 2024. 7.5-03-02-02. Benchmark Database for CFD Validation for Resistance and Propulsion, ITTC Quality System Manual, Recommended Procedures and Guidelines; International Towing Tank Conference, *Specialist Committee on Combined CFD-EFD Methods of 30th ITTC.* https://www.ittc.info/media/11956/75-03-02-02.pdf (accessed 6th March 2025)

[16] Ponkratov, D., 2016. The workshop in ship scale computer simulations, Proceedings, Lloyd's Register, Southampton, UK

[17] Ponkratov, D., Zegos C., 2014. Ship Scale CFD SelfPropulsion Simulation and Its Direct Comparison with Sea Trials Results, *International Conference on Computational and Experimental Marine Hydrodynamics MARHY'14*, Chennai, India

[18] Ponkratov, D., Zegos, C., 2015. Validation of ship scale CFD self-propulsion simulation by the direct comparison with sea trials results. *Proceedings of the Fourth International Symposium on Marine Propulsors*. SMP'15, Austin, Texas, USA, June 2015

[19] Huang, L., Pena, B., Thomas, G., 2023. Towards a full-scale CFD guideline for simulating a ship advancing in open water. *Ship Technology Research*, 70(3), 222–238. https://doi.org/10.1080/09377255.2023.2167537

[20] ITTC, 2024. 7.5-03-01-01. Uncertainty Analysis in CFD Verification and Validation, Methodology and Procedures, ITTC Quality System Manual, Recommended Procedures and Guidelines; International Towing Tank Conference, *Specialist Committee on Combined CFD-EFD Methods of 30th ITTC*. https://www.ittc.info/media/11950/75-03-01-01.pdf (accessed on 06.03.25.)

[21] Jasak, H., Vukčević, V., Gatin, I., Lalović, I, 2019. CFD validation and grid sensitivity studies of full scale ship self-propulsion, *International Journal of Naval Architecture and Ocean Engineering*, 11(1), 33-43. https://doi.org/10.1016/j.ijnaoe.2017.12.004

[22] Pena, B., Muk-Pavic, E., Fitzsimons, P., 2020. Detailed analysis of the flow within the boundary layer and wake of a full-scale ship, *Ocean Engineering*, 218, 108022. https://doi.org/10.1016/j.oceaneng.2020.108022

[23] Luo, W., Yang, B., Sun, Y., 2021. Hydrodynamic analysis of KVLCC2 ship sailing near inclined banks. *Mathematical Problems in Engineering*, 2021, 655971. https://doi.org/10.1155/2021/6655971

[24] Mikulec, M., Piehl, H., 2023. Verification and validation of CFD simulations with full-scale ship speed/power trial data. *Brodogradnja*, 74(1), 41-62. https://doi.org/10.21278/brod74103

[25] Saydam, A. Z., Küçüksu, G. N., İnsel, M., Gökçay, S., 2022. Uncertainty quantification of self-propulsion analyses with rans-cfd and comparison with full-scale ship trials. *Brodogradnja*, 73(4), 107-129. https://doi.org/10.21278/brod73406

[26] Farkas, A., Degiuli, N., Martić, I., 2018. Assessment of hydrodynamic characteristics of a full-scale ship at different draughts. *Ocean Engineering*, 156, 135–152. https://doi.org/10.1016/j.oceaneng.2018.03.002

[27] Orych, M., Werner, S., Larsson, L., 2021, Validation of full-scale delivered power CFD simulations, *Ocean Engineering*, 238, 109654. https://doi.org/10.1016/j.oceaneng.2021.109654

[28] Castro A. M., Carrica P., M., Stern F., 2011. Full scale self-propulsion computations using discretized propeller for the KRISO container ship KCS, *Computers & Fluids*, 51(1), 35-47. https://doi.org/10.1016/j.compfluid.2011.07.005

[29] Farkas, A., Degiuli, N., Martić, I., Dejhalla, R., 2019. Numerical and experimental assessment of nominal wake for a bulk carrier. *Journal of Marine Science and Technology*, 24, 1092–1104. https://doi.org/10.1007/s00773-018-0609-4

[30] Denny, M. E., 1951. B.S.R.A. Resistance Experiments on the Lucy Ashton, Part I – Full Scale Measurements, *International Conference of Naval Architects and Marine Engineers 1951*, Unwin Brothers, 40-57

[31] Schuster, S., 1969. Schiffstechnische Meßfahrten mit dem Forschungsschiff "Meteor" 1967. Meteor Forschungsergebnisse: Reihe A, Allgemeines, *Physik und Chemie des Meeres*, 5, 72-84

[32] Conn, J. F. C., Lackenby, H., Walker, W. P., 1953. B.S.R.A. Resistance Experiments on the Lucy Ashton, Part II – The Ship-Model Correlation for the Naked Hull Conditions, *Spring Meeting of the Institution of Naval Architects*, March 25, 1953, 350-436

[33] Lackenby, H., 1955. Resistance Experiments on the Lucy Ashton, Part III – The Ship-Model Correlation for the Shaft-Appendage Conditions, *Quartetly Transactions of the Institution of Naval Architects*, 97(2), 109-166

[34] Smith, L., 1955. Resistance Experiments on the Lucy Ashton, Part IV – Miscellaneous Investigations and General Appraisal, *Quartetly Transactions of the Institution of Naval Architects*, 97(4), 525-561

[35] Lopes, R., Eslamdoost, A., Johansson, R., RoyChoudhury, S., Bensow, R. E., Hogstrom, P., Ponkratov, D., 2025. Resistance prediction using CFD at model- and full-scale and comparison with measurements, *Ocean Engineering*, 321, 120367. https://doi.org/10.1016/j.oceaneng.2025.120367

[36] Lopes, R., Eslamdoost, A., Bensow, R. E., Ponkratov, D., Kompe, A., Geremia, P., Pekküçük, Ç. B., et al. 2026. A summary of the Lucy Ashton resistance prediction workshop, *Ocean Engineering*, 343, 122951. https://doi.org/10.1016/j.oceaneng.2025.122951

[37] Hirt, C.W., Nichols, B.D., 1981. Volume of Fluid (VOF) Method for the Dynamics of Free Boundaries. *Journal of Computational Physics*, 39, 201-225. https://doi.org/10.1016/0021-9991(81)90145-5

[38] Menter, F. R., 1994. Two-equation eddy-viscosity turbulence models for engineering applications, *AIAA journal*, 32(8), 1598-1605. https://doi.org/10.2514/3.12149

[39] Roache, P. J., 1998, Verification and Validation in Computational Science and Engineering, *Hermosa publishers*, Albuqurque, New Mexico

[40] Xing, T., Stern, F., 2010, Factors of Safety for Richardson Extrapolation, *Journal of Fluids Engineering*, 132(6), 061403. https://doi.org/10.1115/1.4001771

[41] ITTC, 2024. 7.5-03-02-04, Practical Guidelines for Ship Resistance CFD, ITTC Quality System Manual, Recommended Procedures and Guidelines; International Towing Tank Conference, *Specialist Committee on Combined CFD-EFD Methods of 30th ITTC*. https://www.ittc.info/media/11960/75-03-02-04.pdf (accessed 11th March 2025)

[42] ITTC, 2024. 7.5-03-03-01, Practical Guidelines for Ship Self-Propulsion CFD, ITTC Quality System Manual, Recommended Procedures and Guidelines; International Towing Tank Conference, *Specialist Committee on Combined CFD-EFD Methods of 30th ITTC*. https://www.ittc.info/media/11964/75-03-03-01.pdf (accessed 11th March 2025)

ПРИЛОГ 9

Ocean Engineering 343 (2026) 122951

Contents lists available at ScienceDirect

Ocean Engineering

journal homepage: www.elsevier.com/locate/oceaneng

Research paper

A summary of the Lucy Ashton resistance prediction workshop

Rui Lopes [a,*], Arash Eslamdoost [a], Rickard E. Bensow [a], Dmitriy Ponkratov [b], Anja Kömpe [c], Paolo Geremia [d], Çagan Birant Pekküçük [e], Cagri Aydin [f], Diego Villa [g], Dimitris Ntouras [h], Dong Cheol Seo [i], Gennaro Rosano [j], Florian Vesting [k], Gabriele Bigini [l], Guillermo Chillcce [m], Jan Kaufmann [n], Jianfeng Lin [o], João Muralha [p], Lukas Dott [q], Kaan Ilter [r], Dimitrios S. Lampropoulos [s,t], Kristian Sagmo [u], Lars Lübke [v], Masaya Kubota [w], Matija Vasilev [x], Miles Wheeler [y], Muhammed Sahid [z], Carlo Giorgio Grlj [aa], Niklas Kühl [ab], Pierre Crepier [ac], Ramkumar Joga [ad], Rasul Niazmand Bilandi [ae,af], Marcus Boyd [ag], Alvaro Del Toro [ah], Shona Cunningham [ai], Simone Bozzo [g], Fabian Schumacher [aj], Themistoklis Melissaris [ak], Vincent Tissot [al], Vincenzo Sorrentino [j], Wim Van Hoydonck [am], Zhao-Hui Li [an]

[a] *Chalmers University of Technology, Department of Mechanics and Maritime Sciences, Gothenburg, Sweden*
[b] *Siemens Digital Industries Software, London, UK*
[c] *Meyer Werft, Papenburg, Germany*
[d] *Engys, Trieste, Italy*
[e] *SEFT Engineering, Istanbul, Turkey*
[f] *Damen, Gorinchem, the Netherlands*
[g] *University of Genova, Genova, Italy*
[h] *SimFWD, Chalandri, Greece*
[i] *National Research Council, St. John's, Canada*
[j] *University of Naples Federico II, Naples, Italy*
[k] *Volupe, Askim, Sweden*
[l] *Van Oossanen Naval Architects B.V., Wageningen, the Netherlands*
[m] *University of Duisburg-Essen, Duisburg, Germany*
[n] *DST, Duisburg, Germany*
[o] *Institute of Mechanics, Chinese Academy of Sciences, Beijing, China*
[p] *BlueOASIS, Ericeira, Portugal*
[q] *Schottel, Spay, Germany*
[r] *Brookes Bell, Glasgow, UK*
[s] *FEAC Engineering P.C., Patras, Greece*
[t] *Laboratory of Applied Mathematics, School of Science and Technology, Hellenic Open University 18 Aristotelous St, Patras, 26335, Greece*
[u] *SINTEF Ocean AS, Trondheim, Norway*
[v] *SVA-Potsdam, Potsdam, Germany*
[w] *Mitsubishi Heavy Industries, Nagasaki, Japan*
[x] *Ocean Pro-Marine Engineers, Belgrade, Serbia*
[y] *Siemens Digital Industries Software, Seattle, USA*
[z] *Cochin Shipyard Limited, Kochi, India*
[aa] *University of Zagreb Faculty of Mechanical Engineering and Naval Architecture, Ivana Lučića 5, Zagreb, 10000, Croatia*
[ab] *Hamburg Ship Model Basin, Hamburg, Germany*
[ac] *MARIN, Maritime Research Institute Netherlands, Wageningen, the Netherlands*
[ad] *Indian Register of Shipping, Mumbai, India*
[ae] *Estonian Maritime Academy, Tallinn University of Technology, Tallinn, Estonia*
[af] *Department of Aero and Hydrodynamics, Force Technology, Kgs. Lyngby, Denmark*
[ag] *Cape Horn Engineering, Portsmouth, UK*
[ah] *Kongsberg Maritime, Ulstein, Norway*
[ai] *BMT, London, UK*
[aj] *IBMV Maritime Innovationsgesellschaft mbH, Rostock, Germany*
[ak] *Wärtsilä Netherlands B.V., Drunen, the Netherlands*

* Corresponding author.
E-mail address: rui.lopes@chalmers.se (R. Lopes).

https://doi.org/10.1016/j.oceaneng.2025.122951
Received 28 May 2025; Received in revised form 5 September 2025; Accepted 21 September 2025
Available online 23 October 2025

[al] SIREHNA, Bouguenais, France
[am] Waterbouwkundig Laboratorium - Flanders Hydraulics, Antwerpen, Belgium
[an] Marine Design & Research Institute of China, Shanghai, China

ARTICLE INFO

Keywords:
RANS
Resistance
Workshop
Full-scale

ABSTRACT

A blind full-scale CFD resistance prediction workshop was held in 2024, with the Lucy Ashton paddle steamer as its test case. Results from forty participants were received for the three different parts in which the workshop was organised, which consisted of a grid refinement study with common grids, full-scale simulations for varying Froude number, and model-scale simulations at a constant Froude number for varying model sizes. This paper presents a summary of the results gathered for the workshop along with its main findings, and the comparison with the results available from the experimental campaign carried out for the Lucy Ashton in the 1950s. The computational results led to lower ship resistance than the experimental data for all conditions, due to the simulations considering the ship to be hydrodynamically smooth and to not heave or pitch. The scatter of the resistance at full-scale showed a decreasing trend as the Froude number was increased with a median absolute deviation of at most 2.3 %. The spread in the numerical results obtained for the full-scale conditions was equivalent to that observed for the model-scale cases, building further confidence in full-scale CFD.

1. Introduction

Ship design is a complex, multidisciplinary task that involves hydrodynamic, propulsive and structural effects. When it comes to the ship's power performance, two aspects play a central role: the performance of the propeller, and the resistance of the hull. Simply put, this corresponds to the balance between the force that propels the ship (thrust) and the force that opposes the motion of the ship (resistance). These forces are responsible, among other considerations, for driving the design process of the hull and propeller, but they are not directly known for the ship, as their measurement at full-scale is troublesome, and building a prototype is too expensive and time consuming to be done at the design stage.

In order to estimate the full-scale resistance of the ship, experimental tests are conducted on smaller models. To attain the same flow for the model as the real ship experiences, both the Froude and Reynolds numbers of model and ship should match. However, it is practically impossible to do so. In fact, matching the Reynolds number alone is already impractical due to the large speeds that would be required. As a result, the model-scale tests are conducted at the same Froude number as the ship, and the resistance is then scaled for the actual ship, accounting for the difference in Reynolds number between the model and the ship.

With the growth of computational power, Computational Fluid Dynamics (CFD) has established itself as a useful tool in the simulation of all types of flows, and the maritime world is no exception. Nowadays, CFD is commonly employed as a complement to model tests, due to the large amount of information that can be extracted from the simulations which might be impossible or prohibitively expensive to measure in experiments. Methods based on the Reynolds-averaged Navier-Stokes (RANS) equations are by far the most common as a consequence of their accuracy-cost trade-off. Other high-fidelity approaches such as Detached Eddy Simulation (DES), Large Eddy Simulation (LES) or Direct Numerical Simulation (DNS) provide higher accuracy, but their much higher cost excludes these approaches from routine industrial use.

The use of CFD as a tool requires some care due to the sources of possible errors. Not only numerical errors that are related to space and time discretization, but also modelling errors, inherent to the mathematical formulation of the problem and the turbulence model chosen. The use of CFD is often accompanied with experimental measurements for the same conditions, in order to gain confidence in the numerical approach. This has led to the growing maturity of CFD when applied at model-scale. In practice, CFD can be used directly at full-scale, which is sometimes mentioned as one of its main advantages. However, the scarcity of experimental full-scale data is an obstacle in the confidence and use of CFD at full-scale. In the maritime community there has been a growing focus on this topic, which can be highlighted in the full-scale numerical modelling workshop held in 2016 by Lloyd's Register (Ponkratov, 2017). In this workshop, which had a general cargo vessel as a test case, full-scale simulations of resistance, self propulsion, propeller open water performance and propeller cavitation were carried out by the community. Another effort more focused on the gap of full-scale data is the JoRes Joint Industry project, which has gathered full-scale data for six different vessels.

Although there is an increased attention on full-scale measurements, those that have been carried out recently correspond to self-propulsion conditions, which are affected by propeller-hull (and rudder) interaction. However, one of the key quantities used in ship power performance scaling is the bare hull resistance. The measurement of the bare hull resistance at model-scale is typically done in towing tanks, where, as the name indicates, the model is towed through the tank. At ship-scale, this is practically unfeasible. Some attempts have been done to tow a ship at sea through the means of a cable or an outrigger. However, these approaches imply the target ship to be in the wake of the towing vessel or being affected by its wave pattern, which will influence the resistance of the ship being towed. This sort of technique has been employed in experiments carried out for the H.M.S. Greyhound (Froude, 1874) in the late nineteenth century, for the Yudachi in 1928 and 1929 (Hiraga, 1934), for the Wrangel in the 1950s (Nordström, 1953) and for the HMS Penelope in the 1970s (Canham, 1974).

In the 1950s, the issue of how to propel a ship without a propeller was addressed in an extraordinary manner, as the British Shipbuilding Research Association carried out sea trials on the Lucy Ashton, a paddle steamer which was fitted with four jet engines on its deck (Denny, 1951). The use of the jet engines meant neither a propeller or another ship were required, which avoided propeller-hull interaction and wave pattern interference effects. The experimental campaign on the Lucy Ashton also meant to address effects such as surface roughness and bio-fouling, as the tests were carried out for four different surface conditions, corresponding to two coatings (aluminum paint and red-oxide paint) and faired or sharp seams. Other tests such as acceleration and retardation tests were also carried out, and the data was documented in four papers (Denny, 1951; Conn et al., 1953; Lackenby, 1954; Smith, 1955). In spite of the unique setup of this campaign, the value it possesses in full-scale resistance prediction and its previous use in other investigations (Joubert and Matheson, 1970; Smits et al., 1980; Granville, 1974; ITTC, 1999, 2008), it is currently not widely known among the maritime community.

One of the common ways to assess the state of the art when it comes to CFD is the organisation of workshops, where test cases are prepared and instructions are provided to participants so that they conduct their simulations with the code they regularly use. The results from the participants are then gathered and compared in order to assess the discrepancies between the different CFD codes and the spread between participants. The results are also usually compared to available experimental data, which, in light of what has been previously discussed, means that

most of the workshops conducted in the maritime community so far have model-scale conditions as their test cases. When it comes to hydrodynamics, the most notable example is the workshop series on CFD in Ship Hydrodynamics, initiated in 1980 and with follow-ups in 1990, 1994, 2000, 2005, 2010, 2015 and an upcoming workshop (at the time of writing) in 2025, which will be the first one in the series to include a full-scale self-propulsion case.

Considering the value of the Lucy Ashton trials, a blind CFD workshop based on the Lucy Ashton was organised and held in 2024, with the purpose to assess CFD capabilities to predict full-scale resistance. As there had not been any significant CFD work carried out for this geometry, aspects such as hull roughness and dynamic trim and sink were not considered. The main novelty of this workshop was the fact that this unique case corresponds to full-scale bare hull resistance, which is not the case of any of the full-scale cases in workshops mentioned previously. Furthermore, the Lucy Ashton trials were also complemented with a model-scale experimental campaign, and so the topic of resistance scaling can also be addressed with this data. A separate investigation into CFD results with the Lucy Ashton (Lopes et al., 2025) was also performed as part of preparation of the workshop, touching upon the influence of roughness of the predicted resistance.

The structure of the remainder of the paper is as follows: Section 2 details the structure of the workshop, in terms of the conditions that were to be simulated by the participants, quantities of interest and treatment of the submitted data. An overview of the participation on the workshop is given in Section 3, which describes the codes that were used in the simulations, and the number of contributions received for each part of the workshop. The results are summarized in Sections 4–6 according to the different parts of the workshop. An overall discussion of the results is given in Section 7, and the main findings of the workshop are summarized in Section 8.

2. Workshop structure

The initial planning for the workshop began in October of 2023, with the preparation of the instructions for participants, the conditions to be evaluated and the main goals of the workshop. An initial announcement was made in February of 2024, and an online kick-off meeting was held at the end of the month. The groups that showed interest in the workshop received several files consisting of the workshop instructions document, a guideline for results submission along with a template with examples and CAD files with the geometry of the ship. A questionnaire for details about the numerical setup and grids for some of the conditions were also prepared and distributed at a later time. The deadline for most of the results of the workshop was initially set to the end of May, and eventually extended until the 19th of June, which coincided with the date that a second online meeting was held. In this call, a summary of the participation on the workshop was presented, and the name of the ship was disclosed. The results were processed until September, and the workshop took place at Chalmers University of Technology on the 25th of September, with the option to attend online for those who could not join in person. All of the meetings were recorded, and the presentations and recordings were made available to the participants after each meeting.

The ship selected for the workshop was the Lucy Ashton, a paddle steamer that operated as a passenger ferry in the River Clyde in Scotland. The ship first began service in 1888, and was retired in 1949. At this time, the Lucy Ashton was acquired by the BSRA, and the structure corresponding to the paddle wheels was removed. Four jet engines were mounted on the deck of the ship, along with other preparations in order to carry out full-scale resistance measurements. The particulars of the ship are provided in Table 1. A CAD file for the geometry was prepared based on offsets measured when the ship was in dry dock and that were reproduced in Conn et al. (1953) (Fig. 1). Although access to the sea trials data was strictly not restricted, the workshop employed it as a blind case, taking advantage of the fact that the Lucy Ashton campaign was mostly unknown in the community. The name of the ship was not provided to the participants, and no details were provided about the experimental measurements, as that could potentially help identify the ship. The name of the ship and the conditions in which the sea trials were carried out were only disclosed to the participants in the meeting in June, after all relevant results had been received.

Table 1
Main geometrical dimensions of the Lucy Ashton.

Designation	Symbol	Value
Length between perpendiculars	L_{pp}	$58.1m$
Breadth (moulded)	B	$6.4m$
Depth (moulded)	D	$2.18m$
Displaced volume	∇	$386.5m^3$
Wetted surface area	S	$416.9m^2$
Block coefficient	C_b	0.685
Midship area coefficient	C_m	0.972

Table 2
Characteristics of each Set of simulations prepared for the workshop.

	Set 0	Set 1	Set 2
Scale	Full-scale	Full-scale	Model-scale (varying sizes)
Free-surface	No	Yes	Yes
Froude number	Constant	Variable	Constant
Grids	Grid refinement study	Single grid	Single grid
Roughness	No roughness	No roughness	No roughness
Ship motion	Fixed trim and sink	Fixed trim and sink	Fixed trim and sink

The cases for the workshop were selected based on the available data reported in the papers from the trials held in the 1950s. In the extensive campaign conducted at the time, sea trials were carried out for several speeds, and for four different surface finishings. As mentioned, these conditions correspond to two different coatings, aluminum paint and red oxide paint, and sharp and faired seams. In the workshop, participants were asked not to include roughness modelling in their CFD codes, and as such the data is compared against the smoothest experimental condition, which corresponds to the condition with faired seams and the aluminum paint, and this condition was taken to select particular speeds for the simulations. The workshop was divided in three different parts, labelled as Sets, each with its own purpose, and numbered from 0 to 2. The details of each Set are given below, and summarized in Table 2. The draught of the ship was 1.584 m, corresponding to the mean condition referenced in Denny (1951).

The first Set, Set 0, is the verification case of the workshop, a grid refinement study for a single condition at full-scale, which corresponds to a Froude number $Fr = 0.219$ and a ship speed of $V_S = 5.232$ m/s. The grids were prepared by the organisers of the workshop and made available to the participants. Contrary to the remaining Sets of the workshop, participants were explicitly requested to use the $k-\omega$ Shear Stress Transport (SST) model (Menter, 1994) for this case, and the grids were prepared such that a double-body approach was used, i.e. the free-surface was not included in the simulations. The entirety of this Set was planned to be mandatory, as participants had to contribute to it in order for their results submitted to the other Sets to be considered.

The main goal of Set 0 was to act as the main verification case for the workshop, as grid refinement studies were not requested for the remaining Sets. The turbulence model was also set the same for all participants, in order to avoid potential differences due to different turbulence models. These choices, along with participants using the exact same grids, were made so that all participants run, as much as possible outside of code implementation details, the exact same computational problem.

The second part of the workshop consisted of Set 1, which corresponded to the ship scale simulations. A total of five speeds were selected: $V_S = 3.106$, 4.12, 5.232, 6.211 and 7.257 m/s. These five conditions corresponded to groups labeled A through E in Lackenby (1954), and to the Froude numbers of 0.130, 0.173, 0.219, 0.26 and 0.304. Out

Fig. 1. Lucy Ashton CAD model generated from the offsets.

of the five speeds, three were selected as the mandatory part of the Set. These were $V_S = 3.106$, 5.232 and 7.257. The remaining two conditions were optional and their calculation was not required for participation in the Set. Unlike in Set 0, turbulence model selection was unrestricted, and participants were encouraged to use whichever turbulence model they deemed more appropriate. Furthermore, participants had to generate their own grid(s), and the size of the computational domain was not specified either. No suggestions were made regarding grid generation or wall treatment, so participants were free to either employ wall functions or resolve the boundary-layer. The calculations were made for a fixed draught, and participants were also requested to not include the dynamic motions of the ship, so that all simulations were carried out for the even keel condition without any sinkage or dynamic trim.

Set 1 corresponded to the main set of the workshop, as the computation of the full-scale resistance for the five Froude numbers was meant to be compared with the measurements carried out in 1950. The lack of roughness effects and dynamic motion of the ship meant that an underestimation of the resistance was expected. However, this avoided differences that could potentially arise from different roughness implementations, unless details for that were provided too. Although the decisions taken might seem odd for a numerical workshop and were certain to generate differences through, for example, different turbulence models and different grids, they were taken in order to provide participants with a certain degree of freedom, while still trying to solve the same physical problem, and keeping it moderately simple due to the absence of previous numerical work or experience with this geometry. Sufficient information was provided to restrict the problem (geometry, fluid properties, speed), whereas the free parameters (grid settings, turbulence model, domain size) are instead a part of the computational approach. Combined with the fact that the workshop was carried out blindly, this gave the workshop a predictive characteristic, and the scatter observed between participants would reflect the scatter that one would observe for an actual industrial full-scale ship geometry.

The final part of the workshop was comprised of Set 2, where simulations were to be carried out at a constant Froude number ($Fr = 0.219$) and for varying model sizes. The six scaling factors considered were $\lambda = 21.167$, 15.875, 11.906, 9.525, 7.938 and 6.35. The scaling factor is defined as the ratio between the ship's L_{pp} and that of the model. The six conditions were split into a mandatory and optional part of three models each. The mandatory part of this Set consisted of $\lambda = 21.167$, 11.906 and 6.35. It is also noted that participants could choose not to participate in Set 1, but participate in Set 2. In those cases, they also had to carry out one additional simulation for $\lambda = 1$, which would correspond to the full-scale simulation for this Froude number. Similarly to Set 1, no restrictions were enforced on turbulence model, no grids were provided for the simulations, and participants were asked not to include roughness effects or the motion of the models.

Although the novel aspect of the workshop was the available full-scale resistance measurements, Set 2 dedicated to model-scale conditions was prepared in order to take advantage of the different models tested as part of the Lucy Ashton experimental campaign. The Froude number for this case was selected such that it had a reasonably good match with the Froude numbers tested for each of the models. The remaining settings were set in the same manner as for Set 1 for consistency, and since that would enable a fair comparison and assessment of scaling effects. A summary of the conditions requested for the workshop are given in Table 3 in terms of the Froude number and scaling factor.

As previously mentioned, for Set 0, multi-block structured grids were generated and provided to the participants. A total of five grids were generated using Pointwise, covering a grid refinement ratio of 2.33 from the coarsest to the finest grid. The computational domain, illustrated in Fig. 2, is a quarter of a cylinder, with the longitudinal axis corresponding to the main direction of the flow. The inlet is located approximately $1L_{pp}$ upstream of the bow of the ship, and the outlet is approximately $2.1L_{pp}$ downstream of the rudder. The radius of the cylinder is $2L_{pp}$. Since the ship is symmetrical, the grid was generated for only half the ship. The ship was placed so that $x = 0$ corresponds to the location where the surface of the rudder meets the hull, and the bow is located at approximately $x = L_{pp}$. Regarding the boundary-layer treatment, the grids were generated so that wall functions would be used. Since the grids are nearly geometrically similar, the wall distance for the near wall cells on the hull varies from grid to grid. Nonetheless it was carefully selected so that the first cell would lie in the logarithmic region for all grids of the set. Details of the grid set concerning the total number of cells, faces on the ship, and refinement ratio are given in Table 4 and the coarsest grid is illustrated in Figs. 3 and 4.

For the simulations requested for the workshop, the quantities of interest were specified. These were:

- Time history of the resistance, divided into friction and pressure components, and given separately for the rudder, hull and the complete ship;
- Time history of the vertical force, divided into friction and pressure components, for the complete ship;
- Time history of the side force acting on half of the hull, divided in friction and pressure components;
- Wetted surface area of the ship;
- Time-averaged transverse wave cuts at different longitudinal positions: $x/L_{pp} = -0.25$, -0.1, 0, 0.25, 0.5, 0.75, 1.0;
- Time-averaged skin-friction coefficient C_f and pressure cuts at $x/L_{pp} = 0.1$, 0.25, 0.5, 0.75, 0.9, along with one additional cut along the centreline of the ship;
- Time-averaged velocity profile on the boundary-layer at the centreline of the ship ($y/L_{pp} = 0$), and two longitudinal positions corresponding to $x/L_{pp} = 0.49$ and $x/L_{pp} = 0.62$.

The skin-friction coefficient C_f was defined as:

$$C_f = \frac{\tau_w}{0.5\rho V_S^2}. \tag{1}$$

Besides these quantities, additional data concerning the simulations was requested in the form of a questionnaire sent to the participants, in order to gather details about the setup of each participant. The questionnaire asked for data about:

- Software used for grid generation, solver, and post-processing;
- Discretization method, numerical schemes, turbulence model used, free-surface treatment technique, segregated or coupled solver;
- Domain size, boundary condition used at each boundary;
- Whether wall functions were used, the shape of the computational domain and the size of the domain, time discretization and if numerical ventilation was observed;

For each individual simulation, participants also had to report the following in the questionnaire:

- Pressure at a reference location;
- Time step size;
- Total number of cells in the domain and faces in the ship;

Table 3
Froude numbers and scales used for each Set.

	$Fr = 0.130$	$Fr = 0.173$	$Fr = 0.219$	$Fr = 0.260$	$Fr = 0.304$
$\lambda = 1.0$	Set 1 - required	Set 1 - optional	Set 0 and Set 1 - required	Set 1 - optional	Set 1 - required
$\lambda = 6.35$	–	–	Set 2 - required	–	–
$\lambda = 7.938$	–	–	Set 2 - optional	–	–
$\lambda = 9.525$	–	–	Set 2 - optional	–	–
$\lambda = 11.906$	–	–	Set 2 - required	–	–
$\lambda = 15.875$	–	–	Set 2 - optional	–	–
$\lambda = 21.167$	–	–	Set 2 - required	–	–

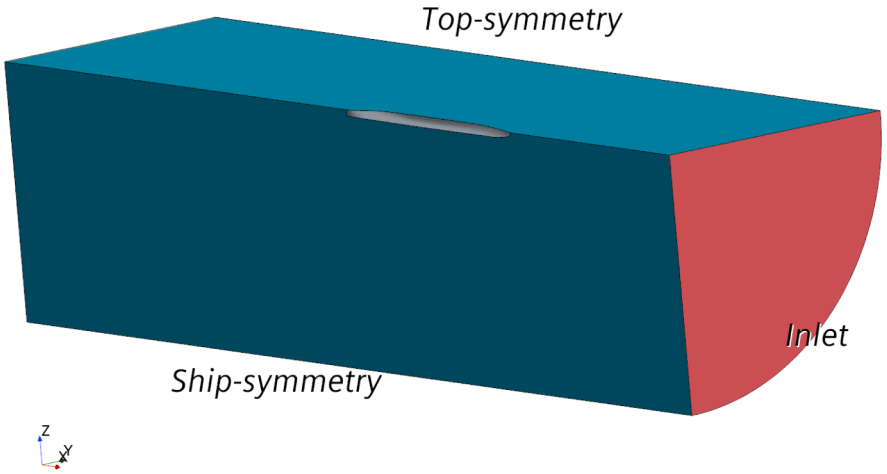

Fig. 2. Computational domain used in the grids prepared for Set 0.

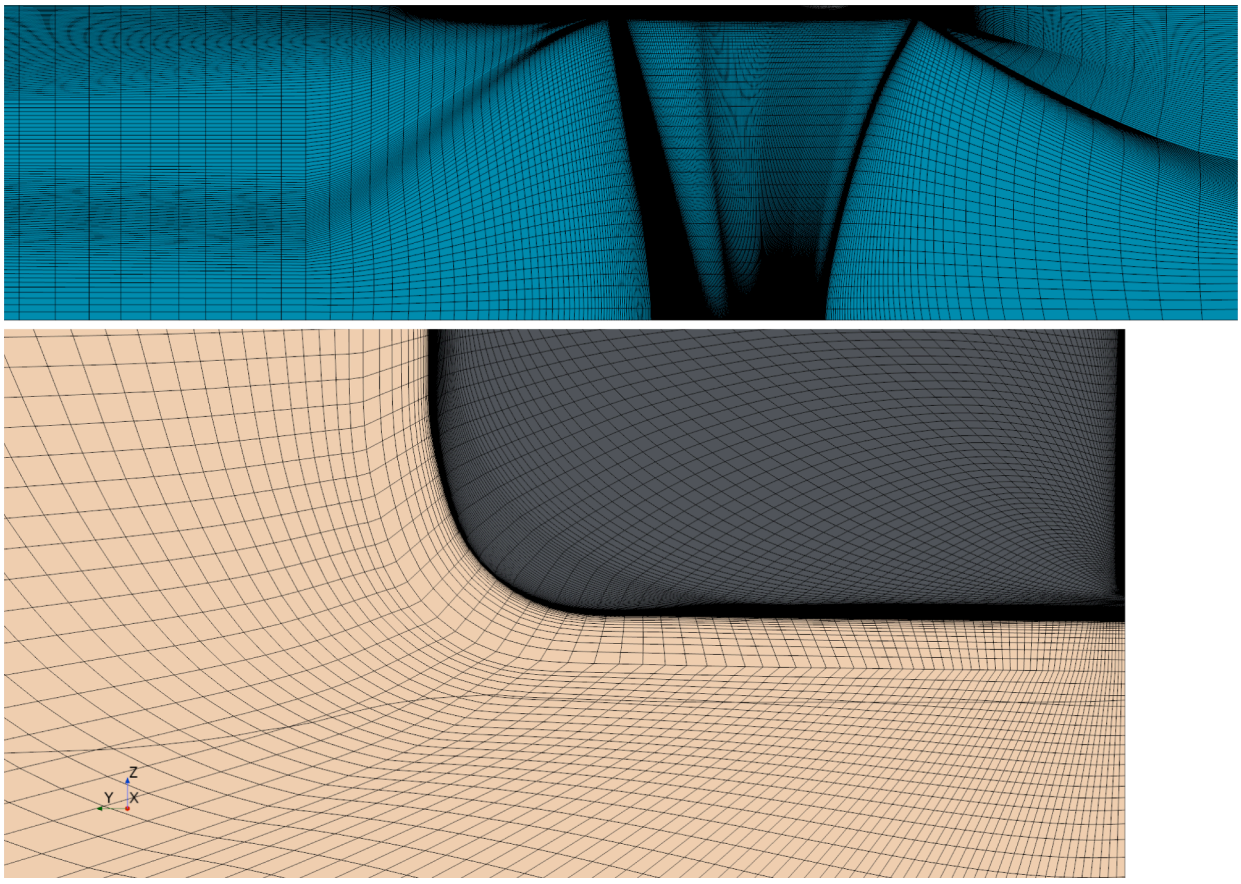

Fig. 3. Coarsest grid of Set 0 on the ship symmetry plane (top) and at mid-ship (bottom).

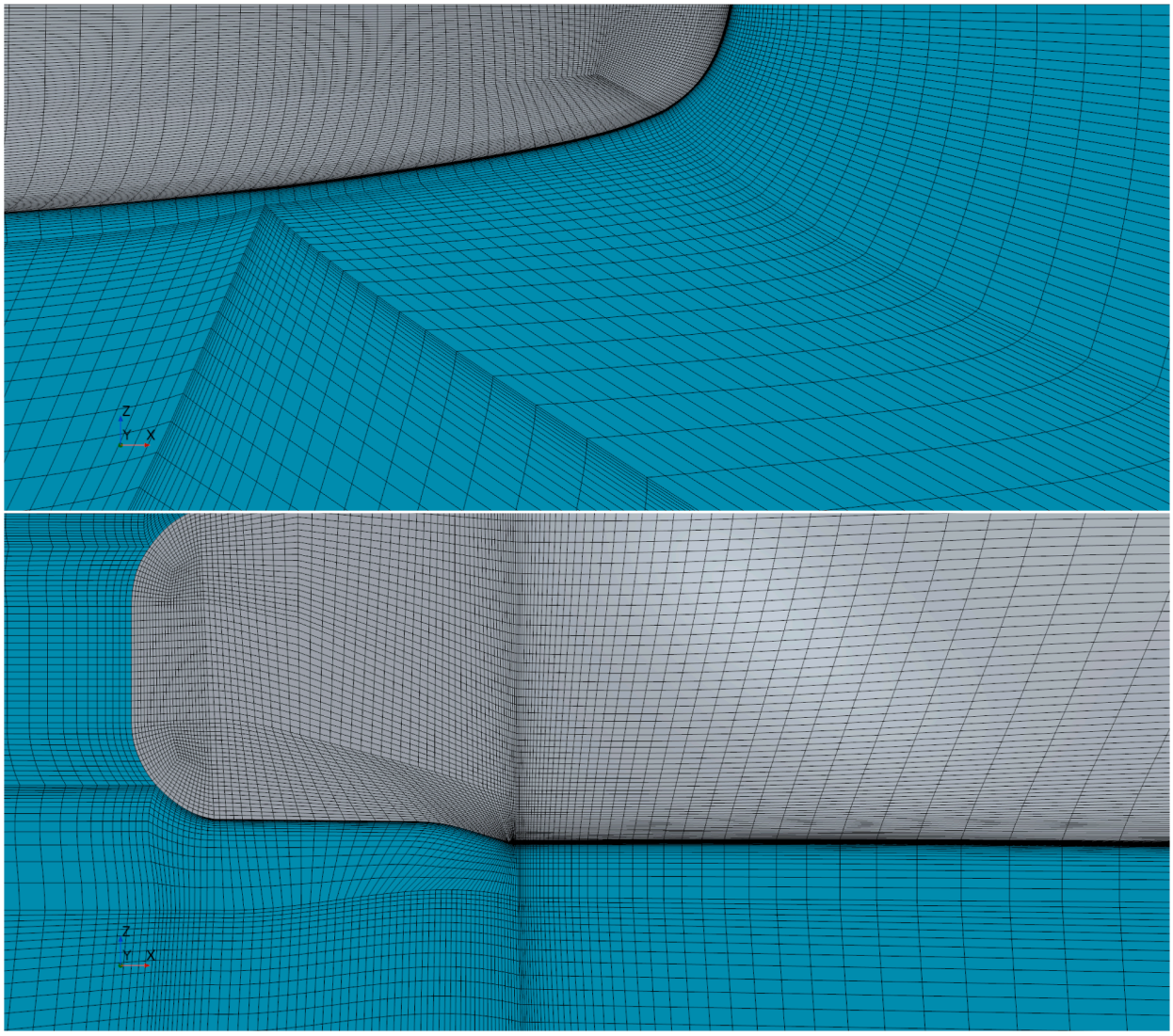

Fig. 4. Coarsest grid of Set 0 on the ship symmetry near the bow (top) and at the aft (bottom).

Table 4
Details of grid refinement level of the grids generated for Set 0.

Grid Designation	Number of Volume Cells	Number of Faces on the Ship	Refinement ratio
Grid 5	2,688,320	27,616	2.32
Grid 4	6,347,956	49,186	1.74
Grid 3	12,557,952	77,728	1.38
Grid 2	21,506,560	110,464	1.16
Grid 1	34,114,300	148,912	1.0

- Minimum, maximum and average y^+ on the hull;
- Number of processors used for the simulation and the total computational time;

The pressure at a reference location, along with the pressure cuts requested on the hull, was used to calculate the pressure coefficient in a manner so that it would be comparable between different participants. The calculation of the pressure coefficient C_p was carried out as

$$C_p = \frac{p - p_{ref} - p_{hydro}}{0.5\rho V_S^2} \quad (2)$$

where p is the pressure on the surface of the hull, p_{ref} is the pressure at the reference location, and p_{hydro} corresponds to the hydrostatic pressure. The reference location was at the inlet, $0.01L_{pp}$ above the undisturbed free-surface, and at plane corresponding to the centreline of the ship, $y/L_{pp} = 0$. In the case of the simulations of Set 0, since these were carried out for a double-body configuration, the reference location corresponded to the intersection between the two symmetry planes and the inlet.

For all the forces that were requested, participants were asked to provide the time history and not a time-averaged result. This was done so that the mean would be calculated consistently for all participants, and its uncertainty estimated according to the Transient Scanning Technique (TST) procedure recommended by the International Towing Tank Conference for single time series measurements (ITTC, 2021), which is further detailed in Brouwer et al. (2013, 2015, 2019). For the workshop, the time histories submitted by the participants varied considerably in terms of length and resolution. In order to calculate the mean for any given force from any given participant, the TST was ran for the complete time history. Then, the mean value was selected based on the time interval that would lead to the smallest uncertainty, with the additional condition that the time interval had to be at least 10 seconds long. As a result, all of the mean forces used in the analysis were the result of an

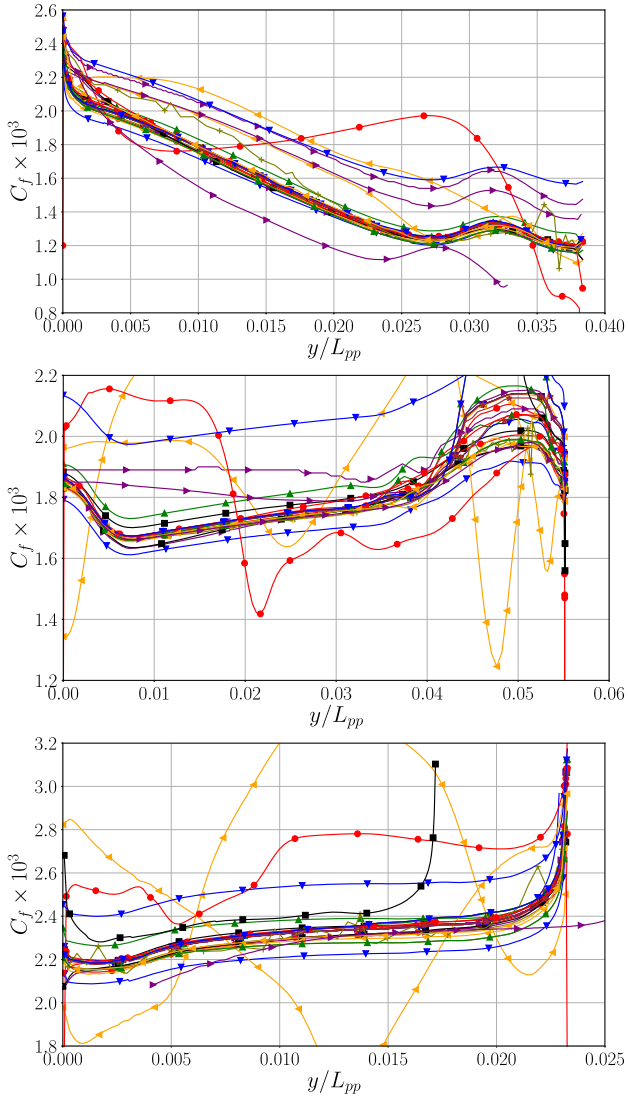

Fig. 5. C_f distributions on the surface of the hull for the finest grid of Set 0 at $x/L_{pp} = 0.1$ (top), $x/L_{pp} = 0.5$ (middle) and $x/L_{pp} = 0.9$ (bottom).

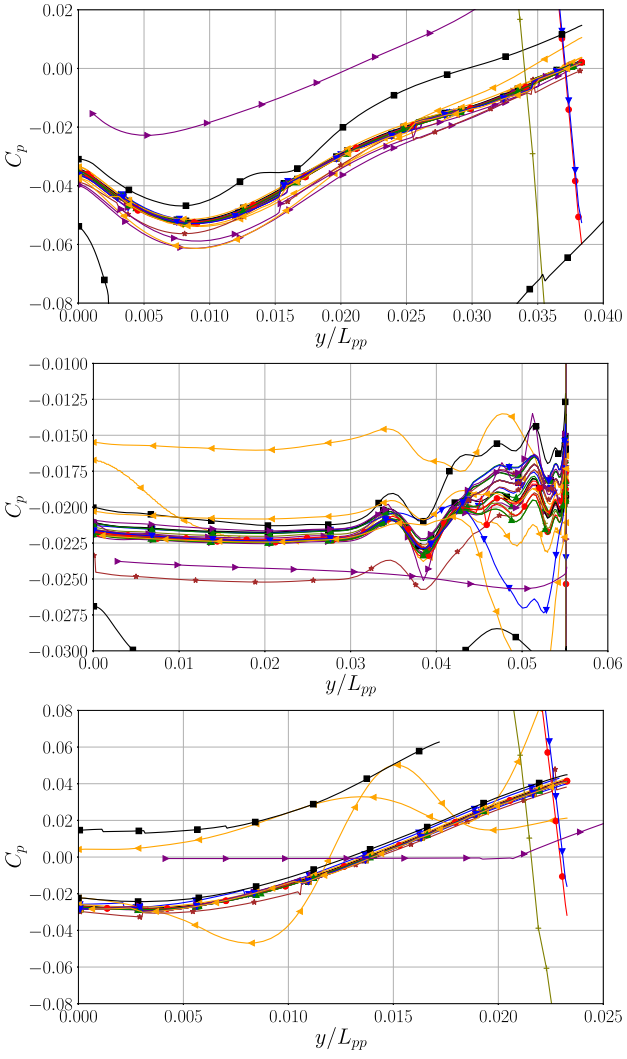

Fig. 6. C_p distributions on the surface of the hull for the finest grid of Set 0 at $x/L_{pp} = 0.1$ (top), $x/L_{pp} = 0.5$ (middle) and $x/L_{pp} = 0.9$ (bottom).

average of at least 10 seconds. For the vast majority of the submissions, the statistical uncertainty is negligible. In this paper, the resistance coefficient C_T is used, defined as

$$C_T = \frac{R}{\frac{1}{2}\rho V_S^2 A_{wetted}}, \tag{3}$$

where R is the resistance and A_{wetted} is the wetted surface area of the ship. Friction and pressure components of the forces are identified by the subscripts f and p, respectively, such that $C_{T,f}$, for example, corresponds to the friction resistance coefficient. Similar definitions are employed for the side force and the vertical force, with the coefficients identified as C_S and C_V.

With regards to Set 0, since a grid refinement study was conducted, the numerical uncertainty of the forces was assessed as well. This was carried out using the procedure detailed in Eça and Hoekstra (2014). The use of grid refinement studies for the estimation of the discretization uncertainty relies on the latter being the dominant component of the numerical error. This means that the remaining components of the numerical error, in this case the iterative error and the round-off error should be negligible when compared to the discretization error. No iterative convergence criteria were directly specified in the workshop, partially since a specific definition of the residuals would be difficult to enforce for the different solvers being used. Regardless, participants were reminded to provide iteratively converged results, and also had to provide a graphical representation of the residual history during the simulations. Concerning the round-off error, this is typically handled by using double precision in the simulations. Although participants were asked to provide the version of the software, details on whether or not a double-precision version was used were not provided. Regardless, for the case at hand, it is not expected that round-off error would have a significant contribution to the numerical error.

All the participants that submitted their results to the workshop received a set of files comparing data for all the variables against a set of reference results, for each of the conditions for which data was submitted. This procedure was also used to identify large discrepancies in the results, with participants being asked to check their data when such differences were observed. Several outliers were detected and corrected in this manner, which improved the overall results of the workshop. Most of the cases identified and corrected were specifically related to post-processing and not to the calculations.

As a large number of results has been received for the workshop, the paper will not focus on individual details of a given submission, but rather on general trends observed for the complete group of results and statistical measures of some quantities. The most commonly used measures for such an analysis are, for a quantity ϕ, its mean value $\overline{\phi}$ and standard deviation $\sigma(\phi)$. However, the mean and standard devia-

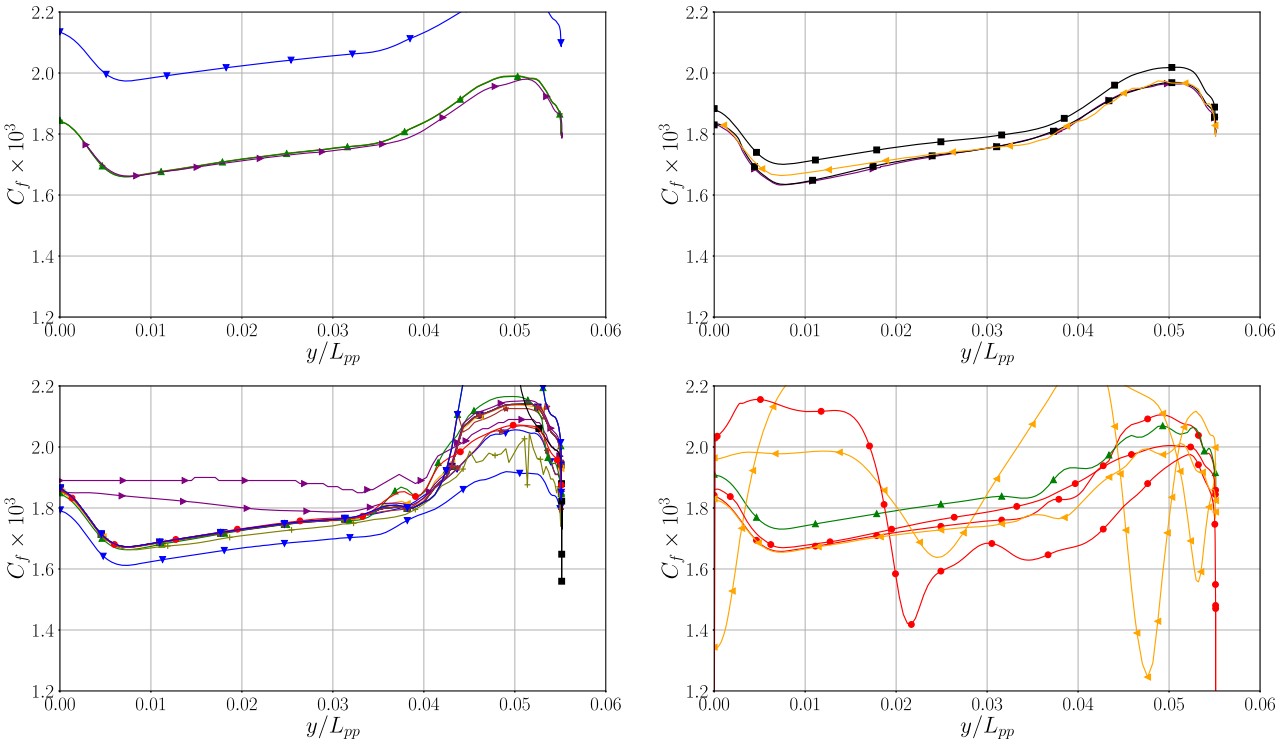

Fig. 7. C_f distribution on the surface of the hull at midship ($x/L_{pp} = 0.5$) obtained on the finest grid of Set 0 for the submissions using FineMarine (top left), OpenFoam (top right), STAR-CCM+ (bottom left) and other codes (bottom right).

tion can be considerably influenced by outliers that differ significantly from the remaining data points. This happens in many of the quantities reported in the workshop due to possible post-processing or typographical errors. In order to avoid this issue, the median $\tilde{\phi}$ and the median absolute deviation $\tilde{\sigma}(\phi)$ are used instead of the mean and standard deviation. Throughout the paper, the mean and standard deviation are occasionally provided to demonstrate how they are affected by the outliers included in the data. Although in some cases the outliers are easily identified and an argument could be made for their removal, this does not hold true for all cases. Since $\tilde{\phi}$ and $\tilde{\sigma}(\phi)$ are more robust measures, no data is ignored in their calculation.

3. Participation overview

A total of forty-seven contributions from different groups were received to the workshop. However, only forty submissions are considered for this paper, mainly due to some contributions being rejected on account of missing or incomplete data for Set 0, which was emphasized as mandatory from the first meeting of the workshop. From the forty participants, twenty-three submitted data for all the cases of Set 1, whereas sixteen only provided the mandatory results. Only one single participant did not submit data for Set 1. For Set 2, fifteen participants submitted results for all the scales, while nineteen only carried out the mandatory conditions, and six participants did not submit any data for Set 2.

Among the forty submissions, eight different CFD codes were used. These were Ansys CFX, Ansys Fluent, Cadence FineMarine, FreSCO+, HELYX-Marine, OpenFOAM, ReFRESCO and Simcenter STAR-CCM+. Details on the number of contributions using each code, along with oldest and newest version are given in Table 5. Details on each of the codes are also provided.

Besides solver version information, details on the software and versions used in mesh generation and post-processing were also gathered. Naturally, there is a large correspondence between the solver and the meshing tool used. All the participants that used STAR-CCM+ as the CFD solver naturally used the same software for mesh generation, those using OpenFOAM used its meshing tools such as snappyHexMesh, CfMesh and blockMesh. The participants that used HELYX-Marine also relied on it for meshing, while those that used Ansys CFX and Fluent used ICEM CFD and Fluent Meshing, respectively. Finally, Hexpress was the meshing tool employed by the participants that used FineMarine, FreSCO+ and ReFRESCO. Regarding the post-processing software, details are given in Table 6.

Ansys CFX uses the finite volume method with a cell-vertex approach for the spatial discretization, and an implicit, second-order accurate scheme for time discretization. A coupled algebraic multigrid method is

Table 5
Flow solvers and corresponding versions used by the participants for the workshop.

Code	# of participants	Oldest version	Newest version
Ansys CFX	1	–	CFX 2023 R2
Ansys Fluent	1	–	Fluent 24R1
Cadence FineMarine	6	8.2	12.1
FreSCO+	1	–	24-1
HELYX-Marine	2	3.2.0	4.1.1
OpenFOAM	5	v2006 / V8	v2312 / V11
ReFRESCO	2	2023.1	2024.1.1
Simcenter STAR-CCM+	22	2020.2.1 (15.04.010)	2402 (19.02.12)

Table 6
Post-processing software and corresponding versions used by the participants for the workshop.

Software	# of participants	Oldest version	Newest version
Ansys CFD-Post	2	24R1	2023R2
CFView	5	11.1	18.1
OpenFOAM	2	–	2312
Paraview	7	5.6	5.12
Simcenter STAR-CCM+	22	2020.2.1 (15.04.010)	2402 (19.02.12)
Tecplot	2	2021 R1	2022 R2

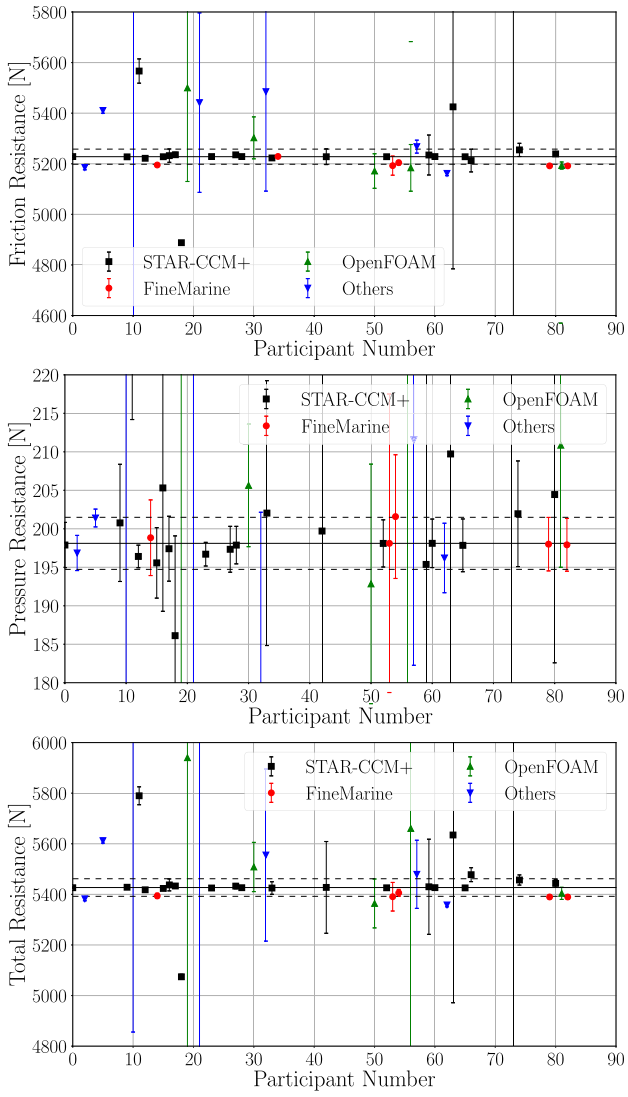

Fig. 8. Friction (top), pressure (middle) and total (bottom) resistance obtained from each participant and CFD code for the finest grid of Set 0, along with the estimated numerical uncertainty, median (solid line) and median absolute deviation (dashed lines).

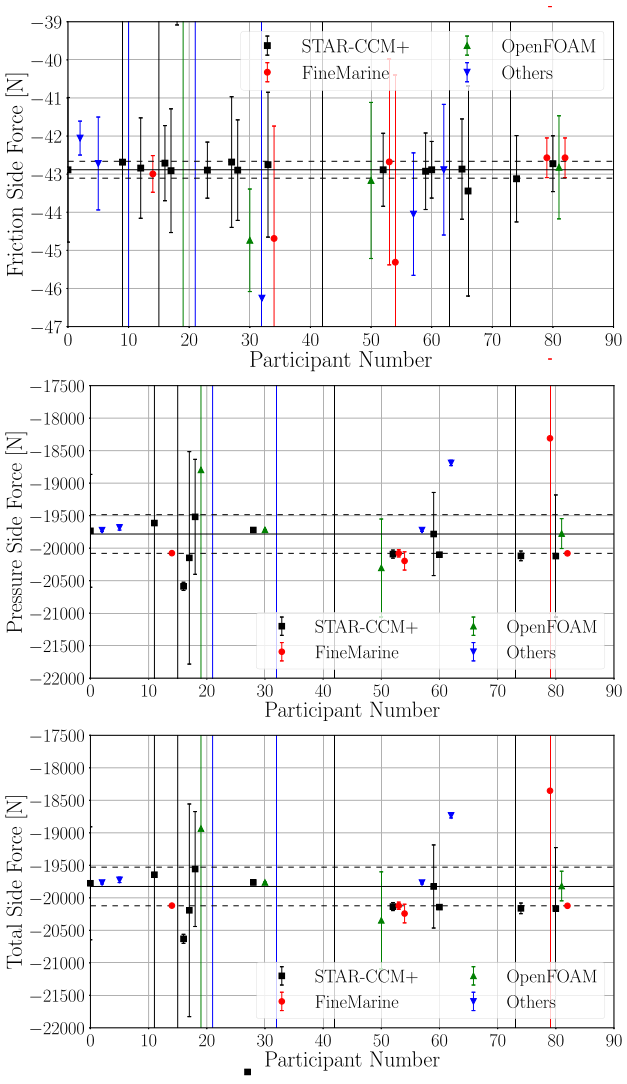

Fig. 9. Friction (top), pressure (middle) and total (bottom) side force obtained from the participants that did not include gravity for the finest grid of Set 0, along with the estimated numerical uncertainty, median (solid line) and median absolute deviation (dashed lines).

used to solve the governing equations. CFX handles unstructured, arbitrary cell shapes such as tetrahedrals, hexahedrals, prisms and pyramid elements.

Ansys Fluent also relies on the finite volume technique, but instead uses a cell-centered approach. The equations can be solved with a segregated or coupled pressure-based method, or with a density-based formulation. Fluent includes several features such as wide range of turbulence models, combustion models, multiphase flows and Fluid Structure Interaction (FSI) capabilities.

Cadence FineMarine uses the ISIS-CFD flow solver developed by the EMN (Equipe Modélisation Numérique), which is an incompressible unsteady RANS flow solver (Queutey and Visonneau, 2007). The solver uses a finite-volume discretisation, and a Rhie & Chow Semi-Implicit Method for Pressure Linked Equations (SIMPLE) type method for the pressure-velocity coupling. The solver accepts unstructured grids with an arbitrary number of arbitrarily shaped faces. In free-surface flows, the water surface is captured by a conservation equation for the volume fraction of water, discretised with specific compressive discretisation schemes (Queutey and Visonneau, 2007). The interface faces on the boundaries between the partitions are shared between the partitions; information on these faces is exchanged with the MPI (Message Passing Interface) protocol.

FreSCo$^+$ employs the finite volume method on a parallel CPU machine with distributed memory (Rung et al., 1999; Kühl, 2021). The approach is based on a second-order approximation associated with arbitrary unstructured grids, and the parallelization follows a domain decomposition approach. The algorithm is based on a cell-centered and co-located arrangement of variables. Temporal derivatives are approximated by an implicit method with two or three time levels and spatial integrals by the midpoint rule. Second-order central differences approximate diffusive fluxes, and higher-order (bounded) upwind-biased methods are generally employed to reconstruct convective fluxes. A modified pressure correction algorithm accounts for the odd-even decoupling of pressure and velocity components (Kühl and Rung, 2022).

HELYX-Marine is a comprehensive set of open-source finite-volume CFD solvers and simulation tools based on OpenFOAM for ship hydrodynamics developed by ENGYS in conjunction with Prof. Kevin Maki of the Department of Naval Architecture and Marine Engineering of the University of Michigan, USA.

OpenFOAM is an open-source CFD software library based on the finite volume approach to discretizing the flow equations. First and

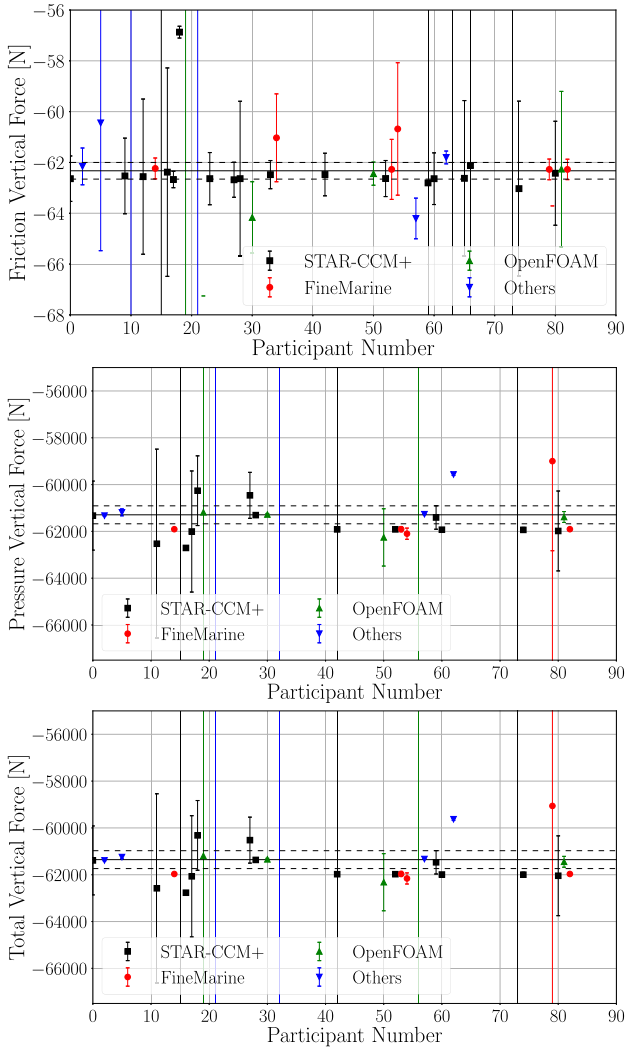

Fig. 10. Friction (top), pressure (middle) and total (bottom) vertical force obtained from the participants that did not include gravity for the finest grid of Set 0, along with the estimated numerical uncertainty, median (solid line) and median absolute deviation (dashed lines).

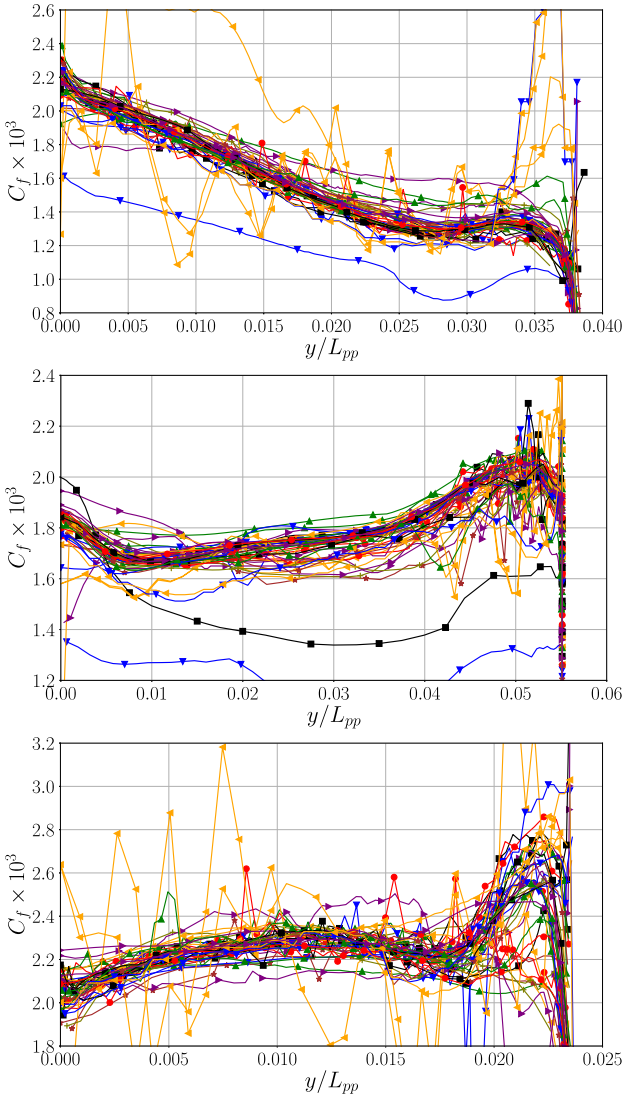

Fig. 11. C_f distributions on the surface of the hull for Set 1 and $Fr = 0.219$ at $x/L_{pp} = 0.1$ (top), $x/L_{pp} = 0.5$ (middle) and $x/L_{pp} = 0.9$ (bottom).

second-order schemes are available for the convective discretization of all flow quantities, and the volume of fluid method is employed as the interface-capturing approach.

ReFRESCO (https://www.refresco.org) discretizes the transport equations using a finite volume method with cell-centred collocated variables. The use of meshes with arbitrary cell shapes, as well as hanging nodes, is possible by the use of a face-based implementation. Mass conservation is ensured using a SIMPLE-type algorithm through a pressure correction equation. At each non-linear iteration, a linear system of equations is obtained using Picard's method. The linearised Navier-Stokes equations are solved in a segregated way, i.e., the equations for velocity, pressure correction, and if required energy, turbulence model and air volume fraction are solved in turn, and when solving for one of the variables, the others are considered known. Time integration is performed through the first or second-order backward differentiation.

STAR-CCM+ is a generic multi-purpose commercial flow solver originally developed and distributed by CD-Adapco, and now part of Siemens PLM Software engineering suite. This is a finite volume based solver running with unstructured meshes composed of arbitrary shaped cells (hexahedra dominant or polyhedra). Surface and volume integrals representing convective and diffusive fluxes are approximated using the midpoint rule. Steady or unsteady flows can be resolved by means of a coupled solver or a segregated solver. The SIMPLE algorithm is used for the segregated solution of the velocity-pressure coupling problem. An implicit second-order three-level scheme is employed for time integration. The free-surface is modeled using the Volume of Fluid (VOF) method with a High- Resolution Interface Capturing (HRIC) scheme for tracking the sharp interface between water and air.

As can be inferred from the code descriptions, all of the simulations for the workshop were carried out with the finite volume approach. The second order upwind scheme was the dominant choice for the discretization of the momentum equations, with some users also using QUICK, TVD Harmonic and AVLSMART. With regards to the discretization of the convective term of the equations of the turbulence model the situation is similar, with most of the users using a second order upwind scheme, followed by AVLSMART, and some participants who used the first order upwind discretization. For time discretization, twenty nine participants used a first order implicit scheme, while five participants relied on a second order implicit scheme. There were also six contributions that used a steady (pseudo-transient) approach with local time stepping. All participants used the Volume of Fluid (VOF) method to capture the free-surface. Three participants used the Realizable $k-\epsilon$ two-layer model for turbulence modelling, whereas the remaining participants used the $k-\omega$ SST model. There were also five cases of participants that submit-

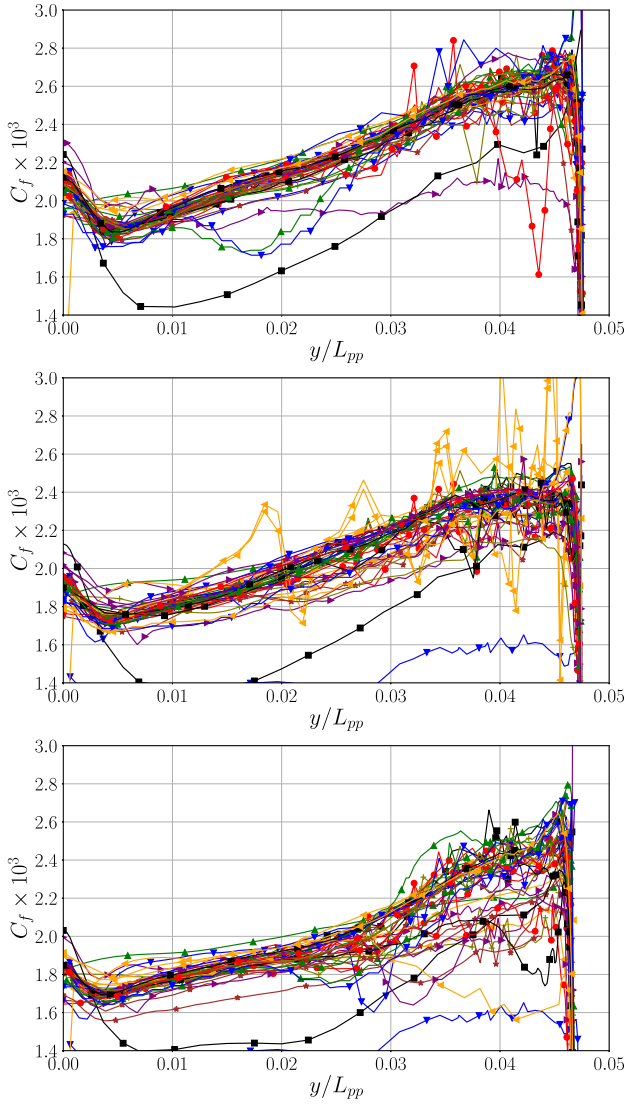

Fig. 12. C_f distributions on the surface of the hull for Set 1 at $x/L_{pp} = 0.75$ for $Fr = 0.13$ (top), $Fr = 0.219$ (middle) and $Fr = 0.304$ (bottom).

ted more than one set of data. These additional submissions, which are included in the results, consist on the use of wall functions instead of fully resolving the boundary layer, the use of the Local Time Step approach in OpenFOAM, and simulations carried out with the $k-\omega$ SST model by one of the participants that submitted results with the realizable $k-\epsilon$ model.

With regards to the computational domain, all participants used a box shaped domain, with the dimensions depending on the contribution. Only one contribution was done for the complete ship, while the remaining participants only simulated half of the ship. Statistics on the length, width and height of the computational domain for Set 1 are presented in Table 7, for the half-ship setup. Statistics for the total number of volume cells and cell faces on the ship are also provided, along with the time step size and y^+_{avg}.

4. Results - Set 0

The discussion of the results starts with Set 0, which is distinct from the remaining Sets in several aspects. Perhaps most importantly, it is the only case where a double-body setup is used and where participants carried out the simulations in the same grids. Consequently, the main expectation would be that this Set would be the one where participants

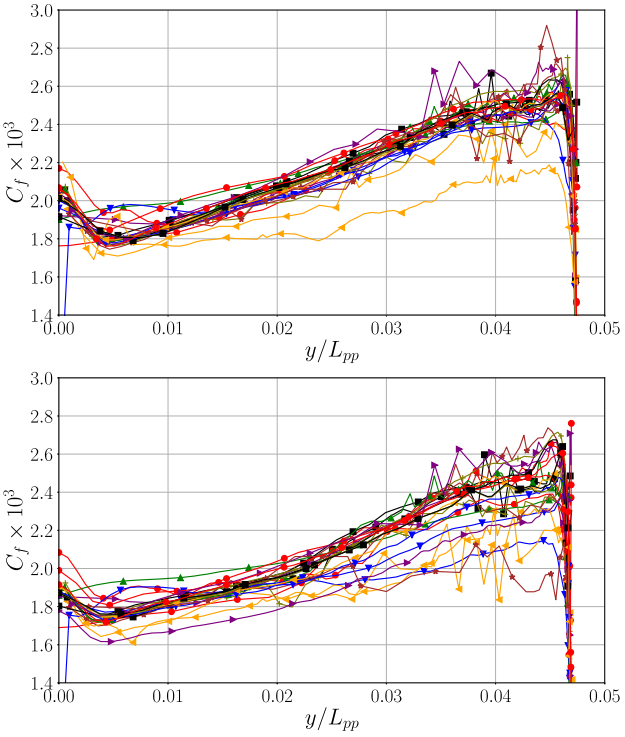

Fig. 13. C_f distributions on the surface of the hull for Set 1 at $x/L_{pp} = 0.75$ for $Fr = 0.173$ (top), and $Fr = 0.26$ (bottom).

would show the closest agreement between each other, with the main differences arising from the CFD code used.

As a starting point, Figs. 5 and 6 display the C_f and C_p distributions along the hull at three different longitudinal positions $x/L_{pp} = 0.1, 0.5$ and 0.9 for the finest grid of Set 0. Results from all participants are included, with each individual line corresponding to the data from a single participant. Considering the large amount of data, a legend is not included. It is also important to highlight that due to the changes in C_f and C_p along the length of the ship, the scales are different at each position.

Analysis of Figs. 5 and 6 shows most of the results to be concentrated relatively close together, with data from a few participants noticeably lying off the trend from the bulk of the results. The most distinguishable outliers are visible regardless of the position at which the C_f and C_p distributions are considered, hinting at some particular issue with the simulations, which might be related to either an incorrect setup or convergence issues. Some scatter in the bulk of the results is observed mainly at $y/L_{pp} = 0.05$ for the cut at midship ($x/L_{pp} = 0.5$) for both quantities.

In Fig. 7 the results for the cut at midship are shown again, but now divided by the CFD solver used. Displaying the results in this manner allows to check for consistency in the results obtained from each code, which was presumed to be the largest source of discrepancies for Set 0. This is mainly confirmed by the good agreement of the results for each solver, with the observation that a large part of the scatter observed at $y/L_{pp} = 0.05$ occurs mainly for the results obtained using STAR-CCM+. However, considering that this code accounts for slightly more than half of submissions (55 %), whereas the remaining solvers, individually, correspond to a much smaller part (at most 15 %) of the results, it is also normal for more scatter to be present in the STAR-CCM+ results due to the large number of results alone. Fig. 7 also shows that the main outliers in this Set are a small group consisting of a mix of codes.

Although results were provided for all five grids prepared for Set 0, the previous discussion has been restricted to the results corresponding to the finest grid. Nonetheless, the results obtained for the remaining

Table 7
Statistics on dimensions and refinement level of the grids used by the participants for the calculations on Set 1. The time step size and y^+_{avg} correspond to $Fr = 0.219$.

	Length [L_{pp}]	Width [L_{pp}]	Height [L_{pp}]	Volume Cells	Cell faces on ship	Time step size [s]	y^+_{avg}
Maximum	13.8	6.8	5	16.9M	787k	1.0	716.0
Minimum	2.5	0.8	0.7	1.3M	41k	0.002	0.451
Mean	6.2	2.4	2.7	6.3M	142k	0.155	128.9
Median	6.0	2.0	2.6	5.4M	114k	0.056	89.41

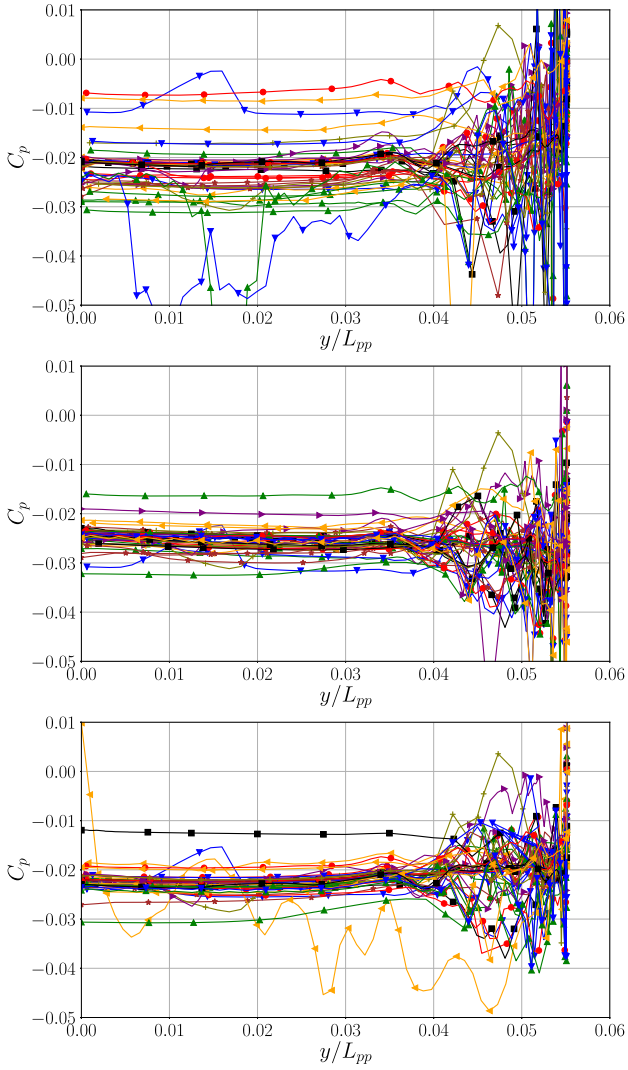

Fig. 14. C_p distributions on the surface of the hull for Set 1 at $x/L_{pp} = 0.5$ for $Fr = 0.13$ (top), $Fr = 0.219$ (middle) and $Fr = 0.304$ (bottom).

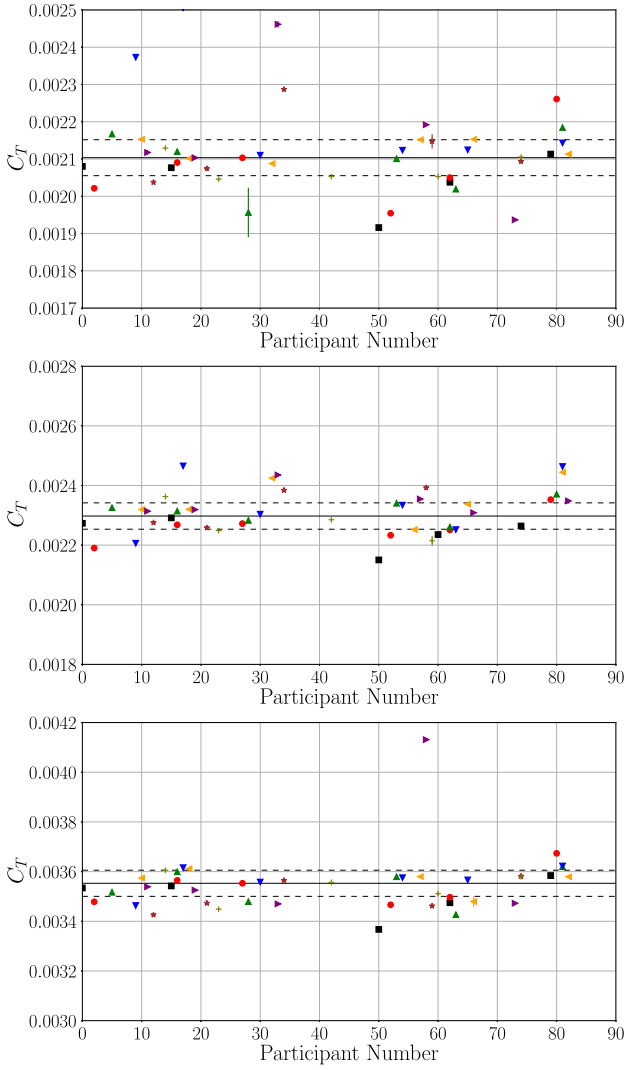

Fig. 15. Resistance coefficient of the ship for each participant and corresponding statistical uncertainty for Set 1 and $Fr = 0.13$ (top), $Fr = 0.219$ (middle) and $Fr = 0.304$ (bottom). Median (solid lines) and median absolute deviation (dashed lines).

grids exhibit the same trends and would be subject to the same discussion. However, data from the remaining grids is used in the uncertainty analysis of the forces, which are the next point of focus.

Fig. 8 illustrates the friction, pressure and total resistance obtained in the finest grid from each participant, along with error bars corresponding to the estimated numerical uncertainty for each result. Also included in these plots are the median of the results, given as the solid line, and the median absolute deviation, which is represented through the dashed lines. Figs. 9 and 10 exhibit a similar analysis but for the side force and the vertical force instead. The choice of the median and the median absolute deviation instead of the mean and standard deviation is motivated due to the large influence that a single outlier can have on the mean and standard deviation. Regardless, Table 8 contains all four statistical measures for each component of the resistance, as well as for their uncertainty. The results for the side and vertical forces are given in Table 9, considering only the median and median absolute deviation. It is noted that for the pressure components of the side force and the vertical force, some of the participants results were not included in the calculation of the statistics. The reason for this is that some of the participants included gravity in their simulations, causing the hydrostatic pressure to become the main contributor of these pressure forces, and leading to significantly different results than the participants who

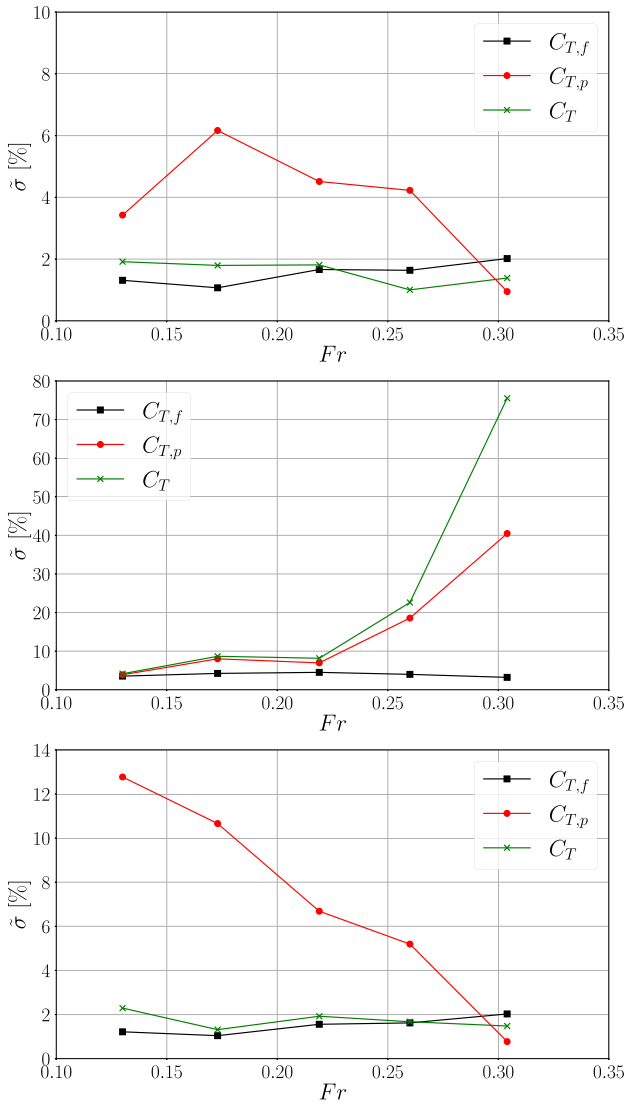

Fig. 16. Variation of the relative median absolute deviation of the friction, pressure and total resistance with the Froude number. Data for the hull (top), rudder (middle) and ship (bottom) surface.

Table 8
Mean, median, standard deviation and median absolute deviation of the friction, pressure and total resistance on the finest grid and of the corresponding estimated numerical uncertainty.

	Mean	Standard deviation	Median	Median Absolute Deviation
R_f [N]	5541	1749	5228	29.9
$U(R_f)$	7.6 %	36.7 %	0.18 %	0.09 %
R_p [N]	43	838	198	3.4
$U(R_p)$	85 %	273 %	3.9 %	3.2 %
R [N]	5584	1391	5427	34.8
$U(R)$	12 %	37 %	0.33 %	0.25 %

did not include gravity in their modelling. Thus, it would not be appropriate to group all results together.

In the results shown in Figs. 8 through 10, the numerical uncertainty has been kept for all the results including those that showed convergence issues. This is visible in the large error bars that go beyond the scale of each plot. It is noted that these cases occurred regardless of the solver used. Although there appears to be a smaller prevalence of numerical issues with the STAR-CCM+ results, given the higher number of results obtained for this code, this is partially justified by the fact that before being sent to the participants, the grids were tested on STAR-CCM+ and not on other solvers. Apart from the cases that exhibit convergence issues, the numerical uncertainty for the total resistance is small to the point that the error bars are barely visible for many results. This is corroborated by the values given in Table 8, as it can be seen that the median uncertainty of the total resistance was 0.33 %, indicating that half of the submissions had an uncertainty lower or equal to this value. When comparing the friction and pressure components of the resistance, it is seen that the pressure resistance exhibits, in general, higher numerical uncertainty, and that some results which provided reasonable values for the friction component appear to be outliers in the pressure resistance.

Table 9
Median and median absolute deviation of the friction, pressure and total side and vertical forces on the finest grid and of the corresponding estimated numerical uncertainty.

	Side force		Vertical force	
	Median	Median Absolute Deviation	Median	Median Absolute Deviation
Friction [N]	–42.9	0.2	–62.3	0.3
U(Friction)	3.6 %	1.9 %	3.1 %	2.4 %
Pressure [N]	–19782	297.5	–61656	364.0
U(Pressure)	0.28 %	0.26 %	0.17 %	0.17 %
Total [N]	–19825	297.2	–61718	363.1
U(Total)	0.28 %	0.26 %	0.16 %	0.16 %

When considering the friction resistance of the ship, it is observed that most of the STAR-CCM+ results show a nearly consistent result, with some small discrepancies perhaps arising from the different versions used. The results obtained with FineMarine are also consistent, with this code displaying a slightly lower friction resistance than that obtained with STAR-CCM+. In the case of OpenFOAM, there is a larger difference between submissions and so it is difficult to extract a general trend. As a whole, the complete set of results shows a relatively low scatter, with only a few results that fall well outside of the bounds marked by the median absolute deviation. The scatter between individual contributions for the pressure resistance is higher than that observed for the friction component, with the behaviour exhibited by the total resistance matching that of the friction resistance, since the latter is the dominant component of the total resistance. The friction resistance can also be taken as an example of how using the mean and the standard deviation would be misleading, as the latter differs by more than one order of magnitude from the median absolute deviation, and the mean value of 5541 N would lie well above the vast majority of the results shown in Fig. 8. These differences arise mainly from a single contribution that reported the friction resistance as 16,000 N. Although such a value could be easily detected as an outlier and removed from the statistical analysis, it was preferred to keep all data points and instead adopt statistical measurements that would not be influenced by single extreme outliers, as defining whether a value is or not an outlier could be difficult in some cases.

In the case of the side and vertical forces, the pressure force is the dominant component of the total force, and so the trends for the former are also reflected on the latter. The friction component of these forces exhibits larger relative uncertainty than that observed for the pressure components and the friction resistance, although the agreement between different solutions is still very good. Furthermore, the uncertainty itself is quite small, showing a median of 1.6 N for the side force and 1.9 N for the vertical force. In the case of the pressure components, the scatter between the simulations is higher than that observed for the friction contribution, a trend similar to that observed for the resistance.

5. Results - Set 1

The results of the study performed at full-scale at varying Froude number starts by considering the C_f distribution obtained for $F_r = 0.219$ at different longitudinal positions, shown in Fig. 11. Comparing these

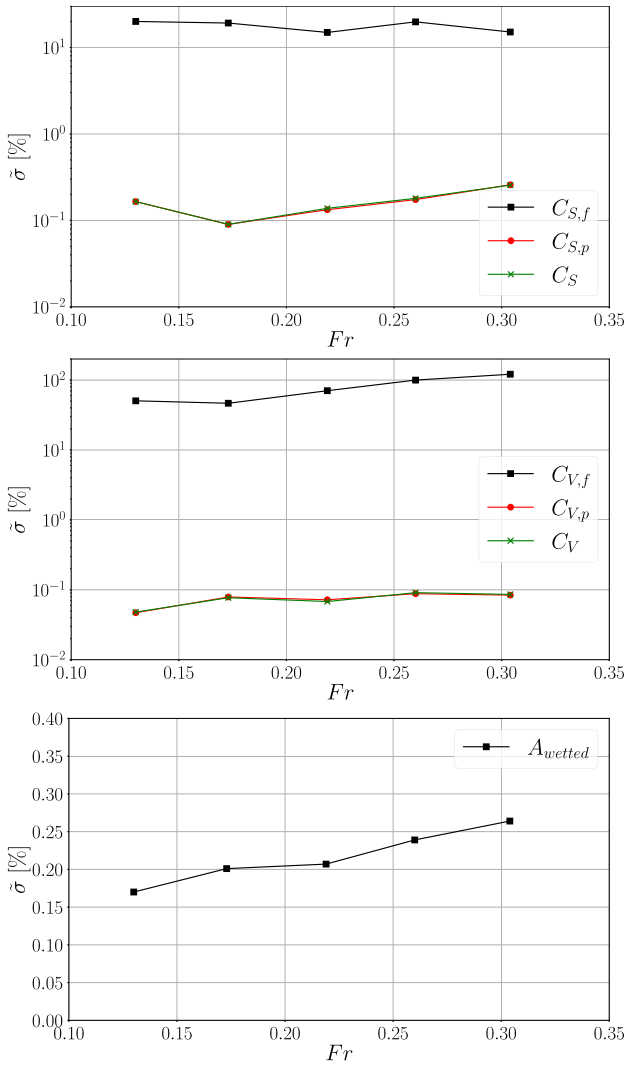

Fig. 17. Variation of the relative median absolute deviation of the side force (top), vertical force (middle) and wetted surface area (bottom) with the Froude number.

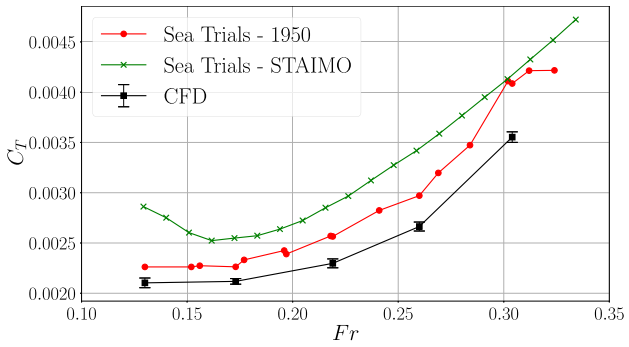

Fig. 18. Comparison of the median of the CFD results with the reported data from the sea trials as processed in the 1950 trials and after adopting current standard procedures. Median absolute deviation of the numerical results given through error bars.

results with those of Set 0, previously displayed in Fig. 5, leads to several relevant observations. In the results for Set 1, strong oscillations are observed in the C_f distribution, a consequence of the unstructured grid topology used by the vast majority of the participants. Disregarding the clear outliers, these oscillations are mainly present at the same locations where deviations were observed in the results for Set 0. Although the irregular evolution of C_f makes the analysis of the results more troublesome as trends become more difficult to distinguish in some regions, it is clear that the scatter in the results is significantly larger than that observed for Set 0. All of these aspects are a logical consequence of the unstructured grid topology, varying grid refinement levels among participants and the lower grid resolution used in Set 1 relative to Set 0. Some results that appear to be outliers are still present in the data, and the scatter seems to be slightly larger close to the bow of the ship, which is located at $x/L_{pp} = 1$.

In Fig. 12 the C_f distribution at $x/L_{pp} = 0.75$ is given for the three mandatory conditions of Set 1, which correspond to Froude numbers of $Fr = 0.13$, 0.219 and 0.304. The evolution of C_f is mainly the same for all the conditions, with the scatter of the results increasing as the Froude number is increased. The C_f distributions obtained at the same location for the two optional conditions of Set 1 are illustrated in Fig. 13. The trend of the increase of the scatter with the increase of the Froude number is again observed. An additional remark is that the results received for the optional conditions exhibit lower scatter and no evident outliers. Furthermore, due to the large variation in the number of contributions received for the mandatory (39) and optional (22) cases, any trends observed with the Froude number should consider these cases separately.

Fig. 14 shows the C_p distributions at mid-ship for the mandatory conditions of Set 1. The large amount of results received, together with the strong oscillations exhibited by C_p make a detailed analysis of the results troublesome. Nonetheless, it is visible that individual results show a closer match as the Froude number is increased, a trend opposite to that observed for C_f. Considering the results for $F_r = 0.13$, and focusing on the area close to the symmetry plane of the ship ($y/L_{pp} = 0$), some variation between individual results is observed. For the case of the pressure coefficient we recall that it was not provided directly by the participants, but rather the pressure on the hull, along with a value for the pressure at a reference location. This latter value was used as the reference pressure in the calculation of C_p, in order to make results comparable, irrespective of the actual reference pressure used in each simulation. However, small changes in this value arising from, for example, whether it was obtained at the cell center or interpolated to the reference location, can lead to the differences in the level of C_p observed at the symmetry plane. Although not shown here, the spread of the results also decreases with Froude number for the optional conditions, and the same trend is present at the other locations on the hull.

The total resistance coefficient of the ship obtained for the mandatory cases of Set 1 is displayed in Fig. 15, along with the median (solid line) and median absolute deviation (dashed lines) of the results. Although the outliers in Set 1 do not influence the mean and standard deviation as much as in Set 0, there are still some large discrepancies in some individual cases, particularly impacting the standard deviation. As an example, the median and mean for the total resistance of the ship differ by only 0.23 % (which corresponds to 40 N). On the other hand, the standard deviation is 5.5 % (1093 N), whereas the median absolute deviation is approximately 1.5 % (296 N). The bounds established by the standard deviation would cover all the results with the exception of a single point. The scale in each of the figures has been adjusted so that it covers a variation of approximately 20 % about the median. This means that individual contributions that deviate from the median by more than 20 % are not visible. The vertical error bars present in some of the results correspond to the uncertainty in the calculation of the mean total resistance, obtained through the TST procedure described in Section 2. In most cases, these bars are not visible, meaning that the uncertainty associated with the calculation of the mean total resistance is negligible. Comparing the results for the different Froude numbers shows that the spread between the results appears to decrease as the Froude number is increased, particularly for those results close to the median value. Furthermore, results that exhibit large deviations from the median for

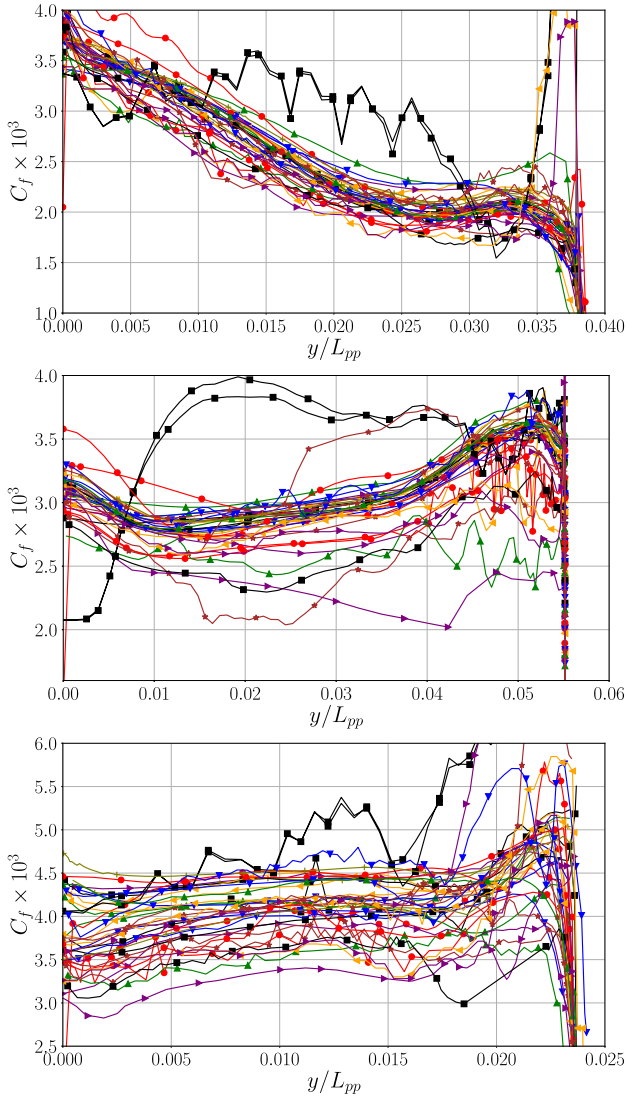

Fig. 19. C_f distributions on the surface of the hull for Set 2 and $\lambda = 11.906$ at $x/L_{pp} = 0.1$ (top), $x/L_{pp} = 0.5$ (middle) and $x/L_{pp} = 0.9$ (bottom).

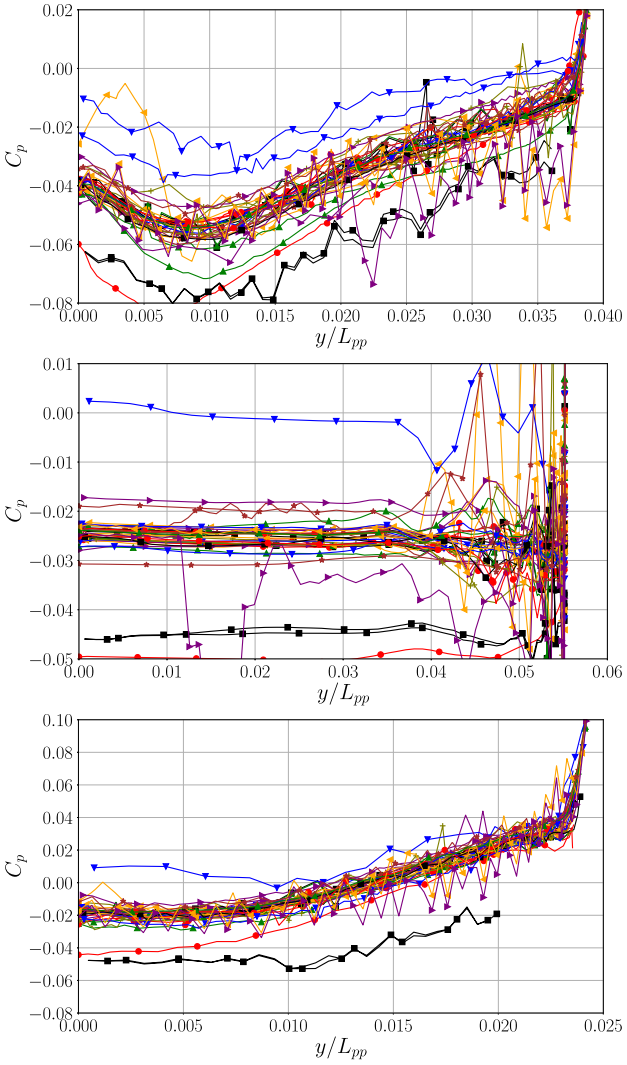

Fig. 20. C_p distributions on the surface of the hull for Set 2 and $\lambda = 11.906$ at $x/L_{pp} = 0.1$ (top), $x/L_{pp} = 0.5$ (middle) and $x/L_{pp} = 0.9$ (bottom).

a given Froude number can exhibit good agreement with the remaining results for different conditions.

An overall summary of the median absolute deviation of the total resistance and its components is given in Fig. 16 for the hull, rudder and complete ship. In the case of the hull surface, the total resistance shows a decrease of the median absolute deviation with the increase of the Froude number, whereas the scatter of the friction resistance increases. We recall again that there is a large discrepancy in the number of results received for the mandatory and optional Froude numbers, and so these should be considered independently. The median absolute deviation of the friction resistance of the hull shows a decrease from $Fr = 0.13$ to $Fr = 0.173$, however this is associated with the discrepancy in received results. The pressure resistance shows a larger scatter than the remaining forces which seems to mainly decrease with the increase of the Froude number, with the exception of the result at $Fr = 0.13$. The results obtained for the rudder show the scatter in pressure and total resistance to increase with the Froude number, and large scatter was observed for these quantities at the highest Froude numbers considered. On the other hand, the friction resistance of the rudder does not show a monotonic trend, and it is higher than that obtained for the hull. The higher scatter observed for the rudder when compared to the hull surface is consistent with higher oscillations observed for C_f and C_p in this area. When considering the complete ship, the scatter of the pressure resistance is considerably higher than that of the other forces, and it exhibits a clear decrease with the increase of the Froude number. It is important to highlight that the data presented in Fig. 16 is given as a percentage, relative to the median. The pressure resistance coefficient increases significantly with the Froude number which contributes to the decrease in the relative median absolute deviation. When considering the absolute deviation, it increases slightly with the Froude number, with the exception of the highest Froude number. On the other hand, the median absolute deviation of the friction resistance shows a slight increase with the Froude number. The overall effect on the total resistance of the ship is a slight decrease of the scatter as the Froude number is increased, with the scatter showing similar levels to that of the friction resistance. The median absolute deviation of the total resistance of the ship is lower than 3 % for all Froude numbers, meaning that half of the results received deviate by less than 3 % from the median.

A similar analysis is presented in Fig. 17 for the side and vertical forces on the ship and the reported wetted surface area. Due to the higher deviation in the friction resistance of the side and vertical forces, the scale for those cases has been changed to logarithmic. Although the friction component of these forces is smaller by several orders of magnitude than the pressure component, it is still noteworthy that it exhibits such a high relative deviation, which shows an increasing trend with

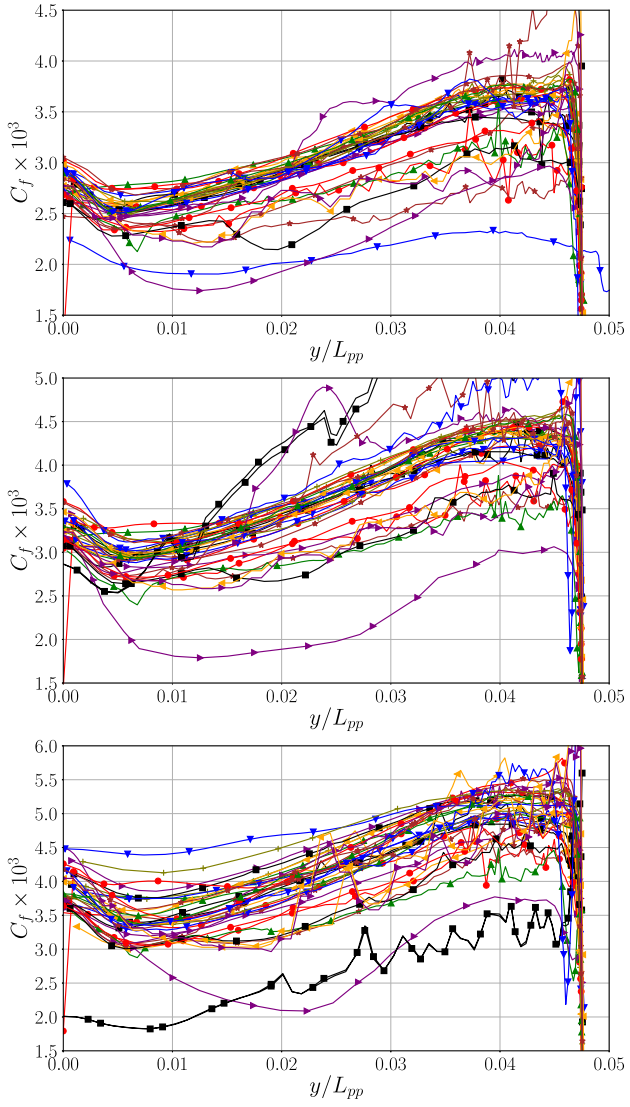

Fig. 21. C_f distributions on the surface of the hull at $x/L_{pp} = 0.75$ for Set 2 and $\lambda = 6.35$ (top), $\lambda = 11.906$ (middle) and $\lambda = 21.167$ (bottom).

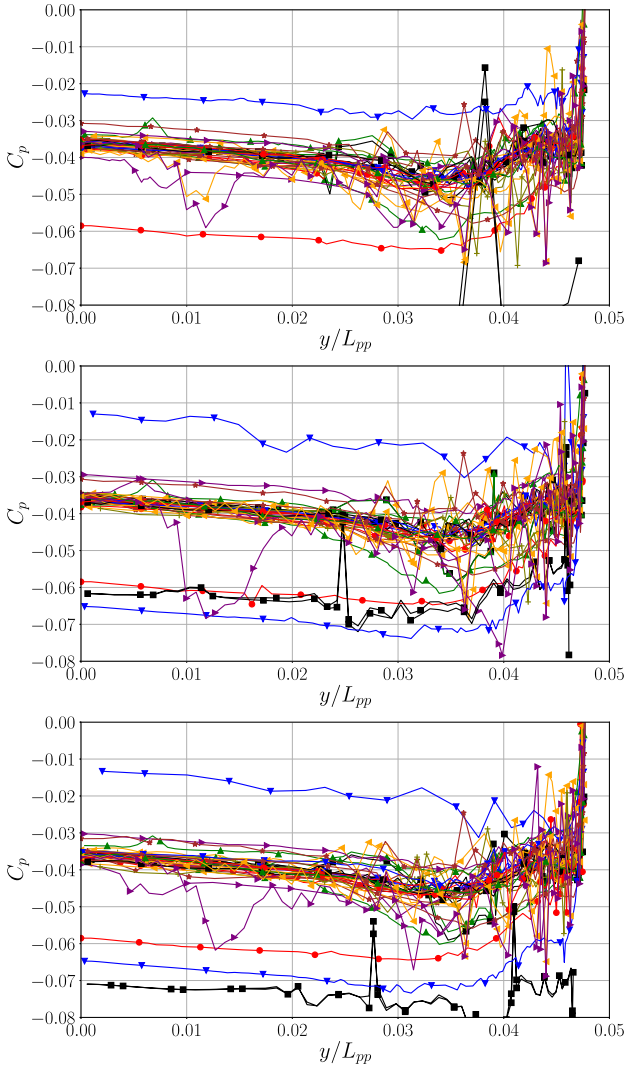

Fig. 22. C_p distributions on the surface of the hull at $x/L_{pp} = 0.75$ for Set 2 and $\lambda = 6.35$ (top), $\lambda = 11.906$ (middle) and $\lambda = 21.167$ (bottom).

increasing Froude number for the case of the vertical force. For the pressure contribution, an increase in the deviation with the Froude number is observed for both side force and vertical force. As the pressure contribution is dominant, the total force follows the same trend. An increase of the deviation of the wetted surface area with the Froude number is also observed, a consequence of the larger waves across the hull, and highlighting possible differences in the capturing of the free-surface in the simulations. Considering that the hydrostatic pressure is the most important factor for the side force and vertical force, it is not surprising to see the trend of the deviation in wetted surface area matching those observed for the side and vertical forces. Regardless, we note that the median absolute deviation in the wetted surface area is lower than 0.3 % for all conditions and increases slightly with the increase of the Froude number. One possible cause for this is numerical ventilation, which was reported to be present in the simulations by some of the participants.

The comparison of the total resistance coefficient obtained in Set 1 with the available data from the Lucy Ashton experimental campaign is carried out in Fig. 18. The experimental results are presented as two distinct lines, one corresponding to the corrected sea trial data given in Conn et al. (1953), and another to corrected data based on ITTC guidelines for speed and power trials, carried out with the STAIMO software according to ISO 15016; 2015. For this comparison, the data corresponding to the smoothest hull condition tested in the 1950s campaign was used. Naturally, the use of STAIMO required some simplifications since no propeller was used in the sea trials. The results obtained with STAIMO exhibit a higher total resistance coefficient than the results obtained with the corrections performed in the original campaign. The numerical results gathered for the workshop show an underprediction of the resistance coefficient for all Froude numbers. This is not a surprising result, given that roughness was not included in the CFD simulations and that the ship was not free to heave or pitch. Regarding the experimental data, there might also be some increased air resistance due to the jet engines and possibly an influence on the trim angle of the ship.

6. Results - Set 2

The analysis of the results for Set 2, where the participants were asked to perform simulations keeping the Froude number constant and equal to 0.219 and varying the ship scale (Reynolds number), begins by looking at the C_f distribution at three different locations for $\lambda = 11.91$, shown in Fig. 19. Again, as in the results for Set 1, the use of unstructured grids by the majority of the participants led to oscillations in the C_f distribution that made the result analysis more difficult. Nevertheless, the same trend observed in Set 1 can easily be identified for model ship size: the data spread increases as the measuring location moves towards

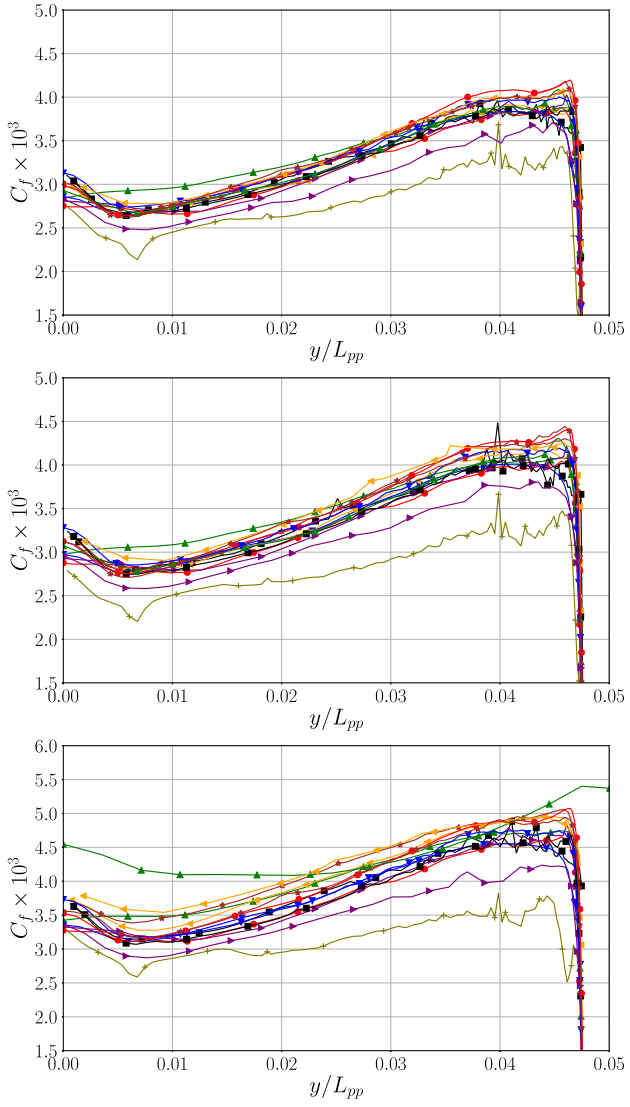

Fig. 23. C_f distributions on the surface of the hull at $x/L_{pp} = 0.75$ for Set 2 and $\lambda = 7.938$ (top), $\lambda = 9.525$ (middle) and $\lambda = 15.875$ (bottom).

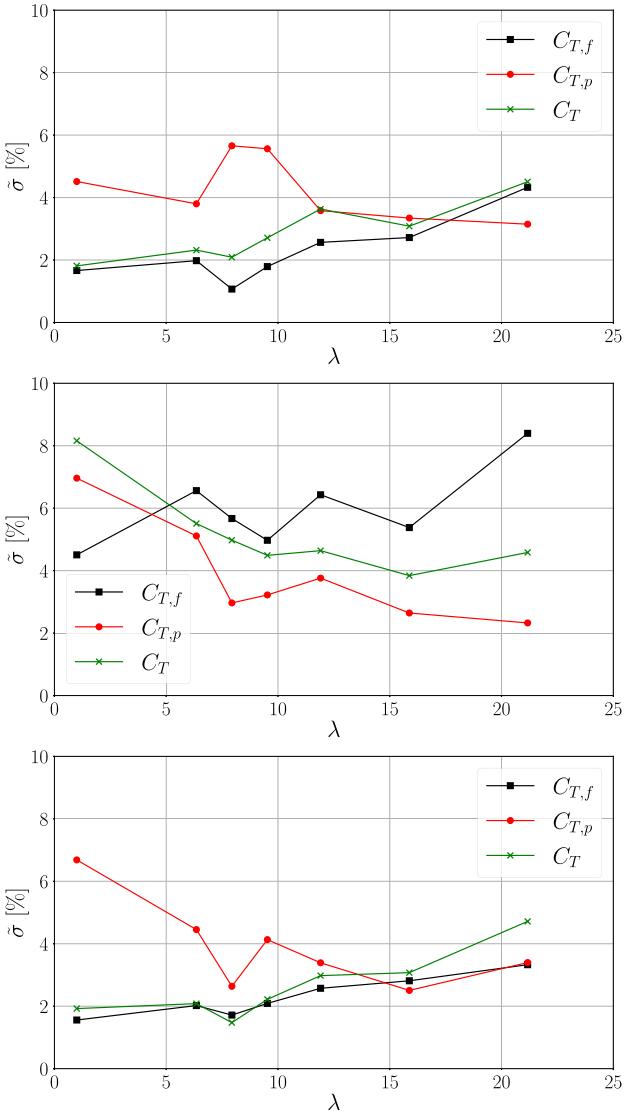

Fig. 24. Variation of the relative median absolute deviation of the friction, pressure and total resistance with the scale factor. Data for the hull (top), rudder (middle) and ship (bottom) surface.

the bow ($x/L_{pp} = 1$). Fig. 20 presents the pressure distribution C_p at the same locations. The presence of outliers is again evident, but unlike for the C_f distribution, the scatter of the data decreases towards the bow. It is also important to notice the increase in data scatter along the vessel beam at the midship location ($x/L_{pp} = 0.5$).

The C_f and C_p distributions for the three mandatory scale factors in Set 2, which are $\lambda = 6.35$, $\lambda = 11.906$ and $\lambda = 21.167$, at $x/L_{pp} = 0.75$ are illustrated in Figs. 21 and 22, respectively. For both quantities, there is a slight reduction of the data scatter as the Reynolds number increases. An increase in C_f as the scale factor is increased is observed, a natural consequence of the decrease of the Reynolds number. The C_p distribution is almost independent of the Reynolds number. Fig. 23 presents the friction distribution for the three optional sets, $\lambda = 7.938$, $\lambda = 9.525$ and $\lambda = 15.875$. As in Set 1, the data for the optional conditions presents reduced scatter and fewer outliers.

Fig. 24 presents $\tilde{\sigma}$ for the total resistance and its components on the different surfaces of the ship. The results from Set 1 for the same Froude number are also included, and correspond to the data at the lowest scale factor, $\lambda = 1$. As was the case for Set 1, it is important to recall the large difference in the number of submitted results between the mandatory and optional conditions, as well as the full-scale condition, which may influence how some trends are visible. The trend of the friction resistance coefficient is similar to that of the total resistance on the hull and for the complete ship. For all of these conditions, a slight increase in the scatter is observed as the scale factor is increased. This corresponds to a decrease of the Reynolds number, meaning that the friction resistance coefficient increases. Furthermore, for these quantities, the deviation obtained in the full-scale condition is lower than for the mandatory cases of Set 2. The deviation of the pressure resistance coefficient seems to decrease slightly as the model size is decreased, and now it is for the full-scale simulation that it exhibits the largest value, when ignoring the optional conditions of Set 2. The trends observed for the total resistance on the rudder show some differences to those observed on the hull, with C_T exhibiting lower scatter for smaller models. In the case of the spread in $C_{T,f}$ it seems to increase slightly as λ increases, although the trend is somewhat erratic. The full-scale simulations exhibit the lowest deviation for the friction resistance and the highest for the pressure and total resistance in the rudder.

One contributing factor to the scatter in the friction resistance is whether the boundary-layer was fully resolved, or if wall functions were used. Fig. 25 presents the friction resistance coefficient of the ship as a function of the average y^+ for all the results received for the workshop for the smallest model, $\lambda = 21.167$. For this condition, some participants

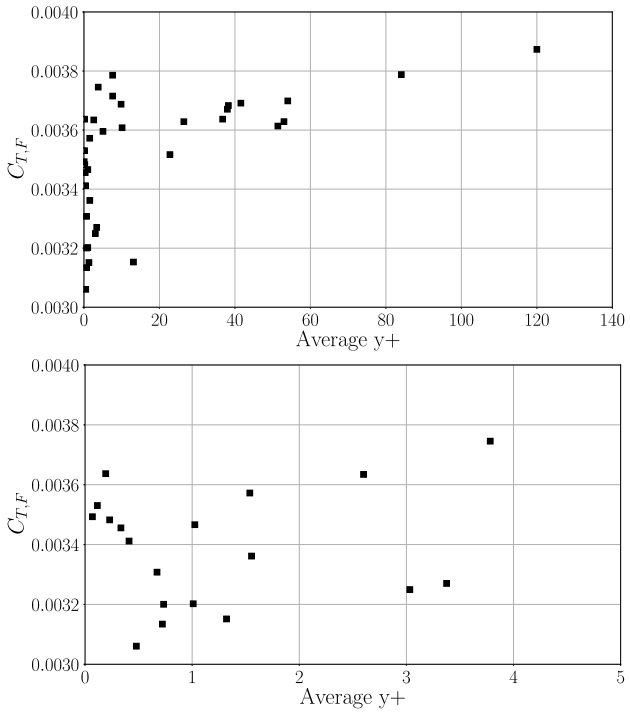

Fig. 25. Friction resistance coefficient of the ship as a function of the average y^+ on the hull for the results at $\lambda = 21.167$.

used wall functions, as evidenced by the number of results that exhibit $y^+ > 30$, whereas others resolved the boundary-layer. Larger deviations are observed for the results that resolve the boundary-layer, particularly in the range $y^+ > 0.5$. In the case of Set 1, there was only a single result that resolved the boundary-layer, while all the others used wall functions. This leads to the lower $\tilde{\sigma}$ observed for the friction resistance for the full-scale condition.

The relative median absolute for the side and vertical forces and the wetted surface area are given in Fig. 26. Similarly to Set 1, higher $\tilde{\sigma}$ is obtained for the friction component of the side and vertical force when compared to the pressure component. There are no clear trends for these forces with the change in model size. The same appears to hold true for the wetted surface area, with the caveat that the full-scale condition exhibits a lower deviation than the conditions for Set 2. Nonetheless, the median absolute deviation for the wetted surface area is under 1 % for all cases.

The final part concerning the results of Set 2 is the comparison between the numerical C_T and the results obtained in the model-scale experiments reported in Conn et al. (1953), which is illustrated in Fig. 27. For the scales considered, the numerical results always underpredict the resistance when compared to the experimental measurements, with the overall trend being well captured. While for the full-scale results the discrepancy was attributed to roughness, that should not be a factor at model-scale. The experimental results correspond to the data available for the measurements with a trip wire, so laminar flow is not a concern either. Regardless, it is stated in Conn et al. (1953) that the effect of the trip wires was at most 2 % on the smallest model. The dynamic motions of the ship remain as the likely cause for the differences, although no information is available from the experiments as to whether the models were constrained or not.

7. Results discussion

This section covers other results that were discussed among the participants during the workshop in September. It is important to note that during the workshop, the mean and standard deviation were used as

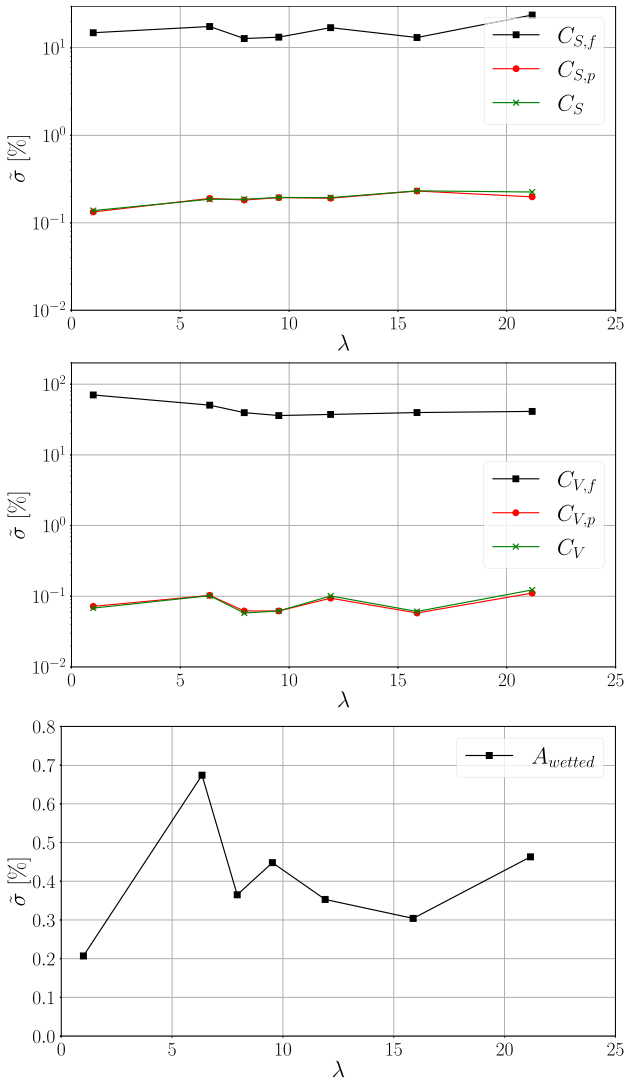

Fig. 26. Variation of the relative median absolute deviation of the side force (top), vertical force (middle) and wetted surface area (bottom) with the scale factor.

the statistical measures of the results. Consequently, the dispersion of the results was discussed as being worse than that presented in this paper.

Regarding this point, a discussion took place about the standard deviation observed for the total resistance of the ship at full-scale, which was approximately 5 %. There was no consensus as to whether this was a positive or negative result. Some participants considered this to be too high of a spread, whereas others argued that such a scatter would also be observed for model-scale experiments. Another point was made that the scatter observed in Set 2 was considerably higher than that obtained in other workshops at model-scale. This was seen as a negative step in the evolution of CFD for maritime applications, especially when taking into the account that the geometry was considered to be simpler than current hull forms.

Besides the previously mentioned use of the standard deviation throughout the workshop, which could at times present high values due to the presence of extreme outliers, there are several other factors that influence the spread in the results and must be mentioned. The first of these is the fact that the workshop was carried out blindly. Participants were unaware of the data available from the campaign carried out in the 1950s and were not told the name of the ship or that the trials were carried out with jet engines, which could have led to the identification

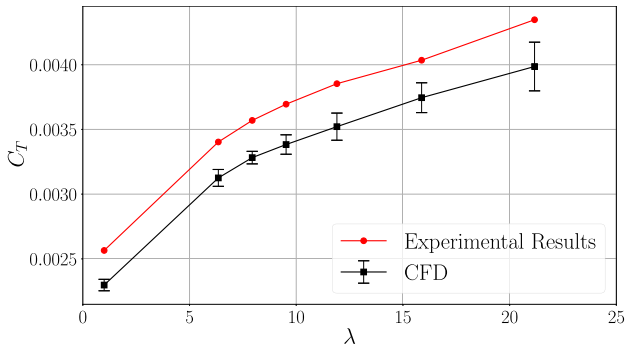

Fig. 27. Comparison of the median of the CFD results with the reported data from the experiments carried out as part of the 1950 campaign. Median absolute deviation of the numerical results given through error bars.

of the case. This contrasts heavily with workshops that rely on well-known benchmark cases such as the KVLCC2, JBC or ONR Tumblehome, which have been subject to numerous studies. For these cases, data is easily available, and participants would be able to check whether their results match already published data and thus potentially eliminating all outliers. This was not the case for the Lucy Ashton, since, as stated in Section 2, the goal for this workshop and in particular Set 1, was to carry it out as a predictive exercise.

The second aspect concerning the scatter in the results is that the results are anonymous and one individual submission can not be linked to a given group, unless they decide to identify themselves. In this manner, one company being an extreme outlier does not influence its standing. Although the decision to have the results being anonymous likely led to higher participation in the workshop, it can also have motivated contributions with lower effort. This can be connected to the trend observed across Set 1 and Set 2 that the optional conditions exhibited a smaller spread than the mandatory ones, and the number of outliers was significantly lower, even when considering the reduced number of submissions for the optional conditions. Participants who take the extra time to run the optional conditions would be putting more time and work into their contribution for the workshop, which would decrease the likelihood of being an outlier.

The final point concerning the spread observed is linked to a shift in the groups that participate in the workshop. Previous numerical workshops had mainly code developers participating, whereas for the present case, the majority of the participants were simply users of the CFD codes, and not developers. Developers being more familiar with their own codes would be more likely to avoid mistakes and produce solutions of good quality, which would contribute to minimizing the differences in the results.

The oscillations in the C_f and C_p distributions, combined with the large number of submissions made it so these quantities did not contribute significantly to the outcome of the workshop. In Set 0, the use of a common, structured grid helped to alleviate this issue and an overall behaviour was easier to identify. However, the unstructured grid topology used by the vast majority of the participants for Sets 1 and 2 leads to oscillations that cause the distributions to be difficult to analyze, particularly if a large number of results is present.

Some of the quantities that were asked from the participants were not included in the previous discussions. One example are the wave cuts, which were provided at several locations for all of the conditions of Set 1 and Set 2. However, these quantities did not prove to be useful for the discussion of the results, as no relevant insight or conclusions were extracted from them and so they were omitted here. The same is valid for the data concerning the number of cells on the domain, cell faces on the ship and the time step size, which were discussed during the workshop. However, there were no visible trends between these quantities and the friction or pressure components of the forces. An example of this is given in Fig. 28.

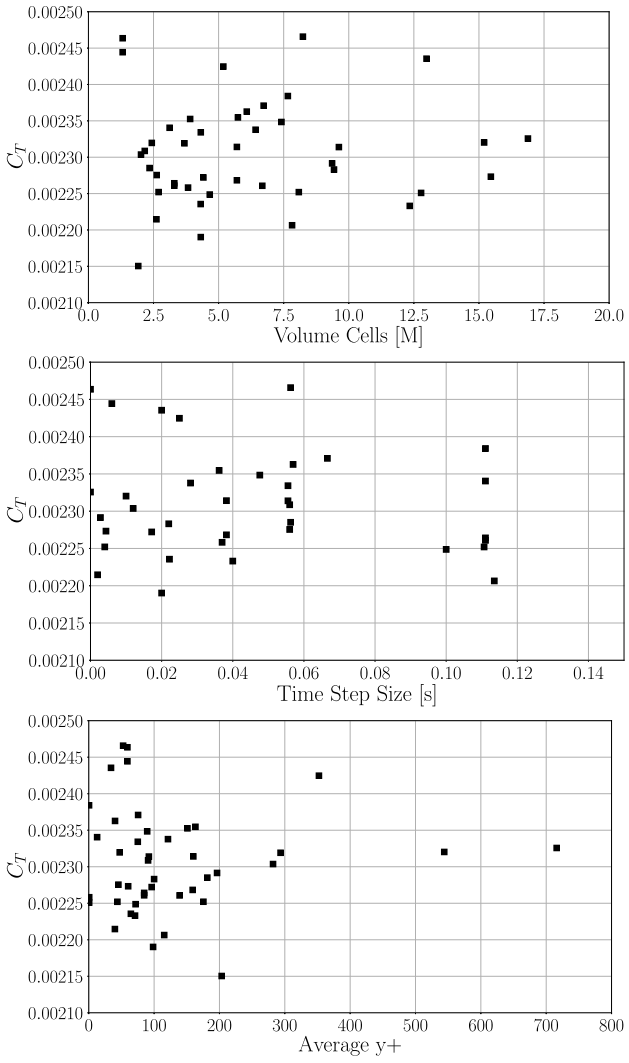

Fig. 28. Resistance coefficient of the ship as a function of the total number of cells (top), time step size (middle) and average y^+ (bottom) for Set 1 and $Fr = 0.219$.

8. Conclusions

This paper presents a summary of a full-scale CFD resistance prediction workshop. The geometry for the workshop was the Lucy Ashton, a paddle steamer which was fitted with jet engines to carry out resistance tests in an experimental campaign carried out in 1950, complemented with model-scale tests. Since the Lucy Ashton experiments are mostly unknown in the maritime community, the workshop was carried out blindly. The name of the ship and details of the measurements were only disclosed to the participants after the results had been received.

The cases for the workshop were divided in three Sets, numbered from 0 to 2. The first Set corresponds to a grid refinement study with multi-block structured grids common for all the participants, for a double-body setup and a single speed at full-scale. This study was mandatory for participation in the workshop. Set 1 was the full-scale part of the workshop, and consisted of five conditions identified by the corresponding Froude number. Out of the five conditions, three were mandatory and two were optional. The last part of the workshop was Set 2, and was comprised of six simulations at a constant Froude number, but for varying scale factors. For this set, three of the conditions were mandatory, and the remaining three were optional. A total of forty different results were received for the workshop, with the vast majority of the participants contributing to the mandatory part of Set 1.

Outliers were present in most of the cases of the workshop, even in Set 0 which corresponded to the simplest simulations to be performed for the geometry, with common grids prepared for all the participants. Outliers were often not the same across different conditions, and in some cases corresponded to post-processing or typographical errors. Even though a large number of results was received for the workshop, outliers could have a large impact on statistical measures such as the mean and the standard deviation, which motivated the use of the median and the median absolute deviation as alternatives for this study.

The main findings of this work are as follows:

- The C_f and C_p distributions showed good agreement between different codes in Set 0, although some slight difference were observed. Some discrepancies were also present between simulations carried out with the same code, although these could be related to different version of the solver. In the case of Set 1 and Set 2, there is no evident agreement between different codes, partially due to the different grids being used, as well as the unstructured grid topology used by the participants which causes large oscillations in these quantities. Regardless, it was possible to conclude that the spread in the C_f distributions increased with the increase of the Froude number, and decreased with the increase in model size. On the other hand, the spread in the results for C_p decreases with the increase of F_r and is mostly independent on the scale factor.
- The scatter in the friction resistance of the ship increases slightly with the increase of the Froude number for Set 1, and decreases as the model size is increased, as shown in the results for Set 2. On the other hand, the pressure resistance exhibits the opposite trend, with a clear decrease in the scatter at full-scale as the Froude number increases. When comparing the two quantities, lower median absolute deviation was obtained for the friction resistance than for the pressure resistance with the exception of the highest Froude number of Set 1, and one of the smallest model sizes in Set 2. The scatter in the friction resistance was lower for Set 1 due to the vast majority of the participants using wall functions, whereas for Set 2 a considerable number of participants resolved the boundary-layer. Finally, the scatter of the total resistance showed a slight decrease with the increase of the Froude number and with the decrease of the scaling ratio.
- The comparison of the results obtained for Set 1 and Set 2 show the numerical ship resistance to be lower than experimental data, both at full-scale (Set 1) and at model-scale (Set 2). At full-scale this is justified by the numerical simulations assuming the hull to be hydrodynamically smooth, and for the configuration with no heave or trim angle in which the simulations were carried out. The latter might also explain the discrepancies at model-scale, where roughness should not be a factor. Regardless, the Lucy Ashton experimental campaign contains more data than that used for the workshop and that can be used to further investigate some of the differences.

Overall, the scatter exhibited by the simulations at full-scale was not higher than the calculations carried out at model-scale. The maximum median absolute deviation for the resistance of the ship for Set 1 was of 2.3 %, meaning that half of the results submitted for the workshop deviated by at most 2.3 % from the median value. This value is lower than that obtained for half of the conditions for Set 2, showing that full-scale simulations did not lead to a deterioration of the agreement between different participants. When considering that the workshop was carried out blindly, this stands as a favourable outcome in building confidence for full-scale simulations.

CRediT authorship contribution statement

Rui Lopes: Writing – original draft, Visualization, Methodology, Investigation, Formal analysis, Data curation, Conceptualization; **Arash Eslamdoost:** Writing – review & editing, Supervision, Resources, Methodology, Conceptualization; **Rickard E. Bensow:** Writing – review & editing, Supervision, Resources, Project administration, Methodology, Funding acquisition, Conceptualization; **Dmitriy Ponkratov:** Writing – review & editing, Methodology, Conceptualization; **Anja Kömpe:** Writing – review & editing, Investigation, Formal analysism; **Paolo Geremia:** Writing – review & editing, Investigation, Formal analysis; **Çagan Birant Pekküçük:** Writing – review & editing, Investigation, Formal analysis; **Cagri Aydin:** Writing – review & editing, Investigation, Formal analysis; **Diego Villa:** Writing – review & editing, Investigation, Formal analysis; **Dimitris Ntouras:** Writing – review & editing, Investigation, Formal analysis; **Dong Cheol Seo:** Writing – review & editing, Investigation, Formal analysis; **Gennaro Rosano:** Writing – review & editing, Investigation, Formal analysis; **Florian Vesting:** Writing – review & editing, Investigation, Formal analysis; **Gabriele Bigini:** Writing – review & editing, Investigation, Formal analysis; **Guillermo Chillcce:** Writing – review & editing, Investigation, Formal analysis; **Jan Kaufmann:** Writing – review & editing, Investigation, Formal analysis; **Jianfeng Lin:** Writing – review & editing, Investigation, Formal analysis; **João Muralha:** Writing – review & editing, Writing – original draft, Investigation, Formal analysis; **Lukas Dott:** Writing – review & editing, Investigation, Formal analysis; **Kaan Ilter:** Writing – review & editing, Investigation, Formal analysis; **Dimitrios S. Lampropoulos:** Writing – review & editing, Investigation, Formal analysis; **Kristian Sagmo:** Writing – review & editing, Investigation, Formal analysis; **Lars Lübke:** Writing – review & editing, Investigation, Formal analysis; **Masaya Kubota:** Writing – review & editing, Investigation, Formal analysis; **Matija Vasilev:** Writing – review & editing, Investigation, Formal analysis; **Miles Wheeler:** Writing – review & editing, Investigation, Formal analysis; **Muhammed Sahid:** Writing – review & editing, Investigation, Formal analysis; **Carlo Giorgio Grlj:** Writing – review & editing, Investigation, Formal analysis; **Niklas Kühl:** Writing – review & editing, Investigation, Formal analysis; **Pierre Crepier:** Writing – review & editing, Investigation, Formal analysis; **Ramkumar Joga:** Writing – review & editing, Investigation, Formal analysis; **Rasul Niazmand Bilandi:** Writing – review & editing, Investigation, Formal analysis; **Marcus Boyd:** Writing – review & editing, Investigation, Formal analysis; **Alvaro Del Toro:** Writing – review & editing, Investigation, Formal analysis; **Shona Cunningham:** Writing – review & editing, Investigation, Formal analysis; **Simone Bozzo:** Writing – review & editing, Investigation, Formal analysis; **Fabian Schumacher:** Writing – review & editing, Investigation, Formal analysis; **Themistoklis Melissaris:** Writing – review & editing, Investigation, Formal analysis; **Vincent Tissot:** Writing – review & editing, Investigation, Formal analysis; **Vincenzo Sorrentino:** Writing – review & editing, Investigation, Formal analysis; **Wim Van Hoydonck:** Writing – review & editing, Investigation, Formal analysis; **Zhao-Hui Li:** Writing – review & editing, Investigation, Formal analysis.

Declaration of competing interest

The authors declare that they have no known competing financial interests or personal relationships that could have appeared to influence the work reported in this paper.

Acknowledgements

This research is supported by the Swedish Energy Agency with Project P2021-00277 and by Kongsberg Maritime Sweden AB through the University Technology Centre in Computational Hydrodynamics hosted by the Department of Mechanics and Maritime Sciences at Chalmers. The computations were enabled by resources provided by Chalmers e-Commons at Chalmers and by resources provided by the National Academic Infrastructure for Supercomputing in Sweden (NAISS) at the National Supercomputer Centre in Linköping University, partially funded by the Swedish Research Council through grant agreement no 2022-06725. The management of Indian Register of Shipping is acknowledged, as well as Mr. Sharad Dhavalikar for his guidance. CMC Marine Srl is gratefully acknowledged. This study has been supported

by the Croatian Science Foundation under project IP-2020-02-8568. We also acknowledge Simone Mancini, Nastia Degiuli, Serge Toxopeus, Ermina Begovic, Maverick Calori, Federico Evangelista, Julian Kimmerl and Lars Larsson for contributions to the workshop.

References

Brouwer, J., Tukker, J., Klinkenberg, Y., van Rijsbergen, M., 2019. Random uncertainty of statistical moments in testing: mean. Ocean Eng. 182, 563–576. https://doi.org/10.1016/j.oceaneng.2019.04.068

Brouwer, J., Tukker, J., Van Rijsbergen, M., 2013. Uncertainty analysis of finite length measurement signals. In: The 3rd International Conference on Advanced Model Measurement Technology for the EU Maritime Industry (AMT'13), Gdansk, Poland, pp. 260–274.

Brouwer, J., Tukker, J., Van Rijsbergen, M., 2015. Uncertainty analysis and stationarity test of finite length time series signals. In: The 4th International Conference on Advanced Model Measurement Technology for the EU Maritime Industry (AMT'15), Istanbul, Turkey.

Canham, H., 1974. Resistance, propulsion and wake tests with HMS penelope. In: Transact. Roy. Instit. Naval Archit., pp. 61–94.

Conn, J.F.C., Lackenby, H., Walker, W.P., 1953. B.S.R.A. resistance experiments on the "Lucy Ashton". Part II - the ship-model correlation for the naked hull conditions. In: Proceedings of the Spring Meeting of the Institution of Naval Architects, London, United Kingdom.

Denny, M.E., 1951. B.S.R.A. resistance experiments on the "Lucy Ashton". Part I - full-scale measurements. In: Proceedings of the International Conference of Naval Architects and Marine Engineers, London, United Kingdom.

Eça, L., Hoekstra, M., 2014. A procedure for the estimation of the numerical uncertainty of CFD calculations based on grid refinement studies. J. Comput. Phys. 262, 104–130. https://doi.org/10.1016/j.jcp.2014.01.006

Froude, W., 1874. On experiments with HMS Greyhound. Transact. Roy. Instit. Naval Archit. 15, 36–73.

Granville, P.S., 1974. A modified froude method for determining full-scale resistance of surface ships from towed models. J. Ship Res. 18 (04), 215–223. https://doi.org/10.5957/jsr.1974.18.4.215

Hiraga, Y., 1934. Experimental investigations on the resistance of long planks and ships. In: Transact. Instit. Naval Archit.. 76, p. 284.

ITTC, 1999. The propulsion committee: final report and recommendations to the 22nd ITTC. In: Proceedings of the 22nd ITTC, Seoul/Shanghai, South Korea/China.

ITTC, 2008. The specialist committee on powering performance prediction: final report and recommendations to the 25th ITTC. In: Proceedings of the 25th ITTC, Fukuoka, Japan.

ITTC, 2021. Determination of a type a uncertainty estimate of a mean value from a single time series measurement. In: ITTC Quality System Manual Recommended Procedures and Guidelines.

Joubert, P.N., Matheson, N., 1970. Wind tunnel tests of two Lucy Ashton reflex geosims. J. Ship Res. 14 (04), 241–276. https://doi.org/10.5957/jsr.1970.14.4.241

Kühl, N., 2021. Adjoint-Based Shape Optimization Constraint by Turbulent Two-Phase Navier-Stokes Systems. Ph.D. thesis. Hamburg University of Technology.

Kühl, N., Rung, T., 2022. Discrete adjoint momentum-weighted interpolation strategies. J. Comput. Phys. 467, 111474. https://doi.org/10.1016/j.jcp.2022.111474

Lackenby, H., 1954. B.S.R.A. resistance experiments on the "lucy ashton". Part III - the ship-model correlation for the shaft-appendage conditions. In: Proceedings of the Autumn Meeting of the Institution of Naval Architects, Torquay, United Kingdom.

Lopes, R., Eslamdoost, A., Johansson, R., RoyChoudhury, S., Bensow, R.E., Hogström, P., Ponkratov, D., 2025. Resistance prediction using CFD at model-and full-scale and comparison with measurements. Ocean Eng. 321, 120367. https://doi.org/10.1016/j.oceaneng.2025.120367

Menter, F.R., 1994. Two-Equation Eddy-viscosity turbulence models for engineering applications. AIAA J. 32 (8), 1598–1605. https://doi.org/10.2514/3.12149

Nordström, H.F., 1953. Full scale tests with the "Wrangel" and comparative model tests. In: SSPA Paper 27.

Ponkratov, D., 2017. Lloyd's Register's full-scale numerical modelling workshop.

Queutey, P., Visonneau, M., 2007. An interface capturing method for free-surface hydrodynamic flows. Comput. Fluid. 36 (9), 1481–1510. https://doi.org/10.1016/j.compfluid.2006.11.007

Rung, T., Wöckner, K., Manzke, M., Brunswig, J., Ulrich, C., Stück, A., 1999. Challenges and perspectives for maritime CFD applications. In: Jahrbuch Der Schiffbautechnischen Gesellschaft.

Smith, S.L., 1955. B.S.R.A. resistance experiments on the "lucy ashton". part IV - miscellaneous investigations and general appraisal. In: Proceedings of the Spring Meeting of the Institution of Naval Architects, London, United Kingdom.

Smits, A.J., Matheson, N., Joubert, P.N., 1980. Some experiments on artificially roughened Lucy Ashton geosims. J. Ship Res. 24 (03), 170–180. https://doi.org/10.5957/jsr.1980.24.3.170

ПРИЛОГ 10

Journal of
Marine Science and Engineering

MDPI

Article

CFD-Powered Ship Trim Optimization: Integrating ANN for User-Friendly Software Tool Development

Matija Vasilev [1,2,*], Milan Kalajdžić [1,2] and Ines Ivković [1]

[1] Faculty of Mechanical Engineering, University of Belgrade, 11000 Belgrade, Serbia; mdkalajdzic@mas.bg.ac.rs (M.K.); iivkovic@mas.bg.ac.rs (I.I.)
[2] Ocean Pro Marine Engineers Ltd., 11000 Belgrade, Serbia
* Correspondence: matija@oceanpro.eu; Tel.: +381-631-076-996

Abstract: This study presents a comprehensive approach to trim optimization as an energy efficiency improvement measure, focusing on reducing fuel consumption for one RO-RO car carrier. Utilizing Computational Fluid Dynamics (CFD) software, the methodology incorporates artificial neural networks (ANNs) to develop a mathematical model for estimating key parameters such as the brake power, daily fuel oil consumption (DFOC) and propeller speed. The complex ANN model is then integrated into a user-friendly software tool for practical engineering applications. The research outlines a seven-phase trim optimization process and discusses its potential extension to other types of ships, aiming to establish a universal methodology for CFD-based engineering analyses. Based on the trim optimization results, the biggest DFOC goes up to 10.5% at 7.5 m draft and up to 8% for higher drafts. Generally, in every considered case, it is recommended to sail with the trim towards the bow, meaning that the ship's longitudinal center of gravity should be adjusted to tilt slightly forward.

Keywords: EEDI; EEXI; CII; CFD; ANN; trim optimization

Citation: Vasilev, M.; Kalajdžić, M.; Ivković, I. CFD-Powered Ship Trim Optimization: Integrating ANN for User-Friendly Software Tool Development. *J. Mar. Sci. Eng.* **2024**, *12*, 1265. https://doi.org/10.3390/jmse12081265

Academic Editors: Nastia Degiuli and Ivana Martić

Received: 17 June 2024
Revised: 17 July 2024
Accepted: 18 July 2024
Published: 27 July 2024

1. Introduction

With the aim to reduce emissions of greenhouse gasses, in 2013, the International Maritime Organization (IMO) introduced the Energy Efficiency Design Index (EEDI) for new ships and later, in 2023, the Energy Efficiency for Existing Ships Index (EEXI). These new measures initiated changes in the shipbuilding industry. By implementing these regulations, it is anticipated to reduce global CO_2 emissions by 40% by the year 2030 and 70% (or at least 50%) by the year 2050, compared to the levels in 2008. All ships that fall under MARPOL Annex VI and have gross tonnage over 400 must meet the set criteria, which are based on nominal ship data. The IMO determined the parameters and procedure for calculating the required EEDI and EEXI, as well as the formula for calculating the attained EEDI/EEXI that must be lower than the required values. The required value for the EEDI is determined by the formula:

$$\text{Required EEDI} = a(\text{DWT})^{-c}, \tag{1}$$

where parameters a and c are based on the regression curve fit [1] of data from ships that were built between 1999 and 2009, and also depend on the type of ship. The required EEDI decreases over the years according to the formula:

$$\text{Attained EEDI} \leq \text{Required EEDI} = (1 - X/100) \cdot \text{Reference line value}, \tag{2}$$

where X is the specified reduction factor given in [2] through four phases. Values for the EEXI are based on the required EEDI, taken into account with the adequate reduction factor from [3]. The requirements for the EEXI are becoming slightly stricter with time, with the plan for the EEXI and EEDI to become equal in 2025. In addition to the two mentioned

energy efficiency parameters, the IMO introduced operational efficiency indicators. In 2009 [4], the Energy Efficiency Operational Indicator (EEOI) was invented and is defined as the ratio of emitted CO_2 per unit of transport work. The EEOI never became mandatory, but it is a representative value of the ship's operational energy efficiency level for a consistent period of time. Another indicator came into force in 2023, the Carbon Intensity Index (CII), which is calculated as the ratio of the total mass of emitted CO_2 to the total transport work undertaken in a specific calendar year, considering the traveled distance, time spent underway and the amount of consumed fuel over a period of one year. As well as for the EEDI and EEXI, the attained [5] and required [6] values are also calculated for the CII, where the attained CII has to be lower than the required, which decreases over time [7]. Based on the attained CII, the ship belongs to one of five energy efficiency categories (A, B, C, D, E). The boundaries between those categories and the calculation method for each ship type are defined in [8] and they depend on the ship's DWT. Since the CII is a mandatory parameter, all ships of gross tonnage of 5000 or more are from 2019 obliged to record the relevant information (traveled distance, time spent underway and the amount of consumed fuel over a period of one year) under the Data Collection System (DCS) [9]. In the case that a ship achieved class E for at least one year, or class D for three years in a row, it must create a plan for reducing CO_2 emissions and satisfy the requirements for at least class C [10]. In 2013, the IMO introduced the Ship Energy Efficiency Management Plan (SEEMP), which consists of three parts: a ship management plan to improve energy efficiency, a ship fuel oil consumption data collection plan and a ship operational carbon intensity plan. Part I applies to all ships that fall under MARPOL Annex VI and have gross tonnage over 400, while Part II and Part III apply for ships that have gross tonnage over 5000 and fall under MARPOL Annex VI.

Various measures can be considered in order to meet the energy efficiency requirements developed by the International Maritime Organization and attain a reduction in CO_2 emissions. Those measures are divided into two categories: operational methods and technical methods. Operational methods include the following: improvement in voyage execution [11,12], reduction in auxiliary power consumption [11,13], weather routing [10,12], "just in time" voyage [13], optimum ballast [10,12], optimum cargo distribution [12], energy-saving utilities [14], optimum use of rudder and heading control systems [10], optimized hull and propeller maintenance [10], speed optimization [12,15], slow steaming [16,17] and trim optimization [12,18].

These measures can be applied for both existing ships as well as new ships. Technical measures are design-related and therefore more favorable for new ships. These measures refer to wind-assisted propulsion, fuel type change [10,16,19], waste heat recovery [12], upgrading and maintenance of propulsion system, hull retrofit (bulb and/or stern modification, installation of energy-saving devices [10], etc.

Optimum trim means that the angle of the trim for a specific operating condition, regarding the displacement and speed, provides minimum resistance, which directly implies the optimal efficiency level [12]. The resistance of the ship changes depending on the trim, although the displacement and speed stay the same [20]. The beneficial aspect of trim optimization is that neither a hull modification nor engine upgrade is needed. The ship is trimmed if the draught at the bow differs from the draught at the aft section of the ship. While a negative trim indicates that the draught at the bow is greater than the draught at the stern, a positive trim implies the opposite. Every vessel is optimized for a number of conditions (even keel at full load and design speed, ballast condition, etc.), but the actual operating conditions usually differ from the expected ones [21]. It was confirmed in [22] that the trim can affect the total resistance of a ship for various service speeds and the optimum trim for every speed is different. The trim optimization method is intended for minimizing the resistance in calm water and therefore minimizing fuel consumption, which can be accomplished with a specially developed program for the ship. The results of [18] indicate the possibility of reducing the total fuel consumption during a whole voyage by 1.2% by utilizing the calculated optimum trim for the whole voyage. A 4250 TEU container ship sea

trial with the use of a trim optimizing program reported a main engine power reduction of 910 kW and energy-saving rate of 9.2% [23]. The trim of the ship can be influenced by the redistribution of ballast, fuel and/or load between tanks. Parameters that change when the ship is trimmed compared to an even-keel condition are a wetted surface area, the length of the waterline and a submerged hull form at the bow as well as at the stern [24]. Potential disadvantages of this method could be a reduction in visibility, reduced freeboard, emergence of the propeller [25], underkeel clearance, seakeeping, maneuverability [26], seakeeping [27] and shipped water on deck [28], and those should as well be taken into account while finding the optimum trim for an operating condition.

Calculating the ship resistance in calm water by conducting model tests and numerical simulations provides data about the resistance for different drafts and trims. As a result, a set of curves with highlighted lowest resistance for a specific draft are obtained, as in [22,29]. While onboard tools have this information at their disposal, model tests are still common and basins are equipped with traditional procedures and up-to-date insights to provide their proper execution, pursuing the measurement of small power variations within a foreseen range of 0 to 4% of the total installed power [30], or a 2% to 4% fuel consumption reduction [31]. With the advancement of technology and computers, CFD software calculations provide trim tables with an accuracy that can compete with the results gained from traditional model tests, with even less investments. Other methods that can be used to determine the optimum trim are sea trials and machine learning methods. The shortcomings of these methods are that sea trials are fuel- and time-consuming for determining the optimum ballast, while for obtaining information about the optimum trim with the machine learning method, a lot of data from a ship's past voyages are needed [32]. In this study, the aim of this work is focused only on applying the CFD method on one RO-RO car carrier in order to optimize the trim for an energy-efficient voyage and exploitation.

The application of the CFD method for trim optimization for different ship types can be found in various existing studies. For example, in the study by [20], the effect of trim optimization for a container ship like MOERI (KCS) was a total resistance reduction of 2%, similar to the results of trim optimization for a US Navy ship [13]. A CFD investigation of the propulsion performance of a low-speed VLCC tanker at various initial trim angles was conducted by [33] and showed a 1.76–2.12% total resistance reduction. The authors of [34] and [35] report even greater profit, such as fuel savings of up to 5% [34] and a 6% reduction in delivered horsepower [35]. Since the trim conditions can vary significantly, so do the results from trim optimization. The authors of [36] highlight that in Series 60, the total resistance between the worst and best trims varies by up to 11%. The trim optimization of a bulk carrier in [37] results in a total resistance reduction possibility of up to 14%. Savings for RO-RO ships were studied by [12] and indicated a possibility of up to a 10.4% reduction in delivered power, or 1.2 t fuel per day. In addition to the calculation of the optimal trim, specialized software for input parameters that quickly provide information about the optimal trim has been mentioned [35,38].

Up to now, artificial neural networks (ANNs) have found application in predicting fuel consumption, as demonstrated in the studies by [39] and [40], which focused on utilizing NOON reports. Furthermore, an ANN has been employed for forecasting the ship speed, as evidenced by the work of [41]. Moreover, research efforts have extended to utilizing ANNs for the joint prediction of the ship speed and fuel consumption, leveraging data from sails, particularly in the case of a barquentine, as explored by [42]. The study by [43] proposes a real-time hybrid electric ship energy efficiency optimization model considering time-varying environmental factors, aiming to optimize the EEOI under wind and wave conditions while maintaining speed limits, resulting in an average reduction in fuel consumption of 13.4% and real-time EEOI of 15.2%. In [44], a real-time prediction model of ship fuel consumption through BP neural network training-related data is presented and further used for ship speed optimization. The research of [45] developed an ANN model to predict the main engine power and pollutant emissions of 3020 container, cargo and tanker

ships using 14 parameters, demonstrating its potential for use in future studies on fuel consumption and energy efficiency in maritime transport.

In today's complex technological landscape, the integration of various disciplines is becoming increasingly vital for tackling engineering challenges. By bridging the fields of naval engineering, CFD, ANN and practical application development, this study not only underscores the importance of multidisciplinary association but also showcases its benefits in addressing real-world problems within the maritime industry. Through the synergy of these varied fields, novel solutions can be developed to optimize ship operations or design, enhance fluid flow analysis accuracy and streamline decision-making processes. Moreover, the utilization of an ANN enables the creation of sophisticated mathematical models that can effectively capture complex relationships and patterns within maritime systems, paving the way for more precise simulations and predictive analytics. Furthermore, the development of user-friendly applications facilitates the seamless implementation of these advanced methodologies, empowering stakeholders to leverage cutting-edge insights for improved vessel performance and operational efficiency. Essentially, this methodology not only promotes scientific comprehension but also encourages innovation and pragmatic breakthroughs in the field of maritime engineering, thus helping in the long-term growth of maritime technologies.

2. Methods

The conducted work consists of several phases: (1) 3D modeling; (2) first-level verification of the reliability of the digital twin (3D model); (3) open water test (OWT); (4) second-level verification of the reliability of the 3D model; (5) trim optimization; (6) determination of a mathematical model for assessing the optimal trim, ship speed, engine (brake) power, daily fuel consumption and propeller speed; (7) programming an application based on previously conducted analyses. In this study, various software has been used: StarCCM+ version 2021.3 for CFD analysis, aNETka for mathematical model determining and MATLAB (version 2020b) for application development. The goal of this paper, in addition to trim optimization, is to establish an initial procedure for setting up CFD simulations. Therefore, this chapter provides only a brief overview of the governing equations used to solve the problem of ship movement through two fluids. More attention is given to functions that are not predefined in the StarCCM+ software, which the user can define. Consequently, this paper includes formulas that can be found in various publications, ensuring that everything complies with the requirements and guidelines issued by relevant institutions in the maritime industry.

In Table 1, the ship's (RO-RO car carrier) principal particulars are given.

Table 1. Principal particulars.

Parameter *	Dimension	Value
L_{pp}	(m)	158
B	(m)	28
H	(m)	30.65
T_s	(m)	7.8

* L_{pp}—length between perpendiculars, B—breadth, H—depth, T_s—draft.

Propeller geometry characteristics are presented in Table 2.

Table 2. Propeller characteristics.

Parameter *	Dimension	Value
D	(m)	5.5
No. of blades	(-)	5
BAR	(-)	0.83
D_{hub}	(m)	0.98

Table 2. *Cont.*

Parameter *	Dimension	Value
Chord length at $0.7R_p$	(m)	2.0988
P/D at $0.7R_p$	(-)	0.9594

* D—diameter, BAR—blade area ratio, D_{hub}—hub diameter, R_p—propeller radius, P—pitch.

2.1. Three-Dimensional Modeling

Three-dimensional modeling is the first necessary step before conducting CFD simulations. Creating a 3D representation of the RO-RO vessel involved using existing documentation: hull construction drawings, rudder construction drawings and propeller drawings. This digital twin includes detailed modeling of the hull, rudder and propeller, with the goal of faithfully capturing the ship's attributes and performance.

2.2. First-Level Verification

First-level verification involves comparing hydrostatic data such as volume displacement (∇), block coefficient (C_b), longitudinal center of buoyancy (LCB) and wetted surface (WS) of the 3D model with data given in the Trim & Stability booklet for various drafts. No parameter should deviate more than 1% from (as per authors' experience, 1% deviation enables enough accuracy) its corresponding value given in the Stability Booklet.

2.3. Open Water Test

The OWT is a method for determining propeller characteristics such as thrust coefficient, torque coefficient and propeller efficiency. The procedure for determining these coefficients through model tests is defined in [46]. In this case, model testing was not conducted; instead, propeller parameters were determined through CFD simulation, following the procedure described in [47]. According to this document, the CFD results of the OWT are considered valid if they do not differ by more than 3% from the results obtained by model testing within the relevant propeller operating range. It is also emphasized that if the model test results of the propeller are not known, an additional OWT with the appropriate B-series propeller model should be conducted. An appropriate B-series propeller is considered one with the same geometric characteristics (diameter, pitch, ratio of characteristic areas) as the original propeller installed on the considered ship. The 3D model of the B-series propeller was obtained using the B-series Propeller Generator available online [48]. The OWT results of the B-series propeller should not deviate by more than 3% from the results obtained with the mathematical model for the same geometric parameters. If this condition is met, the same CFD calculation methodology is applied to the original propeller, and the results obtained this way are considered valid. A mathematical model can be found in [49].

The simulations are conducted using a steady-state numerical flow model, solved in the rotating frame of reference. The numerical method used is called Multiple Reference Frames (MRFs), where in one part of the domain, the equations are solved in a rotating frame of reference, while in the rest of the domain, a stationary frame of reference is used.

Figure 1 shows the domain of the open water test CFD setup. The outer cylinder shows the far-field boundary of the domain, while the inner, smaller cylinder represents the boundary between the rotational frame of reference and stationary frame of reference. The diameter and length of the small cylinder are 4D, while the diameter and length of the large cylinder are 10D. The propeller is positioned downstream from the shaft. All simulations are conducted in full scale.

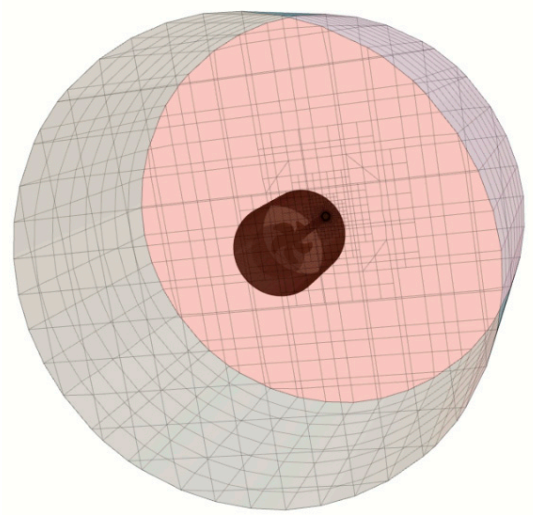

Figure 1. Domain of conducted open water test simulations.

The same grid refinement options were used for both propeller grids (B-series propeller and original propeller) and are presented in Figure 2.

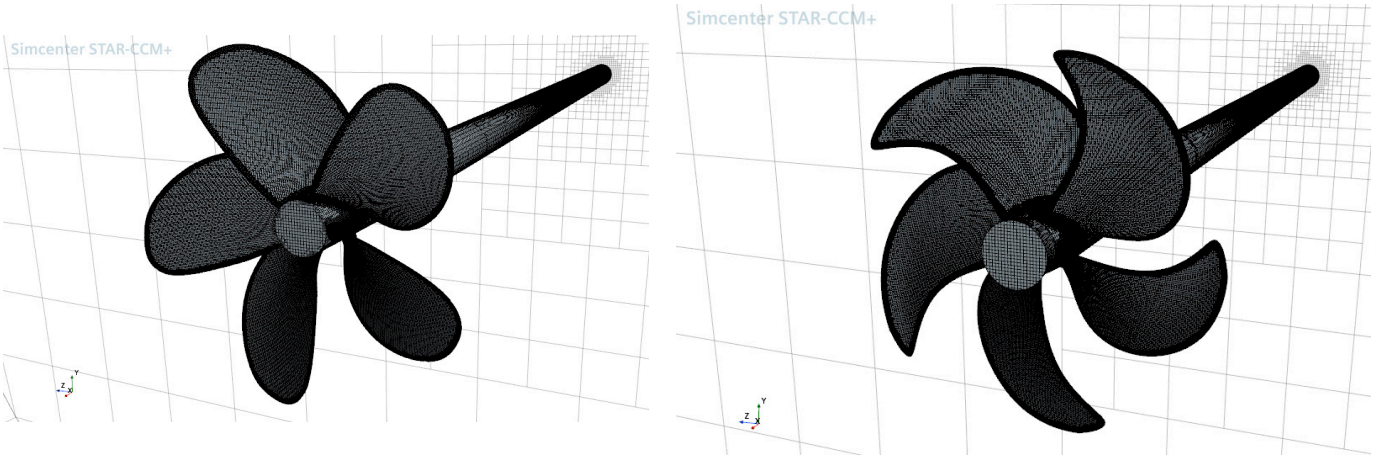

(**a**) (**b**)

Figure 2. Grid of the propellers: (**a**) B-series propeller; (**b**) original propeller.

Turbulence modeling is performed using the k-ω SST model as is required by [47]. The inflow turbulence intensity was set to 1% relative to the inflow speed. The inflow speed conditions and rotation rate of the propeller are selected to closely resemble the conditions expected at self-propulsion conditions.

2.4. Second-Level Verification

Second-level verification involves conducting a CFD simulation for a draft for which there are available results from the model tests or sea trials. The difference between the results obtained by the CFD analysis and model tests/sea trials should not be greater than 5% [47]. This kind of verification is typical in applied CFD analysis in the maritime industry [50,51].

The equations are discretized using the collocated Volume of Fluid (VOF) multiphase method implemented within the software. It is used for large-scale two-phase (in this case, sea water (ρ_w = 1.025 t/m^3) and air (ρ_A = 1.212 kg/m^3) at 18 °C) flows encountered in

naval hydrodynamics. A two-phase, incompressible, turbulent and viscous flow model is employed, governed by the continuity and Navier–Stokes equations:

$$\nabla \cdot (\rho V) = 0, \tag{3}$$

$$\frac{\partial(\rho V)}{\partial t} + \nabla \cdot (\rho V \otimes V) = -\nabla \cdot (p\mathbf{I}) + \nabla \cdot \mathbf{T}_{\mathrm{v}} + f_b, \tag{4}$$

where V stands for the velocity vector field, p is the pressure, $\mathbf{T}_{\mathrm{v}}$ is the viscous stress tensor and f_b is the resultant of the body forces.

The VOF multiphase Eulerian approach model implementation in Simcenter STAR-CCM+ belongs to the family of interface-capturing methods that predict the distribution and the movement of the interface of immiscible phases. This modeling approach assumes that the mesh resolution is sufficient to resolve the position and the shape of the interface between the phases. In this paper, the focus is not on elaborating the theoretical background of the functions in CFD software, but rather on presenting a methodology that can serve as a quick way to set up simulations. Therefore, more about the VOF method can be found in [52], where this concept is detailed.

An important quality of a system of immiscible phases (air and water) is that the fluids always remain separated by a sharp interface. The High-Resolution Interface Capturing (HRIC) scheme is used to mimic the convective transport of immiscible fluid components, resulting in a scheme that is suited for tracking sharp interfaces.

As in the OWT, the k-ω SST turbulence model was used here according to the requirements defined in [47].

2.4.1. Actuator Disk Propeller Model

The body force propeller method is used to model the effects of a propeller such as thrust and thereby creating propulsion without actually resolving the geometry of the propeller. The method employs a uniform volume force distribution over the cylindrical virtual disk. The volume force varies in the radial direction, so the total force can be calculated as the volume integral for the whole modeled cylinder. The radial distribution of the force components follows the Goldstein optimum [53] and is given by

$$f_{bx} = A_x r* \sqrt{1 - r*}, \tag{5}$$

where $r*$ is the normalized disk radius defined as

$$r* = \frac{r' - r'_h}{1 - r'_h}, \tag{6}$$

where $r' = r/R_p$ and $r'_h = R_h/R_p$. Volume force f_{bx} is the body force component in the axial direction, r is the radial coordinate, R_h is the hub radius and R_p is the propeller tip radius. Coefficient A_x is defined as

$$A_x = \frac{105}{8\pi} \frac{T}{t_d (R_p - R_h)(3R_h + 4R_p)}, \tag{7}$$

where T stands for the propeller thrust and t_d is the virtual disk thickness. More about this can be found in [54]. The simulation is performed for a certain operating point specified by the thrust (T). The advance ratio is calculated by solving the following equation numerically (J—advance coefficient, D—propeller diameter):

$$f(J) = K_T - K'_T \tag{8}$$

where K_T is evaluated from the propeller performance curve and K'_T is evaluated as

$$K'_T = \frac{J^2 T_{Operating\ point}}{\rho_w V_A^2 D^2} \tag{9}$$

With K_T available, the thrust is calculated for the propeller:

$$T = \frac{K_T \rho_w V_A^2 D^2}{J^2} \tag{10}$$

With $T(T_{Operating\ point})$ available, the axial body force component can be calculated. Inflow plane is the plane inside the actuator disk where the volume-averaged velocity and density are computed. The input thrust in this part of the simulation is equal to the total resistance that is evaluated as the sum of the pressure resistance and viscous resistance of the hull with the rudder included.

The wake fraction (w) is extracted at the propeller axis plane in a steady resistance simulation.

The thrust deduction factor is calculated as per

$$t = 1 - \frac{R_T}{T}, \tag{11}$$

where R_T is the total resistance of the ship evaluated in the steady resistance simulation.

2.4.2. Steady Resistance Simulations

Total resistance, including viscous and pressure resistance, is obtained by rerunning the self-propulsion simulation with a disabled actuator disk. This procedure implies the same mesh as was used earlier but only without an actuator disk.

2.4.3. Boundary Conditions

Fluid domain dimensions are defined as follows (from origin):

- Inlet: $2.5L_{pp}$—defined as velocity inlet;
- Outlet: $3L_{pp}$—defined as pressure outlet with wave damping boundary option included;
- Bottom: $1.5L_{pp}$—defined as velocity inlet;
- Top: $1L_{pp}$—defined as velocity inlet;
- Port Side: $2L_{pp}$—defined as symmetry plane with wave damping boundary option included;
- Starboard Side: $2L_{pp}$—defined as symmetry plane with wave damping boundary option included.

The wave damping length is defined as two wave lengths, where the wave length is calculated as per

$$2\pi \cdot \mathrm{Fn}_L^2 \cdot L_{pp}, \tag{12}$$

where Fn_L^2 is the Froude number based on the length.

2.4.4. Rigid Body Motion

Two degrees of freedom are allowed for the motion for the vessel, namely pitch and heave, allowing for the dynamic trim and sinkage of the vessel.

2.4.5. Mesh

The triangle surface meshing method has been used to build the mesh. The prism-layer mesher generates prismatic cell layers next to the boundary layer. The number of these layers is calculated as per

$$m = \frac{\ln\left(1 - (1 - sf)\frac{\delta}{y_1}\right)}{\ln(sf)}, \tag{13}$$

where $sf = 1.3$ is the stretch factor, δ is the boundary-layer thickness and y_1 is the first-layer thickness. These cells help to capture the viscous effects in the boundary layer correctly in the region where the thickness is calculated as per [55]

$$\delta = \frac{0.16 L_{wl}}{\sqrt[7]{\mathrm{Re}_{L_{wl}}}}, \tag{14}$$

where L_{wl} is the length at the waterline of the ship and Re is the Reynolds number (L_{wl} in subscription means that the Reynolds number is calculated with the waterline length as a reference value, otherwise L_{pp} is used). The trimmed cell mesher creates a volume mesh by cutting a template mesh with the surface geometry. The first-layer thickness is calculated for y^+ = 150 by following the guidelines in [47] where it is emphasized that y^+ should be in a range from 30 to 300. This value (150) is used as the target factor to ensure that the actual y^+ values will fall within the required range.

$$y_1 = \frac{150\nu}{u_\tau}, \tag{15}$$

where ν is the kinematic viscosity and u_τ is the shear velocity. The shear velocity or frictional velocity is a fictious quantity, it characterizes the shear at the boundary layer, and it is given by

$$u_\tau = \sqrt{\frac{\tau_w}{\rho_w}}, \tag{16}$$

where τ_w is the wall shear stress. This presents a contradiction as follows: determining the thickness of the initial layer requires knowing the stress on the vessel's hull, which in turn needs to be assessed using CFD. Hence, the recommendation from the ITTC [46,56] is utilized in this scenario to compute the wall shear stress for the hull.

$$\tau_w = 0.5((1+k)C_{FS} + C_A)V_s^2 \rho_w, \tag{17}$$

where k is a form factor, C_{FS} is the frictional resistance coefficient and C_A is the correlation allowance.

$$C_{FS} = \frac{0.075}{\left(\log_{10}\mathrm{Re} - 2\right)^2}, \tag{18}$$

$$C_A = \left(5.68 - 0.6\log_{10}\mathrm{Re}\right) \cdot 10^{-3} \tag{19}$$

The form factor is calculated as the mean value of the equations obtained by Grigson, Wright and Conn and Ferguson given in [57]:

$$k = \frac{0.028 + 3.3\left(\frac{WS}{L_{pp}^2}\sqrt{C_B\frac{B}{L_{pp}}}\right) + 18.7\left(C_B\frac{B}{L_{pp}}\right)^2 + 2.48C_B^{0.1526}\left(\frac{B}{T_s}\right)^{0.0533}\left(\frac{B}{L_{pp}}\right)^{0.3856} - 1}{3}. \tag{20}$$

A grid convergence study is performed to assess the convergence of the results by systematically refining a specific input parameter in StarCCM+. In this study, three simulations are conducted, where the chosen input parameter is varied while keeping all other parameters constant. The refinement value used in this study aligns with the guidelines specified in [58] and is set to be uniform ($\sqrt{2}$). By systematically refining the input parameter and comparing the results from the different simulations, the grid convergence study aims to determine the level of convergence and establish the appropriate grid resolution for accurate and reliable results.

The convergence ratio is defined as

$$R = \frac{\varepsilon_{21}}{\varepsilon_{32}}, \tag{21}$$

where ε_{21} is the difference between the solution obtained using medium and fine mesh and ε_{32} is the difference between the solution obtained using coarse and medium mesh. R is used for the estimation of the convergence conditions: monotonic convergence is achieved when $0 < R < 1$, oscillatory convergence is achieved when $-1 < R < 0$ and divergence is achieved when $|R| > 1$. The numerical uncertainty and error for monotonic convergence condition is estimated using generalized Richardson extrapolation (RE). The order of accuracy is calculated as per

$$p = \frac{\ln(\varepsilon_{32}/\varepsilon_{21})}{\ln\sqrt{2}}, \tag{22}$$

$$\delta_{RE} = \frac{\varepsilon_{21}}{\sqrt{2}^p - 1}, \tag{23}$$

The generalized RE solution ($\hat{S}_{RE}$) can be derived by

$$\hat{S}_{RE} = \hat{S}_1 - |\delta_{RE}|. \tag{24}$$

To estimate the grid uncertainty U_G, a safety factor approach is employed, defining U_G as

$$U_G = FS \cdot |\delta_{RE}|, \tag{25}$$

where $FS = 1.25$ is a safety factor. The normalized uncertainties are calculated as follows:

$$\overline{U} = \frac{U_G}{\hat{S}_{RE}} \cdot 100\%. \tag{26}$$

2.4.6. Post-Processing

In the numerical simulations conducted for this study, the direct consideration of the roughness effects and air resistance resulting from the presence of a superstructure is not included. However, these effects are accounted for in the post-processing stage by following the recommended procedures and guidelines outlined in [59]. The ITTC guidelines provide specific methodologies for incorporating the effects of the roughness and air resistance into the analysis, allowing for an assessment of the overall performance and characteristics of the ship. The roughness allowance (ΔC_F) is calculated as per [60]

$$\Delta C_F = 0.044\left[\left(\frac{k_s}{L_{WL}}\right)^{\frac{1}{3}} - 10\mathrm{Re}^{-\frac{1}{3}}\right] + 0.000125 \tag{27}$$

and the air resistance coefficient (C_{AAS}) [54] is

$$C_{AAS} = 0.8\frac{\rho_A \cdot A_{VS}}{\rho_w \cdot WS}, \tag{28}$$

where k_s indicates the roughness of the hull surface equals $150{\cdot}10^{-6}$ m [58], and A_{VS} is the projected area of the ship superstructure to the transverse plane. The new total resistance is calculated as

$$F_T' = \frac{1}{2}V_s^2 \cdot WS \cdot \rho_w \cdot (C_T + \Delta C_F + C_{AAS}), \tag{29}$$

where C_T refers to the total resistance coefficient obtained as a result of the CFD simulation.

The new thrust is calculated as per

$$T' = \frac{R_T'}{1 - t'} \tag{30}$$

Together with the propeller performance data (K_T, K_Q, $\eta_0(J)$), the new operating point is obtained by the numerical solving of equation:

$$\frac{T'}{\rho_w \cdot V_A^2 \cdot D^2} J^2 - K_T(J) = 0 \tag{31}$$

Once the advance ratio coefficient is obtained, the propeller speed (n) and torque (Q_0) can be evaluated:

$$n = \frac{V_A}{JD} = \frac{(1-w')V}{JD}, \tag{32}$$

$$Q_0 = K_Q \rho_w n^2 D^5, \tag{33}$$

where K_Q is evaluated from the propeller performance curve and Q_0 is the torque in the open water condition. Hence, the actuator disk approach has been used in this case and the relative rotative efficiency is adopted to be 1, which means that the torque is calculated as

$$Q = \frac{Q_0}{\eta_R} \approx Q_0 \tag{34}$$

Finally, the brake power can be evaluated as

$$P_b = \frac{2n\pi Q}{\eta_S}, \tag{35}$$

where η_S is the shaft efficiency, adopted to be 0.99. The hull efficiency is considered to be the same as in the steady resistance simulations, i.e., $w' = w$ and $t' = t$, where w' and t' are the wake fraction coefficient and thrust deduction factor in post-processing.

Calibration factors C_n and C_{Pb} are calculated as the average ration between the model test (MT) results and CFD results for the propeller speed (n) and brake power (P_b).

$$C_n = \frac{n_{MT}}{n_{CFD}} \tag{36}$$

$$C_{Pb} = \frac{P_{b_{MT}}}{P_{b_{CFD}}} \tag{37}$$

2.5. Trim Optimization

Trim optimization was conducted for drafts of 7.5 m, 8 m and 8.7 m at speeds of 12.5 kn, 15 kn and 18 kn at 7 different conditions (trims). The range of trims goes from −1.5 m to 1.5 m with a 0.5 m step. A negative sign means the trim by the bow and a positive sign, the trim by the stern. The outcome of trim optimization in CFD analysis typically involves determining the optimal trim settings for a vessel at considered drafts and speeds. This optimization aims to minimize resistance and ensure optimal performance under different operating conditions. By adjusting the vessel's trim, operators can achieve better hydrodynamic characteristics, leading to improved overall performance and operational efficiency. With the available specific fuel oil consumption (SFOC) curve as a function of P_b, a possible reduction in fuel consumption was also calculated.

2.6. Mathematical Model for Assessing the Outcomes from Trim Optimization

The first outcomes from the CFD simulations are the brake power and propeller speed for one ship speed and draft, i.e., trim, i.e., displacement. The results are presented in the form of relative differences between the brake power of the trimmed ship and the ship on an even keel. A negative sign indicates that there is a saving, i.e., a reduction in the required brake power for that case. A graphical example of the results is shown in Figure 3a, where the relative brake power and fuel oil consumption savings are depicted as an area with the ship speed on the x-axis, trim on the y-axis and relative power/fuel oil consumption

savings on the z-axis. The optimal (favorable) sailing zone is depicted in green on the same diagram, meaning that at the current trim and speed, less power or fuel oil consumption is required compared to when the ship is sailing on an even keel. The yellow zone represents the transitional zone where the change in the required brake power/fuel oil consumption is negligible, while the red zone is the zone to be avoided because more power/fuel oil is needed for the ship to sail at the same speed compared to sailing on an even keel. Each point on the surface in Figure 3a corresponds to a certain displacement, where it depends solely on the trim. For easier calculation, a surface ∇ (trim, V_s) is formed from each line ∇ (trim), and the surfaces for all three considered drafts are shown in Figure 3b. In order to have smooth surfaces, all values estimated from the CFD analysis are linearly interpolated. Therefore, the initial matrix 3×7 (3 speeds, 7 trims) is reshaped to 151×111 with a speed step of 0.05 kn and trim step of 0.02 m. The main parameters from the initial matrix are depicted with black lines in Figure 3a.

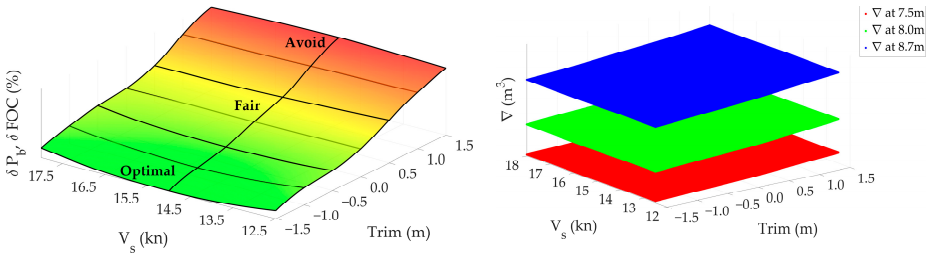

(**a**) (**b**)

Figure 3. Results representation: (**a**) brake power/fuel oil consumption reduction for one draft; (**b**) displacements for three considered drafts and each trim.

Additionally, values between drafts of 7.5 m and 8 m and from 8 m to 8.7 m are linearly interpolated with a step of 0.01 m. Thus, from the initial matrix of $3 \times 7 \times 3$ (3 speeds, 7 trims, 3 drafts), matrices (Σ_m) of size $151 \times 111 \times 120$ are obtained where m is δP_b or ∇.

The daily fuel oil consumption (DFOC) is estimated based on the determined brake power from the CFD simulation and the available specific fuel oil consumption (SFOC) curve for the engine installed on the ship. The SFOC curve is approximated by a sixth-degree polynomial:

$$\text{SFOC} = -5.54 \cdot 10^{-23} {P_b}^6 + 3.75 \cdot 10^{-18} {P_b}^5 - 8.28 \cdot 10^{-14} {P_b}^4 + 8.00 \cdot 10^{-10} {P_b}^3 - 3.11 \cdot 10^{-6} {P_b}^2 - 9.63 \cdot 10^{-4} P_b + 209 \quad (38)$$

The mentioned polynomial provides SFOC values with an average error of 0.02% compared to the exact available values from the reference document.

With the evaluated DFOC for each brake power, the same diagrams as shown in Figure 4 can be created (Figure 5).

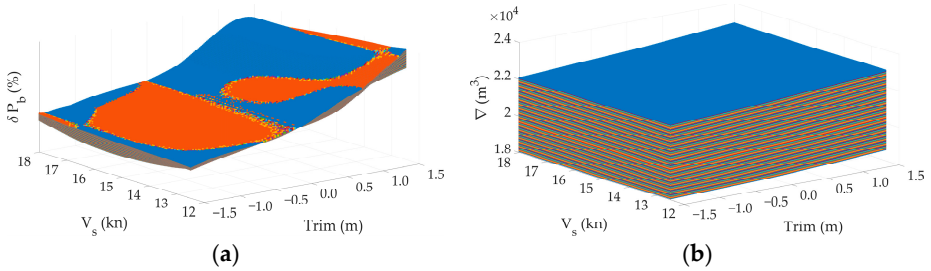

(**a**) (**b**)

Figure 4. Results representation: (**a**) brake power reduction (δP_b) for 120 drafts; (**b**) displacements (∇) for 120 drafts and each trim.

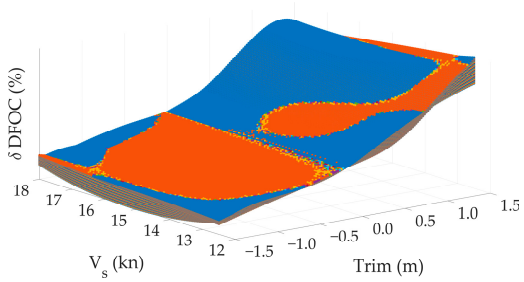

Figure 5. Results representation for DFOC reduction.

In operations, after loading cargo onto the ship, only the displacement is known. The goal of the conducted trim optimization is to find the optimal position, i.e., trim, and recommend the sailing speed based on that single parameter. The optimal trim and recommended speed are those at which the greatest savings in brake power, and consequently fuel consumption, are achieved. The mathematical expression of the above statement is as follows:

$$\delta P_{b_{\min}} = \min_{ijk}\left(\delta P_b{}^{(ijk)} \left| \left| \nabla^{(ijk)} - \nabla_{LC} \right| \leq \varepsilon \cdot \nabla_{LC} \right. \right), \tag{39}$$

where $\delta P_{b_{\min}}$ is the biggest brake power reduction where the corresponding displacement $\nabla^{(ijk)}$ is within a tolerance (ε= 0.0001) of the target displacement (∇_{LC}). Index i represents the speed, j represents the trim and k represents the brake power reduction, i.e., displacement in matrix Σ_m. When $\delta P_{b_{\min}}$ is found, it is easy to extract indices i, j and k therefore to derive the optimum trim and speed for the corresponding displacement, i.e., mean draft. In practice, there may be a need for speed as an input parameter, which depends on the operational requirements, and this case will be addressed in subsequent work.

Mathematical Model for Assessing Brake Power, DFOC and Propeller Speed

A sophisticated mathematical model utilizing artificial neural networks (ANNs) has been developed based on the CFD results. By specifically addressing the challenges posed by non-simulated loading conditions, this model offers a solution for estimating parameters such as the brake power, propeller speed and DFOC.

At its core, the model employs a feedforward artificial neural network (FFANN), a fundamental architecture in machine learning and deep learning. The FFANN's structure comprises interconnected layers of neurons, including an input layer (white circles in Figure 6), one or more hidden layers (gray circles in Figure 6) and an output layer (black circles in Figure 6). Each neuron is equipped with adjustable parameters called biases, which introduce flexibility by allowing for offsets or shifts in output. During training, these biases are fine-tuned to better fit the data and ensure the accurate estimation of the desired parameters.

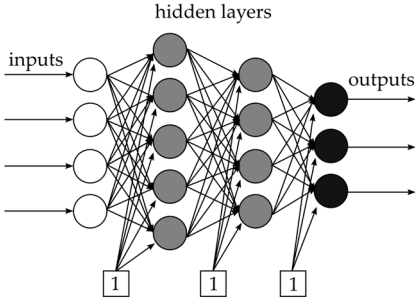

Figure 6. Illustrated ANN structure of interconnected neurons (circles) and biases (squares).

One of the key features of the FFANN is its one-directional flow of information, from the input layer through the hidden layers to the output layer. This design simplifies the learning process and enables the efficient modeling of complex data relationships. Additionally, activation functions embedded within neurons introduce non-linearity, enabling the network to capture patterns present in real-world data.

Overall, this innovative approach represents a significant step forward in the advancement of engineering solutions. It not only addresses the inherent challenges of non-simulated loading conditions but also sets a precedent for the application of artificial intelligence in optimizing the performance of complex systems. As further research and development are conducted in this field, the potential for ANNs to revolutionize engineering practices and transportation systems continues to expand.

In the context of a feedforward artificial neural network (FFANN), the connections between neurons are governed by weights, which dictate the strength of the connections. These weights are adjusted during the training process using an algorithm called backpropagation. The name "backpropagation" stems from its mechanism of iteratively propagating errors backward through the network to adjust the weights and biases of neurons.

The training process involves two phases: the forward pass and the backward pass. During the forward pass, input data are fed into the network, and predictions are made based on the current weights and biases. These predictions are compared to the actual outputs, and the resulting error is calculated.

In the backward pass, this error is propagated backward through the network, layer by layer. The gradient of the error with respect to each weight and bias is computed using techniques like the chain rule of calculus. These gradients indicate the direction and magnitude of adjustment required to minimize the error. The weights and biases are then updated accordingly.

At each neuron, the weighted sum of the inputs is computed by multiplying each input value by its corresponding weight and summing the results. This sum is then combined with the neuron's bias:

$$S_{x,i} = f\left(\sum_i S_{x-1,i} \cdot w_{x,i} + b_{x,i}\right), \tag{40}$$

where f—activation function, $S_{x,i}$—output signal, of ith neuron in xth layer, $S_{x-1,i}$—output of ith neuron in $x-1$th layer, $w_{x,i}$—weights connected to the neuron and $b_{x,i}$—corresponding bias.

The resulting value is passed through an activation function, which introduces non-linearity into the network. Common activation functions include sigmoid, tanh and others, each serving different purposes in facilitating learning and modeling complex data relationships. In this case, the sigmoid function is used as follows:

$$f = \frac{1}{1+e^x} \tag{41}$$

The general form of the function is

$$Y_u = \frac{f_p\left(p + \sum_{w=1}^{r}\left(P_w \cdot f_{p-1}\left(\ldots \cdot f_2\left(b_i + \sum_{j=1}^{m}\left(B_{ij} \cdot f_1\left(a_j + \sum_{k=1}^{n}\left(A_{jk} \cdot (P_k \cdot X_k + R_k)\right)\right)\right)\right)\ldots\right)\right)\right) - G_u}{L_u}, \tag{42}$$

where

- X_k—input parameters (number of neurons in input layer);
- Y_u—output parameters (number of neurons in output layer);
- $f_1, f_2, \ldots, f_{(p-1)}, f_p$—activation function;
- $k, j, i, \ldots, v, w$—number of neurons in each layer;
- $A, B, \ldots, P$—weights between layers;
- $a, b, \ldots, p$—weights between neurons in each layer and bias.

The software that has been used for training the ANN in this study is called aNETka, developed in LabVIEW. The output file from this software is not a direct mathematical model, just weights coefficients and four additional parameters called Down offset Input (DI_k), Down offset Target (DT_u), Up offset Input (UI_k) and Up offset Target (UT_u).

$$DI_k = \min(X_k) \tag{43}$$

$$DT_u = \min(Y_u) \tag{44}$$

$$UI_k = \max(X_k - \min(X_k)) \tag{45}$$

$$UT_u = \max(Y_u - \min(Y_u)) \tag{46}$$

The rest of the parameters are calculated as follows:

$$P_k = \frac{0.9}{UI_k} \tag{47}$$

$$R_k = -\frac{0.9 \cdot DI_k}{UI_k} + 0.05 \tag{48}$$

$$L_u = \frac{0.9}{UT_u} \tag{49}$$

$$G_u = -\frac{0.9 \cdot DT_u}{UT_u} + 0.05 \tag{50}$$

In the trim optimization study, data obtained from CFD analysis, including brake power, DFOC and propeller speed, were utilized as the output layer for training the artificial neural network (ANN), while the draft, speed, trim and displacement are considered as the input layer.

The applicability range of the model is defined within specific boundaries for each parameter: draft (T_s) ranges from 7.5 to 8.7 m, speed (V_s) ranges from 12.5 to 18 kn, trim ranges from −1.5 to +1.5 m and displacement (∇) ranges from 18,079 to 22,884 m^3. The input dataset for training consists of a 63 × 7 matrix, where number 63 represents the total number of CFD simulations conducted and number 7 denotes each parameter. Four parameters are designated as the input layer (draft, displacement, trim, speed), while the remaining three represent the output layer (propeller speed, brake power, DFOC).

Prior to training, all data were normalized within the range of 0.05 to 0.95 to ensure the stability of activation functions, which can be sensitive to extremely small or large input values. This normalization step enhances the convergence and effectiveness of the training process.

For testing purposes, 8% of the total input parameters (5 out of 63) were reserved, while the remaining data were allocated for training. The training process was programmed to iteratively adjust the weights and biases of the network, stopping when the Root Mean Square (RMS) percentage error reached the target threshold of 1%:

$$RMS = \sqrt{\left(\frac{\Sigma \left[\left(\frac{TV - OV}{TV} \right)^2 \right]}{N} \right)}, \tag{51}$$

where TV—target values, OV—ANN output values, N—number of values.

When creating a neural network model, it is vital to carefully consider the number of neurons in each layer and the presence of hidden layers. These decisions must be well informed and tailored to match the complexity of the problem at hand and the specific attributes of the dataset.

In practice, just before leaving the port, the parameters that are categorized into the input layer are usually known, but until now, the fuel consumption could never be predicted in advance. It is very common that fuel consumption and the power engaged by the engine are not monitored during the journey, and the amount of fuel used was always determined retroactively. With such mathematical models and conducted CFD simulations for a larger number of loading conditions, it is possible not only to predict the fuel consumption in advance but also to determine the optimal speed at which the ship should sail to minimize consumption. Knowing the fuel consumption, it is easy to determine the amount of CO_2 emitted and predict the energy rating to which the ship will belong according to [8], which is a direct indicator of energy efficiency.

2.7. Trim Optimization Software Application

Formulas derived for a particular purpose may not always be user-friendly, leading to the creation of an application to facilitate their use. In this case, an application developed using MATLAB's App Designer package offers a user-friendly interface for utilizing these formulas. The application allows users to input only one parameter, i.e., displacement and obtain corresponding output values efficiently: optimum trim, speed, propeller speed, brake power and DFOC. This enables users to quickly obtain results without the need for manual calculations.

3. Results

The results in this section will be presented in subsections in the same order, i.e., following the phases outlined in Section 2 (Methods).

3.1. Three-Dimensional Modeling

In Figure 7, a 3D model and characteristic sections of the waterlines (a), buttocks (b) and frames (c) are depicted in various projections obtained based on the construction drawings.

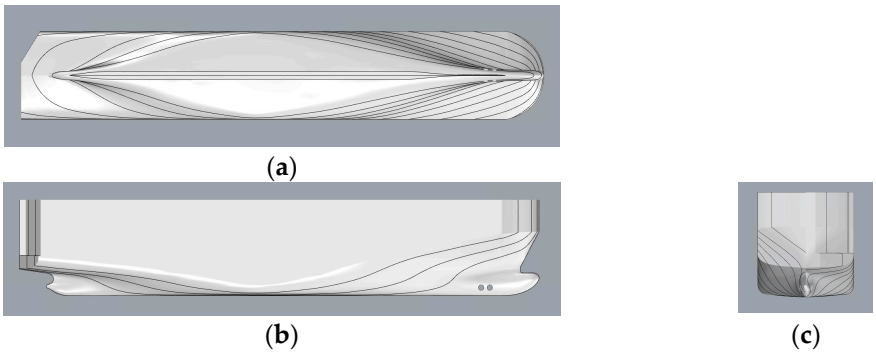

Figure 7. The 3D model of the RO-RO ship: (**a**) bottom view—waterlines; (**b**) starboard side view—buttocks; (**c**) aft view—frames.

The propeller underwent a modeling process, aligning with the specifications outlined in the reference drawing. A comparison was conducted between the 3D model of the propeller and the reference drawing to ensure precise adherence to the intended design. The findings of this comparison are visually presented in Figure 8, offering a clear representation of the propeller's details and shape. The 3D model of the propeller (Figure 9a) enables engineers and designers to perform CFD simulations and evaluate performance characteristics. The rudder was modeled to faithfully represent its original design but without any gaps between the rudder shaft and rudder shell (Figure 9b).

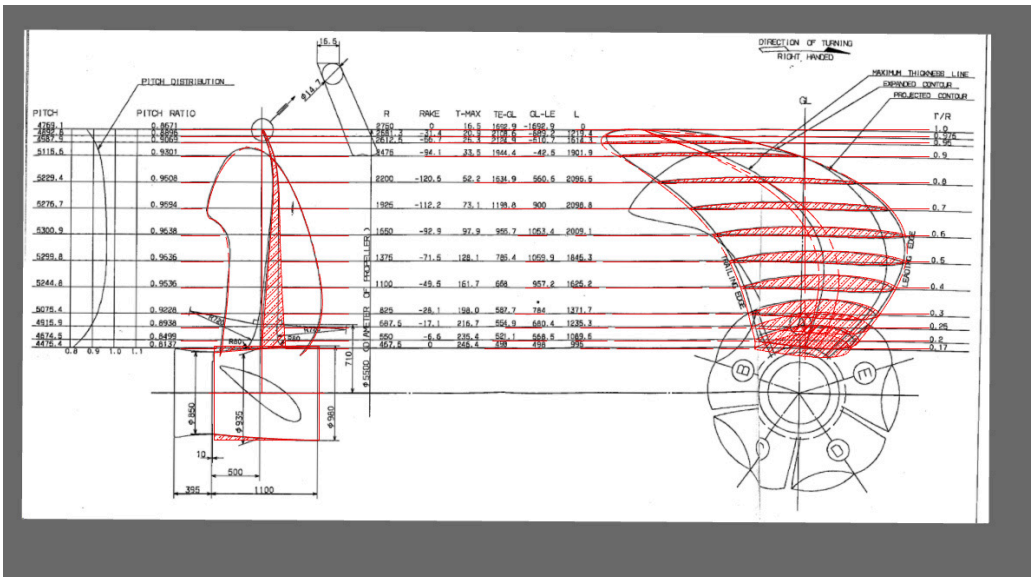

Figure 8. Propeller: comparison between drawing of 3D modeled propeller (red colored) and scanned reference drawing.

(**a**) (**b**)

Figure 9. Propeller and rudder: (**a**) original propeller; (**b**) rudder.

3.2. First-Level Verification

The reliability of the developed 3D model was assessed by comparing its calculated hydrostatic parameters against the corresponding ones given in the Trim & Stability booklet. The corresponding percentage deviations between C_b, ∇, *LCB* and *WS* are listed in Table 3.

Table 3. Comparison between hydrostatics data obtained on the basis of 3D model and Trim & Stability booklet.

T_s (m) (Trim = 0)	C_b	∇	*LCB*	*WS*
4	0.52%	0.88%	−0.03%	0.54%
5	0.43%	0.77%	−0.03%	0.74%
6	0.34%	0.62%	−0.01%	0.63%
7	0.27%	0.51%	0.01%	0.38%
7.5	0.22%	0.43%	0.03%	0.42%
8	0.21%	0.42%	0.03%	0.74%
8.7	0.23%	0.42%	0.03%	0.79%
9	0.31%	0.40%	0.03%	0.82%
10	0.14%	0.31%	0.03%	0.87%

It can be easily observed that deviations between the calculated and reference values of the hydrostatic data are less than 1%, especially for the range of interest (drafts 7.5 m, 8.0 m and 8.7 m).

3.3. Open Water Test

A graphical representation of the CFD results (K_T, K_Q, η_0) from the conducted OWT with the B-series propeller with data obtained with the mathematical model is presented in Figure 10a, while the relative differences between each evaluated parameter are presented in Table 4.

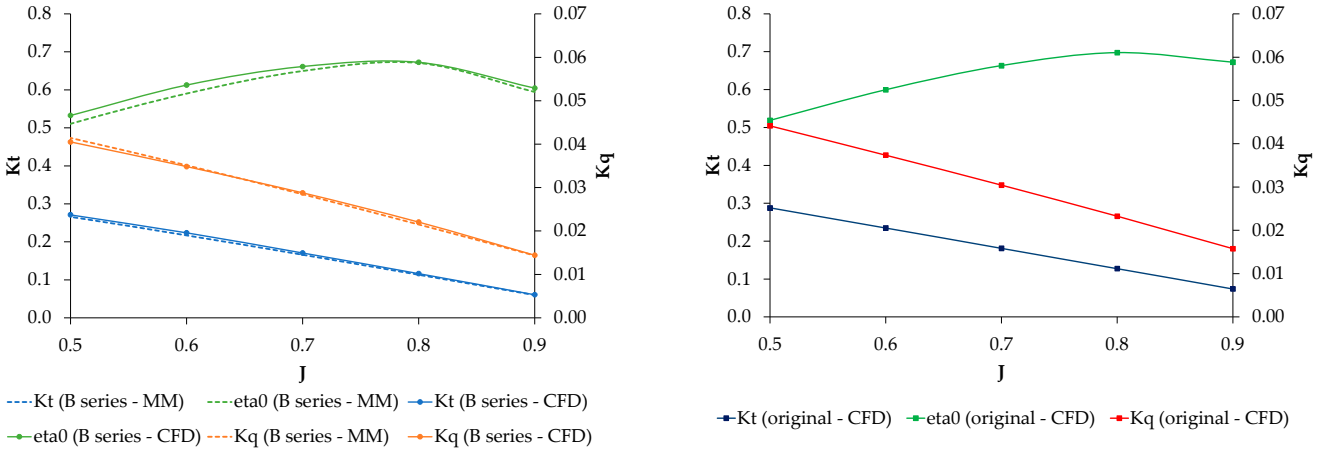

(**a**) (**b**)

Figure 10. Propeller characteristics. MM—results based on mathematical model, CFD—results based on OWT CFD simulations: (**a**) B-series propeller; (**b**) original propeller.

Table 4. Relative differences between data obtained with mathematical model and results from CFD.

J	δK_T	δK_Q	$\delta \eta_0$
0.5	1.9%	−2.3%	2.2%
0.6	2.9%	−0.8%	2.3%
0.7	2.8%	1.1%	1.2%
0.8	2.7%	2.4%	0.2%
0.9	2.2%	0.6%	1.0%

As the results for each of the advance coefficients are within the prescribed 3%, the CFD calculation methodology is considered valid; therefore, with the same setup, the original propeller OWT was conducted, and the results are presented in Figure 10b.

3.4. Second-Level Verification

The obtained results from the CFD OWT simulation with the original propeller are used as the input propeller characteristics data in self-propulsion simulations. The first group of simulations were conducted at a design draft (7.8 m) and speeds of 17 kn, 19 kn and 21 kn because for these draft and speeds model tests, data are available.

In Figure 11, the meshed domain is shown. For a better evaluation of the free surface, additional refinement zones are defined in wave field zones and near the hull (Figure 12a,b).

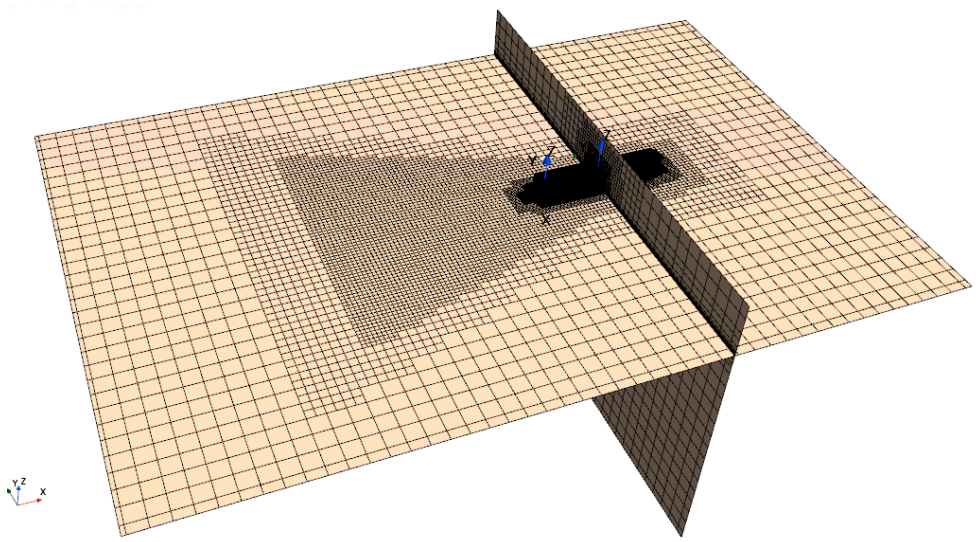

Figure 11. Domain—mesh.

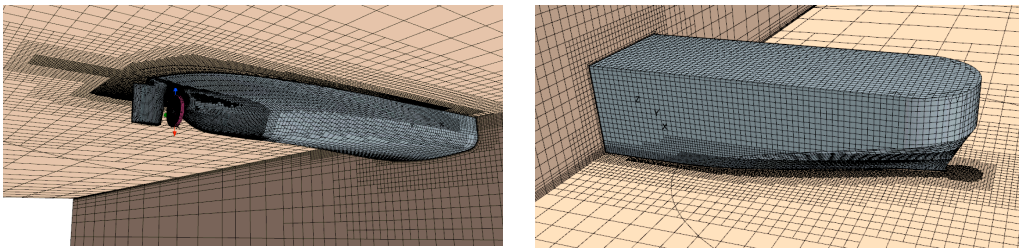

(**a**) (**b**)

Figure 12. Refinement zones: (**a**) stern part; (**b**) bow part.

The results from the completed self-propulsion simulations and steady resistance simulations by following the procedure described in Section 2.4 are presented in Table 5, where R_p is the pressure resistance and R_v is the viscous resistance.

Table 5. Results from CFD analysis for design draft.

V_s (kn)	R_p (kN)	R_v (kN)	R_T (kN)	t (-)	w (-)	T' (kN)	Q (kNm)	η_0 (-)	n (rpm)	P_b (kW)
17	125.454	292.216	475.936	0.1746	0.2487	576.644	466.316	0.6736	103.1	5083
19	178.852	366.869	622.133	0.1579	0.2479	738.831	595.864	0.6721	116.0	7309
21	321.762	438.076	857.035	0.1600	0.2458	1020.295	820.407	0.6656	132.8	11,523

The results from the CFD analysis and model test data are graphically presented in Figure 13. In Figure 13a, the brake power as a function of the ship speed curve is depicted while in Figure 13b, the brake power as a function of the propeller speed is presented.

The calibration factors are C_n = 1.05 and C_{P_b} = 1.04, which means that a 5% deviation requirement in the results compared to the model test is met. Differences in the results obtained from the CFD analysis and model testing can arise from several factors, such as the reliability of the model testing results, the reliability of the method used to extrapolate the results from the model to full scale, as well as the CFD analysis itself. A portion of the difference undoubtedly stems from the differences in the OWT results presented in Table 4. Due to all the aforementioned reasons, an acceptable margin of 5% exists according to [47].

In Figure 14, the y+ values for the underwater part of the hull are presented and the average y+ value is pointed out (average y^+ = 70.61). A particular case is extracted from the steady resistance simulation at a speed of 18 kn at 7.5 m draft. For all other speeds, the y^+ values do not deviate from those aforementioned.

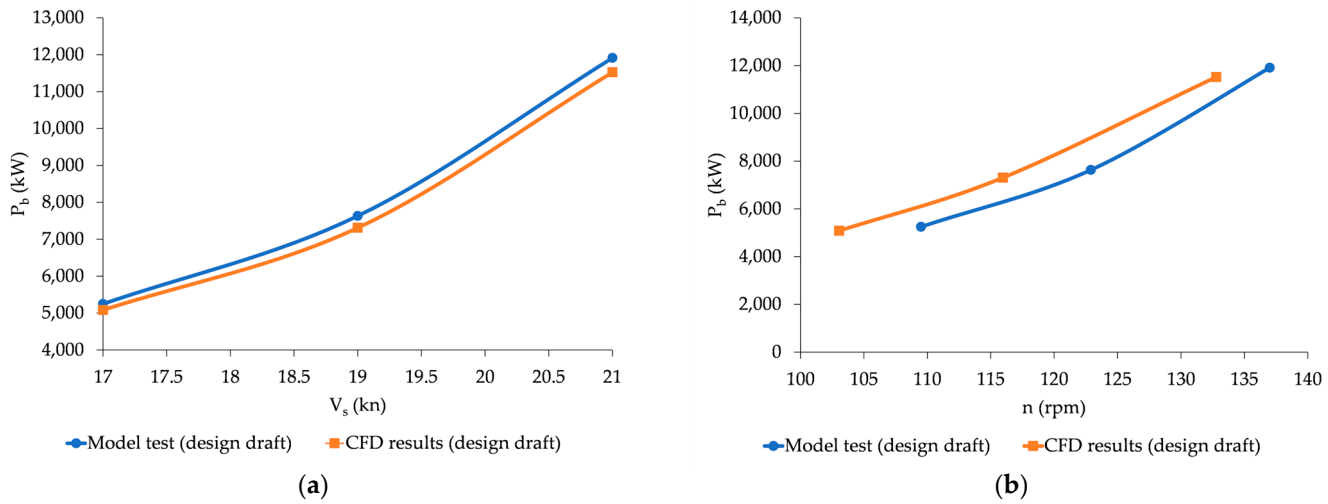

Figure 13. CFD results for design draft: (**a**) P_b as a function of V_s; (**b**) P_b as a function of n.

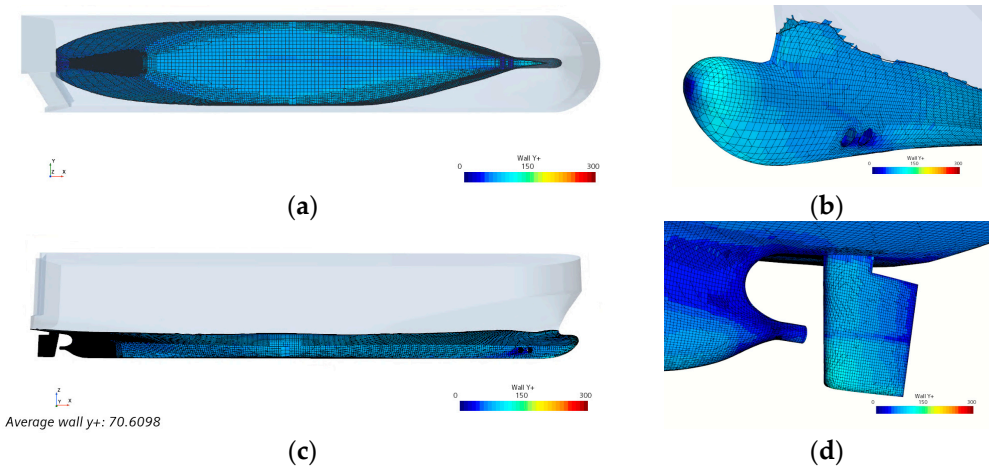

Figure 14. y^+ values: (**a**) bottom view; (**b**) bow part—perspective view; (**c**) starboard side view; (**d**) stern part—perspective view.

Three different meshes were considered for the grid uncertainty study with mesh sizes of 1.852 million cells (coarse), 3.628 million cells (medium) and 7.454 million cells (fine). The study was conducted at a speed of 18 knots at a 7.5 m draft (even keel). The results of the study, including the grid uncertainties for thrust, are presented in Table 6.

Table 6. Grid uncertainty results for thrust.

Mesh Quality	T (kN)
Coarse	544.445
Medium	539.287
Fine	535.586
$\overline{U}$	2.2%

3.5. Trim Optimization

The trim optimization CFD study was performed at a 7.5 m, 8 m and 8.7 m draft for a range of speeds, 12.5 kn, 15 kn and 18 kn, at seven different loading (trim) conditions and coarse mesh. Therefore, the results obtained for the propeller speed, brake power and estimated DFOC are presented in Tables 7–9, respectively.

Table 7. Propeller speed (n [rpm]): CFD analysis results.

		Trim by Bow (m)			Even Keel		Trim by Stern (m)	
	V_s (kn)	−1.5	−1	−0.5	0	0.5	1	1.5
7.5 m	12.5	82.7	83.6	84.2	85.0	86.6	87.9	88.9
	15	97.2	98.3	99.3	100.9	102.2	103.5	105.3
	18	116.8	117.9	119.0	119.7	121.1	122.6	125.1
8.0 m	12.5	82.4	83.1	84.0	84.7	85.7	87.7	89.5
	15	98.3	99.3	100.2	100.7	102.3	103.5	105.8
	18	120.4	120.2	121.2	122.3	123.5	126.1	127.4
8.7 m	12.5	84.4	85.0	85.7	86.4	87.3	89.1	91.2
	15	101.9	102.3	103.1	104.0	105.3	107.1	108.9
	18	125.1	125.6	126.0	127.4	129.1	131.3	132.9

Table 8. Brake power (P_b [kW]): CFD analysis results.

		Trim by Bow (m)			Even Keel	Trim by Stern (m)		
	V_s (kn)	−1.5	−1	−0.5	0	−1.5	−1	−0.5
7.5 m	12.5	2248	2335	2370	2447	2601	2739	2837
	15	3509	3665	3772	3965	4130	4414	4642
	18	5957	6187	6345	6441	6667	7124	7480
8.0 m	12.5	2155	2221	2285	2357	2450	2664	2882
	15	3587	3719	3818	3869	4073	4352	4639
	18	6595	6567	6750	6942	7120	7879	7991
8.7 m	12.5	2293	2353	2403	2478	2564	2771	3048
	15	4018	4072	4181	4303	4504	4890	5113
	18	7531	7663	7707	8003	8405	9143	9361

Table 9. DFOC [t fuel/day]: CFD analysis results.

		Trim by Bow (m)			Even Keel	Trim by Stern (m)		
	V_s (kn)	−1.5	−1	−0.5	0	−1.5	−1	−0.5
7.5 m	12.5	10.70	11.08	11.24	11.57	12.25	12.84	13.26
	15	16.11	16.75	17.20	18.00	18.68	19.85	20.79
	18	26.22	27.18	27.83	28.23	29.18	31.09	32.58
8.0 m	12.5	10.29	10.58	10.86	11.18	11.59	12.52	13.46
	15	16.43	16.98	17.39	17.60	18.45	19.60	20.78
	18	28.88	28.76	29.53	30.33	31.08	34.26	34.73
8.7 m	12.5	10.90	11.16	11.38	11.71	12.08	12.98	14.16
	15	18.22	18.44	18.89	19.39	20.22	21.81	22.73
	18	32.80	33.35	33.53	34.78	36.46	39.56	40.48

3.6. Mathematical Model for Assessing the Outcomes from Trim Optimization

Brake power reduction and DFOC reduction are linearly interpolated for additional trims and speeds (values considered in CFD analysis) and the results are graphically presented for the three considered drafts in Figures 15 and 16. The optimum trim and speed are also depicted with red points in Figure 16. The black line in Figures 15 and 16 represents a neutral line, i.e., the state of the even keel against which the brake power savings and DFOC savings are calculated.

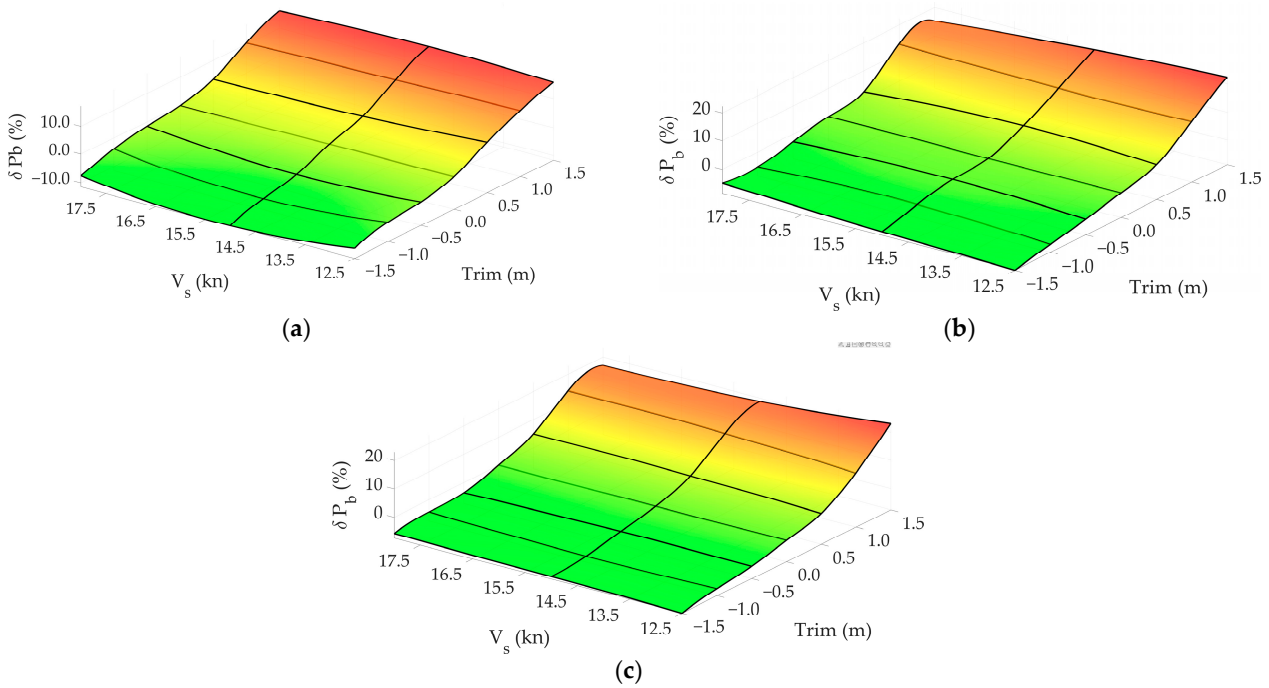

Figure 15. Brake power reduction: (**a**) T_s = 7.5 m; (**b**) T_s = 8.0 m; (**c**) T_s = 8.7 m.

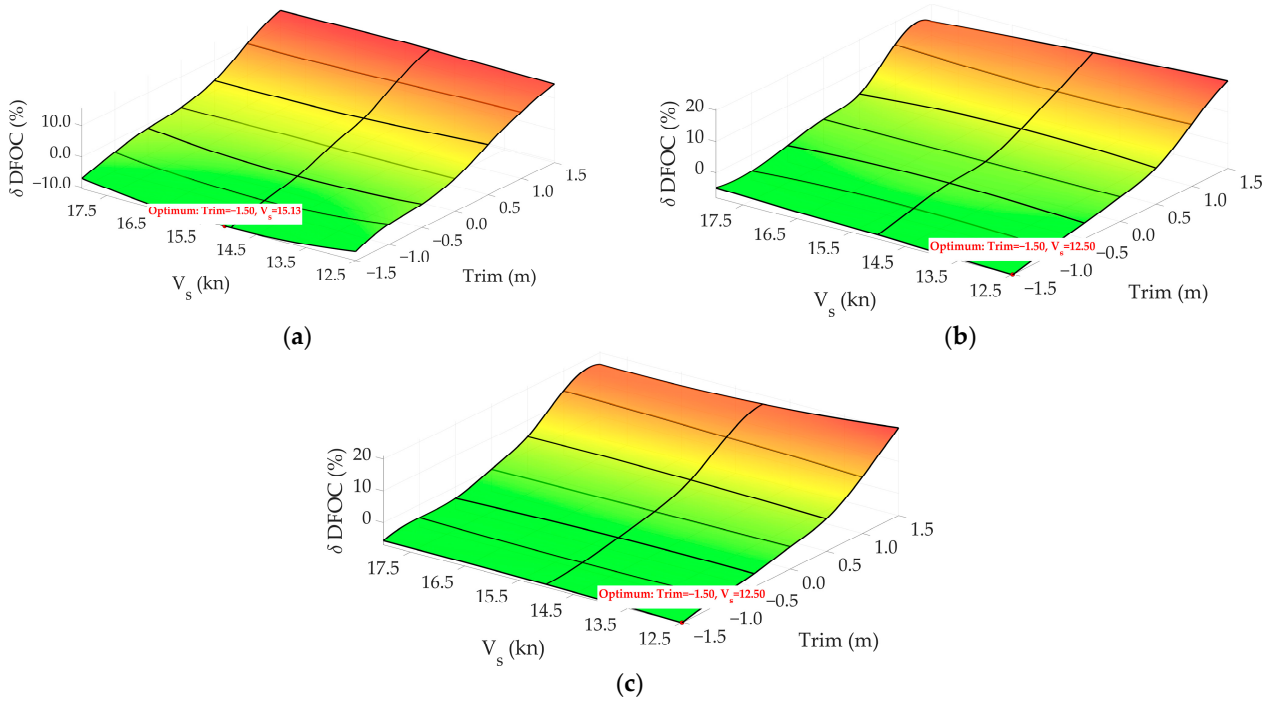

Figure 16. DFOC reduction: (**a**) T_s = 7.5 m; (**b**) T_s = 8.0 m; (**c**) T_s = 8.7 m.

The biggest reduction in the DFOC can be achieved at a 1.5 m trim by the bow, 7.5 m draft and speed of 15.17 kn (10.5%), while for the 8 m and 8.7 m draft, the biggest reduction in brake power is at 12.5 kn (8%, 7%, respectively). Sailing at 12.5 kn instead of 15 kn or 18 kn, and maintaining an even keel, can result in greater fuel savings for higher drafts. Although greater fuel savings might be achievable with a greater trim by the bow, any condition more than −1.5 m trim by the bow cannot be attained on the current ship.

In Figure 17, wave fields are depicted for the case of V_s = 15 kn, T_s = 7.5 m at trim = 0 m (Figure 17a) and at trim = −1.5 m (Figure 17b). It is evident that the total wave amplitude

when trimmed towards the bow by 1.5 m is reduced by 0.25 m, indicating a decrease in the pressure resistance–displacement ratio of 15% (see Table 10). The volume displacement is multiplied by the gravity constant (9.81 m/s^2) and sea water density.

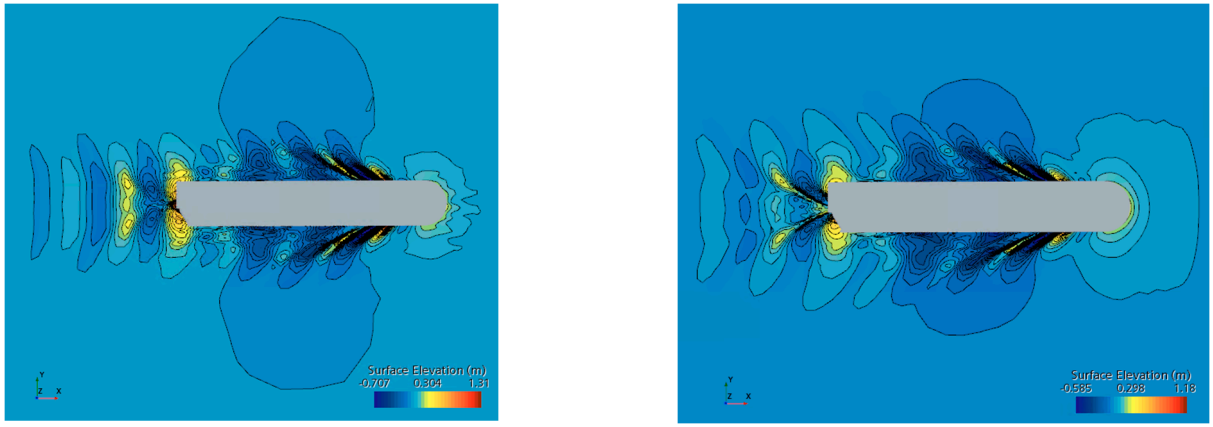

(**a**) (**b**)

Figure 17. Wave patterns: (**a**) V_s = 15 kn, T_s = 7.5 m, trim = 0 m; (**b**) V_s = 15 kn, T_s = 7.5 m, trim = −1.5 m.

Table 10. Pressure resistance decrease.

V_s = 15 kn, T_s = 7.5 m	Trim = 0 m	Trim = −1.5 m
$R_p/\nabla \cdot 10^3$ (-)	0.6039	0.5127

In Figure 18, the free surfaces in the center line and along the hull are presented at two different conditions: trim = 0 m (white hull) and trim = −1.5 m (yellow hull). The black line corresponds to the free-surface level at a zero trim condition while the red line corresponds to the free-surface level at a 1.5 m trim by the bow. In Figure 18a, the bow waves are presented, while in Figure 18b, the stern waves are presented. The peak-to-peak amplitude of the bow wave is reduced by 0.64 m while the stern wave is reduced by nearly 1 m when the ship is trimmed towards the bow by 1.5 m.

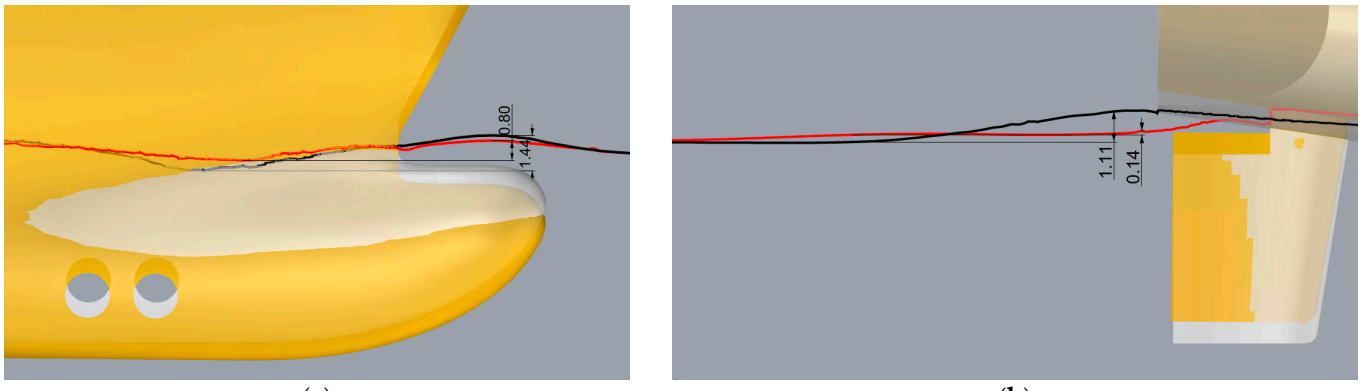

(**a**) (**b**)

Figure 18. Free-surface cuts (V_s = 15 kn, T_s = 7.5 m): (**a**) bow part—white-colored even keel hull; black line represents free-surface elevation for even keel hull, yellow-colored (−1.5 m) trimmed hull; red line represents free-surface elevation for trimmed hull; (**b**) stern part—white-colored even keel hull; black line represents free-surface elevation for even keel hull, yellow-colored (−1.5 m) trimmed hull; red line represents free-surface elevation for trimmed hull.

For other drafts and trims, the impact of the bow trim remains similar; nevertheless, there is a less noticeable reduction in the pressure resistance. It seems that this kind of bulb has a better effect when it is more submerged into the water at lower drafts. This contradicts what is highlighted in numerous literature sources, including [61,62] but it is not the first time that the same conclusion with a fully submerged bulb has been set [63,64].

Mathematical Model for Assessing Brake Power, DFOC and Propeller Speed

Unfortunately, a single mathematical model did not attain the desired RMS within a reasonable training timeframe and iteration count. As a result, two separate mathematical models were devised as follows: one focusing on the brake power and DFOC and the other dedicated to propeller speed prediction. The formula for brake power follows a general form:

$$P_b = \frac{f_3\left(c_{P_b} + \sum_{i=1}^{7}\left(C_{iP_b} \cdot f_2\left(b_i + \sum_{j=1}^{10}\left(B_{ij} \cdot f_1\left(a_j + \sum_{k=1}^{4}\left(A_{jk} \cdot (P_k \cdot X_k + R_k)\right)\right)\right)\right)\right)\right) - G_{P_b}}{L_{P_b}}. \quad (52)$$

The general form of the function for DFOC is

$$DFOC = \frac{f_3\left(c_{DFOC} + \sum_{i=1}^{7}\left(C_{iDFOC} \cdot f_2\left(b_i + \sum_{j=1}^{10}\left(B_{ij} \cdot f_1\left(a_j + \sum_{k=1}^{4}\left(A_{jk} \cdot (P_k \cdot X_k + R_k)\right)\right)\right)\right)\right)\right) - G_{DFOC}}{L_{DFOC}}. \quad (53)$$

The general form of the function for propeller speed is

$$n = \frac{f_3\left(c_n + \sum_{l=1}^{5}\left(C_{ln} \cdot f_2\left(b_l + \sum_{m=1}^{8}\left(B_{lm} \cdot f_1\left(a_m + \sum_{s=1}^{4}(A_{ms} \cdot (P_s \cdot X_s + R_s))\right)\right)\right)\right)\right) - G_n}{L_n}. \quad (54)$$

Configurations of the neurons for both mathematical models are presented in Figure 19a,b.

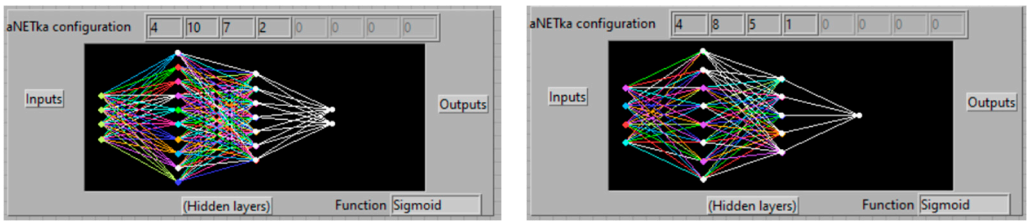

(**a**) (**b**)

Figure 19. Configurations of neurons: (**a**) for brake power and DFOC; (**b**) for propeller speed.

The obtained coefficients for Equations (52) and (53) are given in Tables 11–15, while the coefficients for Equation (54) are given in Tables 16–19.

Table 11. Coefficients A and a for Equations (52) and (53).

A_{j1}	A_{j2}	A_{j3}	A_{j4}	a_j
1.39544	4.80982	−1.76190	−1.30478	−0.75004
0.22339	3.25659	−0.04068	2.23871	−1.54100
−2.10995	3.49346	−0.21458	1.21715	−1.63827
3.03760	4.14154	−2.40221	1.04647	−6.47006
−0.04455	0.71422	1.58515	−0.98086	−0.02750
−1.50944	0.27102	−1.41296	1.52488	1.06833
−0.97408	−0.21472	−0.34123	−0.58728	0.38679
1.83711	2.00358	−9.92587	−1.27416	3.94278
0.08588	0.39723	1.06558	−0.68159	−0.95401
−1.45797	−0.49383	3.67284	−2.41111	0.23743

Table 12. Coefficients B and b for Equations (52) and (53).

B_{i1}	B_{i2}	B_{i3}	B_{i4}	B_{i5}	B_{i6}	B_{i7}	B_{i8}	B_{i9}	B_{i10}	b_i
−3.94741	−1.10676	−1.51183	−3.90542	1.28454	1.37817	1.67905	10.13879	0.82581	2.39590	3.05951
−0.83685	−0.80410	−0.84916	−0.74439	−0.53931	1.20460	0.17759	−0.26222	−0.48840	−0.58512	0.76405
−1.21006	−1.28977	−1.53713	−0.74023	−1.04296	0.87026	0.00654	0.35832	−0.85771	−1.31206	0.45529
0.79825	−0.92382	−0.16195	−3.22868	0.48528	0.41493	0.29515	−2.64142	0.12449	1.60271	0.59712
−0.83157	−1.72121	−1.74315	−1.78391	−0.13521	2.35956	0.85288	1.08050	−0.61823	−0.66071	2.10411
−1.03458	−1.10428	−1.25646	−0.56187	−0.81983	0.76972	−0.00495	0.29741	−0.77011	−1.13999	0.35562
−0.48851	−0.49214	−0.56036	−0.16494	−0.22853	0.26762	−0.48143	1.41729	−0.31051	−1.40889	0.36591

Table 13. Coefficients C_{P_b} and c_{P_b} for Equations (52) and (53).

C_{P_b1}	C_{P_b2}	C_{P_b3}	C_{P_b4}	C_{P_b5}	C_{P_b6}	C_{P_b7}	c_{P_b}
−3.60944	−1.69300	−1.92004	−2.15282	−2.51012	−1.80109	−2.08429	7.38079

Table 14. Coefficients C_{DFOC} and c_{DFOC} for Equations (52) and (53).

C_{DFOC1}	C_{DFOC2}	C_{DFOC3}	C_{DFOC4}	C_{DFOC5}	C_{DFOC6}	C_{DFOC7}	c_{DFOC}
−3.60911	−1.64363	−2.01584	−2.11789	−2.49256	−1.76852	−2.02170	7.32870

Table 15. Coefficients P_k, R_k, G_{P_b}, L_{P_b}, G_{DFOC} and L_{DFOC} for Equations (52) and (53).

P_k	R_k	G_{P_b}	L_{P_b}	$G_{\mathbf{DFOC}}$	$L_{\mathbf{DFOC}}$
0.75000	−5.57500	−0.21915	0.00012	−0.25636	0.02980
0.16364	−1.99545				
0.30000	0.50000				
0.00019	−3.33586				

Table 16. Coefficients A and a for Equation (54).

A_{m1}	A_{m2}	A_{m3}	A_{m4}	a_m
1.60283	1.91017	−1.71984	0.23942	−1.93017
1.62613	2.44722	−0.17892	−1.00908	−3.09041
1.09543	1.09342	2.08237	0.00351	−0.00032
−0.17611	2.37242	0.49469	1.22030	−2.13783
−1.12935	5.25606	−0.88296	−1.08825	−0.79561
−1.10799	−0.07232	−2.85448	0.21127	3.80378
−2.76944	2.04227	4.00000	−0.90497	−1.59122
−0.09699	1.92632	1.05398	−0.48593	−0.22092

Table 17. Coefficients B and b for Equation (54).

B_{l1}	B_{l2}	B_{l3}	B_{l4}	B_{l5}	B_{l6}	B_{l7}	B_{l8}	b_l
−0.85076	−0.86022	−0.92193	−1.21839	−1.28573	0.12384	−0.42344	−0.84941	0.72250
−2.21759	−3.16121	1.26550	−1.20003	−2.78787	4.04679	−1.95753	0.95956	3.10950
−1.04299	−0.99883	−1.19340	−1.29826	−1.50607	0.14846	−0.49616	−1.15469	1.08981
−1.11884	−0.96068	−1.18134	−1.19153	−1.62624	0.20455	−0.46174	−1.00754	1.02576
−0.43893	−1.02698	−1.08333	−1.41701	−0.49332	1.67727	0.33505	−0.39926	1.34012

Table 18. Coefficients C and c for Equation (54).

C_{n1}	C_{n2}	C_{n3}	C_{n4}	C_{n5}	c_n
−2.44334	−5.02627	−2.91111	−2.88484	−2.67661	6.86984

Table 19. Coefficients P_s, R_s, G_n and L_n for Equation (54).

P_s	R_s	G_n	L_n
0.75000	−5.57500	−1.41852	0.01782
0.16364	−1.99545		
0.30000	0.50000		
0.00019	−3.33987		

The standard deviations of the relative differences in the brake power, DFOC and propeller speed calculated the values using Equations (52)–(54), and the results obtained from the CFD analysis for the same three parameters are 0.6%, 0.6% and 0.2%, respectively.

3.7. Trim Optimization Software Application

The development of software focusing on trim optimization is another step forward that demonstrates how engineering and technical practice can be more effectively connected. The equations obtained (52), (53) and (54) are very complex and not suitable for manual calculation. Additionally, the matrix obtained through interpolation of the CFD analysis results contains over 2 million elements (a 151 × 111 × 120 matrix), meaning tabular or graphical representation of the results will be impractical for the average user. Therefore, the most elegant solution is to develop an application with a graphical interface. Today, there are many software tools that operate based on writing in various programming languages, but this task is addressed to other engineering disciplines. This paper demonstrates the development of a software tool within MATLAB App Designer. MATLAB App Designer is highly suitable for the rapid development of simple applications as it has certain functions predefined within the Component Library. In this specific case, only three predefined functions were used: "Button", "Edit Field" and "Label". The interface design is depicted in Figure 20:

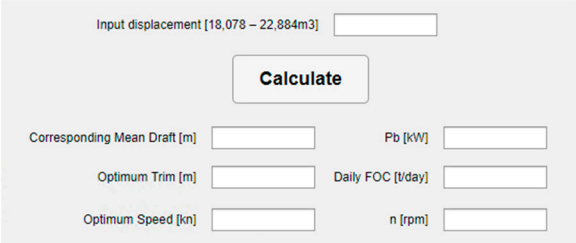

Figure 20. Application interface design.

In the "Input displacement" label, the user should insert the current displacement in cubic meters in the range from 18,078 to 22,884 m^3. The estimation of the optimal trim, corresponding mean draft, estimated speed, brake power, DFOC and propeller speed is performed by simply clicking the "Calculate" button. In case the user inputs a displacement below or above the specified values, despite the stated applicability limits of the mathematical model, and initiates the calculation, a message will appear on the screen: "Displacement is out of range" (see Figure 21).

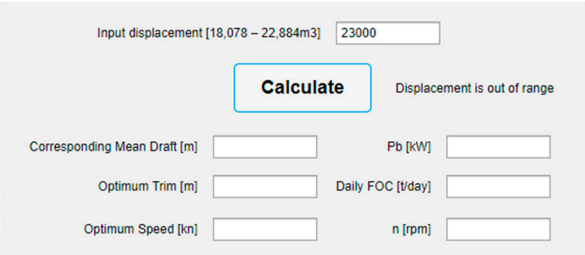

Figure 21. Wrong input.

If a displacement within the specified limits is entered, and the "Calculate" button is clicked, all the data are instantly displayed (see Figure 22).

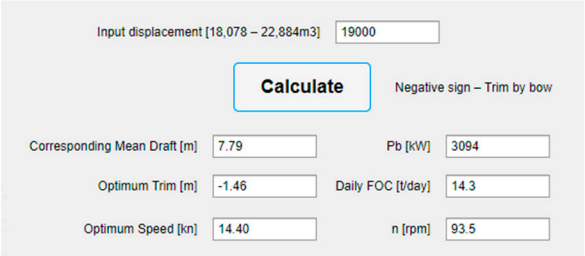

Figure 22. An example input.

The application provides results based on previously obtained mathematical models for estimating the optimal trim, speed, corresponding mean draft, brake power, DFOC and propeller speed. There is also a note that sign "−" in the Optimum Trim label corresponds to the trim by the bow. Due to the specified project task, which required trim optimization at certain speeds, trims and drafts rather than displacements, it is clear that for the same mean draft and different trims, the vessel has different displacements (due to the different position of the ship, the C_b is different and therefore displacement). Considering the upper limit of the performed calculations with a draft of 8.7 m and taking into account various trims, accordingly, the upper limit of displacements for which the calculations were performed at this draft (8.7 m) is variable (refer to Figure 4b). Considering the obtained results, there is a displacement range where the optimal trim is 0 m, meaning that sailing on an even keel is recommended (see Figure 23). This zone starts from the displacement corresponding to a draft of 8.7 m and even-keel position.

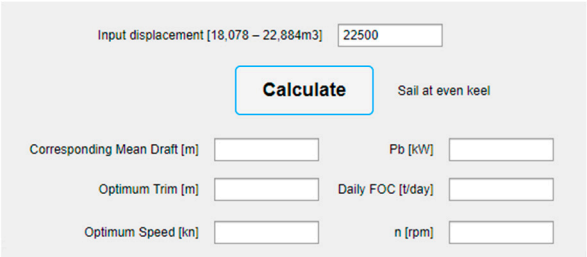

Figure 23. An example input of displacement that is at the upper limit of the mathematical model's application.

The mathematical model does not take draft as an input parameter but determines the mean draft by seeking the optimal trim for a given displacement. It is logical to apply the recommendation of the optimal trim obtained from the mathematical model only through the additional ballasting of the vessel if achieving the optimal trim cannot be attained with the existing ballast water in the tanks (if any). This is manifested by further increasing the displacement. Therefore, it is necessary to rerun the application with the new displacement. Through a few iterations, the optimal trim can be achieved, thus obtaining the estimated ship speed, propeller speed, brake power and DFOC in a reliable manner. It should be noted that the application is not part of the Loading Computer nor does it track stability data for a specific loading condition for a recommended optimal trim. However, it can be integrated into the Loading Computer system to enhance its functionality.

4. Discussion and Conclusions

In this work, not only trim optimization aiming to improve the energy efficiency of the ship, but specifically the CII parameter by reducing the fuel consumption, was presented. The methodology for approaching this issue using CFD software, the application of results

obtained from CFD analysis, i.e., using an ANN to develop a mathematical model that provides estimates of the parameters (brake power, DFOC and propeller speed) for all conditions for which CFD calculations were performed, as well as for all intermediate conditions, was also introduced. Since the use of an ANN resulted in a complex mathematical model that is not straightforward to use in engineering practice, it went a step further, incorporating it into a simple software tool (application).

The entire trim optimization process is described through seven phases that should be applied to other types of ships in future research to develop a universal methodology, not only for trim optimization but also for CFD calculations based on which various engineering analyses such as the optimization of the bow or stern, determination of V_{ref} for EEXI, efficiency of energy-saving devices, etc., can be conducted. For now, the applied methodology, which includes 3D modeling of a digital twin whose hydrostatic parameters differ by up to 1% when comparing the same parameters with data from the Trim & Stability booklet, has proven to be sufficiently good. With additional assumptions about determining the boundary-layer thickness and shear wall stress, i.e., shear velocity, satisfactory accuracy of the y+ parameters, which are very significant for obtaining reliable results, was achieved. The obtained values of y^+(approximately 70–72) differ from the initial target y+ of 150, which is to be expected because the equations used to estimate both the boundary-layer thickness and wall shear stress are not the only ones that can be applied and are very general. For example, the formula for the boundary-layer thickness applies to a flat plate, but in calculating the shear stress, a form factor is included, which is itself obtained based on empirical expressions. Therefore, these formulas cannot provide exact parameter values because these parameters are actually calculated by CFD analysis. However, they can be used to determine enough fine mesh (parameters) so that the results obtained by CFD analysis fall within prescribed limits, according to currently published requirements (up to 5% difference in power brake and shaft speed) for a specific ship case.

The application of an ANN to develop a mathematical model has proven to be very reliable. Generally speaking, artificial intelligence (AI) is increasingly finding applications in various engineering industries, where new design approaches can be developed, and existing ones significantly accelerated based on machine learning. It should be noted that the obtained mathematical model applies to navigation in calm waters, which is practically an almost impossible scenario. This approach, which encompasses multidisciplinarity (CFD analysis, ANN application, software tool programming), can lay the foundation for the further development of the shipbuilding industry from an engineering perspective. In the future, research should further focus on the impact of trim optimization on maneuverability and seakeeping, as these characteristics are crucial for safe navigation. Currently, these aspects are often overlooked in trim optimization projects, as they are not typically included in the project assignments. Addressing this gap will enhance the overall safety and performance of maritime ships.

The further idea is to collect real (measured) data on fuel consumption, engine power, ship speed and navigation conditions during voyages. Monitoring and recording some of these parameters have already become mandatory through [10]. Based on the stored parameters and the formed database, and with the help of machine learning and AI, it will be possible in the future to predict in advance to which energy class the ship belongs and what can be changed during real-time operation to make the ship "green". This can lead to a global reduction in exhaust gas emissions instantly, without ship owners being exposed to penalties imposed by the system because the CII is determined retroactively.

Author Contributions: Conceptualization, M.V. and M.K.; methodology, M.V.; software, M.V.; validation, M.V., M.K. and I.I.; formal analysis, M.V.; investigation, I.I.; resources, M.K.; data curation, M.V. and M.K.; writing—original draft preparation, M.V. and I.I.; writing—review and editing, M.V. and M.K.; visualization, M.V.; supervision, M.K.; project administration, M.V. and I.I.; funding acquisition, M.K. All authors have read and agreed to the published version of the manuscript.

Funding: This research received no external funding.

Informed Consent Statement: Not applicable.

Data Availability Statement: The raw data supporting the conclusions of this article will be made available by the authors on request.

Acknowledgments: Authors would like to thank Ocean Pro Marine Engineers LTD who provided necessary support in CFD simulations and guidelines and Argo Navis Ltd. who provided technical software support. This work was supported by the Ministry of Education, Science and Technological Development of Serbia (Project no. 451–03−65/2024−03/200105 from 5 February 2024).

Conflicts of Interest: Author Matija Vasilev, Milan Kalajdžić was employed by the company Ocean Pro Marine Engineers Ltd. The remaining authors declare that the research was conducted in the absence of any commercial or financial relationships that could be construed as a potential conflict of interest.

References

1. IMO. *2013 Guidelines for Calculation of Reference Lines for Use with the Energy Efficiency Design Index (EEDI)*; Resolution MEPC.231(65), Annex 14; IMO: London, UK, 2013.
2. IMO. *Amendments to the Annex of the Protocol of 1997 to Amend the International Convention for the Prevention of Pollution from Ships. 1973, as Modified by the Protocol of 1978 Relating Thereto*; Resolution MEPC.203(62); IMO: London, UK, 2011.
3. IMO. *Amendments to the Annex of the Protocol of 1997 to Amend the International Convention for the Prevention of Pollution from Ships, 1973, as Modified by the Protocol of 1978 Relating Thereto*; Resolution MEPC.328(76); IMO: London, UK, 2021.
4. IMO. *Guidelines for Voluntary Use of the Ship Energy Efficiency Operational Indicator (EEOI)*; Resolution MEPC.1/Circ.684; IMO: London, UK, 2009.
5. IMO. *2022 Guidelines on Operational Carbon Intensity Indicators and the Calculation Methods (CII Guidelines, G1)*; Resolution MEPC.352(78), Annex 14; IMO: London, UK, 2022.
6. IMO. *2022 Guidelines on the Reference Lines for Use with Operational Carbon Intensity Indicators (CII Reference Lines Guidelines, G2)*; Resolution MEPC.353(78), Annex 15; IMO: London, UK, 2022.
7. IMO. *2021 Guidelines on the Operational Carbon Intensity Reduction Factors Relative to Reference Lines (CII Reduction Factors Guidelines, G3)*; Resolution MEPC.338(76), Annex 12; IMO: London, UK, 2021.
8. IMO. *2022 Guidelines on the Operational Carbon Intensity Rating of Ships (CII Rating Guidelines, G4)*; Resolution MEPC.354(78), Annex 16; IMO: London, UK, 2022.
9. IMO. *Amendments to the Annex of the Protocol of 1997 to Amend the International Convention for the Prevention of Pollution from Ships, 1973, as Modified by the Protocol of 1978 Relating Thereto*; Resolution MEPC.278(70); IMO: London, UK, 2016.
10. IMO. *2022 Guidelines for the Development of a Ship Energy Efficiency Management Plan (SEEMP)*; Resolution MEPC.346(78), Annex 8; IMO: London, UK, 2022.
11. Islam, H.; Carlos, G.-S. Effect of trim on container ship resistance at different ship speeds and drafts. *Ocean. Eng.* **2019**, *183*, 106–115. [CrossRef]
12. Demir, U. Evaluation of Operational Factors for the Energy Efficiency Optimization of High-Speed RORO Vessels by Trim Optimization. Master's. Thesis, Piri Reis University, Istanbul, Turkey, 2019.
13. Le, T.-H.; Vu, M.-T.; Bich, V.-N.; Phuong, N.-K.; Ha, N.-T.-H.; Chuan, T.-Q.; Tu, T.-N. Numerical investigation on the effect of trim on ship resistance by RANSE method. *Appl. Ocean. Res.* **2021**, *111*, 102642. [CrossRef]
14. Hüffmeier, J.; Johanson, M. State-of-the-art methods to improve energy efficiency of ships. *J. Mar. Sci. Eng.* **2021**, *9*, 447. [CrossRef]
15. Sun, C.; Wang, H.; Liu, C.; Zhao, Y. Dynamic prediction and Optimization of Energy Efficiency Operational Index (EEOI) for an Operating Ship in Varying Environments. *J. Mar. Sci. Eng.* **2019**, *7*, 402. [CrossRef]
16. Peričić, M.; Vladimir, N.; Fan, A.; Jovanović, I. Holistic Energy Efficiency and Environmental Friendliness Model for Short-Sea Vessels with Alternative Power Systems Considering Realistic Fuel Pathways and Workloads. *J. Mar. Sci. Eng.* **2022**, *10*, 613. [CrossRef]
17. Zincir, B. Slow steaming application for short-sea shipping to comply with the CII regulation. *Brodogradnja* **2023**, *74*, 2. [CrossRef]
18. Yu, Y.; Zhang, H.; Mu, Z.; Li, Y.; Sun, Y.; Liu, J. Trim and Engine Power Joint Optimization of a Ship Based on Minimum Energy Consumption over a Whole Voyage. *J. Mar. Sci. Eng.* **2024**, *12*, 475. [CrossRef]
19. Prados, J.M.M.; Fernandez, I.A.; Gomez, M.R.; Parga, M.N. The decarbonisation of the maritime sectior: Horizon 2050. *Brodogradnja* **2024**, *75*, 2. [CrossRef]
20. Sherbaz, S.; Duan, W. Ship Trim Optimization: Assessment of Influence of Trim on Resistance of MOERI Container Ship. *Hindawi Publ. Corp.* **2014**, *2014*, 603695. [CrossRef] [PubMed]
21. Korkmaz, K.-B.; Werner, S.; Bensow, R. Investigations on experimental and computational trim optimisation methods. *Ocean Eng.* **2023**, *288*, 116098. [CrossRef]
22. Thiha, S.; Jin, Y. Study on Energy Efficient Operation by ship's Trim Optimization based on Computational Fluid Dynamics. *J. Sci. Res. Sci. Eng. Technol.* **2023**, *10*, 18–28.

23. Jianglong, S.; Haiwen, T.; Yongnian, C.; De, X.; Jiajian, Z. A study on trim optimization for a container ship based on effects due to resistance. *J. Ship Res.* **2016**, *60*, 30–47.
24. Ziylan, K.; Nas, S. A Study on the Relationship Between Ship Resistance and Trim, Supported by Experimental and Software-Based Analysis. *Trans. Mar. Sci.* **2022**, *11*, 5. [CrossRef]
25. Kishev, R.; Georgiev, S.; Kirilova, S.; Milanov, E.; Kyulevcheliev, S. Global View on Ship Trim Optimization. In Proceedings of the 2nd International Symposium on Naval Architecture and Maritime INT-NAM 2014, Istanbul, Turkey, 23–24 October 2014.
26. Park, B.-S.; Donghoon, K.; Kang, I.-K.; Kim, H.-M. The Analysis of the Ship's Maneuverability According to the Ship's Trim and Draft. *J. Fish. Mar. Sci. Educ.* **2015**, *27*, 1865–1871. [CrossRef]
27. Wen, P.; Fadillah, A. The Effect of Trim on Stability and Seakeeping of Tanker, Container and Bulk Carrier. In *IOP Conference Series: Earth and Environmental Science, Volume 972, Proceedings of the 6th International Conference on Marine Technology (SENTA 2021), Surabaya, Indonesia, 27th November 2021*; IOP Publishing Ltd.: Bristol, UK, 2022.
28. Hydrocompinc. Available online: https://www.hydrocompinc.com/blog/article-trim-optimization-using-navcad-for-prediction-confidence/ (accessed on 30 April 2024).
29. Chuan, T.Q.; Phuong, N.K.; Tu, T.N.; Quan, M.V.; Anh, N.D.; Le, T.-H. Numerical Study of Effect of Trim on Performance of 12500DWT Cargo Ship Using RANSE Method. *Pol. Marit. Res.* **2022**, *29*, 3–12. [CrossRef]
30. ABS. *Ship Energy Efficiency Measures. Status and Guidance*; TX 05/13 50000 13015; ABS: Spring, TX, USA, 2013.
31. Ziarati, R.; Bhuizan, Z.; de Melo, G.; Koivisto, H.; Lahiry, H.; OzTurker, E.; Akdemir, B. *MariEMS Train the Trainee (MariTTT) Courses on Energy Efficient Ship Operation. MariEMS*; MTCC-Asia, Guidelines on Ship Trim Optimization—Based on Machine Learning Method; The Global MTCC Network: London, UK, 2017.
32. MTCC-Asia. *Guidelines on Ship Trim Optimization—Based on Machine Learning Method*; The Global MTCC Network: London, UK, 2017.
33. Mahmoodi, H.; Ghamari, I.; Hajivand, A.; Mansoori, M. A CFD investigation of the propulsion performance of a low-speed VLCC tanker at different initial trim angles. *Ocean Eng.* **2023**, *275*, 114148. [CrossRef]
34. Petursson, S. Predicting Optimal Trim Configuration of Marine Vessel with Respects to Fuel Usage. Master's Thesis, Faculty of Industrial Engineering, Mechanical Engineering and Computer Science, School of Engineering and Natural Sciences, University of Iceland, Reykjavík, Iceland, 2009.
35. Lee, J.; Yoo, S.; Choi, S.; Kim, H.; Hong, C.; Seo, J. Development and Application of Trim Optimization and Parametric Study Using an Evaluation System (SoLuTion) Based on the RANS for Improvement EEOI. In Proceedings of the ASME 2014 33rd International Conference on Ocean, Offshore and Arctic Engineering OMAE2014, San Francisco, CA, USA, 8–13 June 2014.
36. Lyu, X.; Tu, H.; Xie, D.; Sun, J. On Resistance Reduction of a Hull by Trim Optimization. *Brodogradnja* **2018**, *69*, 1. [CrossRef]
37. Moustafa, M.M.; Yehia, W.; Hussein, A.W. Energy Efficient Operation of Bulk Carriers by Trim Optimization. In Proceedings of the 18th International Conference on Ships and Shipping Research 2015, NAV 2015, Lecco, Italy, 24–26 June 2015.
38. Reichel, M.; Minchev, A.; Larsen, N.L. Trim Optimization—Theory and Practice. *TransNav Int. J. Mar. Navig. Saf. Sea Transp.* **2014**, *8*, 3.
39. Bal Beşikçi, E.; Arslan, O.; Turan, O.; Ölçer, A.I. An Artificial Neural Network Based Decision Support System for Energy Efficient Ship Operations. *Comput. Oper. Res.* **2016**, *66*, 393–401. [CrossRef]
40. Jeon, M.; Noh, Y.; Shin, Y.; Lim, O.-K.; Lee, I.; Cho, D. Prediction of Ship Fuel Con-sumption by Using an Artificial Neural Network. *J. Mech. Sci. Technol.* **2018**, *32*, 5785–5796. [CrossRef]
41. Bassam, A.M.; Phillips, A.B.; Turnock, S.R.; Wilson, P.A. Artificial Neural Network Based Prediction of Ship Speed Under Operating Conditions for Operational Optimization. *Ocean Eng.* **2023**, *278*, 114613. [CrossRef]
42. Tarelko, W.; Rudzki, K. Applying Artificial Neural Networks for Modelling Ship Speed and Fuel Consumption. *Neural Comput. Appl.* **2020**, *32*, 17379–17395. [CrossRef]
43. Liu, B.; Gao, D.; Yang, P.; Hu, Y. An Energy Efficiency Optimization Strategy of Hybrid Electric Ship Based on Working Condition Prediction. *J. Mar. Sci. Eng.* **2022**, *10*, 1746. [CrossRef]
44. Lin, H.; Chen, S.; Luo, L.; Wang, Z.; Zeng, Y. Research on the Speed Optimization Model Based on BP Neural Network and Genetic Algorithm (GA). In Proceedings of the 29th International Ocean and Polar Engineering Conference, Honolulu, HI, USA, 16–21 June 2019.
45. Ozsari, I. Predicting main engine power and emissions for container, cargo and tanker ships with artificial neural network analysis. *Brodogradnja* **2023**, *74*, 2. [CrossRef]
46. ITTC. 7.5-02-03-02.1—Open Water Test, ITTC Quality System Manual, Recommended Procedures and Guidelines; International Towing Tank Conference, Resistance and Propulsion Committee of the 29th ITTC, 13–18 June 2021. Available online: https://www.ittc.info/media/9621/75-02-03-021.pdf (accessed on 31 March 2024).
47. IMO. *Development of Draft 2022 IACS Guidelines for the Use of Computational Fluid Dynamics (CFD) for the Purposes of Deriving the in the Framework of the EEXI Regulation, Resolution MEPC.78/INF.16*; Internation Maritime Organization: London, UK, 2022.
48. B-Series Propeller Generator. Available online: https://www.wageningen-b-series-propeller.com/ (accessed on 31 March 2024).
49. Bernitsas, M.M.; Ray, D.; Kinley, P. *K_T, K_Q and Efficiency Curves for the Wageningen B-Series Propellers*; College of Engineering, The University of Michigan: Ann Arbor, MI, USA, 1981.
50. Saydam, A.Z.; Küçüksu, G.N.; İnsel, M.; Gökçay, S. Uncertainty quantification of self-propulsion analyses with RANS-CFD and comparison with full-scale ship trials. *Brodogradnja* **2022**, *73*, 107–129. [CrossRef]

51. Mikulec, M.; Piehl, H. Verification and validation of CFD simulations with full-scale ship speed/power trial data. *Brodogradnja* **2023**, *74*, 41–62. [CrossRef]
52. Hirt, C.W.; Nichols, B.D. Volume of Fluid (VOF) Method for the Dynamics of Free Boundaries. *J. Comput. Phys.* **1981**, *39*, 201–225. [CrossRef]
53. Goldstein, S. On the Vortex Theory of Screw Propellers. Proceedings of the Royal Society of London. Series A, Containing Papers of a Mathematical and Physical Character, Volume 123, Issue 792, pp. 440–465. Available online: https://royalsocietypublishing.org/doi/abs/10.1098/rspa.1929.0078 (accessed on 31 March 2024).
54. Šeb, B. Numerička Karakterizacija Brodskog Propelera. Ph.D. Thesis, University of Zagreb, Faculty of Mechanical Engineering and Naval Architecture, Zagreb, Croatia, 2017.
55. White, F.M.; Majdalani, J. *Viscous Fluid Flow*, 4th ed.; McGraw Hill LLC: New York, NY, USA, 2021; pp. 578–583.
56. ITTC. 7.5-02-03-01.4, 1978 ITTC Performance Prediction Method, ITTC Quality System Manual, Recommended Procedures and Guidelines; International Towing Tank Conference, Resistance and Propulsion Committee of the 29th ITTC, 13–18 June 2021. Available online: https://www.ittc.info/media/9872/75-02-03-014.pdf (accessed on 31 March 2024).
57. Molland, A.F.; Turnock, S.R.; Hudson, D.A. *Ship Resistance and Propulsion: Practical Estimation of Propulsive Power*; Cambridge University Press: Cambridge, UK, 2011; p. 108.
58. ITTC. 7.5-03-01-01, Uncertainty Analysis in CFD Verification and Validation, Methodology and Procedures, ITTC Quality System Manual, Recommended Procedures and Guidelines; International Towing Tank Conference, Resistance and Propulsion Committee of the 29th ITTC, 13–18 June 2021. Available online: https://www.ittc.info/media/9765/75-03-01-01.pdf (accessed on 31 March 2024).
59. ITTC. 7.5-03-03-01, Practical Guidelines for Ship Self-Propulsion CFD, ITTC Quality System Manual, Recommended Procedures and Guidelines; International Towing Tank Conference, Qualitu Systems Group of the 28th ITTC, Wuxi, China, 2017. Available online: https://www.ittc.info/media/8169/75-03-03-01.pdf (accessed on 31 March 2024).
60. ITTC. 7.5-03-02-04, Practical Guidelines for Ship Resistance CFD, ITTC Quality System Manual, Recommended Procedures and Guidelines; International Towing Tank Conference, Resistance and Propulsion Committee of the 29th ITTC, 13–18 June 2021. Available online: https://www.ittc.info/media/8167/75-03-02-04.pdf (accessed on 31 March 2024).
61. Kracht, A.M. Design of Bulbous Bows. *SNAME Trans.* **1978**, *86*, 197–217.
62. Molland, A.F.; Turnock, S.R.; Hudson, D.A. *Ship Resistance and Propulsion, Practical Estimation of Ship Propulsive Power*, 2nd ed.; Cambridge Univeristy Press: Cambridge, UK, 2017.
63. Vasilev, M.; Kalajdžić, M.; Suvačarov, A. A Practical Approach to Bulbous Bow Retrofit Analysis for Enhanced Energy Efficiency. In Proceedings of the 25th Numerical Towing Tank Symposium (NuTTS), Ericeira, Portugal, 15–17 October 2023; pp. 191–196.
64. Schneekluth, H.; Bertram, V. *Ship Design for Efficiency and Economy*, 2nd ed.; Butterworth Heinemann: Oxford, UK, 1998.

ПРИЛОГ 11

A Practical Approach to Bulbous Bow Retrofit Analysis for Enhanced Energy Efficiency

Matija Vasilev[*†], Milan Kalajdžić[*†], Aleksa Suvačarov[*]
[*]Ocean Pro Marine Engineers LTD & [†]Faculty of Mechanical Engineering University of Belgrade, Serbia
matija@oceanpro.eu, mdkalajdzic@mas.bg.ac.rs, energy@oceanpro.eu

1 Introduction

The bulbous bow is a significant feature integrated into ship designs to improve their overall performance. However, relying solely on original design assumptions may lead to suboptimal results, potentially hindering the vessel's efficiency during operation. To address this issue and optimize ship performance, this paper proposes a practical methodology for retrofitting the bulbous bow to suit the actual operational profile of container ships. By analyzing four years' worth of operational data, this study identifies the most frequent sailing conditions, including speed, draft, trim, and displacement. Using this information, multiple bulbous bow configurations by following Kracht (1978) are derived and subjected to numerical simulations, tailored to various sailing conditions. The proposed framework not only optimizes the bulbous bow for container ships but also extends its application to other vessel types such as bulk carriers, tankers, and large commercial ships. By customizing the bulbous bow design to match specific operational profiles, significant improvements in fuel efficiency, environmental sustainability, and overall operational performance can be achieved. This research underscores the significance of accounting for real-world operational conditions when designing and optimizing the bulbous bow. Leveraging operational data and conducting numerical simulations facilitates the identification of optimal configurations, aligning vessel performance with its actual sailing conditions. Implementing these optimized bulbous bow designs has the potential to revolutionize the maritime industry by enhancing ship performance and promoting energy efficiency. By prioritizing the practical considerations of real-world operational conditions, this paper presents a valuable approach to improve the overall efficiency of ships, contributing to a more sustainable and eco-friendly maritime sector. CFD, or Computational Fluid Dynamics, has revolutionized the process of bulb optimization. Before its introduction, research was primarily based on physical model testing. However, CFD has made it significantly easier and faster to refine bulb designs. This technological advancement has allowed for the incorporation of economic and ecological considerations into bulb design, going beyond just hydrodynamics (refer to Schneekluth et al 1998). This advancement enables engineers and designers to not only improve the hydrodynamic performance of the bulb, but also to take into account factors such as cost-effectiveness and environmental impact. As a result, bulb optimization has become a more comprehensive and efficient process, ultimately leading to better-designed vessels and a more sustainable approach to shipbuilding. The first serious attempts to improve ship design using CFD began during the previous decades which includes parametric design Lu et al (2016), Yang et al (2016), Peri et al (2001), Sharma et al (2008), Wagner et al (2014) and many others. A common characteristic among all of them is that the bulbous bow has a positive effect at higher speeds (refer to Schneekluth et al (1998)). In this paper, bulb optimization is presented as a measure to improve the energy efficiency of a container vessel in order to meet the Carbon Intensity Indicator (CII) criteria defined in Resolution MEPC.353(78) (2022). The concept of a CII within the shipping industry, designed to gauge and manage the carbon emissions associated with maritime activities, has emerged as a crucial tool in addressing environmental concerns and reducing the sector's carbon footprint. The aim of the measures is to improve the fleet average carbon intensity by at least 40% in 2030, relative to 2008 (refer to Resolution MEPC.377(80), (2023)).

2 Methodology

The container vessel used for analysis was built in 2006 and is currently still in operation. The vessel in question belongs to the 2550TEU class with a maximum displacement of 45740t and a deadweight of 34248t at a design (and scantling) draft of 11.5m. The length between perpendiculars is 199m, and the moulded beam is 30.2m. Based on available construction drawings, the ship's 3D model has been created. The reference hull model is depicted in Figure 1.

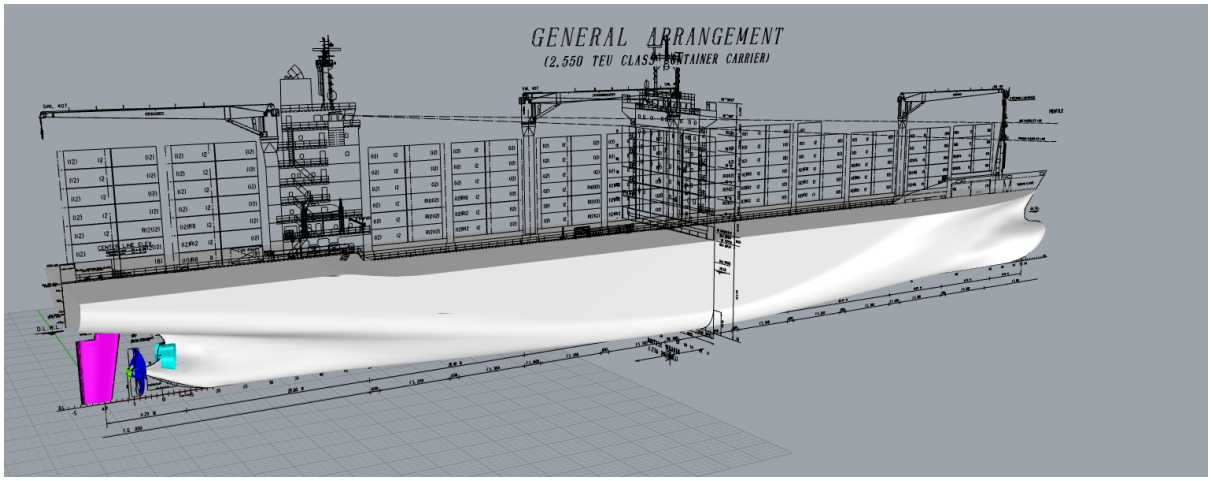

Fig. 1: Reference hull model

The analysis of operational profile is based on NOON reports submitted by the ship's crew for the period of 2018-2021. Excluding arrival, departure and port inputs and focusing only on seagoing logs the most common operational profile is derived. The average speed over four years of exploitation is 14kn which is a lot less than the design speed of 22.5kn and even less than described in Hochkirch et al (2009) where 70% of design speed was considered as usual reaction of containership operators to the high fuel prices. The most common loading condition is also nowhere near the design draft of 11.5m at even keel. The actual loading condition is closer to aft draft T_A = 9.15m and fore draft T_F = 8.15m with the displacement of approximately 32000t.

Operational data was used to obtain CII values in accordance with Resolution MEPC.352(78) (2022). The calculation results show that for the three consecutive years the ship is graded "D" [refer to Resolution MEPC.354(78) (2022). Therefore SEEMP Part III containing ship operational carbon intensity plan should be created and serve as the implementation plan for achieving the required CII (refer to Resolution MEPC.347(78) (2022)).

Based on provided operational data numerical simulation parameters are formed. Vessel simulation speeds are set at 10, 14, 18, 20 and 22.5 knots. The main draft for the simulations is T_A = 9.15m and T_F = 8.15m (aft and fore respectively). The ballast draft of T_A = 7.82m, T_F = 4.12m is used to verify the simulations methodology and setup against the model test and sea trial results. In Figure 2 are presented brake power (*Pb*) versus speed (*V*) curves extracted from available model test report and sea trial report, together with simulated same loading condition. Numerical simulations match the model test and sea trial results with 2% deviation. In all numerical simulations, self-propulsion with actuator disk (body force propeller) method was used.

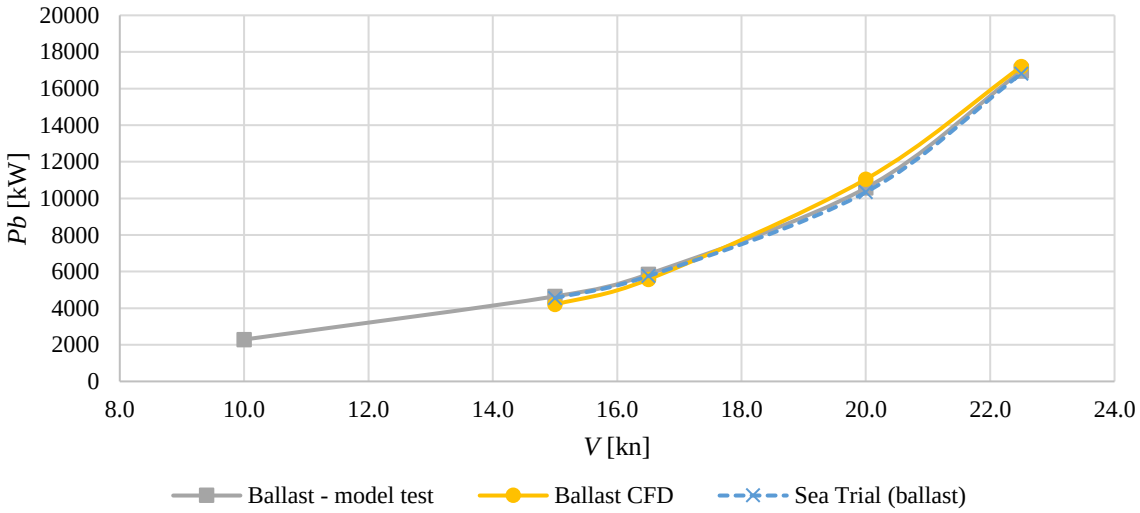

Fig. 2: CFD vs model test vs sea trial

Different bulbous bow configurations are tested for the determined operational draft. Three significant bulbous bow shapes were tested: nabla-type (∇-current design bow), delta-type (Δ), O-type (refer to Kracht (1978)) and vertical stem due to the fact that the average speed is slightly below the threshold of Fn=0.17, which represents the lower limit for the beneficial impact of bulbous bows (refer to Schneekluth et al (1998)). Bulbous bows additionally varied in length since the operational speeds were lower than the design speed. The bulbous bow lengths were originally planned at their designated designed bulb length, as well as in two reduced variations: one at 10% shorter and another at 20% shorter than the originally specified dimension. Designed bulb length is the length measured from forward perpendicular to the most prominent point of the bulb. A longer bulb was not considered due to the ship's operating speed being lower than its design speed. Increasing the bulb's length could potentially result in a longer overall length of the ship, which in turn might affect the floodable length. The floodable length is critical as it defines the maximum length of the ship that can be flooded without submerging the margin line. The margin line of a ship is an imaginary waterline located 75 mm below the uppermost continuous watertight deck.

In total, ten different bow configurations were tested at five different speeds at the most common draft. In the Figure 3 are presented all bow configurations and their centers of volumes. To gauge the effectiveness of the new bulbous bow design at the original design draft, an additional simulation was carried out. This simulation entailed a comparison between the new design and the original bulbous bow, providing insights into the new design's performance under the initial design draft conditions. A dimensionless parameter, specifically the ratio of thrust to displacement (T/D), has been determined In to compare the results for all configurations.

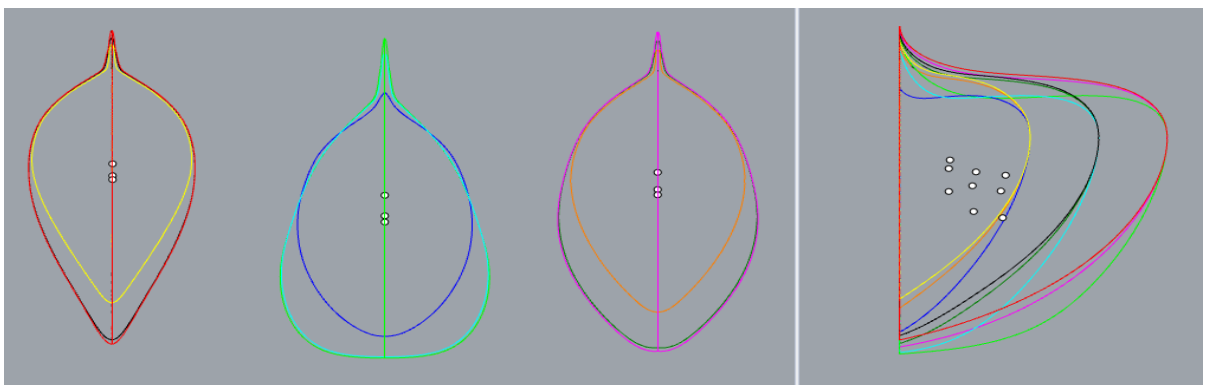

Fig. 3: ∇-type, Δ-type, O-type bulbous bows, respectively (transverse view (left) and longitudinal view (right))

3 Results

Figure 4 presents the results obtained from conducted simulations in the form of a 3D surface plot. On the x-axis, ship speed is varied within the range of 10 to 22 knots. On the y-axis, ten different considered configurations are depicted, ranging from 1 to 10. Configuration no. 1 corresponds to the best design, while configuration no. 10 represents the least favorable design. The "best" configuration is determined as the one that exhibits the most significant relative reduction in *T/D* (Thrust-to-Displacement ratio) on average across all speeds when compared to the original design. On the z-axis, denoted in Figure 4, a non-dimensional ratio $T/D \cdot 10^3$ is illustrated, defining the surfaces within the figure. The green-colored surface represents a reduction in *T/D*, indicating improved performance, while the red surface represents an increase in *T/D*, suggesting decreased performance. Ship no. 4 serves as the reference one, representing the original design, and is distinguished by a bold line in the figure. Each red dot on the plot corresponds to a specific configuration and is accompanied by a number indicating the relative reduction or increase in *T/D* compared to the originally designed bulb, presented as a percentage. In the accompanying Table 1, appropriate labels are provided for each configuration. The letter 'V' is used to represent a vertical stem in the design configurations, ∇ represents nabla-type bow, Δ represents delta-type bow and O represents O-type bow. Extensions such as -0, -10, and -20 indicate the original bulb length, a bulb length 10% shorter than the original, and a bulb length 20% shorter than the original, respectively.

Table 1: The order of effectiveness of the bow design configurations and their labels

Ship No.	1	2	3	4	5	6	7	8	9	10
Label	V	∇-20	∇-10	∇-0	Δ-10	Δ-20	Δ-0	O-20	O-0	O-10

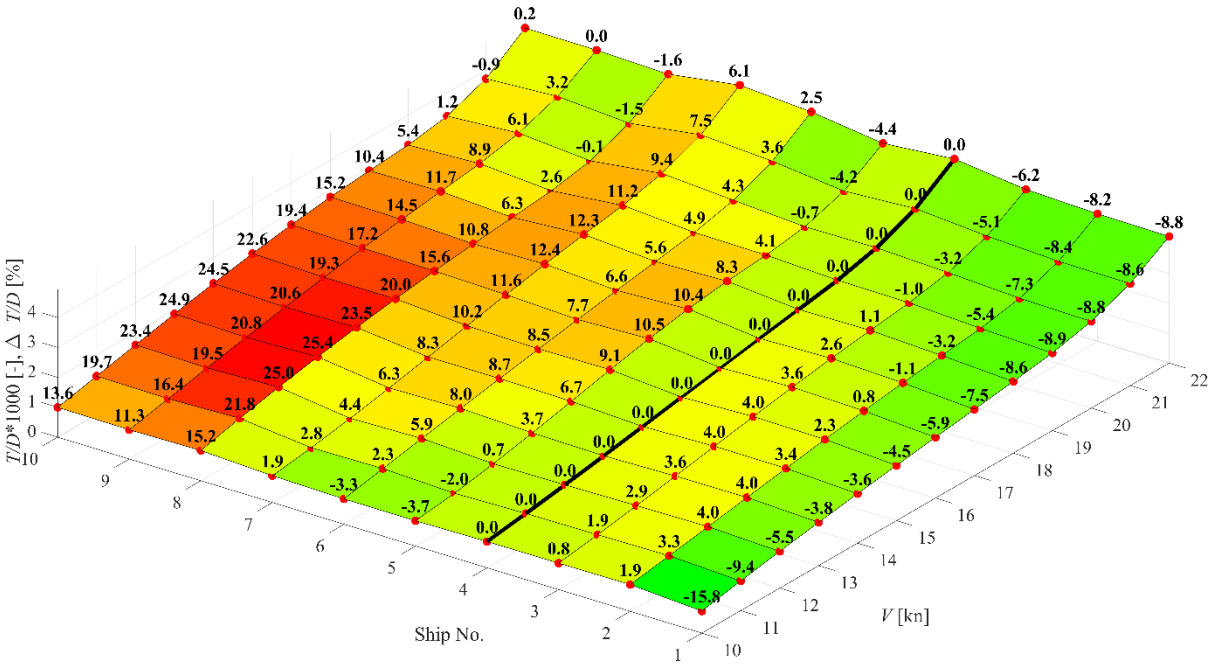

Fig. 4: Comparative analysis of *T/D* ratios for diverse ship bow configurations and speeds

In the context of the analyzed scenario, the vertical configuration has emerged as the most advantageous choice, showcasing an average *T/D* enhancement of 9.1%. It is followed by the ∇-20 and ∇-10 configurations, which exhibit 2.7% and 0.7% reductions in the *T/D* ratio, respectively. Conversely, all other configurations have demonstrated inferior performance when compared to the original design, with deviations reaching as high as 10%. This indicates that, in this specific context, the vertical configuration offers the most favorable balance between thrust and drag, resulting in significant efficiency gains, while alternative configurations present varying degrees of inefficiency, with some significantly falling short of the original design's performance. Furthermore, it's worth highlighting that

the daily fuel oil consumption with this V configuration would be reduced by 9%, a significant improvement that would likely enable the ship to achieve a grade of C for the next three years.

To further enhance the analysis, an additional simulation of the optimal V configuration was conducted at the design draft, and the results are depicted in Figure 5 where the results at new draft are also presented. According to findings at design draft, the V configuration exhibits inferior characteristics in terms of the *T/D* ratio compared to the original design (∇-0), with an average increase of 6.5%. Additionally, at a speed of 14 knots, it lags behind by 2.8%. This outcome aligns with expectations since the original design (∇-0) was optimized specifically for that loading condition (design draft). However, it's worth noting that the ship has never sailed at the design draft during the last four years. This suggests that the V configuration may be a better choice than the original design (∇-0) under the current operational conditions, emphasizing the importance of considering operational conditions and optimization criteria when selecting the appropriate configuration for a given application. In Figure 6, the design configurations of the original bulb (∇-0) and the vertical stem (V) are displayed at new draft. The red part, depicted in red, will be replaced with a green part, and it encompasses the section in front of the bow collision bulkhead and below the upper deck.

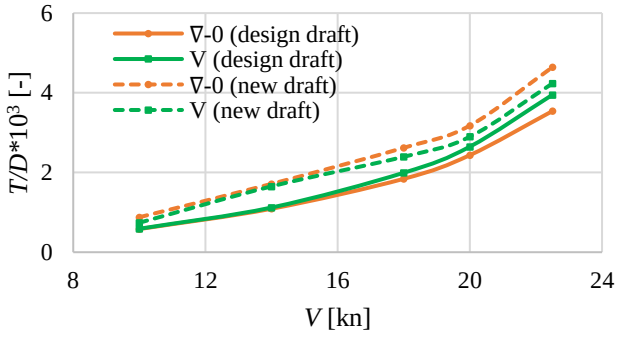

Fig. 5: V design compared to original ∇-0 design at design draft (solid lines) and new draft (dashed lines)

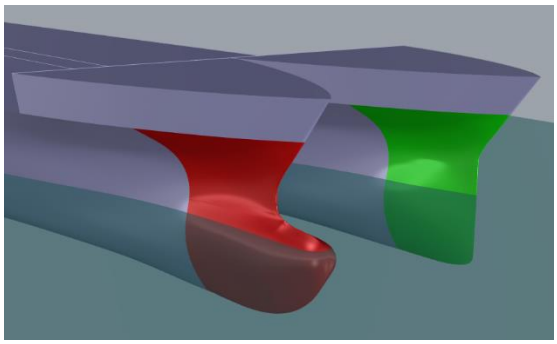

Fig. 6: ∇-0 (left) and V design (right)

By implementing a vertical stem instead of a bulb, the amplitude of the bow wave is reduced by as much as 28%. The wave profile is illustrated in Figure 7, where the green curve represents the wave corresponding to the vessel with a vertical (V) bow stem, and the orange curve represents the wave corresponding to the original (∇-0) design. The x-axis depicts the non-dimensional parameter of the ratio between the reference length (*X*) and the length between perpendiculars (*Lpp*), while the y-axis represents the free surface height measured from the even keel.

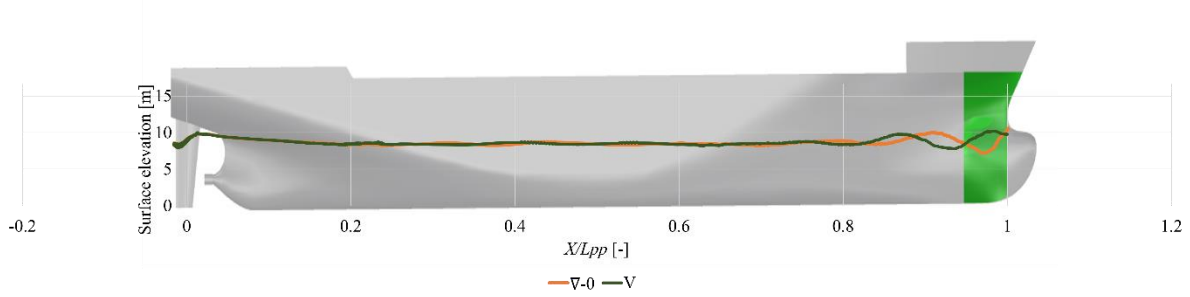

Fig. 7: Water surface elevation

4 Conclusion

The conducted numerical simulations for the most common load case of a container ship have yielded compelling results, showcasing the superiority of the simple vertical bow configuration. This outcome is not surprising, given the significant deviations between actual sailing conditions and the originally intended design condition. It underscores a critical point: adapting the vessel's design to real-world operational scenarios can lead to substantial improvements in efficiency. Specifically, by transitioning

from a bulb to a vertical stem, the potential for enhanced efficiency becomes evident, with fuel consumption and CO_2 emissions potentially reduced by up to 9%.

Furthermore, the study challenges conventional wisdom by revealing that the commonly recommended practice of having the bulb protrude slightly above the free surface (matching the new draft) may not universally apply. Instead, a fully submerged bulb, akin to the design draft, proves to be more effective in this particular case.

The vertical stem configuration emerges as a favorable choice, particularly for vessels frequently navigating at varying drafts and trims. Its advantages include simplicity and cost-effectiveness in manufacturing. To achieve an optimized design during retrofit, it is imperative to conduct meticulous analyses of operational data collected during voyages. For new ship construction projects, the vessel's future usage must be a central consideration, ensuring that the design is adaptable to multiple drafts and trims. This dynamic approach was previously impractical with traditional model tests, which were time-consuming and costly. However, the adoption of CFD and artificial neural networks offers a faster and more cost-efficient means of arriving at optimal solutions, ultimately enhancing the performance and sustainability of modern maritime transportation.

Acknowledgements

Authors would like to thank to Ocean Pro Marine Engineers LTD who provided necessary support in CFD simulations and guidelines. This work was supported by Ministry of Education, Science and Technological Development of Serbia (Project no. 451-03-47/2023-01/ 200105 from 3 February 2023).

References

Kracht A. M. (1978). Design of Bulbous Bows, *SNAME Transactions*, Vol. 86, pp. 197-217, 1978.
Schneekluth, H., Bertram, V. (1988). Ship Design for Efficiency and Economy, *Butterworth-Heinemann, Second edition*.
Lu Y. Chang, X., An-kang Hu A. (2016). A hydrodynamic optimization design methodology for a ship bulbous bow under multiple operating conditions, *Engineering Applications of Computational Fluid Mechanics*, 10:1, 330-345. DOI: 10.1080/19942060.2016.1159987.
Yang C., Huang F. (2001). An overview of simulation-based hydrodynamic design of ship hull forms, *Journal of Hydrodynamics*, 28(6):947-960, 2016, DOI: 10.1016/S1001-6058(16)60696-0.
Peri D., Campana E. F., Design Optimization of Ship Hulls via CFD Techniques, *Journal of Ship Research*. DOI: 10.5957/jsr.2001.45.2.140.
Sharma R., Sha O.P. (2008). Practical Hydrodynamic Design of Bulbous Bows for Ships, *Naval Engineers Journal*. DOI: 10.1111/j.1559-3584.2005.tb00321.x.
Wagner J., Binkowski E., Bronsart R. (2014). Scenario based optimization of a container vessel with respect to its projected operating conditions, *Int. J. Nav. Archit. Ocean Eng*. 6:496-506. DOI: 10.2478/IJNAOE-2013-0195.
Resolution MEPC.353(78) (2022). 2022 Guidelines on the reference lines for use with operational carbon intensity indicators (CII reference lines guidelines, G2), MEPC 78/17/Add/1, Annex 15.
Resolution MEPC.377(80) (2023). 2023 IMO Strategy on reduction of GHG emissions from ships, MEPC 80/WP.12, Annex 1.
Hochkirch K., Bertram V. (2009). Slow Steaming Bulbous Bow Optimization for a Large Containership, *8th International Conference on Computer and IT Applications in the Maritime Industries, COMPIT'09*.
Resolution MEPC.352(78) (2022). 2022 Guidelines on operational carbon intensity indicators and the calculation methods (CII guidelines, G1), MEPC 78/17/Add/1, Annex 14.
Resolution MEPC.354(78) (2022). 2022 Guidelines on the operational carbon intensity rating of ships (CII rading guidelines, G4), MEPC 78/17/Add/1, Annex 16.
Resolution MEPC.347(78) (2022). 2022 Guidelines for the verification and company audits by the administration of part III of the ship energy efficiency management plan (SEEMP), MEPC 78/17/Add/1, Annex 9.

ПРИЛОГ 12

The Influence of Roughness Change on Ship Resistance in CFD Simulations

Matija Vasilev, Milan Kalajdžić
Ocean Pro Marine Engineering LTD - Belgrade, Faculty of Mechanical Engineering University of Belgrade
matija@oceanpro.eu, mdkalajdzic@mas.bg.ac.rs

Abstract
The biofouling of ship hulls has a significant impact on both the environment and the ship. A negative effect on the environment is manifested by an increase in pollution with greenhouse gasses and disrupting the ecosystem by translocating microorganisms, sea plants or animals from one place to another. Biofouling film which appears on the immersed hull part through the years increases surface roughness and therefore induces a streamlines disturbance and together with increased wet surface affects the increase in total resistance. As a result of greater total resistance, a larger amount of fuel combusts over time, thus greenhouse emission is being increased. A numerical model based on Reynolds Averaged Navier-Stokes (RANS) equations with incorporated different roughness effects as equivalent sand grain roughness height in one Computational Fluid Dynamics (CFD) software has been conducted in this paper. Simulation has been applied to one bulk carrier and represents the effect of dry-docking the ship after several years in operation and treating the hull with high-performance coat such as self-polishing coating (SPC) or silicone- and fluorine-based fouling coatings (FRC).

1 Introduction

Biofouling is one of the problems that appeared together with the invention of the first ships. It could be said that fauna and flora don't want us in their environment, therefore they try to conquer every foreign thing that enters their habitat by fouling. This effect is negative for both sides, the natural ecosystem could be damaged when various species arrive with a ship from one destination to another. On the other side, the biofouling layer increases the wetted surface of the ship and together with streamlines disturbance due to non-smooth surface, affects the increase in total resistance, whence it implies power increase, consequently implies to increase in fuel combustion, and finally increase in air pollution. Air pollution is the main reason why is this topic very attractive nowadays.

Until today, many attempts were carried out in order to find the relation between roughness that represent fouled hull surface and the total resistance of a ship. Schultz (2005) conducted an experimental study to compare the frictional resistance of several ship hull coatings in unfouled, fouled and cleaned conditions with a flat plate. The increase in friction coefficient (C_F) compared to smooth surface in the unfouled condition ranged from 3% to 6%, in fouled 50%-217% and cleaned 3%-11%. Song et al. (2020a) presented an experimental investigation into the effect of roughness on ship resistance and provided validation of Granville's similarity law scaling (Granville (1958, 1978)) by using test results of a flat plate and a model ship. Frictional resistance of towed plate was increased up to 94% and the total resistance of the model ship up to 32%. This is validated later in CFD analysis and shown in Song et al. (2020b). The „orange peel" surface roughness drag penalty was empirically estimated by Utama et al (2017) and got a 31% increase compared to the hydrodynamically smooth surface without suffering and fouling. Hakim et al (2018) continued previous work and tried to verify the previous estimation by CFD with scanned recently cleaned and painted hull. The hull surface had an „orange peel" type of roughness ranging from 0.1 to 0.5 mm and they got an increase of 7.5% to 28% in total resistance. More detailed research was described in Demirel et al (2017) where a formula for hydrodynamic roughness as a function of barnacle height and percentage coverage is presented. In this case, roughness range from 2.5 mm to 5 mm leads to an increase in total resistance from 30% to 100%. As per Song et al. (2021) and experimental results with Wigley hull with various hull roughness conditions it is concluded

that added resistance is dominantly affected by the bow than at the aft with the same wetted surface. Over the years, CFD has become more and more popular in these kinds of research. So, the influence of roughness is not only checked on friction resistance, but also on wave resistance. Song et al. (2019) and Farkas et al. (2019, 2020) in three independent investigations have discovered that wave resistance can increase or decrease depending on the dominance of the wave-making resistance and the viscous pressure resistance. Moreover, Farkas and Song continued their work together and published Farkas, Song et al. (2020) the impact of biofilm on ship propulsion and concluded that the efficiency of the propeller decreases from 2.8% to 9.4% and therefore increases the power from 1.4% to 36.3%. According to Olmer et al. (2017), on average, hull fouling increases the power by about 7% and ranges from 2% to 11% depending on the ship's age and maintenance schedule. The increase in power leads to an increase in fuel consumption and as per some research (see Schultz et al, (2011)) 10.3% more fuel will be needed each year but together with applied anti-fouling coatings this value could be lower. The assessment of return on investment varied approximately from 1.5 to 3 years (see Farkas et al. (2021)). Extended research for the world fleet gives a total annual saving of about 3000 million USD (see Milne et al. (1971)).

2 Integration of roughness effect in CFD

As per Schultz (2007) there are several types of roughness i.e. fouled hull surfaces: 1) Hydraulically smooth surface; 2) Typical as applied anti-fouling coating; 3) Deteriorated coating or light slime; 4) Heavy slime; 5) Small calcareous fouling or weed; 6) Medium calcareous fouling; 7) Heavy calcareous fouling. Each type of mentioned roughness corresponds to one value of equivalent sand grain roughness (k_{eq}) and average hull roughness (*AHR*), see Demirel et al. (2017), Schultz (2007).

The equivalent sand grain roughness is an input parameter for Naval Hydro Pack CFD software based on CFD code within Open-FOAM used in this calculation. Idea is to represent the effect of dry-docking the ship after several years in operation and treating the hull with high-performance coatings such as self-polishing coating (SPC) or silicone- and fluorine-based fouling coatings (FRC). According to Doulgeris et al. (2012), average hull roughness amplitude increases gradually by 30 microns each year due to biofouling. If ITTC guidelines are being followed (see ITTC (2021)) where is indicated that for a new-built ship standard value of 150 microns for roughness should be used. So, a ship after five years in operation which is an usual period between dry-docking will have at least 300 microns of hull roughness. Haslbeck et al. (1992) described interesting research when for one ship sea trials have been conducted just after coating the ship and 22 months later. The results show that the difference in shaft power was 8-9%.

One of the available mathematical models for sand grain roughness can be found in Hadžić et al. (2022):

$$k_{eq}=0.0013AHR^2-0.3723AHR+70.144, \text{ if } AHR \leq 1000\ \mu m \text{ and } k_{eq}=AHR, \text{ else.} \quad (1)$$

This polynomial is based on Schultz (2007) and it is already used in software Naval Hydro Pack as described in Hadžić et al (2022). Within this research, the effects of biofouling are applied to the bulk carrier with the following particulars:

Table 1: Ship particulars.

L_{pp} [m]	186.65
B [m]	30
T [m]	10.7
Δ [m^3]	52106

Three speeds are considered: 11, 13 and 15 knots. Five simulations were performed for each speed with different average hull roughness: smooth hull, 75, 150, 300 and 600 μm. Calm water resistance

simulations are performed in full scale without appendages and results are compared with the available results of model tests. The 3D model of the considered ship is shown in the following Fig. 1 and Fig. 2:

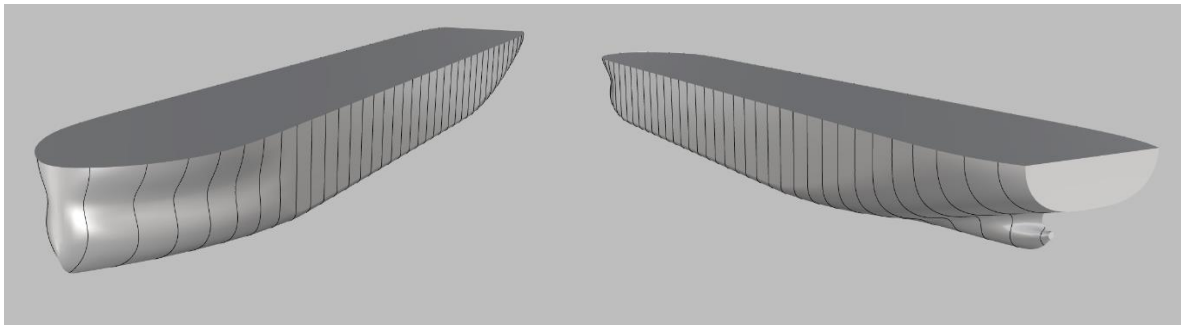

Fig. 1: Bow view.

Fig. 2: Aft view.

2 Results and discussion

Obtained results, shown in the following Table 2, are presented as differences in viscous (ΔFv), pressure (ΔFp) and total resistances (ΔFt) between considered rough hulls and the smooth hull.

Table 2: Results.

	ΔFv			ΔFp			ΔFt		
AHR	11 kn	13 kn	15 kn	11 kn	13 kn	15 kn	11 kn	13 kn	15 kn
75 μm	12.0%	14.2%	15.9%	-1.5%	-3.3%	-9.5%	8.9%	9.9%	9.1%
150 μm	10.2%	12.2%	13.7%	-2.5%	-3.6%	-10.1%	7.3%	8.3%	7.3%
300 μm	19.2%	22.0%	24.3%	-1.2%	-0.7%	-7.8%	14.4%	16.4%	15.7%
600 μm	55.7%	59.0%	61.4%	14.6%	13.0%	2.8%	46.2%	47.7%	45.7%

Roughness allowance significantly affects the increase in viscous resistance, but it has also been proven again that pressure resistance (wave-making resistance) could be increased or decreased just as in Song et al. (2019) and Farkas et al. (2019, 2020). To verify this procedure, the estimated total resistance with included roughness of 150 μm has been compared with the available model-scale test results for a range of speeds 11-15 kn and the differences are from -2 to -7% (on average -3.8% (see Fig. 3)). The minus sign means that CFD simulations underestimate results, which is expected in this case because the model used for tests was equipped with the rudder. Besides, it can be noticed that the character of results obtained by CFD simulations doesn't agree with the expected for the lowest considered *AHR*. Namely, it is concluded that evaluated added resistance is lower at *AHR*=150 μm than at *AHR*=75 μm. The reason is exactly in polynomial which has a global minimum at approximately 143 μm of *AHR*. In the Fig. 4 can be seen that differences in resistances follow the trend of the used polynomial (1).

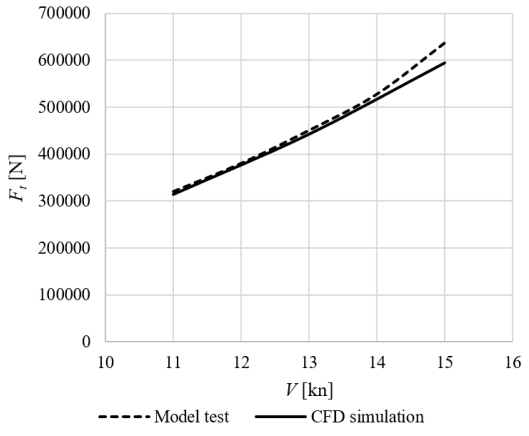

Fig. 3: Comparison: Model test vs CFD

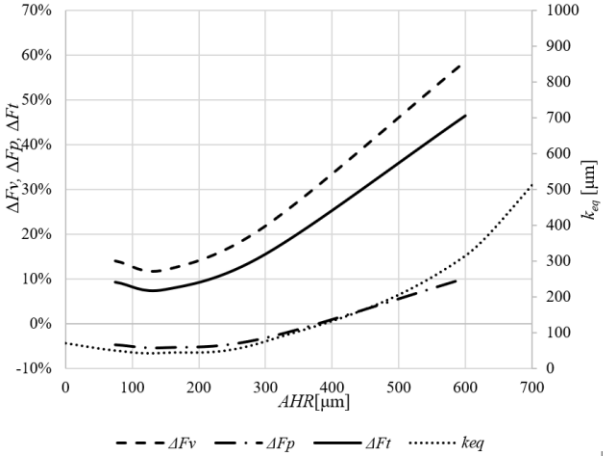

Fig. 4: Trend of k_{eq} polynomial and resistances.

The average differences in total resistance for 300 μm and 600 μm compared to total resistance with 150 μm of *AHR* are 7.3% and 36.1%, respectively. So, if the hull before cleaning had 300 μm or 600 μm of *AHR*, the expected savings in brake power after cleaning/painting are 8.8% and 45.5%, respectively. However, there is still a question if the hull is treated with a high-performance coating, with roughness lower than 150 μm. By using the aforementioned polynomial (1), there is no doubt that power saving will be less than expected. However, in some articles, such as Dean et al. (2010) and Ibrahim et al. (2018), fluid drag reduction could be achieved with a non-smooth surface like shark skin. This effect can reduce resistance from 3.9% to 5%.

However, Marine Environment Protection Committee through MEPC 78/INF.16 (2022) still didn't approve the previous method for roughness inclusion in CFD. The only accepted method is to calculate the resistance roughness allowance according to ITTC (2021) formula:

$$\Delta C_{F(\mathrm{ITTC})} = 0.044((AHR/L_{WL})^{1/3}\text{-}10\mathrm{Re}^{-1/3})+0.000125, \quad (2)$$

where L_{WL} is the length at the waterline, and Re is the Reynolds number.
The new total resistance coefficient C_T is calculated as follows:

$$C_T = C_v + C_p + \Delta C_{F(ITTC)}, \quad (3)$$

where C_v and C_p are viscous and pressure resistance coefficients obtained in CFD simulation.

After each provided CFD simulation with implemented sand grain roughness, roughness allowance can be computed as:

$$\Delta C_{F(\mathrm{CFD})} = C_{T(\text{hull with roughness})} - C_{T(\text{smooth hull})}\ , \quad (4)$$

and assuming that:

$$\Delta C_{F(\mathrm{CFD})} = \Delta C_{p(\text{hull with roughness})} + \Delta C_{v(\text{hull with roughness})}\ , \quad (5)$$

because it is proven that roughness affects both pressure and viscous parts of resistance. New simulations have been done in an iterative way for various values of k_{eq} until:

$$\Delta C_{F(\mathrm{CFD})} \approx \Delta C_{F(\mathrm{ITTC})} \quad (6)$$

is reached with an accuracy of less than 5%.

If formula (1) is applied, differences between $\Delta C_{F(\mathrm{CFD})}$ and $\Delta C_{F(\mathrm{ITTC})}$ are shown in Table 3. Significant differences are noted between two coefficients.

Table 3: Differences between roughness allowances.

AHR	75 μm	150 μm	300 μm	600 μm
$\Delta C_{F(\mathrm{CFD})}/\ \Delta C_{F(\mathrm{ITTC})}$-1	840%	40%	45%	170%

Every new k_{eq} were being interpolated between previously computed and after several iterations, new differences between roughness allowances are presented in Table 4:

Table 4: Differences between roughness allowances.

AHR	75 μm	150 μm	300 μm	600 μm
$\Delta C_{F(\mathrm{CFD})}/\ \Delta C_{F(\mathrm{ITTC})}$-1	N/A	2.5%	4.8%	3.7%

For 75 μm of *AHR*, an accuracy of less than 5% couldn't be achieved. For the rest of *AHR*, the required accuracy has been accomplished. Second order polynomial trendline has been set to approximate the results and therefore new formula for sand grain roughness has been presented:

$$k_{eq} = \text{-}1.62626\mathrm{E}\text{-}04AHR^2 + 2.26394\mathrm{E}\text{-}01AHR + 1.28182, \quad (7)$$

for $k_{eq} \geq 150$ μm and $k_{eq} \leq 600$ μm.

A summarized table with values of sand grain roughness according to formula from Hadžić et al. (2022), data from Schultz (2007) and the new polynomial (7), based on CFD results, are shown in Table 5, while the corresponding graph is presented in Fig. 5.

Table 5: Summarized sand grain roughness values.

	Hadžić et al (2022)	Schultz (2007)	New polynomial
AHR [μm]	k_{eq} [μm]	k_{eq} [μm]	k_{eq} [μm]
0	70	0	0
75	50	N/A	N/A
150	44	30	32
300	75	100	55
600	315	300	79

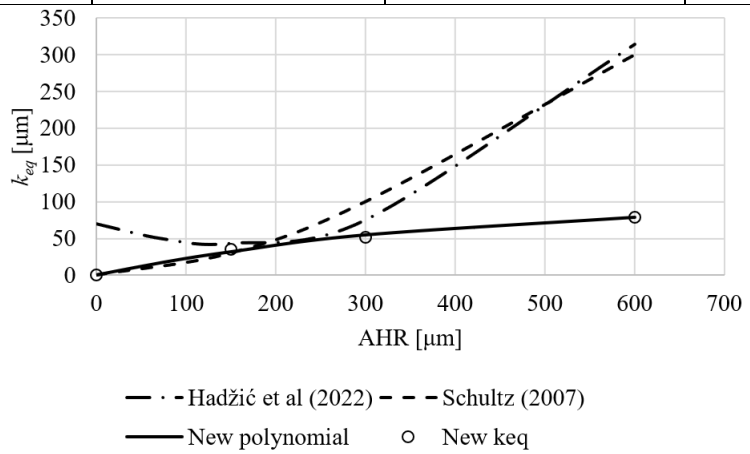

Fig. 5: Sand grain roughness curves.

With polynomial (7), new simulations are conducted and results are presented in the same way as they are in Table 2:

Table 6: Results with new polynomial.

	Δ*Fv*			Δ*Fp*			Δ*Ft*		
AHR	11 kn	13 kn	15 kn	11 kn	13 kn	15 kn	11 kn	13 kn	15 kn
150 μm	8.1%	9.6%	10.9%	-3.7%	-4.9%	-10.5%	5.4%	6.0%	5.2%
300 μm	13.4%	15.8%	17.7%	-0.2%	-3.6%	-1.0%	10.2%	11.0%	12.7%
600 μm	22.4%	25.6%	28.2%	3.3%	0.2%	-1.5%	18.0%	19.3%	20.3%

The average differences in total resistance for 300 μm and 600 μm compared to total resistance with 150 μm of *AHR* are 5.5% and 12.9%. If the hull before cleaning had 300 μm or 600 μm of *AHR*, the expected savings in brake power after cleaning/painting are 6.6% and 15.7%, respectively. This is in accordance with Olmer et al. (2017) if five years are considered to be a maintenance schedule.

3 Conclusion

Obtained new formula (7) can be applicable for bulk carriers similar to the considered ship with a range of Froude numbers Fn=0.13÷0.18. It should be noted that Schultz (2007) presented data for the US Navy ship. In future work, limits of applicability should be extended to cover larger numbers and kinds of ships, together with *AHR* higher than 600 μm. With new polynomial (7), wave resistance can again be increased or decreased depending on ship speed, while the effect of roughness is decreased compared to a polynomial (1). However, with provided iterative process, the satisfactory accuracy could not be met for 75 μm of *AHR*. More detailed analysis has to be performed for values of *AHR* less than 75 μm. Moreover, Anderson et al. (2020) could not find any strong correlation between *AHR* only and sand grain roughness. They suggest including hydrodynamic characterization of hull coating and expected fouling in CFD setup.

Acknowledgements

Authors would like to thank to Cloud Towing Tank who provided necessary support in CFD simulations and guidelines. This work was partially supported by Ministry of Education, Science and Technological Development (Project no. TR 35009) of Serbia.

References

M. P. Schultz (2005). Frictional Resistance of Antifouling Coating Systems. *J. Fluids Eng*. Nov 2004, 126(6): 1039-1047 (9 pages). https://doi.org/10.1115/1.1845552

S. Song, S. Dai, Y. K. Demirel, M. Atlar, S. Day, O. Turan (2020a). Experimental and theoretical study of the effect of hull roughness on ship resistance. *J Ship Res* 65 (01): 62–71. Paper Number: SNAME-JSR-07190040. https://doi.org/10.5957/JOSR.07190040

S. Song, Y. K. Demirel, M. Atlar, S. Dai, S. Day, O. Turan (2020b). Validation of the CFD approach for modelling roughness effect on ship resistance. *Ocean Engineering* 200 (2020) 107029. https://doi.org/10.1016/j.oceaneng.2020.107029

P. S. Granville (1958). The frictional resistance and turbulent boundary layer of rough surfaces. *J. Ship Res., 2*(3),52-74.

P. S. Granville (1978). Similarity-law characterization methods for arbitrary hydrodynamic roughnesses. In P.

S. Granville (Ed.), Final Report Naval Ship Research and Development Center, Bethesda, MD. Ship Performance Dept. (pp. 31). Bethesda, MD: David Tayler Naval Ship Research and Development Center.

I. K. A. P. Utama, B. Nugroho, C. Chin, M. L. Hakim, F. A. Prasetyo, M. Yusuf, I. K. Suastika, J. Monty, N. Hutchins, B. Ganapathisubramani (2017). A Study of Skin Friction Drag from Realistic Roughness of a Freshly Cleaned and Painted Ship Hull. *Proceedings of the International Symposium on Marine Engineering* (ISME) October 15-19, 2017, Tokyo, Japan.

M. L. Hakim, B. Nugroho, R. C. Chin, T. Putranto, I. K. Suastika (2018). Assessment of Drag Penalty Resulting from the Roughness of Freshly Cleaned and Painted Ship-hull using Computational Fluid Dynamics. *11th International Conference on Marine Technology*, MARTEC 2018.

Y. K. Demirel, D. Uzun, Y. Zhang, H. C. Fang, A. H. Day, O. Turan (2017). Effect of barnacle fouling on ship resistance and powering, *Biofouling*. http://dx.doi.org/10.1080/08927014.2017.1373279

S. Song, R. Ravenna, S. Dai, C. D. M. Fenech, G. Tani, Y. K. Demirel, M. Atlar, S. Day, A. Incecik (2021). Experimental investigation on the effect of heterogeneous hull roughness on ship resistance. *Ocean Engineering* 223 (2021) 108590. https://doi.org/10.1016/j.oceaneng.2021.108590

S. Song, Y. K. Demirel, M. Atlar (2019). An investigation into effect of biofouling on the ship hydrodynamic charactesitics using CFD. *Ocean Engineering* 175 (2019) 122-137. https://doi.org/10.1016/j.oceaneng.2019.01.056

A. Farkas, N. Degiuli, I. Martić (2019). Impact of biofilm on the resistance characteristics and nominal wake. *Journal of Engineering for the Maritime Environment*. DOI: 10.1177/1475090219862897

A. Farkas, N. Degiuli, I. Martić (2020a). An investigation into the effect of hard fouling on the ship resistance using CFD. *Applied Ocean Research* (2020) 102205. https://doi.org/10.1016/j.apor.2020.102205

A. Farkas, S. Song, N. Degiuli, I. Martic, Y. K. Demirel (2020b). Impact of biofilm on the ship propulsion characteristics and the speed reduction. *Ocean Engineering* 199 (2020) 107033. https://doi.org/10.1016/j.oceaneng.2020.107033

N. Olmer, B. Comer, B. Roy, X. Mao, D. Rutherford (2017). Greenhouse gas emissions from global shipping, 2013-2015. *The International Council on Clean Transportation*

M. P. Schultz, J. A. Bendick, E. R. Holm, W. M. Hertel (2011) Economic impact of biofouling on a naval surface ship, *Biofouling*, 27:1, 87-98, https://doi.org/10.1080/08927014.2010.542809

A. Farkas, N. Degiuli, I. Martic, M. Vujanovic (2021). Greenhouse gas emissions reduction potential by using antifouling coatings in a maritime transport industry. *Journal of Cleaner Production* 295 (2021) 126428 https://doi.org/10.1016/j.jclepro.2021.126428.

A. Milne, G. Hails (1971). British Patent 1457590.

M. P. Schultz (2007). Effects of coating roughness and biofouling on ship resistance and powering. *Biofouling: The Journal of Bioadhesion and Biofilm Research*.
http://dx.doi.org/10.1080/08927010701461974
Y. K. Demirel, O. Turan, A. Incecik (2017). Predicting the effect of biofouling on ship resistance using CFD. *Applied Ocean Research* 62 (2017) 100-118. http://dx.doi.org/10.1016/j.apor.2016.12.003
G. Doulgeris, T. Korakianitis, P. Pilidis, E. Tsoudis (2012). Techno-economic and environmental risk analysis for advanced marine propulsion systems. *Applied Energy* 99 (2012) 1-12.
http://dx.doi.org/10.1016/j.apenergy.2012.04.026
ITTC – Recommended Procedures and Guidelines (2021). 7.5-02-03-01.4 1978 *ITTC Performance Prediction Method*.
EG. Haslbeck, G. Behrends (1992), Microbial biofilm effects on drag – lab and field. *Proc SNAME Ship Production Symp*. Paper No. 3A-1. 7p.
N. Hadžić, I. Gatin, T. Uroić, V. Ložar (2022). Biofouling dynamic and its impact on ship powering and dry-docking. *Ocean Engineering* 245 (2022) 110522.
https://doi.org/10.1016/j.oceaneng.2022.110522
B. Dean, B. Bhushan (2010). Shark-skin surfaces for fluid-drag reduction in turbulent flow: a review. *Phil. Trans. R. Soc.* A 2010 368. doi: 10.1098/rsta.2010.0201
M.D. Ibrahim, S.N.A. Amran, Y.S. Yunos, M.R.A. Rahman, M.Z. Mohtar, L.K. Wong, A. Zulkarnain (2018). The Study of Drag Reduction on Ships Inspired by Simplified Shark skin Imitation. *Hindawi, Applied Bionics and Biomechanics.* Volume 2018, article ID 7854321.
https://doi.org/10.1155/2018/7854321
Marine Environment Protection Committee (2022). MEPC 78/INF.16 Reduction of GHG Emissions from Ships. 78th session, Agenda item 7. IACS.
J. Andersson, D.R. Oliveira, I. Yeginbayeva, M. L. Andersen, R. E. Bensow (2020). Review and comparison of methods to model ship hull roughness. *Applied Ocean Research* 99 (2020) 102119.
https://doi.org/10.1016/j.apor.2020.102119

ПРИЛОГ 13

From Lucy Ashton to Future CFD Case Studies: Benchmarking Ship Resistance at Full and Model Scales

Matija Vasilev [*,†], **Milan Kalajdžić** [*,†], **Dmitriy Ponkratov** [§]
[*] *Department of Naval Architecture, Faculty of Mechanical Engineering, University of Belgrade, Serbia*
[†] *Ocean Pro Marine Engineers LTD, Belgrade, Serbia*
[§] *Siemens Digital Industries Software, London, UK*
matija@oceanpro.eu

1 Introduction

Accurate prediction of ship resistance using Computational Fluid Dynamics (CFD) requires thorough validation against both model-scale and full-scale data. However, full-scale ship resistance measurements are extremely difficult to carry out, which is why throughout the entire history of shipbuilding, only a few such cases have ever been recorded. In 1874, William Froude towed an English corvette *HMS Greyhound* to demonstrate the transferability of model test results to full-scale ships (Froude, (1874)). In 1950/51, the British Shipbuilding Research Association performed extensive testing on the 390-ton ferry *Lucy Ashton* using four externally mounted Rolls-Royce jet engines (Denny (1951)). In 1953, SSPA (Sweden) towed a 70 m long destroyer *Wrangel*, built in 1918, using a nylon rope to reach 20 knots (Nordström (1953)). For the first time, the nominal wake field of a full-scale vessel was measured. This was followed by wake measurements on *HMS Penelope* in 1974 (Canham (1974)).

This study presents a comprehensive summary of benchmarking efforts for CFD simulations of ship resistance, starting with the *Lucy Ashton* vessel, a historical case supported by full-scale resistance measurements with installed jet engines on her deck. To broaden the evaluation, an additional vessel with an extensive experimental dataset-comprising model-scale and full-scale resistance measurements, full-scale self-propulsion data, wake field measurements-was analyzed. This expanded dataset enabled a more detailed assessment of simulation accuracy and scale effects. The outcomes from this study will support the organization of a dedicated CFD workshop, using the additional vessel as a reference case to promote standardized practices and improve simulation accuracy in maritime hydrodynamics.

The *Lucy Ashton*, originally a Clyde paddle steamer built in 1888, was repurposed in the mid-20th century as a floating laboratory for hydrodynamic research. After its retirement in 1949, the vessel underwent significant modifications to eliminate confounding variables and optimize its suitability for resistance testing. The removal of paddle wheels, machinery and deckhouses streamlined the hull, while sand ballast and structural reinforcements stabilized the ship for precise measurements. To enhance hydrodynamic smoothness, the hull surface was meticulously faired, with plate edges sharpened to reduce turbulence. A notable innovation was the installation of four Rolls Royce Derwent V jet engines on a custom gantry, generating over six tons of thrust to propel the ship to speeds of approximately 15 knots. This jet propulsion system eliminated the wake interference and unstable towing forces typical of conventional tugboat methods, enabling controlled resistance measurements. Emergency water brakes-steel flaps beneath the gantry-were added to counteract the jets' inability to reverse thrust, ensuring safe deceleration. A soundproof cabin designed by BBC engineers shielded the crew from the deafening engine noise, while strain gauges on the engine mounts provided precise thrust data. These modifications underscored the ingenuity required to adapt retired vessels for scientific rigor, balancing operational practicality with experimental accuracy.

The *Lucy Ashton* experiments, documented across multiple studies between 1951 and 1955 (Denny (1951), Conn et al. (1953), Lackenby (1955), Smith (1955)), pursued several interrelated objectives. First, they sought to correlate full-scale resistance measurements with predictions from model tests, using Froude's skin-friction coefficients to bridge scale differences. This involved testing six geometrically similar models ranging from 9 to 30 feet in length, with results highlighting discrepancies in skin-friction corrections and the influence of hull surface conditions. Aluminum paint, red oxide paint, faired versus unfaired seams and the effects of paint deterioration were systematically evaluated,

revealing measurable differences in resistance that underscored the importance of surface finish in hydrodynamic performance. A second focus was quantifying the resistance increments caused by twin-screw appendages, such as bossings and shaft brackets-a novel contribution, as prior studies had relied solely on model-scale data. The findings revealed scale-dependent effects, with appendage resistance increasing disproportionately at smaller scales, challenging assumptions about geometric similitude. Later phases of the program explored operational factors like fouling, virtual mass during acceleration trials and boundary layer dynamics using Pitot traverses. These investigations provided a holistic view of resistance contributors, from microscopic surface roughness to macroscopic appendage interactions. Decades later, the *Lucy Ashton* resurfaced as a benchmark for CFD validation during a 2024 blind workshop organized by Chalmers University of Technology. Participants simulated the ship's resistance using 1950s trial data, focusing on the smoothest hull condition-faired seams with aluminum paint-to isolate hydrodynamic effects without the confounding variable of surface roughness. The study by Lopes et al. (2025) revealed both the promise and limitations of modern computational tools. While simulations broadly captured trends across Froude numbers and scaling ratios, challenges emerged in accurately resolving the free surface interaction near the hull. Artificial viscosity in the numerical models led to underpredicted resistance at full scale, a discrepancy attributed to the "smearing" of turbulent structures. Incorporating hull roughness and allowing limited degrees of freedom in heave and pitch motions improved agreement with experimental data, though the double-body approach-a common simplification-proved inadequate at higher Froude numbers where wave-making resistance dominates. Additionally, Prohaska's classical method for estimating form factors yielded inconsistent results compared to CFD-derived values, suggesting a need for updated empirical correlations. Despite these challenges, the ITTC-78 extrapolation procedure aligned well with full-scale resistance when air drag and roughness were excluded, reaffirming its utility in practical ship design.

Parallel to the *Lucy Ashton* efforts, the 1967 trials of another vessel in the Baltic Sea addressed similar questions for large vessels. Using a family of models at three different model scales, the study aimed to validate extrapolation methods for resistance, propeller thrust and power demand. Her propulsion system-three water jets inspired by the *Lucy Ashton*'s design-delivered 12,000 HP of thrust, measured via strain gauges on the jet mounts. Unique to this experiment was the removal of the propeller to isolate total resistance, a technically demanding maneuver that required recalibrating thrust measurements. Pitot tubes and Prandtl tubes mapped the wake and boundary layer velocity distributions, while a force balance on the rudder shaft quantified steering forces. The results critiqued the ITTC 1957 skin-friction line, which was found to underpredict resistance increases at higher Reynolds numbers due to its insufficient slope. However, the study confirmed the universality of the logarithmic boundary layer profile (with von Kármán constants $K = 0.41$ and $C = 5.0$) and revealed that thrust deduction fractions remained scale-invariant, simplifying extrapolation procedures. These findings reinforced the importance of boundary layer physics in resistance prediction while highlighting gaps in mid-century extrapolation practices.

Instrumentation played a pivotal role in both studies. On the *Lucy Ashton*, two Pitot logs positioned 72 and 97 feet aft of the bow provided boundary layer profiles and speed measurements during trials. These devices, extended up to three feet from the hull, faced challenges during traversal, with data stability issues requiring rigorous filtering. Calibration via measured-mile runs ensured reliability within ±3%, though only data for a single speed (10.18 knots) were fully validated. The logs revealed a 50% thicker boundary layer at the aft position (0.46m vs 0.3m forward), illustrating the progressive growth of viscous effects along the hull.

The first CFD workshop that considered full-scale conditions was organized in 2016 with the now well-known ship *Regal* (Ponkratov (2016)). The same author had already addressed this topic earlier, validating CFD results against full-scale sea trial measurements (Ponkratov and Zegos (2014), Ponkratov and Zegos (2015)).

The main question is whether CFD results are more reliable than full-scale measurements, as there are many disturbance factors that can affect measurement results, such as sea currents, waves, wind and hull surface roughness. Recommendations for correcting measured data have been published through the ISO 15016 standard (ISO, 2025). The aim of CFD workshops is precisely to draw conclusions on whether CFD can be used as an adequate substitute for experiments. According to the results of past CFD workshops, there has been no indication of optimism regarding achieving the desired agreement

between experimental and numerical results. Moreover, over the past decade, a decline in the reliability of CFD code results has been observed, reflected in increased deviations in resistance prediction for the same model and mesh quality among workshop participants (Hino et al. (2021)).
In 2025, additional workshops are planned that will reach a higher level by organizing the following test cases: turbulent wake, wave breaking, course keeping in waves and cavitation. In addition, two more workshops will focus on full-scale powering performance for single-propeller and twin-propeller ships.
This paper presents an initiative for organizing an additional workshop that would cover basic resistance prediction analyses at multiple model scales as well as at full scale, propeller performance in open water in full scale (Open Water Test – OWT) and full-scale powering performance. No CFD workshop organized so far has covered all four of these research areas simultaneously.
The chapter on CFD results presents the reliability of numerical methods in predicting total resistance for both model-scale and full-scale ships for two different vessels, as well as OWT and powering performance predictions for one of them.
For setting up and analyzing the CFD simulations, the IACS (2024) guidelines were followed along with an internal methodology developed in-house.

2 CFD Results

Fig. 1 presents the total resistance coefficient (C_T) for the *Lucy Ashton* model obtained through both experimental measurements and CFD analysis across six different geometric scales. The dashed lines represent experimental data (labeled M in legend), while the solid lines correspond to CFD results. All values are plotted as a function of the Reynolds number. In Fig. 2, full-scale resistance measurements (discrete points), a fitted resistance curve derived from those measurements (dashed line) and the CFD-predicted full-scale resistance (solid line) are shown as a function of vessel speed. Full scale measured resistance data during sea trials (ST) were corrected to standard temperature, displacement, for the effect of helm while wind and air resistance and tide effect were eliminated, as per standards of the time when ST were conducted. The CFD results accounted for hull surface roughness, which was included in post-processing according to Denny (1951). A more accurate agreement between CFD predictions and experimental measurements was observed at higher speeds for the model-scale tests, whereas in full scale, better agreement was obtained at lower speeds.
Across all considered cases, both model and full scale, the discrepancy between CFD-predicted and experimentally measured total resistance values did not exceed 5%, demonstrating the reliability and accuracy of the applied simulation methodology.

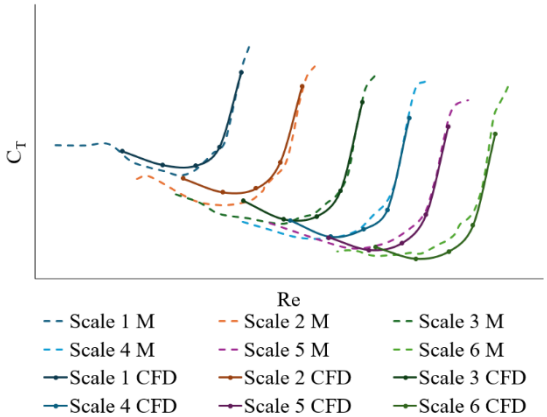

Fig. 1: Total resistance coefficient, six different model scales, Lucy Ashton, comparison between model test data (M) and CFD

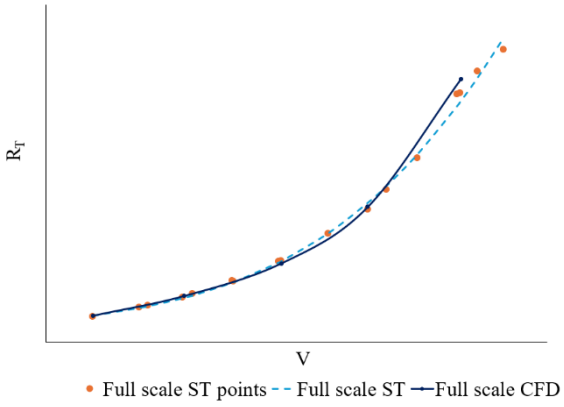

Fig. 2: Total resistance coefficient, full scale, Lucy Ashton, comparison between full scale data from ST and CFD

The same CFD methodology applied to *Lucy Ashton* was used for a second vessel, which will be the focus of an upcoming CFD workshop. Fig. 3 shows the estimated total resistance values of the bare hull model (labeled M in legend) in three different scales, obtained both experimentally (dashed lines) and

via CFD (solid lines). In order to protect proprietary experimental data before the workshop is concluded, the x-axis is represented using a transformed function *f*(Re), known only to the authors.
For each scale, CFD simulations were conducted at six different speeds while ensuring Froude number similarity between scales. The comparison revealed that the CFD results deviated by no more than 5% from the experimental measurements. Fig. 4 shows full-scale resistance values obtained through CFD (solid line) and a trendline (dashed line) based on full-scale measurements (points) during ST for a ship wothout propeller but with all appandages. Once again, the deviation between CFD-predicted and experimentally measured resistance remained within 5%, confirming the applicability of the method to ships of different dimensions and operational conditions.

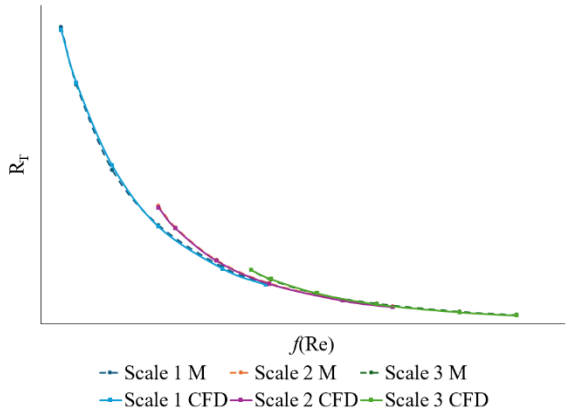

Fig. 3: Total resistance, three different model scales, comparison between model test data (M) and CFD

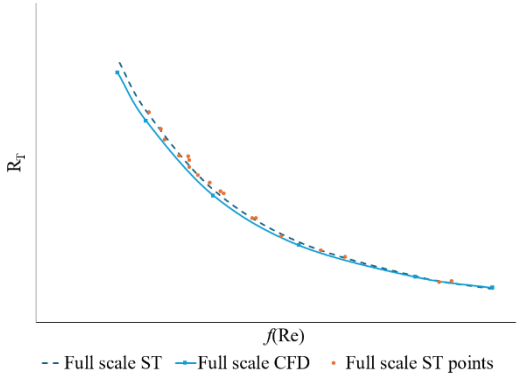

Fig. 4: Total resistance, full scale, comparison between full scale data from ST and CFD

To estimate delivered power, an OWT was simulated using CFD for the vessel's propeller. The propeller had predetermined geometric properties and simulations were conducted for six different advance coefficients. The objective was to derive hydrodynamic performance characteristics, namely the thrust coefficient (Kt), torque coefficient (Kq) and propeller efficiency (Eta0). These results are shown in Fig. 5, where the x-axis again uses *f*(Re) to ensure data protection. Since experimental open water tests were not available for the specific propeller design in full scale nor in model scale, the CFD results were benchmarked against a mathematical model (MM) corresponding to the propeller series installed on the vessel. Deviations between the CFD results and the mathematical model remained within 3% across all advance coefficients, further validating the CFD methodology.

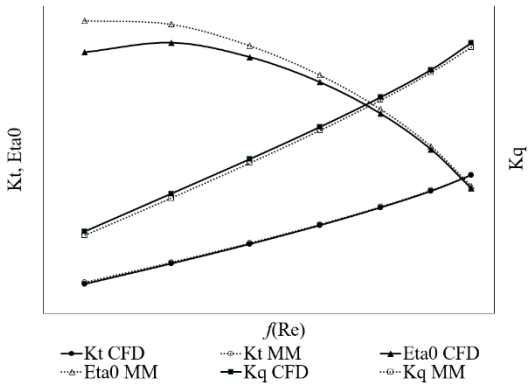

Fig. 5: Propeller characteristics, comparison between CFD and MM

Based on the previously determined propeller characteristics and resistance predictions, self-propulsion simulations were performed to assess powering performance. The actuator disk method was used to model the propeller's effect and estimate the required thrust for each of the six speeds analyzed. In the post-processing stage, a hull roughness value of 300 μm was introduced in accordance with ITTC (2024)

recommendations. Since specific roughness data were not explicitly documented for the vessel, this standard value was adopted due to explanation that it could be exptected. Additionally, air resistance due to the superstructure was included as per ITTC (2021) guidelines. Fig. 6 shows the delivered power estimated from CFD (solid line), the trendline based on ST measurements (dashed line) and the original data points. Fig. 7 presents shaft speed in the same format. The x-axis for both figures again uses the protected function *f*(Re). In both cases, deviations between CFD results and ST measurements did not exceed 5%.

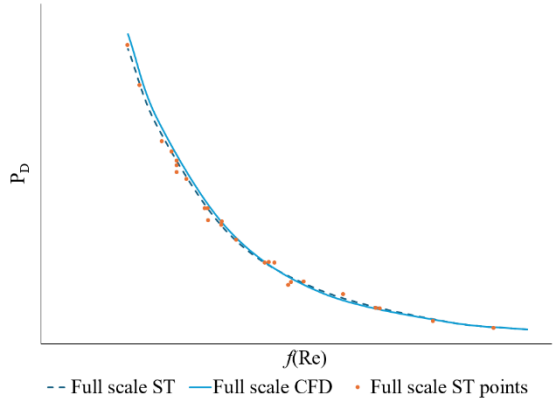

Fig. 6: Delivered power, measured during ST and CFD results

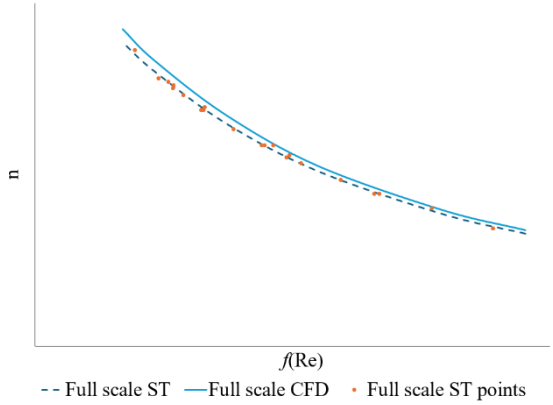

Fig. 7: Shaft speed, achieved during ST and CFD results

3 Conclusions

The results of the conducted CFD simulations, which included analysis of total ship resistance, open water propeller characteristics and self-propulsion performance, indicate that a universal and reliable methodology can be applied to ships of different types and sizes, across both model and full scales. This methodology demonstrated reliability for a range of Froude numbers from 0.1 to 0.3, with deviations between CFD predictions and experimental results consistently within the limits recommended by relevant international standards - 5% for total resistance and delivered power estimates and 3% for open water tests (OWT). The comparative analysis conducted for the historical ship *Lucy Ashton* across six model scales and full-scale conditions showed that CFD methods can replicate experimental resistance values with minimal discrepancy. Similarly, the methodology was successfully applied to a second vessel, the subject of an upcoming CFD workshop, confirming its applicability to a hull form with entirely different geometric characteristics. Importantly, in both cases, full-scale CFD simulations were post-processed to include hull surface roughness and air resistance in accordance with ITTC (2021, 2024) guidelines. The consistent agreement between numerical and experimental results across all studied domains reinforces the validity of this CFD approach and its potential to complement, or even substitute, physical model tests in certain design phases. This is particularly relevant given the logistical and financial constraints associated with full-scale trials and tank testing.
Looking forward, the goal is to organize a CFD workshop that will, for the first time, integrate four key analysis domains: multi-scale resistance prediction, full-scale resistance validation, open water test and delivered power estimation. No previously held CFD workshop has covered this full scope simultaneously.
Future research will also involve the application of this methodology to more different hull forms and propulsion configurations to evaluate its versatility.

References

D. Ponkratov, C. Zegos (2014). Ship Scale CFD Self Propulsion Simulation and Its Direct Comparison with Sea Trials Results, International Conference on Computational and Experimental Marine Hydrodynamics MARHY'14, Chennai, India

D. Ponkratov, C. Zegos (2015). Validation of ship scale CFD self-propulsion simulation by the direct comparison with sea trials results. In Proceedings of the Fourth International Symposium on Marine Propulsors. SMP'15, Austin, Texas, USA, June 2015

D. Ponkratov (2016). The workshop in ship scale computer simulations, Proceedings, Lloyd's Register, Southampton, UK

H.F. Nordström (1953). Full scale tests with the "Wrangel" and comparative model tests, SSPA paper no.27

H. Lackenby (1955). Resistance Experiments on the Lucy Ashton, Part III – The Ship-Model Correlation for the Shaft-Appendage Conditions, Quartetly Transactions of the Institution of Naval Architects, Vol. 97 No. 2, 109-166

H. J. S. Canham (1974). Resistance, propulsion and wake tests with HMS "Penelope", paper presented at Spring Meetings of Roy. Inst. of Naval Architects, 1974

IACS, 2024. EEXI Implementation Guidelines, Recommendation No. 172. London, England. URL https://iacs.org.uk (01.03.25.)

International Organization for Standardization (2025). Ships and marine technology – Specification for the assessment of speed and power performance by analysis of speed trial data (ISO stadndard No. 15016:2025, Third edition 2025-02).

ITTC, 2021. 7.5-02-03-01.4. 1978 ITTC Performance Prediction Method, ITTC Quality System Manual, Recommended Procedures and Guidelines; International Towing Tank Conference, Propulsion Committee of the 29th ITTC. URL https://www.ittc.info/media/8017/75-02-03-014.pdf (accessed 06.05.25.)

ITTC, 2024. 7.5-03-03-01, Practical Guidelines for Ship Self-Propulsion CFD, ITTC Quality System Manual, Recommended Procedures and Guidelines; International Towing Tank Conference, Specialist Committee on Combined CFD-EFD Methods of 30th ITTC. URL https://www.ittc.info/media/11964/75-03-03-01.pdf (accessed 06.05.25)

J. F. C. Conn, H. Lackenby, W. P. Walker, (1953). B.S.R.A. Resistance Experiments on the Lucy Ashton, Part II – The Ship-Model Correlation for the Naked Hull Conditions, Spring Meeting of the Institution of Naval Architects on March 25, 1953, 350-436

L. Smith (1955). Resistance Experiments on the Lucy Ashton, Part IV – Miscellaneous Investigations and General Appraisal, Quartetly Transactions of the Institution of Naval Architects, Vol. 97 No. 4, 525-561

M. E. Denny (1951). B.S.R.A. Resistance Experiments on the Lucy Ashton, Part I – Full Scale Measurements, International Conference of Naval Architects and Marine Engineers 1951, Unwin Brothers, 40-57

R. Lopes, A. Eslamdoost, R. Johansson, S. RoyChoudhury, R. E. Bensow, P. Hogstrom, D. Ponkratov, (2025). Resistance prediction using CFD at model- and full-scale and comparison with measurements, Ocean Engineering, Volume 321, 2025, 120367. doi: https://doi.org/10.1016/j.oceaneng.2025.120367

T. Hino, F. Stern, L. Larsson, M. Visonneau, N. Hirata, J. Kim, 2021. Numerical ship hydrodynamics. An assessment of the Tokyo 2015 Workshop, Springer, Switzerland

W. Froude, (1874). On experiments with HMS "Greyhound", Trans Inst. Naval Architects, Vol 15, p. 36

Биографија аутора

Матија Н. Василев, маст. инж. маш., рођен је 24. октобра 1994. године у Крушевцу, Република Србија. Основну школу „Миодраг Чајетинац Чајка“ у Трстенику завршио је 2009. године са одличним успехом. Након тога је похађао Гимназију „Вук Караџић“ у Трстенику, природно-математички смер, коју је завршио 2013. године, такође са одличним успехом.

Школске 2013/2014. године уписао је Основне академске студије – машинско инжењерство на Универзитету у Београду – Машинском факултету. Основне студије завршио је 2016. године са укупном просечном оценом 9,93 (девет и 93/100). За изванредан успех био је похваљен на првој, другој и трећој години студија. Током друге и треће године студија био је добитник стипендије Министарства просвете Републике Србије, а на трећој години добио је и престижну стипендију Фонда за младе таленте Министарства омладине и спорта Републике Србије – „Доситеја“. Поред тога, био је добитник стипендије за младе таленте општине Трстеник, а 2016. године и стипендије за изузетно надарене студенте Министарства просвете, науке и технолошког развоја Републике Србије.

Школске 2016/2017. године уписао је Мастер академске студије – машинско инжењерство, модул Бродоградња, на Машинском факултету Универзитета у Београду. Мастер студије завршио је 2018. године са укупном просечном оценом 9,55 (девет и 55/100). Мастер рад на тему „Истраживања могућности за побољшање пропулзивних карактеристика такмичарских пловних објеката Сава и Дунав“ одбранио је у октобру 2018. године са оценом 10 (десет), под менторством проф. др Александра Симића. На обе године мастер студија био је добитник похвале за изванредан успех, као и стипендије Министарства просвете Републике Србије (прва година) и стипендије Фонда за младе таленте Министарства омладине и спорта – „Доситеја“ (друга година). Поново је добио стипендију за младе таленте општине Трстеник.

У периоду 2016–2018. освајао је прва места на такмичењима Машинских факултета (Машинијадама) из области математике и механике. Такође, од 2017. до 2018. године био је члан студентског тима Машинског факултета „Confluence Belgrade“ (одсек Бродоградња), са којим је постигао запажене резултате – освојивши прво, друго и треће место на међународном такмичењу „Hydrocontest“ у различитим категоријама.

Од 2018. до 2020. године био је запослен као инжењер бродоградње у компанији „NTL Ship Design“, у сектору за бродске конструкције, где је радио на изради техничке документације, димензионисању конструктивних елемената и оптимизацији бродских структура.

Од 2020. до 2025. године био је запослен у компанији „Ocean Pro Marine Engineers“ као машински инжењер – конструктор, у сектору за енергетску ефикасност бродова, где учествује у развоју и примени иновативних решења за унапређење енергетске ефикасности постојећих и нових пловила, са посебним акцентом на примену CFD анализа и оптимизацију погонских система.

Школске 2021/2022. године уписао је Докторске академске студије – машинско инжењерство на Машинском факултету Универзитета у Београду, где тренутно спроводи истраживања из области хидродинамике и нумеричких симулација у поморској индустрији, са посебним фокусом на развој параметарских формула за оптимизацију мрежа у CFD симулацијама и унапређење енергетске ефикасности бродова.

Од октобра 2024. године на Машинском факултету Универзитета у Београду, стиче звање истраживача приправника на Катедри за бродоградњу, а од јануара 2026. године је и званично запослен на Машинском факултету Универзитета у Београду као стручно-технички сарадник

и изводи наставу из предмета Отпор брода, Пропулзија брода, Кормиларење брода и Рачунарских алата у бродоградњи.

Познавање страних језика

- Енглески језик - говори, чита и пише.

Познавање рада на рачунару

- Има значајне вештине кодирања у програмским софтверима Matlab/Simulink, Latex.
- Има вишегодишње искуство у коришћењу софтвера Microsoft Office, Autodesk AutoCAD, CorelDraw, 3D Beam, Genie, Rhino, Siemens StarCCM+ као и SolidWorks, Inkscape и DelftShip.

Истраживачке области

- Бродоградња.

Остало

- Возачка дозвола за Б категорију возила.
- Суоснивач Удружења студената бродоградње.
- Оснивач Међународног удружења машинских инжењера.
- Вишегодишњи члан Удружења бродограђевних инжењења и техничара.
- Члан међународног удружења високоинтелигентних људи „Mensa“.

Изјава о ауторству

Име и презиме аутора Матија Н. Василев
Број индекса Д31/21

Изјављујем

да је докторска дисертација под насловом

Параметарско подешавање мреже у CFD прорачунима са применом у анализи енергетске ефикасности бродова

- резултат сопственог истраживачког рада;
- да дисертација у целини ни у деловима није била предложена за стицање друге дипломе према студијским програмима других високошколских установа;
- да су резултати коректно наведени и
- да нисам кршио/ла ауторска права и користио/ла интелектуалну својину других лица.

Потпис аутора

У Београду, _____ _____

Изјава о истоветности штампане и електронске верзије докторског рада

Име и презиме аутора	Матија Н. Василев
Број индекса	Д31/21
Студијски програм	Докторске студије – Машинско инжењерство
Наслов рада	Параметарско подешавање мреже у CFD прорачунима са применом у анализи енергетске ефикасности бродова
Ментор	редовни професор др Милан Калајџић, Универзитет у Београду, Машински факултет

Изјављујем да је штампана верзија мог докторског рада истоветна електронској верзији коју сам предао/ла ради похрањивања у Дигиталном репозиторијуму Универзитета у Београду.

Дозвољавам да се објаве моји лични подаци везани за добијање академског назива доктора наука, као што су име и презиме, година и место рођења и датум одбране рада.

Ови лични подаци могу се објавити на мрежним страницама дигиталне библиотеке, у електронском каталогу и у публикацијама Универзитета у Београду.

Потпис аутора

У Београду, _____ _____

Изјава о коришћењу

Овлашћујем Универзитетску библиотеку „Светозар Марковић“ да у Дигитални репозиторијум Универзитета у Београду унесе моју докторску дисертацију под насловом:

Параметарско подешавање мреже у CFD прорачунима са применом у анализи енергетске ефикасности бродова

која је моје ауторско дело.

Дисертацију са свим прилозима предао/ла сам у електронском формату погодном за трајно архивирање.

Моју докторску дисертацију похрањену у Дигиталном репозиторијуму Универзитета у Београду и доступну у отвореном приступу могу да користе сви који поштују одредбе садржане у одабраном типу лиценце Креативне заједнице (Creative Commons) за коју сам се одлучио/ла.

1. Ауторство (CC BY)
2. Ауторство – некомерцијално (CC BY-NC)
3. Ауторство – некомерцијално – без прерада (CC BY-NC-ND)
4. Ауторство – некомерцијално – делити под истим условима (CC BY-NC-SA)
5. Ауторство – без прерада (CC BY-ND)
6. Ауторство – делити под истим условима (CC BY-SA)

Потпис аутора

У Београду, _____ _____

1. Ауторство. Дозвољавате умножавање, дистрибуцију и јавно саопштавање дела, и прераде, ако се наведе име аутора на начин одређен од стране аутора или даваоца лиценце, чак и у комерцијалне сврхе. Ово је најслободнија од свих лиценци.
2. Ауторство – некомерцијално. Дозвољавате умножавање, дистрибуцију и јавно саопштавање дела, и прераде, ако се наведе име аутора на начин одређен од стране аутора или даваоца лиценце. Ова лиценца не дозвољава комерцијалну употребу дела.
3. Ауторство – некомерцијално – без прерада. Дозвољавате умножавање, дистрибуцију и јавно саопштавање дела, без промена, преобликовања или употребе дела у свом делу, ако се наведе име аутора на начин одређен од стране аутора или даваоца лиценце. Ова лиценца не дозвољава комерцијалну употребу дела. У односу на све остале лиценце, овом лиценцом се ограничава највећи обим права коришћења дела.
4. Ауторство – некомерцијално – делити под истим условима. Дозвољавате умножавање, дистрибуцију и јавно саопштавање дела, и прераде, ако се наведе име аутора на начин одређен од стране аутора или даваоца лиценце и ако се прерада дистрибуира под истом или сличном лиценцом. Ова лиценца не дозвољава комерцијалну употребу дела и прерада.
5. Ауторство – без прерада. Дозвољавате умножавање, дистрибуцију и јавно саопштавање дела, без промена, преобликовања или употребе дела у свом делу, ако се наведе име аутора на начин одређен од стране аутора или даваоца лиценце. Ова лиценца дозвољава комерцијалну употребу дела.
6. Ауторство – делити под истим условима. Дозвољавате умножавање, дистрибуцију и јавно саопштавање дела, и прераде, ако се наведе име аутора на начин одређен од стране аутора или даваоца лиценце и ако се прерада дистрибуира под истом или сличном лиценцом. Ова лиценца дозвољава комерцијалну употребу дела и прерада. Слична је софтверским лиценцама, односно лиценцама отвореног кода.